Synthesis of renewable polycarboxylic acids and their application in polymer science

Zur Erlangung des akademischen Grades eines

DOKTORS DER NATURWISSENSCHAFTEN

(Dr. rer. nat.)

von der KIT-Fakultät für Chemie und Biowissenschaften

des Karlsruher Instituts für Technologie (KIT)

genehmigte

DISSERTATION

von

Luis Santos Correa (M.Sc.)

aus Villingen-Schwenningen

1. Referent: Prof. Dr. Michael A. R. Meier

2. Referent: Prof. Dr. Joachim Podlech

Tag der mündlichen Prüfung: 10.02.2025

“*An expert is a person who has made all the mistakes*
that can be made in a very narrow field.“

Niels Bohr

Declaration of Authorship

Die vorliegende Arbeit wurde von Februar 2022 bis Januar 2025 unter Anleitung von Prof. Dr. Michael A. R. Meier am Institut für Organische Chemie (IOC) und am Institut für Biologische und Chemische Systeme – Funktionelle Molekulare Systeme (IBCS-FMS) des Karlsruher Instituts für Technologie (KIT) angefertigt.

Erklärung

Hiermit versichere ich, dass ich die Arbeit selbstständig angefertigt, nur die angegebenen Quellen und Hilfsmittel benutzt und mich keiner unzulässigen Hilfe Dritter bedient habe. Insbesondere habe ich wörtlich oder sinngemäß aus anderen Werken übernommene Inhalte als solche kenntlich gemacht. Die Satzung des Karlsruher Instituts für Technologie (KIT) zur Sicherung wissenschaftlicher Praxis habe ich beachtet. Des Weiteren erkläre ich, dass ich mich derzeit in keinem laufenden Promotionsverfahren befinde, und auch keine vorausgegangenen Promotionsversuche unternommen habe. Die elektronische Version der Arbeit stimmt mit der schriftlichen Version überein und die Primärdaten sind gemäß Abs. A (6) der Regeln zur Sicherung guter wissenschaftlicher Praxis des KIT beim Institut abgegeben und archiviert.

Karlsruhe den 07.01.2025

Luis Santos Correa

Abstract

The development and production of new materials from renewable resources is of paramount importance to reduce humanity's high dependency on depleting fossil resources. Especially research on polymers must be performed, since to date still less than 1% of the worldwide production of plastics is bio-based.

This work focused on the utilization of renewable resources for the synthesis of new mono and polycarboxylic acids that serve as monomers for the production of bio-based polymers. The performed reactions were optimized in each project considering sustainability aspects of the *Twelve Principles of Green Chemistry*, such as waste production and toxicity of the involved chemicals. This work therefore contributes to the transition from conventional fossil-based chemistry towards the use of renewable resources.

First, a new three-step reaction sequence was developed to synthesize renewable fatty acid based dimethyl esters from saturated fatty acids. The sequence consists of a catalytic dehydrogenation with molecular oxygen as oxidant, an esterification with methanol, and a dimerization reaction with dithiols *via* thia-Michael addition. Three new dimethyl esters were thus synthesized from lauric acid and subsequently polymerized with 1,12-dodecanediol to obtain polyesters with high molecular weights (up to 31.8 kDa). Methyl crotonate-based polymers were prepared for comparison with the fatty acid derived materials. Thermogravimetric analysis revealed that an increasing carbon content led to improved thermal stability and differential scanning calorimetry showed side chain crystallization for one polymer.

In a second project, a literature known ruthenium catalyzed oxidative cleavage of alkenes was utilized to synthesize a tricarboxylic acid from high oleic sunflower oil. A statistical concept was devised for the prediction of the yields of mono-, di- and trifunctional derivatives that can be formed, depending on the overall conversion of double bonds into carboxylic acids and the overall oleic acid content of the used oil. This concept proofed to be highly useful for the explanation of seemingly moderate triacid yields, which are inherently dependent on the unsaturated fatty acid content of the used oil. In addition, a more sustainable purification procedure was developed to obtain a polymerizable mixture of polyacids containing more than 2.0 carboxylic acid groups per molecule on average.

The sunflower oil-based tricarboxylic acid was utilized in a following project to synthesize cross-linked thermosets *via* the Passerini three-component reaction. Ten different polymers were synthesized from the triacid in combination with two diisocyanides and five monoaldehydes and subsequently characterized *via* infrared spectroscopy, swelling tests, thermogravimetric analysis, differential scanning calorimetry, and tensile tests. The characterization of the insoluble polymeric networks was complemented by the synthesis of model compounds to enable analysis in solution *via* nuclear magnetic resonance spectroscopy. Due to the fast curing of all polymers at room temperature, adhesive tests were performed to demonstrate their potential application as glues. At last, the circularity of these new materials was shown by chemical recycling of one polymer *via* transesterification with methanol and catalytic amounts of sulfuric acid to recycle azelaic acid dimethyl ester and a difunctional *α*-hydroxyamide in yields of 75%. Repolymerization of the *α*-hydroxyamide to a polyurethane was performed to demonstrate a potential second life of these compounds.

In a final project, a synthetic route was established for the synthesis of organosolv lignin-based polycarboxylic acids. Carboxylic acid moieties were thus introduced by functionalization of organosolv lignin with succinic anhydride. Through variation of temperature, concentration and amount of succinic anhydride, different degrees of substitution (DS) between 10% and 70% of all alcohol groups were achieved. For the succinylated lignin sample with the highest DS of 70%, quantitative conversion of all aliphatic alcohol groups was observed by ^{31}P NMR spectroscopy, while aromatic alcohol groups only reached a maximum degree of substitution of 35%, presumably due to the thermodynamic instability of the produced phenyl esters. In another approach, a synthetic route *via* hydroxyethylation was chosen to first transform all aromatic alcohol groups into their corresponding hydroxyethyl ethers. The newly introduced hydroxyethyl groups as well as the originally present aliphatic alcohol groups of organosolv lignin were subsequently reacted with succinic anhydride to synthesize a polycarboxylic acid sample with a high DS of 99.6%. All samples were furthermore characterized *via* ^{1}H NMR spectroscopy, infrared spectroscopy, and size exclusion chromatography. The synthesized renewable polycarboxylic acids from lignin are promising compounds for future syntheses of cross-linked polymers, as was demonstrated in a proof of concept for one Passerini three-component polymerization.

Zusammenfassung

Die Entwicklung und Herstellung neuer Materialien aus nachwachsen Ressourcen ist von größter Bedeutung, um die Abhängigkeit der Menschheit vom Erdöl zu reduzieren. Speziell im Bereich der Polymerchemie muss dieser Ansatz implementiert werden, da bis heute immer noch weniger als 1% der gesamten weltweiten Plastik Produktion biobasiert sind.

Diese Arbeit beschäftigte sich mit der Nutzung von nachwachsenden Ressourcen für die Synthese von neuen Mono- und Polycarbonsäuren, welche als Monomere für die Produktion von biobasierten Polymeren dienen. Die benutzten Reaktionen wurden in jedem Projekt in einer nachhaltigen Weise optimiert, um die Produktion von Müll zu minimieren und die Benutzung von toxischen Chemikalien zu vermeiden. Die Arbeit trägt daher zum Wandel von konventioneller erdölbasierter Chemie zur Nutzung nachwachsender Ressourcen bei.

Zuerst wurde eine neue drei Stufen Reaktionssequenz entwickelt, um Dimethylester aus gesättigten Fettsäuren herzustellen. Die Reaktionssequenz besteht aus einer katalytischen Dehydrogenierung mit molekularem Sauerstoff als Oxidationsmittel, einer Veresterung mit Methanol und einer Dimerisierungsreaktion mit Dithiolen durch Thia-Michael Addition. Drei neue Dimethylester wurden aus Laurinsäure hergestellt und anschließend mit 1,12-Dodecandiol polymerisiert, um Polyester mit molekularen Gewichten von bis zu 31.8 kDa zu erhalten. Methylcrotonat basierte Polymere wurden zum Vergleich mit den fettsäurebasierten Materialien hergestellt. In thermogravimetrischer Analyse wurde gezeigt, dass ein größerer Kohlenstoff Anteil die thermische Stabilität der Materialien erhöht hat. Zudem wurde für ein Polymer in dynamischer Differenzkalorimetrie Kristallisation der Seitenketten beobachtet.

In einem zweiten Projekt wurde eine literaturbekannte Ruthenium katalysierte oxidative Spaltung von Alkenen benutzt, um eine Tricarbonsäure aus high oleic Sonnenblumenöl herzustellen. Es wurde darüber hinaus ein statistisches Konzept entwickelt, um die Ausbeuten von mono-, di- und trifunktionalen Derivaten in Abhängigkeit von der gesamten Umwandlung von Doppelbindung in Carbonsäuren und dem Anteil an Ölsäure im Öl vorherzusagen. Dieses Konzept ermöglichte die Erklärung scheinbar mittelmäßiger Ausbeuten an Trisäure, welche inhärent abhängig vom Anteil ungesättigter Fettsäuren im benutzten Öl sind. Zudem wurde ein nachhaltigeres Verfahren zur Aufreinigung entwickelt, um ein Gemisch von Carbonsäuren zu erhalten, welche im Schnitt über 2.0 Carbonsäuregruppen pro Molekül enthalten.

Die sonnenblumenölbasierte Tricarbonsäure wurde in einem Folgeprojekt benutzt, um quervernetzte Duroplaste durch die Passerini Dreikomponenten Reaktion herzustellen. Zehn unterschiedliche Polymere wurden aus der Trisäure in Kombination mit zwei Diisocyaniden und fünf Monoaldehyden hergestellt und mittels Infrarot Spektroskopie, thermogravimetrischer Analyse, dynamischer Differenzkalorimetrie und Zugversuchen analysiert. Die Charakterisierung der unlöslichen Polymernetzwerke wurde durch Modellsubstanzen komplementiert, da diese eine Analyse in Lösung durch Kernspinresonanzspektroskopie ermöglichten. Aufgrund der schnellen Aushärtung der Polymere bei Zimmertemperatur, wurden Klebetests durchgeführt um ihre Anwendung als Kleber zu demonstrieren. Zuletzt wurde die Zirkularität dieser Materialien durch chemisches Recycling von einem Polymer gezeigt. Azelainsäure Dimethylester und ein bifunktionelles *α*-Hydroxyamid konnten durch Umesterung mit Methanol und katalytischen Mengen Schwefelsäure in einer Ausbeute von 75% rezykliert werden. Die erneute Polymerisation des *α*-Hydroxyamids zu einem Polyurethan wurde durchgeführt, um eine erneute Anwendung zu demonstrieren.

In einem letzten Projekt wurde eine synthetische Route entwickelt, um Lignin basierte Polycarbonsäuren herzustellen. Carbonsäuregruppen wurden durch Funktionalisierung mit Bernsteinsäureanhydrid in das Lignin Gerüst eingebaut. Durch Variation der Temperatur, der Konzentration und der Menge an Bernsteinsäureanhydrid, konnten unterschiedliche Funktionalisierungsgrade zwischen 10% und 70% von allen Alkoholgruppen erreicht werden. Es wurde mittels ^{31}P NMR-Spektroskopie für die succinylierte Lignin Probe mit einem DS von 70% ein quantitativer Umsatz für aliphatische Alkoholgruppen beobachtet, während aromatische Alkoholgruppen nur einen Umsatz von 35% erreichten, vermutlich aufgrund der thermodynamischen Instabilität der gebildeten Phenylester. In einer anderen Herangehensweise, wurden durch Hydroxyethylierung alle aromatischen Alkoholgruppen in ihre entsprechenden Hydroxyethylether umgewandelt. Die in diesem Schritt eingebauten Hydroxyethylgruppen und die ursprünglich vorhandenen aliphatischen Alkoholgruppen vom Organosolv Lignin wurden anschließend mit Bernsteinsäureanhydrid reagiert, um eine weitere Polycarbonsäure Probe mit einem hohen Funktionalisierungsgrad von 99.6% herzustellen. Alle Proben wurden zudem mittels ^{1}H NMR-Spektroskopie, Infrarotspektroskopie, und Größenausschluss-Chromatographie untersucht. Die hergestellten Polycarbonsäuren sind vielversprechend für zukünftige Synthesen von quervernetzten Polymeren. Dies wurde als Proof of Concept mit einer Passerini Dreikomponenten Polymerisation demonstriert.

Table of Contents

1 Introduction

In chemistry, almost every industrial process for the synthesis of bulk chemicals is based on fossil resources and thus the vast majority of chemical products we use in our everyday life is as well.[1-3] The current rate at which humanity consumes fossil resources however exceeds their natural regeneration by several orders of magnitude and will therefore eventually result in their depletion within the next centuries. The demand of these limited resources will most likely rise even more due to the increasing global population. In 1987, the UN World Commission on Environment and Development defined sustainability as a “development that meets the needs of the present without comprising the ability of future generations to meet their own needs”.[4] The chemical sector is therefore, without doubt, unsustainable and a major transition must ensue to guarantee the same quality of life in all three pillars of sustainability for the next generations. One key aspect in chemistry is the utilization of renewable resources, which is inevitable with regard to the foreseeable exhaustion of fossil resources. Moreover, chemical processes must be designed to be inherently safer to have the least adverse consequences for humans and the environment. In this context, several concepts such as *Green Chemistry*,[5] *Green Engineering*[6-7] and the circular economy[8-9] were implemented to consider aspects within the whole life cycle of chemical products, from their production, their use, and the disposal or recycling of wastes after their end of life.

Especially in the field of polymer chemistry these concepts must be realized, since to date still more than 90% of the global production of plastics depend fossil resources with only 10% of them being recycled after their use.[10] Moreover, certain polymers such as polyurethanes, polyvinylchloride, or polyacrylonitrile, which are produced in several million tons per year, heavily rely on extremely hazardous substances such as isocyanates, vinyl chloride and acrylonitrile, respectively.[11] This thesis aims to elaborate new synthetic routes for the production of polymerizable compounds from renewable resources, while abiding by the *Twelve Principles of Green Chemistry*, and thus ultimately aims to contribute to a sustainable development in polymer chemistry.

2 Theoretical Background

2.1 Green Chemistry

The concept of sustainable chemistry emerged in the early 1990s due to many environmental problems that were caused by the thoughtless use of chemicals with dangerous attributes, such as physical (e.g., explosiveness), toxicological (e.g., mutagenic), as well as global (climate change) properties.[12] One prominent example of an unpredictable impact of hazardous chemical substances is the chlorinated pesticide DDT (dichlorodiphenyl-trichloroethane) that was used during the 1940s to 1970s. It turned out to be persistent and accumulated in several species of raptorial birds, causing a thinning of their eggshells and ultimately a catastrophic decline of their population due to breakages of eggs during the hatching time.[13-14]

Paul Anastas and John Warner performed pioneering work in this scientific field and developed *Green Chemistry* as a methodology, which is defined as the "utilization of a set of principles that reduces or eliminates the use or generation of hazardous substances in the design, manufacture and application of chemical products".[5, 15-16] Furthermore, the *Twelve Principles of Green Chemistry* were devised as a set of cohesive guidelines to pursue chemistry in the most responsible and sustainable manner possible (Table 2.1).[5, 17] In short, these principles encourage chemists to strive for perfection, by designing chemical reactions and their products on a molecular level to be inherently more efficient, less waste generating, non-toxic, safer, based on renewable instead of depleting feedstocks, and biodegradable to form non-hazardous degradation products.[17] Green chemistry metrics (Principles number 1 and 2), and renewable resources (Principle number 7) will be discussed in chapter 2.2 and chapter 2.3, respectively, as they represent the most important principles for this thesis.

The twelve principles were furthermore condensed into mnemonics such as PRODUCTIVELY or IMPROVEMENTS to be more memorable and easier to understand.[7, 18] In 2009, Anastas and Eghbali summarized that *Green Chemistry* "1.) designs across all stages of the chemical life-cycle, 2.) seeks to design the inherent nature of the chemical products and processes to reduce their intrinsic hazards, and 3.) works as a cohesive system of principles or design criteria".[17]

Table 2.1: The Twelve Principles of Green Chemistry.[5]

The Twelve Principles of Green Chemistry
1. **Prevention:** It is better to prevent waste than to treat or clean up waste after it is formed.
2. **Atom Economy:** Synthetic methods should be designed to maximize the incorporation of all materials used in the process into the final product.
3. **Less Hazardous Chemical Synthesis:** Wherever practicable, synthetic methodologies should be designed to use and generate substances that possess little or no toxicity to human health and the environment.
4. **Designing Safer Chemicals:** Chemical products should be designed to preserve efficacy of function while reducing toxicity.
5. **Safer Solvents and Auxiliaries:** The use of auxiliary substances (e.g. separation agents, solvents, etc.) should be made unnecessary wherever possible and, when used, innocuous.
6. **Design for Energy Efficiency:** Energy requirements should be recognized for their environmental and economic impacts and should be minimized. If possible, synthetic methods should be conducted at ambient temperature and pressure.
7. **Use of Renewable Feedstocks:** A raw material or feedstock should be renewable rather than depleting whenever technically and economically practicable.
8. **Reduce Derivatives:** Unnecessary derivatization steps (use of blocking groups, protection/deprotection, temporary modification of physical/chemical processes) should be avoided whenever possible.
9. **Catalysis:** Catalytic reagents are superior to stoichiometric reagents.
10. **Design for Degradation:** Chemical products should be designed so that at the end of their function they break down into innocuous degradation products and do not persist in the environment.
11. **Real-Time Analysis for Pollution Prevention:** Analytical methodologies need to be further developed to allow for real-time, in-process monitoring and control prior to the formation of hazardous substances.
12. **Inherently Safer Chemistry for Accident Prevention:** Substances and the form of a substance used in a chemical process should be chosen to minimize the potential for chemical accidents, including releases, explosions, and fires.

2.2 Metrics used in the field of sustainable chemistry

The assessment of the sustainability of chemical processes is very complex as it depends on many factors that cannot be quantified easily. Certain metrics have therefore been introduced in the field of chemistry to allow a facile and preliminary evaluation of the sustainability of chemical reactions.[19-21] It is, for instance, possible to quantify the minimum amount of waste that will be generated during a reaction with the so-called atom economy (*AE*), which was introduced by Trost in 1991.[22-24] This simplified metric only requires the reaction equation and is thus purely theoretical. The *AE* is calculated by dividing the molecular weight (MW) of the product by the sum of all starting materials MWs in the stoichiometric equation (Equation (1)).

$$AE\,(\%) = \frac{MW_{\text{product}}}{\sum MW_{\text{starting materials}}} \times 100 \qquad (1)$$

Atom economy therefore quantifies the amount of the starting materials weight that will be incorporated into the final product or inversely the amount of waste that will be generated (waste = 100%−*AE*). One prominent example for poor atom economies is the Wittig olefination.[25] If for instance methylenetriphenylphosphorane (Ph_3PCH_2, MW = 276.32) is used for the methylenation of a carbonyl compound, only the methylene group (CH_2, MW = 14.03), i.e. 5% of the reagents' mass, will be transferred to the product. Thus 95 wt% of the used Wittig reagent will be obtained as waste. In contrast, addition reactions such as the Diels-Alder reaction do not generate waste in form of byproducts as all atoms of the reaction are incorporated into the product. *AE* thus represents a useful tool for the initial assessment of waste generation. It is however evident that in practice more waste will be generated, as *AE* assumes quantitative yields, use of reactants in stoichiometric amounts and does not include chemicals such as solvents that do not appear in the reaction equation.

The most widely used metric is the environmental factor (*E* factor) that was introduced by Sheldon in 1992.[26-27] In contrast to *AE*, the *E* factor describes the actual mass of waste that is produced during a process in proportion to the mass of isolated product (Equation (2)).[28]

$$E\text{ factor} = \frac{m_{\text{waste}}}{m_{\text{product}}} = \frac{\sum m_{\text{starting materials}} - m_{\text{product}} - m_{\text{recycled materials}}}{m_{\text{product}}} \qquad (2)$$

It is worth mentioning here that solvent losses are usually the major source of waste.[29] Recycled materials, such as solvents or catalysts, can therefore be considered for the calculation, as they significantly contribute to a lower *E* factor (Equation (2)).

Usually, when comparing literature with no experimental data on solvent recovery, it is assumed that 90% of all used solvents were recovered.[29] Moreover, water used during a process is generally excluded from calculations, since inclusion would lead to exceptionally high *E* factors, rendering meaningful comparisons difficult.[28] Problems associated with the lack of experimental data were furthermore addressed by the introduction of the simple *E* factor (*sEF*) and complete *E* factor (*cEF*).[30] The *sEF* is more appropriate for early stage development of processes, as only raw materials and neither solvents nor water are taken into account (Equation (3)).[29] The *cEF* on the other hand includes solvents as well as process water and furthermore assumes no recycling, representing the maximum amount of waste that can be formed during the process (Equation (4)).[29] The true commercial *E* factor will be somewhere between the simple and the complete *E* factor.[29]

$$sEF = \frac{\sum m_{\text{raw materials}} + \sum m_{\text{reagents}} - m_{\text{product}}}{m_{\text{product}}} \tag{3}$$

$$cEF = \frac{\sum m_{\text{raw materials}} + \sum m_{\text{reagents}} + \sum m_{\text{solvents}} + m_{\text{water}} - m_{\text{product}}}{m_{\text{product}}} \tag{4}$$

Interestingly, due to its simplicity, the *E* factor can be calculated quite easily for industrial production sites by dividing the mass of raw materials that were purchased by the mass of product that was produced or sold.[29] Typical *E* factors of different segments in the chemical industry are listed in Table 2.2.[31-32] These values were published in 1992 by Sheldon based on his personal experience and are intended to give an indication only.[31] The incredibly high *E* factors of 25−100 (or higher) for pharmaceuticals and 5−50 for fine chemicals inherently correlate with their complex chemical structures that usually require multistep syntheses.[33] Moreover, usually stoichiometric reagents are used in this field rather than catalytic reactions as for bulk chemicals.[33] It is therefore important to develop more step economical syntheses of these compounds to further reduce the amount of waste formed.[34] Function-oriented synthesis, aiming to reproduce the function of an active compound with simpler scaffolds that are designed for ease of synthesis, can be implemented as well.[35]

Table 2.2: *E* factors of different industrial segments (by Sheldon in 1992).[31-32]

Industry Segment	Volume (tons per annum)	*E* factor
Oil Refining	10^6–10^8	<0.1
Bulk Chemicals	10^4–10^6	<1–5
Fine Chemicals	10^2–10^4	5–50
Pharmaceuticals	10–10^3	25–100 (or higher)

Various other metrics have been implemented so far to evaluate the efficiency of chemical reactions even more precisely. However, they usually do not offer significant advantages compared to the *E* factor in the early-stage development of processes and will therefore only be mentioned briefly. For instance, the actual atom economy (*AAE*) was introduced to correct *AE* by the yield that was obtained experimentally in the laboratory (*AAE* = *AE* × yield).[36] The reaction mass efficiency (*RME*) is another correction that furthermore includes experimental stoichiometry (*RME* (%) = m(isolated product) / m(starting materials) × 100).[37] *AAE* and *RME* thus offer a more accurate result than *AE* by the utilization of experimental data. The mass intensity (*MI*) describes the total amount of mass used in a process divided by the mass of product, which basically equals the *E* factor plus one. The process mass intensity (*PMI*) includes process water and is therefore equal to *cEF* plus one.[38]

Mass-based metrics are very useful for fundamental research as they allow an easy and fast comparison between several experimental procedures to decide in an early stage which process will be the most efficient and the least waste generating. These metrics are however not suitable to estimate the true negative effects of a process on the environment as no social and environmental aspects are considered (e.g., toxicity of the involved chemicals). Thus, a comprehensive Life Cycle Assessment (LCA)[39-42] must be performed to evaluate the absolute environmental impact of a product within its whole life cycle, from raw material acquisition to manufacture, distribution, use, and disposal of wastes after its use (from “cradle-to-grave”).[43] LCAs are highly sophisticated and require huge amounts of data about a process and its materials to result in an adequate representation of the environmental impact of a product and are thus best adapted to compare processes that are already in commercial use.[41] As a consequence, mass-based metrics such as *AE* and *E* factor remain the most widely used tools for an assessment of the environmental impact since LCAs are too difficult and time consuming at the research or development stage.[41, 44]

2.3 Renewable resources

An incredibly large amount of approximately 170 billion tons of biomass is produced annually by earth, from which less than 10% are used worldwide (mainly for feed, food or energy purposes).[1, 45-46] Despite these large amounts of unused biomass, the field of chemistry still highly depends on fossil resources as most commodity chemicals and virtually all polymers are made from crude oil.[47-49] For instance, in 2022, less than 1% of the global production of >400 million tons of plastics were bio-based.[10] This chapter therefore introduces the class of renewable resources and shortly discusses how they can be utilized in chemistry using one of the two following approaches: i) the targeted synthesis of conventional fossil-derived chemicals (e.g., bioethanol through fermentation of sugars[50]), so-called drop-in solutions, or ii) the production of new compounds, which can compete with fossil derived materials (e.g., polylactic from fermentation of starch[51]).[52]

The biomass on earth consists of approximately 75% carbohydrates, 20% lignin, and 5% of oils, fats, terpenes and natural products, such as proteins and alkaloids (Figure 2.1).[45]

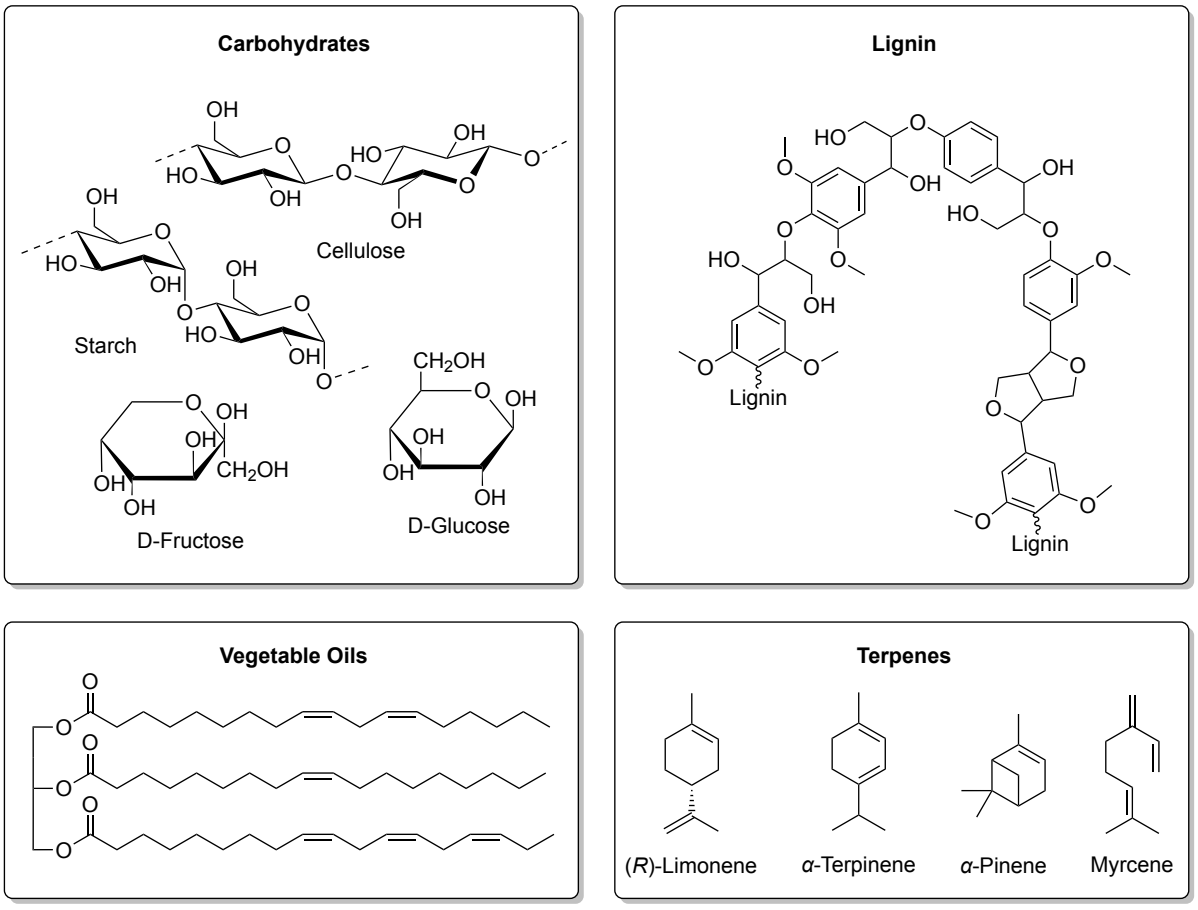

Figure 2.1: Representative structures of plant-derived renewable resources for the synthesis of more sustainable chemicals.

Carbohydrates

Carbohydrates are by far the most abundant renewable resource on earth, with an estimated production of 150 billion tons per year, from which only 1% is used by humanity delivery (see Figure 2.1 for some selected examples).[52] Polysaccharides such as chitin, hyaluronic acid and cellulose deliver many intriguing properties such as biocompatibility, biodegradability, and non-toxicity and thus allow biomedical applications, such as tissue engineering, wound healing, or drug delivery.[53] Monosaccharides such as glucose and fructose can be fermented into valuable building-blocks for polymer syntheses or further chemical modification.[54-55] In this regard, the U.S. Department of Energy published a report about top value added chemicals that could potentially be produced from sugars by biological or chemical processes in high volumes.[56-57] The list includes directly polymerizable compounds such as succinic acid, 2,5-furandicarboxylic acid (FDCA), and lactic acid, which can be converted to plastics such as poly(butylene succinate), poly(ethylene furanoate) (PEF), and polylactide, respectively. For instance, PEF represents a fully bio-based polymer with superior properties compared to fossil-derived poly(ethylene terephthalate), such as a higher glass transition temperature and improved gas barrier properties for carbon dioxide and oxygen.[58] Recently, in October 2024, the Dutch company Avantium opened the world's first commercial plant for the production of FDCA from sugars in a volume of 5000 tons p.a., which is an important milestone for the utilization of carbohydrates as renewable resource.[59]

Lignin

Lignin is the second most abundant organic material on earth after cellulose and is produced in an estimated amount of 20 billion tons each year by photosynthesis.[60-61] The aromatic biopolymer is produced in plants by polymerization of *para*-coumaryl, coniferyl and sinapyl alcohol, which are all derived from the amino acid phenylalanine (see Figure 2.1 for a representative structure of lignin).[62] In plant cell walls, lignin acts as a "glue", which is cross-linked with cellulose and hemicellulose to confer structural strength and rigidity to the system.[63] Thus, inflexible plants such as trees have high lignin contents between 15%−40%, while herbs for instance have <15% lignin.[62] Research focuses either on the utilization of lignin as raw material for aromatic compounds (e.g., vanillin *via* oxidation[64] or phenols *via* hydrogenolysis[65]),[66-68] or on its use in polymer chemistry,[69-71] for instance in polymer blends[71] or as macromonomer for cross-linked materials such as epoxy resins[72-73] or polyurethanes.[74-75]

Terpenes

Terpenes are naturally occurring hydrocarbons, which are formally made up of multiple isoprene units and thus belong to the class of isoprenoids (see Figure 2.1 for a few selected examples).[76-77] Terpenes are subdivided into hemi (C_5), mono (C_{10}), sesqui (C_{15}), di (C_{20}), sester (C_{25}), tri (C_{30}), tetra (C_{40}), and polyterpenes ((C_5)$_n$ with n > 8) according to the number of isoprene subunits (C_5H_8) within their scaffold.[78] Together with terpenoids (i.e., isoprenoids that contain oxygen atoms in various functional groups),[77] they represent the largest and most diverse class of secondary metabolites, with >50000 isolated compounds to date.[79-80] Monoterpenes such as *α*-pinene and *β*-pinene are predominantly obtained from turpentine oil, a mixture of different terpenes that is produced in a volume of more than 300000 tons per year by steam distillation of the resin from conifers or from sulfate turpentine, which is obtained as by-product during the kraft pulping of pine wood.[81-83] (*R*)-Limonene, another monoterpene, is the main component of oil from citrus fruit peels and is produced in a high volume of 70000 tons per year.[81, 84] Further monoterpenes (e.g., camphene) are synthesized by isomerization of *α*-pinene.[81, 85-87] Applications of terpenes include flavors, fragrances and pharmaceuticals,[78, 88] solvents,[84] asymmetric catalysis,[89] and polymers.[90-93]

2.4 Fatty acids and vegetable oils

Plant oils are triesters of glycerol and three fatty acids, with a varying composition of diverse fatty acids depending on the crop, the season, and the growing conditions (see Figure 2.1 for an exemplary triglyceride structure).[94] [95] For instance, high oleic sunflower oil contains up to 90% of oleic acid, while castor oil is mainly composed of ricinoleic acid. The chemical structure of fatty acids is constituted of one carboxylic acid moiety linked to an aliphatic chain, typically of an even number of carbon atoms.[96] They can generally be divided into saturated and unsaturated fatty acids (see Scheme 2.1 for selected examples).

Vegetable oils are one of the most important renewable feedstocks of the chemical industry. Typical applications include cosmetics,[97] lubricants,[98] surfactants,[99] and coatings[100] such as alkyd resins[101] and linoleum.[102]. A large amount of 208 million tons of vegetable oils were thus produced globally in 2019, from which about 25% were used for industrial applications (e.g. biodiesel, oleochemicals), whereas the remaining 75% were consumed as food.[103] Due to ethical concerns that arise with the industrial/chemical use of vegetable oils instead of their use as food, research focuses on the implementation of new resources such as algae[104-106] and yeast[107-109] to further increase the global production of oils. Microalgae represent a promising alternative to terrestrial crops as they rapidly accumulate lipids (up to 77% of dry cell mass) and more importantly can be cultivated in a saline water medium and therefore do not compete with the arable land area that is needed for vegetable oils.[104]

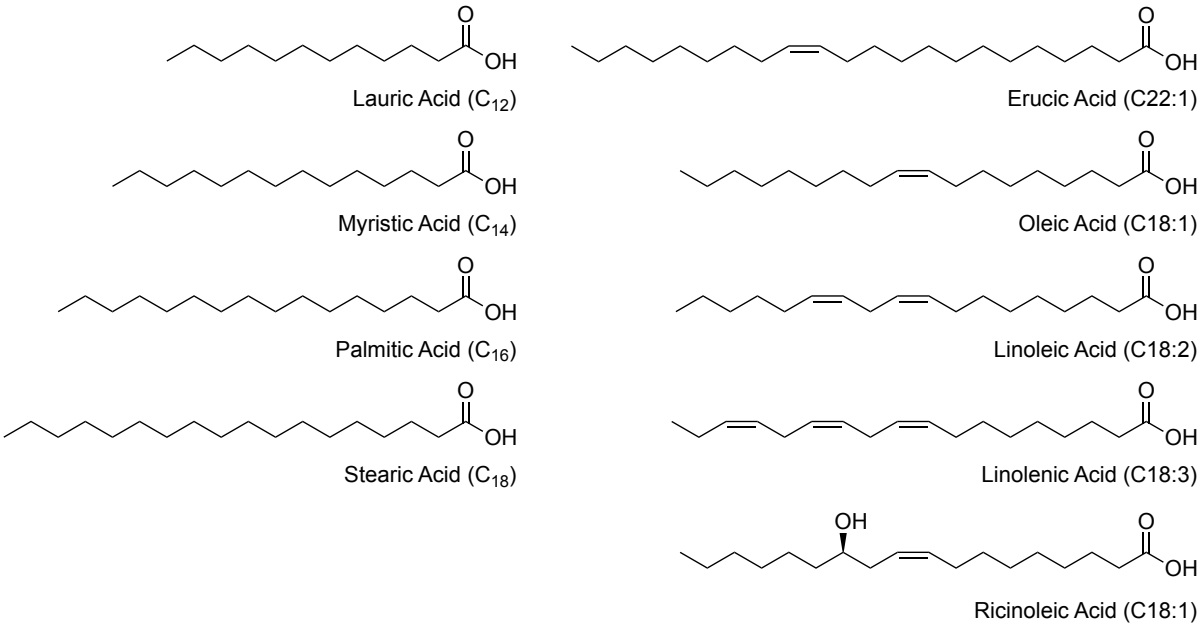

Scheme 2.1: Selected examples of naturally occurring saturated (left) and unsaturated fatty acids (right).[110]

It has for instance been calculated that biodiesel, i.e. fatty acid methyl esters, produced from food crops cannot realistically satisfy the overall demand of transport fuels as this would require a substantial amount of land area.[111] A high-yielding crop such a palm oil would for instance require 24% of the total cropland of the United States to meet 50% of the U.S. transport fuel needs, while microalgae with 30 wt% of lipids in their dry cell mass would only require 2.5% of the total cropland, thus being ten times more productive than conventional vegetable oils.[111] However, various technological obstacles must be overcome to realize the large-scale production of microalgae. Current limitations include the development of effective harvesting and lipid extraction protocols,[104] and the adjustment of optimal growing conditions (e.g., nutrients, temperature, and concentration of gases such as carbon dioxide and oxygen).[112]

In this chapter, oleochemical reactions will be discussed focusing mainly on polymer applications. Unsaturated fatty acids and saturated fatty acids will be addressed separately due to their different and distinct reactivities. Thus, double bond reactions will be discussed in chapter 2.4.1 for unsaturated fatty acids and in chapter 2.4.2 for vegetable oils. At last, the chemistry of saturated fatty acids will be discussed in chapter 2.4.3.

2.4.1 Unsaturated fatty acids

Monounsaturated fatty acids are usually preferred over polyunsaturated fatty acids in the synthesis of renewable step-growth polymerization monomers.[113] Reasoning for this is the inherent bifunctionality of monounsaturated fatty acids (i.e., one carboxylic acid and one double bond) that enables the facile and selective synthesis of new bifunctional monomers. Therefore, only an overview of functionalizations of monounsaturated fatty acids and their applications in polymer science will be given. Note: Oxidative cleavages of fatty acid double bonds will be discussed in chapter 2.5.3.

The thiol-ene reaction is a widely applied reaction for the functionalization of double bonds due to its high efficiency.[114-115] Dithiols can for instance be utilized for the synthesis of fatty acid dimers, which are polymerizable by polycondensation with diamines or diols.[116-118] Monothiols such as 2-mercaptoethanol,[116, 119] thioglycerol,[116] 3-mercaptopropionic acid,[120-121] methyl thioglycolate,[116] and cysteamine[122] were used for the introduction of new functional groups into the fatty acid scaffold. For instance, directly polymerizable AB-type monomers were obtained from methyl oleate and methyl erucate *via* thiol-ene addition of 2-mercaptoethanol under UV irradiation using 2,2-dimethoxy-2-phenylacetophenone (DMPA) as photoinitiator (Scheme 2.2).[119] Homopolymerization of the methyl oleate and methyl erucate based monomers (functionalized with 2-mercaptoethanol) in bulk with 10 mol% of 1,5,7-triazabicyclo[4.4.0]dec-5-ene (TBD) as catalyst was then performed at 130 °C to obtain two polyesters with 17 kDa and 19 kDa, respectively, and melting points of −59 °C and −9 °C, respectively (Scheme 2.2). At last, the thermal properties of the polyesters were altered by oxidation of the thioether moieties within the polymer backbone into their corresponding sulfones with hydrogen peroxide as oxidant. Amorphous polymers with low glass transition temperatures of approximately −35 °C were thus obtained after oxidation.[119]

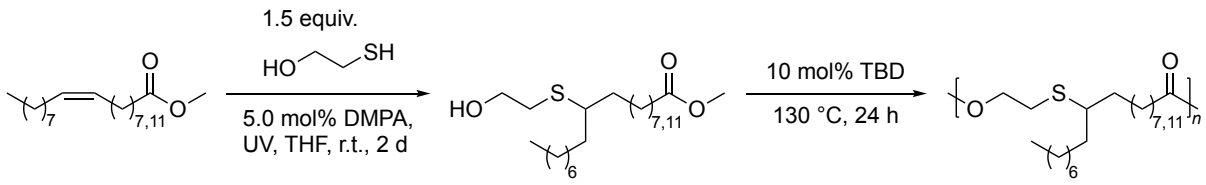

Scheme 2.2: Synthesis of polyester by thiol-ene addition of 2-mercaptoethanol to either methyl oleate or methyl erucate and subsequent polymerization.[119]

Olefin metathesis is another powerful tool that can be directly employed on fatty acid methyl esters (FAMEs) to synthesize their corresponding diesters by self-metathesis or to introduce new functional groups by cross-metathesis.[123-124] For instance, Rybak and Meier reported the cross-metathesis of methyl acrylate with either methyl oleate or methyl erucate to synthesize new mono-unsaturated *α*,*ω*-dicarboxylic acid dimethyl esters, which represent monomers for polyester and polyamide syntheses (Scheme 2.3).[125] Moreover, the *α*,*β*-unsaturated methyl undecenoate that is formed as second product of the cross-metathesis is considered valuable for the synthesis of detergents due to its short 11 carbon chain length. The metathesis reaction was performed solvent-free at 50 °C with 10 equivalents of methyl acrylate and only 0.2 mol% of Grubbs-Hoveyda II catalyst loading. High conversion as well as high selectivity were achieved, as 92% of the desired cross-metathesis products and only 5% of self-metathesis products formed during the reaction (determined by gas chromatography).[125]

Ethenolysis of FAMEs can be utilized as well to synthesize monomethyl esters (or their free carboxylic acids) with terminal double bonds for subsequent syntheses of new monomers.[126-127] For instance, Moser *et al*. esterified the ethenolysis product of oleic acid (i.e., 9-decenoic acid) with its reduced derivative 9-decen-1-ol using *para*-toluenesulfonic acid as catalyst to obtain a new *α*,*ω*-diene with one internal ester moiety in a high yield of 93% (Scheme 2.4).[128-129] A subsequent thiol-ene polymerization with either 1,2-ethanedithiol or 1,3-popanedithiol yielded two bio-based poly(thioether-ester)s with high molecular weights of 149 kDa and 31 kDa, respectively, and melting points of 71 °C and 65 °C, respectively.[128] The same *α*,*ω*-diene was furthermore polymerized by acyclic diene metathesis (ADMET) polymerization to obtain a fully renewable polyester with an average molecular weight of 8.3 kDa and a melting point of 48 °C.[129] In another study by Moser *et al*., 9-decen-1-ol was esterified with azelaic acid, a dicarboxylic acid obtained by oxidative cleavage of oleic acid,[130] to synthesize another *α*,*ω*-diene, which was then polymerization *via* thiol-ene with 1,2-ethanedithtiol or *via* ADMET to obtain two polymers with M_n values of 191 kDa and 28 kDa, respectively, and melting points of 70 °C and 48 °C, respectively.[131]

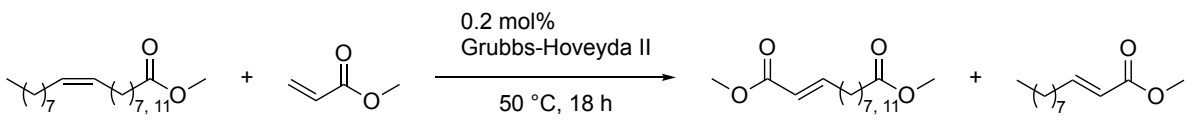

Methyl oleate or methyl erucate + Methyl acrylate → Monounsaturated *α*,*ω*-dimethyl ester + *α*,*β*-Unsaturated methyl undecenoate

Scheme 2.3: Cross-metathesis of methyl acrylate with either methyl oleate of methyl erucate.[125]

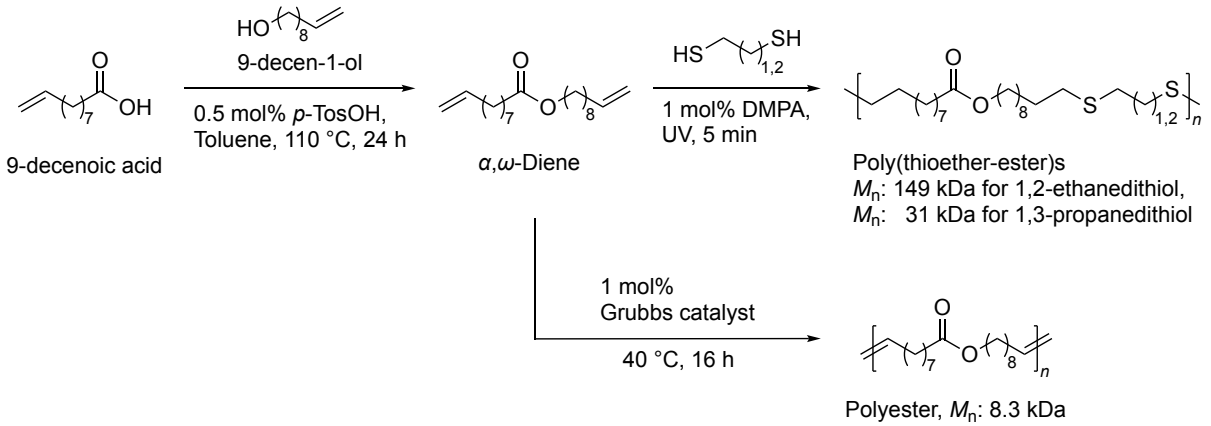

Scheme 2.4: Synthesis of *α*,*ω*-diene from 9-decenoic acid and 9-decen-1-ol and the subsequent polyester synthesis either by thiol-ene reaction with dithiols or by acyclic diene metathesis polymerization.[128-129]

Wacker oxidation of internal double bonds from fatty acids into ketones represents an interesting approach to enable subsequent carbonyl functionalizations. Historically, the Wacker oxidation describes the palladium(II) catalyzed oxidation of terminal alkenes into their corresponding methyl ketones. The reaction is usually conducted in a DMF/water solvent mixture with copper(II)chloride as co-catalyst and oxygen as final oxidant.[132] One prominent example is the industrial production of acetaldehyde from ethylene.[133-134] The selective oxidation of internal double bonds was however difficult to achieve with the original Wacker-Tsuji procedure due to their low reactivity and the formation of undesired oxygenated side products.[135] In 2006, Kaneda *et al*. developed a practical modification of the Wacker oxidation that enabled the co-catalyst free oxidation of terminal olefins with $PdCl_2$ and oxygen in a solvent mixture of *N*,*N*-dimethylacetamide (DMAc) and water (6:1).[136] DMAc was here vitally important to the system, as cyclic-voltammetry measurements revealed that Pd(0) oxidized more readily in DMAc compared to other amide group containing solvents such as *N*-methyl-2-pyrrolidone or *N*,*N*-dimethylformamide. It was furthermore demonstrated that the catalyst is easily separated from the oxidized products by simple washing with *n*-heptane to remove oxygenated products. The DMAc solution that still contained the catalyst after extraction was then reused for another two reaction cycles without any loss in catalytic activity.[136] Kaneda *et al*. furthermore showed that this catalytic system was selective for the oxidation of internal double bonds.[135] Thus, Winkler and Meier utilized this modification of the Wacker oxidation for the synthesis of renewable ketones from methyl oleate and methyl erucate (Scheme 2.5).[137] Both ketones were extracted with *n*-heptane after the reaction and recrystallized to obtain high yields of 85%.

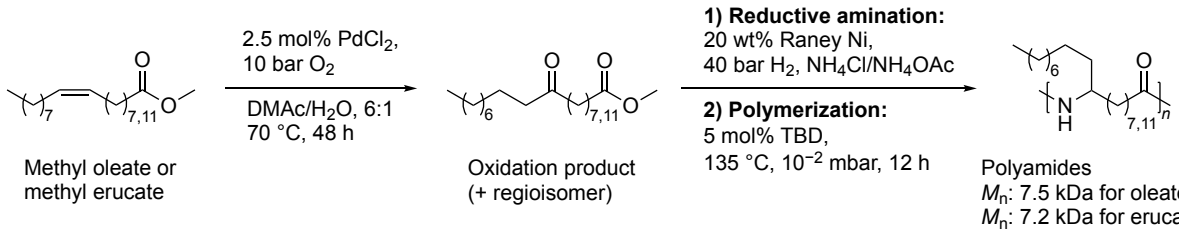

Scheme 2.5: Synthesis of polyamides from methyl oleate and methyl erucate by reaction sequence of 1) Wacker oxidation, 2) reductive amination and 3) polymerization.[137]

The catalyst remaining in the DMAc phase was used for another two reaction cycles without any significant loss in catalytic activity to demonstrate the efficiency of this system. A subsequent reductive amination[138] with Raney nickel and 40 bar of hydrogen atmosphere yielded the respective amines in yields >90%. At last, homopolymerizations of the methyl oleate and methyl erucate derived amines were performed to obtain two renewable polyamides with average molecular weights of 7.5 kDa and 7.2 kDa, respectively, and melting points of 45 °C and 90 °C, respectively (Scheme 2.5).[137] Copolymerization with Nylon 6,6 was conducted as well to fine tune properties such as melting point and hydrophobicity.

10-Undecenoic acid is another interesting fatty acid for the synthesis of various polymers due to its terminal double bond that allows the facile introduction of functional groups. This fatty acid is produced industrially by pyrolysis of either methyl ricinoleate or castor oil, which contains up to 90% of ricinoleic acid.[139-141] The pyrolysis of methyl ricinoleate is usually preferred due to a higher viscosity and the formation of side products when castor oil is employed.[140-141] Heptanal and methyl 10-undecenoate are thus obtained by pyrolysis of methyl ricinolate in yields of 50%−60% (Scheme 2.6).[142] A subsequent ester hydrolysis then yields 10-undecenoic acid. The most prominent polymer application of 10-undecenoic acid is the industrial production of polyamide 11 (Scheme 2.7).[113, 143-144] The necessary monomer, 11-aminoundecanoic acid, is synthesized in two synthetic steps. First, a radical bromination with hydrobromic acid in the presence of oxygen is conducted in toluene at 30 °C to selectively form the anti-Markovnikov[145] product 11-bromoundecanoic acid in yields between 95%−97%.[143] A subsequent nucleophilic substitution in aqueous ammonia at 20 °C yields the desired 11-aminoundecanoic acid, which precipitates from the reaction solution in its zwitterionic form and does not react in further substitution reactions to form side products.[143]

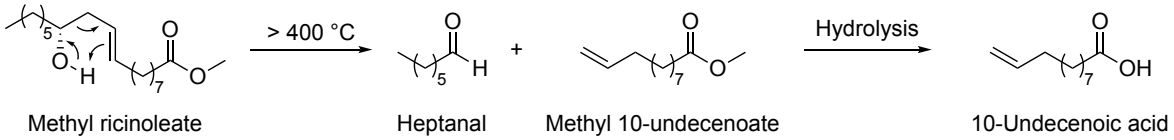

Scheme 2.6: Pyrolysis of methyl ricinoleate to yield heptanal and methyl 10-undecenoate.[140]

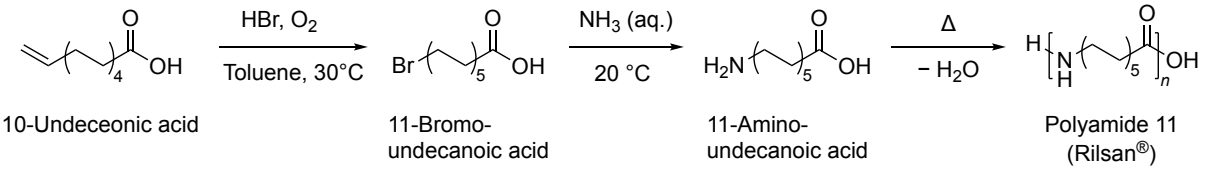

Scheme 2.7: Industrial production of 11-aminoundecanoic acid and polyamide 11 from 10-undecenoic acid.[143]

It should however be noted that this process uses toxic and corrosive hydrobromic acid and ammonia and therefore requires suitable safety measures. Moreover, stoichiometric amounts of ammonium bromide are formed as waste, which should ideally be recycled to render this process more sustainable.[113] At last, polycondensation is performed at elevated temperatures under removal of water to obtain 100% bio-based polyamide 11, which is currently sold under the brand name Rilsan® by Arkema.[146] Noteworthy, this process was commercialized already 70 years ago in the 1950s.[147] The excellent chemical resistance combined with a high melting point of 189 °C and a low density of 1.03 g cm^{-3} render polyamide 11 suitable for applications such as automotive fuel lines, cable sheathings, and lightweight products for sports utilities.[145]

Besides the industrial production of polyamide 11, much fundamental research has been conducted to incorporate 10-undecenoic acid and its ester derivatives into polymers. The terminal double bond is thus frequently utilized to synthesize bifunctional and polymerizable derivatives with reactions such as Wacker oxidation,[136, 148] thiol-ene,[116, 121-122] or olefin metathesis[149] that have already been discussed for oleic acid and erucic acid (see above). In contrast to oleic acid with an internal double bond, here the thiol-ene reaction does not result in a new stereocenter with long pending alkyl side chains. In fact, the thiol-ene reaction is very selective for terminal double bonds, delivering the linear anti-Markovnikov product without any side chain.[120] It is therefore quite interesting to compare thermal properties of materials made *via* thiol-ene reaction from 10-undecenoic acid with the ones made from fatty acids such as oleic acid or erucic acid with one internal double bond. For instance, Meier *et al*. reported the synthesis of new ω-amino carboxylic acid methyl esters **M1.1**−**M1.3** in yields >66% by thiol-ene addition of cysteamine hydrochloride to methyl 10-undecenoate, methyl oleate, and methyl erucate, respectively (Scheme 2.8).[122] Polyamides with molecular weights ranging from 6.2 kDa−15.9 kDa were then obtained by homopolymerizations with TBD as catalyst.

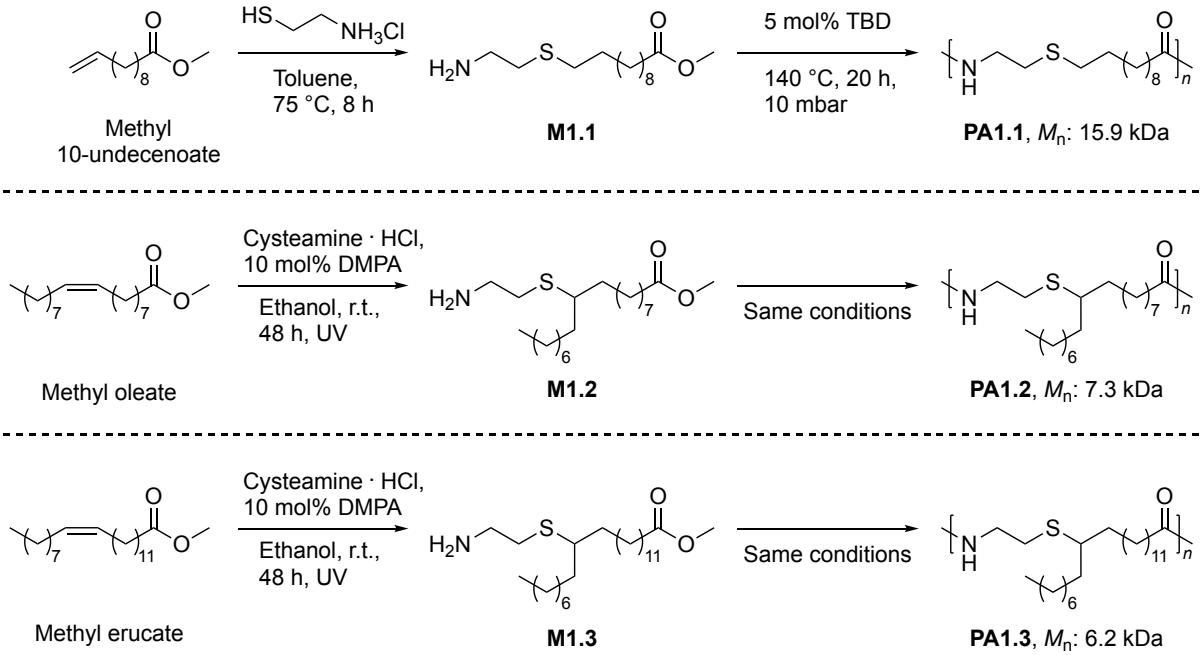

Scheme 2.8: Thiol-ene addition of cysteamine hydrochloride to unsaturated fatty acids to yield monomers **M1.1**–**M1.3** and their polymerizations to yield polyamides **PA1.1**–**PA1.3**.[122]

The influence of the dangling alkyl chains on the thermal properties of the polyamides was revealed by differential scanning calorimetry. **PA1.1** was solid at room temperature and had a high melting point of 138 °C, while **PA1.2** remained highly viscous and did not show any thermal transition. **PA1.3** on the other hand had a melting point of 43°C, presumably due to the higher amount of carbon atoms in the backbone compared to **PA1.2**. Fine-tuning of thermal properties was moreover demonstrated by copolymerization of 50% **PA1.1** with 50% **PA1.3** to result in a melting point of 86 °C in between the melting points of both polymers.[122]

The self-metathesis of methyl 10-undecenoate was performed by Mutlu and Meier to obtain the renewable long chain dimethyl(*E*)icos-10-enedioate in a yield of 57% (Scheme 2.9).[149] Subsequent polymerization in bulk at 150 °C with either 1,2-ethane, 1,4-butane, 1,6-hexane, or 1,8-octane diamine resulted in molecular weights ranging from 5.5 kDa–14.7 kDa and dispersities between 1.9–2.4. The melting points of the polyamides increased incrementally from 180 °C for the longest diamine to 226 °C for the shortest diamine due to the increasing amide groups density and thus a higher amount of hydrogen bonding. Interestingly, it was shown that the same polyamides are accessible if the two reactions are conducted in a reverse order.

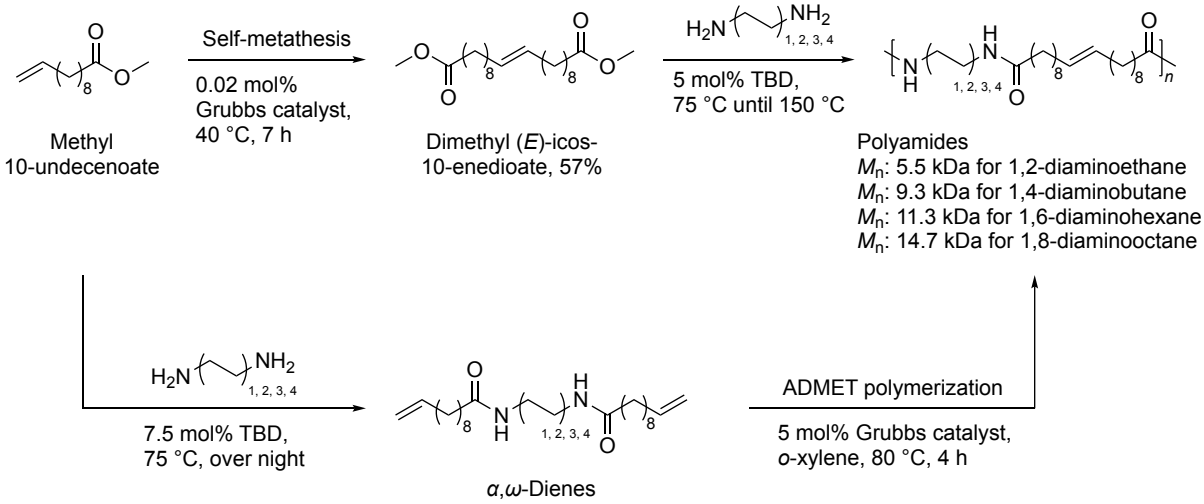

Scheme 2.9: Self-metathesis of methyl 10-undecenoate and the polymerization of dimethyl (*E*)-icos-10-enedioate with four diamines to yield polyamides (top) and the reverse order of both reactions (bottom).[149]

α,*ω*-Dienes were thus obtained by reaction of the four diamines with methyl 10-undecenoate in yields >70%. However, due to the solid nature of all *α*,*ω*-dienes and their bad solubility in a variety of solvents, only low M_n values of 4 kDa and 6 kDa were obtained in the subsequent ADMET polymerization of the 1,6-hexanediamine and the 1,8-octanediamine derived dienes, respectively. The ADMET approach is moreover inferior to the polymerization of dimethyl(*E*)icos-10-enedioate considering sustainability, as solvent and a 100-fold higher Grubbs catalyst loadings was required.[149]

2.4.2 Vegetable oils

The chemistry of vegetable oils with a high content of double bonds (e.g., high oleic sunflower oil) is very similar to the chemistry of unsaturated fatty acids (chapter 2.4.1). Reactions such as thiol-ene reaction[150-151] or metathesis[152-153] that were already discussed have thus been performed on oils as well. However, in this case, polyfunctional instead of difunctional compounds are obtained, offering the possibility to produce cross-linked polymers in a subsequent polymerization step. In this chapter only selected examples with new approaches, compared to the ones presented in chapter 2.4.1, will be discussed to prevent unnecessary repetition of chemical reactions.

Epoxidized oils derived from soybean oil or linseed oil (i.e., oils with a high content of double bonds) are frequently used for the preparation of bio-based epoxy resins by curing with either cyclic acid anhydrides or polyamine hardeners.[154-156] However, as most hardeners are fossil-based, research focused furthermore on the synthesis of bio-based curing agents to produce epoxy resins that are 100% renewable.[157-158] One prominent example of a fully bio-based epoxy resin was reported by Lapinte *et al*. in 2011.[150] In this study, grapeseed oil was utilized for the synthesis of a renewable polyamine and subsequently polymerized with commercially available epoxidized linseed oil. Grapeseed oil was chosen due to its generally high content of linoleic and oleic acid. Prior to the experiments, the fatty acid content of the used grapeseed oil was determined by transesterification with methanol and quantitative gas chromatography analysis of the formed fatty acid methyl esters, which resulted in an average value of 4.75 double bonds per triglyceride.[150] The polyamine compound was then synthesized by thiol-ene addition of cysteamine under UV irradiation with DMPA as photoinitiator. A maximum conversion of 87% was achieved after 8 h of reaction to obtain a polyamine with 4.13 amino groups per molecule on average. Finally, curing with epoxidized linseed oil (5.3 epoxy groups per molecule) at 100 °C resulted in the formation of a renewable epoxy resin with a glass transition temperature of −38 °C (Scheme 2.10).[150] The rather low T_g was ascribed to the high molecular flexibility of the aminated grapeseed oil. For instance, higher glass transition temperatures of 113 °C and 148 °C were achieved for linseed oil epoxy resins cured with smaller and less flexible hardeners such as tetrahydrophthalic anhydride and phthalic anhydride, respectively.[154]

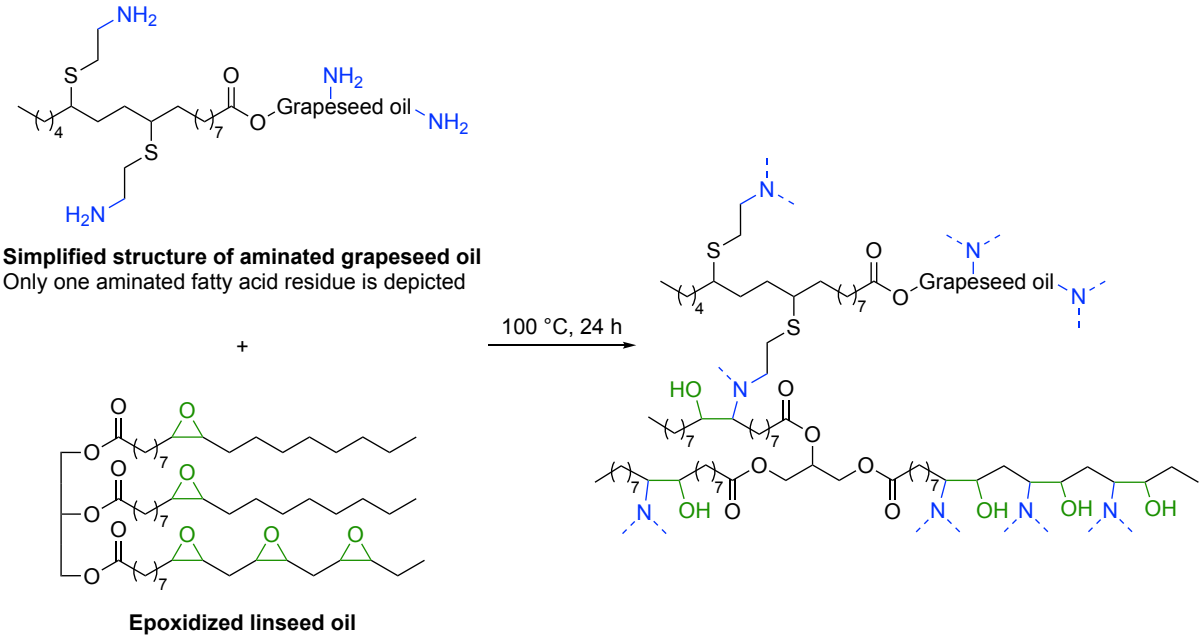

Scheme 2.10: Synthesis of epoxy resin from aminated grapeseed oil and epoxidized linseed oil.[150]

Renewable polyols are furthermore accessible from epoxidized vegetable oils by nucleophilic ring-opening reaction with methanol (Scheme 2.11).[159] In 2003, Petrović *et al*. utilized this approach for the synthesis of six polyols with a varying degree of functionality from vegetable oils. Thus, one polyol with 3 hydroxyl groups per molecule was obtained from midoleic sunflower oil, four polyols with approximately 3.5 hydroxyl groups per molecule were obtained from canola, soybean, sunflower and corn oil, and at last one polyol with 5.2 hydroxyl groups per molecule was obtained from linseed oil. The degrees of functionality of the obtained polyols directly correlated with the content of double bonds in the respective oils, as expected (e.g., 3.7 double bonds per molecule for midoleic sunflower oil and 6.4 double bonds per molecule for linseed oil). Polyurethanes with high gel-contents of >97% were then obtained by reaction of each polyol with methylene diphenyl diisocyanate (MDI) at 100 °C.[159]

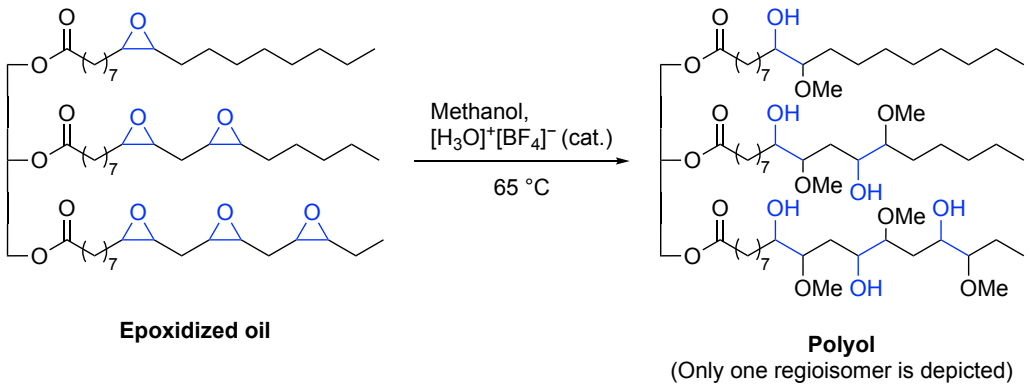

Scheme 2.11: Synthesis of polyol by ring-opening reaction of epoxidized oil with methanol and catalytic amounts of tetrafluoroboric acid.[159]

A linear relationship was observed for the number of hydroxyl groups per molecule (i.e. the resulting cross-linking density) and the T_g as well as the ultimate tensile strength. Thus, the PU derived from linseed-oil had the highest T_g of 77 °C and a tensile strength of 56 MPa, while the midoleic sunflower-oil derived PU hat a T_g of 24 °C and a tensile strength of 15 MPa. The other four PUs derived from polyols with similar hydroxyl values had a T_g of about 30 °C and a tensile strength of approximately 20 MPa. In a different study by Auvergne *et al*., a polyol with 3.6 hydroxyl groups per molecule was synthesized by thiol-ene addition of 2-mercaptoethanol to rapeseed oil.[151] Polymerization of this polyol with MDI resulted in a T_g of 25 °C.[159]

It should be noted here that castor oil, consisting of up to 90% of ricinoleic acid,[141] represents a fully renewable polyol which can directly be used in polyurethane syntheses without any prior functionalization steps.[160-162] Polymerizing pure castor oil with diisocyanates usually results in rubbery materials with low glass transition temperatures of about 10 °C due to its low content of hydroxyl groups.[160] This issue can however be resolved by the addition of low molecular weight polyols such as glycerol to increase cross-linking density. One interesting example from literature utilized hydroxypropylated lignin as second polyol component to introduce rigid domains into the polyurethane.[163] It was thus possible to increase the T_g of a castor oil and MDI based polyurethane from 18 °C up to 47 °C by addition of 20 wt% of lignin. Moreover, mechanical properties such as Young's modulus and elongation at break increased from 1.9 MPa to 13.6 MPa and from 53% to 89%.[163]

The synthesis of bio-based polyurethanes from oils however still suffers from the use of toxic diisocyanates, which themselves are produced from toxic phosgene.[164-165] One study by Meier and Johansson, thus investigated the synthesis of polythionourethanes from castor oil as potential substitutes for polyurethanes.[166] A multicomponent reaction approach was utilized to synthesize diisothiocyanates from elemental sulfur and diisocyanides under DBU catalysis in castor oil as solvent (Scheme 2.12). Interestingly, the initially heterogeneous reaction between the diisocyanides and the sulfur proceeded readily at 55 °C, while the subsequent polymerization step of castor oil and the *in situ* formed diisocyanate required a temperature of 100 °C.

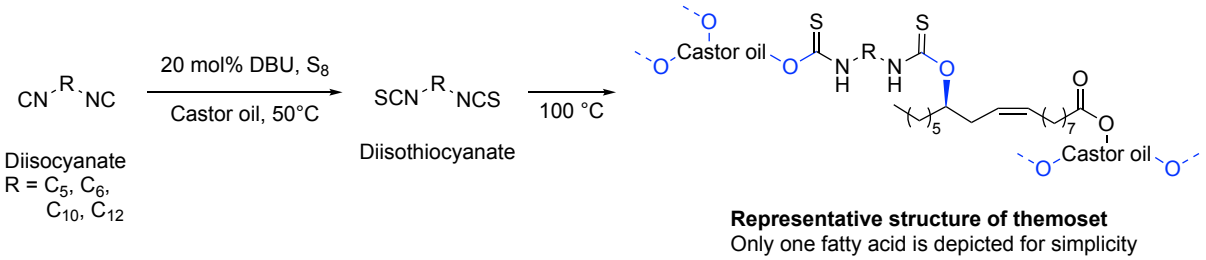

Scheme 2.12: Synthesis of Polythionourethanes from castor oil, diisocyanides and elemental sulfur in a DBU catalyzed multicomponent reaction.[166] Note: the former hydroxyl groups of ricinoleic acids are depicted in blue.

It was thus possible to prevent heterogeneity problems as the mixture became homogeneous after full conversion of elemental sulfur at 55 °C. Polythionourethanes with glass transition temperatures ranging from −42 °C to −31 °C were thus synthesized from diisocyanides and castor oil. In addition, analogous polyurethanes (PUs) were synthesized form diisocyanates to allow comparison. The PUs did not show a significant difference for the glass transition temperature. However, in thermogravimetric analysis, the PUs proved to be thermally more stable as they degraded at about 300 °C, while the polythionourethanes started degrading between 212−265 °C.[166] Despite the reduced thermal stability of these materials compared to PUs, this multicomponent approach proved to be more sustainable for the production of new materials, since the polymerizations were performed solvent-free and with less toxic chemicals.

2.4.3 Saturated fatty acids

In polymer chemistry, unsaturated fatty acids such as oleic acid, linoleic acid, and linolenic acid are easily functionalized at their double bonds by oxidations, thiol-ene reaction, olefin metathesis or isomerizing functionalization to obtain difunctional monomers for polymer syntheses.[167-168] In contrast, the chemistry of saturated fatty acids is restricted mainly to the carboxylic acid moiety and therefore less versatile. Esterification of saturated fatty acids is a common approach to either introduce new functional groups (e.g., double bonds) or increase acidity of α-CH_2 protons (e.g., methyl ester) and hence enable further functionalization through enolate chemistry. For instance, radical polymerization and ring-opening metathesis polymerization (ROMP) can be performed with fatty acid vinyl esters[169-171] and fatty acid norbornene esters,[172] respectively.

In one study by Mutlu and Meier, 5-norbornene-2-methanol (**NBM**) was esterified with several saturated fatty acids using 1,1'-carbonyldiimidazole (**CDI**) as activation agent to obtain monomers suitable for ROMP in high yields of 73% up to 99% (Scheme 2.13).[172] ROMPs were then performed with the third generation Grubbs catalyst (**Grubbs 3**) to achieve molecular weights of 10 kDa up to 140 kDa, depending on the employed monomer to catalyst ratio. Moreover, it was observed that the polymerization behaved like a living polymerization as very low dispersities of 1.06−1.25 were obtained.[172] In differential scanning calorimetry (DSC) experiments, a decreasing glass transition temperature (T_g) was observed with an increasing side chain length of the polymers, thereby indicating that the alkyl side chains behaved like internal plasticizers. The T_g decreased incrementally from 102 °C for hexanoic acid to −32 °C for stearic acid. Moreover, side chain crystallization was observed for polymers with long alkyl chains of 14 or more carbon atoms and the corresponding melting points decreased from 30 °C for C_{14} to 15 °C for C_{16} and ultimately to 6 °C for C_{18}.

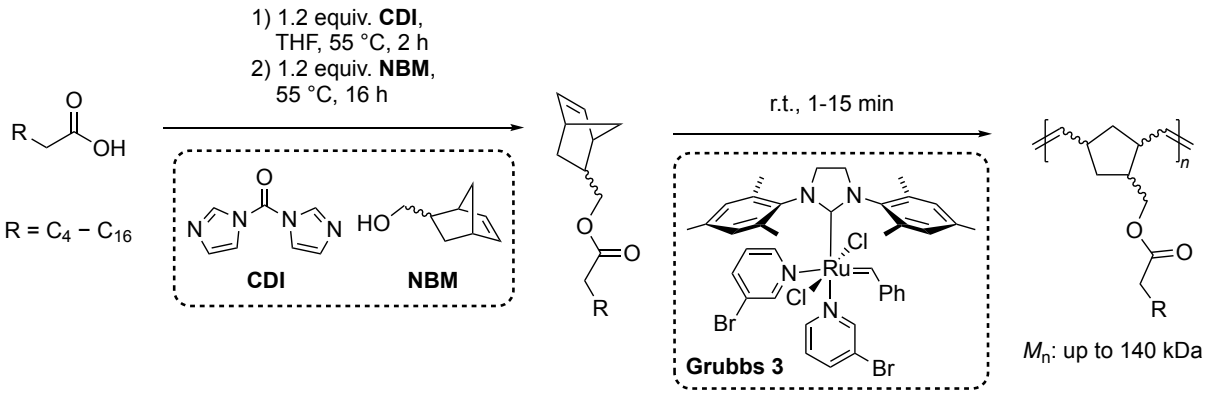

Scheme 2.13: Ring-opening metathesis polymerization of fatty acid norbornene-methanol esters.[172]

The reduction of saturated fatty acids to their corresponding alcohols broadens the scope of possible ester syntheses. For instance, Çayli and Meier reported the synthesis of fatty alcohol derived methacrylates from methacryloyl chloride and fatty alcohols with chain lengths from C_{10} to C_{18} (Scheme 2.14). A subsequent atom transfer radical polymerization (ATRP) with CuCl/pentamethyldiethylenetriamine(PMDETA) as catalytic system and ethyl 2-bromoisobutyrate (**EBIB**) as initiator yielded polymers with molecular weights ranging from 9 kDa−121 kDa depending on the used ratio of monomer to initiator (Scheme 2.14). Methyltrioctylammonium chloride (Aliquat 336) was added as phase transfer catalyst to provide a homogeneous polymerization mixture in bulk and stabilize the copper salts, preventing them from precipitation.[173] The controlled/living character of the polymerization was confirmed by an observed first-order kinetic for the concentration of acrylate monomer against reaction time. Moreover, a linear correlation of the average molecular weight against conversion of monomer, which is expected for controlled polymerizations, was confirmed by SEC. Investigation of these polymers by DSC revealed that side chain crystallization happened only when the fatty alcohol length was at least 12 carbon atom or longer. However, in contrast to the polymers made *via* ROMP (see above), here the melting point increased incrementally with a longer chain length from −34 °C for C_{12} to 47 °C for C_{18}, indicating that the polymer backbone has a significant influence on this behavior.[173]

One example for the use of enolate chemistry in polymer applications is the reaction between fatty acid methyl ester (FAME) enolates and dimethyl carbonate (DMC) to yield dimethyl malonates.[174] In the developed reaction procedure from Kolb and Meier, FAMEs are deprotonated with sodium hydride and reacted with a high excess of dimethyl carbonate (20.0 equiv.) to suppress a Claisen-condensation from happening as side reaction (Scheme 2.15, **top**).[175] For instance, with 10.0 equiv. or 5.0 equiv. of DMC already 5% and 14% of Claisen-product were formed, respectively. The reaction was moreover performed in the presence of dimethyl formamide (DMF), which was observed to accelerate the reaction, presumably due to a better solvation of reactants and/or intermediates.[174]

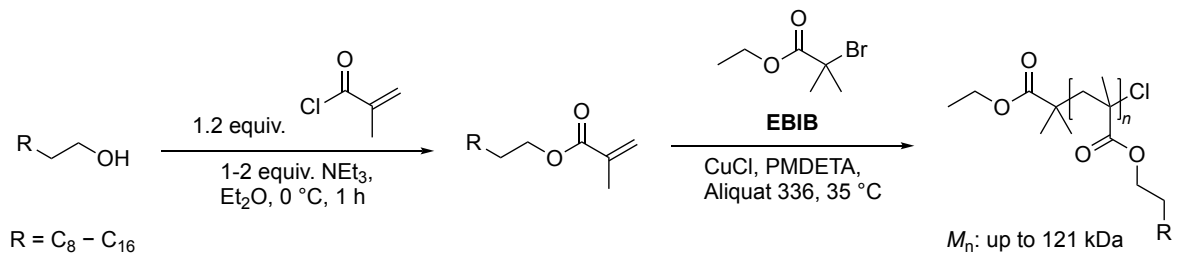

Scheme 2.14: Atom transfer radical polymerization of fatty alcohol methacrylates.[173]

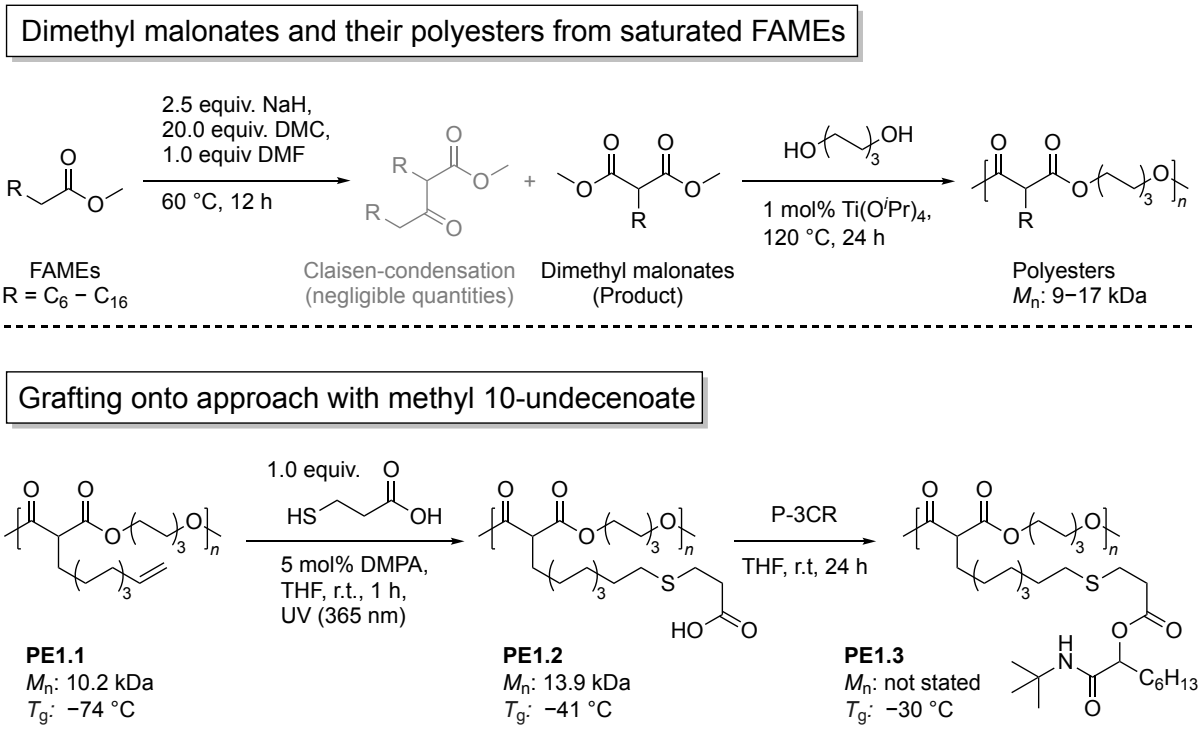

Scheme 2.15: Synthesis of dimethyl malonates and their derived polyesters from fatty acid methyl esters and dimethyl carbonate (top).[174] Grafting onto approach with methyl 10-undecenoate-based polyester **PE1.1** *via* Thiol-ene reaction (**PE1.2**) and subsequent Passerini three-component reaction (**PE1.3**).[176]

Thus, six dimethyl malonates were synthesized from methyl octanoate up to methyl stearate (C_8−C_{18}) and subsequently polymerized with 1,6-hexanediol to obtain renewable polyesters with molecular weights between 9 kDa−17 kDa (Scheme 2.15, **top**). In DSC measurements, side chain crystallization was observed for all polyesters with side chain lengths of at least 10 carbon atoms. The melting point increased incrementally from −36 °C for a C_{10} side chain (methyl palmitate) to 27 °C for C_{16} (methyl stearate).[174] Polymerizations with 1,6-hexanediamine were performed as well to obtain polyamides with molecular weights from 7 kDa−15 kDa and high melting points, which increased gradually with an increasing side chain length (114 °C−159 °C). Thermal properties of the polymers were thus altered by introduction of amide groups capable of hydrogen bonding.[174] The dimethyl malonate synthesis was further applied on unsaturated fatty acids to allow the polyesters to be grafted onto.[176] Hence, polyester **PE1.1** was synthesized with the same synthetic pathway from 10-undecenoic acid, which is obtained by the pyrolysis of castor oil (Scheme 2.15, **bottom**).[140-141] The introduced terminal double bonds of **PE1.1** could be grafted onto by either cross-metathesis with acrylates (e.g., methyl, *tert*-butyl, 2-hydroxyethyl acrylate) or thiol-ene addition with thiols (e.g., 2-mercaptoethanol, thioglycerol, methyl thioglycolate) to introduce functional groups such as esters and alcohols into the polymer scaffold.

In one grafting reaction, 3-mercaptopropionic acid was added to **PE1.1** *via* thiol-ene reaction using 5 mol% of 2,2,-dimethoxy-2-acetophenone (DMPA) as radical initiator under UV irradiation to obtain polyester **PE1.2** with an increased molecular weight of 13.9 kDa compared to **PE1.1** with 10.2 kDa (Scheme 2.15, **bottom**).[176] The introduced carboxylic acid moieties were then used to demonstrate further grafting possibilities *via* the Passerini three-component reaction (P-3CR). Thus, **PE1.2** was reacted with heptanal and *tert*-butyl isocyanide to obtain polyester **PE1.3** after 24 h of reaction at room temperature. The hydrodynamic radius of the polyester increased, as expected, stepwise with each grafting step from **PE1.1** to **PE1.3**. Moreover, it was possible to increase the glass transition temperature of −74 °C for **PE1.1** up to −30 °C for **PE1.3** with this grafting onto approach.[176] The high versatility of the dimethyl malonate approach was furthermore shown in another study by Cramail *et al*. who synthesized a 6-membered cyclic carbonate with a terminal double bond from methyl 10-undecenoate.[177] Dimerization *via* self-metathesis or thiol-ene reaction was performed to obtain difunctional cyclic carbonates, which were then polymerized with 1,12-diaminododecane to obtain poly(hydroxyurethane)s, a subclass of non-isocyanate polyurethanes, with molecular weights between 9 kDa−23 kDa.[177]

Another interesting synthetic pathway to yield dimethyl esters from saturated fatty acids is the oxidative coupling of methyl ester enolates with copper(II)bromide as oxidant to obtain dialkylated dimethyl succinate derivatives (Scheme 2.16).[178] The deprotonation of FAMEs was performed with lithium diisopropylamide (LDA) at a low temperature of −78 °C to suppress the competing Claisen-condensation to an extent of 4%. Hence, dimethyl esters were synthesized in yields higher than 65% from saturated FAMEs with chain lengths ranging from C_8 (octanoic acid) to C_{14} (myristic acid). A subsequent polymer synthesis was not reported.[178]

Besides esterification and enolate chemistry, the introduction of double bonds into the carbon chain of saturated fatty acids represents a desirable transformation to allow for further modification and thus increase the scope of their applications. Catalytic dehydrogenations of carboxylic acids will be discussed in chapter 2.5.1.

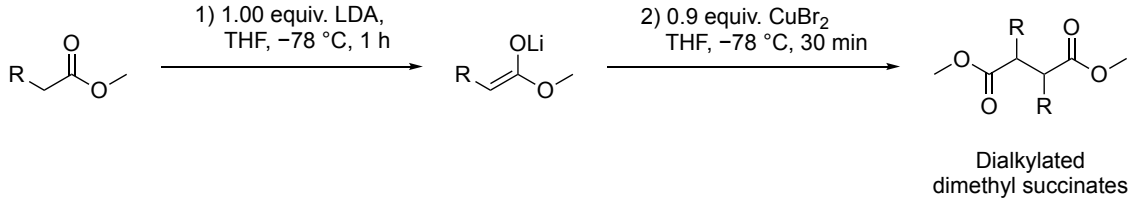

Scheme 2.16: Oxidative coupling of two fatty acid methyl ester enolates with copper(II)bromide as oxidant.[178]

2.5 Reactions used within this thesis

In the following subchapters, specific reactions used within this thesis will be discussed. The mechanism of each reaction will be discussed shorty, followed by a few examples for applications in polymer chemistry.

A palladium catalyzed dehydrogenation of carboxylic acids (chapter 2.5.1) as well as the thia-Michael addition (chapter 2.5.2) were used for the synthesis of renewable dimethyl esters from saturated lauric acid (results are discussed in chapter 4.1).

A ruthenium catalyzed oxidative cleavage of double bonds (chapter 2.5.3) was used for the synthesis of a renewable tricarboxylic acid from high oleic sunflower oil (results are discussed in chapter 4.2).

At last, the Passerini three-component reaction (chapter 2.5.4) was used for the synthesis of cross-linked polymeric networks (results are discussed in chapter 4.3).

2.5.1 Catalytic *α,β*-dehydrogenation of carboxylic acids

Over the past decade, a few catalytic methods have been developed for the *α,β*-dehydrogenation of saturated carbonyl compounds such as aldehydes, ketones, carboxylic acids, esters and amides.[179-183] The selective introduction of double bonds is however challenging due to the difficulty of selectively activating methylene C(sp^3)-H bonds in the molecule, while simultaneously preventing C(sp^2)-H activation of the products' more reactive double bond. Especially for carboxylic acids, few catalysts have been reported so far, which are based on transition metals such as palladium[184-187] and iridium.[188]

One example for a selective and catalytic dehydrogenation of aliphatic carboxylic acids was reported by Newhouse *et al*. in 2017.[184] In this study, carboxylic acids were first transformed into their corresponding zinc enediolates by deprotonation with bis(2,2,6,6-tetramethyl-piperidinyl)zinc ($Zn(TMP)_2$) and then dehydrogenated under palladium catalysis with allyl acetate as final oxidant (Scheme 2.17, **top**).[184] It was assumed that the zinc enediolates react with an allyl-palladium complex to form palladium enolates, which subsequently undergo *β*-hydride elimination to release the desired product (Scheme 2.17, **bottom**).[184] The catalytically active allyl-palladium complex is then regenerated after reductive elimination of propene and oxidative addition of allyl acetate. The dehydrogenation proved to be highly efficient as yields higher than 80% were obtained for fatty acids with chain lengths from octanoic acid up to palmitic acid.[184]

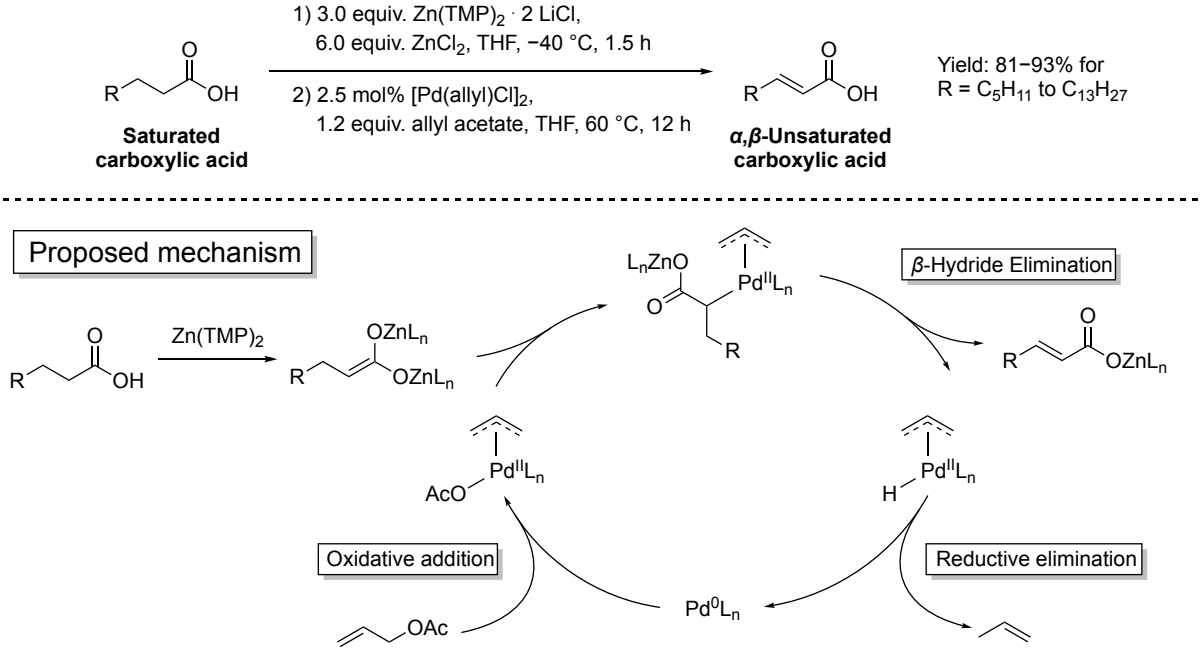

Scheme 2.17: Palladium catalyzed dehydrogenation of zinc enediolates with allyl acetate as oxidant (top) and the proposed mechanism for this reaction (bottom).[184]

The procedure itself is however considered impractical on large scale and rather unsustainable as highly reactive *n*-butyllithium, low temperatures of −40 °C and protective gas atmosphere are required for the synthesis of the used zinc enediolates. Moreover, overstoichiometric amounts of $Zn(TMP)_2$ (3.00 equiv.) and the additive $ZnCl_2$ (6.00 equiv.) were needed for the reaction to achieve high yields.

More recently, in 2021, Yu *et al*. reported another palladium catalyzed dehydrogenation method for the synthesis of *α*,*β*-unsaturated carboxylic acids from their saturated derivatives.[187] The development of this dehydrogenation procedure was possible through careful design of pyridine-pyridone ligands with different bite angles. Thus, the five-membered chelating **ligand 1.1** with a bite angle of 79° selectively formed the desired *α*,*β*-unsaturated product (Scheme 2.18, **top**). In contrast, six-membered chelating **ligand 1.2** with a wider bite angle of 89° further reacted in C(sp^2)-H activation of the products' double bond and therefore enabled the development of a tandem reaction with (bromoethynyl)triisopropylsilane to yield *γ*-alkylidene butenolides (Scheme 2.18, **middle**).[187]

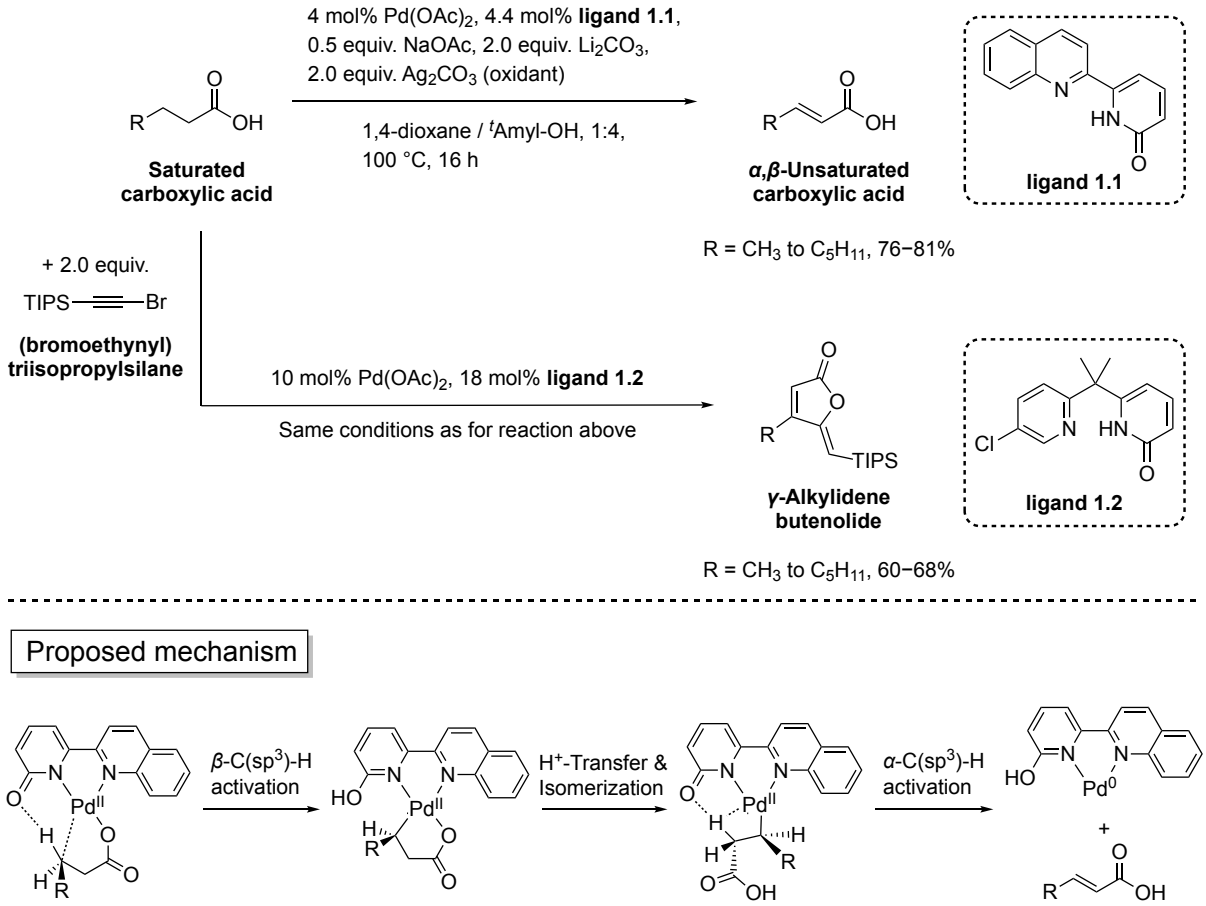

Scheme 2.18: Ligand-controlled palladium catalyzed dehydrogenation of saturated aliphatic carboxylic acids to yield either *α*,*β*-unsaturated carboxylic acids with **ligand 1.1** (top) or *γ*-alkylidene butenolides with **ligand 1.2** (middle) and the proposed C-H activation mechanism (bottom).[187, 189]

The mechanism of this transformation was thoroughly investigated by density functional theory (DFT) in a proceeding publication.[189] The calculations revealed that the ligands most likely act as intramolecular bases to activate the *β*-methylene C(sp^3)-H bond of the carboxylic acid as rate determining step of the reaction. Subsequent proton transfer, isomerization and *α*-C(sp^3)-H activation presumably yields the *α*,*β*-unsaturated product (Scheme 2.18, **bottom**).[189] Energy barriers were then calculated for the *β*-methylene C(sp^3)-H activation of butyric acid as well as for the *β*-vinyl C(sp^2)-H activation of the product butenoic acid. The calculations resulted for **ligand 1.1** in an increase of activation barrier from 28.2 kcal/mol (for butyric acid activation) to 30.1 kcal/mol (for butenoic acid activation), while calculations for **ligand 1.2** resulted in a decrease in activation barrier from 28.6 kcal/mol to 27.9 kcal/mol.[189] The performed DFT calculations were thus consistent with the observed selectivity of both ligands.

In practice, both reactions were performed with the same conditions at a temperature of 100 °C for 16 h in a solvent mixture of 1,4-dioxane and *tert*-amyl alcohol (1:4) with 2.00 equivalents of silver carbonate as oxidant.[187] Furthermore, 2.00 equivalents of lithium carbonate were added to guarantee complete deprotonation of all carboxylic acids, thereby facilitating their coordination to the Pd(II) center of the catalyst. Yields higher than 75% were achieved for the *α*,*β*-dehydrogenation of linear aliphatic carboxylic acids with chain lengths up to octanoic acid (Scheme 2.18, **top**), while slightly lower yields of 60%−68% were achieved for the tandem procedure with **ligand 1.2** (Scheme 2.18, **middle**).

Noteworthy, Yu *et al*. demonstrated for the synthesis of *α*,*β*-unsaturated carboxylic acids that molecular oxygen could be used as more sustainable oxidant instead of silver carbonate. Within this thesis, the original procedure from Yu *et al*. was optimized for the synthesis of *α*,*β*-unsaturated lauric acid in a sustainable manner. Subsequent esterification with methanol and dimerization with dithiols *via* thia-Michael addition enabled the synthesis of bio-based dimethyl esters and their polymers. The results from this project are discussed in chapter 4.1.

2.5.2 Thia-Michael addition

The Michael reaction generally describes the conjugate 1,4-addition of a nucleophile ("Michael donor") to the *β*-carbon atom of an *α*,*β*-unsaturated carbonyl ("Michael acceptor") to form an enolate intermediate, which after protonation yields the so-called "Michael adduct".[190] The reaction is however not restricted to *α*,*β*-unsaturated carbonyls, as other electron deficient olefins such as acrylonitrile, vinyl sulfones, nitro ethylenes, vinyl phosphonates, vinyl pyridines, and azo compounds can be employed as well.[191-192] Moreover, depending on the type of nucleophile, the reaction is termed Michael (carbon),[191] aza-Michael (nitrogen),[191, 193] oxa-Michael (oxygen),[194-195] or thia-Michael addition (sulfur).[190, 196]

In this chapter, additions of thiols to *α*,*β*-unsaturated carbonyls (Scheme 2.19, **top**) will be discussed, as the thia-Michael addition was conducted within this thesis for the synthesis of bio-based dimethyl esters (chapter 4.1). The thia-Michael addition can in principle be catalyzed by various compounds such as Lewis acids,[197-200] Brønsted acids,[201-202] Brønsted bases,[203-205] and nucleophiles[206-208]. However, acid catalysts are not employed often since they are typically the least efficient catalysts.[190] For basic catalysts, the proposed reaction mechanism begins with deprotonation of the thiol to form its corresponding thiolate anion, along with the conjugate acid of the base (Scheme 2.19, **bottom left**). Next, the *α*,*β*-unsaturated carbonyl is attacked by the thiolate in *β*-position to form an enolate anion, which itself is a very strong base (pK_a ~25)[206] and thus deprotonates another thiol (or alternatively the conjugate acid) to generate another thiolate and the Michael adduct (Scheme 2.19, **bottom right**).[190]

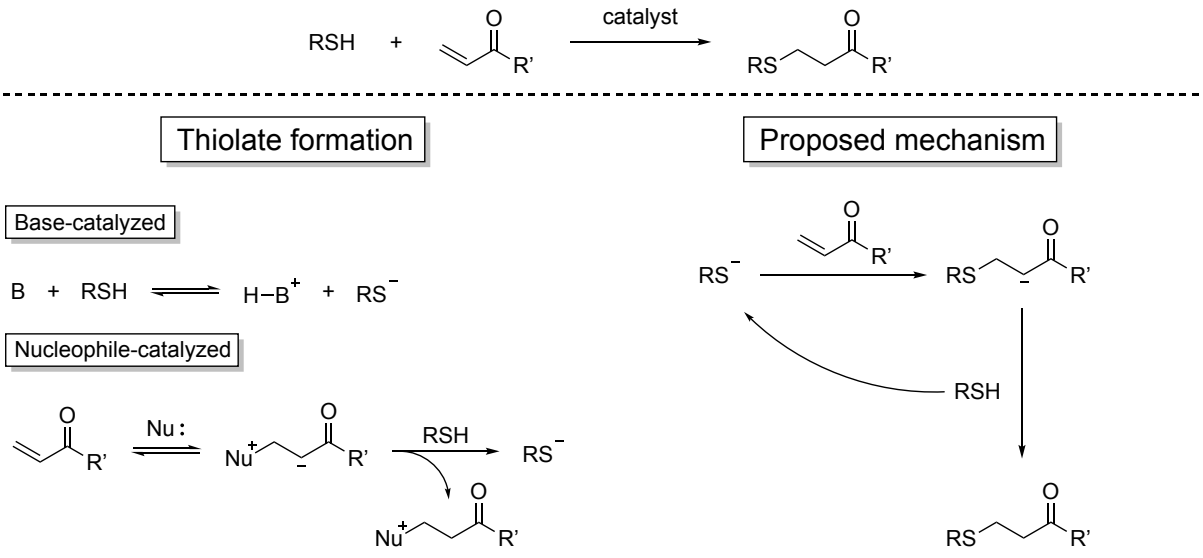

Scheme 2.19: Thia-Michael addition of a thiol to an *α*,*β*-unsaturated carbonyl (top), the base and nucleophile catalyzed thiolate formation (bottom left), and the mechanism of the thia-Michael addition (bottom right).

The rate-limiting step of the reaction is generally the Michael-addition. Therefore, the overall reaction rate is second order and first order with respect to thiolate and the *α*,*β*-unsaturated carbonyl. Moreover, the reaction rate will be of pseudo-first order in the concentration of the *α*,*β*-unsaturated carbonyl, if the pK_a of the conjugate acid of the catalyst is much higher than that of the thiol, as this results in full deprotonation and a steady state concentration of the thiolate.[191]

Several studies in the past observed that nucleophilic and non-basic compounds, such as phosphines, were not only suitable catalysts for the thia-Michael addition but also significantly more active than bases.[192, 206, 209-210] One study by Haddleton *et al*. showed that phosphine catalyzed thia-Michael additions of thiols to (meth)acrylates proceeded much more rapidly and resulted in less side reactions compared to the analogous amine catalyzed reactions.[211] For instance, the addition of 2-mercaptoethanol to poly(ethylene glycol) methacrylate achieved a conversion of 33% after 4 h when 130 mol% of *n*-pentylamine were added as catalyst, while 20 mol% of dimethylphenylphosphine as catalyst resulted in quantitative conversion already after 30 minutes.[211] The mechanism of the nucleophile-mediated reaction begins with the thia-Michael addition of the nucleophile to the *α*,*β*-unsaturated carbonyl. The formed enolate, being a strong base, then deprotonates the thiol to generate a thiolate (Scheme 2.19, **bottom left**).[206] Afterwards, the reaction proceeds in the same way as already explained for the base-catalyzed reaction (Scheme 2.19, **bottom right**). The reaction kinetics of the nucleophilic pathway thus strongly depend on the nucleophilicity of the catalyst as a higher concentration of thiolate anions will be generated with an increasing nucleophilicity.[190]

Both, the base-catalyzed and the nucleophile-mediated thia-Michael addition are generally very selective, achieve high yields and proceed readily at room temperature, and therefore fit many criteria of efficient click reactions.[190, 212] Moreover, waste generation is kept to a minimum due to the atom economy of 100%.

Within this thesis, the thia-Michael addition was utilized for the solvent-free synthesis of new dimethyl esters from aliphatic dithiols and *α*,*β*-unsaturated methyl laurate with 1,1,3,3-tetramethylguanidine as catalyst (results are discussed in chapter 4.1).

2.5.3 Ruthenium catalyzed oxidative cleavage of alkenes

The oxidative cleavage of carbon-carbon double bonds is a practical method for the introduction of oxygen bearing functional groups into the scaffold of unsaturated renewable resources such as terpenes and fatty acids.[213-214] Ozonolysis represents the most famous reaction in this field of chemistry and describes the reaction between an alkene and ozone to form oxidized cleavage products.[215-217] The reaction is highly versatile as different functional groups such as alcohols, aldehydes, ketones, and carboxylic acids can be obtained depending on the employed reaction conditions (e.g., solvent and work-up procedure).[217] Additional benefits are a high selectivity, high yields, and good scale-up properties (under extreme safety precautions).[216] A prominent example from industry is the ozonolysis of oleic acid to produce nonanoic acid and azelaic acid (> 1000 tons p.a.).[130, 218] In the first step of the process, ozone is reacted with oleic acid at moderate temperatures of 25 °C−45 °C to form the so-called secondary ozonide *via* a sequence of three [2+3] cycloadditions and cyclo-reversions (Scheme 2.20).[130, 219] Subsequent thermolysis and oxidation are performed at 75−120 °C in oxygen atmosphere to yield the cleaved carboxylic acids, nonanoic acid and azelaic acid.[130] The former is used for the production of lubricants and plasticizers,[220] while the latter is used for cosmetics, plasticizers, lubricants and the production of polymers such as polyamide 6,9. [97, 221-222] Although this process is quite efficient, it is still considered unsustainable due to the associated safety risks caused by the toxicity[223-224] and explosiveness[225-226] of ozone. Moreover, the high electricity demand required for the production of ozone from oxygen renders industrial processes expensive.[227] The development of less hazardous oxidative cleavages is thus desired.[221]

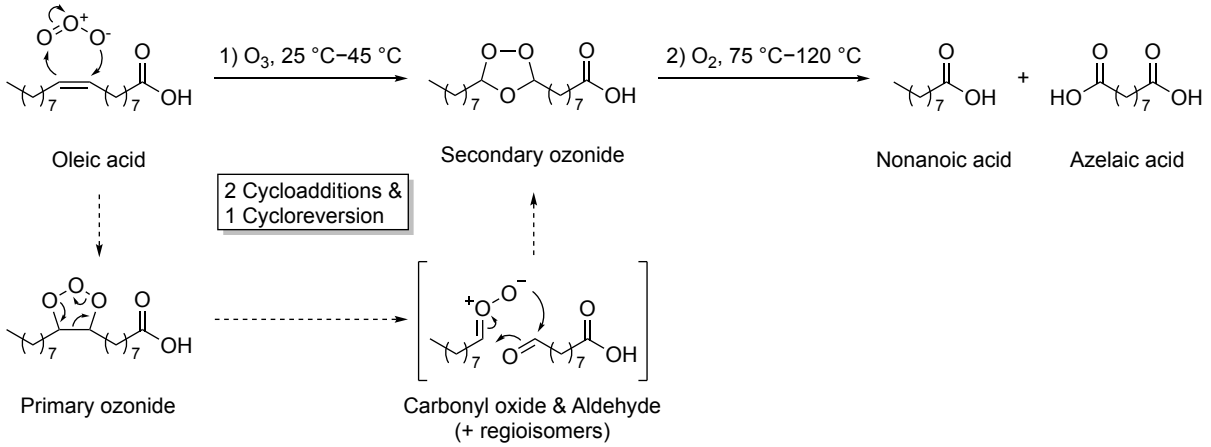

Scheme 2.20: Ozonolysis of oleic acid to yield nonanoic acid and azelaic acid and the proposed mechanism for the formation of the secondary ozonide.[130, 217, 219]

Many reactions with highly reactive oxidation agents such as potassium permanganate,[228] sodium hypochlorite,[227] sodium periodate,[229-234] and potassium peroxymonosulfate[230, 235] have been reported so far. These reactions are however not considered sustainable due to the hazardousness of the employed oxidants as well as the concomitant generation of stoichiometric amounts of waste (e.g., heavy iodine containing waste from sodium periodate).[97] Thus a lot of research focused on the development of transition metal-based catalysts that use more sustainable oxidants such as hydrogen peroxide or even molecular oxygen.[213-214, 221] Within this thesis, a ruthenium-based catalyst from literature was utilized for the synthesis of a tricarboxylic acid from sunflower oil (chapter 4.2).[236] The procedure and the proposed reaction mechanism will thus be discussed in the following:

In 2013, Behr *et al*. developed a homogeneous ruthenium catalyst for the oxidative cleavage of methyl oleate.[236] The optimized reaction is performed at 80 °C in *tert*-butanol and water, with 1 mol% of ruthenium(III)acetylacetone and 20 mol% of pyridine-2,6-dicarboxylic acid as catalytic system, and with hydrogen peroxide as more sustainable oxidant. Yields higher than 80% were obtained for both cleavage products of methyl oleate, i.e. nonanoic acid and azelaic acid monomethyl ester (Scheme 2.21, **top**).[236] The reaction is a sequence of: i) **epoxidation** to 9,10-epoxystearic acid methyl ester, ii) **hydrolysis** to 9,10-dihydroxystearic acid methyl ester, and iii) **oxidative cleavage** (Scheme 2.21, **bottom**). Three control experiments were performed to prove this mechanism. First it was shown that the epoxidation product is obtained in a yield of 92%, when the reaction is performed at room temperature instead of 80 °C.[237] Secondly, heating the pure epoxide to 80 °C in an aqueous solution with the same pH value as in the reaction (pH = 2.4) yields 97% of vicinal diol.[236] At last, it was shown that the catalyst oxidized the pure diol to obtain both products in yield >60%.[236]

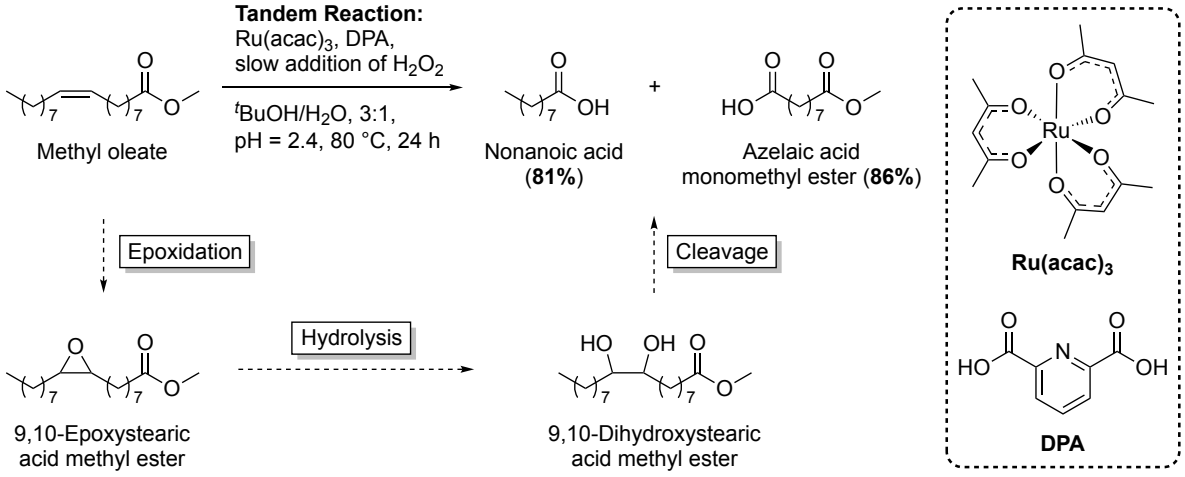

Scheme 2.21: Ruthenium catalyzed oxidative cleavage of methyl oleate.[236]

The reaction was further monitored by quantitative gas chromatography (GC) to investigate the mechanism. The obtained GC results showed that epoxidation of methyl oleate was quite fast as already after 3 h of reaction full conversion of methyl oleate was achieved. The epoxide that was detected as first intermediate hydrolyzed readily to yield 48% of diol after 3 h of reaction. Next, the cleavage products nonanal and 9-oxononanoic acid methyl ester were detected, indicating that the diol was first oxidatively cleaved to yield aldehydes. At last the formation of the desired carboxylic acids was observed, which reached the maximum yield after 12 h of reaction. The monitoring by gas chromatography thus supports the proposed reaction sequence.[236] In summary, the ruthenium catalyzed oxidative cleavage of methyl oleate proved to be very efficient and high yielding. A further improvement to this reaction could be the development of a heterogeneous catalyst to allow recycling and reuse by simple filtration.

2.5.4 Passerini three-component reaction (P-3CR)

The Passerini three-component reaction (P-3CR) was discovered in 1921 by Mario Passerini and describes the addition reaction between a carboxylic acid, an aldehyde, and an isocyanide to form an *α*-acyloxy amide (Scheme 2.22, **top**).[238-239] The proposed reaction mechanism begins with activation of the aldehyde component by the carboxylic acid *via* hydrogen-bonding (Scheme 2.22, **middle**).[239] In a following cyclic transition state, the isocyanide component reacts in a nucleophilic *α*-addition with the aldehyde component, while the carboxylic acid component simultaneously adds nucleophilic to the isocyanide. The postulated *α*-adduct, which has not been isolated yet, rearranges in an irreversible intramolecular transacylation step to form the *α*-acyloxy amide.[239] The mechanism being non-ionic is supported by the observation that the reaction proceeds faster in aprotic solvents such as dichloromethane instead of highly polar solvents, which besides could compete in hydrogen bonding during the activation step.[240] The mechanism is furthermore supported by an observed third order reaction rate with first order in each of the reactants.[241] Based on quantum-chemical calculations, Maeda *et al*. proposed a different mechanism, in which two carboxylic acids participate in the rearrangement, thereby rendering the P-3CR actually a four-component reaction.[242] The second carboxylic acid is a catalyst that lowers the activation barrier of the reaction by being a proton donor and a proton acceptor (Scheme 2.22, **bottom**).

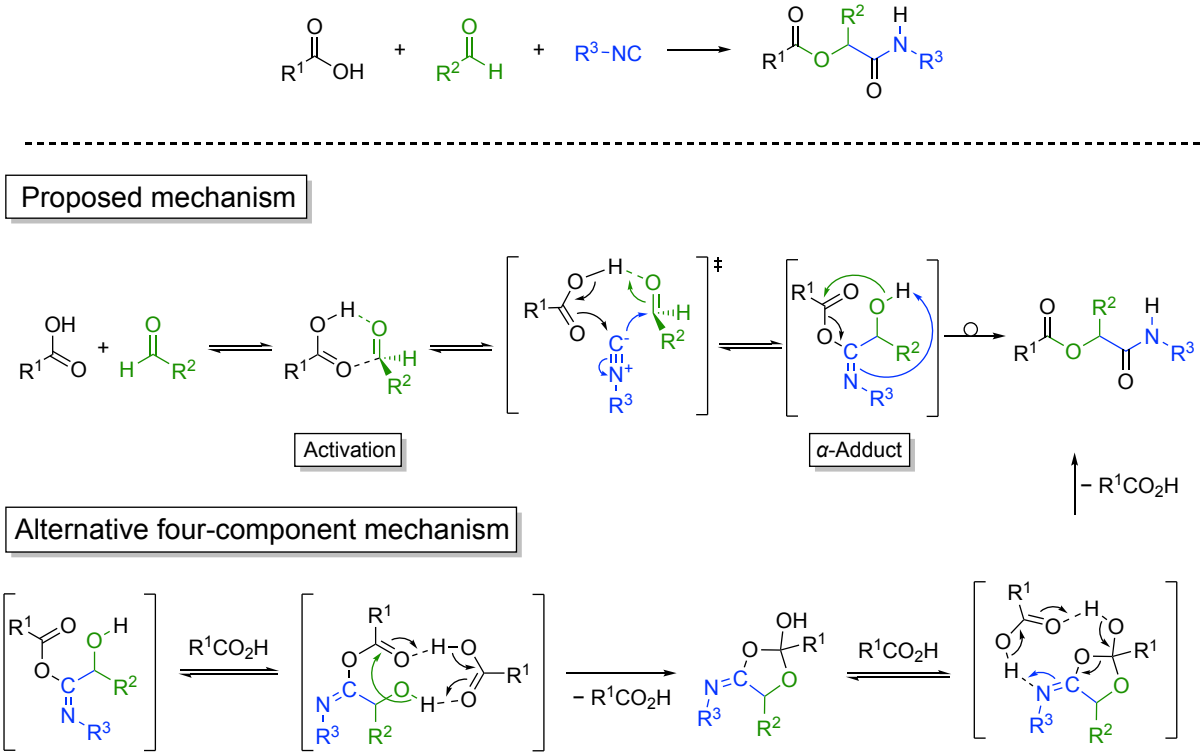

Scheme 2.22: Passerini reaction and the proposed reaction mechanisms.[239, 242]

Although the Passerini reaction is known to achieve near quantitative conversions at room temperature, its utilization as step-growth polymerization reaction was first reported 90 years after its discovery.[243] Thus, in 2011, Meier *et al*. reported the synthesis of two polyesters with amide side chains and high molecular weights of 56.5 kDa and 42.3 kDa by reaction of dicarboxylic acid **M1.4**, dialdehyde **M1.5**, and either cyclohexyl isocyanide or *tert*-butyl isocyanide (Scheme 2.23a). It is worth mentioning that mild conditions of 40 °C and a reaction time of 24 h were already enough to achieve these results due to the high efficiency of the Passerini three-component reaction. Interestingly, the two difunctional monomers **M1.4** and **M1.5** were synthesized from 10-undecenoic acid, which is obtained industrially by pyrolysis of castor oil.[140-141] As a consequence, both difunctional monomers as well as both polyesters are (partially) bio-based, thereby increasing the sustainability of this approach.

Shortly after, Li *et al*. utilized the P-3CR polymerization approach by Meier to synthesize poly(ester-amide)s and polyamides by simple permutation of the difunctional starting materials' functional groups.[244-245] For instance, poly(ester-amide)s were obtained by reaction of dicarboxylic acids with diisocyanides and monoaldehydes.[244] Thus, Li *et al*. reported the synthesis of two polymers with M_n values of 15.2 kDa and 6.6 kDa by polymerization of either adipic acid (hexanedioic acid) or sebacic acid (decanedioic acid) with 1,6-diisocyanohexane and phenylacetaldehyde at 30 °C in dichloromethane for 36 h (Scheme 2.23b). It was observed by ^{1}H NMR spectroscopy that already after 2 h of reaction at room temperature, 98% of the monomers had reacted, again revealing the fast reaction rates of the P-3CR polymerization.[244] Polyamides with ester side-chains are obtained with the last permutation of difunctional monomers, i.e. the combination of dialdehyde, diisocyanide and monocarboxylic acid. For instance, Li *et al*. reported the synthesis of three polyamides with ester side chains by reaction of adipaldehyde with 1,6-diisocyanohexane and either undecanoic acid, 10-undecenoic acid, or 10-undecynoic acid (Scheme 2.23c).[245] The polymerizations were performed at 40 °C in chloroform for 48 h to yield polymers with high molecular weights between 10.6 kDa−17.7 kDa and dispersities between 1.52−1.98.[245]

$A_2 + B_2 + C$

a) Dicarboxylic acid + Dialdehyde:

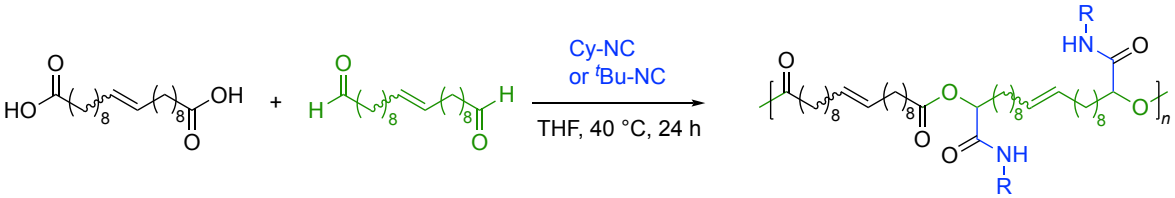

M1.4 **M1.5**

Polyesters with amide side chains
M_n: 56.5 kDa for Cy-NC
M_n: 42.3 kDa for ^{t}Bu-NC

b) Dicarboxylic acid + Diisocyanide:

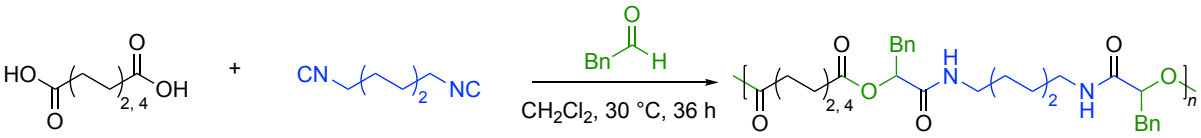

Adipc acid or
Sebacic acid

1,6-Diisocyanohexane

Poly(ester-amide)s
M_n: 15.2 kDa for adipic acid
M_n: 6.6 kDa for sebacic acid

c) Dialdehyde + Diisocyanide:

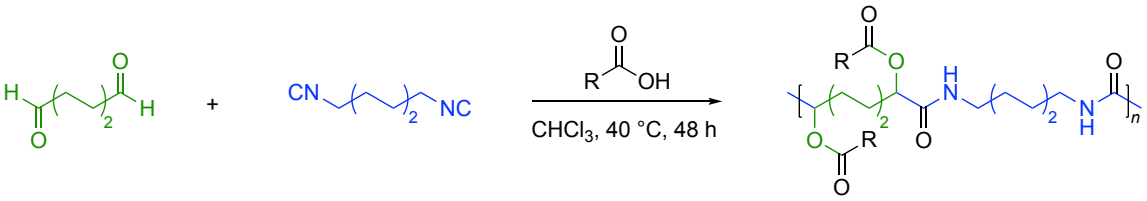

Adipaldehyde

1,6-Diisocyanohexane

Polyamides with ester side chains
M_n: 16.6 kDa for Undecanoic acid
M_n: 10.6 kDa for 10-Undecenoic acid
M_n: 17.7 kDa for 10-Undecynoic acid

AB + C

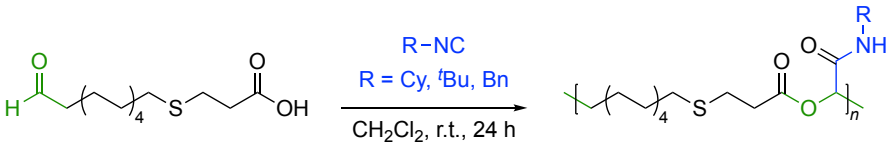

M1.6

Polyesters with amide side chains
M_n: 31.7 kDa−34.6 kDa

Scheme 2.23: Synthesis of linear polymers *via* the Passerini three-component reaction by combination of either A_2, B_2 and C-type monomers (top) or AB and C-type monomers (bottom). Polyesters, poly(ester-amide)s, and polyamides are obtained depending on the distribution of functional groups among all monomers.[121, 243-245]

The multicomponent polymerization approach moreover easily allows the polymers to be grafted onto by introduction of additional functional groups during the MCR step.[245-246] For instance, in the mentioned examples from Li *et al*. (Scheme 2.23c), the two polyamides made from 10-undecenoic acid and 10-undecynoic acid bearing terminal double bonds and terminal triple bonds in their side chains, respectively, were grafted onto *via* thiol-ene reaction and *via* copper-catalyzed azide-alkyne cycloaddition, respectively.[245]

In contrast to the combination of A_2, B_2 and C-type monomers, only two components are required when AB-type monomers are employed. Noteworthy, the "AB + C" system moreover intrinsically fulfills the stoichiometric balance that is needed for step-growth polymerizations to achieve high molecular weights, even if the C component is used in excess. In 2014, Meier *et al*. reported the AB-type monomer **M1.6** bearing an aldehyde and a carboxylic acid group, which was synthesized from 10-undecenal and 3-mercaptopropionic acid *via* thiol-ene reaction with UV irradiation and DMPA as photoinitiator (Scheme 2.23, **bottom**).[121] **M1.6** was reacted with several isocyanides (e.g., cyclohexyl, *tert*-butyl, benzyl) in dichloromethane for 24 h at room temperature to obtain polymers with molecular weights ranging from 31.7 kDa−34.6 kDa and dispersities between 1.79−2.29. Post-polymerization modification was performed by oxidation with 3-chloroperbenzoic acid to transform the thioether moieties within the polymer backbone into their corresponding sulfones. As a result, the glass transition temperature of all polyesters increased by approximately 30 °C after oxidation (e.g., for *tert*-butyl isocyanide-based polymer from 2 °C to 35 °C).[121] In two other studies by Li *et al*., 4-oxobut-3-enoic acid and 6-oxohexanoic acid were used as AB-type monomers in combination with monoisocyanides to synthesize polyesters with amide side chains.[246-247] However, to the best of this author's knowledge, there have been no reports about polymerizations of AB-type monomers bearing either one aldehyde and one isocyanide group or one carboxylic acid and one isocyanide group.

So far, the synthesis of cross-linked polymers *via* isocyanide based MCRs has been reported scarcely. In 1999, Crescenzi *et al*. reported the first synthesis of a P-3CR derived hydrogel from carboxymethylcellulose (CMC), which was reacted with glutaraldehyde and cyclohexyl isocyanide (Scheme 2.24, **left**).[248] In addition, Ugi four-component derived hydrogels were synthesized by combination of CMC with formaldehyde, cyclohexyl isocyanide and 1,5-diaminopentane (Scheme 2.24, **right**).[248]

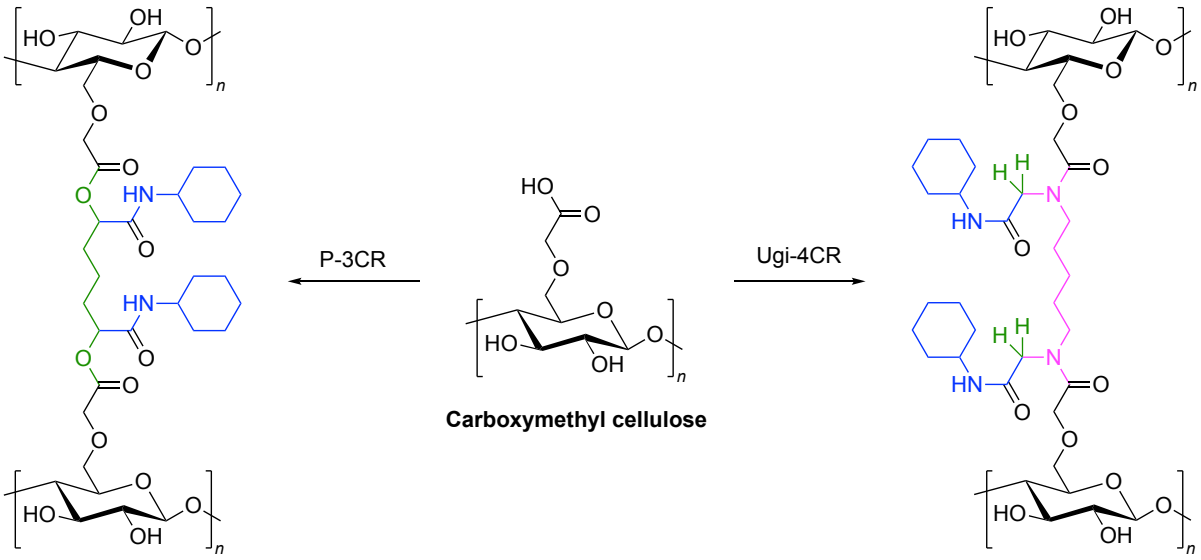

Scheme 2.24: Cross-linked hydrogels from carboxymethylcellulose *via* Passerini three-component reaction (left) and Ugi four-component reaction (right).[248]

Both MCRs were performed in acidic aqueous solution (pH = 4) and proceeded within 30 minutes at room temperature to yield transparent hydrogels with cross-linking degrees ranging from 5%−15%. The degree of cross-linking was defined as ratio between the moles of difunctional compound (i.e. glutaraldehyde or 1,5-diaminopentane) and the moles of carboxylic acid groups of the carboxymethylcellulose.[249] Hence, only substoichiometric amounts of difunctional compounds were used for these hydrogels (0.1−0.3 equiv.). Degradation studies in alkaline aqueous solution (pH = 9.5) revealed that the P-3CR hydrogels with ester groups as cross-links degraded within few days, while the Ugi-4CR derived hydrogels with amide cross-links were completely stable for up to 60 days.[248] It was therefore possible to deliberately manipulate the stability of the materials by choice of the applied MCR. Apart from carboxymethylcellulose,[248, 250] other carboxylic acid group bearing polysaccharides such as alginic acid[250-253] and hyaluronic acid[249-250] have been used for the synthesis of hydrogels *via* MCRs. Furthermore, chitosan was used as polyamine component for the synthesis of Ugi-4CR based microgels.[254] It should be noted here that in all of these reports, the cross-linking was performed only with already polymeric starting materials and not by polymerization of monomers. To the best of this author's knowledge, so far only one report by Xie *et al*. described the synthesis of a cross-linked P-3CR polymer from the low molecular weight compounds terephthalaldehyde, 1,6-diisocyanohexane, and sebacic acid.[255] It was moreover possible to incorporate a ruthenium complex with one ligand bearing an aldehyde group into the thermoset to synthesize a heterogenous catalyst (Scheme 2.25).

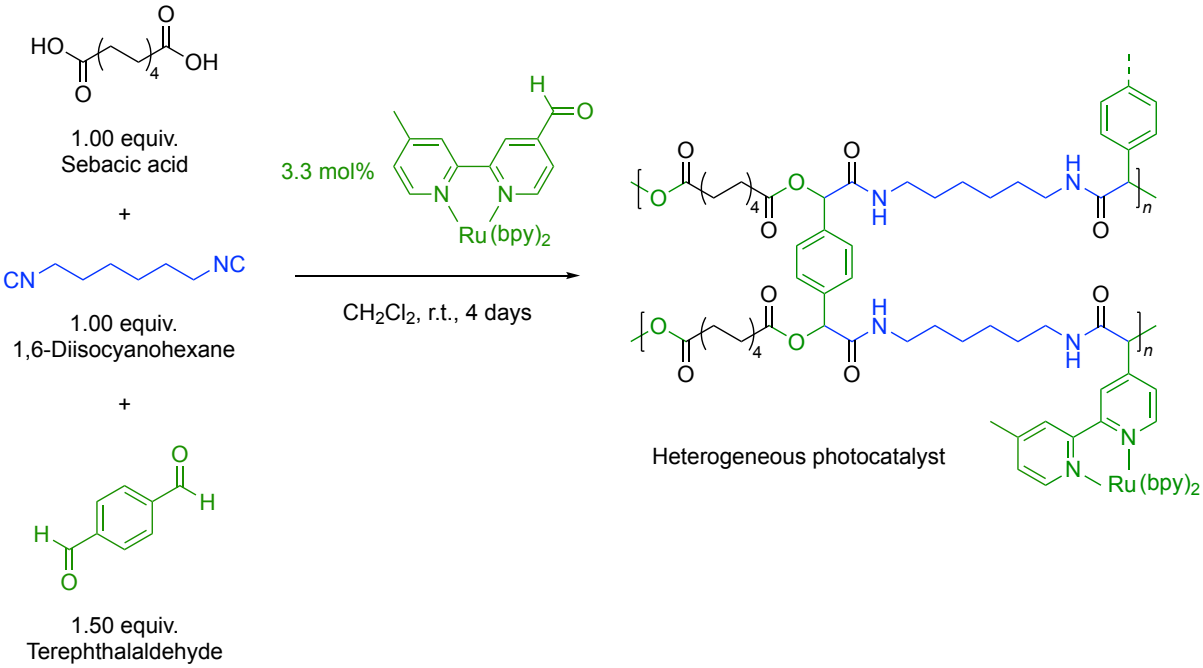

Scheme 2.25: Synthesis of a cross-linked polymer *via* Passerini three-component reaction of sebacic acid, 1,6-diisocyanohexane, terephthalaldehyde, and a photo catalytically active ruthenium complex.[255]

It is however most likely that these materials exhibited a low degree of cross-linking and a high share of unreacted aldehyde groups due to molar excess of 50 mol% terephthalaldehyde that was used.[255] Xie *et al*. demonstrated that this thermoset efficiently catalyzed the oxidation of thioanisole with molecular oxygen to yield 92% of methyl phenyl sulfoxide (for comparison: 5% yield without catalyst). The catalyst was separated from the reaction mixture by simple filtration and then reused for another three reactions without any significant decrease in its catalytic activity (92% for first use vs. 85% for third reuse).[255]

To the best of this author's knowledge, no cross-linked polymers have hitherto been synthesized *via* the Passerini reaction in a solvent-free manner since both, the hydrogel approach and the polymer reported by Xie *et al*. relied on solvents during the polymerization.

Thus, within this thesis, the P-3CR was utilized for the synthesis of new cross-linked polymers from a renewable tricarboxylic acid in combination with two diisocyanides and five monoaldehydes. All polymerizations were conducted without any solvents due to the liquid nature of all monomers. The results from this project are discussed in chapter 4.3.

3 Aim

The substitution of depleting fossil resources by renewable materials is crucial to guarantee a more sustainable future. Especially research on polymers must be performed, since to date still less than 1% of the worldwide production of plastics is bio-based. Thus, this work aimed to utilize various renewable resources for the synthesis of polycarboxylic acids that serve as monomers for the production of bio-based polymers. This functional group was targeted since it can be polymerized in various ways to provide diverse plastic materials. For instance, polyesters are yielded by reaction of dicarboxylic acids with diols, while polyamides are obtained with diamines as second monomer. Furthermore, poly(ester-amide)s are accessible by reaction of dicarboxylic acids with diisocyanides and monoaldehydes in a Passerini three-component reaction (P-3CR). The performed reactions within this thesis were deliberately chosen to be inherently as sustainable as possible and furthermore optimized in each project considering sustainability aspects of the *Twelve Principles of Green Chemistry*, such as waste production and toxicity of the involved chemicals.[5]

In the first project, saturated fatty acids were chosen as renewable resource. It was aimed to elaborate a new three-step reaction sequence to transform saturated lauric acid into dimethyl esters as monomers for the synthesis of polyesters. The selective dehydrogenation of lauric acid at its *α* and *β* positions was planned to be performed with a recently established palladium catalyzed dehydrogenation procedure that uses molecular oxygen as sustainable oxidant.[187] Esterification of the obtained *α*,*β*-unsaturated lauric acid with methanol to its corresponding methyl ester as second step and a subsequent dimerization reaction with dithiols *via* thia-Michael reaction as third step were devised to yield new dimethyl esters (Scheme 3.1, **top**). At last, polymerization with 1,12-dodecanediol was aimed to yield bio-based polyesters.

Secondly, it was targeted to synthesize a tricarboxylic acid from high oleic sunflower oil by oxidative cleavage of its double bonds to obtain a new cross-linker for thermoset applications. A literature reported ruthenium catalyzed oxidative cleavage of alkenes into carboxylic acids using hydrogen peroxide as more sustainable oxidant was thus planned to be employed on high oleic sunflower oil to yield the desired triacid (Scheme 3.1, **middle**).[236] It was aimed to synthesize thermosets from this triacid in combination with diisocyanides and monoaldehydes *via* P-3CR. Alternatively, curing of epoxy resins with this triacid was considered.

Finally, it was aimed to utilize lignin for the synthesis of polycarboxylic acids by reaction with succinic anhydride (Scheme 3.1, **bottom**). It was planned to functionalize lignin in a solvent-free system and at lower temperatures in solution to synthesize several lignin samples with different degrees of substitution. The lignin-based polycarboxylic acids will presumably be more rigid than the targeted sunflower oil-based triacid due to their aromatic scaffold. Furthermore, the amount of functional groups per molecule will be significantly higher. It was therefore aimed to synthesize similar thermosets *via* P-3CR from these cross-linkers to compare their influence on the thermal properties of the resulting materials with the sunflower oil-based triacid.

Overall, this work aimed to establish new and environmentally benign synthetic routes to renewable carboxylic acids as monomers for plastics and thus to contribute to the transition from conventional fossil-based polymer chemistry to the use of renewable resources.

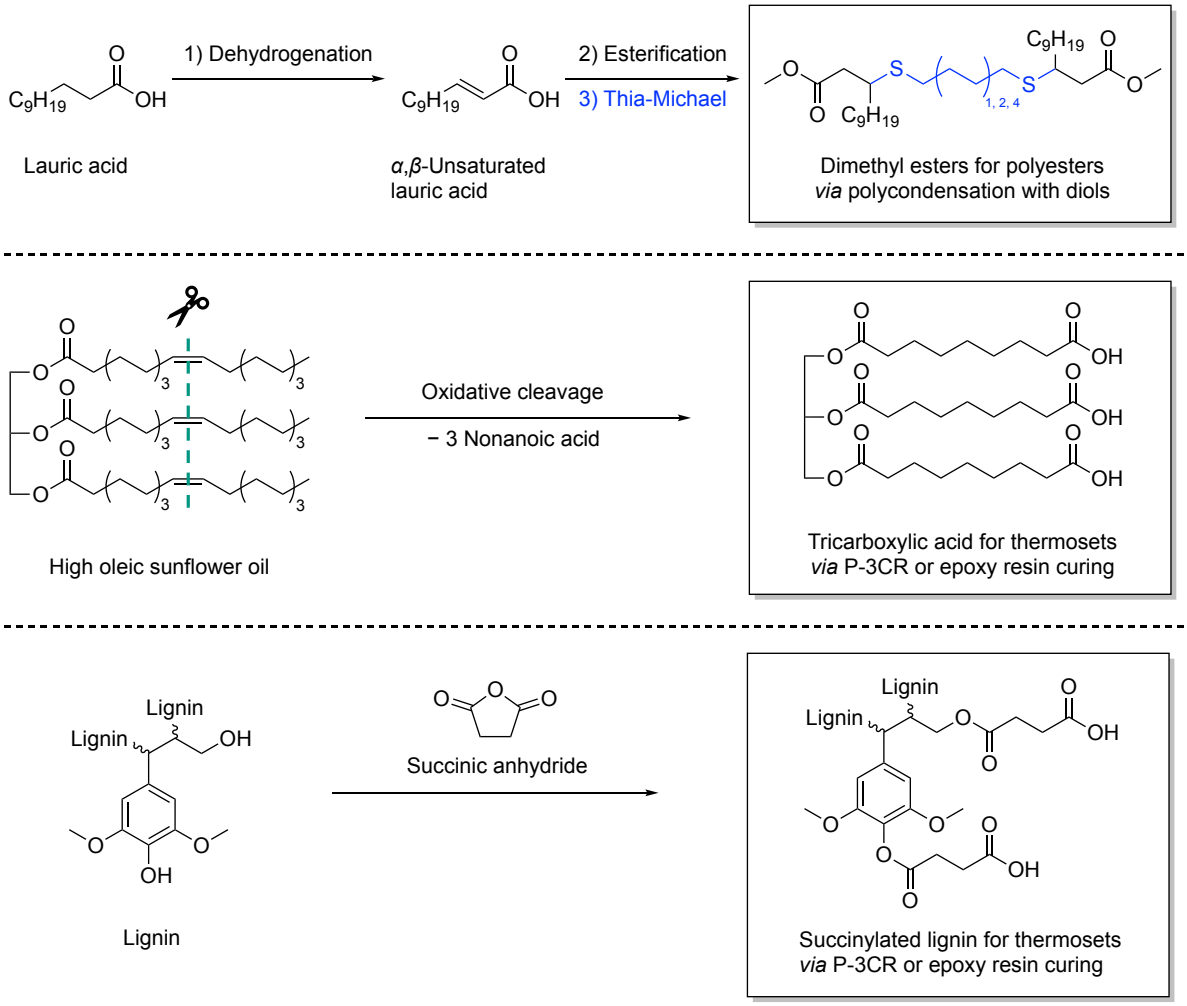

Scheme 3.1: Summarized aim of this thesis that is divided into the synthesis of dimethyl esters from saturated lauric acid as monomers for polyesters (top), the synthesis of a new tricarboxylic acid from high oleic sunflower oil as cross-linker for thermosets (middle), and the synthesis of polycarboxylic acids from organosolv lignin as cross-linkers for thermosets (bottom).

4 Results and Discussion

In this chapter, the experimental results obtained within this thesis are presented and discussed in detail. This chapter is subdivided into four parts, each describing a different research project, yet all chapters contribute to the general aim of this thesis and are thus thematically connected. In chapter 4.1, a new three-step reaction sequence was developed for the synthesis of dimethyl esters from renewable lauric acid. The sequence consists of a catalytic dehydrogenation with molecular oxygen as oxidant, an esterification with methanol, and a dimerization reaction with dithiols *via* thia-Michael addition. This approach enabled the subsequent synthesis of bio-based polyesters by polycondensation with 1,12-dodecanediol. In chapter 4.2, a literature known ruthenium catalyzed oxidative cleavage was employed to high oleic sunflower oil to synthesize a novel tricarboxylic acid. A simple statistical concept was devised to explain seemingly moderate triacid yields, emphasizing furthermore that a high content of at least 90% unsaturated fatty acids in the used oil is necessary to achieve high yields of trifunctional derivatives. In chapter 4.3, the obtained tricarboxylic acid was utilized for the synthesis of renewable cross-linked polymers *via* the Passerini three-component reaction. Adhesive tests were performed to demonstrate a potential application of these new materials as “three component glues”. One Passerini thermoset was chemically recycled by transesterification with methanol and catalytic amounts of sulfuric acid to establish a proof of concept of the circularity of these materials. At last, in chapter 4.4, organosolv lignin was functionalized at its hydroxyl groups by reaction with succinic anhydride to synthesize succinic acid lignin esters. Two lignin-based polycarboxylic acids with functionalization degrees of 69% and 34% were synthesized in a solvent-free reaction at 150 °C and a solvent containing reaction at 80 °C, respectively. In another approach, lignin was first hydroxyethylated to transform aromatic alcohol groups into hydroxyethyl ethers and hence achieve a more uniform chemical functionality of 99% aliphatic alcohol groups instead of the initially present 53% aliphatic and 47% aromatic alcohol groups. A polycarboxylic acid with a high functionalization degree of 99.6% was then obtained by reaction of the hydroxyethylated lignin with succinic anhydride.

4.1 Catalytic dehydrogenation of lauric acid and a polyester synthesis

This chapter is based on previously published results by the author of this thesis:

L. Santos Correa, E. Stapf, T. Nonner, M. A. R. Meier, “Catalytic Dehydrogenation of Lauric Acid and a Potential Use in Polyester Synthesis”, *Eur. J. Lipid Sci. Technol.* **2025**, e70003.[256]

The author of this thesis developed the synthetic procedure, planned and evaluated the experiments, and wrote the original draft of the publication. E. Stapf synthesized the ligand for the catalysis and conducted all solvent containing lauric acid dehydrogenation experiments under the co-supervision of the author of this thesis. T. Nonner conducted all thia-Michael addition experiments under the co-supervision of the author of this thesis.

Note: Before reading this chapter, the reader is advised to read chapter 2.5.1 and chapter 2.5.2 for a theoretic introduction to catalytic *α*,*β*-dehydrogenations of carboxylic acids and thia-Michael additions, respectively.

Abstract

The substitution of depleting fossil resources by renewable resources is of paramount importance especially for polymer chemistry with its large production volume in order to guarantee a more sustainable future. Herein, a new three-step reaction sequence was developed to synthesize renewable fatty acid-based dimethyl esters from saturated fatty acids. The sequence consists of a catalytic dehydrogenation with molecular oxygen as oxidant, an esterification with methanol, and a dimerization reaction with dithiols *via* thia-Michael addition. Three new dimethyl esters were thus synthesized from lauric acid and fully characterized *via* infrared, ^{1}H NMR and ^{13}C NMR spectroscopy as well as mass spectrometry. Polyesters with molecular weights ranging from 26.0 kDa−31.8 kDa were obtained by polycondensation of each dimethyl ester with 1,12-dodecanediol. Methyl crotonate-based polymers were prepared for comparison with the fatty acid derived materials. Thermogravimetric analysis revealed that the long side chains led to improved thermal stability and differential scanning calorimetry showed side chain crystallization for one polymer.

Results and discussion

At first, the original palladium catalyzed dehydrogenation procedure from Yu *et al*. was employed to octanoic acid and to four fatty acids (C_{12}, C_{14}, C_{16}, C_{18}) to assess whether the length of the aliphatic chain has an impact on the dehydrogenation efficiency of the catalyst (Scheme 4.1, see chapter 2.5.1 for theory).[187] The procedure uses 1,4-dioxane and *tert*-amyl alcohol as solvents, 2.50 equivalents of lithium carbonate and sodium acetate as bases to deprotonate the carboxylic acid, and 2.00 equivalents of silver carbonate as oxidant. For all five reactions, a high selectivity was observed in ^{1}H NMR spectroscopy as all proton signals were either assigned to the product or to the unreacted starting material. Exemplarily, the ^{1}H NMR spectrum of the dehydrogenation of octanoic acid is depicted in Figure 4.1 (all other spectra can be found in the Experimental section chapter 6.3.2). The ratio of starting material to product was determined *via* ^{1}H NMR spectroscopy by integration of the *α*-CH_2 protons of the saturated acid at 2.35 ppm and the CH_2 protons adjacent to the double bond of the *α*,*β*-unsaturated acid at 2.22 ppm. In case of octanoic acid, this results in integrals of 0.48 and 2.19, respectively, and thus in a starting material to product ratio of 18:82 (Figure 4.1, signals 3 and 4; Table 4.1, Entry 1). Moreover, the absence of side products allowed the reaction yield to be calculated directly from the ratio of starting material to product. The dehydrogenation of octanoic acid thus achieved a yield of 82% and served as control experiment to demonstrate reproducibility, as the same reaction was performed in the original publication with a yield of 76%.[187] For the fatty acids, a lower reactivity was observed with an increasing chain length. Already for lauric acid (C_{12}), the NMR yield reduced drastically to 48% and further decreased steadily to 6% for stearic acid (C_{18}). An optimization of the reaction procedure was therefore desired to improve reaction yields. Moreover, it should be noted that the original protocol is considered rather unsustainable due to the large amount of waste that is generated by 2.50 equivalents of inorganic bases and 2.00 equivalents of silver carbonate.

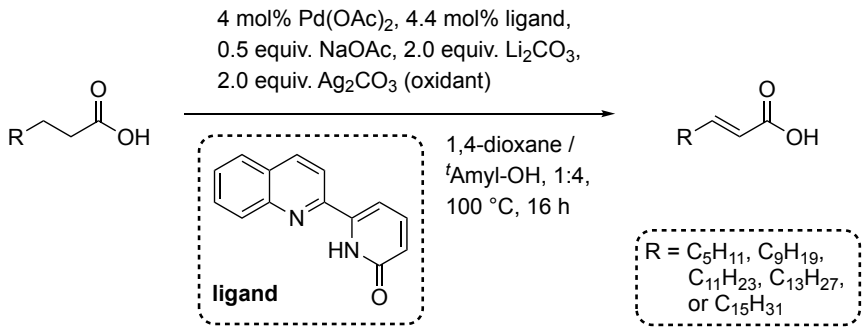

Scheme 4.1: Palladium catalyzed dehydrogenation of aliphatic carboxylic acids.[187]

Table 4.1: Carboxylic acid dehydrogenation performed with silver carbonate as oxidant. Reaction yields were estimated *via* ^{1}H NMR spectroscopy (Experimental section chapter 6.3.2).

Carboxylic acid	Starting material to product ratio	NMR-Yield / %
Octanoic acid (C_8)	18:82	82
Lauric acid (C_{12})	52:48	48
Myristic acid (C_{14})	70:30	30
Palmitic acid (C_{16})	86:14	14
Stearic acid (C_{18})	94:6	6

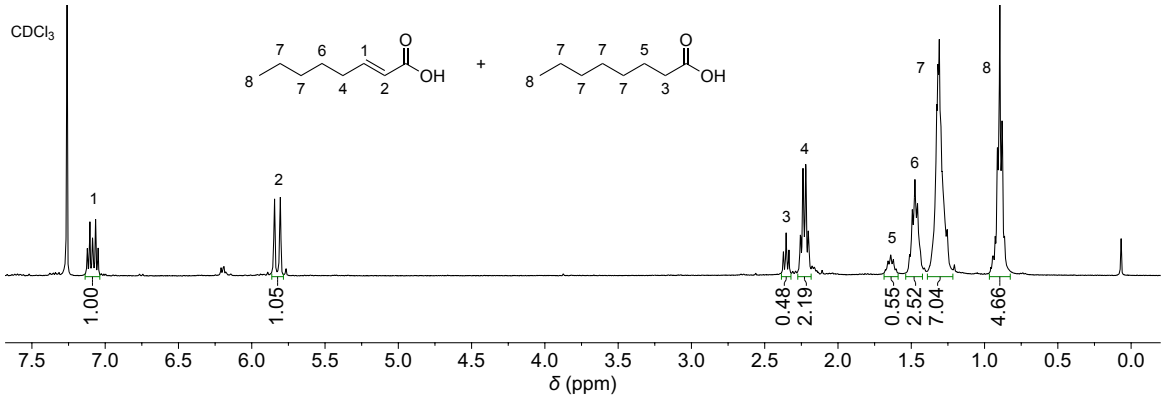

Figure 4.1: ^{1}H NMR spectrum of the dehydrogenation of octanoic acid with silver carbonate as oxidant.

In fact, Yu *et al*. demonstrated that molecular oxygen can be used as oxidant to substitute silver carbonate.[187] However, not only was the toxic solvent DMF used,[257] but also stoichiometric amounts of toxic *p*-benzoquinone as co-catalyst.[258] The herein conducted optimization therefore included the use of molecular oxygen as oxidant in combination with the more sustainable solvents *tert*-butanol and water.[259-260] Co-catalysts were fully excluded to reduce the amount of waste formed and the equivalents of inorganic base were reduced to a minimum (Table 4.2). Reaction time and temperature of 24 h and 100 °C, respectively, were initially kept identical to the original procedure. The first experiment showed that 1.00 equivalent of lithium carbonate was sufficient for the reaction to proceed (Entry 1). Moreover, no loss in reaction yield was observed when lithium carbonate was replaced by the more abundant sodium carbonate (Entry 2). Higher amounts of sodium carbonate led to phase separation due to an increased polarity of the aqueous phase and therefore resulted in heterogeneous reactions with reduced yields (Entries 2−5). Replacing sodium carbonate by potassium carbonate and cesium carbonate further increased the yield to 24.6% and 32.4%, respectively (Entries 6−7). As expected, a reduced reaction temperature resulted in a lower reaction yield of 16.1% (Entry 8). A too high temperature however led to lower yields due to the formation of side products (Entries 9−10, see chapter 6.3.3 for ^{1}H NMR spectra).

Table 4.2: Optimization of the palladium catalyzed dehydrogenation of lauric acid with molecular oxygen. Reaction conditions were the following unless stated otherwise: 10 bar O_2, 4.0 mol% $Pd(OAc)_2$, 4.4 mol% ligand, 24 h of reaction time, concentration of 50 mmol l^{-1} in mixture of *tert*-butanol and water (1:1). Notes: [a]Reaction time of 72 h; [b]Double the amount of catalyst and ligand were used; [c]Four times the amount of catalyst and ligand were used; [d]Solvent-free; [e]Octanoic acid was used instead of lauric acid.

Entry	Base		Temperature	NMR-Yield with CH_2Br_2 as external standard / %
	Base	Equiv.		
1	Li_2CO_3	1.00	100 °C	17.6
2	Na_2CO_3	1.00	100 °C	18.0
3	Na_2CO_3	1.25	100 °C	19.3
4	Na_2CO_3	1.50	100 °C	7.2
5	Na_2CO_3	2.00	100 °C	6.2
6	K_2CO_3	1.00	100 °C	24.6
7	Cs_2CO_3	1.00	100 °C	32.4
8	Cs_2CO_3	1.00	90 °C	16.1
9	Cs_2CO_3	1.00	115 °C	19.5
10	Cs_2CO_3	1.00	130 °C	0.9
11[a]	Cs_2CO_3	1.00	100 °C	37.9
12[b]	Cs_2CO_3	1.00	100 °C	58.8
13[c]	Cs_2CO_3	1.00	100 °C	80.3
14[d]	–	–	100 °C	38.3
15[d,b]	–	–	100 °C	26.5
16[d,e]	–	–	100 °C	46.0

A prolonged reaction time of 72 h did not result in a significantly higher yield (37.9%, Entry 11). An increased reaction yield was observed with higher catalyst loadings (Entries 12−13). Hence, double and four times the amount of catalyst achieved yields of 58.8% and 80.3%, respectively. The very low concentration of 50 mmol l^{-1} seemed unsustainable and impractical, since 10 grams of starting material would already require one liter of reaction volume, therefore generating large amounts of solvent waste. Several attempts to increase the concentration resulted in lower reaction yields, again presumably due to phase separation caused by the increased concentration of inorganic base. It was therefore decided to exclude the inorganic base and the solvents to prevent phase separations. Indeed, neither solvents, nor bases were actually needed for the reaction to proceed. Reacting molten lauric acid at 100 °C with 4.0 mol% of palladium(II)acetate and 4.4 mol% of ligand under 10 bar of oxygen atmosphere resulted in a yield of 38.3%, which is comparable to the yield of 48% that was obtained with the silver carbonate procedure (Table 4.2, Entry 14 vs. Table 4.1, Entry 2). A higher catalyst loading however did not result in a higher yield for this solvent-free approach (Entry 15). For octanoic acid, a higher yield of 46% was achieved, again confirming the reduced reactivity of longer chain carboxylic acids (Entry 16).

In summary, with the solvent-free approach, toxic DMF, toxic benzoquinone, and overstoichiometric amounts of lithium carbonate were avoided and thus the amount of waste formed is reduced significantly. The reaction was performed again with 40 grams of lauric acid to demonstrate its easy scalability. The black residue of the reaction was distilled *in vacuo* at 150 °C and 0.1 mbar to obtain a light-yellow liquid, presumably consisting of the fatty acids that were separated from the catalyst. ^{1}H NMR spectra of pure lauric acid and of the distilled liquid are depicted in Figure 4.2 (**top** and **middle**, respectively). The conversion of the reaction corresponded to 42% and was calculated from the integral of the product's methylene group at 2.23 ppm (integral = 2.21, signal e, Figure 4.2 **middle**) and the integral of lauric acid's *α*-methylene group at 2.35 ppm (integral = 3.07, signal a, Figure 4.2 **middle**; calculation: 2.21/(2.21+3.07) = 42%). Separation of both compounds was not possible due to their chemical and physical similarity. However, it was rationalized that separation and purification should be straightforward after conducting a double bond specific reaction to transform the *α*,*β*-unsaturated lauric acid into a new compound with different properties.

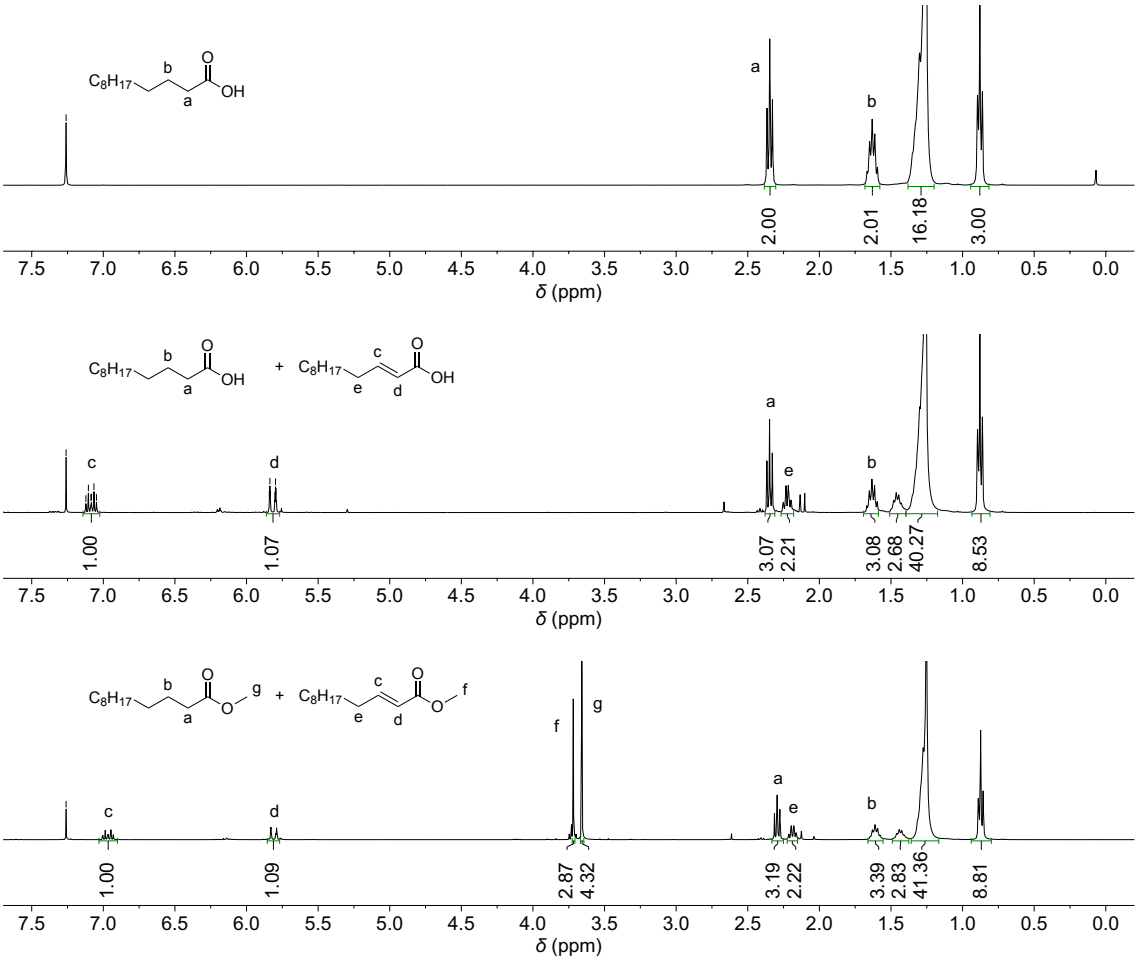

Figure 4.2: Stacked ^{1}H NMR spectra (in $CDCl_3$) of lauric acid (top), mixture of *α*,*β*-unsaturated lauric acid and lauric acid before esterification (middle) and after esterification (bottom).

Thus, the thia-Michael addition was utilized as specific reaction for *α*,*β*-unsaturated compounds (see chapter 2.5.2 for theory).[190, 196] It is used for functional groups such as acrylates,[261-262] maleates,[205] *α*,*β*-unsaturated cyclic ketones,[197, 204] as well as acyclic *α*,*β*-unsaturated ketones.[197-198] Basic catalysts such as triethylamine, TBD and DBU are commonly employed for thia-Michael additions. It was therefore reasonable to first conduct an esterification with methanol to convert the mixture of lauric acid and *α*,*β*-unsaturated lauric acid into their corresponding methyl esters. Otherwise, more than 100 mol% of base catalyst would be needed as the first equivalent is directly neutralized by the free carboxylic acid moieties. Additionally, strong acids would be needed during work-up to protonate the carboxylic acid groups and hence generate stoichiometric amounts of ammonium salt as waste. The mixture of carboxylic acids was hence esterified with methanol and catalytic amounts of sulfuric acid. The esterification proceeded quantitatively and was further characterized by NMR and IR spectroscopy. In comparison to the ^{1}H NMR spectrum of the starting materials, two additional methyl ester signals at 3.72 ppm and 3.66 ppm with an integral ratio of 40:60 indicate the successful esterification of the mixture of *α*,*β*-unsaturated lauric acid and lauric acid (Figure 4.2, **bottom**). In the IR spectrum, the C=O vibration signal of the carboxylic acid moiety at 1696 cm^{-1} shifted to 1741 cm^{-1}, which is characteristic for ester groups (Figure 4.3). Moreover, disappearance of the broad O-H stretching vibration signal between 3300 cm^{-1}−2500 cm^{-1} indicated a full conversion of carboxylic acids.

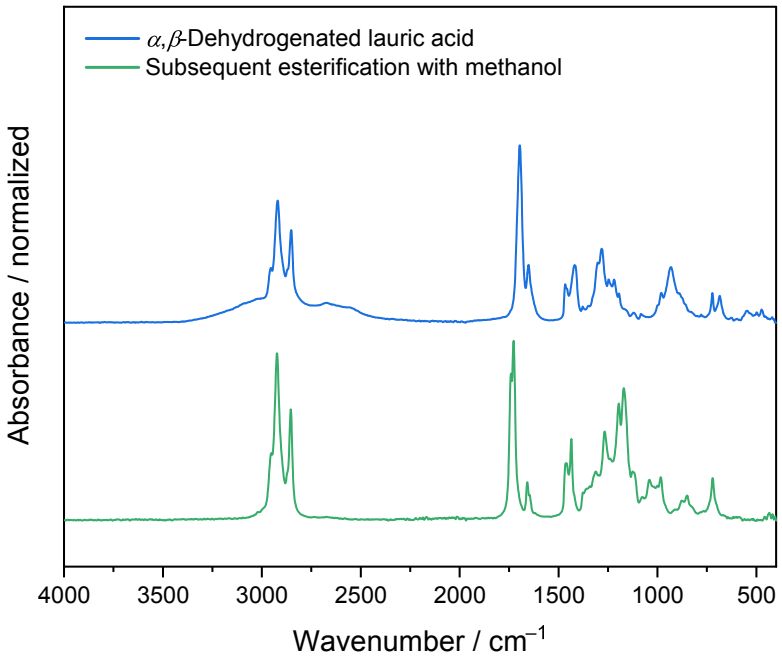

Figure 4.3: Stacked IR spectra of the dehydrogenation of lauric acid (top) and the subsequent esterification with methanol (bottom).

After successful dehydrogenation and esterification, the synthesis of three methyl laurate-based dimers (**LD1−LD3)** *via* thia-Michael addition from *α*,*β*-unsaturated methyl laurate and three dithiols was performed (Scheme 4.2, **top**). This approach was chosen as it enables the subsequent synthesis of bio-based polyesters (Scheme 4.2, **bottom**). The three dithiols 1,4-butanedithiol, 1,6-hexanedithiol, and 1,10-decanedithiol were used to investigate the influence of the dithiol length on the final properties of the resulting polyesters.

The reaction conditions of the thia-Michael addition were however first optimized for the addition of 1,4-butanedithiol to methyl crotonate before transferring them to the *α*,*β*-unsaturated methyl laurate (Scheme 4.2, **top**). Reasoning for this was the commercial availability of methyl crotonate in a high purity of 98%, which simplified monitoring of the reaction in contrast to the mixture of methyl esters that was obtained from the dehydrogenation. First, triethylamine was tested as catalyst because it was reported to be efficient for thia-Michael additions of thiols to cyclohexenone and methyl acrylate.[204, 261] The reaction was performed with 10 mol% of NEt_3 and was stirred for 24 h at room temperature. It was possible to measure the ratio of methyl crotonate to the crotonate-based dimer **CD1** *via* ^{1}H NMR spectroscopy by integration of the double bond proton signal at 5.83 ppm and the signal of newly formed thioether moiety at 3.18 ppm (Experimental section chapter 6.5.1, Figure 6.16). Hence, a conversion of 29% was achieved with NEt_3 as catalyst at room temperature, which could further be increased to 53% when the reaction was performed at 90 °C (Table 4.3, Entries 1−2). The organic superbase 1,5-diazabicyclo[4.3.0]non-5-ene (DBN) was tested as next catalyst, since multiple reports in literature described that such nitrogen bases were more active catalysts for thia-Michael additions than triethylamine.[205-207]

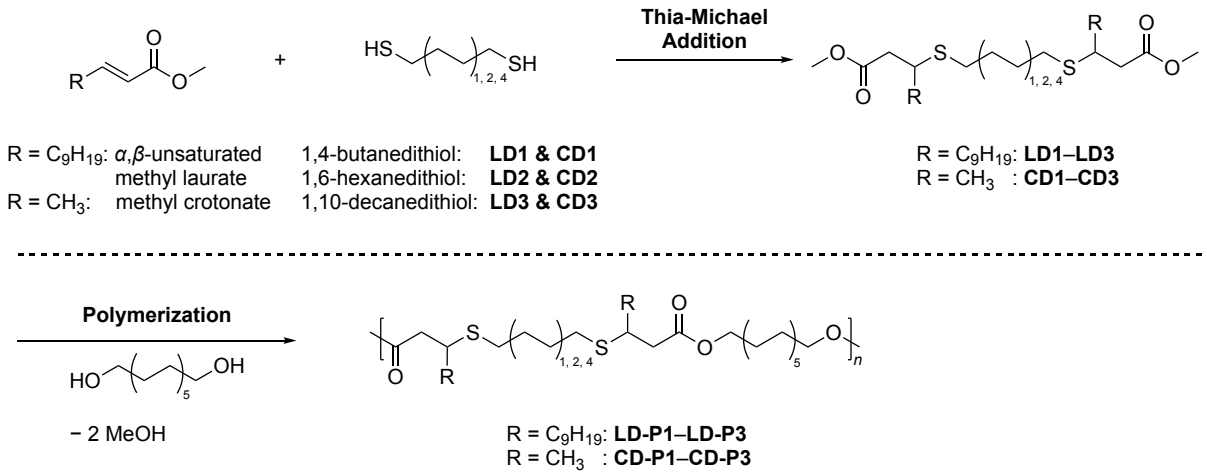

Scheme 4.2: Thia-Michael addition of dithiols to methyl crotonate and *α*,*β*-unsaturated methyl laurate to yield dimethyl esters (top) and polymerization with 1,12-dodecanediol (bottom).

Table 4.3: Optimization of thia-Michael addition of 1,4-butanedithiol to methyl crotonate. Note: [a]Reaction was performed at 90 °C.

Entry	Catalyst	Time	Methyl crotonate : product ratio determined by ^{1}H NMR spectroscopy
1	10 mol% NEt_3	24 h	71:29
2[a]	10 mol% NEt_3	24 h	47:53
3	10 mol% DBN	1 h	0:100
4	1 mol% DBN	1 h	26:74
		20 h	14:86
5	1 mol% DBU	2 h	02:98
6	1 mol% TMG	2 h	03:97

Indeed, a conversion of 100% was achieved already after 1 h at room temperature with 10 mol% of DBN (Entry 3). It was therefore aimed to further decrease the catalyst loading to reduce the amount of waste formed. However, 1 mol% of DBN achieved a lower conversion of 86% after 20 h of reaction time (Entry 4). 1,8-Diazabicyclo[5.4.0]undec-7-ene (DBU) was a more active catalyst at 1% loading and achieved a conversion of 98% after 2 h (Entry 5). DBU was however undesired as catalyst for this reaction due to its expensiveness and more importantly its toxicity.[263] The cheaper and less toxic superbase 1,1,3,3-tetramethyl-guanidine (TMG) proved to be as effective as DBU with a conversion of 97% at 1% loading and was therefore chosen as more sustainable catalyst for all further reactions (Entry 6; ^{1}H NMR spectrum in chapter 6.5.1, Figure 6.17).[264-265] Purification of **CD1** was performed in a sustainable manner by distillation *in vacuo* to achieve a high yield of 93%. In ^{1}H NMR spectroscopy, characteristic signals of methyl ester and thioether moieties were observed at 3.68 ppm and 3.17 ppm, respectively (Figure 4.4, **top**). Two diastereomeric protons were detected at 2.61 ppm and 2.44 ppm due to the newly formed stereocenter, and protons of the 1,4-butanedithiol scaffold were detected at 2.54 ppm and 1.67 ppm. The structure of **CD1** was further confirmed by ^{13}C NMR spectroscopy, as characteristic signals of the quaternary ester carbon and the new thioether moiety were observed at 172 ppm and 36.3 ppm, respectively (chapter 6.5.2, Figure 6.19). The two other methyl crotonate dimers, **CD2** and **CD3**, were obtained with the same procedure and obtained in yields of 94% and 84%, respectively. **CD2** was purified by distillation *in vacuo*, while **CD3** had to be purified by flash column chromatography due to its very high boiling point.

With TMG as the optimal catalyst, the thia-Michael addition of 1,4-butanedithiol was employed to the mixture of *α*,*β*-unsaturated methyl laurate and methyl laurate. The reaction was conducted with 3 mol% of TMG to ensure full conversion and stirred for 16 h at 80 °C due to the reduced reactivity of the *α*,*β*-unsaturated methyl laurate compared to methyl crotonate.

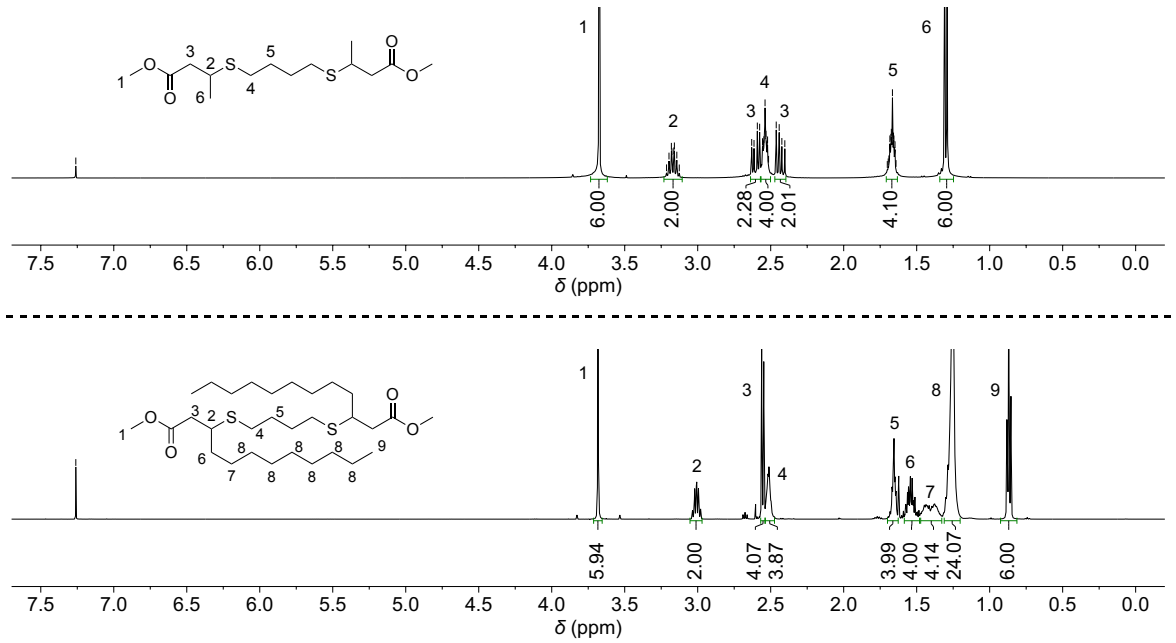

Figure 4.4: Stacked ^{1}H NMR spectra (in $CDCl_3$) of methyl crotonate dimer **CD1** (top) and methyl laurate dimer **LD1** (bottom).

Noteworthy, it was possible to recover the unreacted methyl laurate by distillation in a yield of 93%, which corresponds to 51% of the initially used amount of lauric acid in the dehydrogenation step, thus minimizing waste generation. The initial separation issue of *α*,*β*-unsaturated lauric acid and lauric acid was therefore no longer present after the double bond specific thia-Michael reaction had been performed, as reasoned before. Methyl laurate dimer **LD1** was isolated from the distillation residue by flash column chromatography in a yield of 75%, which corresponds to an overall yield of 27% over the three reactions. In ^{1}H NMR spectroscopy, all characteristic signals that were observed for **CD1** were detected as well for **LD1** (Figure 4.4, **bottom**). The diastereomeric protons however appeared as one doublet in contrast to the two separated signals that were observed for **CD1**. The successful isolation of **LD1** was further confirmed by ^{13}C NMR and IR spectroscopy and mass spectrometry (Experimental section chapter 6.5.3).

In summary, the reaction sequence of dehydrogenation, esterification and thia-Michael addition was performed successfully with 40 g of lauric acid. The product **LD1** was isolated in an overall yield of 27% and it was demonstrated that 51% of the unreacted lauric acid could be recovered as methyl laurate by distillation. The development of this reaction sequence ultimately allowed the preparation of three fatty acid-based dimethyl esters (**LD1**−**LD3**) for the synthesis of renewable polyesters (Scheme 4.2, **bottom**).

It should however be noted here that the samples of **LD1**−**LD3** that were actually used for polymerizations were synthesized *via* a different reaction pathway, since optimization of the dehydrogenation and the polymerizations themselves were conducted in parallel in the laboratory. Hence, *α*,*β*-unsaturated lauric acid was synthesized from decanal and malonic acid *via* a Knoevenagel-Doebner condensation.[266] Esterification with methanol and subsequent thia-Michael additions yielded **LD1**−**LD3** (Experimental section chapter 6.6). The analytic data of the final products derived from the two different synthesis routes are identical.

Renewable 1,12-dodecanediol was polymerized with methyl laurate-based dimers **LD1**−**LD3** to synthesize bio-based polyesters **LD-P1**−**LD-P3** (Scheme 4.2, **bottom**).[267] In addition, **CD1**−**CD3** were polymerized with 1,12-dodecanediol as well to synthesize analogous polymers which differ from the methyl laurate polymers only in the length of the side chain in the repeating unit (C_1 vs. C_9) (**CD-P1**−**CD-P3**). The influence of the long C_9 side chain on the thermal properties of the polymers was afterwards evaluated by comparing each **LD** polymer with its respective **CD** polymer analogue. All polymerizations were performed solvent-free with 5 mol% of titanium(IV)isopropoxide and applying a temperature/pressure gradient starting at 140 °C and 700 mbar and ending at 200 °C and 10 mbar to remove the condensation product methanol and to achieve full conversion. In size exclusion chromatography (SEC), high average molecular weights (M_n) ranging from 26.0 kDa−31.8 kDa and dispersities ($Đ$) from 1.75−1.85 were obtained for polymers **LD-P1**−**LD-P3** (Table 4.4). Polymerizations of **CD1**−**CD3** resulted in lower M_n values between 13.0 kDa−29.1 kDa and dispersities of 1.52−1.74. The general observation that polymers of the **CD** series resulted in lower molecular weights than the **LD** series is exemplarily depicted in Figure 4.5 for **CD-P1** and **LD-P1**.

Table 4.4: List of polyesters from methyl crotonate and methyl laurate based dimethyl esters (**CD1**−**CD3**, **LD1**−**LD3**) and 1,12-dodecanediol together with their average molar mass (M_n), dispersity ($Đ$), temperature of 5 weight% loss ($T_{d,5\%}$) and melting temperature (T_m).

Polymer	M_n (SEC) / kDa	$Đ$	M_n (NMR) / kDa	$T_{d,5\%}$ / °C	T_m / °C
CD-P1	20.6	1.52	26.3	306	10
LD-P1	31.8	1.75	27.4	332	−31 & 16
CD-P2	13.0	1.71	12.2	321	13
LD-P2	28.1	1.85	35.7	341	–
CD-P3	29.1	1.74	21.8	334	36
LD-P3	26.0	1.83	25.6	344	0 & 15

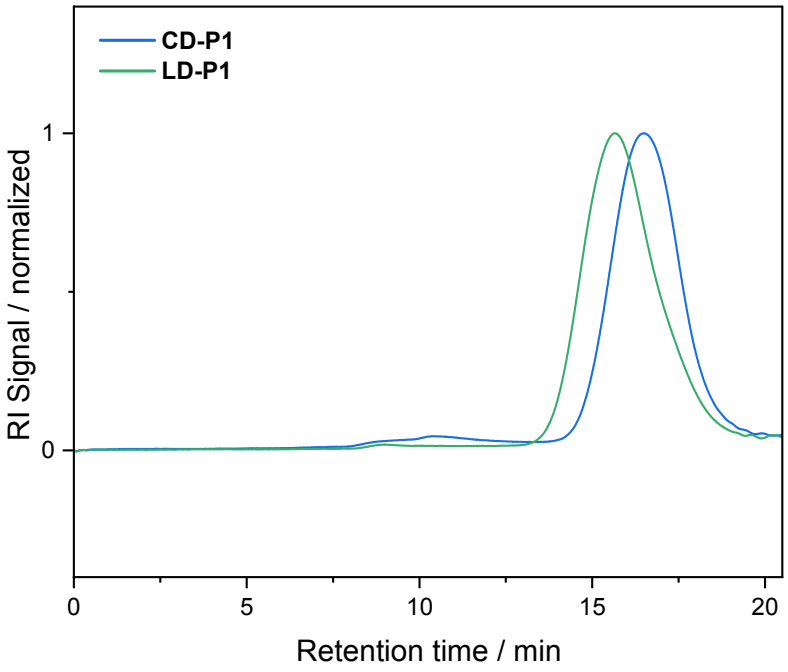

Figure 4.5: SEC (Poly THF) measurements of **CD-P1** and **LD-P1**.

The molecular weight of all polymers was furthermore estimated *via* ^{1}H NMR spectroscopy by integration of the end group signals of methyl esters and hydroxymethyl groups at 3.69 ppm and 3.63 ppm, respectively (Table 4.4, Experimental section chapter 6.7). The M_n values obtained by ^{1}H NMR spectroscopy deviated from the respective SEC results by 2%−25% and confirmed high molecular weight polycondensates. The results from ^{1}H NMR spectroscopy revealed that every **LD** polymer had a higher M_n than its respective **CD** polymer, which is reasonable due to the molecular weight difference of the starting materials.

The temperature of 5 weight% loss ($T_{d,5\%}$) determined by thermogravimetric analysis (TGA) increased incrementally from **LD-P1** with the short 1,4-butanedithiol linker (332 °C) to **LD-P3** with the longer 1,10-decanedithiol linker (345 °C). The same trend was observed for the methyl crotonate based polymers (from 306 °C to 336 °C), indicating that a higher relative content of methylene groups improved thermal stability. Moreover, it was noted that every **LD** polymer had an improved $T_{d,5\%}$ value (up to 20 °C higher) than the respective **CD** polymer (Table 4.4). This indicates that also the longer side chain had a positive influence on the thermal stability of the materials.

At last, differential scanning calorimetry (DSC) experiments were performed to evaluate the influence of the nonyl side chains on the thermal properties of the polymers (Table 4.4). Exemplarily, DSC measurements of **CD-P1** and **LD-P1** are depicted in Figure 4.6. For polymer **CD-P1**, a glass transition temperature (T_g) of −44 °C and a cold crystallization at −29 °C together with a melting point at 10 °C were observed. Cold crystallization and melting point were observed as well for polymer **LD-P1** at slightly higher temperatures of −11 °C and 16 °C, respectively. Moreover, one additional melting point was observed at −31 °C, which most like originates from crystallization of the nonyl side chains. The crystallization of side chains was reported in several studies for polymers with long aliphatic side chains.[172-174, 268] For instance, Beiner *et al*. observed a melting point at −26 °C for poly(*n*-lauryl methacrylate) with a C_{12} side chain, while no melting point was detected for (*n*-decyl methacrylate) with a C_{10} side chain. In another study by Meier *et al*., side chain crystallization was observed for a malonate derived polyester with a side chain length of 10 carbon atoms at −36 °C, which is similar to the herein observed melting point at −31 °C. The side chain crystallization effect was however not observed for the other two fatty acid-based polymers. A low T_g of −50 °C and no melting point at all were observed for **LD-P2,** while **CD-P2** had a T_g at −52 °C and a melting point at 13 °C (chapter 6.7.6, Figure 6.46). Interestingly, **CD-P3** exhibited a higher T_g and melting point of −30 °C and 36 °C, respectively (chapter 6.7.9, Figure 6.52). **LD-P3** exhibited a lower T_g of −40 °C and two melting points at 0 °C and 15 °C, respectively. It is thus possible to alter thermal transitions of these polymers by replacement of short side chains with longer ones.

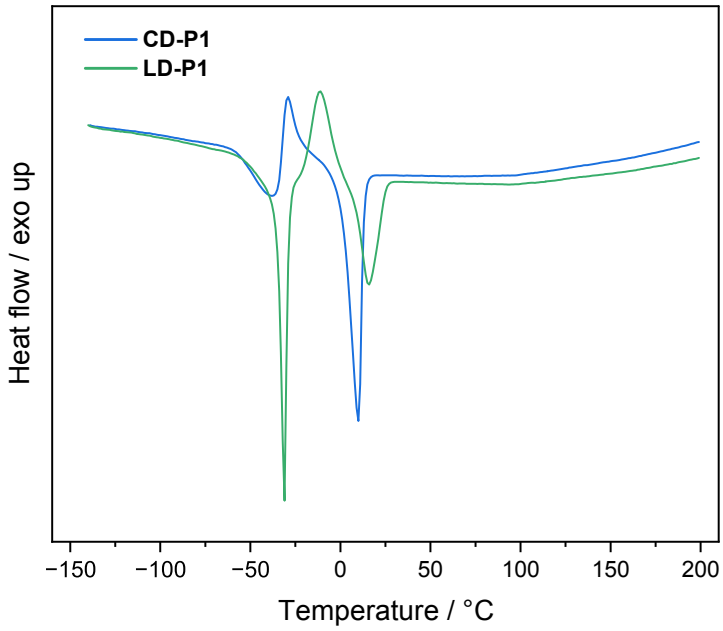

Figure 4.6: DSC measurements of **CD-P1** and **LD-P1** (second heating run).

Conclusion

In this project, a new three-step reaction sequence was developed for the synthesis of bio-based dimethyl esters and their polyesters starting from renewable saturated fatty acids. The sequence consists of a catalytic dehydrogenation with molecular oxygen as oxidant, an esterification with methanol, and a dimerization reaction with dithiols *via* thia-Michael addition. A recently established method for the catalytic dehydrogenation of carboxylic acids was thus utilized for the synthesis of *α*,*β*-unsaturated lauric acid.[187] The original procedure was first optimized considering sustainability aspects to exclude solvents, cocatalysts, and overstoichiometric amounts of inorganic bases, thereby reducing the amount of waste formed immensely. The dehydrogenation was performed on a 40 g scale to obtain a mixture consisting of 60% lauric acid and 40% *α*,*β*-unsaturated lauric acid, which was directly esterified in a second step with methanol and catalytic amounts of sulfuric acid to obtain a mixture of the respective methyl esters in quantitative yield. A subsequent thia-Michael addition with 1,4-butanedithiol allowed not only the synthesis of a new fatty acid-based dimethyl ester in a yield of 27% over all three reactions, but also the recovery of 51% of the initially used lauric acid in the dehydrogenation step as methyl laurate. The developed reaction sequence is thus quite sustainable, as waste generation is kept to a minimum. The sequence further allows the use of otherwise difficult to functionalize saturated fatty acids. The thia-Michael addition was moreover performed with 1,6-hexanedithiol and 1,10-decanedithiol to produce two more dimethyl esters with longer aliphatic linkers between both ester groups. At last, all dimethyl esters were polymerized with 1,12-dodecanediol to produce bio-based polyesters with high molecular weights ranging from 26.0 kDa−31.8 kDa. The influence of the long C_9 side chain on the thermal properties of the materials was evaluated by comparison of each polymer with its analogous methyl crotonate-based polymer bearing only a short methyl side chain. It was observed that the long side chain had a positive impact on the thermal stability of all polymers, as the temperature of 5 weight% loss increased by up to 20 °C compared to the polymers with methyl side chains. Generally, it was possible to alter thermal properties of these materials by incorporating longer side chains into the polymer repeating unit.

4.2 Ruthenium catalyzed oxidative cleavage of high oleic sunflower oil

This chapter is based on previously published results by the author of this thesis:

L. Santos Correa, M. A. R. Meier, "Ruthenium Catalyzed Oxidative Cleavage of High Oleic Sunflower Oil: Considerations Regarding the Synthesis of a Fully Biobased Triacid", *Eur. J. Lipid Sci. Technol.* **2023**, *125*, 2200171.[269]

Text, figures, and data are reproduced from this article and were partially edited and extended with permission from the European Journal of Lipid Science and Technology, copyright 2023.

Note: The oxidative cleavage of high oleic sunflower was already investigated by this author during his master thesis, in which the author successfully isolated the targeted tricarboxylic acid from high oleic sunflower oil by applying the optimized reaction conditions from Behr *et al*.[236, 270] The purification technique as well as the performed analytical measurements (i.e., IR and NMR spectroscopy, mass spectrometry) of the triacid belong to the master thesis and are presented for context reasons. All other results were generated during this PhD thesis.

Before reading this chapter, the reader is advised to read chapter 2.5.3 for a theoretic introduction to the ruthenium catalyzed oxidative cleavage of carbon-carbon double bonds.

Abstract

Tricarboxylic acids are molecules of interest for the synthesis of highly cross-linked polymers, for instance for the curing of epoxy resins. Herein, a synthesis route to a novel high oleic sunflower oil-based tricarboxylic acid is described by applying a ruthenium catalyzed oxidative cleavage of its double bonds. A statistical concept was devised for the prediction of the yields of mono-, di- and trifunctional derivatives that can be formed from high oleic sunflower oil, depending on the overall conversion of double bonds into carboxylic acids and the overall oleic acid content of the used oil. This concept proofed to be highly useful for the explanation of seemingly moderate triacid yields, which are inherently dependent on the unsaturated fatty acid content of the used oil. All obtained sunflower oil based polyacids were fully analyzed by IR spectroscopy, mass spectrometry, ^{1}H NMR, ^{13}C NMR and quantitative ^{31}P NMR spectroscopy. In addition, a more sustainable purification procedure was developed to obtain a polymerizable mixture of polyacids containing more than 2.0 carboxylic acids per molecule on average.

Theoretical Considerations

The aim of this investigation was the synthesis of glyceryl triazelate, a tricarboxylic acid, by applying a literature known ruthenium catalyzed oxidative cleavage of double bonds on high oleic sunflower oil (Scheme 4.3, see chapter 2.5.3 for theory). Before the discussion of actual synthesis results, considerations are reported to estimate the amount of triacid being formed from high oleic sunflower oil (**HOSO**). The first evaluation was conducted with the assumption that every double bond has an 80% probability (P) to be cleaved into carboxylic acids and a 20% probability for no reaction or, more realistically, to be transformed into possible side products (e.g., diol, acyloin, diketone).[236] Moreover, triolein was used as model substrate as it simplifies the calculation. A tree diagram is depicted in Figure 4.7 to illustrate these statistical considerations. Therefore, the expected yield of triacid equals 51.2%, which is the probability for an oxidative cleavage to the power of 3, since every oleic acid residue (out of three per molecule) has a respective probability of 80% to get cleaved (Equation (5)).

$$\text{Yield(Triacid)} = P(\text{cleavage})^3 = 0.8^3 = 0.512 = 51.2\% \quad (5)$$

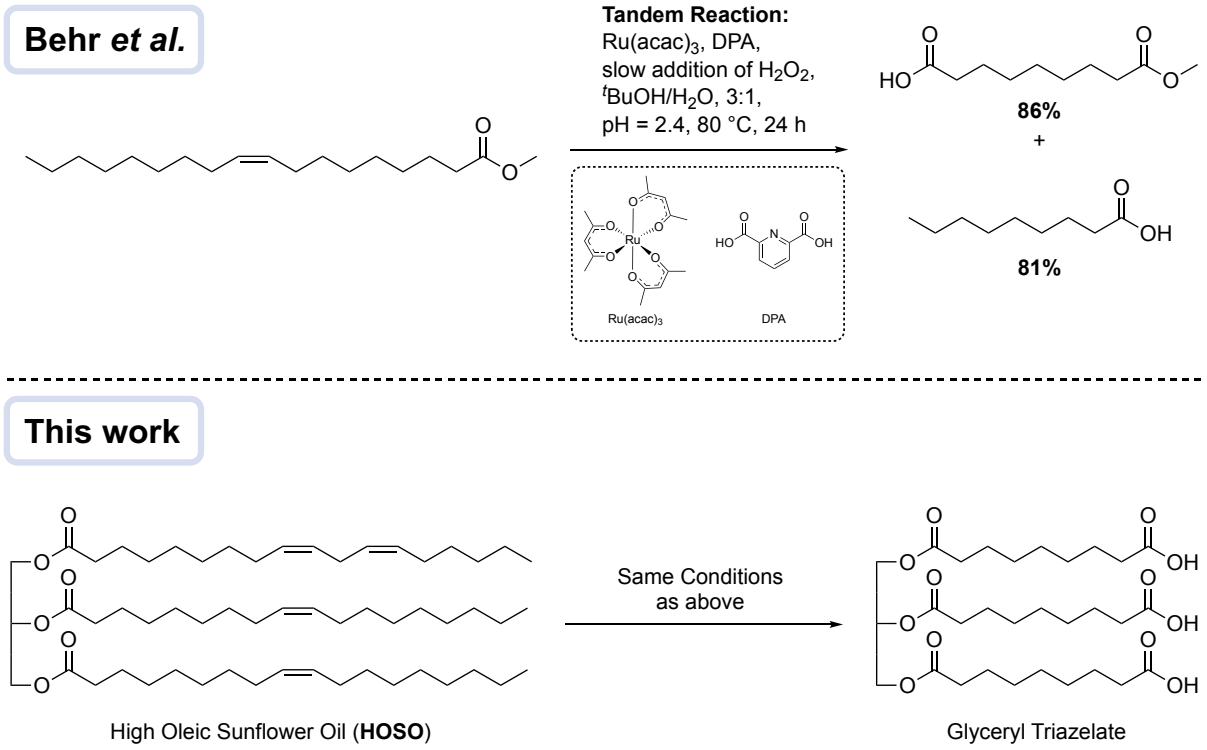

Scheme 4.3: Ruthenium catalyzed oxidative cleavage of methyl oleate by Behr *et al*. (top) and the ruthenium catalyzed oxidative cleavage of high oleic sunflower oil that was conducted within this thesis (bottom).[236, 269]

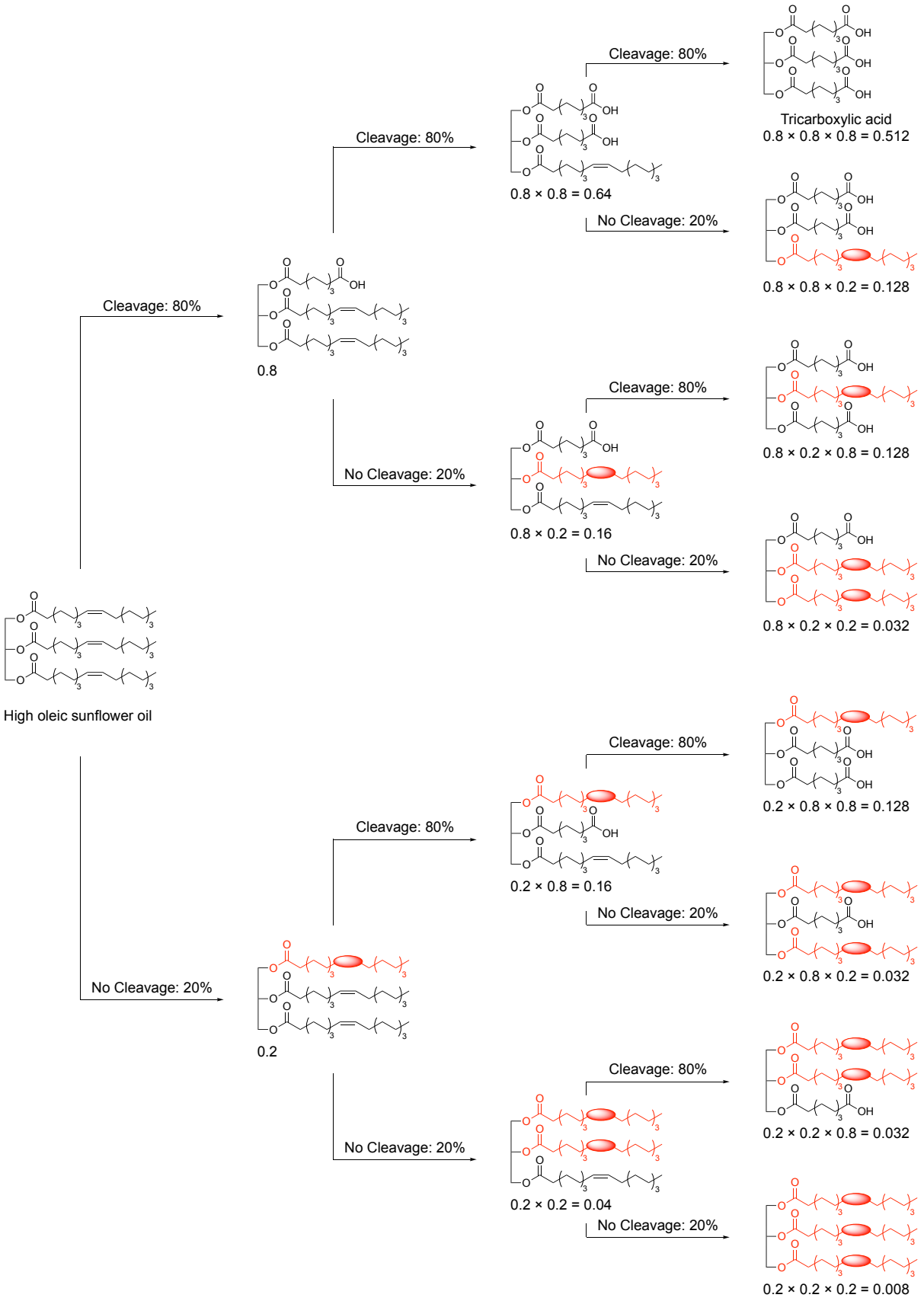

Figure 4.7: Tree diagram of the oxidative cleavage of triolein. The possible product acids are calculated with a probability of 80% for an oxidative cleavage and a probability of 20% for a side reaction or no reaction. The red spheres depict an uncleaved chain bearing any functional groups (e.g., diol, acyloin, diketone).

This calculation points out why only oxidative cleavages that generally result in yields higher than 80% for a monofunctionalized molecule should be used. Furthermore, it is also possible to calculate the amount of monoacid, diacid and side products being formed, using the tree diagram depicted in Figure 4.7. Multiplication of the number of permutations of the respective product (e.g., 3 permutations for a diacid) with the probability of one permutation being formed results in the overall expected yield. It should be noted that the number of permutations of each individual acid can be obtained from the tree diagram or alternatively be calculated with binomial coefficients (Experimental section chapter 6.9, Equations (14) to (17)). The probability of one permutation being formed is a product of P(cleavage) to the power of acid moieties and P(no cleavage) to the power of no acid moieties. An example calculation is given for the yield of diacid with an overall conversion of double bonds into carboxylic acids (**CDBCA**) of 80% (Equation (6)).

$$\begin{aligned} \text{Yield(Diacid)} &= \text{permutations} \times \text{probability(2 cleavages)} \\ &= 3 \times P(\text{cleavage})^2 \times P(\text{no cleavage}) \\ &= 3 \times 0.8^2 \times 0.2 = 0.384 = 38.4\% \end{aligned} \qquad (6)$$

For each possible product (monoacid, diacid, triacid, unreacted starting material (or side products bearing no carboxylic acid)), a function of the reaction yield was devised with x being the **CDBCA** having values between 0 and 1:

$$\begin{aligned} f(x;\ \text{Triolein, 0 cleavages}) &= (1-x)^3 \\ f(x;\ \text{Triolein, 1 cleavage}) &= 3 \times x^1 \times (1-x)^2 \\ f(x;\ \text{Triolein; 2 cleavages}) &= 3 \times x^2 \times (1-x)^1 \\ f(x;\ \text{Triolein, 3 cleavages}) &= x^3 \end{aligned}$$

The devised functions are plotted in Figure 4.8. High amounts of diacid only form if a **CDBCA** higher than 0.6 is achieved. For a high amount of triacid, a **CDBCA** higher than 0.8 is needed. It should be noted that this statistical approach is only viable with some assumptions, the first one being that every double bond in every intermediate has the same reactivity and the second one being that the catalyst and all reagents show the same reactivity and selectivity to every double bond in every intermediate.

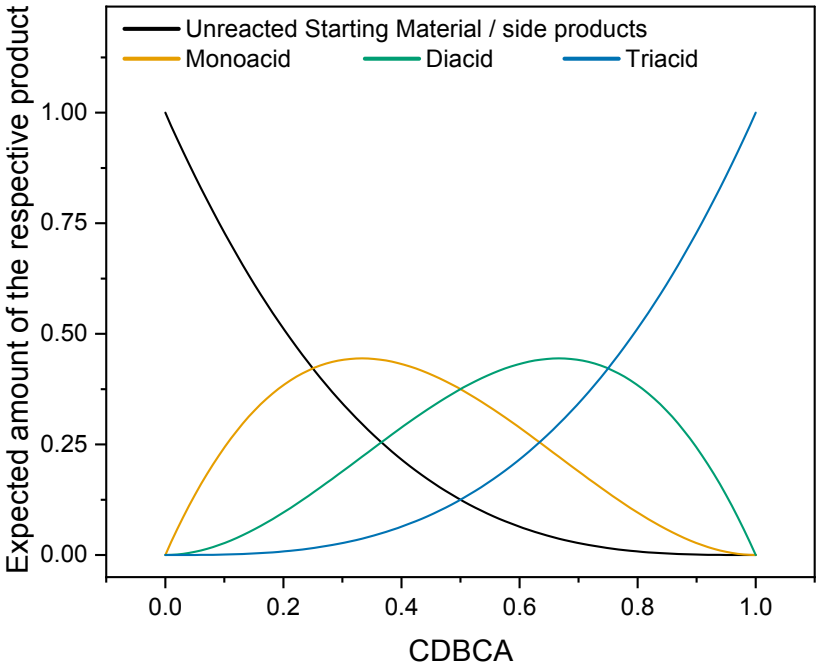

Figure 4.8: Statistical product distribution for the oxidative cleavage of triolein; **CDBCA**: Conversion of double bonds into carboxylic acid.

Hence, all molecules should react according to the statical distribution depicted in Figure 4.8. Practically, another issue has to be considered, since no pure triolein is used, but **HOSO**. It was assumed that the above used statistical approach can also be used for the calculation of the distribution of fatty acid residues in triglycerides. As a simplification, it was assumed that the glyceride molecule either contains an oleic acid residue or a saturated fatty acid. The resulting functions are hence analogues to the ones devised for the oxidative cleavage of triolein (distribution of two objects on three places). For each possible triglyceride (3 saturated fatty acids, 1 oleic acid, 2 oleic acids, or 3 oleic acids (triolein)), a function of the amount of the respective molecule within the mixture of triglycerides was devised with y as the overall oleic acid content of the used oil having values between 0 and 1:

f(y; 0 oleic acids) $= (1-y)^3$
f(y; 1 oleic acid) $= 3 \times y^1 \times (1-y)^2$
f(y; 2 oleic acids) $= 3 \times y^2 \times (1-y)^1$
f(y; 3 oleic acids) $= y^3$

Assuming an oleic acid content of 90%, this results in a distribution of 0.1% triglycerides bearing no oleic acid, 2.7% bearing one oleic acid, 16.2% bearing two oleic acids and 72.9% triolein. Again, it should be noted that this calculation is purely statistical and does not consider realistically observed triglyceride compositions.[271] Nevertheless, these simplified considerations are important to understand the synthetic challenge of preparing a tricarboxylic acid from **HOSO**. By connection of these two functions, it is possible to calculate the amount of a certain type of acid (e.g., monoacid) being formed depending on the overall **CDBCA** (x) and the overall oleic acid content of the used oil (y). The simplest of these equations is the one for the desired triacid (Equation (7)).

$$\begin{aligned} f(x,y;\ 3\ \text{cleavages}) &= f(y,\ 3\ \text{oleic acids}) \times f(x,\ \text{Triolein},\ 3\ \text{cleavages}) \\ &= y^3 \times x^3 \end{aligned} \tag{7}$$

Hence, the above calculated yield of 51% triacid diminishes to 37% if an oleic acid content of 90% is assumed. It was therefore desired to use a high oleic acid sunflower oil with at least 85% oleic acid content. The derivation of all other functions f(x,y) for side products, i.e. mono acids and diacids being formed, is described in the Experimental section chapter 6.9.2. 3D plots of the functions for the calculated amount of monoacid, diacid and triacid are depicted in Figure 4.9. The chronological formation of the respective intermediates is clearly visible, with the amount of monoacid and diacid being formed first and then being consumed towards the desired triacid. The exponential dependency of triacid formation is also observable. Table 4.5 shows some calculated distributions for an oil with 80%, 90% and 100% oleic acid content and different **CDBCA**.

Table 4.5: Calculated distribution of products of the oxidative cleavage of high oleic sunflower oil using a statistical approach with x as the overall conversion of double bonds into carboxylic acids (CDBCA) and y as the oleic acid content of the used oil. The derivation of the functions f(x,y) is listed in chapter 6.9.

Entry	Oleic Acid content (y)	CDBCA (x)	Unreacted starting material or side products / %	Monoacid / %	Diacid / %	Triacid / %	Sum / %	Carboxylic acids per molecule
1	0.8	0.7	8.52	32.52	41.40	17.56	100	1.680
2	0.8	0.8	4.67	24.88	44.24	26.21	100	1.920
3	0.8	0.83	3.69	22.17	44.44	29.70	100	2.002
4	0.8	0.9	2.20	16.93	43.55	37.32	100	2.160
5	0.8	1.0	0.80	9.60	38.40	51.20	100	2.400
6	0.9	0.7	5.07	25.87	44.06	25.00	100	1.890
7	0.9	0.74	3.70	22.20	44.44	29.66	100	2.001
8	0.9	0.8	2.20	16.93	43.55	37.32	100	2.160
9	0.9	0.9	0.69	8.77	37.40	53.14	100	2.430
10	0.9	1.0	0.10	2.70	24.30	72.90	100	2.700
11	1.0	0.8	0.80	9.60	38.40	51.20	100	2.400
12	1.0	0.9	0.10	2.70	24.30	72.90	100	2.700
13	1.0	1.0	–	–	–	100.00	100	3.000

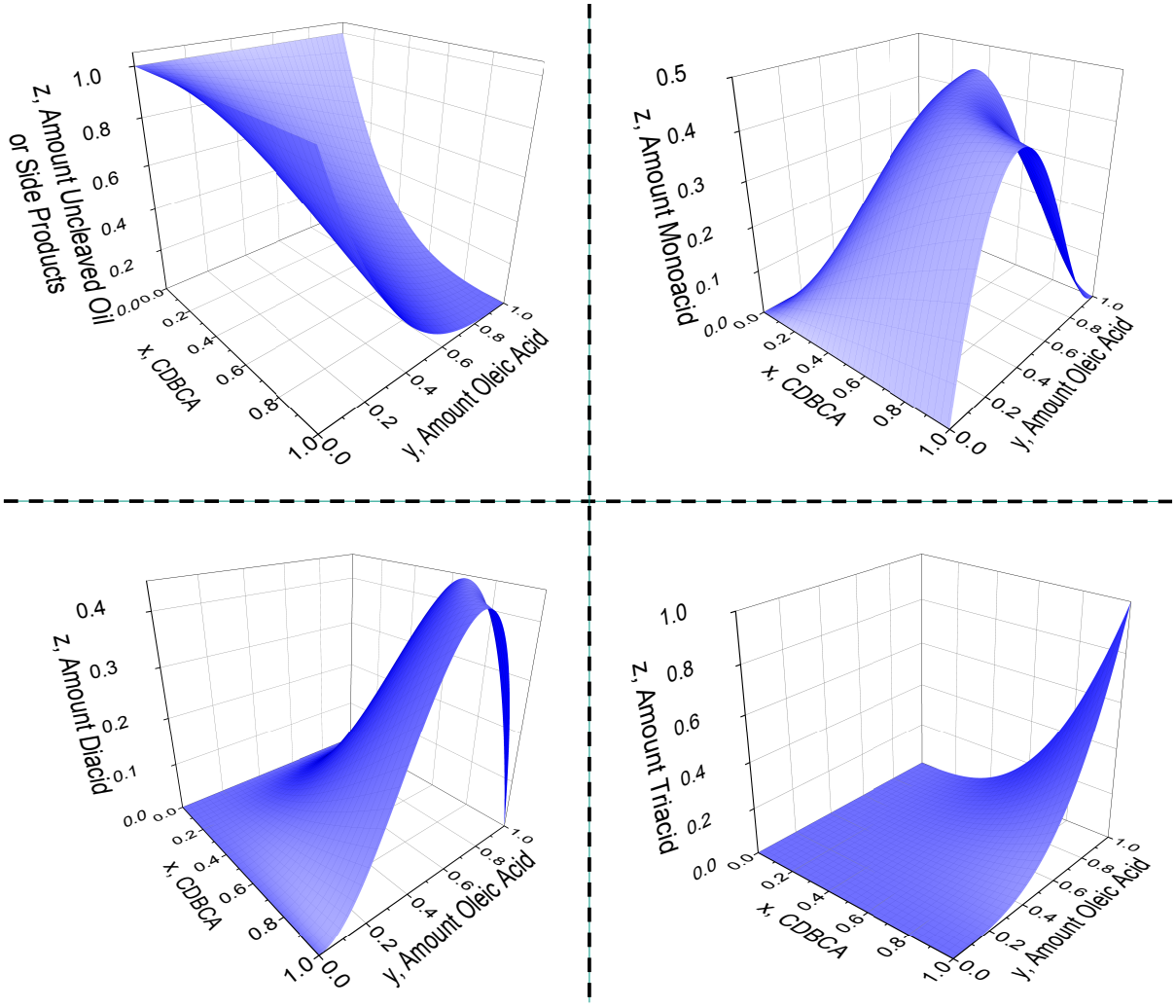

Figure 4.9: 3D plots of the statistically calculated product distribution of the oxidative cleavage of high oleic sunflower oil with x as the overall conversion of double bonds into carboxylic acids (CDBCA) and y as the amount of oleic acid inside the used oil. **Top, Left:** amount uncleaved oil; **Top, Right:** amount monoacid; **Bottom, Left:** amount diacid; **Bottom, Right:** amount triacid.

The calculated results show that a high amount of triacid can only be obtained with a high amount of oleic acid and a reaction yield above 80% due to the exponential dependency on both variables (Table 4.5, Entries 5, 9-13). Hence, going from 80% oleic acid content to 100% oleic acid content with a **CDBCA** of 100% the triacid yield increases from 51% to 100% (Entries 5, 10, 13). The same dependency is visible for 100% oleic acid content with a **CDBCA** from 80% to 100% (Entries 11-13). These calculations show that the last 20 percentage points are crucial for an increase of 49% triacid yield. Having this in mind it was sought to use an oil containing 90% oleic acid and using an oxidative cleavage that generally results in yields higher than 80% for monofunctionalized molecules to isolate triacid in a reasonable yield of at least 37% (Entry 8). However, it will not be possible to isolate more than 73% triacid if an oil containing 90% oleic acid is used and the reaction is optimized to 100%

yield, considering this simple model. For that reason, another approach concerned the isolation of all formed acids as one mixture and using it as received. Therefore, the average number of carboxylic acids per molecule must surpass the margin of 2.0 to be polymerizable. Looking at the calculated average number of carboxylic acids per molecule, the yield needs to be higher than 74% if an oil with an oleic acid content of 90% is used (Entry 7). Pursuing the principles of Green Chemistry, this approach is the most sustainable one, since all products are used as received without tedious separation of mono-, di- and triacid. However, glyceryl triazelate is considered as a highly valuable compound depending on the nature of the application. Hence, both approaches were considered to be useful for the synthesis of new sunflower oil-based polyacids.

Synthetic Results

The theoretical considerations discussed above suggest the use of an oil containing the largest amount of oleic acid possible for the aimed synthesis of a triacid. Hence, four different high oleic sunflower oils were bought at local supermarkets and a transesterification with methanol under acid catalysis was performed, according to an already reported literature procedure.[272] The formed methyl esters were then quantified *via* GC-MS (see Experimental section chapter 6.8 for all data and chromatograms). The resulting fatty acid composition of all oils is listed in Table 6.8. High oleic sunflower oil 04 (**HOSO04**) was chosen as substrate for the oxidative cleavage investigations as it contained the highest amount of oleic acid (88.7%). After choosing the oil with the appropriate amount of oleic acid, the ruthenium catalyzed oxidative cleavage was optimized for **HOSO04** to achieve the highest yield possible (see Scheme 4.3 for reaction equation). First, the optimized conditions for methyl oleate reported by Behr *et al*. were applied, of course adjusting catalyst and ligand loading to the amount of double bonds.[236] The molar concentration of **HOSO04** was reduced by a factor of three to guarantee the same concentration of double bonds, catalyst and ligand as previously reported. All other reaction conditions and the equivalents of hydrogen peroxide per double bond were kept the same. During the first hours of the reaction, it was noticed that the solution is slightly heterogenous with small oil droplets floating around the mixture. However, over the course of the reaction, the reaction mixture transformed from a red emulsion into a yellow, homogeneous liquid phase. After stopping the reaction and extracting the products, all characteristic signals of carboxylic acid moieties and glyceryl ester moieties were visible in ^{1}H NMR spectroscopy (Figure 4.10).

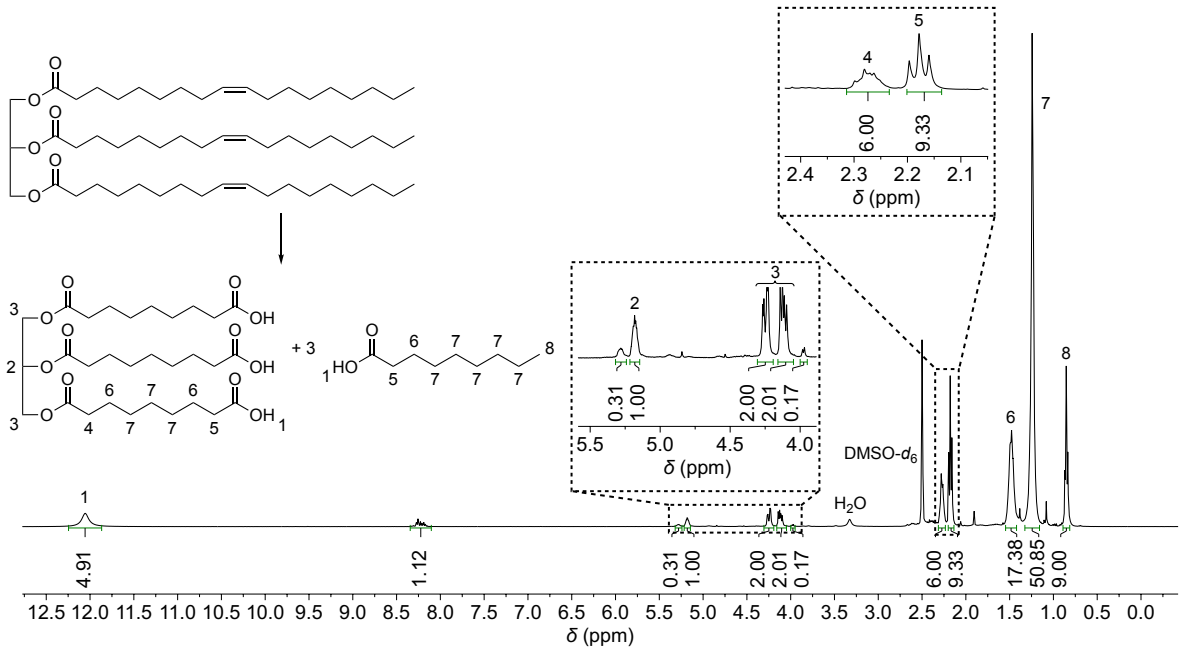

Figure 4.10: ^{1}H NMR spectrum (in DMSO-d_6) of the ruthenium catalyzed oxidative cleavage of high oleic sunflower oil (simplified by triolein in the figure) after extraction.

The small signals at 5.29 ppm and 3.98 ppm indicate unreacted double bonds and probably alcohol groups of not fully oxidized intermediates (e.g., diol, acyloin, see also ESI-MS data in Experimental section chapter 6.10.1). For one double bond cleavage, two carboxylic acids form (reaction equation in Figure 4.10). Hence, for a yield of 100%, the integral of carboxylic acid protons should be the same as the initially present number of vinylic protons of the used oil and the characteristic signal of the *α*-CH_2 protons of carboxylic acids (2.18 ppm) should duplicate. The number of initially present vinylic protons per triglyceride was calculated from the oil composition determined *via* GC-MS and resulted in 5.81 vinylic protons per triglyceride (Experimental section chapter 6.10, Equation (18)). Conversion of double bonds into carboxylic acids, i.e. a yield estimated by ^{1}H NMR spectroscopy, can thus be calculated with Equation (8) by division of the integral of *α*-CH_2 protons of carboxylic acids (for this reaction: 9.33) by 2 and the calculated number of vinylic protons inside the oil, after normalizing the spectrum relative to the signal of the glyceryl moiety. An NMR-Yield of 80.3% for the above-mentioned test reaction was thus observed.

$$\text{NMR-Yield} = \frac{\text{integral}\ (\alpha\text{-}CO_2H)}{2 \times 5.81} \times 100 \qquad (8)$$

Integration of the characteristic signal of α-CH_2 protons of ester functionalities (2.28 ppm) results in exactly six protons representing three ester moieties. The oxidative cleavage is therefore applicable to high oleic sunflower oil without concurring hydrolysis of the glyceryl ester functionalities of the oil, despite the acidic pH of 2.4. It should be noted that in the original publication of Behr *et al*. one test reaction with a high oleic sunflower oil of unknown fatty acid composition was performed. A yield of 82% nonanoic acid methyl ester and 79% azelaic acid dimethyl ester was determined by GC after transesterification of the glyceryl moieties with methanol.[236] Despite the test reaction having a surprisingly high yield of 80%, it was attempted to improve the reaction yield further to increase the statistically possible yield of triacid and additionally increase the sustainability of the used procedure, for instance by reducing amount of catalyst and ligand needed. Therefore, varying amounts of catalyst were screened by keeping all other reaction parameters constant (Table 4.6, Entries 1−5). The ^{1}H NMR data suggested a maximum yield of 84.8% at 2 mol% catalyst loading (Entry 2). Afterwards, the ligand (pyridine-2,6-dicarboxylic acid) concentration was optimized by using the same procedure with 2 mol% catalyst and varying amounts of ligand (Entries 6−12). At 40 mol% of ligand loading, the reaction reaches a maximum of 85.9% NMR-Yield (Entry 10). Loadings higher or lower than 40% resulted in lower yields, which is probably due to the ligand being a carboxylic acid and therefore influencing the pH value of the reaction mixture. Behr *et al*. reported that the epoxide intermediate is hydrolyzed more efficiently, if the pH value stays at 2.4 and that almost no conversion was observable if the pH increased above 4.0.[236] The overall CDBCA could therefore be improved by 5.6% from 80.3% up to 85.9%. Further yield improvements failed.

Table 4.6: Optimization of the ruthenium catalyzed oxidative cleavage of high oleic sunflower oil. Reaction conditions: **HOSO04** (4.43 g, 5.00 mmol), $Ru(acac)_3$ (variable amount) and pyridine-2,6-dicarboxylic acid (variable amount), ^{t}BuOH (45 ml), H_2O (15 ml), H_2O_2 (24 equiv. = 8 equiv. per double bond), 80 °C, 24 h.

Entry	Catalyst / mol%	Ligand / mol%	NMR-Yield / %
1	1.00	60.0	74.5
2	**2.00**	**60.0**	**84.8**
3	3.00	60.0	80.3
4	4.00	60.0	82.5
5	6.00	60.0	80.9
6	2.00	10.0	57.7
7	2.00	15.0	77.0
8	2.00	20.0	79.5
9	2.00	30.0	83.5
10	**2.00**	**40.0**	**85.9**
11	2.00	50.0	85.7
12	2.00	70.0	83.1

Confirming initial results of Behr *et al*., the reaction resulted in worse NMR-Yields at lower temperatures (62.6% at 70°C and 46.7% at 60°C).[236] Hydrolysis of the intermediate epoxide as well as the oxidative cleavage of the formed diol are preferred at higher temperatures. Reaction times longer than 24 h were not investigated, since earlier results investigating methyl oleate indicated that the reaction is finished after at least 12 h.

After this optimization, different purification procedures, for either separation and isolation of all reaction products (i.e., nonanoic acid, sunflower oil-based monoacid, diacid and triacid) or separation of nonanoic acid from a mixture of all sunflower oil-based acids, were investigated. After extraction and removal of solvent, a heterogeneous mixture of reaction products and pyridine-2,6-dicarboxylic acid (DPA) as solid impurity was obtained. Although several filtration attempts were performed, it was not possible to remove 100% of DPA since it appears to be soluble inside the products to a certain extent. A flash column chromatography of the extracted product was thus performed to separate all compounds. Three fractions were isolated using this approach. The first one being nonanoic acid and the second and third fraction being sunflower oil-based polyacids with a different content of diacids and triacid. Representative structures of glyceryl triazelate and a diacid bearing one stearic acid residue and the ^{1}H NMR spectra of fractions 2 and 3 are depicted in Figure 4.11. The integrals of fraction 3 suit the triacid structure (Figure 4.11, **bottom**). However, it seems that there are alcohol groups inside the product (doublet at 3.98 ppm), which may be formed due to side reactions leading to alcohol moieties, which do not oxidize further.

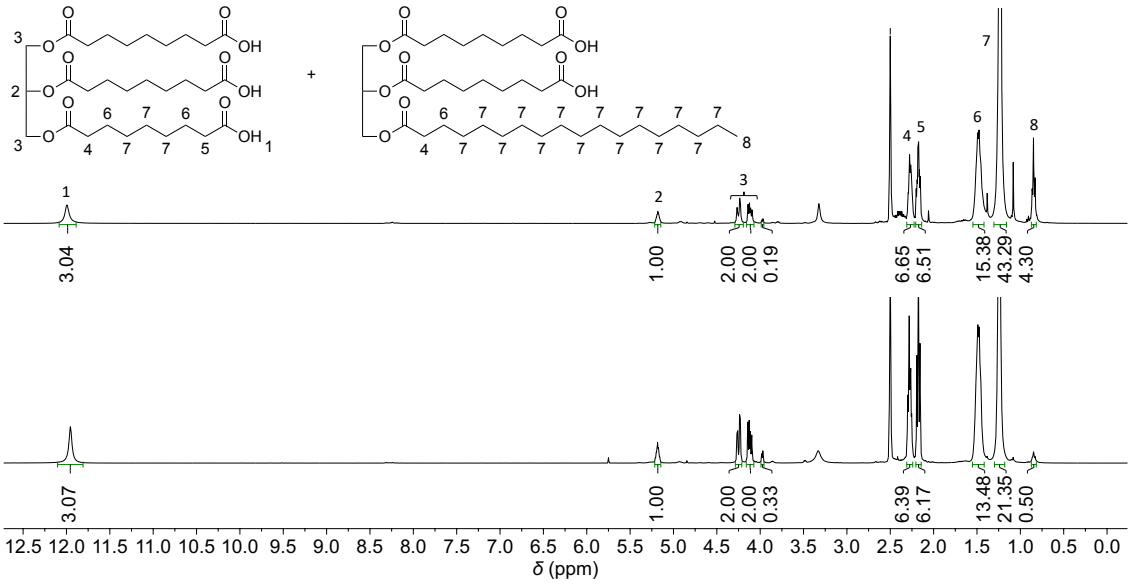

Figure 4.11: Stacked ^{1}H NMR spectra of fraction 2 (top) and fraction 3 (bottom) obtained by flash column chromatography from the oxidative cleavage of high oleic sunflower oil.

Additionally, there is an impurity of about 14.3% of diacid visible due to the methyl group integral of 0.5 at 0.85 ppm. This calculation is however only accurate if there are no other molecules containing methyl groups in this fraction. Although several flash column attempts were performed, it was not possible to obtain a product of higher purity. A purity of 85.7% corresponds to an isolated triacid yield of 40.5%, if the yield is compared to the molar amount of **HOSO** that was used. However, if the statistical considerations are taken into account, the yield of triacid corresponds to an estimated yield between 88.6% and 100%. An estimated range of yields was calculated since it is not known how reactive linoleic and linolenic acid are compared to oleic acid. All yield calculations are explained and listed in chapter 6.10.1.1 of the Experimental section. The average number of carboxylic acids per molecule was calculated from the residual CH_3 group integral of the ^{1}H NMR spectrum after normalizing the spectrum relative to the glyceryl moiety (Equation (9)).

$$\mathrm{CO_2H\ per\ molecule} = 3 - \frac{\mathrm{Integral\ (CH_3)}}{3} \tag{9}$$

Hence, fraction 3 of the flash column contains an average of 2.83 carboxylic acids per molecule and represents therefore a new sunflower oil-based polyacid for the synthesis of cross-linked thermosets. In ESI-MS measurements, molecular signals of the deprotonated tricarboxylic acid and dicarboxylic acids with one partially oxidized oleic acid residue (e.g., diol, acyloin) were detected (Experimental section chapter 6.10.1), thus confirming that the polyacid consists of a mixture of trifunctional and difunctional carboxylic acids. Fraction 2 showed an average carboxylic acid number of 1.57 and therefore presumably contains a large share of monoacids (Figure 4.11, **top**).

After the successful isolation of an almost pure triacid, it was targeted to isolate all formed sunflower oil-based carboxylic acids formed during the reaction as one mixture. This mixture should then have more than two carboxylic acids per molecule on average to be polymerizable. The minimum yield required for this condition was calculated to be 75.2%. Hence, the same optimized reaction conditions (NMR-Yield of first work-up: 83.1%) were applied again and after extraction, the crude product was purified by a filter flash column (5 cm height) to remove pyridine-2,6-dicarboxylic acid. The cleavage products (mainly nonanoic acid) were then removed *via* vacuum distillation in a Kugelrohr oven to obtain the mixture of sunflower oil-based carboxylic acids as residue. The average number of carboxylic acids per molecule was determined *via* ^{1}H NMR spectroscopy to be 2.11 (Equation (9)).

Hence, it was possible to isolate a polymerizable mixture of sunflower oil-based carboxylic acids by applying the same conditions. To further improve the sustainability of this reaction, one might imagine omitting column chromatography completely to reduce waste generation. However, as already stated above, the crude extract turns out to be a heterogeneous mixture after removal of solvent due to pyridine-2,6-dicarboxylic acid (DPA). It was considered that a certain amount of DPA may be soluble in the formed sunflower oil-based acids. Hence, the reaction were performed multiple times with varying amounts of DPA to find the conditions that deliver the highest yield possible and simultaneously delivering a homogenous extract in which the amount of DPA dissolves (Table 4.6, Entries 6−12). An amount of 15 mol% DPA resulted in an NMR-Yield of 77.0% and a homogenous extract (Entry 7). Reducing the amount of DPA to 10 mol% resulted in an NMR-Yield of 57.7% (Entry 6). Hence, 15 mol% DPA were used to try the last purification method. The crude extract was then purified by removal of the cleavage products *via* vacuum distillation in a Kugelrohr oven to obtain a mixture of sunflower polyacids and DPA in a yield of 97.7% (excluding DPA) with an average number of carboxylic acids per oil molecule of 2.09 (Table 4.7, sample 4). As DPA bears two carboxylic acid moieties, it is certainly polymerizable but would of course influence polymer properties. Besides the characterization of the isolated samples *via* NMR spectroscopy, it was possible to observe the deprotonated molecule signals of several sunflower oil based polyacids *via* ESI-MS. Hence, for all samples the deprotonated molecule signal of glyceryl triazelate was observed. Furthermore, for samples 1, 3 and 4, signals for diacids bearing either one palmitic acid, one stearic acid or one arachidic acid residue were observed, emphasizing the natural composition of the oil. Two carbonyl vibrations at 1700 cm^{-1} were visible in IR spectroscopy for each sample, one corresponding to ester moieties and the other one to carboxylic acid moieties. For each sample, the amount of carboxylic acids and hydroxyl groups per mg of sample was determined *via* ^{31}P NMR spectroscopy analogous to a procedure reported by Kilpeläinen *et al*.[273]

Table 4.7: Isolated yields, carboxylic acids per molecule (*via* ^{1}H NMR), carboxylic acid value and OH value (*via* ^{31}P NMR) of the four polyacid samples. The given error is the standard deviation from three measurements.

Polyacid sample	Purification	Yield nonanoic acid	Yield polyacid / %	Integral (CH_3)	Carboxylic acids per molecule (^{1}H NMR)	µmol CO_2H per mg of sample (^{31}P NMR)	µmol OH per mg of sample (^{31}P NMR)
1	Flash Column	80.8	34.8	4.30	1.57	3.342±0.039	0.237±0.026
2	Flash Column		43.8	0.50	2.83	4.621±0.023	0.303±0.034
3	Filter Column, Distillation	75.1	82.3	2.67	2.11	3.731±0.052	0.166±0.025
4	Distillation	72.4	97.7	2.73	2.09	3.592±0.035	0.516±0.032

This method uses 2-chloro-4,4,5,5-tetramethyl-1,3,2-dioxaphospholane (2-Cl-TMDP) as phosphitylation agent to transform carboxylic acid moieties and hydroxyl groups into the corresponding phosphite derivatives which can be detected by ^{31}P NMR spectroscopy. Quantification is then realized by addition of the internal standard endo-*N*-Hydroxy-5-norbornene-2,3-dicarboximide. The results show an increase of carboxylic acids per mg of sample for higher functionalized samples (increasing from sample 1 to 4 to 3 to 2, see Table 4.7) due to the rising number of carboxylic acids and the concurrent decrease of molecular weight during cleavage. It is however not possible to determine an average number of carboxylic acids per molecule from these experiments, since the samples consist of molecular mixtures rather than pure molecules. Furthermore, it should be noted that hydroxyl groups were visible in the ^{31}P NMR and quantified. These hydroxyl groups were thought to originate from side products (e.g., diol, acyloin) and were also visible in ^{1}H NMR spectra (see above). The characterization of sunflower polyacid samples 3 and 4 resulted in very similar parameters. Since sample 4 was purified and isolated *via* a considerably more sustainable procedure, producing less waste, the preparation and usage of this sample should be favored for proceeding research. However, it should be noted that the color of sample 4 differs from the other samples (Experimental section chapter 6.10, Figure 6.76 for picture), which can be considered disadvantageous depending on the desired application.

Conclusion

A literature known ruthenium catalyzed oxidative cleavage of alkenes using hydrogen peroxide as oxidant was optimized for the synthesis of a novel polyacid, bearing 2.83 carboxylic acids per molecule on average, from high oleic sunflower oil. The novel triacid was fully characterized by NMR spectroscopy, IR spectroscopy and mass spectrometry. Moreover, quantitative ^{31}P NMR spectroscopy was conducted to determine the exact amount of carboxylic acid per mg of sample. A simple statistical concept was devised to explain seemingly low yields, which are inherently dependent on the unsaturated fatty acid content of the used oil. Hence, such transformations for the isolation of trifunctinalized molecules from sunflower oil are only feasible with a high content of unsaturated fatty acids. The procedure was furthermore used to obtain mixtures of polyacids containing more than 2.0 carboxylic acids per molecule on average in a sustainable manner. The synthesized samples open access to new sunflower oil-based polymer chemistry, for instance for epoxy resin curing or the direct synthesis of new polymers *via* multicomponent reactions.

4.3 Sunflower oil-based thermosets *via* the Passerini three-component reaction

This chapter is based on previously published results by the author of this thesis:

L. Santos Correa, S. Leidenheimer, M. A. R. Meier, “Sunflower oil-based thermosets *via* the Passerini three-component reaction”, *Polym. Chem.* **2025**, *16*, 821-832.

The author of this thesis developed the synthetic procedure, planned, evaluated and performed the experiments, and wrote the original draft of the publication. S. Leidenheimer synthesized isocyanides and two model compounds under supervision of this author.

Note: Before reading this chapter, the reader is advised to read chapter 2.5.3 and chapter 2.5.4 for a theoretic introduction to the ruthenium catalyzed oxidative cleavage of carbon-carbon double bonds and the Passerini three-component reaction, respectively.

Abstract

Tricarboxylic acids are molecules of interest for the synthesis of cross-linked polymers. Herein, a recently established route to a tricarboxylic acid from high oleic sunflower oil was utilized to synthesize cross-linked polymers *via* the Passerini three-component reaction. Ten different polymers were synthesized by variation of the diisocyanide and monoaldehyde components and subsequently characterized *via* infrared spectroscopy, swelling tests, thermogravimetric analysis, differential scanning calorimetry, and tensile tests. The characterization of the insoluble polymeric networks was complemented by the synthesis of model compounds to enable analysis in solution *via* nuclear magnetic resonance spectroscopy. Due to the fast curing of all polymers at room temperature, adhesive tests were performed to demonstrate their potential application as glues. At last, one Passerini polymer was chemically recycled by transesterification with methanol and catalytic amounts of sulfuric acid to establish a proof of concept of the circularity of these materials. Azelaic acid dimethyl ester, an industrially relevant compound used for the synthesis of polyamides, and a difunctional *α*-hydroxyamide were recycled in yields of 75%. Repolymerization of the *α*-hydroxyamide to a polyurethane was performed to demonstrate a potential second life cycle of these compounds.

Results and discussion

A literature known ruthenium catalyzed oxidative cleavage was used to synthesize the tricarboxylic acid glyceryl triazelate from high oleic sunflower oil (Scheme 4.4).[236] The catalytic reaction was first reported by Behr *et al*. in 2013 for the oxidative cleavage of methyl oleate and was further optimized for the oxidative cleavage of high oleic sunflower oil within this thesis (chapter 4.2).[269] Key features are the use of hydrogen peroxide as greener oxidant, use of the benign solvents *tert*-butanol and water, and the tolerance towards ester groups as they remain uncleaved during this transformation. The successful isolation of the sunflower oil-based tricarboxylic acid was confirmed by ^{1}H NMR, ^{13}C NMR, and IR spectroscopy as well as mass spectrometry (Experimental section chapter 6.10.3: “sunflower polyacid sample 5”). In the ^{1}H NMR spectrum, a minor methyl proton integral is visible at 0.85 ppm (chapter 6.10.3, Figure 6.83). It was assumed that this signal corresponds to the formation of dicarboxylic acids due to the presence of saturated fatty acid residues in the used sunflower oil, which are inert to the performed reaction. This is reasonable, since the used sunflower oil contained 7% saturated palmitic acid and stearic acid. The small integral of 0.17 corresponds to approximately 5% dicarboxylic acids. Hence, the isolated compound is practically a tricarboxylic acid and will therefore be referred to as “triacid” in the following. The amount of carboxylic acid groups per gram of sample was determined quantitatively by ^{31}P NMR spectroscopy according to a procedure introduced by Kilpeläinen *et al*.[273-274] In this method, carboxylic acid and hydroxyl groups of the sample are first transformed to their corresponding phosphite esters by reaction with 2-chloro-4,4,5,5-tetramethyl-1,3,2-dioxaphospholane and then quantified by ^{31}P NMR spectroscopy. The determined carboxylic acid value of 4.95 µmol CO_2H per mg of sample is almost identical to the carboxylic acid value of glyceryl triazelate (4.98 µmol CO_2H per mg), again confirming the successful synthesis of the triacid.

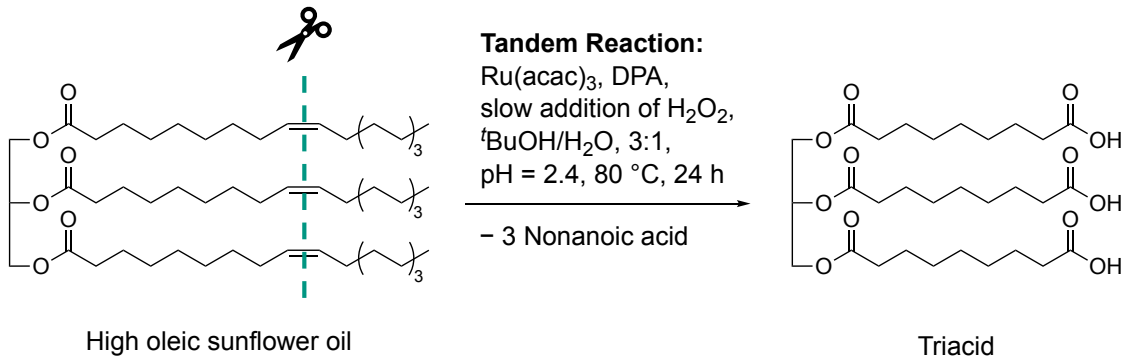

Scheme 4.4: Ruthenium catalyzed oxidative cleavage of high oleic sunflower oil (DPA: pyridine-2,6-dicarboxylic acid, $Ru(acac)_3$: ruthenium(III)acetylacetonate).

Five model substances (**M1**−**M5**) were synthesized from the sunflower oil-based triacid, *n*-hexylisocyanide, and the five aldehydes acetaldehyde (**1**), butanal (**2**), hexanal (**3**), nonanal (**4**), and 2-ethylbutyraldehyde (**5**) to investigate the suitability of the triacid for Passerini three-component reactions and to obtain soluble compounds that allow full molecular characterization (Scheme 4.5). Each model compound was synthesized by stirring all three components for 3 days at room temperature. After purification by flash column chromatography, good yields between 50% and 70% were achieved. All model compounds were fully characterized by ^{1}H NMR, ^{13}C NMR and IR spectroscopy as well as mass spectrometry (Experimental section, chapter 6.12). Exemplarily, the ^{1}H NMR spectrum of compound **M4** is depicted in Figure 4.12. Characteristic signals for Passerini products such as amide protons at 6.03 ppm as well as CH protons of the newly formed *α*-acyloxy amide group at 5.13 ppm were detected.[245-246] Moreover, signals of the glyceryl ester moiety at 5.23 ppm and 4.12−4.27 ppm and signals of *α*-CH_2 protons of ester groups at 2.29 ppm and 2.36 ppm were observed and therefore confirmed the successful isolation of the trifunctional Passerini product as a proof of concept. All molecular signals of **M1**−**M5** were furthermore detected in ESI-MS measurements (Experimental section chapter 6.12). The sunflower oil-based triacid was then reacted with aldehydes **1−5** and the two difunctional isocyanides 1,6-diisocyanohexane (**a**) and 1,9-diisocyanononane (**b**) for the synthesis of ten different cross-linked polymers *via* the Passerini three-component reaction (Scheme 4.5). All aldehyde and isocyanide components were chosen to be aliphatic and at least in principle renewable.

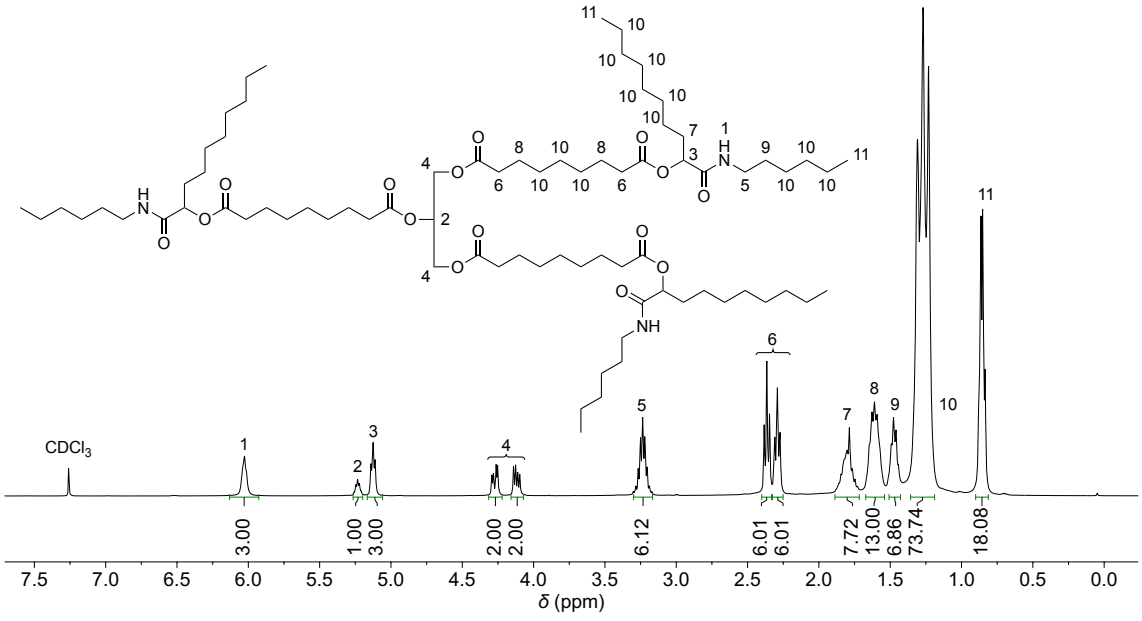

Figure 4.12: ^{1}H NMR spectrum of **M4** in $CDCl_3$. Integrals are referenced to protons **4** of the glyceryl moiety.

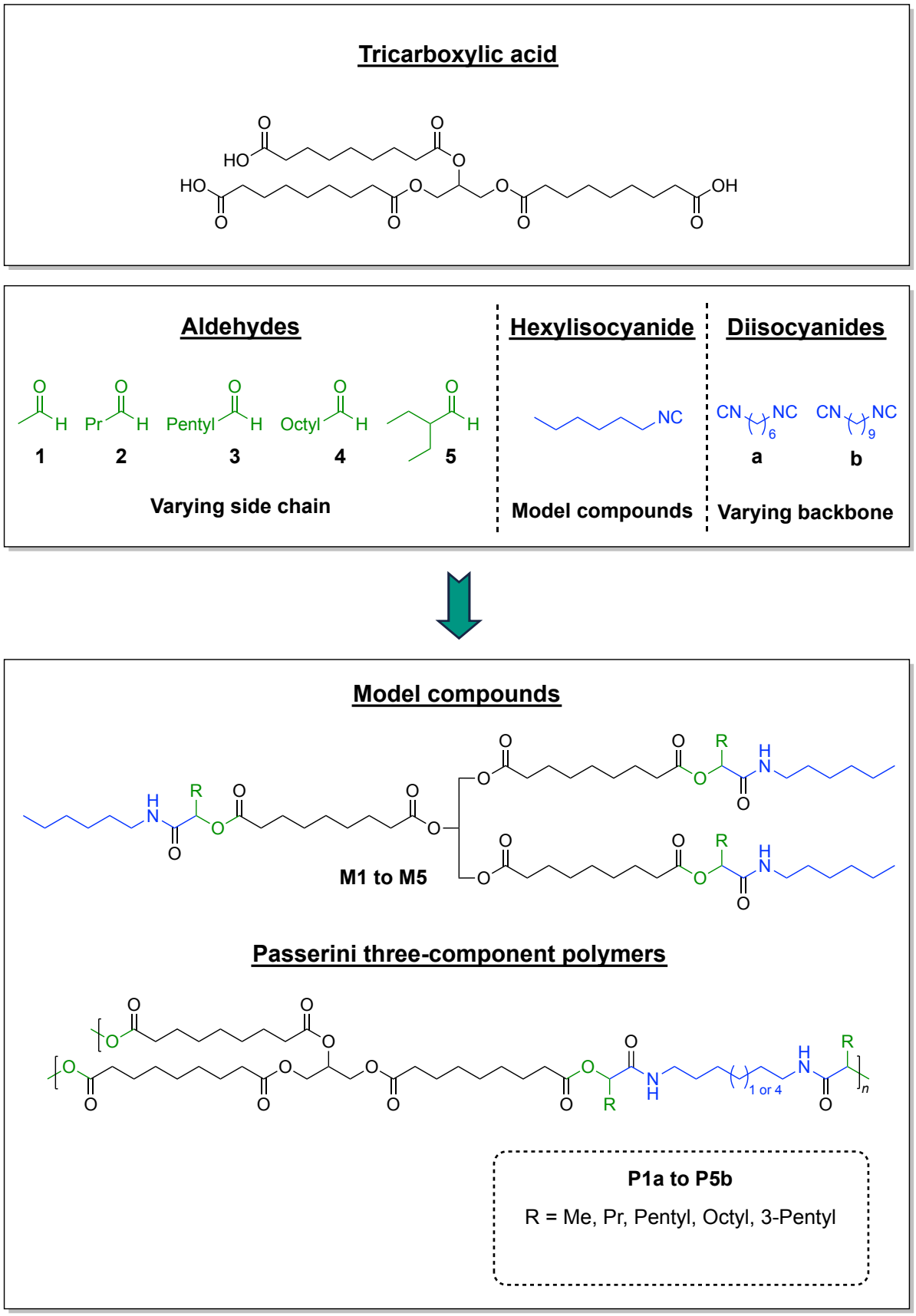

Scheme 4.5: Synthesis of model compounds **M1**−**M5** and polymers **P1a**−**P5b** *via* Passerini three-component reaction from the sunflower oil-based tricarboxylic acid, the five aldehydes acetaldehyde (**1**) butanal (**2**), hexanal (**3**), nonanal (**4**), 2-ethylbutyraldehyde (**5**), and the three isocyanides *n*-hexylisocyanide, 1,6-diisocyanohexane (**a**) and 1,9-diisocyanononane (**b**).

For instance, 1,6-diisocyanohexane was synthesized from hexamethylenediamine, which can be produced from adiponitrile by hydrogenation.[275] Adiponitrile can be synthesized from ammonia and adipic acid, which in turn can be produced biotechnologically from sugars.[276-278] Another feasible route to hexamethylenediamine from adipic acid is the reduction of adipic acid ester to 1,6-hexanediol, which is then reacted with ammonia to yield the diamine.[275] 1,9-Diaminononane, the starting material for 1,9-diisocyanononane, can most likely be produced in the same way from azelaic acid, which is obtained industrially by oxidative cleavage of oleic acid.[130, 218] A biotechnological route to 1,9-diaminononane starting from oleic acid was recently reported by Park *et al*.[279] All unbranched aldehydes occur in natural oils and can further be synthesized by dehydrogenation of the primary alcohols.[133, 280-281] 2-Ethylbutyraldehyde is obtained by aldol condensation of butanal with acetaldehyde and subsequent hydrogenation.[281]

All polymerizations were performed in bulk, as all compounds were liquid at room temperature. First, the three components were mixed at −20 °C to guarantee a homogeneous mixture of all compounds before the polymerization started, as very rapid curing was observed in bulk. Then, the mixture was casted into a PTFE form to produce bone shaped samples for tensile strength measurements. Polymers **P1a** to **P3b** (please see Scheme 4.5 for compound labeling) were cured at 5 °C for 30 minutes to prevent evaporation of the volatile aldehyde components, while polymers **P4a** to **P5b** were cured at room temperature for 30 minutes. All polymers were further cured at 50 °C for 24 h to guarantee full conversion of functional groups. For polymers **P4a** and **P4b**, a fast reaction was observed as the samples completely solidified after 5 minutes of curing at room temperature, while polymers **P5a** and **P5b** with the sterically more demanding 2-ethylbutyraldehyde took longer to solidify (10 minutes). It is therefore potentially possible to further increase the curing time by incorporating sterically more demanding and/or less reactive substrates into the polymer formulation. The reaction completeness was investigated qualitatively *via* infrared spectroscopy. IR spectra of the sunflower-oil based triacid, nonanal (**4**), 1,6-diisocyanohexane (**a**), model compound **M4**, and polymer **P4a** are exemplarily depicted in Figure 4.13. Characteristic IR signals of the starting materials such as the C=O stretching vibration of carboxylic acids at 1703 cm^{-1}, the COH combination band of aldehydes at 2823 cm^{-1} and 2714 cm^{-1}, and the stretching vibration of isocyanides at 2146 cm^{-1} were neither visible in the IR spectra of model compound **M4** nor for polymer **P4a**.

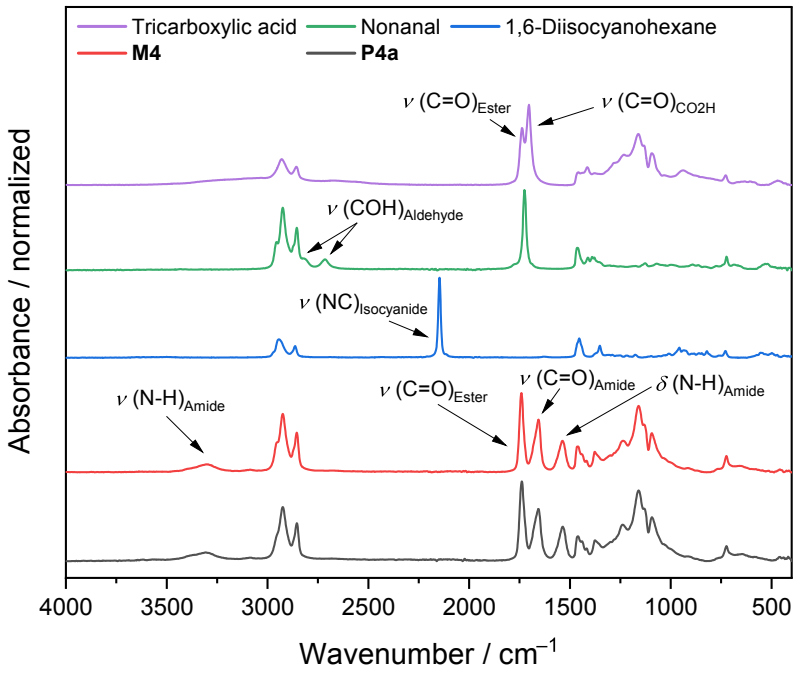

Figure 4.13: Stacked IR spectra of sunflower oil-based tricarboxylic acid, nonanal (**4**), 1,6-diisocyanohexane (**a**), model compound **M4**, and polymer **P4a**. Each IR spectrum is normalized to the strongest absorbance vibration.

In the IR spectrum of **M4**, characteristic signals for amide groups such as the N−H stretching vibration (3305 cm^{-1}), the C=O stretching vibration (1655 cm^{-1}), and N−H deformation vibration (1537 cm^{-1}) were observed. The IR spectrum of polymer **P4a** was completely identical to the one of **M4**, thereby confirming the successful P-3CR polymerization with near quantitative conversion of all functional groups.

Swelling tests of all polymers were performed to further evaluate the degree of cross-linking. Each polymer was weighed and immersed in tetrahydrofuran for 3 days at room temperature to allow the complete solubilization of residual unreacted monomeric and oligomeric compounds inside the material. The polymer was then removed from the solvent, dried at 70 °C and 10 mbar, and weighed again. The gel content is the percentage of mass that is insoluble in THF and is therefore calculated by division of the dried sample's mass m_1 by the initial sample's mass m_0 (Equation (10)).

$$\text{Gel content}\ (\%) = \frac{m_1}{m_0} \times 100 \tag{10}$$

The determined gel content values of all polymers were between 96% and 99% (Table 4.8). Hence, both the results obtained from IR spectroscopy and the high gel contents from the swelling tests show that the P-3CR polymerization is suitable for thermosetting applications as very high conversions and high degrees of cross-linking were achieved.

The thermal stability of all materials was analyzed using thermogravimetric analysis (TGA). The obtained values for the temperature of 5 wt% loss ($T_{d,5\%}$) of polymers **P1a**−**P5b** ranged from 340 °C to 365 °C and were approximately 20 °C higher than the $T_{d,5\%}$ values of model compounds **M1**−**M5** (321 °C to 344 °C). Variation of aldehyde and isocyanide components had almost no influence on the thermal stability, as all polymers as well as all model compounds decomposed in a temperature range of 10 °C, respectively. Studies by Li *et al*. reported a $T_{d,5\%}$ value of 335 °C for a P-3CR polymer synthesized from adipaldehyde, 1,6-diisocyanohexane, and undecanoic acid as well as $T_{d,5\%}$ values ranging from 291 °C to 316 °C for polycaprolactone derivatives synthesized *via* P-3CR from 6-oxohexanoic acid and aliphatic isocyanides.[245-246] For aliphatic poly(ester-amide)s, $T_{d,5\%}$ values ranging from 267 °C to 290 °C were reported.[282] A degradation temperature of 313 °C was reported for renewable isosorbide containing P-3CR polymers.[283] The herein synthesized cross-linked polymers therefore exhibit an improved thermal stability compared to many linear P-3CR polymers.

Differential scanning calorimetry experiments revealed that all polymers showed glass transition temperatures (T_g) below room temperature (Table 4.8). Exemplarily, all DSC measurements of the polymer series **a** are depicted in Figure 4.14.

Table 4.8: Polymers **P1a** to **P5b** with their gel content in tetrahydrofuran, temperature of 5 weight% loss ($T_{d,5\%}$), glass transition temperature (T_g), Young's modulus, ultimate tensile strength, and their elongation at break. The given error values are standard deviations calculated from three measurements.

Polymer	Gel content in THF / %	$T_{d,5\%}$ / °C	T_g / °C	Young's Modulus / MPa	Ultimate Tensile Strength / MPa	Elongation at break / %
P1a	98 ± 2	363	9	2.16 ± 0.41	1.64 ± 0.29	104 ± 8
P1b	96 ± 2	362	4	1.78 ± 0.40	1.34 ± 0.31	101 ± 2
P2a	96 ± 1	346	3	1.84 ± 0.10	1.45 ± 0.20	105 ± 10
P2b	98 ± 1	365	1	2.11 ± 0.08	1.68 ± 0.21	109 ± 13
P3a	97 ± 2	357	−8	1.86 ± 0.08	1.24 ± 0.03	84 ± 4
P3b	96 ± 2	363	−12	1.44 ± 0.09	0.92 ± 0.14	81 ± 16
P4a	97 ± 1	362	−12	1.24 ± 0.02	0.85 ± 0.01	91 ± 1
P4b	97 ± 1	364	−18	1.27 ± 0.04	0.87 ± 0.05	90 ± 6
P5a	98 ± 1	333	3	1.35 ± 0.04	2.20 ± 0.33	214 ± 26
P5b	99 ± 1	343	0	1.95 ± 0.05	1.98 ± 0.23	146 ± 14

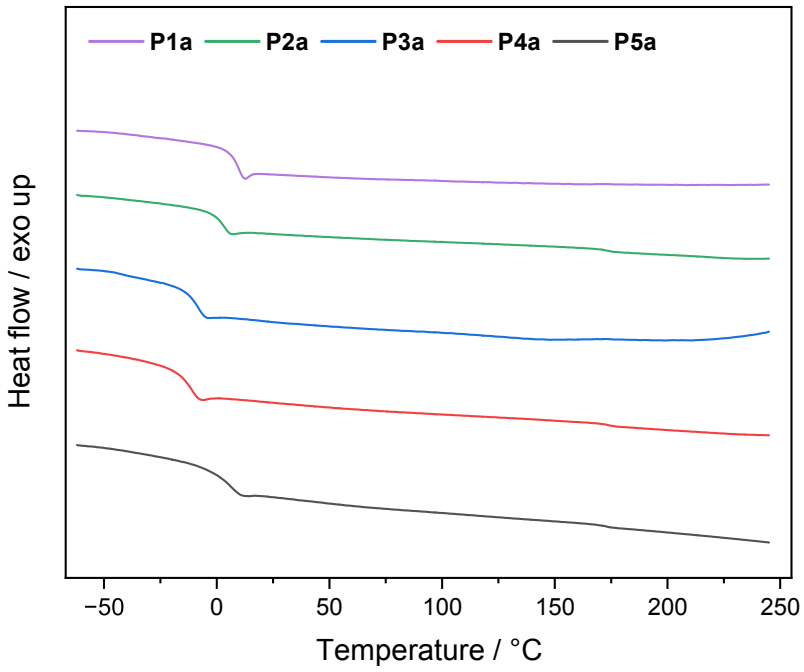

Figure 4.14: Differential scanning calorimetry measurements of polymer series **a**.

The glass transition temperature decreased gradually with an increasing aldehyde side chain length from acetaldehyde (**P1a**) with 9 °C to nonanal (**P4a**) with −12 °C. The T_g of **P5a** was identical to **P2a**, presumably due to the similar steric hindrance of 2-ethylbutyraldehyde and butanal. The same relationship between T_g and side chain length is observed for the polymer series **b** (Table 4.8, chapter 6.13.5). Interestingly, every **a** polymer had a slightly higher T_g than the respective polymer from the **b** series. 1,9-Diisocyanononane (series **b**) is three carbon atoms longer than 1,6-diisocyanohexane (series **a**), resulting, on the one hand, in a lower density of amide groups and thus in less hydrogen bonding and on the other hand in a larger mesh size. Both factors contribute to a higher T_g in the **a** series. The DSC experiments thus show that the glass transition temperature can be fine-tuned in a temperature range of 30 K through simple variation of aldehyde and diisocyanide components.

Tensile strength measurements were performed to evaluate the mechanical properties of all samples. The manufactured samples as well as one exemplary measurement of **P4a** are depicted in Figure 4.15a. All samples behaved flexible and could be bent by 180 °C without breaking. Moreover, linear elastic regions of at least 20% were observed for each measurement (Experimental section chapter 6.13.6, Figure 6.114−Figure 6.123).

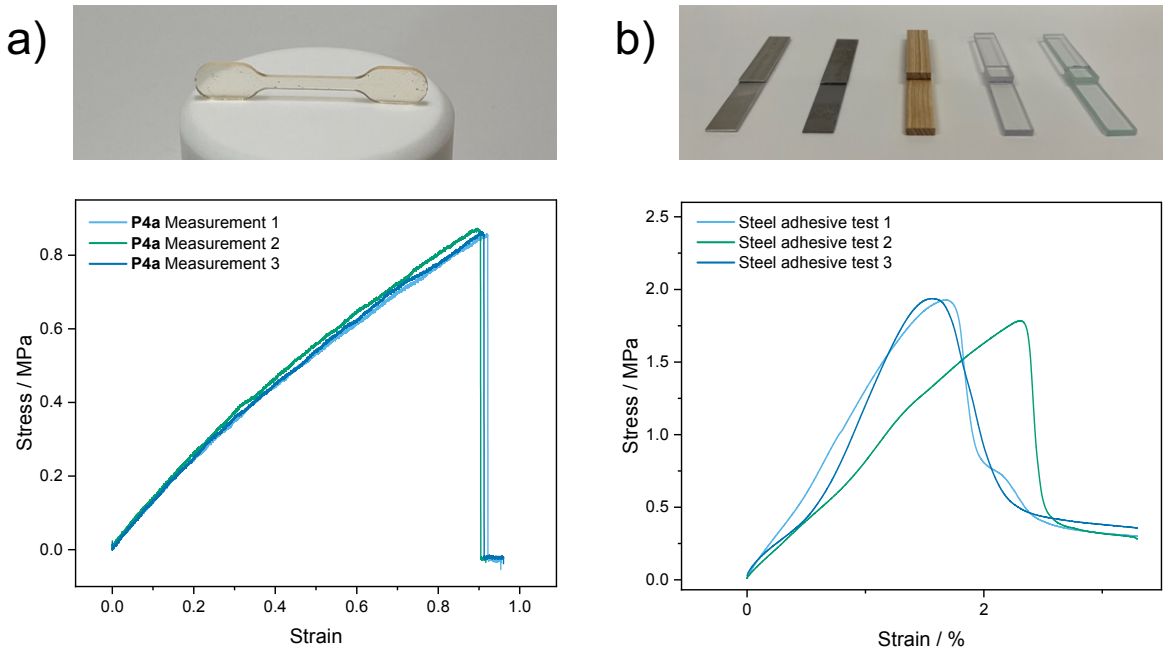

Figure 4.15: Dog bone sample of polymer **P4a** with the associated tensile strength measurements (a) and adhesive test samples prepared from polymer **P5a** and different substrates (aluminum, stainless-steel, wood, PMMA, borosilicate glass) with the adhesive tests of stainless-steel after 2 h of curing at room temperature (b).

The determined Young's moduli are in the region on rubber-like materials and ranged from 1.24 MPa to 2.16 MPa (Table 4.8). Ultimate tensile strengths were in the range of 0.85 MPa to 2.20 MPa and the determined elongations at break ranged from 81% up to a maximum of 214%. It was observed that the Young's modulus decreases slightly but gradually with an increasing side chain length from **P1a** to **P4b**. Polymers **P2a** to **P5b** showed great reproducibility in preparation of samples and had standard deviations between 1% to 5% for the Young's modulus and a maximum of 15% for the ultimate tensile strength. The high standard deviations of approximately 20% for **P1a** and **P1b** are attributed to the low boiling point of acetaldehyde and hence a more difficult reproducibility.

Due to the fast curing of all polymers at room temperature, a potential application as "three component glues" was imagined. For this proof of concept, polymer **P5a** was chosen since the sterically more demanding 2-ethylbutyraldehyde significantly increased the curing time and enabled a reproducible manufacturing of adhesive test samples. The substrates to be glued together were prepared by cutting aluminum alloy, stainless-steel, wood, poly(methyl methacrylate) (PMMA), and borosilicate glass into rectangular pieces. Polymer **P5a** was freshly prepared and applied onto two pieces of the same substrate. The two surfaces were then pressed together and cured at room temperature for 2 h. Afterwards, each substrate was measured in triplicate to determine the ultimate tensile strength.

The prepared samples and the measurements performed with stainless-steel as substrate are depicted in Figure 4.15b. The adhesion of **P5a** ranged from 0.94 MPa to 1.17 MPa for all surfaces expect for steel, for which a stronger adhesion of 1.88 MPa was accomplished. In further experiments, wood surfaces were glued together and measured after 30 minutes, 60 minutes, and 120 minutes had passed (chapter 6.13.7, Figure 6.127). Already after one hour of curing at room temperature, no further increase in tensile strength could be detected, indicating a fully cured glue. These results prove that a multicomponent approach can be used to manufacture new thermosetting glues and that different substrates can be glued efficiently.

At last, chemical recycling of polymer **P4a** was investigated to demonstrate a possible way to reutilize all components in a second life cycle after the materials have reached their end of life. It was assumed that transesterification of **P4a** with methanol yields the three products glycerol, azelaic acid dimethyl ester, and the difunctional *α*-hydroxyamide **6** (Scheme 4.6). It should be noted that this approach of P-3CR reaction and subsequent transesterification has already been utilized in literature for the targeted synthesis of *α*-hydroxyamides.[284-285] Hence, three grams of **P4a** were suspended in methanol and catalytic amounts of sulfuric acid were added. Intriguingly, the thermoset had completely dissolved after heating the reaction mixture to 65 °C for 5 h. Diol **6** precipitated as a white powder from the reaction mixture while cooling to room temperature and was thus easily isolated by filtration in a yield of 74% (1.26 g). The compound had a high melting point of 162 °C and was poorly solubility in common organic solvents due to the strong hydrogen bonding that originates from its amide groups.

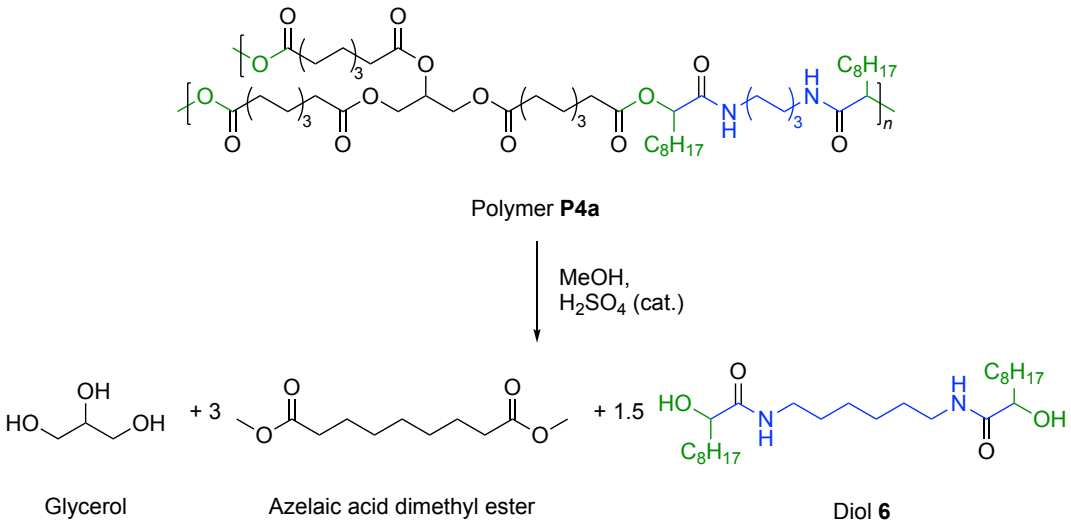

Scheme 4.6: Chemical recycling of polymer **P4a** by transesterification with methanol and catalytic amounts of sulfuric acid.

The molecular structure was confirmed by mass spectrometry and by NMR spectroscopy in deuterated trifluoroacetic acid (chapter 6.13.8, Figure 6.130 and Figure 6.131). In the ^{1}H NMR spectrum, the alpha amide proton signal is shifted downfield to 4.63 ppm due to the electron withdrawing effect of the hydroxy group. This was further confirmed by heteronuclear multiple bond correlation (HMBC) spectroscopy that showed correlation between this signal and the quaternary carbon atom of the amide at 180.7 ppm (Experimental section Figure 6.132). Moreover, characteristic signals of the amide functionality such as the C=O stretching vibration at 1638 cm^{-1}, the N−H stretching vibration at 3242 cm^{-1}, and the N−H deformation vibration at 1543 cm^{-1} were observed in IR spectroscopy.

Methanol was then removed from the filtrate under reduced pressure. The residue that still contained a mixture of azelaic acid dimethyl ester and glycerol was extracted with ethyl acetate and washed with water to separate both compounds. Azelaic acid dimethyl ester was obtained in high purity by vacuum distillation of the organic phase in a yield of 75% (1.18 g) and glycerol was isolated by vacuum distillation of the aqueous phase in a yield of 30% (68 mg). The low glycerol yield is attributed to the small scale of recycling as 227 mg of glycerol corresponded to 100% yield. The chemical recycling of **P4a** was therefore successful with a simple transesterification approach. Noteworthy, azelaic acid dimethyl ester is an industrially relevant compound, which is used for cosmetic applications and the manufacture of polymers such as polyamides and polyesters.[97, 221-222] It was desired to repolymerize diol **6** with azelaic acid dimethyl ester to show that the recycled compounds can directly be incorporated into a new material. However, several polymerization efforts in bulk at 160 °C under TBD catalysis yielded only oligomeric compounds with an average molecular weight of 1900 Da (Experimental section chapter 6.14, Figure 6.135). The apparently low reactivity of **6** towards transesterification renders this diol with secondary hydroxyl groups impractical for poly(ester-amide) synthesis. Alternatively, it was discovered that diol **6** reacted readily with isocyanates in bulk. A reaction with hexamethylene diisocyanate yielded a poly(amide-urethane) with an average molecular weight of 17 kDa already after one hour of reaction time at 160 °C (Figure 4.16). The polymer structure was further elucidated *via* NMR spectroscopy (Experimental section Figure 6.137 and Figure 6.138). In the ^{1}H NMR spectrum, characteristic amide and urethane protons were visible at 6.89 ppm and 5.85 ppm, respectively. The corresponding quaternary carbon signals were observed at 171.5 ppm and 155.8 ppm in the ^{13}C NMR spectrum.

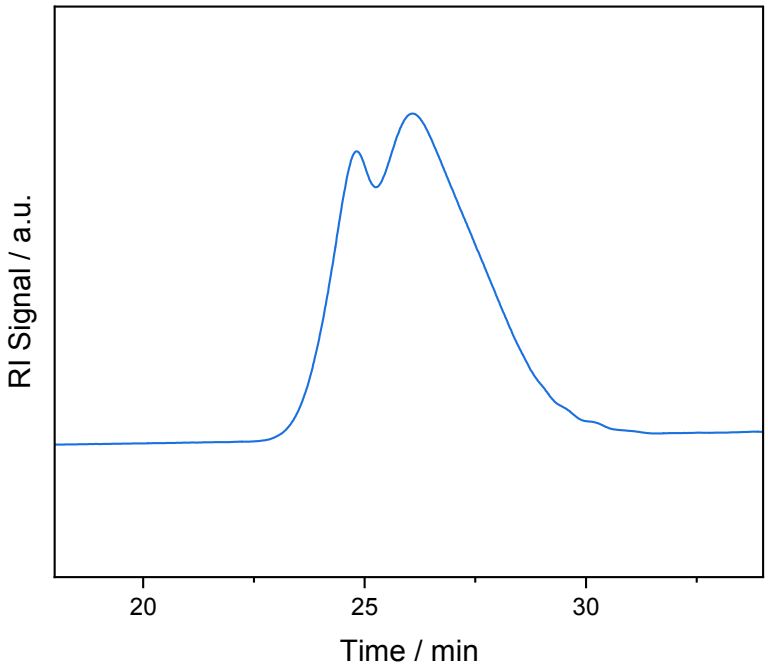

Figure 4.16: SEC (DMAc) measurement of poly(amide-urethane) made from diol **6** and hexamethylene diisocyanate (M_n, M_w and dispersity are listed in Experimental section chapter 6.14.2).

Although the use of isocyanates is rather unsustainable, one possible way to reuse this difunctional *α*-hydroxyamide was demonstrated. Apart from this polymer application, *α*-hydroxyamides are found in pharmaceutical, and natural products.[286-287]

Conclusion

A multicomponent polymerization approach for the synthesis of thermosets from a sunflower oil-derived tricarboxylic acid is presented. The triacid was produced from commercial sunflower oil *via* a ruthenium catalyzed oxidative cleavage which uses hydrogen peroxide as greener oxidant.[236, 269] As proof of concept for the multicomponent approach, five model compounds were synthesized *via* the Passerini three-component reaction (P-3CR) and fully characterized *via* ^{1}H NMR, ^{13}C NMR, and IR spectroscopy and mass spectrometry. Afterwards, a set of ten P-3CR thermosets was synthesized from the triacid in combination with five monoaldehydes and two diisocyanides. The polymerization proceeds readily at room temperature and was performed without any additional solvents, rendering this process more sustainable. IR spectroscopy of the cured thermosets indicated a quantitative conversion of all aldehyde and isocyanide groups. Gel contents between 96% and 99% in THF point towards high degrees of cross-linking in all materials. Differential scanning calorimetry experiments revealed structure property relationships as it was possible to fine-tune the glass transition temperature in a range from −18 °C to 9 °C by variation of aldehyde and diisocyanide components. With increasing side chain length as well as increasing length of the diisocyanide, a gradual decrease of the T_g was observed. In tensile strength measurements, Young's moduli ranging from 1.24 MPa to 2.16 MPa, and elongations at break between 81% and 214% were determined. The presented system can be used as a "three component glue" since all compounds are liquid and no additional heating was required for curing. After 60 minutes of curing at room temperature, the adhesive exhibited ultimate tensile strengths between 0.94 MPa and 1.88 MPa on aluminum, steel, wood, PMMA, and glass surfaces. At last, chemical recycling of polymer **P4a** was achieved by transesterification with methanol and catalytic amounts of sulfuric acid. The difunctional *α*-hydroxyamide **6** precipitated during recycling and was isolated in a good yield of 74%, while azelaic acid dimethyl ester was obtained by vacuum distillation in a yield of 75%. Eventually a new polyurethane was synthesized from diol **6** and hexamethylene diisocyanate to exemplify a second life cycle of the recycled compound.

4.4 Renewable polycarboxylic acids from organosolv lignin and succinic anhydride

Abstract

In this work, a synthetic route was established for the synthesis of organosolv lignin-based polycarboxylic acids. In the first approach, carboxylic acid moieties were introduced by functionalization of organosolv lignin with succinic anhydride. Through variation of temperature, concentration and amount of succinic anhydride, different degrees of substitution between 10% and 70% of all alcohol groups were achieved. For the succinylated lignin sample with the highest DS of 70%, quantitative conversion of all aliphatic alcohol groups was observed by ^{31}P NMR spectroscopy, while aromatic alcohol groups only reached a maximum degree of substitution of 30%, presumably due to the thermodynamic instability of the produced phenyl esters. Thus, an alternative synthetic route *via* hydroxyethylation was chosen to first transform all aromatic alcohol groups into their corresponding hydroxyethyl ethers. The newly introduced hydroxyethyl groups as well as the originally present aliphatic alcohol groups of organosolv lignin were subsequently reacted with succinic anhydride to synthesize a new polycarboxylic acid without any residual aromatic hydroxyl groups. In ^{31}P NMR spectroscopy, a DS of 99.6% and thus a quantitative conversion of all alcohol groups was determined. All samples were furthermore characterized *via* ^{1}H NMR spectroscopy, infrared spectroscopy, and size exclusion chromatography. At last, as a proof of concept, one thermoset was synthesized from the lignin-based polycarboxylic acid *via* the Passerini three-component reaction to obtain a polymer with a gel content of 95% and a glass transition temperature of 59 °C.

Results and discussion

The organosolv lignin used within this project was kindly donated by the Fraunhofer-Zentrum für Chemisch-Biotechnologische Prozesse CBP (Leuna, Germany). In the so-called *Organosolv process*, mixtures of ethanol and water are used to fractionate wood under high pressure and high temperature into its components cellulose, hemicellulose and lignin.[288] Organosolv lignin precipitates from the solution after evaporation of ethanol or dilution with water. It is then filtered off, washed several times with water and dried under reduced pressure. The pilot plant at the Fraunhofer institute uses beech wood to produce organosolv lignin with an average molecular weight of 1100 Da in reproducible quality.[289]

Prior to the conducted experiments, the used organosolv lignin was characterized *via* size exclusion chromatography (SEC), IR, ^{1}H NMR, and ^{31}P NMR spectroscopy. In SEC, a number molecular average of 800 Da and a dispersity of 1.50 were determined (chapter 6.15.1, Figure 6.139). In IR spectroscopy, a characteristic broad vibration signal of hydroxyl groups was detected between 3200 cm^{-1} and 3600 cm^{-1} (Figure 4.17). The stretching vibration of the aromatic scaffolds' C=C double bonds was detected at 1594 cm^{-1} and 1512 cm^{-1}. In ^{1}H NMR spectroscopy, methoxy groups were detected in the range from 3.00 ppm to 4.00 ppm (chapter 6.15.1, Figure 6.140). Aromatic protons and phenolic hydroxyl groups were detected between 6.00 ppm and 9.00 ppm. At last, the OH value of lignin was determined quantitatively *via* ^{31}P NMR spectroscopy to allow calculation of stoichiometry in reactions (5.46 µmol OH groups per mg lignin, Experimental section chapter 6.15.3).

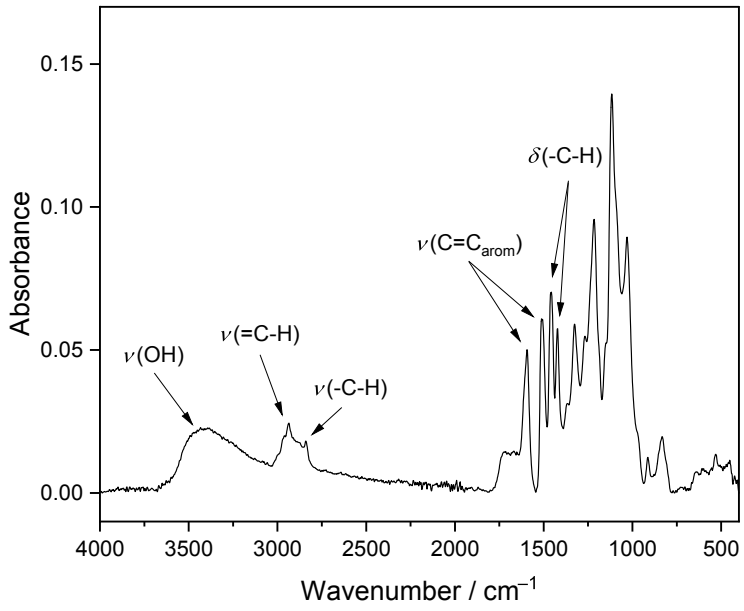

Figure 4.17: IR spectrum of organosolv lignin used within this thesis.

It was targeted to synthesize new polycarboxylic acids from lignin by formal addition reaction of its alcohol groups to succinic anhydride (Scheme 4.7). It is worth mentioning that succinic anhydride is potentially bio-based, as it can be produced from succinic acid, which in turn can be obtained by fermentation of sugars, thus rendering this approach fully renewable.[290-291]

The modification of an alcohol with succinic anhydride can generally be realized either in solution (with[292] or without catalyst[293]) or in molten succinic anhydride[294] (melting point 119°C). Initial experiments were conducted solventless in molten succinic anhydride at elevated temperatures. Hence, organosolv lignin was functionalized in 10 equivalents of succinic anhydride (SAn) at 140 °C with varying reaction times (Table 4.9, **Lignin 1.1**−**Lignin 1.4**). A degree of substitution (DS) of 55% was observed already after 10 minutes of stirring and further increased to about 65% after 60 minutes of stirring (determined *via* ^{31}P NMR spectroscopy, see chapter 6.15.4 of experimental section for details). To further assess the selectivity of this transformation, the integral of phosphitylated carboxylic acids in the ^{31}P NMR spectrum was divided by the sum of all integrals (Table 4.9). This integration ratio should approximately equal to the degree of substitution as one carboxylic acid moiety is formed by the reaction of one alcohol moiety with succinic anhydride. Indeed, this integration ratio has similar values as the quantitative determination by ^{31}P NMR spectroscopy. The modification in molten succinic anhydride therefore shows high selectivity, and it is reasonable that almost no side reactions occur. A longer reaction time of 2 h (**Lignin 1.5**) did not lead to higher functionalization. Moreover, increasing the reaction temperature to 150 °C and 160 °C did not increase the degree of substitution (**Lignin 1.6** and **Lignin 1.7**).

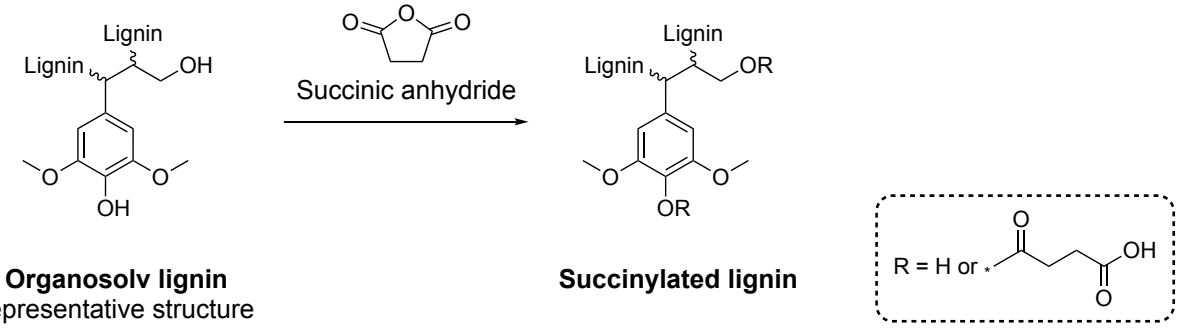

Organosolv lignin
representative structure

Succinylated lignin

Scheme 4.7: Functionalization of organosolv lignin with succinic anhydride to yield succinylated lignin.

Table 4.9: Solventless functionalization of organosolv lignin with molten succinic anhydride (SAn). The degree of substitution (DS) and the conversion of hydroxyl groups were determined *via* ^{31}P NMR spectroscopy.

Sample	Temperature / Reaction Time	SAn (equiv.)	DS (%)	CO_2H Integral *via* ^{31}P NMR / %	Conversion / %	
					$OH_{Aliphatic}$	$OH_{Aromatic}$
Lignin 1.1	140 °C / 10 min	10.0	54.9	58.2	73.1	34.0
Lignin 1.2	140 °C / 20 min	10.0	61.2	63.9	84.4	34.7
Lignin 1.3	140 °C / 40 min	10.0	66.4	68.8	91.3	37.9
Lignin 1.4	140 °C / 60 min	10.0	65.3	68.2	93.3	33.2
Lignin 1.5	140 °C / 2 h	5.00	66.0	71.1	97.7	29.8
Lignin 1.6	150 °C / 2 h	5.00	69.6	69.8	99.1	35.8
Lignin 1.7	160 °C / 2 h	5.00	68.7	68.7	99.0	34.0

Noteworthy, the conversion of aliphatic OH groups in samples **Lignin 1.5** to **Lignin 1.7** was almost quantitative, while aromatic OH groups reached a functionalization limit of about 30% to 35%. These results indicate that there is an equilibrium for the reaction of aromatic alcohol groups with succinic anhydride in contrast to the observed quantitative conversion of aliphatic alcohol groups. Indeed, this can be explained with observations made in the past for a method for the quantitative determination of alcohols. This method used cyclic anhydrides like phthalic anhydride, pyromellitic dianhydride or succinic anhydride as functionalization agents (Scheme 4.8).[295] After conversion of all alcohol groups, the excess amount of anhydride was hydrolyzed and the amount of alcohol groups of the sample was determined by titration with sodium hydroxide. This method showed selectivity towards aliphatic OH groups and can therefore be conducted, if aromatic OH groups are present. In 1975, Cohen and Fong showed that this selectivity is due to the equilibrium constant of this reaction.[296] The equilibrium lies on the product side for alcohols with a pK_a higher than 14 (e.g., aliphatic alcohols) and to the starting materials side for more acidic alcohols (e.g., phenols). For instance, conversions of 99%, 93% and 31% were determined for the reaction of methanol (pK_a = 15.5),[297] trifluoroethanol (pK_a = 12.4),[297] and phenol (pK_a = 10.0)[298] with succinic anhydride, respectively.[296] The herein obtained selectivity is in agreement with the results obtained by Cohen and Fong (31% for phenol[296] vs. 30 to 35% for lignin aromatic OH). The functionalization in molten succinic anhydride is so fast at 140 °C that this equilibrium is almost fully reached after 60 minutes of reaction time.

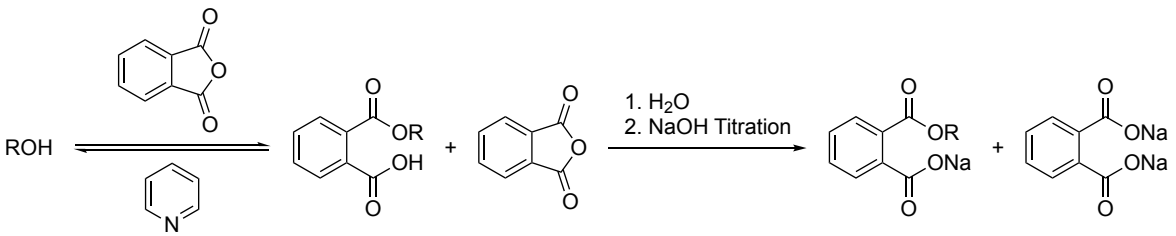

Scheme 4.8: Method for the quantitative determination of alcohol groups by reaction with phthalic anhydride and subsequent titration.[295]

Furthermore, it was observed that this equilibrium depends on the steric nature of the used anhydride and the propensity of the neighboring CO_2H group to cleave the formed monoester and form back the cyclic anhydride (phthalic anhydride > maleic anhydride > succinic anhydride).[296, 299] Thus, Monteil-Rivera and Paquet reported a quantitative conversion of aliphatic OH groups in lignin for the functionalization with maleic anhydride, while aromatic OH groups stayed unfunctionalized.[300]

Lignin 1.1 to **Lignin 1.7** were further analyzed *via* IR spectroscopy and SEC. Upon esterification, a broadening of the signal in the range of 3600−2400 cm^{-1} is visible due to the stretching vibration ν (OH) of the formed carboxylic acid moieties (Figure 4.18 for exemplary IR spectrum of **Lignin 1.5**). In contrast to unfunctionalized lignin, two major vibrations overlapping at 1730 cm^{-1} and 1715 cm^{-1} can be assigned to ester and carboxylic acid carbonyl stretching vibrations ν (C=O). In size exclusion chromatography (SEC), a shift towards higher retention times was observed for **Lignin 1.1** to **Lignin 1.4** (Figure 4.19). The modification with succinic anhydride therefore reduced the overall hydrodynamic radius of organosolv lignin. However, if reaction times were too long and high temperatures were employed, a high molecular weight shoulder appeared (**Lignin 1.5** to **Lignin 1.7**). This indicates cross-linking, for instance by transesterification reactions, between lignin molecules.

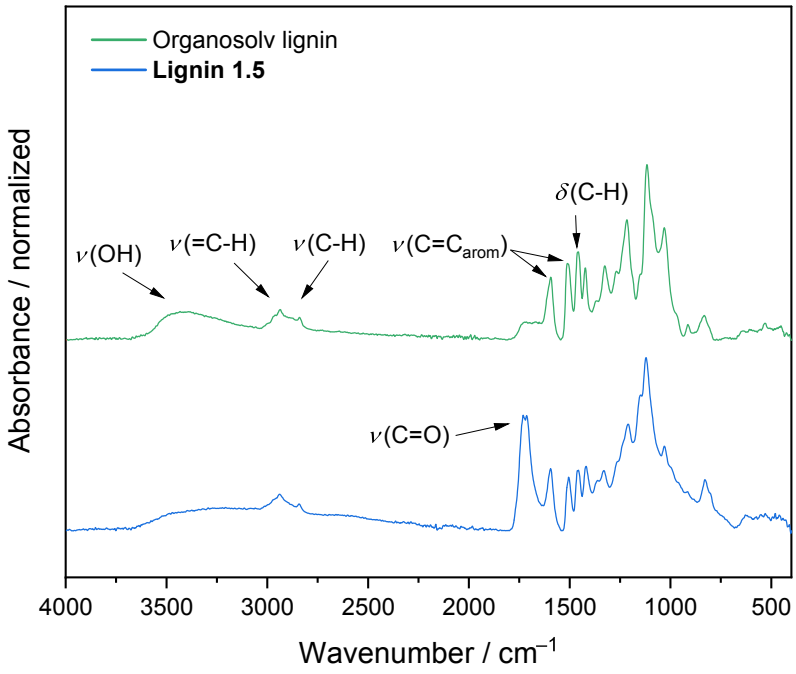

Figure 4.18: Stacked IR spectra of organosolv lignin and succinylated lignins **Lignin 1.5**.

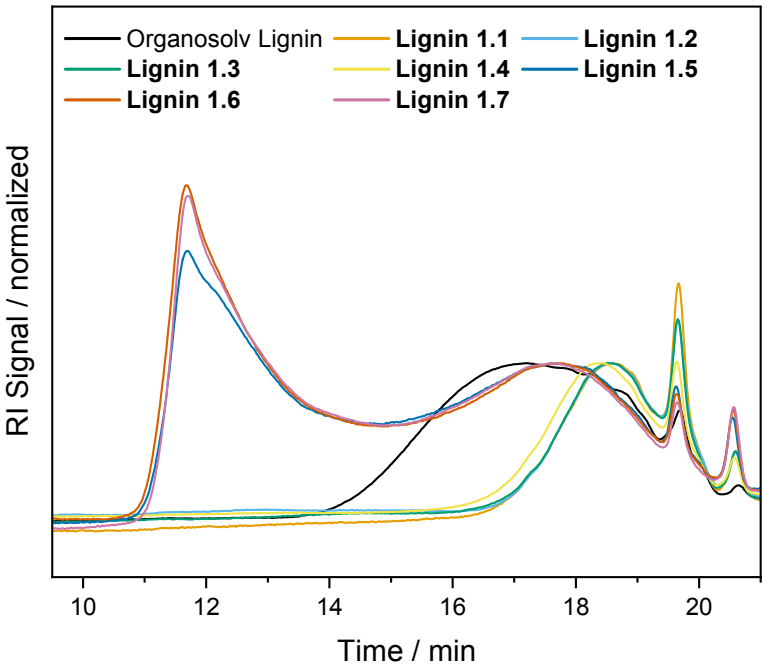

Figure 4.19: SEC (Oligo THF) of organosolv lignin and **Lignin 1.1** to **Lignin 1.7** (M_n, M_w and $Đ$ value are listed in Experimental section chapter 6.15.9).

Griffini *et al*. modified Kraft lignin under milder conditions with succinic anhydride and 1-methylimidazole as catalyst at 60 °C.[301] The obtained samples showed full conversion of aliphatic OH groups and no signal broadening in SEC measurements. It is hence possible to suppress cross-linking between lignin molecules by applying a lower reaction temperature than the one used herein for the solventless modification. For further research this is a viable option if a lower dispersity is desired.

The functionalization of lignin with succinic anhydride was afterwards conducted in solution (THF and Me-THF) to lower the reaction temperature, as without solvent a melt had to be achieved, and thus enable the synthesis of samples with lower degrees of substitution (Table 4.10). First, lignin was functionalized in THF at 60°C (**Lignin 1.8**) and in Me-THF at 80 °C (**Lignin 1.9**) with 5.00 equivalents of succinic anhydride. The obtained degrees of substitution were 14.9% and 26.3% for **Lignin 1.8** and **Lignin 1.9**, respectively. It is therefore possible to adjust different degrees of substitution with varying reaction temperatures. Then, different equivalents of succinic anhydride were applied to improve the overall sustainability of this transformation (2.50 equivalents for **Lignin 1.10** and 1.00 equivalents for **Lignin 1.11**).

Table 4.10: Functionalization of organosolv lignin with succinic anhydride (SAn) in solution (reaction time: 18 h). Degree of substitution (DS) and conversion of hydroxyl groups were determined *via* ^{31}P NMR spectroscopy.

Sample	Temperature (°C) / Solvent / Lignin concentration	SAn (equiv.)	DS (%)	CO_2H Integral *via* ^{31}P (%)	Conversion (%)	
					$OH_{Aliphatic}$	$OH_{Aromatic}$
Lignin 1.8	60 / THF / 25 mg ml^{-1}	5.00	14.9	10.5	10.3	20.3
Lignin 1.9	80 / Me-THF / 25 mg ml^{-1}	5.00	26.3	24.6	33.8	17.8
Lignin 1.10	80 / Me-THF / 25 mg ml^{-1}	2.50	24.6	20.9	30.6	17.7
Lignin 1.11	80 / Me-THF / 25 mg ml^{-1}	1.00	18.3	10.7	27.5	7.6
Lignin 1.12	80 / Me-THF / 50 mg ml^{-1}	1.00	29.6	22.7	38.4	19.7
Lignin 1.13	80 / Me-THF / 75 mg ml^{-1}	1.00	30.3	24.9	41.4	17.7
Lignin 1.14	80 / Me-THF/100 mg ml^{-1}	1.00	33.8	28.4	46.4	19.4

Due to the lower obtained functionalization degrees with less equivalents of succinic anhydride (DS = 18.3% for 1.00 equiv. SAn, **Lignin 1.11**), the lignin concentration was increased from 25 mg ml^{-1} up to 100 mg ml^{-1} to increase the reaction rate (**Lignin 1.12**-**Lignin 1.14**). The degree of substitution thus increased up to a maximum of 33.8% for a lignin concentration of 100 mg ml^{-1} (**Lignin 1.14**). Higher concentrations were not feasible due to the restricted solubility of lignin. SEC measurements of **Lignin 1.4**, **Lignin 1.8**, **Lignin 1.9** and **Lignin 1.13** are depicted in Figure 4.20. In agreement with the observation made for the solventless reactions, the retention time increases with an increasing degree of substitution from **Lignin 1.8** to **Lignin 1.9** to **Lignin 1.13** to **Lignin 1.4**.

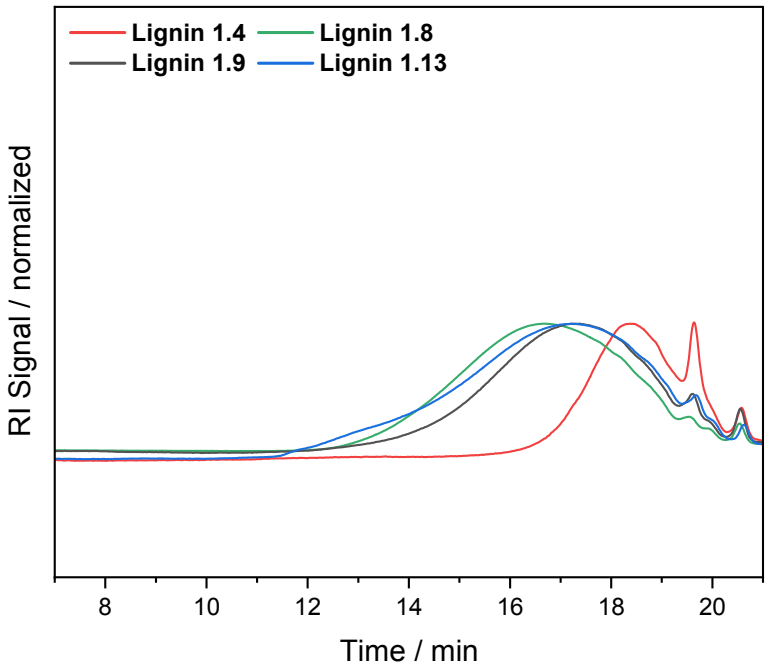

Figure 4.20: SEC (Oligo THF) of **Lignin 1.4**, **Lignin 1.8**, **Lignin 1.9**, **Lignin 1.13** (M_n, M_w and $Đ$ value are listed in Experimental section chapter 6.15.9).

However, for **Lignin 1.13**, which has approximately the same DS as **Lignin 1.9**, the formation of a higher molecular weight shoulder is visible (dispersity of 2.58 compared to 1.83 for **Lignin 1.9**). These results support the assumption that higher concentrations lead to cross-linking reactions between lignin molecules.

In summary, the functionalization of organosolv lignin with succinic anhydride was investigated in a solvent-free reaction and in a solvent containing reaction to achieve DS values of 60%−70% and 15%−35%, respectively. Finally, the two samples **Lignin 1.15** and **Lignin 1.16** with DS values of 69% and 34%, respectively, and carboxylic acid values of 0.00263 mol g^{-1} and 0.00127 mol g^{-1}, respectively, were synthesized on a larger scale of up to 10 grams and fully characterized by IR, ^{1}H NMR and ^{31}P NMR spectroscopy as well as SEC (Experimental section chapter 6.15.7 and chapter 6.15.8). Multiplication of the carboxylic acid values of **Lignin 1.15** and **Lignin 1.16** with their average molecular weights (determined by SEC: 2000 g mol^{-1} and 2200 g mol^{-1}) results in a number of 5.26 and 2.79 carboxylic acids per lignin molecule, respectively. It was thus possible to synthesize polycarboxylic acids from lignin and succinic anhydride in a one-step procedure. However, it should be noted that the calculated number of carboxylic acids per molecule is probably very inaccurate, since SEC is no method for the quantitative determination of molecular weights. The calculation was merely performed to visualize the polyfunctional nature of these compounds.

Since the presented results for the solventless functionalization suggested that phenolic esters of the succinic anhydride are labile, a derivatization with ethylene carbonate was performed to transform all aromatic alcohols into hydroxy ethyl ethers and therefore introduce aliphatic alcohol groups (Scheme 4.9). Renneckar *et al.* optimized the hydroxyethylation of Kraft lignin using 10 mol% of potassium carbonate as catalyst to achieve a conversion of 95% aromatic alcohols into hydroxyethyl ethers.[302] Thus, herein, organosolv lignin was reacted with 7.50 equivalents of ethylene carbonate in the presence of 10 mol% of potassium carbonate at 90 °C for 4 h (**Lignin 1.17**). In ^{31}P NMR spectroscopy, 99% of all detected alcohol groups of **Lignin 1.17** were aliphatic after the reaction, thus confirming a successful and near quantitative hydroxyethylation. The hydroxyethylated **Lignin 1.17** was furthermore characterized by ^{1}H NMR, IR spectroscopy and SEC (Experimental section chapter 6.15.9).

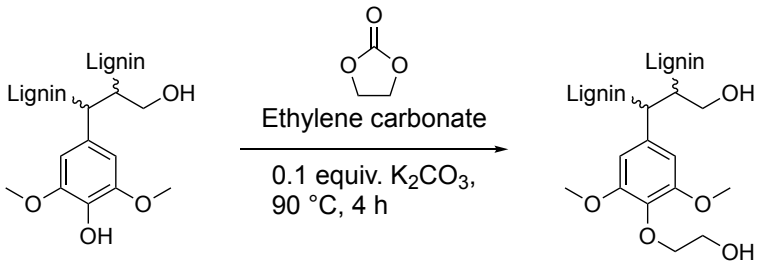

Organosolv lignin
representative structure

Hydroxyethylated lignin

Scheme 4.9: Functionalization of organosolv lignin with ethylene carbonate to yield hydroxyethylated lignin.

The disappearance of phenolic proton signals in the ^{1}H NMR spectrum at 8.00−9.00 ppm furthermore confirmed the successful conversion of aromatic alcohols (Experimental section chapter 6.15.9, Figure 6.151). It should however be noted that this reaction is not 100% selective, as aliphatic hydroxyl groups reacted as well with ethylene carbonate in a nucleophilic addition to the quaternary carbon atom to form linear carbonates.[302] This side reaction was observed in IR spectroscopy, where a new vibration signal of carbonyl C=O bonds was detected at 1742 cm^{-1} (chapter 6.15.9, Figure 6.152). Moreover, the dispersity increased from 1.50 to 2.67, which may be explained by transesterification reactions occurring between lignin carbonates to form dimers and oligomers. The hydroxyethylated sample **Lignin 1.17** was afterwards reacted with succinic anhydride at 150 °C for 2 h to synthesize the polycarboxylic acid **Lignin 1.18**. In ^{1}H NMR spectroscopy, carboxylic acid protons and methylene protons of ester groups were observed at 12.19 ppm and 4.20 ppm, respectively (chapter 6.15.10, Figure 6.155). The successful functionalization was furthermore confirmed by IR spectroscopy, where two characteristic C=O stretching vibration signals for ester and carboxylic acid groups were observed at 1734 cm^{-1} and 1713 cm^{-1}, respectively (chapter 6.15.10, Figure 6.156). Intriguingly, a degree of substitution of 99.6% and thus a quantitative conversion of all alcohol groups was determined by ^{31}P NMR spectroscopy (chapter 6.15.10, Figure 6.154). It was therefore indeed possible to further increase the degree of substitution up to 100% by prior transformation of unreactive aromatic hydroxyl groups into more reactive hydroxyethyl ethers. The carboxylic acid value of 0.00285 mol g^{-1} and the molecular weight of 1100 g mol^{-1} (determined by SEC) correspond to an approximate number of 3.14 carboxylic acids per lignin molecule, rendering this polycarboxylic acid suitable for cross-linking reactions.

At last, **Lignin 1.18** was utilized for the synthesis of one thermoset *via* the Passerini three-component reaction (P-3CR) to demonstrate, as a proof of concept, that these polycarboxylic acids are suitable for polymer syntheses. Unfortunately, the solvent 2-methyltetrahydrofuran was necessary to dissolve the succinylated lignin sample to guarantee a homogenous polymerization, which renders this process less sustainable compared to the solvent-free thermosets that were performed in chapter 4.3. After complete dissolution of **Lignin 1.18**, nonanal and 1,9-diisocyanononane were added to the solution and the mixture was stirred vigorously for 1 minute to guarantee homogeneity. The mixture was then casted into a PTFE form and cured at room temperature for 48 h until the solvent had completely evaporated to obtain a polymer in form of a black solid. The IR spectrum of the cured thermoset indicated a quantitative conversion of functional groups, since no characteristic signals of the starting materials such as the C=O stretching vibration of carboxylic acids at 1711 cm^{-1}, the COH combination band of aldehydes at 2817 cm^{-1} and 2714 cm^{-1} and the stretching vibration of isocyanides at 2146 cm^{-1} were detected (Figure 4.21). The signals at 3403 cm^{-1}–3298 cm^{-1} and 1659 cm^{-1} were assigned to the newly formed amide group. In addition, a high gel content of 95% was determined after immersing the polymer for 72 h in 2-methyltetrahydrofuran and thus proved a successful polymerization.

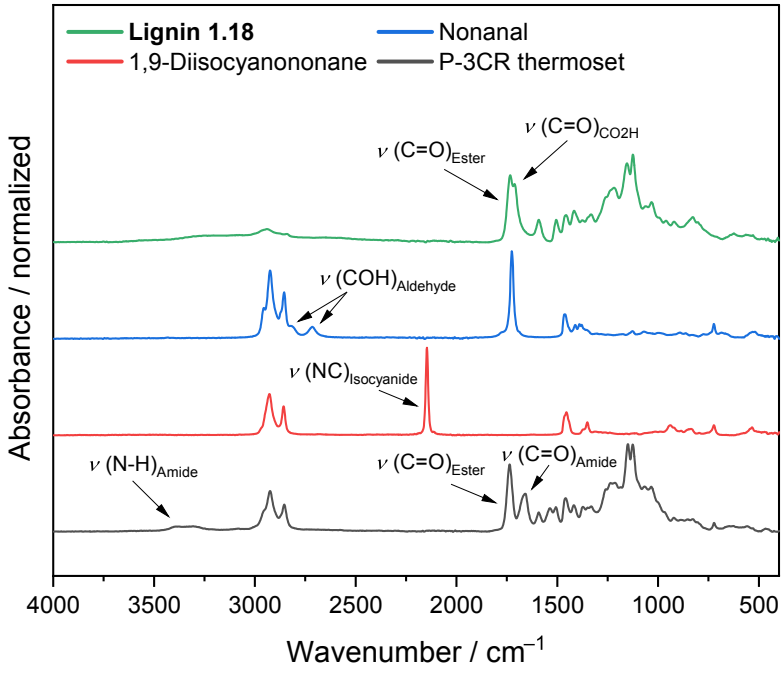

Figure 4.21: Stacked IR spectra of **Lignin 1.18**, nonanal, 1,9-diisiocyanononane, and their P-3CR thermoset.

In differential scanning calorimetry, a glass transition temperature of 59 °C was determined for the lignin-based P-3CR thermoset. This T_g value is approximately 80 °C higher than the one of polymer **P4b**, which was made from the high oleic sunflower oil-based tricarboxylic acid, nonanal and 1,9-diisocyanononane (Figure 4.22, see chapter 4.3). It was thus indeed possible to achieve a higher glass transition temperature by exchange of the flexible triglyceride scaffold with a more rigid lignin scaffold. A T_g value in between both polymers can most likely be achieved by addition of a second and more flexible dicarboxylic acid compound to the succinylated lignin polymer formulation (e.g., azelaic acid).

Due to time limitation within this thesis, no further experiments were conducted. Future research should therefore investigate more polymerizations with the herein synthesized lignin based polycarboxylic acids samples **Lignin 1.15**, **1.16**, and **1.18**. Potential applications include Passerini reactions and the curing of epoxy resins.

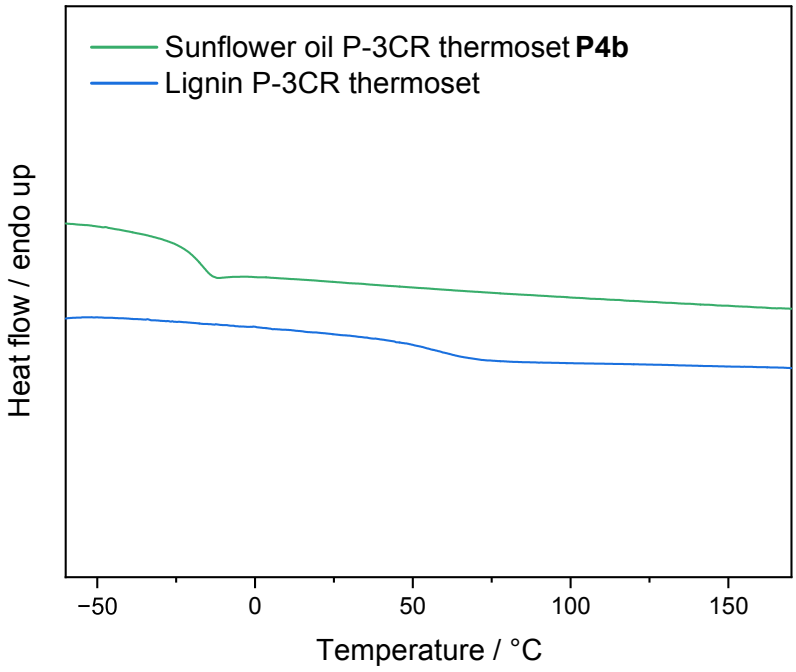

Figure 4.22: Differential scanning calorimetry measurements of Polymer **P4b** (chapter 4.3) and the thermoset made from lignin *via* a P-3CR.

Conclusion

Organosolv lignin was used as renewable resource to synthesize polycarboxylic acids by reaction with succinic anhydride. It was demonstrated that different degrees of substitutions can be adjusted by variation of the reaction conditions. Thus, solvent-free reactions at high temperatures of >140 °C delivered high DS values between 55% and 70% in short reaction times of 10 minutes up to 2 hours. A DS of 100% was not viable, presumably due to the thermodynamic instability of succinic acid phenyl esters. It was moreover possible to deliberately achieve low degrees of substitution between 15% and 35%, if the reaction was performed in 2-methyltetrahydrofuran at 80 °C using different concentrations of lignin. At last, a hydroxyethylation of organosolv lignin was conducted to transform all aromatic alcohol groups into their corresponding hydroxyethyl ethers. The newly introduced hydroxyethyl ether groups as well as originally present aliphatic alcohol groups of organosolv lignin were then reacted with succinic anhydride to synthesize a polycarboxylic acid with a DS of 99.6%. At last, as a proof of concept, one thermoset was synthesized from the lignin based polycarboxylic acid, nonanal and 1,9-diisocyanohexane *via* the Passerini three-component reaction. The polymerization proceeded readily at room temperature to obtain a polymer with a gel content of 95% and a glass transition temperature of 59 °C.

5 Conclusion and Outlook

Within this thesis, new synthetic pathways were developed for the synthesis mono and polycarboxylic acids from renewable resources. These carboxylic acids serve as monomers for the production of bio-based polymers. Three synthetic approaches were investigated to utilize saturated fatty acids, high oleic sunflower oil, and lignin as renewable resources:

In the first project, a new three-step reaction sequence was developed for the synthesis of dimethyl esters and their polyesters from renewable lauric acid. The saturated fatty acid was first dehydrogenated with a literature established palladium catalyzed procedure using molecular oxygen as oxidant to yield *α*,*β*-unsaturated lauric acid. The original procedure was optimized considering sustainability aspects to exclude solvents, cocatalysts, and stoichiometric amounts of bases, thereby reducing the amount of waste formed immensely. The optimized dehydrogenation was then performed on a 40-gram scale to obtain a mixture consisting of 60% lauric acid and 40% *α*,*β*-unsaturated lauric acid. A subsequent esterification with methanol yielded a mixture of the respective methyl esters, which was reacted with 1,4-butanedithiol in a solvent-free thia-Michael addition. It was possible to isolate the desired dimethyl ester in an overall yield of 27% and to recover 51% of the initially used lauric acid as methyl laurate. The thia-Michael addition was moreover performed with 1,6-hexanedithiol and 1,10-decanedithiol to produce two more dimethyl esters. At last, polymerization of the three dimethyl esters with renewable 1,12-dodecanediol was performed to produce polyesters with high molecular weights (up to 32 kDa). The herein developed reaction sequence thus enables the utilization of otherwise difficult to functionalize saturated fatty acids.

In a second project, a new tricarboxylic acid was synthesized from high oleic sunflower oil using a literature known procedure for a ruthenium catalyzed oxidative cleavage of alkenes with hydrogen peroxide as more sustainable oxidant. The procedure was first optimized for the used sunflower oil to achieve a high conversion of double bonds into carboxylic acids of up to 86%. The optimized reaction conditions were then employed on the sunflower oil to obtain a tricarboxylic acid in a seemingly moderate yield of 44%. A simple statistical concept was devised to explain that not only the efficiency of the employed oxidative cleavage, but also the unsaturated fatty acid content of the used oil had a high impact on the amount of tricarboxylic acid that was formed during the reaction. The isolated yield of 44% thus corresponded to >88% of triacid, if statistical calculations were considered.

The sunflower oil-based tricarboxylic acid was utilized in a following project to synthesize cross-linked thermosets *via* the Passerini three-component reaction. A set of ten different polymers was obtained from the triacid in combination with two diisocyanides and five monoaldehydes. All components were by design chosen to be liquid and therefore allowed the facile preparation of solvent-free formulations, rendering this process more sustainable. Due to the high efficiency of the Passerini reaction, near quantitative conversions of all functional groups and high gel contents between 96% and 99% were achieved already at room temperature without any additional heating. Differential scanning calorimetry experiments revealed the glass transition temperature could be fine-tuned in a broad range from −18 °C to 9 °C by variation of aldehyde and diisocyanide components. A potential application as “three component glues” of the herein developed multicomponent approach was demonstrated, since all polymer formulations polymerized within 60 minutes at room temperature. At last, the circularity of these new materials was shown by chemical recycling of one polymer *via* transesterification with methanol and catalytic amounts of sulfuric acid to recycle azelaic acid dimethyl ester and a difunctional *α*-hydroxyamide in a yield of 75%.

In a final project, organosolv lignin (extracted from beech wood) was reacted with succinic anhydride to synthesize polycarboxylic acids in a one-step procedure. The functionalization was optimized for a solvent-free reaction at 150 °C and for a solvent containing reaction at 80 °C to synthesize two lignin samples with degrees of functionalization of 69% and 34%, respectively. The obtained results suggested that phenolic esters of succinic acid were labile and therefore prevented quantitative functionalization of all alcohol groups. Thus, derivatization with ethylene carbonate was performed to quantitatively transform aromatic alcohols into hydroxy ethyl ethers. A third polycarboxylic acid sample with a high functionalization degree of 99.6% was then obtained by reaction of the hydroxyethylated lignin with succinic anhydride at 150 °C. The synthesis of a thermoset from one lignin polycarboxylic acids *via* P-3CR was performed as a proof of concept. Further research on this subject is of great interest to establish these monomers in polymer science.

In summary, fundamental research was performed to establish new synthetic pathways to renewable polycarboxylic acids and their polymers. The herein presented approaches therefore contribute to the substitution of fossil resources in chemistry by renewable resources.

6 Experimental Section

6.1 Materials and methods

Parts of the general information are standardized descriptions and were adapted from previous group members.

6.1.1 General remarks

All starting materials, solvents and reagents were purchased from chemical suppliers and used without further purification unless stated otherwise.

Liquids were added with a stainless-steel cannula and solids were added in powdered shape.

Solvents were evaporated under reduced pressure at 45 °C using a rotary evaporator unless stated otherwise.

6.1.2 Used solvents

Table 6.1 lists all solvents used in this thesis together with the corresponding suppliers they were obtained of, specifications, and purities.

Anhydrous solvents were purchased sealed under inert atmosphere (nitrogen or argon) over molecular sieve.

Dichloromethane (OQEMA, technical) was purified by distillation prior to use.

DMSO-d_6 (<99.8% D) and $CDCl_3$ (<99.8% D) were purchased from Eurisotop. Trifluoroacetic acid-*d* (99.5% D) was purchased from Sigma-Aldrich.

Table 6.1: Solvents used within this thesis with the suppliers they were obtained of, specifications, and purities.

Solvent	Supplier	Specification, Purity
tert-Amyl alcohol	Sigma-Aldrich	99%
tert-Butanol	Acros Organics	99.5%
Chloroform	Thermo Fisher Scientific	HPLC grade
Chloroform-*d*	Eurisotop	>99.8%D
Cyclohexane	VWR	HPLC grade
Dichloromethane	OQEMA	technical
Dimethylformamide (anhydrous)	Thermo Scientific	99.8%
Dimethyl sulfoxide-d_6	Eurisotop	>99.8%D
1,4-Dioxane	Sigma-Aldrich	99.8%
Ethanol	Thermo Fisher Scientific	HPLC grade
Ethyl acetate	VWR	HPLC grade
Methanol	Thermo Fisher Scientific	HPLC grade
2-Methyltetrahydrofuran	Acros Organics	99.9%
Tetrahydrofuran	Honeywell	>99.9%
Tetrahydrofuran (anhydrous)	Sigma-Aldrich	≥99.9%, contains 250 ppm BHT as inhibitor
Trifluoroacetic acid-*d*	Sigma-Aldrich	99.5%D

6.1.3 Used compounds

Table 6.2 lists all compounds other than solvents used in this thesis together with the corresponding suppliers they were obtained of, specifications, and purities.

High oleic sunflower oils were bought at local supermarkets in Karlsruhe, Germany: "**HOSO01**" (Alnatura), "**HOSO02**" (Alnatura), "**HOSO03**" (Scheck-in-Center), "**HOSO04**" (dm).

The Organosolv Lignin used in this thesis was produced by Fraunhofer institute *via* the *Organosolv process*. In this process, mixtures of ethanol and water are used to fractionate wood under high pressure and high temperature into its components cellulose, hemicellulose and lignin.[288] Organosolv lignin precipitates out of the solution after evaporation of ethanol or dilution by addition of water. It is then filtered off, washed several times with water and dried under reduced pressure. The pilot plant at Fraunhofer institute uses beech wood to produce organosolv lignin with an average molecular weight of 1100 Da in reproducible quality.[289]

Table 6.2: Compounds other than solvents used within this thesis with the suppliers they were obtained of, specifications, and purities.

Compound	Supplier	Specification, Purity
Acetaldehyde	Acros Organics	99.5%
2-Acetyl-6-bromopyridine	ChemPUR	98%
Anthranilaldehyde	abcr	95%
Bromocresol green	Tokyo Chemical Industry	>99%
Butanal	Acros Organics	99%
1,4-Butanedithiol	Sigma-Aldrich	≥97%
Cerium(IV)sulfate	ChemPUR Feinchemikalien	98%
Cesium carbonate	Sigma-Aldrich	99%
2-Chloro-4,4,5,5-tetramethyl-1,3,2-dioxaphospholane	Sigma-Aldrich	95%
Crotonic acid	Thermo Fisher Scientific	98%
18-Crown-6	abcr	99%
1,10-Decanedithiol	Tokyo Chemical Industry	>98%
1,6-Diaminohexane	Sigma-Aldrich	≥97.5%
1,9-Diaminononane	abcr	98%
1,5-Diazabicyclo[4.3.0]non-5-ene (DBN)	Thermo Fisher Scientific	98%
1,8-Diazabicyclo[5.4.0] undec-7-ene (DBU)	Thermo Fisher Scientific	>98%
1,12-Dodecanediol	Thermo Fisher Scientific	98%
Dibromomethane	Sigma-Aldrich	≥98.5%
2-Ethylbutyraldehyde	Sigma-Aldrich	≥92%
Ethylene carbonate	Sigma-Aldrich	98%
Ethyl formate	Thermo Scientific	≥98%
Formic acid	Acros Organics	99%
Hexamethylene diisocyanate	Sigma-Aldrich	For synthesis
Hexanal	Sigma-Aldrich	98%
1,6-Hexanedithiol	Alfa Aesar	97%
n-Hexylamine	Sigma-Aldrich	99%
Hydrogen peroxide	abcr	35% aqueous solution
endo-*N*-Hydroxy-5-norbornene-2,3-dicarboximide	Alfa Aesar	97%
Lauric acid	Thermo Scientific	99%
Lithium carbonate	Tokyo Chemical Industry	>98%
Magnesium sulfate	Carl Roth	≥99%
4-Methoxybenzylalcohol	Sigma-Aldrich	98%
Methyl arachidate	ChemPUR Feinchemikalien	98%
Methyl crotonate	Sigma-Aldrich	98%
Methyl elaidate	Sigma-Aldrich	>99%
Methyl linoleate	Sigma-Aldrich	>98%
Methyl linolenate	Sigma-Aldrich	>99%
Methyl myristate	Sigma-Aldrich	>99%
Methyl oleate	abcr	96%
Methyl palmitate	Sigma-Aldrich	>99%
Methyl stearate	Sigma-Aldrich	99%
Myristic acid	Sigma-Aldrich	For synthesis
Nonanal	Alfa Aesar	97%
Octanoic acid	Sigma-Aldrich	≥99%
Palladium(II)acetate	Sigma-Aldrich	For synthesis
Palmitic acid	Sigma-Aldrich	For synthesis
Phosphomolybdic acid	Sigma-Aldrich	>99%

Potassium carbonate	Sigma-Aldrich	>99%
Potassium hydroxide	Honeywell	≥85%
Potassium permanganate	Sigma-Aldrich	>99%
Pyridine	Sigma-Aldrich	>99%
Pyridine-2,6-dicarboxylic acid	Acros Organics	99%
Ruthenium(III)acetylacetonate	abcr	99%
Sea Sand	Bernd Kraft	p.a.
Silver carbonate	ChemPUR Feinchemikalien	99.7%
Sodium acetate	Bernd Kraft	For analysis
Sodium carbonate	Thermo Scientific	99.5%
Sodium chloride	Sigma-Aldrich	>99%
Sodium hydroxide	Sigma-Aldrich	>99%
Sodium sulfate	Thermo Fisher Scientific	99%
Stearic acid	abcr	98%
Succinic anhydride	Tokyo Chemical Industry	>95%
Sulfuric acid	Sigma-Aldrich	98%
1,1,3,3-Tetramethylguanidine	Thermo Fisher Scientific	99%
Titanium(IV)isopropoxide	Sigma-Aldrich	97%
p-Toluenesulfonyl chloride	Sigma-Aldrich	≥99%
Triethylamine	Sigma-Aldrich	>99.5%

6.1.4 Kugelrohr distillation

Distillations of volumes smaller than 5 ml were performed with a Büchi Labortechnik Kugelrohr model B-585.

6.1.5 Addition of liquids with a syringe pump

The slow addition of liquids over time was performed with a Landgraf Laborsysteme syringe pump model LA-30.

6.1.6 Thin-Layer Chromatography (TLC)

Aluminum plates coated with fluorescent silica gel of the type F_{254} (Zn_2SiO_4 as fluorescent material) obtained by Sigma-Aldrich were used for TLC measurements. TLC plates with the applied samples were placed in a glass chamber filled with eluent (filling height ca. 0.5 cm). The plates were removed once the eluent front had reached a height of ~3 cm and cautiously dried with a heat gun. The compounds on the plates were visualized with either UV light (254 nm or 365 nm), potassium permanganate stain, Seebach stain, or bromocresol green stain. Note: Jork *et al*. published an extensive documentation about reagents and detection methods for thin-layer chromatography.[303]

The used staining solutions within this thesis were prepared as follows:

Permanganate solution: 1.5 g potassium permanganate, 10 g potassium carbonate, 1.25 ml sodium hydroxide solution (10 wt%), 200 ml water.

Seebach stain: 2.0 g cerium(IV)sulfate, 5.0 g phosphomolybdic acid, 16 ml sulfuric acid, 200 ml water.

Bromocresol green stain: 40 mg bromocresol green, 100 ml ethanol, addition of 0.1 M $NaOH_{(aq)}$ until a persistent blue color appears.

6.1.7 Flash column chromatography

The purification of compounds by flash column chromatography was conducted according to the publication of Still *et al*.[304] Silica gel, obtained from Sigma Aldrich, with a pore size of 60 Å, a mesh size of 230–240, and a particle size of 40–63 µm was used as stationary phase. A set of glass columns, with different diameters, with and without frits, and all fitted with Teflon stopcocks, was used. For columns without frits, a small plug of glass wool was placed in the tube connecting the stopcock to the column body and was subsequently covered by a small layer of sea sand (glowed and purified with hydrochloric acid). Columns were filled with a slurry of silica gel and eluent to a height of 20 cm unless stated otherwise. Liquid samples were applied using glass Pasteur pipettes. Solid samples were dissolved in a volatile solvent (e.g. dichloromethane) and the threefold amount of silica gel was added. The dry mixture of product and silica gel obtained after evaporation of the solvent was then applied on the column. The pressure for faster eluent flow was applied with a manual pump. After a successful purification the desired fractions were poured together, and the eluent was removed under reduced pressure to obtain the purified product.

6.2 Reaction monitoring and analytical methods

6.2.1 Infrared (IR) spectroscopy

Infrared spectra of all compounds were recorded on a Bruker Alpha Fourier transform infrared spectrometer with attenuated total reflection (ATR) technology in the range from 4000 cm^{-1} to 400 cm^{-1}. The resulting absorbance spectra are averaged over 24 scans per measurement. By convention, the signals are noted from large to small wavenumbers. Characterization of the absorption bands was done in dependence of the absorption strength with the following abbreviations: vs (very strong), s (strong), m (medium), w (weak), vw (very weak).

6.2.2 Nuclear Magnetic Resonance (NMR) spectroscopy

All NMR spectra were recorded on a Bruker Ascend™ 400 spectrometer and a Bruker Avance DRX spectrometer.

^{1}H NMR spectra were recorded either on a Bruker Ascend™ 400 spectrometer at 400 MHz with 16 scans and a delay time D_1 of 1 s at 298 K or on a Bruker Avance DRX spectrometer at 500 MHz with 16 scans and a delay time D_1 of 1 s at 298 K. The chemical shift δ is reported in parts per million and referenced to the solvent signal of DMSO-d_5 at 2.50 ppm, $CHCl_3$ at 7.26 ppm, or trifluoroacetic acid at 11.5 ppm. Additionally, gradient selected correlation spectroscopy (COSY) was carried out for signal assignment of protons. The following abbreviations are used to describe the proton splitting pattern: s = singlet, d = doublet, t = triplet, m = multiplet. All coupling constants J are given in Hz and decreasing order.

^{1}H NMR spectra of lignin samples were recorded on a Bruker Ascend™ 400 spectrometer at 400 MHz with 128 scans and a delay time D_1 of 5 s at 298 K.

^{13}C NMR spectra were recorded either on a Bruker Ascend™ 400 spectrometer at 101 MHz with 1024 scans and a delay time D_1 of 2 s at 298 K or on a Bruker Avance DRX spectrometer at 126 MHz with 1024 scans and a delay time D_1 of 2 s at 298 K. The chemical shift δ is reported in parts per million and referenced to the solvent signal of DMSO-d_6 at 39.52 ppm, $CDCl_3$ at 77.16 ppm, or trifluoroacetic acid-d at 164.2 ppm. Furthermore, phase-edited heteronuclear single quantum coherence ($HSQC_{ed}$) and heteronuclear multiple bond correlation (HMBC) spectroscopy were carried out for signal assignment of carbon atoms and structure elucidation. Signals of carbon atoms were specified as follows: C_q = quaternary carbon atom, CH, CH_2, or CH_3.

Quantitative ^{31}P NMR spectra were recorded on a Bruker Avance DRX spectrometer at 202 MHz with an inverse gated decoupling pulse program, 1024 scans and a delay time D_1 of 10 s at 298 K.

For sample preparation, 15 mg of analyte were dissolved in 500 µl of deuterated solvent. For lignin samples, 25 mg of analyte were dissolved in 550 µl of deuterated solvent.

6.2.3 Mass Spectrometry (MS)

Electrospray ionization (ESI) experiments were recorded on a Q Exactive Plus (Orbitrap) mass spectrometer (Thermo Fisher Scientific) equipped with a HESI II probe to record high

resolution. The spectra of most compounds were evaluated by molecular signals $[M]^+$, signals of protonated molecules $[M+H]^+$, signals of adducts such as $[M+Na]^+$ and characteristic fragment peaks and indicated with their mass-to-charge ratio (*m/z*). Moreover, spectra of carboxylic acids were evaluated by signals of deprotonated molecules $[M-H]^-$.

6.2.4 Melting point

The Melting point of diol **6** was recorded on a Stanford Research Systems OptiMelt – Automated Melting Point System with Digital Image Processing Technology. The measurement was performed from 25 °C to 200 °C with a heating rate of 10 K min^{-1}.

6.2.5 Gas Chromatography (GC)

Gas chromatography measurements were performed using an Agilent 8860 gas chromatography instrument with a HP-5 column (30 m × 0.32 mm × 0.25 µm) and a flame ionization detector (FID). If not stated otherwise, the measurements proceeded *via* the standard heating program, which starts at 95 °C, heats up to 200 °C with a rate of 15 K min^{-1}, retains 200°C for 4 min, heats to 300°C with a rate of 15 K min^{-1} and then retains 300 °C for 2 min. The injector transfer line temperature was set to 250 °C. Measurements were performed with a split ratio of 50:1 using nitrogen as make-up gas and helium as carrier gas with a flow rate of 1.0 ml min^{-1}.

For the sample preparation, 1.5–5.0 mg of analyte was dissolved in 1.5 ml of ethyl acetate. All samples were filtered by syringe filter (PTFE, 13 mm diameter, 0.2 µm pore size, Agilent) prior to use, to avoid plugging of the injection setup or the column.

6.2.6 Gas Chromatography-Mass Spectrometry (GC-MS)

Gas chromatography-mass spectrometry measurements were performed on a Varian 431 gas chromatography instrument with a HP-5 (30 m × 0.32 mm × 0.25 µm) column and a Varian 210 ion trap mass detector. Scans were performed from 40 to 650 m/z at a rate of 1.0 scan s^{-1}. The fatty acid composition of sunflower oils was determined *via* GC-MS with the following heating program that has been reported by Lee *et al*.:[305] Initial temperature at 100 °C for 1 min, heating to 195 °C with a rate of 15 K min^{-1}, heating to 210 °C with a rate of 1 K min^{-1}, heating to 240 °C with a rate of 10 K min^{-1}, retaining 240 °C for 10 min. The injector transfer line temperature was set to 250 °C. Measurements were performed with a split ratio of 50:1 using helium as carrier gas with a flow rate of 1.0 ml min^{-1}. For the sample preparation,

1.5−5.0 mg of analyte was dissolved in 1.5 ml of ethyl acetate. All samples were filtered by syringe filter (PTFE, 13 mm diameter, 0.2 µm pore size, Agilent) prior to use, to avoid plugging of the injection setup or the column.

6.2.7 Size Exclusion Chromatography (SEC)

SEC analyses were performed in one of the three following systems.

System I (Oligo THF SEC): A PSS SECcurity^2 SEC system based on Agilent Infinity 1260 II hardware was used for the measurements. The system is equipped with a refractive index detector SECcurity^2 RI, a column oven (Bio)SECcurity^2 column compartment TCC6500, a standard SECcurity^2 autosampler, and an isocratic pump SECcurity^2 isocratic pump. Anhydrous tetrahydrofuran stabilized with 250 ppm butylated hydroxytoluene (BHT, ≥99.9%) was used at a flow rate of 1.0 ml min^{-1} and at 30 °C as mobile phase. The analysis was performed on the following column system: PSS SDV analytical precolumn (3 µm, 8 mm × 50 mm) with two PSS SDV analytical columns (3 µm, 8 mm × 300 mm, 1000 Å). For the calibration, narrow linear poly(methyl methacrylate) standards (Polymer Standards Service, PSS, Germany) ranging from 102 to 62200 Da were used.

System II (Poly THF SEC): A Shimadzu Size Exclusion Chromatography system equipped with a Shimadzu isocratic pump model LC-20AD, a Shimadzu autosampler model SIL-20A, and a Shimadzu refractive index detector model RID-20A was used for the measurements. A mixture of anhydrous tetrahydrofuran stabilized with 250 ppm butylated hydroxytoluene (BHT, ≥99.9%) and triethylamine (2 vol% of THF) was used at a flow rate of 1.0 ml min^{-1} and at 30 °C as mobile phase. The analysis was performed on the following column system: PSS SDV analytical precolumn (5 µm, 8 mm × 50 mm), PSS SDV analytical column (5 µm, 8 mm × 300 mm, 1000 Å), and a PSS SDV analytical column (5 µm, 8 mm × 300 mm, 100000 Å). For the calibration, narrow linear poly(methyl methacrylate) standards (Polymer Standards Service, PSS, Germany) ranging from 1100 to 981000 Da were used.

System III (DMAc SEC): A PSS SECcurity^2 SEC system based on Agilent Infinity 1260 II hardware was used for the measurements. The system is equipped with a refractive index detector. DMAc with 0.03 wt% lithium bromide was used at a flow rate of 1.0 ml min^{-1} and at 35 °C as mobile phase. The analysis was performed on the following column system: Agilent Mixed-C column and Agilent Mixed-E column. For the calibration, polystyrene standards ranging from 370 to 2520000 Da were used.

For sample preparation, 2.00 mg of analyte was dissolved in 1.50 ml of solvent/solvent mixture used in the respective SEC system. All samples were filtered by syringe filter (PTFE, 13 mm diameter, 0.2 µm pore size, Agilent) prior to use, to avoid plugging of the injection setup or the column.

6.2.8 Differential Scanning Calorimetry (DSC)

DSC measurements were recorded either on a Mettler Toledo DSC3 STAR^e system or on a 214 Polyma DSC device from NETZSCH (Selb, Germany). All experiments were carried out under nitrogen atmosphere using 40 µl aluminum crucibles and a sample mass of 4−7 mg. Physical changes (T_g) and phase transitions (T_{cc}, T_m) were determined from the second heating run to eliminate possible interference from the polymer's thermal history.

Mettler Toledo DSC3 STAR^e system: The samples were measured using the following program: first heating from 25 °C to 250 °C, then cooling from 250 °C to −70 °C and a final heating step from −70 °C to 250 °C with a heating/cooling rate of 10 K min^{-1}.

214 Polyma: The samples were measured using the following program: first heating from −150 °C to 200 °C, then cooling from 200 °C to −150 °C and a final heating step from −150 °C to 200 °C with a heating/cooling rate of 10 K min^{-1}.

6.2.9 Thermogravimetric Analysis (TGA)

TGA measurements were performed on a TA Instruments TGA 5500 under a nitrogen atmosphere using platinum TGA sample pans and a heating rate of 10 K min^{-1} over a temperature range from 25 °C to 600 °C. $T_{d,5\%}$ is defined as the temperature of 5% weight loss.

6.2.10 Tensile strength measurements

Tensile strength measurements were performed on an Inspect table 10kN from Hegewald & Peschke equipped with a 1.5 kN load cell. Tensile strength measurements and adhesive tests were performed with an elongation of 5 mm min^{-1} and 1 mm min^{-1}, respectively.

6.3 Palladium catalyzed dehydrogenation of lauric acid

6.3.1 Ligand Synthesis

2-(6-bromopyridin-2-yl)quinoline:

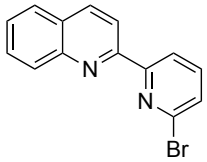

$C_{14}H_9BrN_2$
M = 285.14 g/mol

Freshly bought *o*-aminobenzaldehyd (9.50 g, 78.4 mmol, 1.00 equiv.) was dissolved in ethanol (600 ml). Then, 1-(6-bromopyridin-2-yl)ethan-1-one (15.7 g, 78.4 mmol, 1.00 equiv.) and potassium hydroxide (2.64 g, 47.1 mmol, 0.60 equiv.) were added. The reaction mixture was stirred at 85 °C for 12 h. After cooling to room temperature, the yellow suspension was filtrated to obtain the product as a beige solid (18.8 g, 65.9 mmol, 84%).

^{1}H NMR (400 MHz, $CDCl_3$, ppm): δ = 8.65 (dd, J = 7.8, 0.9 Hz, 1H), 8.51 (d, J = 8.6 Hz, 1H), 8.31 (d, J = 8.6 Hz, 1H), 8.22−8.11 (m, 1H), 7.89 (dd, J = 8.2, 1.5 Hz, 1H), 7.80−7.66 (m, 2H), 7.66−7.46 (m, 2H).

^{13}C NMR (101 MHz, $CDCl_3$, ppm): δ = 158.0, 155.0, 148.4, 142.0, 140.0, 137.5, 130.3, 130.3, 129.0, 128.9, 128.2, 127.7, 120.9, 119.2, 54.3.

IR (ATR, cm^{-1}): $\tilde{\nu}$ = 1595 (m), 1579 (w), 1543 (m), 1503 (m), 1465 (w), 1434 (m), 1421 (m), 1398 (m), 1377 (w), 1350 (w), 1332 (m), 1319 (m), 1296 (m), 1239 (w), 1211 (w), 1154 (m), 1146 (w), 1118 (s), 1079 (w), 1067 (m), 1011 (w), 986 (s), 955 (w), 943 (m), 915 (w), 871 (m), 844 (vs), 802 (vs), 783 (vs), 771 (m), 747 (s), 728 (vs), 684 (m), 650 (s), 622 (m), 569 (w), 482 (w), 470 (m), 394 (w).

ESI-MS ($[M+H]^+$, $C_{14}H_{10}BrN_2$) calcd.: 285.0022; found: 285.0019.

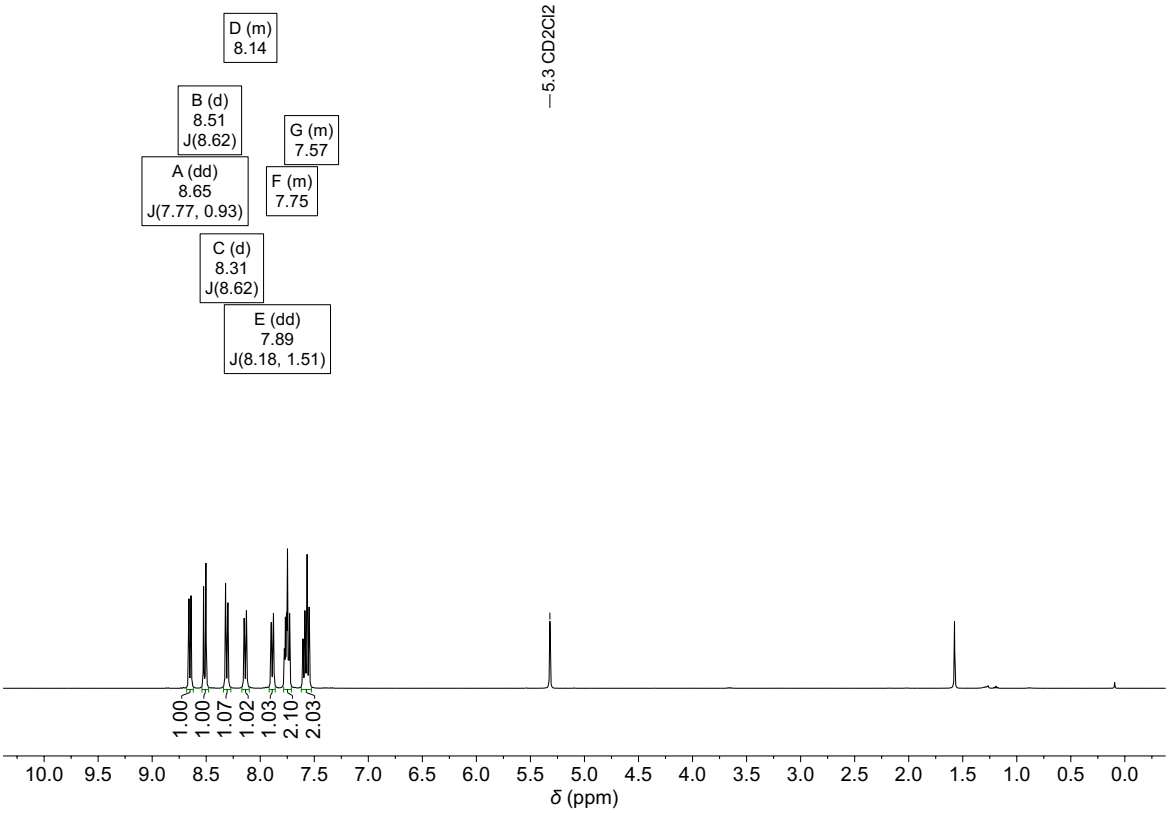

Figure 6.1: ^{1}H NMR spectrum of 2-(6-bromopyridin-2-yl)quinoline in $CDCl_3$.

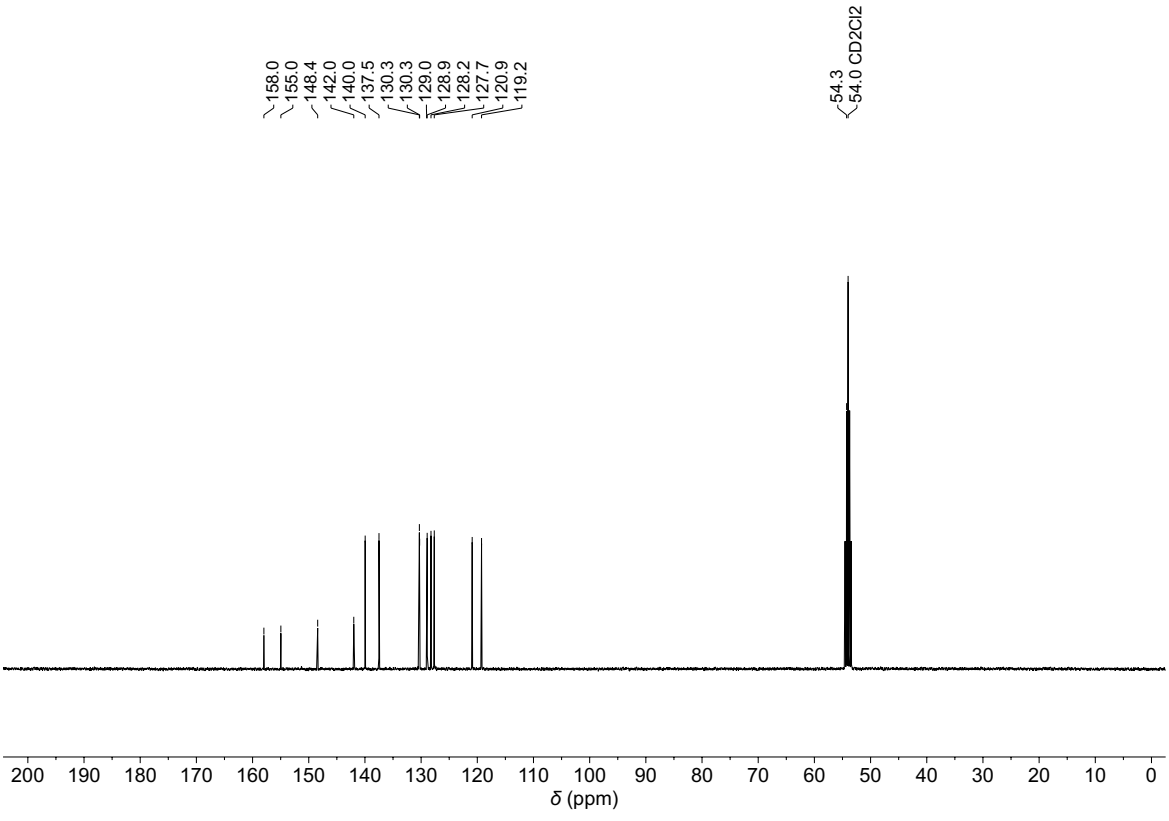

Figure 6.2: ^{13}C NMR spectrum of 2-(6-bromopyridin-2-yl)quinoline in $CDCl_3$.

6-(quinolin-2-yl)pyridin-2(1*H*)-one:

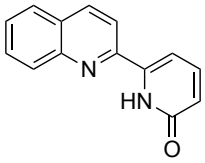

$C_{14}H_{10}N_2O$
M = 222.25 g/mol

A mixture of 2-(6-bromopyridin-2-yl)quinoline (2.00 g, 7.00 mmol, 1.00 equiv.), 4-methoxybenzyl alcohol (98%, 887 µl, 987 mg, 7.00 mmol, 1.00 equiv.), potassium hydroxide (471 mg, 8.40 mmol, 1.2 equiv), 18-crown-6 (185 mg, 700 µmol, 0.10 equiv.) and toluene (35 ml) was stirred at 100 °C for 12 hours. After cooling to room temperature, the solvent was removed under reduced pressure before dichloromethane (70.0 ml) was added. The organic layer was washed with saturated sodium chloride solution (2 × 30 ml), dried over sodium sulfate, and filtered. The dichloromethane solution was then transferred into a flask and trifluoroacetic acid (700 µl, 9.10 mmol, 1.30 equiv.) was added. The mixture was stirred at room temperature for 1 hour before saturated sodium hydrogencarbonate solution (40.0 ml) was added. The mixture was extracted with chloroform (3 × 40 ml). The combined organic layers were dried over sodium sulfate, filtered and the solvent was removed under reduced pressure. The ligand was purified by flash chromatography (ethyl acetate/methanol, 20:1) to obtain a pale-yellow compound (1.05 g, 4.73 mmol, 67%).

R_f (dichloromethane/methanol, 99:1): 0.21.

^{1}H NMR (400 MHz, $CDCl_3$, ppm): δ = 10.80 (s, 1H), 8.29 (d, J = 8.7 Hz, 1H), 8.18−8.04 (m, 1H), 7.94−7.84 (m, 2H), 7.78 (ddd, J = 8.4, 6.8, 1.5 Hz, 1H), 7.61 (ddd, J = 8.1, 6.8, 1.2 Hz, 1H), 7.52 (dd, J = 9.2, 6.9 Hz, 1H), 6.94 (dd, J = 6.9, 0.9 Hz, 1H), 6.60 (dd, J = 9.1, 0.9 Hz, 1H).

^{13}C NMR (101 MHz, $CDCl_3$, ppm): δ = 162.9, 148.0, 147.6, 142.3, 140.9, 138.2, 131.1, 129.9, 128.8, 128.2, 128.2, 123.3, 117.4, 104.5.

IR (ATR, cm^{-1}): $\tilde{\nu}$ = 1642 (vs), 1604 (s), 1587 (vs), 1558 (s), 1504 (s), 1449 (m), 1425 (w), 1409 (w), 1290 (w), 1231 (w), 1179 (w), 1169 (w), 1145 (w), 992 (m), 943 (w), 836 (w), 813 (vs), 802 (vs), 779 (m), 764 (s), 752 (vs), 714 (s), 677 (w), 616 (w), 578 (w), 568 (w), 551 (s), 538 (w), 521 (w), 506 (w), 476 (w), 449 (w), 438 (w).

ESI-MS ($[M+H]^+$, $C_{14}H_{11}N_2O$) calcd.: 223.0866; found: 223.0866.

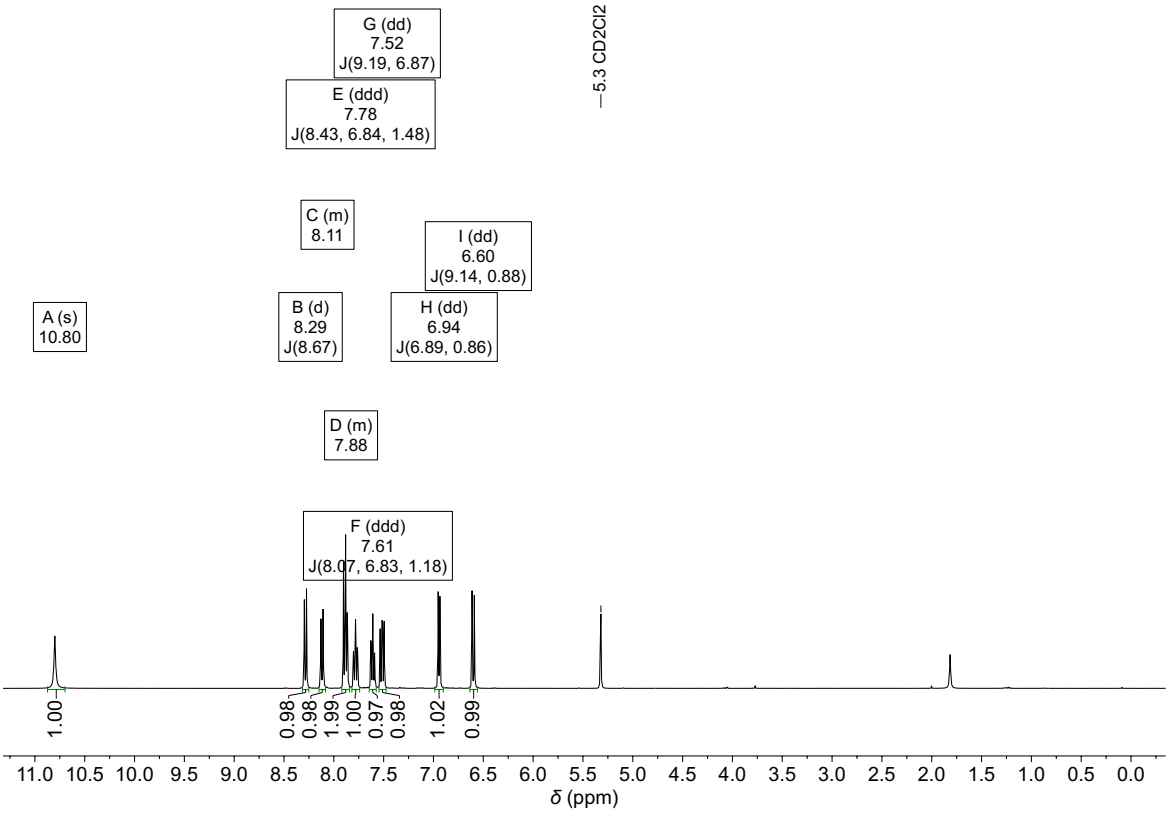

Figure 6.3: ^{1}H NMR spectrum of 6-(quinolin-2-yl)pyridin-2(1*H*)-one in $CDCl_3$.

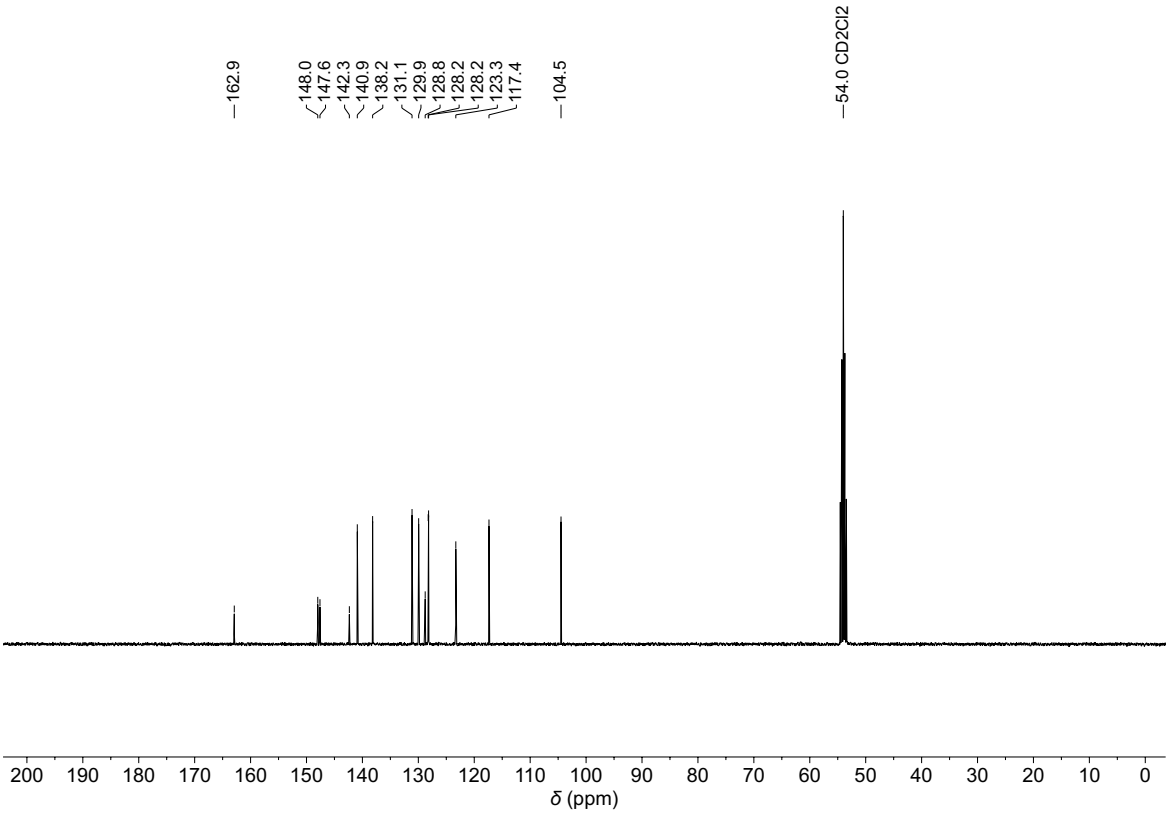

Figure 6.4: ^{13}C NMR spectrum of 6-(quinolin-2-yl)pyridin-2(1*H*)-one in $CDCl_3$.

6.3.2 Dehydrogenation with silver carbonate as oxidant

Five palladium catalyzed dehydrogenations with silver carbonate as oxidant were performed with octanoic acid, lauric acid, myristic acid, palmitic acid, and stearic acid.[187] The ^{1}H NMR spectra after work-up of these five reactions are depicted in Figure 6.5−Figure 6.9.

General procedure:[187]

The carboxylic acid (i.e., octanoic, lauric, myristic, palmitic, or stearic acid) (700 µmol, 1.00 equiv.), silver carbonate (386 mg, 1.40 mmol, 2.00 equiv.), lithium carbonate (103 mg, 1.40 mmol, 2.00 equiv.), and sodium acetate (28.7 mg, 350 µmol, 0.50 equiv.) were weighed into a 10 ml screw-cap vial. A solution of palladium(II)acetate (6.29 mg, 28.0 µmol, 4.00 mol%) and 6-(quinolin-2-yl)pyridin-2(1*H*)-one (6.85 mg, 30.8 µmol, 4.40 mol%) in 1,4-dioxane (1.40 ml) was premixed and added to the tube. Then, *tert*-amyl alcohol (5.60 ml) was added, and the tube was briefly flushed with argon and the vial was capped. The reaction mixture was then stirred at the rate of 300 rpm at 100 °C for 16 h. After cooling to room temperature, the mixture was acidified with formic acid (158 µl, 4.20 mmol, 6.00 equiv.). The mixture was passed through a pad of Celite with a solvent mixture (methanol/formic acid/dichloromethane = 5:5:90) as the eluent to remove any insoluble precipitate. The solvent of the filtrate was removed under reduced pressure and a ^{1}H NMR spectrum was measured in $CDCl_3$.

Dehydrogenation of octanoic acid (C_8):

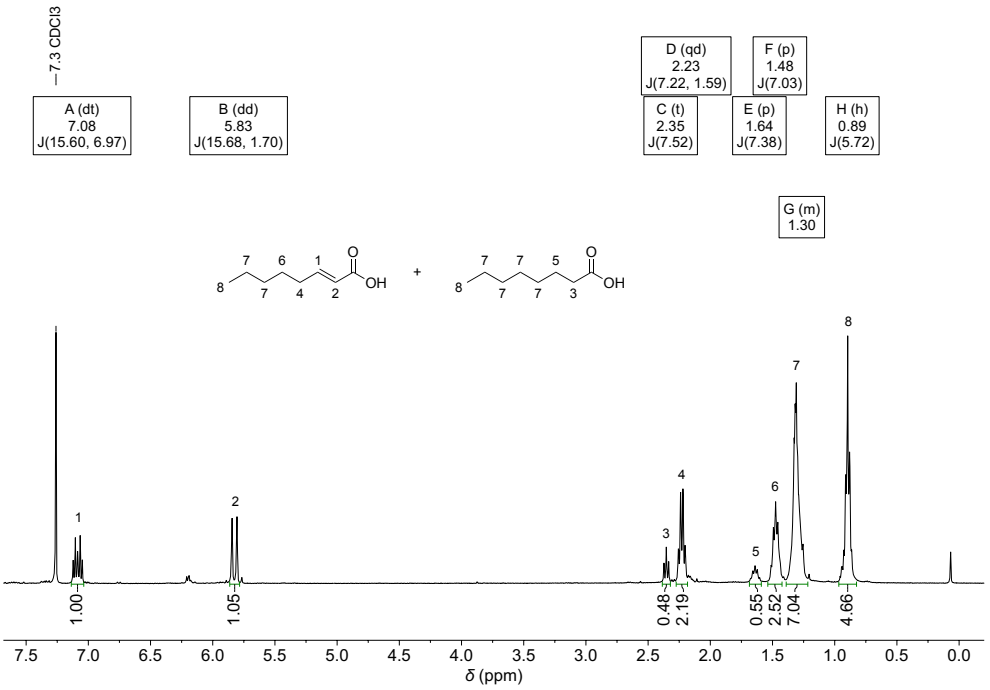

Figure 6.5: ^{1}H NMR spectrum of the dehydrogenation of octanoic acid with silver carbonate as oxidant.

Dehydrogenation of lauric acid (C_{12}):

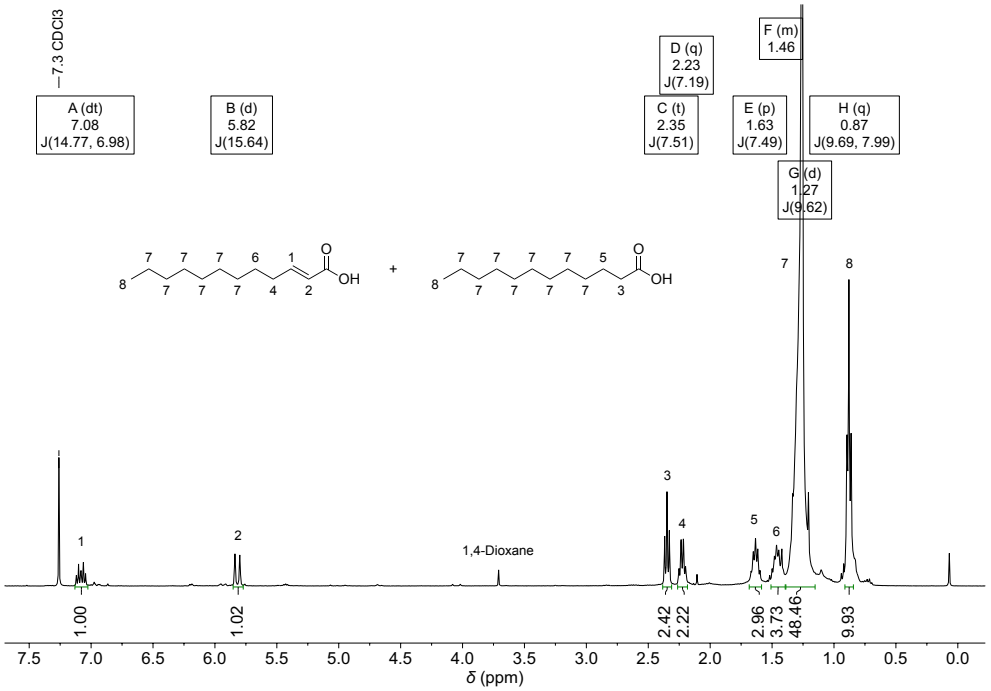

Figure 6.6: ^{1}H NMR spectrum of the dehydrogenation of lauric acid with silver carbonate as oxidant.

Dehydrogenation of myristic acid (C_{14}):

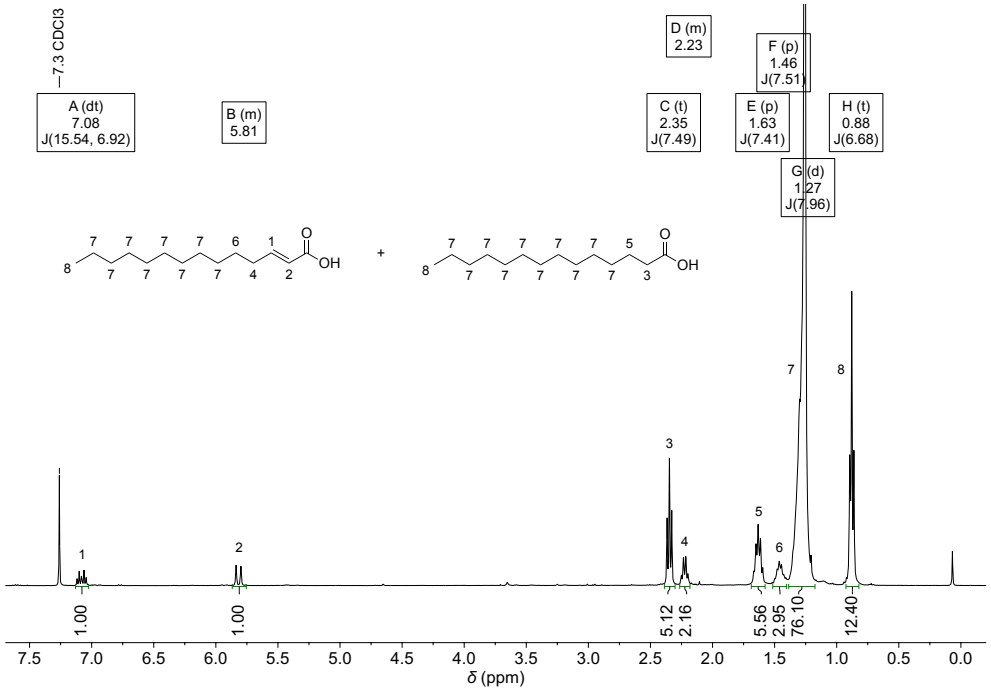

Figure 6.7: ^{1}H NMR spectrum of the dehydrogenation of myristic acid with silver carbonate as oxidant.

Dehydrogenation of palmitic acid (C_{16}):

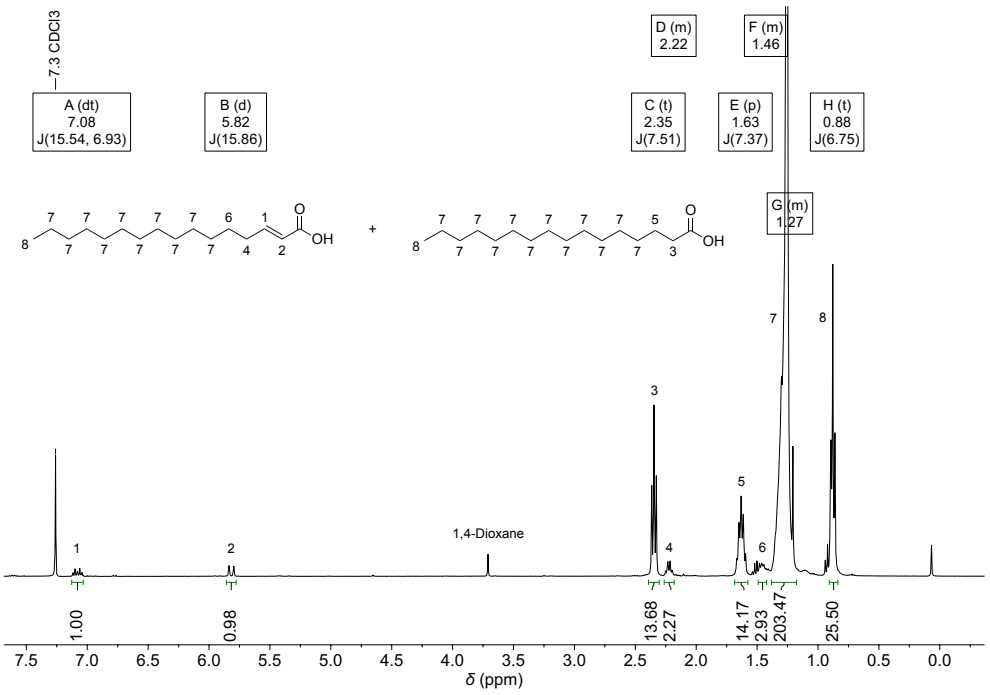

Figure 6.8: ^{1}H NMR spectrum of the dehydrogenation of palmitic acid with silver carbonate as oxidant.

Dehydrogenation of stearic acid (C_{18}):

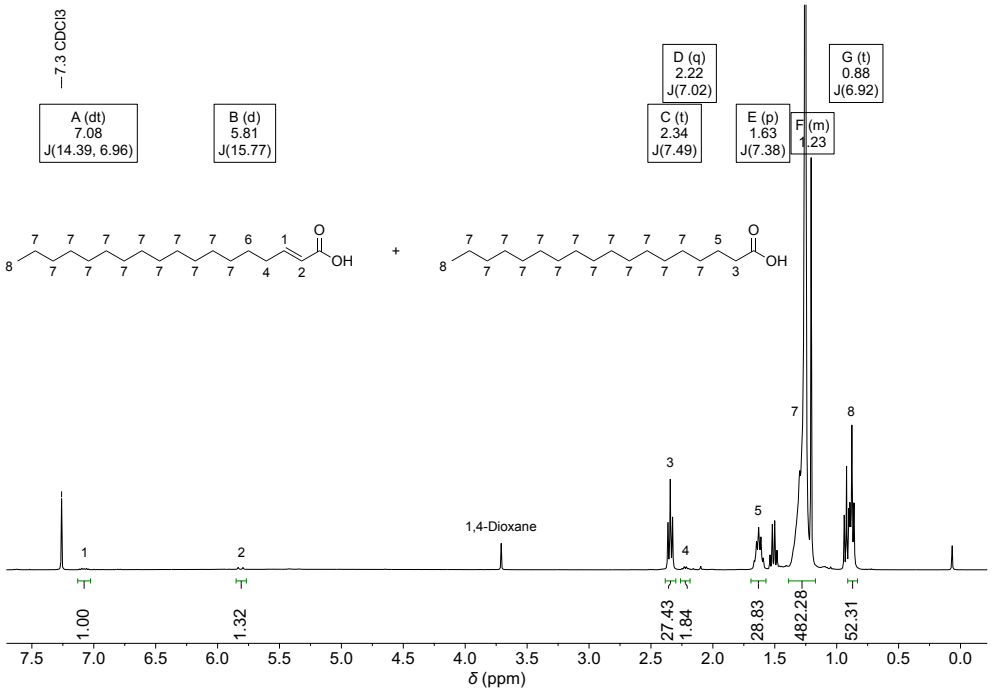

Figure 6.9: ^{1}H NMR spectrum of the dehydrogenation of stearic acid with silver carbonate as oxidant.

6.3.3 Optimization of lauric acid dehydrogenation

The palladium catalyzed dehydrogenation procedure from Yu *et al*. was optimized for lauric acid and included molecular oxygen as oxidant and the solvents *tert*-butanol and water.[187]

General procedure:

Lauric acid (100 mg, 500 µmol, 1.00 equiv.) and the respective base (Table 6.3) were dissolved in a mixture of *tert*-butanol and water (10 ml, 1:1). Palladium(II)acetate (4.49 mg, 20.0 µmol, 4.00 mol%) and 6-(quinolin-2-yl)pyridin-2(1*H*)-one (4.89 mg, 22.0 µmol, 4.40 mol%) were added and the mixture was stirred at 60 °C until all compounds dissolved. Then, the solution was added to a 50 ml PTFE Inlet of a pressure reactor. The pressure reactor was sealed, and the reaction mixture was stirred at the rate of 600 rpm at the respective temperature (Table 6.3) under pure oxygen atmosphere (10 bar) for 24 h. After cooling to room temperature, the mixture was acidified with formic acid (57.2 µl, 1.50 mmol, 3.00 equiv.) and diluted with water (10 ml). The reaction mixture was extracted with dichloromethane (3 × 15 ml). The combined organic layers were washed with saturated sodium chloride solution (2 × 10 ml), dried over sodium sulfate, filtered, and the solvent was removed under reduced pressure. A ^{1}H NMR spectrum was measured in $CDCl_3$ after the addition of dibromomethane (9.00 µl, 22.3 mg, 128 µmol, 0.26 equiv.) as external standard to determine the reaction yield (see Figure 6.10 for exemplary ^{1}H NMR spectrum).

Table 6.3: Optimization of the palladium catalyzed dehydrogenation of lauric acid with molecular oxygen. Reaction conditions were the following unless stated otherwise: 10 bar O_2, 4.0 mol% $Pd(OAc)_2$, 4.4 mol% ligand, 24 h of reaction time, concentration of 50 mmol l^{-1} in mixture of *tert*-butanol and water (1:1). Notes: [a]Reaction time of 72 h; [b]Double the amount of catalyst and ligand were used; [c]Four times the amount of catalyst and ligand were used; [d]Solvent-free; [e]Octanoic acid was used instead of lauric acid.

Entry	Base		Temperature	NMR-Yield with CH_2Br_2 as external standard / %
	Base	Equiv.		
1	Li_2CO_3	1.00	100 °C	17.6
2	Na_2CO_3	1.00	100 °C	18.0
3	Na_2CO_3	1.25	100 °C	19.3
4	Na_2CO_3	1.50	100 °C	7.2
5	Na_2CO_3	2.00	100 °C	6.2
6	K_2CO_3	1.00	100 °C	24.6
7	Cs_2CO_3	1.00	100 °C	32.4
8	Cs_2CO_3	1.00	90 °C	16.1
9	Cs_2CO_3	1.00	115 °C	19.5
10	Cs_2CO_3	1.00	130 °C	0.9
11[a]	Cs_2CO_3	1.00	100 °C	37.9
12[b]	Cs_2CO_3	1.00	100 °C	58.8
13[c]	Cs_2CO_3	1.00	100 °C	80.3
14[d]	–	–	100 °C	38.3
15[d,b]	–	–	100 °C	26.5
16[d,e]	–	–	100 °C	46.0

Exemplary ^{1}H NMR spectrum of the dehydrogenation at 100 °C:

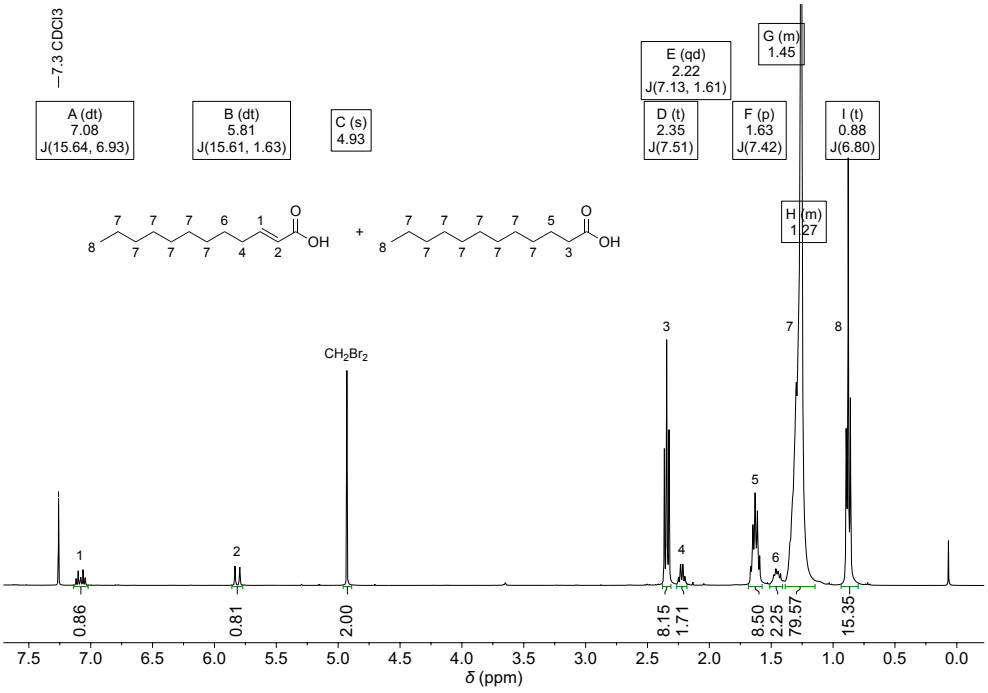

Figure 6.10: ^{1}H NMR spectrum of dehydrogenation of lauric acid after addition of dibromomethane as external standard. Used conditions are: ^{t}BuOH/H_2O, 1:1; 1.00 equiv. Na_2CO_3; 100 °C; 24 h.

Exemplary ^{1}H NMR spectrum of side product formation at 115 °C:

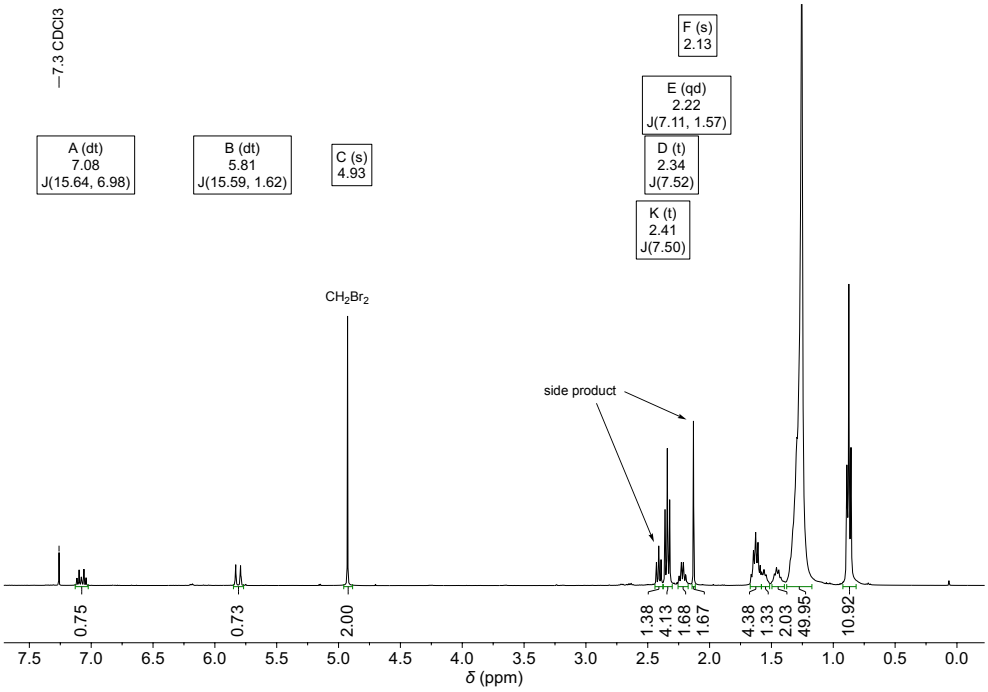

Figure 6.11: ^{1}H NMR spectrum of dehydrogenation of lauric acid after addition of dibromomethane as external standard. Used conditions are: ^{t}BuOH/H_2O, 1:1; 1.00 equiv. Na_2CO_3; 115 °C; 24 h.

6.4 Synthesis of *α,β*-unsaturated methyl laurate in large scale

6.4.1 Dehydrogenation of lauric acid

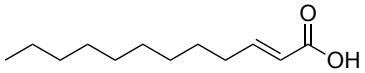

$C_{12}H_{22}O_2$
M = 198.31 g/mol

Lauric acid (40.1 g, 200 mmol, 1.00 equiv.), palladium(II) acetate (1.80 g, 8.00 mmol, 4.00 mol%), and 6-(quinolin-2-yl)pyridin-2(1*H*)-one (1.96 g, 8.80 mmol, 4.40 mol%) were added into a 150 ml PTFE inlet of a pressure reactor. The pressure reactor was sealed, and the reaction mixture was stirred at the rate of 600 rpm at 100 °C under pure oxygen atmosphere (10 bar) for 24 h. The reaction mixture was distilled *in vacuo* in a Kugelrohr oven (150 °C, 0.1 mbar) to obtain a mixture of lauric acid and *α,β*-unsaturated lauric acid in a ratio of 60:40, as determined by ^{1}H NMR spectroscopy (38.6 g, 195 mmol, 97%) (Figure 6.12).

^{1}H NMR (400 MHz, $CDCl_3$, ppm): δ = 7.08 (dt, J = 15.7, 7.0 Hz, 1H, H^1), 5.82 (dt, J = 15.6, 1.6 Hz, 1H, H^2), 2.35 (t, J = 7.5 Hz, 3H, H^3), 2.23 (qd, J = 7.1, 1.6 Hz, 2H, H^4), 1.62 (q, J = 7.3 Hz, 3H, H^5), 1.51−1.40 (m, 2H, H^6), 1.28 (d, J = 16.2 Hz, 40H, H^7), 0.88 (t, J = 6.8 Hz, 8H).

^{13}C NMR (101 MHz, $CDCl_3$, ppm): δ = 180.5 (C_q, $C_{SaturatedCOOH,}$ C^1), 172.3 (C_q, $C_{UnsaturatedCOOH,}$ C^2), 152.7 (CH, $C_{DoubleBond}$, C^3), 120.7 (CH, $C_{DoubleBond}$, C^4), 34.2 (CH_2, C^5), 32.5 (CH_2, C^6), 32.1 (CH_2, C^6), 32.0 (CH_2, C^6), 29.7 (CH_2, C^6), 29.6 (CH_2, C^6), 29.6 (CH_2, C^6), 29.5 (CH_2, C^6), 29.5 (CH_2, C^6), 29.4 (CH_2, C^6), 29.4 (CH_2, C^6), 29.3 (CH_2, C^6), 29.2 (CH_2, C^6), 28.0 (CH_2, C^6), 24.8 (CH_2, C^6), 22.8 (CH_2, C^6), 22.8 (CH_2, C^6), 14.3 (CH_3, C^7), 14.2 (CH_3, C^7).

IR (ATR, cm^{-1}): $\tilde{\nu}$ = 2953 (w), 2919 (s), 2870 (w), 2851 (m), 1696 (vs), 1652 (w), 1466 (w), 1419 (w), 1302 (w), 1282 (m), 1247 (w), 1220 (w), 1194 (w), 980 (w), 932 (w), 890 (w), 722 (w), 686 (w).

ESI-MS ($[M-H]^-$, $C_{12}H_{21}O_2$, *α,β*-unsaturated lauric acid) calcd.: 197.1547; found: 197.1535.

ESI-MS ($[M-H]^-$, $C_{12}H_{23}O_2$, lauric acid) calcd.: 199.1704; found: 199.1690.

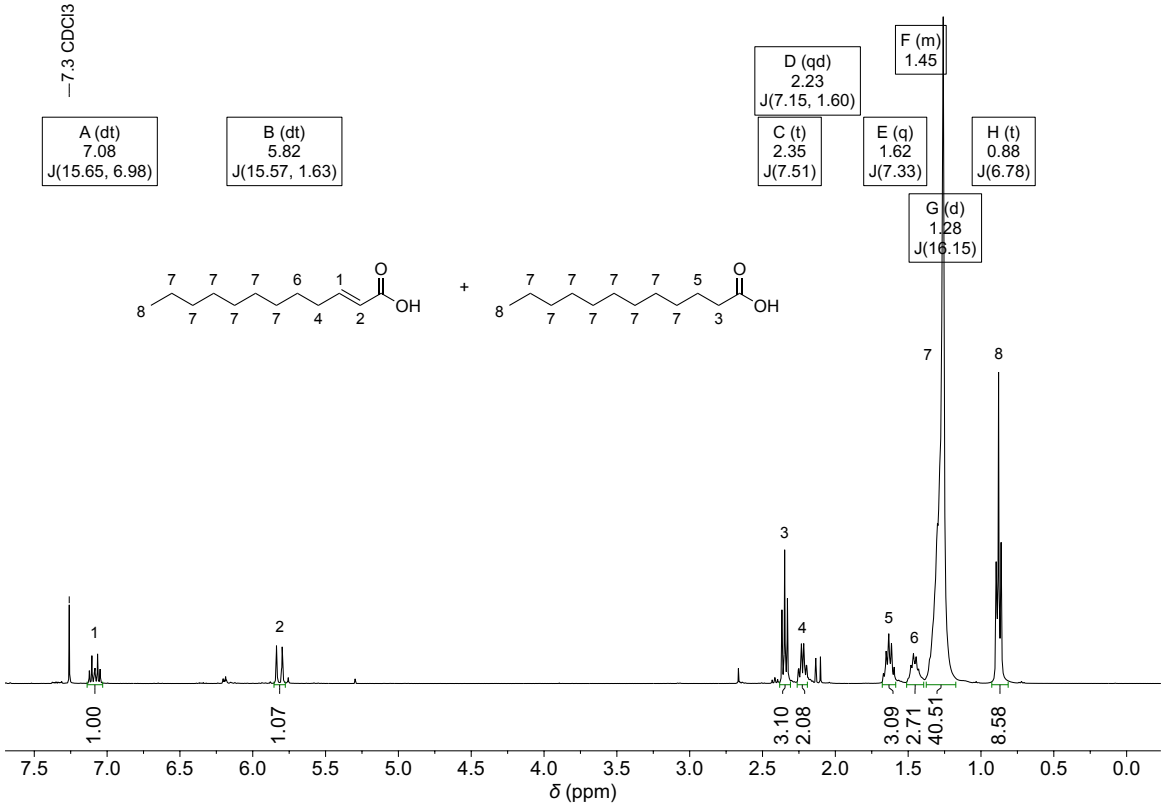

Figure 6.12: ^{1}H NMR spectrum of mixture of lauric acid and α,β-unsaturated lauric acid in $CDCl_3$.

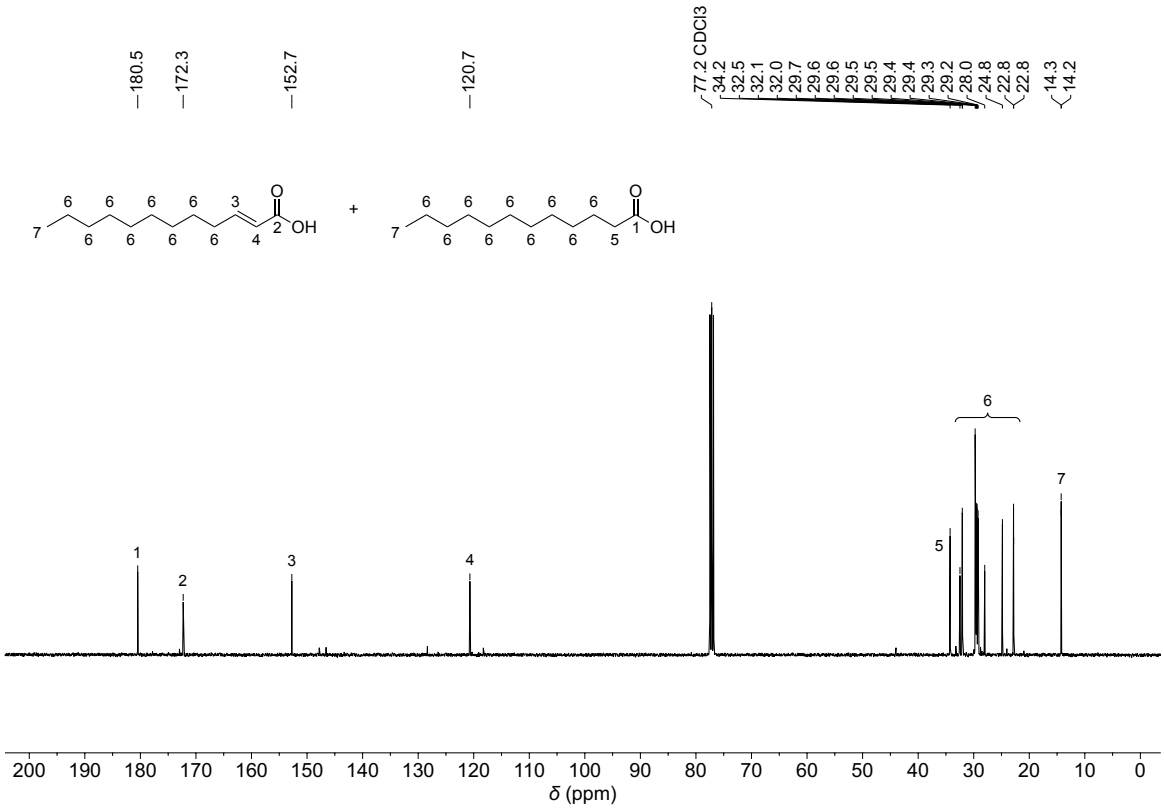

Figure 6.13: ^{13}C NMR spectrum of mixture of lauric acid and α,β-unsaturated lauric acid in $CDCl_3$.

6.4.2 Esterification of *α,β*-unsaturated lauric acid with methanol

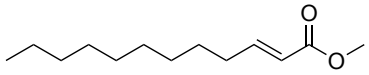

$C_{13}H_{24}O_2$
M = 212.33 g/mol

The mixture of lauric acid and *α,β*-unsaturated lauric acid (38.5 g, 194 mmol, 1.00 equiv.), methanol (315 ml, 7.77 mol, 40.0 equiv.), and sulfuric acid (96%, 1.08 ml, 19.4 mmol, 10 mol%) were added into a 500 ml round bottom flask. The reaction solution was stirred at 65 °C for 4 h. After cooling to room temperature, the solvent methanol was removed under reduced pressure. The residue was diluted with ethyl acetate (200 ml) and washed with water (2 × 100 ml) and saturated sodium chloride solution (100 ml). The organic phase was dried over sodium sulfate, filtered, and the solvent was removed under reduced pressure to obtain a mixture of methyl laurate and *α,β*-unsaturated methyl laurate in a ratio of 60:40, as determined by ^{1}H NMR spectroscopy (39.1 g, 184 mmol, 95%) (Figure 6.14).

^{1}H NMR (400 MHz, $CDCl_3$, ppm): δ = 6.97 (dt, J = 15.7, 7.0 Hz, 1H, H^1), 5.81 (dt, J = 15.6, 1.6 Hz, 1H, H^2), 3.72 (s, 3H, H^3), 3.66 (s, 4H, H^4), 2.29 (t, J = 7.5 Hz, 3H, H^5), 2.19 (qd, J = 7.2, 1.6 Hz, 2H, H^6), 1.61 (p, J = 7.3 Hz, 3H, H^7), 1.43 (q, J = 7.1 Hz, 2H, H^8), 1.26 (d, J = 7.9 Hz, 41H, H^9), 0.87 (t, J = 6.8 Hz, 9H, H^{10}).

^{13}C NMR (101 MHz, $CDCl_3$, ppm): δ = 174.5 (Cq, $C_{SaturatedEster}$, C^1), 167.4 (Cq, $C_{UnsaturatedEster}$, C^2), 150.0 (CH, $C_{DoubleBond}$, C^3), 120.9 (CH, $C_{DoubleBond}$, C^4), 51.6 (CH_3, C_{Ester}, C^5), 51.5 (CH_3, C_{Ester}, C^5), 34.3 (CH_2, C^6), 32.4 (CH_2, C^7), 32.0 (CH_2, C^7), 32.0 (CH_2, C^7), 29.7 (CH_2, C^7), 29.6 (CH_2, C^7), 29.6 (CH_2, C^7), 29.5 (CH_2, C^7), 29.5 (CH_2, C^7), 29.4 (CH_2, C^7), 29.4 (CH_2, C^7), 29.3 (CH_2, C^7), 29.3 (CH_2, C^7), 28.2 (CH_2, C^7), 25.1 (CH_2, C^7), 22.8 (CH_2, C^7), 22.8 (CH_2, C^7), 14.2 (CH_3, C^8).

IR (ATR, cm^{-1}): $\tilde{\nu}$ = 2952 (w), 2924 (vs), 2854 (s), 1741 (vs), 1727 (vs), 1657 (w), 1646 (vw), 1459 (w), 1435 (m), 1377 (w), 1341 (w), 1312 (w), 1266 (m), 1238 (w), 1196 (s), 1170 (vs), 1126 (w), 1075 (vw), 1041 (w), 1000 (w), 983 (w), 877 (vw), 850 (vw), 721 (w).

ESI-MS ($[M+H]^+$, $C_{13}H_{25}O_2$, *α,β*-unsaturated methyl laurate) calcd.: 213.1849;
found: 213.1849.

ESI-MS ($[M+H]^+$, $C_{13}H_{27}O_2$, methyl laurate) calcd.: 215.2006; found: 215.2001.

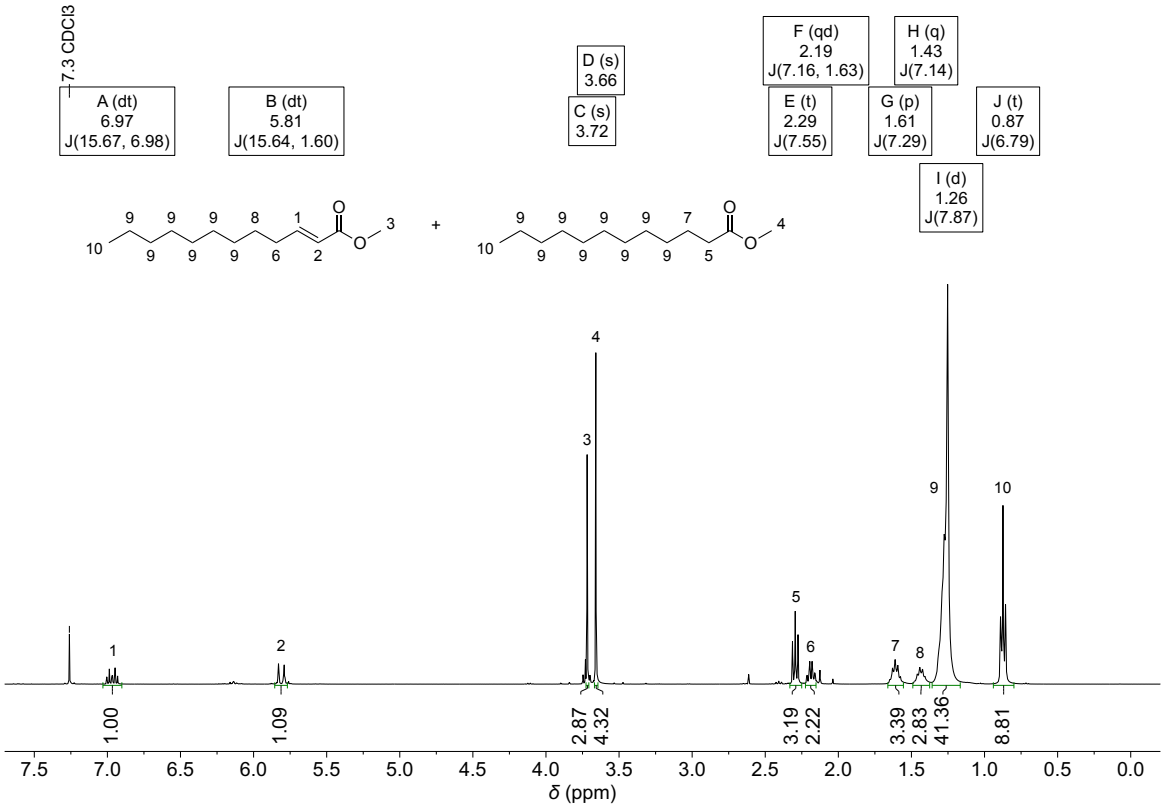

Figure 6.14: ^{1}H NMR spectrum of mixture of methyl laurate and *α*,*β*-unsaturated methyl laurate in $CDCl_3$.

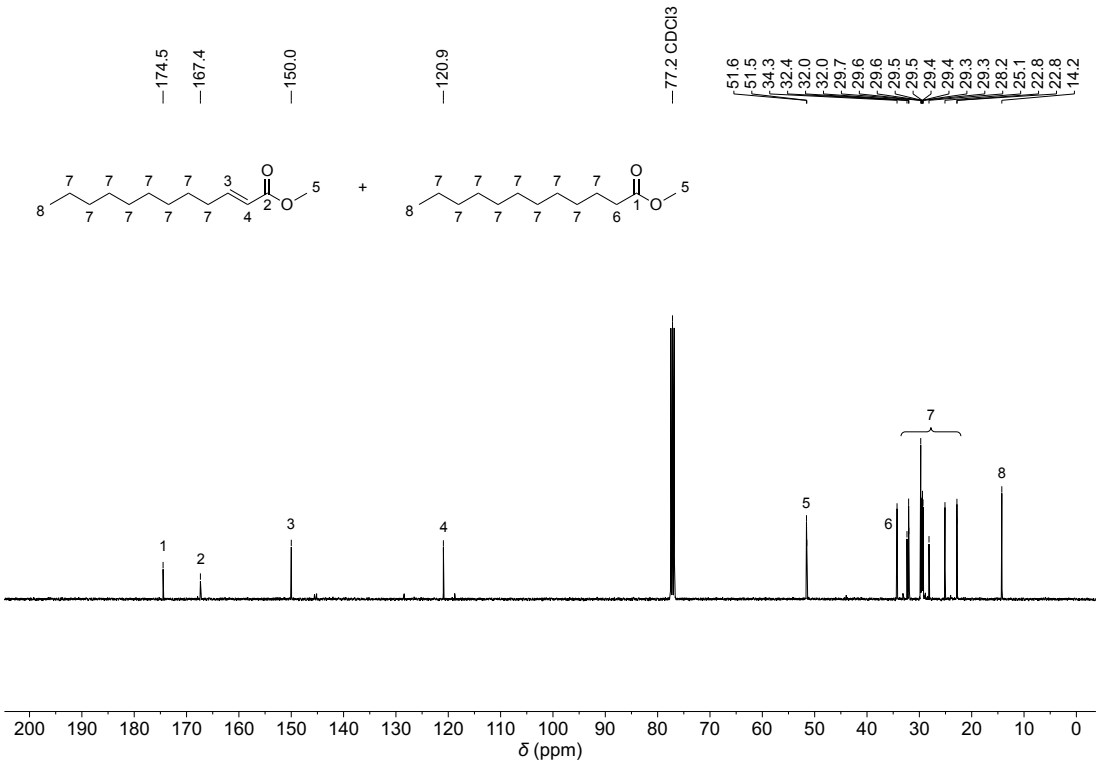

Figure 6.15: ^{13}C NMR spectrum of mixture of methyl laurate and *α*,*β*-unsaturated methyl laurate in $CDCl_3$.

6.5 Thia-Michael additions to *α,β*-unsaturated methyl esters

6.5.1 Optimization of thia-Michael addition

General procedure:

A mixture of methyl crotonate (98%, 511 mg, 5.00 mmol, 1.00 equiv.) 1,4-butanedithiol (97%, 309 mg, 2.50 mmol, 0.50 equiv.), and the respective catalyst (Table 6.4) was stirred in a 10 ml screw-cap vial at either room temperature or 90 °C. ^{1}H NMR spectra of the reaction mixture were measured after certain time intervals in $CDCl_3$ to monitor the conversion of methyl crotonate (Table 6.4, see Figure 6.16 and Figure 6.17 for exemplary ^{1}H NMR spectra).

Table 6.4: Optimization of thia-Michael addition of 1,4-butanedithiol to methyl crotonate. Note: [a]Reaction was performed at 90 °C.

Entry	Catalyst	Time	Methyl crotonate : product ratio determined by ^{1}H NMR spectroscopy
1	10 mol% NEt_3	24 h	71:29
2[a]	10 mol% NEt_3	24 h	47:53
3	10 mol% DBN	1 h	0:100
4	1 mol% DBN	1 h	26:74
		20 h	14:86
5	1 mol% DBU	2 h	02:98
6	1 mol% TMG	2 h	03:97

Thia-Michael addition of 1,4-butanedithiol to methyl crotonate with 10 mol% of NEt_3:

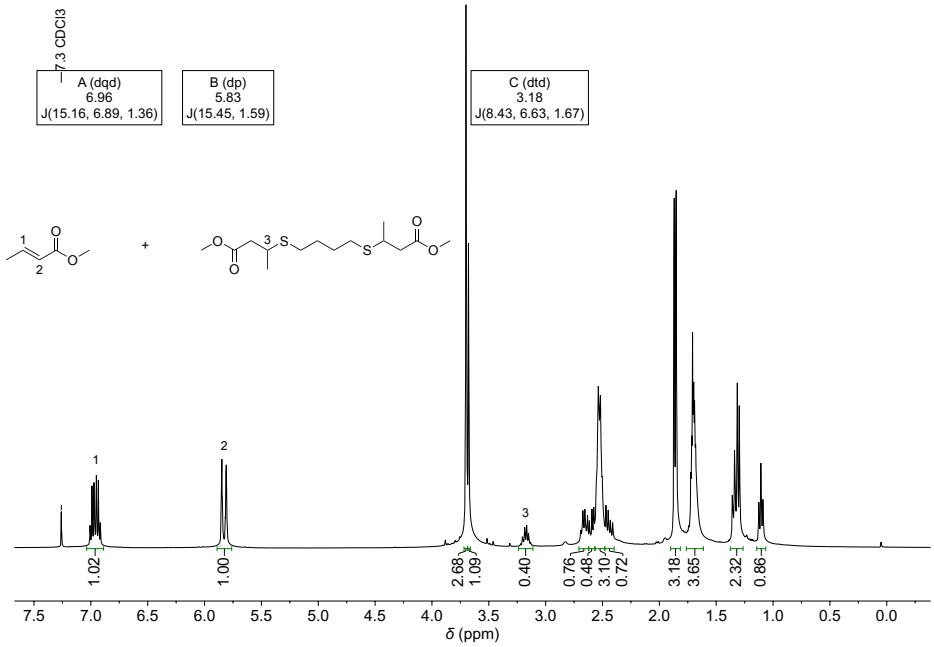

Figure 6.16: ^{1}H NMR spectrum (in $CDCl_3$) of the thia-Michael addition of 1,4-butanedithiol to methyl crotonate with 10 mol% NEt_3 after 24 h at room temperature.

Thia-Michael addition of 1,4-butanedithiol to methyl crotonate with 1 mol% of TMG:

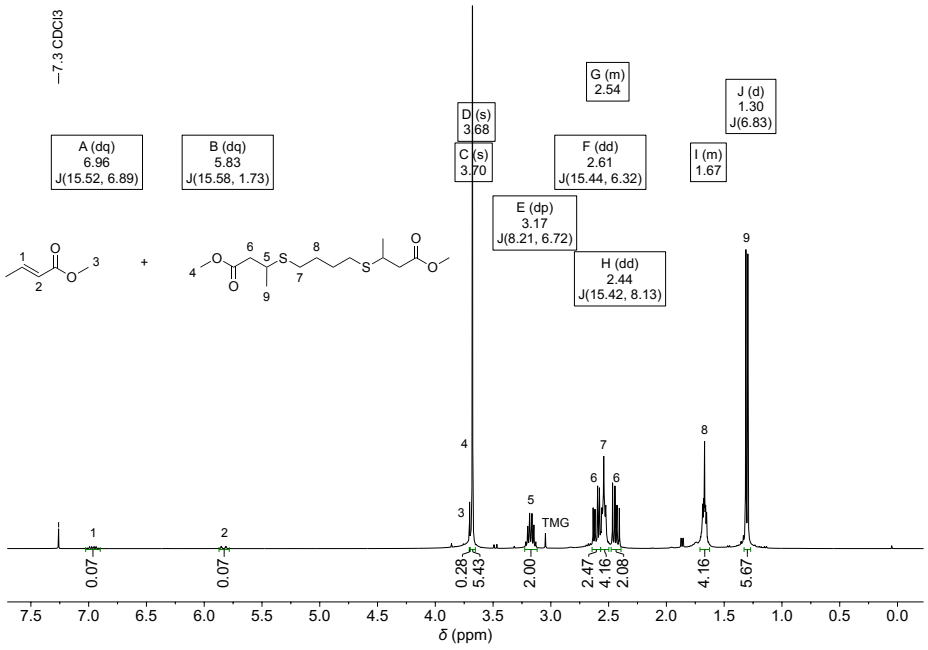

Figure 6.17: ^{1}H NMR spectrum (in $CDCl_3$) of the thia-Michael addition of 1,4-butanedithiol to methyl crotonate with 1 mol% TMG after 2 h at room temperature.

6.5.2 Thia-Michael additions to methyl crotonate

General procedure:

Methyl crotonate (1.00 equiv.), the respective dithiol (0.50 equiv.) and 1,1,3,3-tetramethylguanidine (1.00 mol%) were mixed and stirred for 4 hours at room temperature. The reaction mixture was diluted with ethyl acetate (50 ml) and acidified with 2 molar hydrochloric acid. The organic phase was washed with water (2 × 50 ml) and saturated sodium chloride solution (50 ml), dried over magnesium sulfate, filtered, and the solvent was removed under reduced pressure. The crude product was purified either by distillation or by flash column chromatography (cyclohexane/ethyl acetate).

6.5.2.1 Addition of 1,4-butanedithiol (CD1)

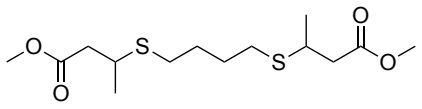

$C_{14}H_{26}O_4S_2$
M = 322.48 g/mol

7.66 g (98%, 75.0 mmol) of methyl crotonate were used for this reaction. After work-up and purification by vacuum distillation in a Kugelrohr oven (95 °C, 0.1 mbar), 11.2 g of product (34.7 mmol, 93%) were obtained.

The general procedure for the thia-Michael addition is described in the beginning of this chapter (page 125).

^{1}H NMR (400 MHz, $CDCl_3$, ppm): δ = 3.67 (s, 6H, H^1), 3.17 (dp, J = 8.3, 6.7 Hz, 2H, H^2), 2.60 (dd, J = 15.4, 6.3 Hz, 2H, H^3), 2.57−2.50 (m, 4H, H^4), 2.43 (dd, J = 15.4, 8.1 Hz, 2H, H^3), 1.72−1.62 (m, 4H, H^5), 1.30 (d, J = 6.8 Hz, 6H, H^6).

^{13}C NMR (101 MHz, $CDCl_3$, ppm): δ = 172.0 (C_q, C_{Ester}, C^1), 51.8 (CH_3, C_{Ester}, C^2), 42.2 (CH_2, α-C_{Ester}, C^3), 36.3 (CH, β-C_{Ester}, C^4), 30.3 (CH_2, C^5), 28.8 (CH_2, C^6), 21.6 (CH_3, C^7).

IR (ATR, cm^{-1}): $\tilde{\nu}$ = 2951 (w), 2927 (vw), 2866 (vw), 1732 (vs), 1435 (w), 1375 (vw), 1356 (w), 1299 (w), 1283 (w), 1221 (m), 1187 (w), 1157 (vs), 1109 (w), 1077 (w), 1023 (w), 996 (w), 880 (vw), 839 (vw), 742 (vw), 657 (vw), 594 (vw).

ESI-MS ($[M+H]^+$, $C_{14}H_{27}O_4S_2$) calcd.: 323.1345; found: 323.1343.

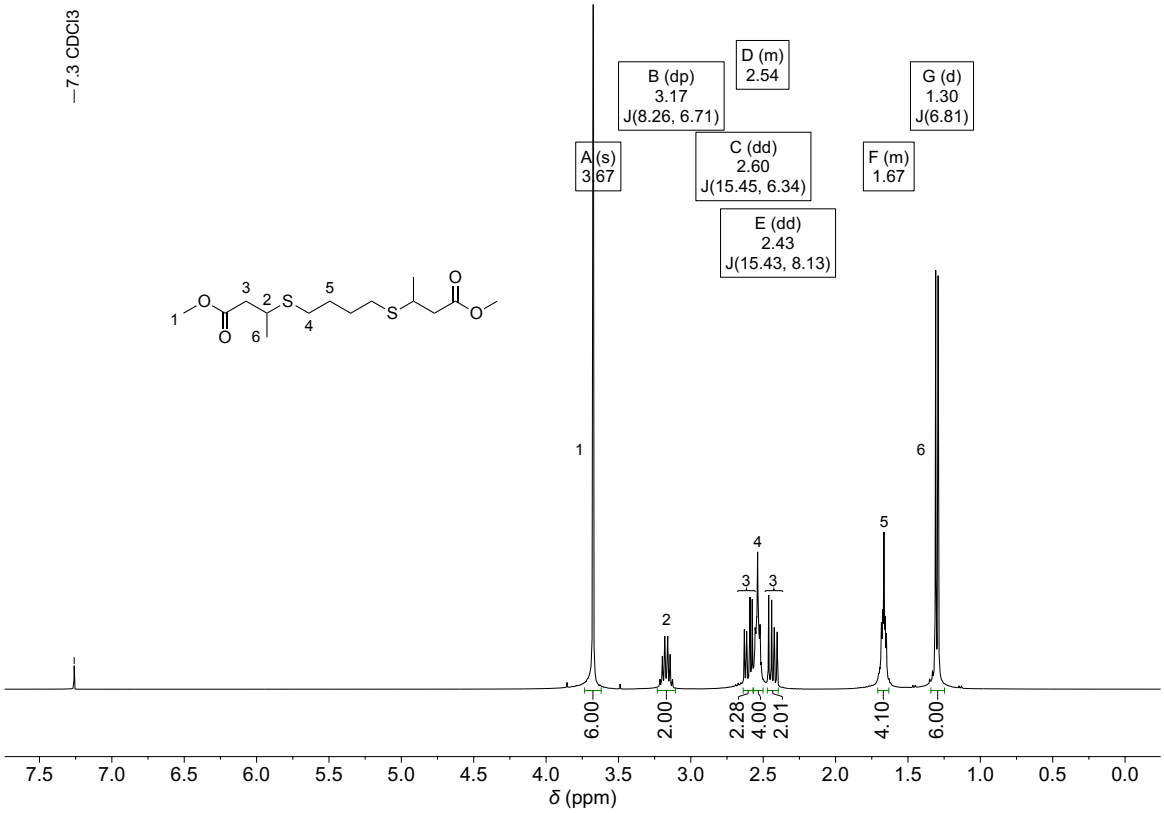

Figure 6.18: ^{1}H NMR spectrum of **CD1** in $CDCl_3$.

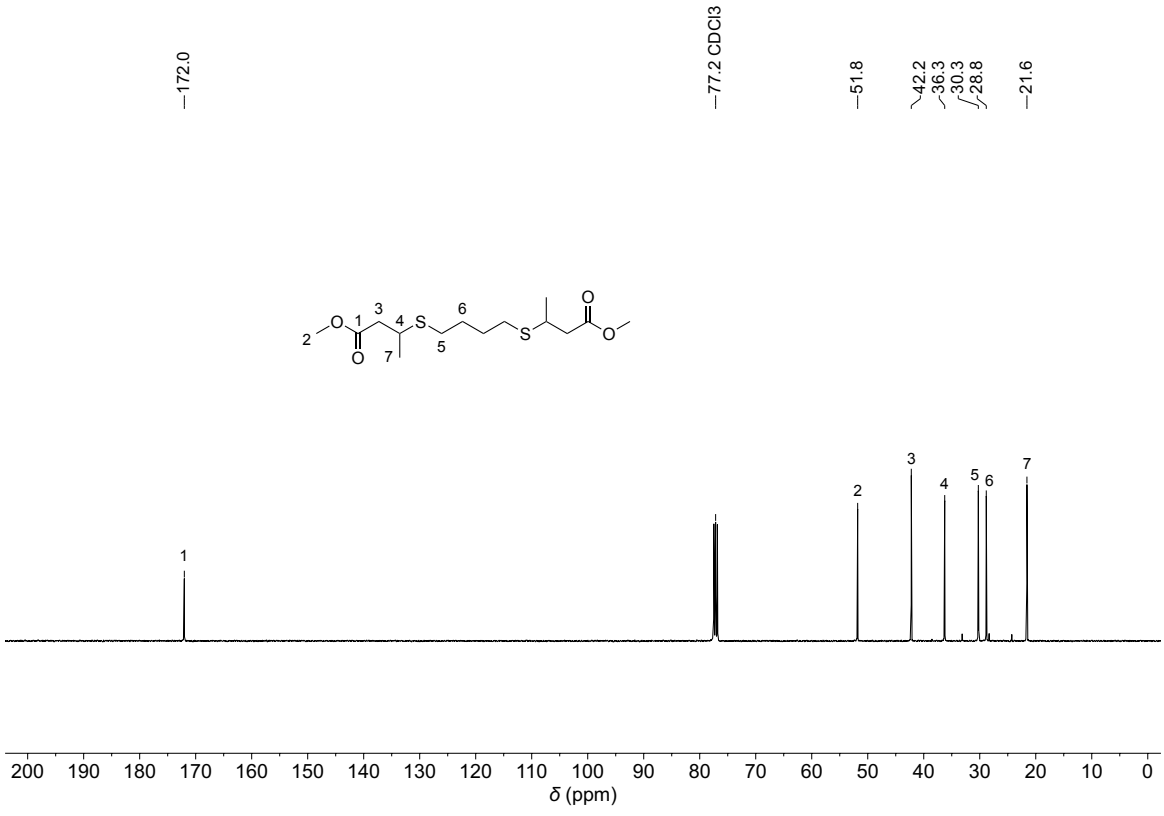

Figure 6.19: ^{13}C NMR spectrum of **CD1** in $CDCl_3$.

6.5.2.2 Addition of 1,6-hexanedithiol (CD2)

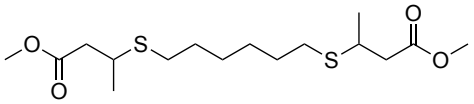

$C_{16}H_{30}O_4S_2$
M = 350.53 g/mol

7.66 g (98%, 75.0 mmol) of methyl crotonate were used for this reaction. After work-up and purification by vacuum distillation in a Kugelrohr oven (150 °C, 0.1 mbar), 12.4 g of product (35.4 mmol, 94%) were obtained.

The general procedure for the thia-Michael addition is described in the beginning of this chapter (page 125).

^{1}H NMR (500 MHz, $CDCl_3$, ppm): δ = 3.68 (s, 6H, H^1), 3.17 (dp, J = 8.2, 6.7 Hz, 2H, H^2), 2.61 (dd, J = 15.4, 6.2 Hz, 2H, H^3), 2.53 (t, J = 7.6 Hz, 4H, H^4), 2.44 (dd, J = 15.4, 8.2 Hz, 2H, H^3), 1.57 (d, J = 7.4 Hz, 4H, H^5), 1.42−1.35 (m, 4H, H^6), 1.30 (d, J = 6.8 Hz, 6H, H^7).

^{13}C NMR (126 MHz, $CDCl_3$, ppm): δ = 172.1 (C_q, C_{Ester}, C^1), 51.8 (CH_3, C_{Ester}, C^2), 42.3 (CH_2, α-C_{Ester}, C^3), 36.3 (CH, β-C_{Ester}, C^4), 30.7 (CH_2, C^5), 29.6 (CH_2, C^6), 28.6 (CH_2, C^7), 21.6 (CH_3, C^8).

IR (ATR, cm^{-1}): $\tilde{\nu}$ = 2927 (w), 2856 (vw), 1734 (vs), 1453 (w), 1435 (w), 1374 (vw), 1356 (w), 1288 (w), 1254 (w), 1221 (m), 1187 (w), 1157 (vs), 1109 (w), 1077 (w), 1024 (w), 997 (w), 881 (vw), 839 (vw), 734 (vw), 657 (vw).

ESI-MS ($[M+H]^+$, $C_{16}H_{31}O_4S_2$) calcd.: 351.1658; found: 351.1655.

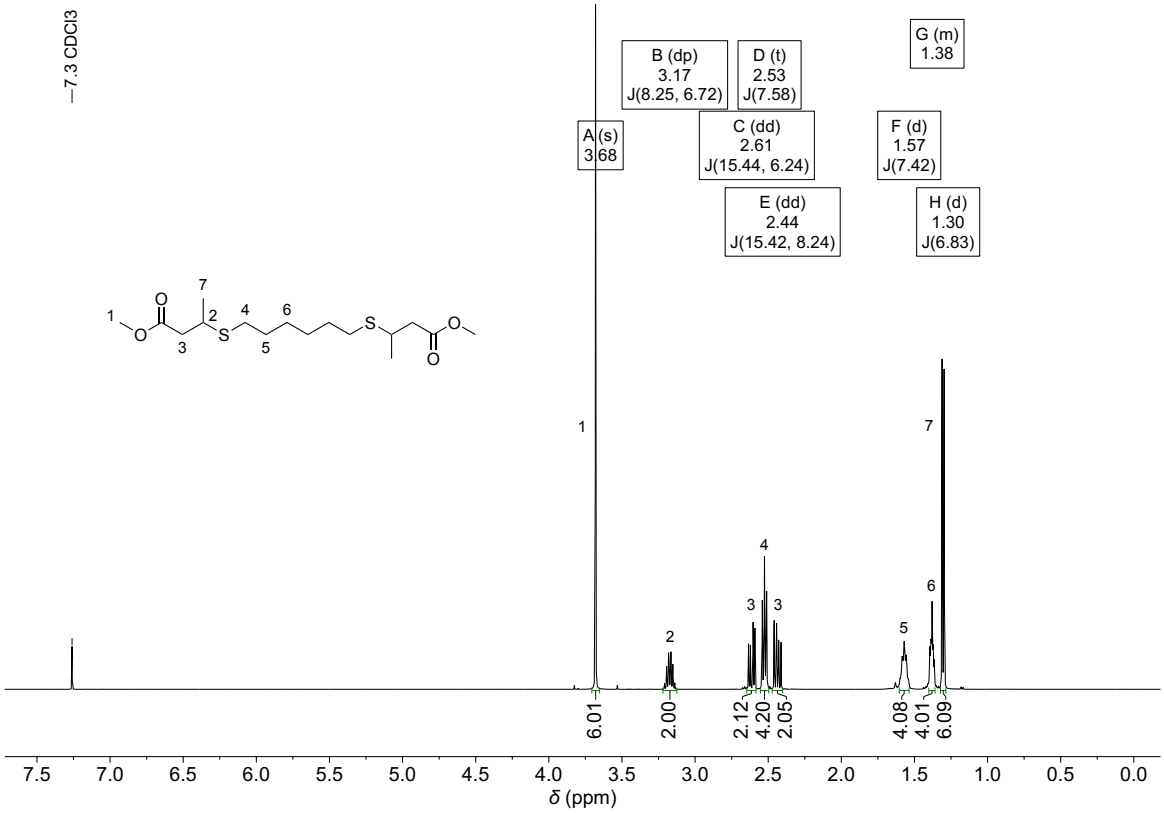

Figure 6.20: ^{1}H NMR spectrum of **CD2** in $CDCl_3$.

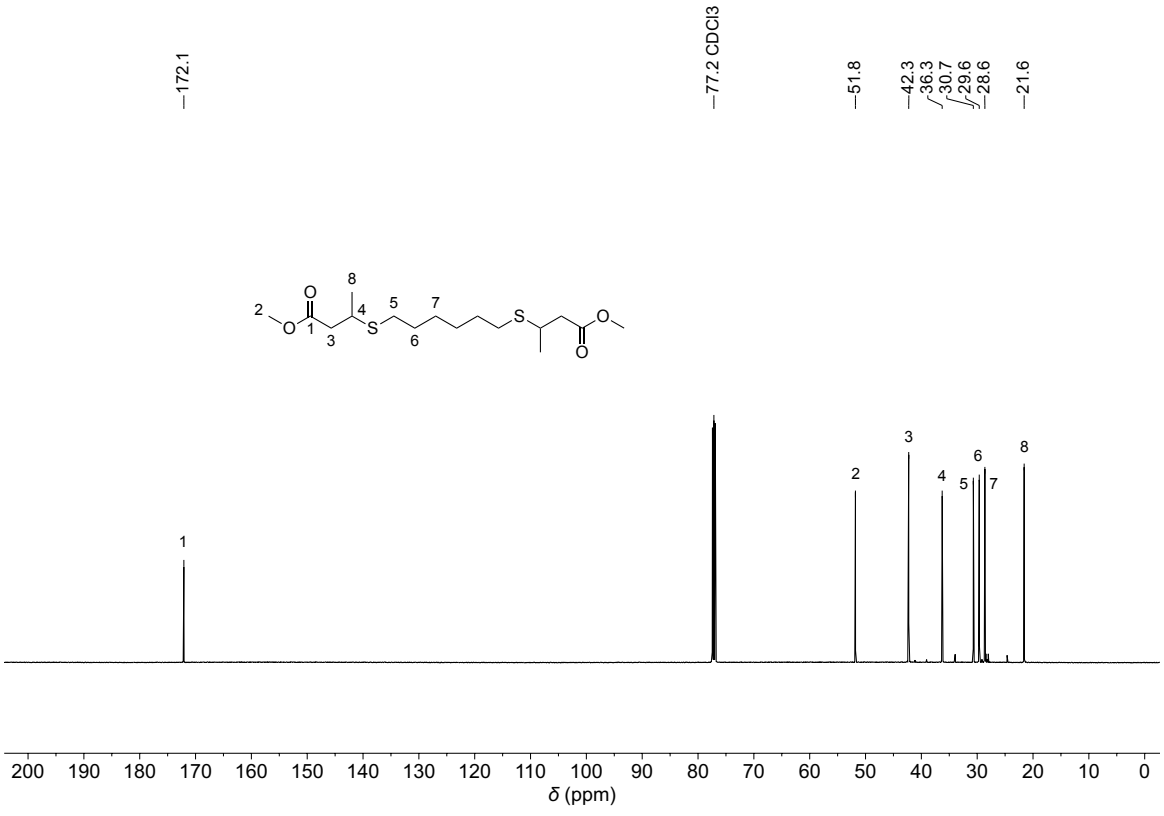

Figure 6.21: ^{13}C NMR spectrum of **CD2** in $CDCl_3$.

6.5.2.3 Addition of 1,10-decanedithiol (CD3)

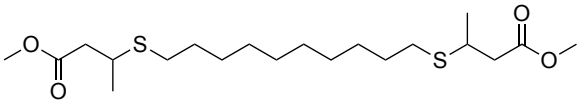

$C_{20}H_{38}O_4S_2$
M = 406.64 g/mol

6.13 g (98%, 60.0 mmol) of methyl crotonate were used for this reaction. After work-up and purification by flash column chromatography (cyclohexane/ethyl acetate), 10.3 g of product (25.3 mmol, 84%) were obtained.

The general procedure for the thia-Michael addition is described in the beginning of this chapter (page 125).

***R*f** (cyclohexane/ethyl acetate, 9:1): 0.30.

^{1}H NMR (500 MHz, $CDCl_3$, ppm): δ = 3.68 (s, 6H, H^1), 3.17 (dp, J = 8.3, 6.7 Hz, 2H, H^2), 2.61 (dd, J = 15.4, 6.2 Hz, 2H, H^3), 2.52 (t, J = 7.4 Hz, 4H, H^4), 2.43 (dd, J = 15.4, 8.2 Hz, 2H, H^3), 1.55 (p, J = 7.4 Hz, 4H, H^5), 1.35 (t, J = 7.4 Hz, 4H, H^6), 1.30 (d, J = 6.8 Hz, 6H, H^7), 1.28−1.22 (m, 8H, H^8).

^{13}C NMR (126 MHz, $CDCl_3$, ppm): δ = 172.1 (C_q, C_{Ester}, C^1), 51.8 (CH_3, C_{Ester}, C^2), 42.3 (CH_2, α-C_{Ester}, C^3), 36.2 (CH, β-C_{Ester}, C^4), 30.8 (CH_2, C^5), 29.8 (CH_2, C^6), 29.5 (CH_2, C^6), 29.3 (CH_2, C^6), 29.1 (CH_2, C^6), 21.6 (CH_3, C^7).

IR (ATR, cm^{-1}): $\tilde{\nu}$ = 2924 (m), 2853 (w), 1735 (vs), 1451 (w), 1435 (w), 1354 (w), 1300 (w), 1283 (w), 1221 (m), 1187 (w), 1157 (vs), 1109 (w), 1077 (w), 1024 (w), 997 (w), 882 (vw), 837 (vw), 722 (vw), 660 (vw).

ESI-MS ($[M+H]^+$, $C_{20}H_{39}O_4S_2$) calcd.: 407.2284; found: 407.2282.

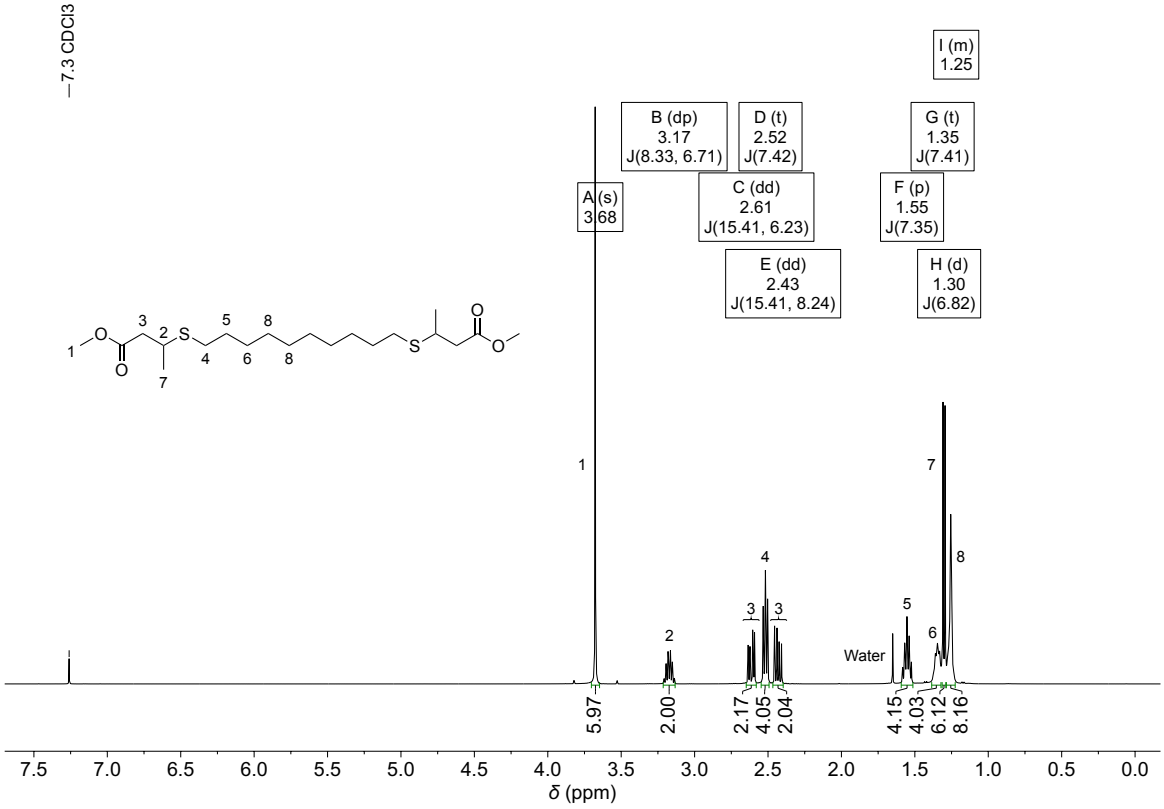

Figure 6.22: ^{1}H NMR spectrum of **CD3** in $CDCl_3$.

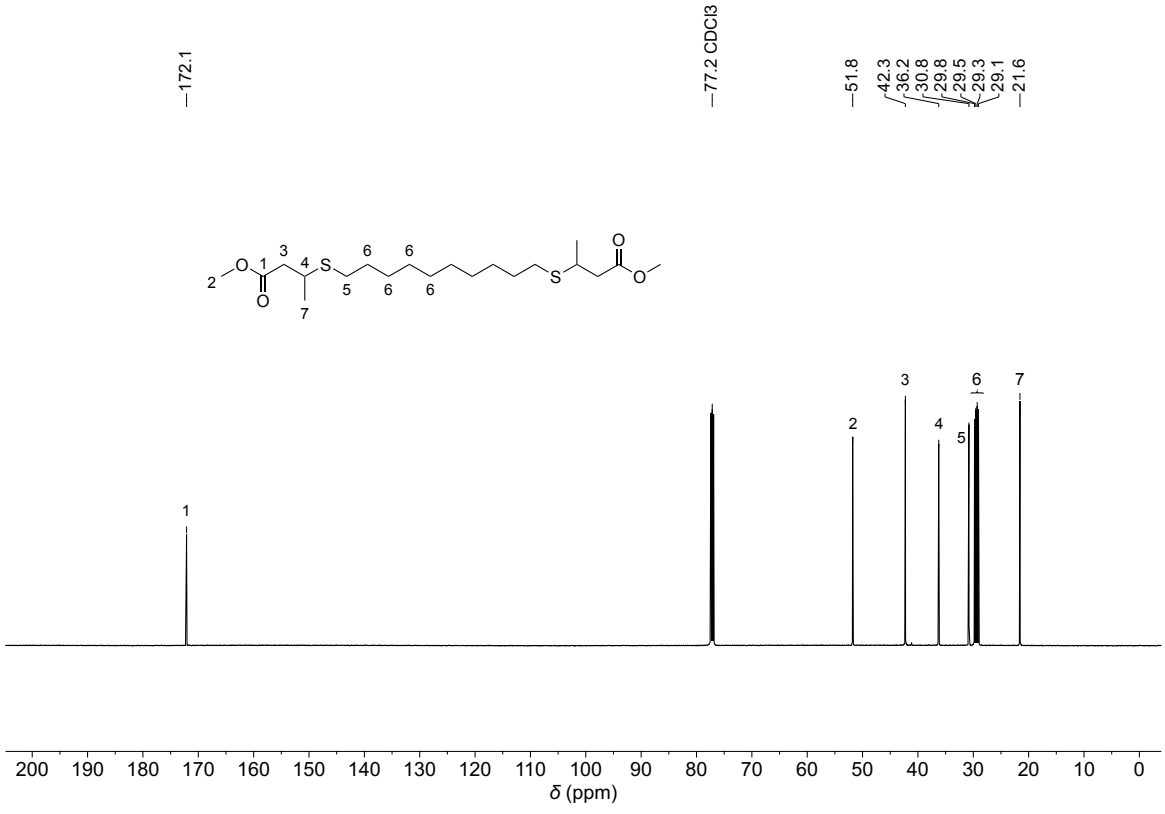

Figure 6.23: ^{13}C NMR spectrum of **CD3** in $CDCl_3$.

6.5.3 Thia-Michael addition of 1,4-butanedithiol to *α,β*-unsaturated methyl laurate

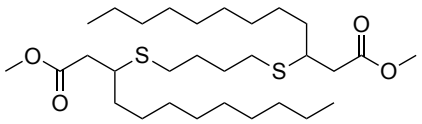

$C_{30}H_{58}O_4S_2$
M = 546.91 g/mol

α,β-Unsaturated methyl laurate (40% NMR purity, 39.0 g, 73.5 mmol, 1.00 equiv.), 1,4-butanedithiol (97%, 4.63 g, 4.44 ml, 36.7 mmol, 0.50 equiv.) and 1,1,3,3-tetramethylguanidine (277 µl, 254 mg, 2.20 mmol, 3.00 mol%) were mixed at room temperature and the mixture was then stirred for 16 h at 80 °C. After cooling to room temperature, the reaction mixture was diluted with ethyl acetate (200 ml) and acidified with 2 molar hydrochloric acid. The organic phase was washed with water (2 × 100 ml) and saturated sodium chloride solution (100 ml), dried over sodium sulfate, filtered, and the solvent was removed under reduced pressure. The crude product was distilled *in vacuo* (100 °C, 0.1 mbar) to recover the unreacted methyl laurate (21.7 g, 101 mmol, 93%). The residue of the distillation was purified by flash column chromatography (cyclohexane/ethyl acetate, 40:1) to obtain the title compound (15.0 g, 27.4 mmol, 75%).

Methyl laurate:

^{1}H NMR (400 MHz, $CDCl_3$, ppm): δ = 3.66 (s, 3H, H^1), 2.30 (t, J = 7.6 Hz, 2H, H^2), 1.61 (p, J = 7.3 Hz, 2H, H^3), 1.35−1.14 (m, 16H, H^4), 0.88 (t, J = 6.9 Hz, 3H, H^5).

Methyl laurate dimer (LD1):

***R*$_f$** (cyclohexane/ethyl acetate, 20:1): 0.23.

^{1}H NMR (500 MHz, $CDCl_3$, ppm): δ = 3.68 (s, 6H, H^1), 3.01 (qd, J = 7.3, 5.7 Hz, 2H, H^2), 2.55 (d, J = 7.2 Hz, 4H, H^3), 2.54−2.48 (m, 4H, H^4), 1.69−1.63 (m, 4H, H^5), 1.59−1.49 (m, 4H, H^6), 1.48−1.33 (m, 4H, H^7), 1.32−1.19 (m, 24H, H^8), 0.87 (t, J = 7.0 Hz, 6H, H^9).

^{13}C NMR (126 MHz, $CDCl_3$, ppm): δ = 172.3 (C_q, C_{Ester}, C^1), 51.8 (CH_3, C_{Ester}, C^2), 42.0 (CH, *β*-C_{Ester}, C^3), 41.0 (CH_2, *α*-C_{Ester}, C^4), 35.3 (CH_2, C^5), 32.0 (CH_2, C^6), 30.3 (CH_2, C^6), 29.7 (CH_2, C^6), 29.6 (CH_2, C^6), 29.6 (CH_2, C^6), 29.4 (CH_2, C^6), 29.0 (CH_2, C^6), 26.9 (CH_2, C^6), 22.8 (CH_2, C^6), 14.2 (CH_3, C^7).

IR (ATR, cm^{-1}): $\tilde{\nu}$ = 2949 (w), 2922 (vs), 2853 (m), 1737 (vs), 1458 (w), 1435 (m), 1354 (w), 1307 (w), 1279 (w), 1237 (m), 1221 (m), 1153 (s), 1125 (w), 1017 (w), 986 (vw), 881 (vw), 841 (vw), 722 (w).

ESI-MS ($[M+H]^+$, $C_{30}H_{59}O_4S_2$) calcd.: 547.3849; found: 547.3848.

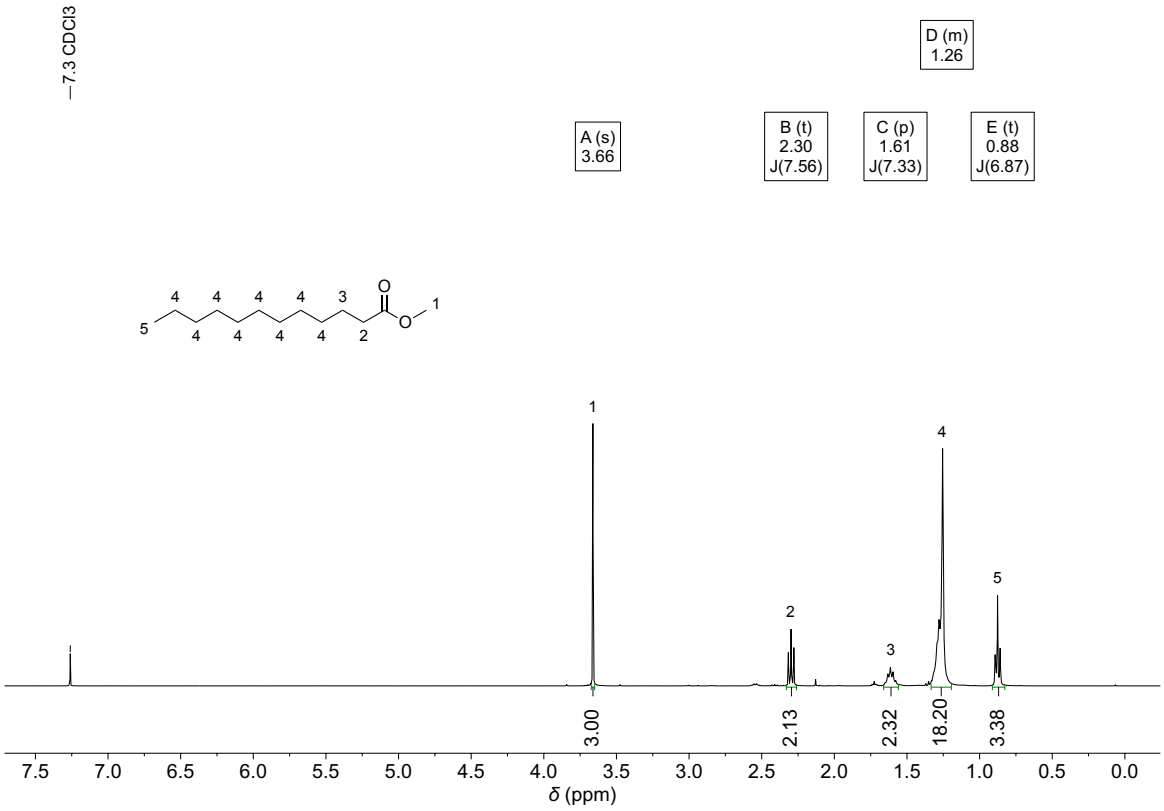

Figure 6.24: ^{1}H NMR spectrum of recovered methyl laurate in $CDCl_3$.

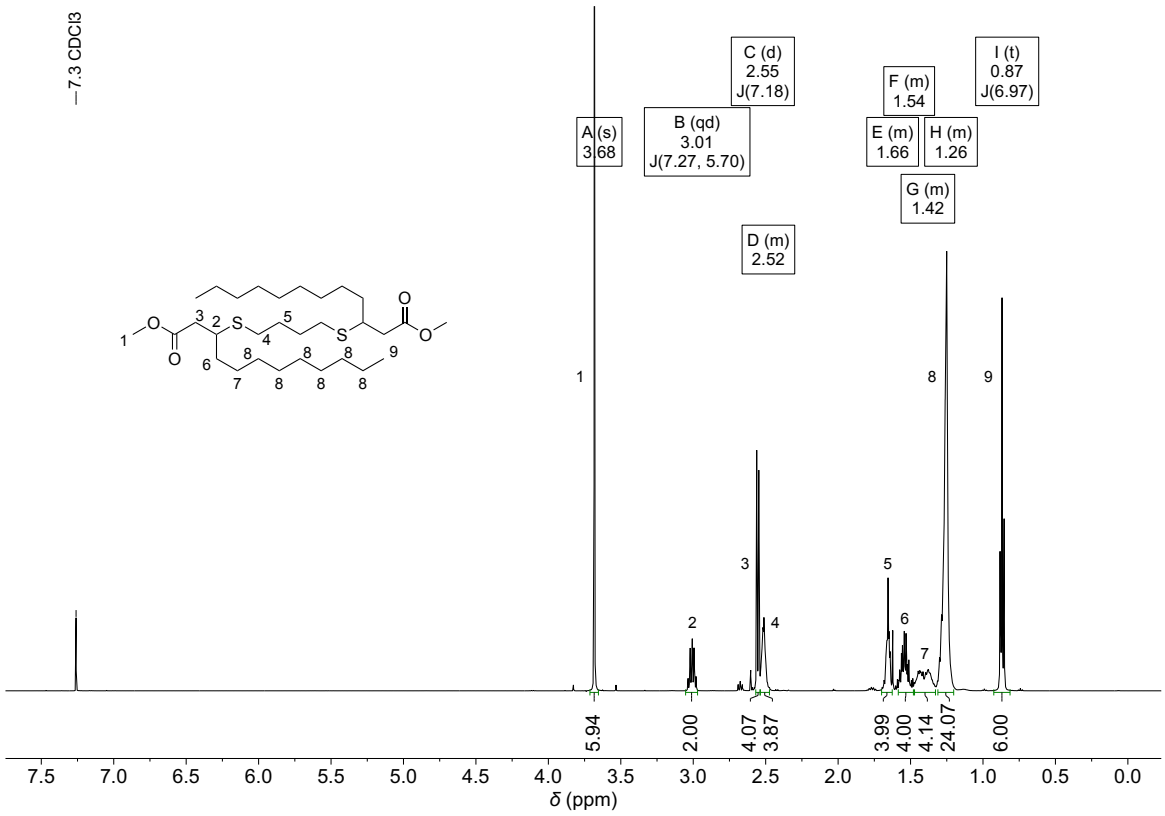

Figure 6.25: ^{1}H NMR spectrum of **LD1** in $CDCl_3$.

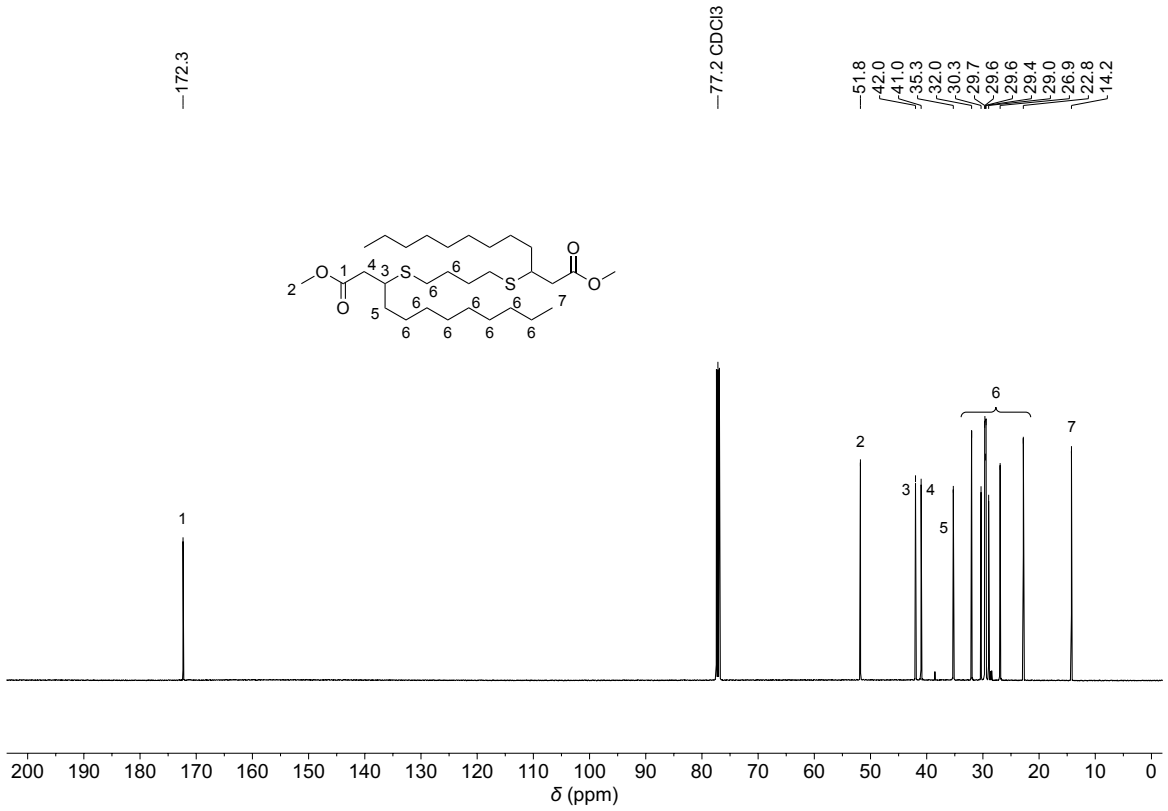

Figure 6.26: ^{13}C NMR spectrum of **LD1** in $CDCl_3$.

6.6 Alternative synthesis of methyl laurate dimers LD1−LD3

6.6.1 Knoevenagel-Doebner condensation of decanal and malonic acid

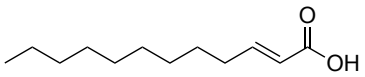

$C_5H_{22}O_2$
M = 198.31 g/mol

The reaction was performed according to a literature reported procedure.[266]

A solution of decanal (30.0 g, 192 mmol, 1.00 equiv.), malonic acid (20.0 g, 192 mmol, 1.00 equiv.), and pyridine (38.7 ml, 38.0 g, 480 mmol, 2.50 equiv.) was stirred at room temperature for 4 days. Afterwards, the reaction mixture was stirred for another two days at 50 °C. After cooling to room temperature, the reaction mixture was carefully neutralized and acidified with 2 molar hydrochloric acid to a pH value of 1 and water (200 ml) was added. The aqueous phase was extracted with ethyl acetate (3 × 200 ml). The combined organic layers were washed with water (2 × 100 ml) and saturated sodium chloride solution (100 ml), dried over sodium sulfate, filtered, and the solvent was removed under reduced pressure. The crude product was distilled *in vacuo* (120 °C, 0.1 mbar) to obtain the title compound (23.2 g, 117 mmol, 61%).

^{1}H NMR (500 MHz, $CDCl_3$, ppm): δ = 7.08 (dt, J = 15.5, 6.9 Hz, 1H, H^1), 5.82 (dd, J = 15.7, 1.7 Hz, 1H, H^2), 2.23 (qd, J = 7.2, 1.6 Hz, 2H, H^3), 1.46 (p, J = 7.3 Hz, 2H, H^4), 1.37−1.14 (m, 12H, H^5), 0.88 (t, J = 6.8 Hz, 3H, H^6).

^{13}C NMR (126 MHz, $CDCl_3$, ppm): δ = 172.0 (C_q, $C_{CarboxylicAcid}$, C^1), 152.7 (CH, $C_{DoubleBond}$, C^2), 120.7 (CH, $C_{DoubleBond}$, C^3), 32.5 (CH_2, C^4), 32.0 (CH_2, C^4), 29.6 (CH_2, C^4), 29.5 (CH_2, C^4), 29.4 (CH_2, C^4), 29.3 (CH_2, C^4), 28.0 (CH_2, C^4), 22.8 (CH_2, C^4), 14.3 (CH_2, C^5).

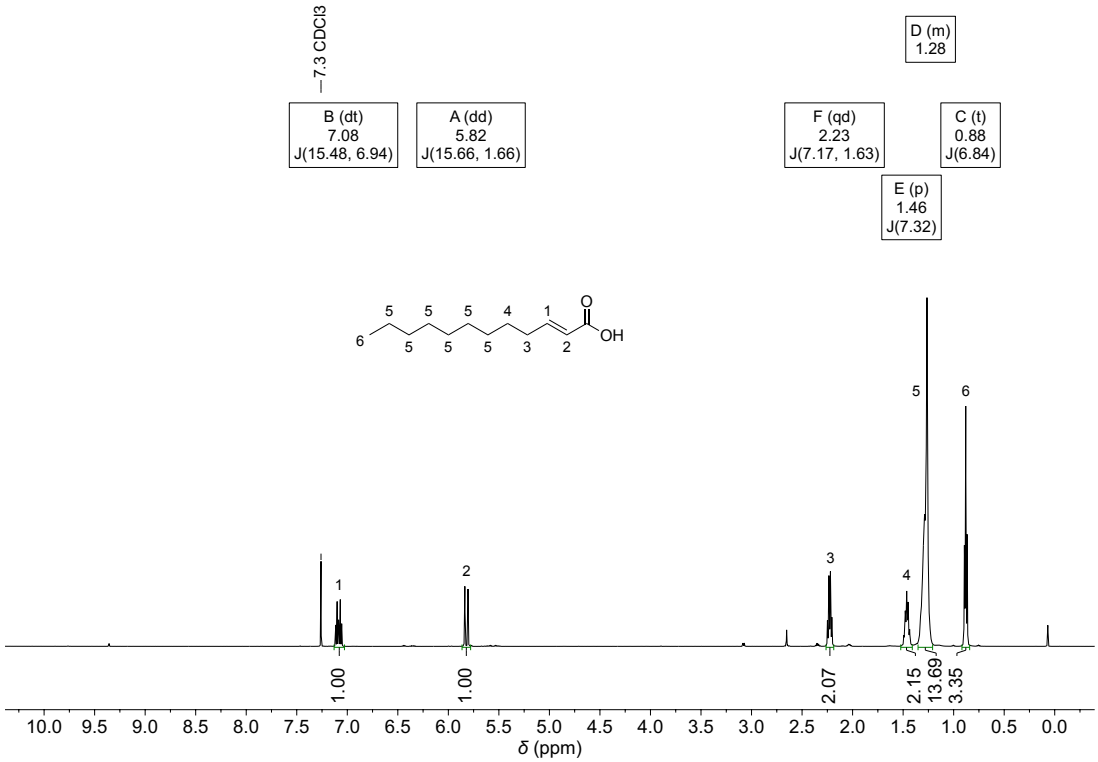

Figure 6.27: ^{1}H NMR spectrum of *α*,*β*-unsaturated lauric acid synthesized *via* Knoevenagel-Doebner condensation in $CDCl_3$.

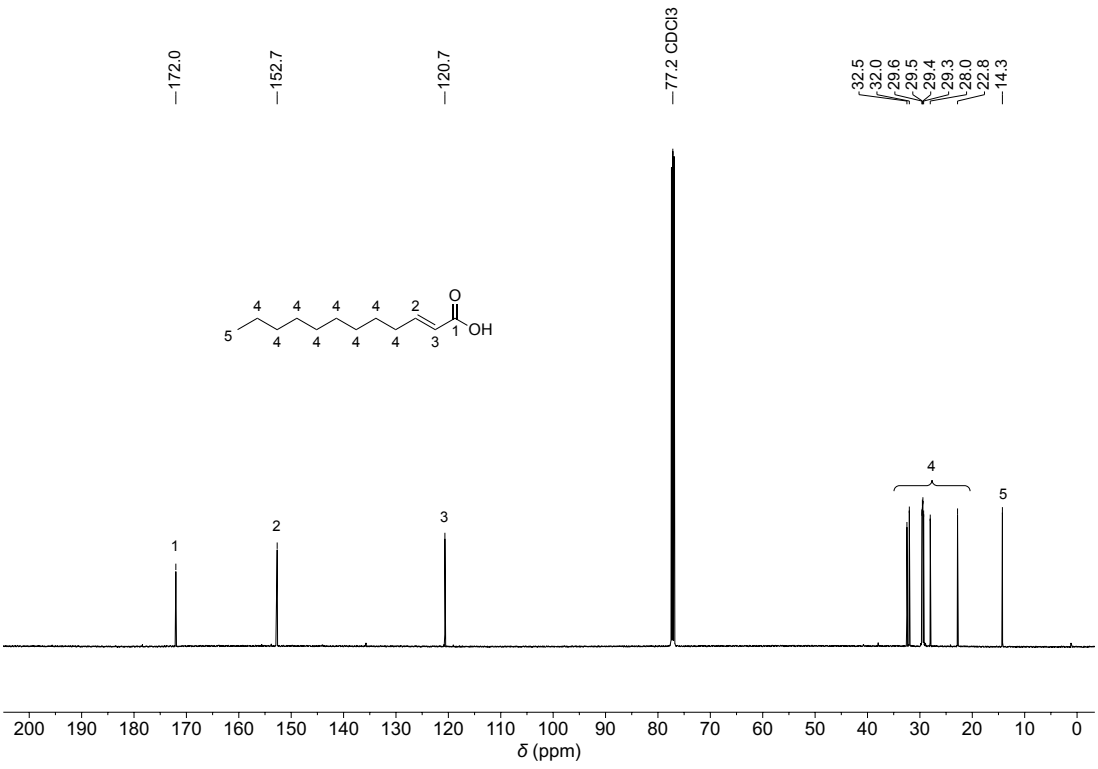

Figure 6.28: ^{13}C NMR spectrum of *α*,*β*-unsaturated lauric acid synthesized *via* Knoevenagel-Doebner condensation in $CDCl_3$.

6.6.2 Esterification of *α,β*-unsaturated lauric acid with methanol

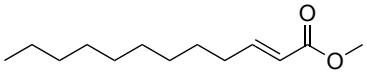

$C_{13}H_{24}O_2$
M = 212.33 g/mol

α,β-Unsaturated lauric acid from Knoevenagel-Doebner condensation (23.2 g, 117 mmol, 1.00 equiv.), methanol (189 ml, 4.67 mol, 40.0 equiv.) and sulfuric acid (650 µl, 11.7 mmol, 0.100 equiv.) were added into a 500 ml round bottom flask. The reaction solution was stirred at 65 °C for 4 h. After cooling to room temperature, the solvent methanol was removed under reduced pressure. The residue was dissolved in ethyl acetate (100 ml) and washed with water (2 × 100 ml) and saturated sodium chloride solution (100 ml). The organic phase was dried over $MgSO_4$, filtered, and the solvent was removed under reduced pressure to obtain the title compound (23.4 g, 110 mmol, 94%).

^{1}H NMR (500 MHz, $CDCl_3$, ppm): δ = 6.97 (dt, J = 15.7, 7.0 Hz, 1H, H^1), 5.81 (dt, J = 15.8, 1.6 Hz, 1H, H^2), 3.72 (s, 3H, H^3), 2.19 (qd, J = 7.1, 1.6 Hz, 2H, H^4), 1.44 (p, J = 7.2 Hz, 2H, H^5), 1.34−1.20 (m, 12H, H^6), 0.87 (t, J = 7.0 Hz, 3H, H^7).

^{13}C NMR (126 MHz, $CDCl_3$, ppm): δ = 167.4 (C_q, C_{Ester}, C^1), 150.0 (CH, $C_{Double\ bond}$, C^2), 120.9 (CH, $C_{Double\ bond}$, C^3), 51.5 (CH_3, C_{Ester}, C^4), 32.4 (CH_2, C^5), 32.0 (CH_2, C^5), 29.6 (CH_2, C^5), 29.5 (CH_2, C^5), 29.4 (CH_2, C^5), 29.3 (CH_2, C^5), 28.2 (CH_2, C^5), 22.8 (CH_2, C^5), 14.2 (CH_3, C^6).

IR (ATR, cm^{-1}): $\tilde{\nu}$ = 2952 (w), 2924 (s), 2854 (m), 1725 (vs), 1657 (w), 1459 (w), 1435 (w), 1312 (w), 1268 (m), 1196 (m), 1173 (m), 1128 (w), 1041 (w), 982 (w), 850 (w), 720 (w).

ESI-MS ($[M+H]^+$, $C_{13}H_{25}O_2$) calcd.: 213.1849; found: 213.1847.

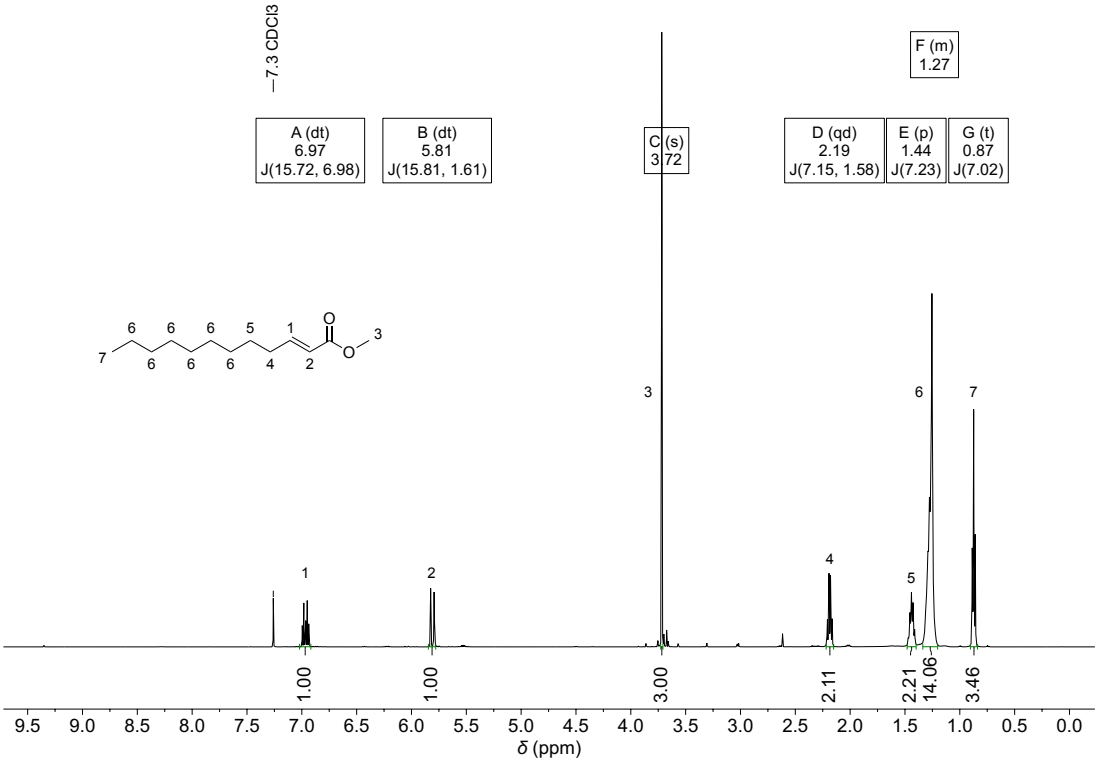

Figure 6.29: ^{1}H NMR spectrum of *α*,*β*-unsaturated methyl laurate synthesized *via* the alternative reaction pathway in $CDCl_3$.

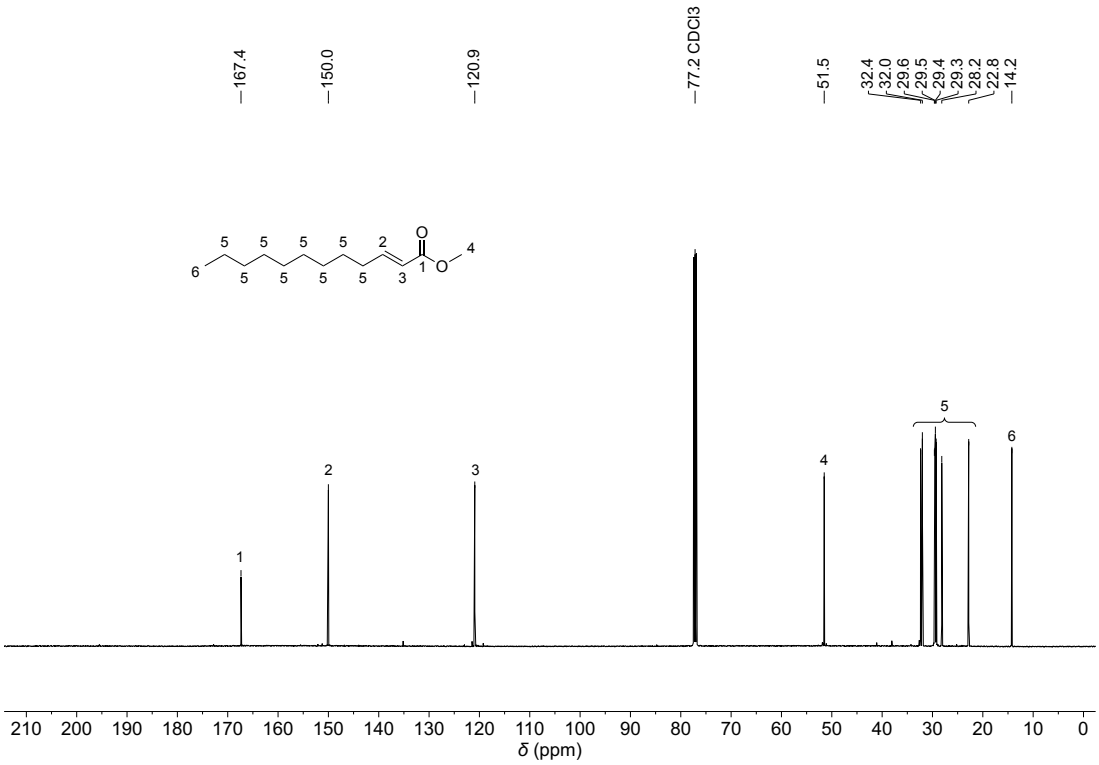

Figure 6.30: ^{13}C NMR spectrum of *α*,*β*-unsaturated methyl laurate synthesized *via* the alternative reaction pathway in $CDCl_3$.

6.6.3 Thia-Michael addition of 1,4-butanedithiol (LD1)

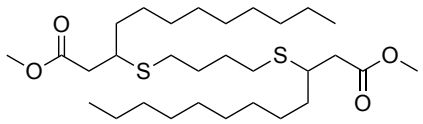

$C_{30}H_{58}O_4S_2$
M = 546.91 g/mol

α,*β*-Unsaturated methyl laurate (92% GC purity, 6.00 g, 26.0 mmol, 1.00 equiv.), 1,4-butanedithiol (97%, 1.64 g, 1.57 ml, 13.0 mmol, 0.50 equiv.) and 1,1,3,3-tetramethylguanidine (97.9 µl, 89.8 mg, 780 µmol, 3.00 mol%) were mixed at room temperature and the mixture was then stirred for 16 h at 80 °C. After cooling to room temperature, the reaction mixture was diluted with ethyl acetate (50 ml) and acidified with 2 molar hydrochloric acid. The organic phase was washed with water (2 × 50 ml) and saturated sodium chloride solution (50 ml), dried over magnesium sulfate, filtered, and the solvent was removed under reduced pressure. The crude product was purified by flash column chromatography (cyclohexane/ethyl acetate, 40:1) to obtain the title compound (5.90 g, 10.8 mmol, 83%).

The analytical data is consistent with the one listed in chapter 6.5.3.

6.6.4 Thia-Michael addition of 1,6-hexanedithiol (LD2)

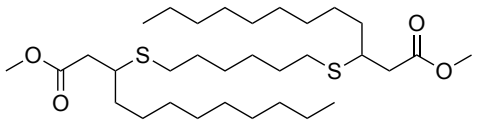

$C_{32}H_{62}O_4S_2$
M = 574.96 g/mol

α,*β*-Unsaturated methyl laurate (92% GC purity, 6.00 g, 26.0 mmol, 1.00 equiv.), 1,6-hexanedithiol (97%, 2.01 g, 2.03 ml, 13.0 mmol, 0.50 equiv.) and 1,1,3,3-tetramethylguanidine (97.9 µl, 89.8 mg, 780 µmol, 3.00 mol%) were mixed at room temperature. The mixture was heated to 80 °C and stirred for 16 h. After cooling to room temperature, the reaction mixture was diluted with ethyl acetate (50 ml) and acidified with 2 molar hydrochloric acid. The organic phase was washed with water (2 × 50 ml) and saturated sodium chloride solution (50 ml), dried over magnesium sulfate, filtered, and the solvent was removed under reduced pressure. The crude product was purified by flash column chromatography (cyclohexane/ethyl acetate, 40:1 to 15:1) to obtain the title compound (6.10 g, 10.6 mmol, 82%).

R_f (cyclohexane/ethyl acetate, 20:1): 0.27.

^{1}H NMR (500 MHz, $CDCl_3$, ppm): δ = 3.69 (s, 6H, H^1), 3.01 (qd, J = 7.3, 5.7 Hz, 2H, H^2), 2.56 (dd, J = 7.2, 1.5 Hz, 4H, H^3), 2.54−2.47 (m, 4H, H^4), 1.62−1.51 (m, 8H, H^5), 1.47−1.34 (m, 8H, H^6), 1.32−1.21 (m, 24H, H^7), 0.87 (t, J = 6.9 Hz, 6H, H^8).

^{13}C NMR (126 MHz, $CDCl_3$, ppm): δ = 172.4 (C_q, C_{Ester}, C^1), 51.8 (CH_3, C_{Ester}, C^2), 42.0 (CH, β-C_{Ester}, C^3), 41.0 (CH_2, α-C_{Ester}, C^4), 35.3 (CH_2, C^5), 32.0 (CH_2, C^5), 30.8 (CH_2, C^5), 29.8 (CH_2, C^5), 29.7 (CH_2, C^5), 29.7 (CH_2, C^5), 29.6 (CH_2, C^5), 29.4 (CH_2, C^5), 28.7 (CH_2, C^5), 26.9 (CH_2, C^5), 22.8 (CH_2, C^5), 14.3 (CH_3, C^6).

IR (ATR, cm^{-1}): $\tilde{\nu}$ = 2922 (vs), 2853 (m), 1738 (vs), 1459 (w), 1435 (w), 1353 (w), 1238 (w), 1220 (w), 1153 (s), 1123 (w), 1071 (vw), 1017 (w), 987 (vw), 881 (vw), 841 (vw), 722 (w).

ESI-MS ($[M+H]^+$, $C_{32}H_{63}O_4S_2$) calcd.: 575.4162; found: 575.4169.

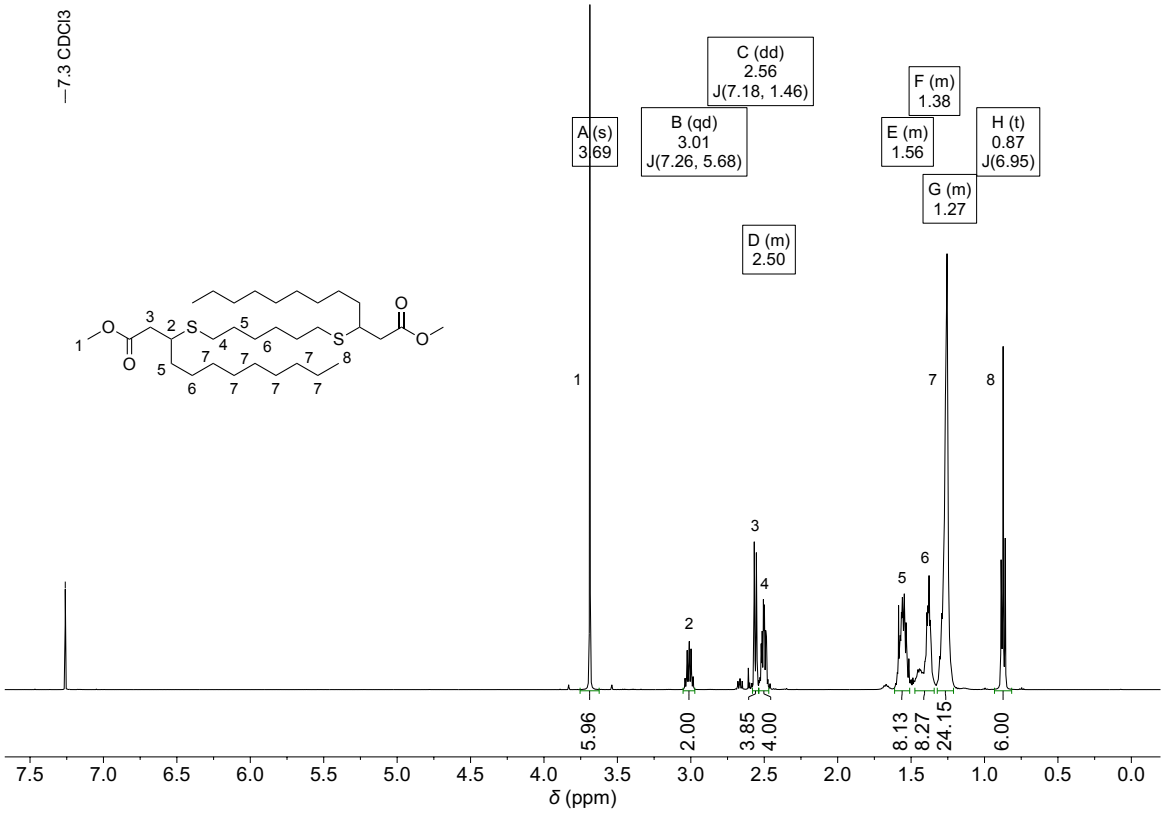

Figure 6.31: ^{1}H NMR spectrum of **LD2** in $CDCl_3$.

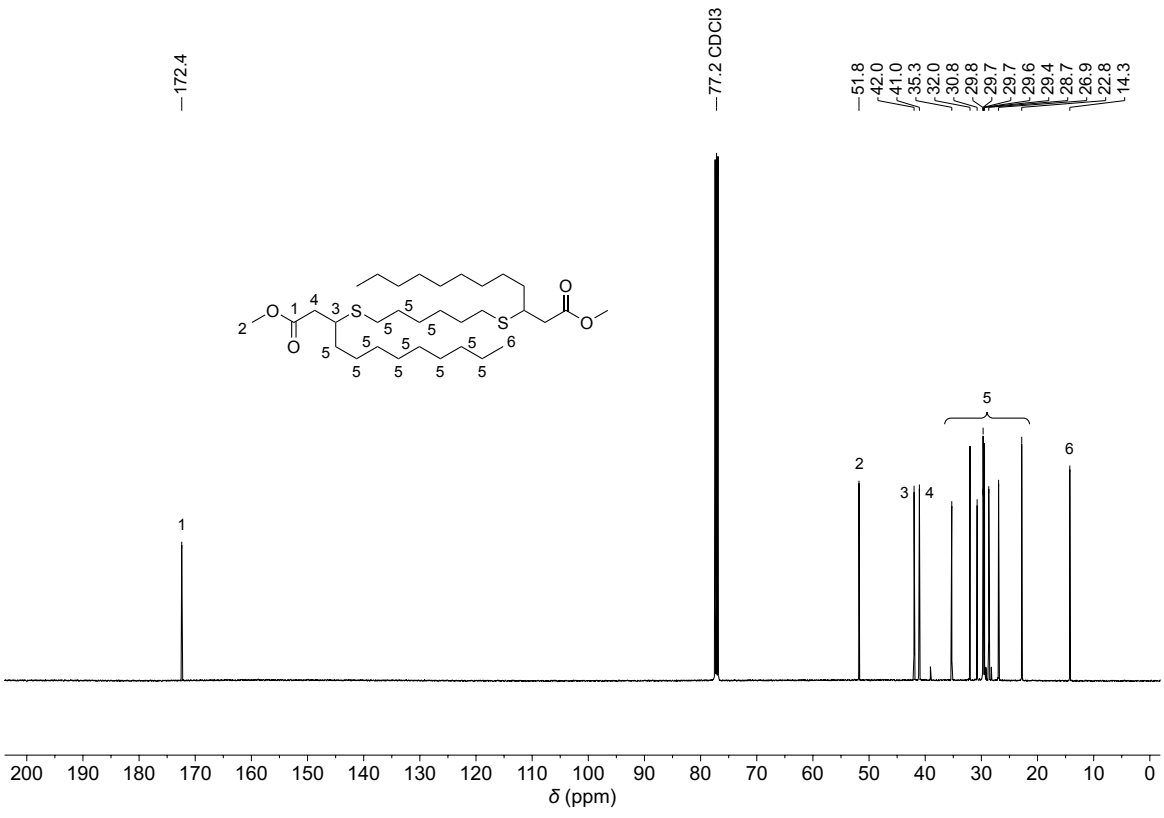

Figure 6.32: ^{13}C NMR spectrum of **LD2** in $CDCl_3$.

6.6.5 Thia-Michael addition of 1,10-decanedithiol (LD3)

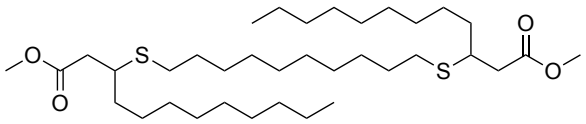

$C_{36}H_{70}O_4S_4$
M = 631.07 g/mol

α,*β*-Unsaturated methyl laurate (92% GC purity, 6.00 g, 26.0 mmol, 1.00 equiv.), 1,10-decanedithiol (98%, 2.74 g, 13.0 mmol, 0.50 equiv.) and 1,1,3,3-tetramethylguanidine (97.9 µl, 89.8 mg, 780 µmol, 3.00 mol%) were mixed at room temperature. The mixture was heated to 80 °C and stirred for 16 h. After cooling to room temperature, the reaction mixture was diluted with ethyl acetate (50 ml) and acidified with 2 molar hydrochloric acid. The organic phase was washed with water (2 × 50 ml) and saturated sodium chloride solution (50 ml), dried over magnesium sulfate, filtered, and the solvent was removed under reduced pressure. The crude product was purified by flash column chromatography (cyclohexane/ethyl acetate, 9:1) to obtain the title compound (6.17 g, 9.78 mmol, 76%).

R_f (cyclohexane/ethyl acetate, 20:1): 0.3.

^{1}H NMR (500 MHz, $CDCl_3$, ppm): δ = 3.69 (s, 6H, H^1), 3.02 (qd, J = 7.2, 5.6 Hz, 2H, H^2), 2.56 (dd, J = 7.2, 2.5 Hz, 4H, H^3), 2.53−2.47 (m, 4H, H^4), 1.59−1.51 (m, 8H, H^5), 1.47−1.32 (m, 8H, H^6), 1.32−1.20 (m, 32H, H^7), 0.87 (t, J = 7.0 Hz, 6H, H^8).

^{13}C NMR (126 MHz, $CDCl_3$, ppm): δ = 172.4 (C_q, C_{Ester}, C^1), 51.8 (CH_3, C_{Ester}, C^2), 42.0 (CH, β-C_{Ester}, C^3), 41.1 (CH_2, α-C_{Ester}, C^4), 35.3 (CH_2, C^5), 32.0 (CH_2, C^5), 30.9 (CH_2, C^5), 29.9 (CH_2, C^5), 29.7 (CH_2, C^5), 29.7 (CH_2, C^5), 29.6 (CH_2, C^5), 29.6 (CH_2, C^5), 29.4 (CH_2, C^5), 29.4 (CH_2, C^5), 29.1 (CH_2, C^5), 26.9 (CH_2, C^5), 22.8 (CH_2, C^5), 14.3 (CH_3, C^6).

IR (ATR, cm^{-1}): $\tilde{\nu}$ = 2922 (vs), 2851 (s), 1738 (vs), 1459 (w), 1435 (m), 1353 (w), 1278 (w), 1237 (w), 1220 (w), 1153 (s), 1125 (w), 1069 (vw), 1017 (w), 986 (vw), 881 (vw), 841 (vw), 721 (w).

ESI-MS ($[M+H]^+$, $C_{36}H_{71}O_4S_2$) calcd.: 631.4788; found: 631.4794.

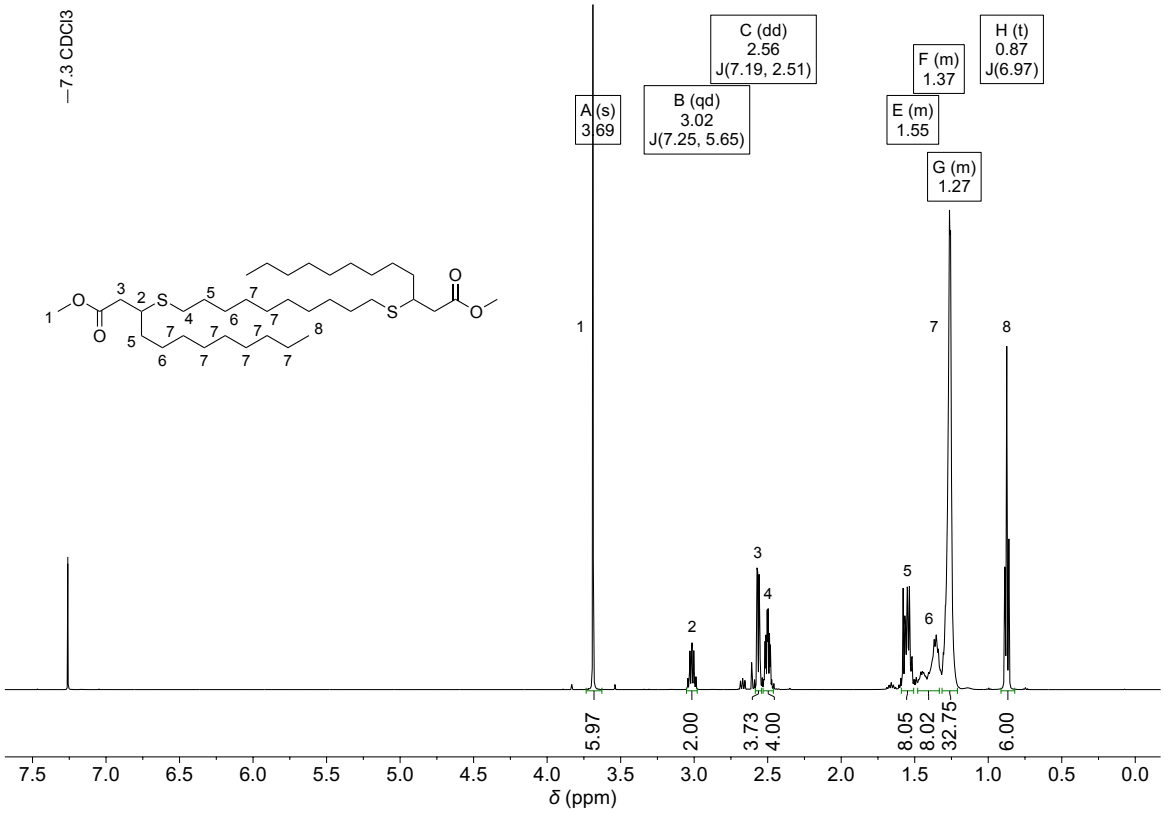

Figure 6.33: ^{1}H NMR spectrum of **LD3** in $CDCl_3$.

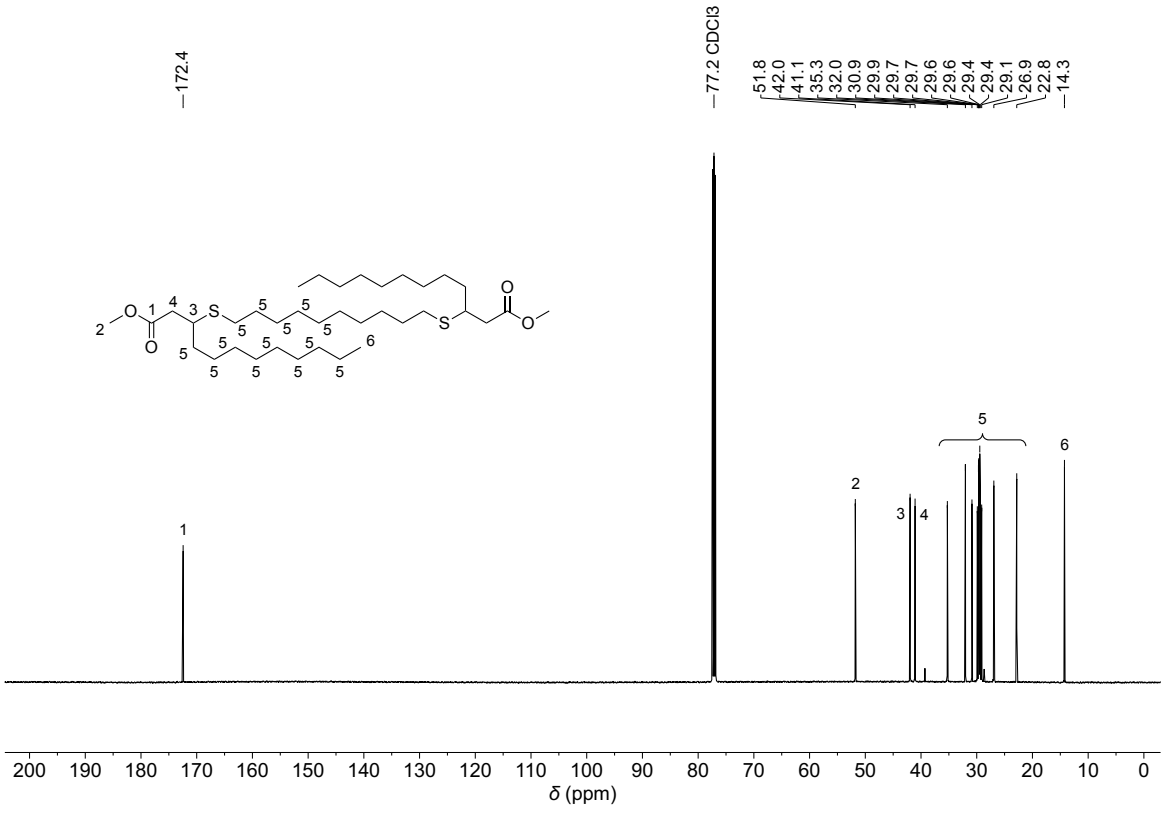

Figure 6.34: ^{13}C NMR spectrum of **LD3** in $CDCl_3$.

6.7 Polymerizations of thia-Michael-based dimethyl esters

General procedure:

Dimethyl ester (**CD1**-**CD3**, or **LD1**-**LD3**) (1.00 equiv.), 1,12-dodecanediol (1.00 equiv.), and titanium(IV)isopropoxide (5.00 mol%) were weighed into a 10 ml screw-cap vial. Methanol (2 ml) and dichloromethane (2 ml) were added, and the compounds were mixed for 10 minutes to obtain a homogeneous solution. The mixture was then transferred into a Schlenk tube equipped with a mechanical stirrer. The pressure was reduced to 700 mbar and the reaction was stirred at 140 °C for 3 h and then at 180 °C for 15 h. Afterwards, the pressure was reduced to 100 mbar and the reaction was stirred at 200 °C for 1 h. The pressure was further reduced to 10 mbar and the reaction was stirred for another 4 h at 200 °C. After cooling to room temperature, the residue was dissolved in chloroform and precipitated in a cold methanol/chloroform mixture (2:1). The polymer was isolated by filtration and dried at 70 °C and 10 mbar.

6.7.1 Polymerization of CD1 with 1,12-dodecanediol (CD-P1)

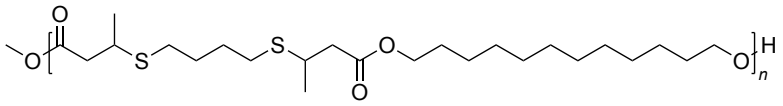

Repeating unit:
$C_{24}H_{44}O_4S_2$
M = 460.73 g/mol

1.00 g (3.10 mmol) of **CD1** was used for this reaction. After work-up, 560 mg of polymer was obtained. The general procedure for the polymerization is described in the beginning of this chapter (page 143).

SEC (THF): M_n = 20600 Da, M_w = 31400 Da, $Đ$ = 1.52.

^{1}H NMR (500 MHz, $CDCl_3$, ppm): δ = 4.07 (t, J = 6.8 Hz, 4H, H^1), 3.24−3.11 (m, 2H, H^2), 2.60 (dd, J = 15.4, 6.2 Hz, 2H, H^3), 2.57−2.52 (m, 4H, H^4), 2.42 (dd, J = 15.4, 8.3 Hz, 2H, H^3), 1.72−1.65 (m, 4H, H^5), 1.62 (p, J = 6.9 Hz, 4H, H^6), 1.37−1.21 (m, 22H, H^7).

***M*$_n$ *via* ^{1}H NMR**: The end group at 3.63 ppm (signal “b” in Figure S35) shows an integral value of 0.07 if the two CH groups of the thioether moieties in the repeating unit are set to an integral value of 2. Due to the higher volatility of **CD1** compared to 1,12-dodecanediol, there is a significantly smaller methyl ester end group integral of 0.02 at 3.69 ppm (signal “a” in Figure S35). For simplicity, it is therefore assumed that each polymer/oligomer bears two end groups “b”. Therefore, the integral of 0.07 corresponds to 57.1 repeating units on average and hence a number average molar mass of 26300 Da.

^{13}C NMR (126 MHz, $CDCl_3$, ppm): δ = 171.7 (C_q, C_{Ester}, C^1), 64.9 (CH_2, C_{Ester}, C^2), 42.5 (CH_2, α-C_{Ester}, C^3), 36.3 (CH, β-C_{Ester}, C^4), 30.3 (CH_2, C^5), 29.7 (CH_2, C^5), 29.7 (CH_2, C^5), 29.4 (CH_2, C^5), 28.9 (CH_2, C^5), 28.7 (CH_2, C^5), 26.0 (CH_2, C^5), 21.6 (CH_3, C^6).

IR (ATR, cm^{-1}): $\tilde{\nu}$ = 2922 (m), 2853 (w), 1731 (vs), 1453 (w), 1375 (vw), 1350 (w), 1300 (w), 1282 (w), 1220 (m), 1156 (vs), 1106 (w), 1072 (w), 1021 (w), 989 (w), 722 (vw).

TGA ($T_{d,5\%}$): 306 °C.

DSC (−150 °C to 200 °C, 10 K min^{-1}): T_g = −44 °C, T_{cc} = − 29 °C, T_m = 10 °C.

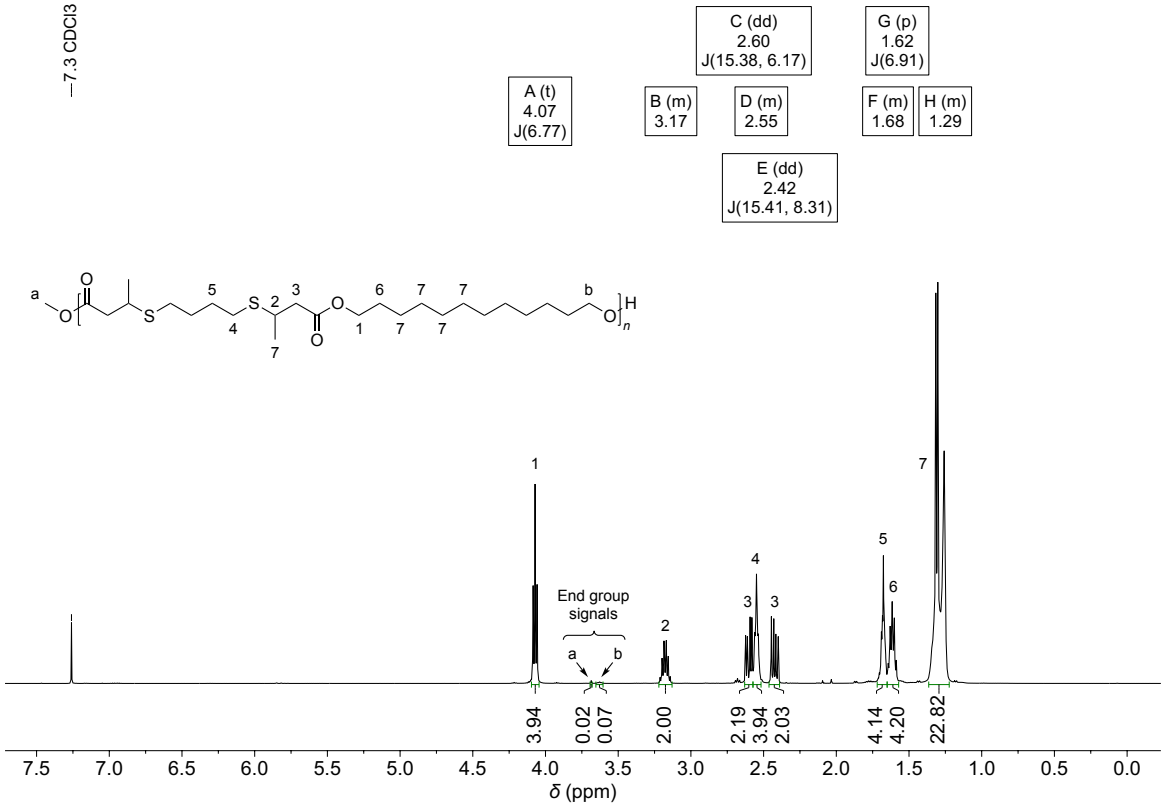

Figure 6.35: ^{1}H NMR spectrum of **CD-P1** in $CDCl_3$.

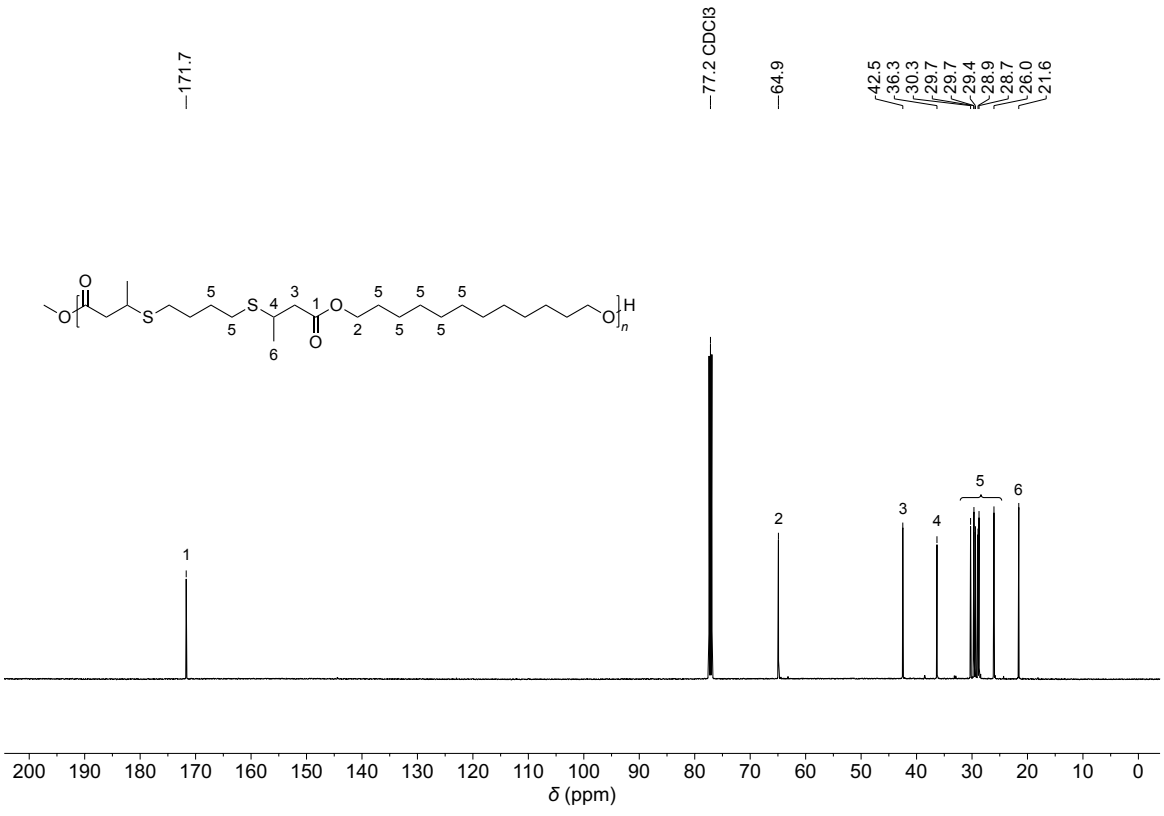

Figure 6.36: ^{13}C NMR spectrum of **CD-P1** in $CDCl_3$.

6.7.2 Polymerization of LD1 with 1,12-dodecanediol (LD-P1)

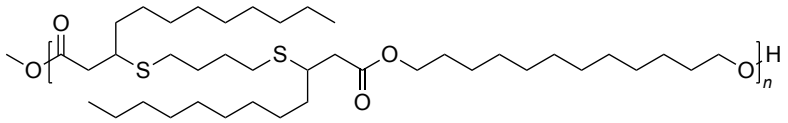

Repeating unit:
$C_{40}H_{76}O_4S_2$
M = 685.16 g/mol

1.26 g (2.30 mmol) of **LD1** was used for this reaction. After work-up, 1.22 g of polymer was obtained.

The general procedure for the polymerization is described in the beginning of this chapter (page 143).

SEC (THF): M_n = 31800 Da, M_w = 55500 Da, $Đ$ = 1.75.

^{1}H NMR (500 MHz, $CDCl_3$, ppm): δ = 4.07 (t, J = 6.8 Hz, 4H, H^1), 3.01 (qd, J = 7.3, 5.5 Hz, 2H, H^2), 2.57−2.47 (m, 8H, H^3), 1.69−1.64 (m, 4H, H^4), 1.64−1.59 (m, 4H, H^5), 1.59−1.51 (m, 4H, H^6), 1.47−1.20 (m, 44H, H^7), 0.87 (t, J = 6.9 Hz, 6H, H^8).

***M_n via* ^{1}H NMR**: The end group at 3.63 ppm (signal “b” in Figure S37) shows an integral value of 0.05 if the two CH groups of the thioether moieties in the repeating unit are set to an integral value of 2. For simplicity, it is assumed that each polymer/oligomer bears one end group “a” and one end group “b”. Therefore, the integral of 0.05 corresponds to 40 repeating units on average and hence a number average molar mass of 27400 Da.

^{13}C NMR (126 MHz, $CDCl_3$, ppm): δ = 172.0 (C_q, C_{Ester}, C^1), 64.9 (CH_2, C_{Ester}, C^2), 42.0 (CH, β-C_{Ester}, C^3), 41.2 (CH_2, α-C_{Ester}, C^4), 35.2 (CH_2, C^5), 32.0 (CH_2, C^5), 30.3 (CH_2, C^5), 29.8 (CH_2, C^5), 29.7 (CH_2, C^5), 29.7 (CH_2, C^5), 29.6 (CH_2, C^5), 29.5 (CH_2, C^5), 29.5 (CH_2, C^5), 29.1 (CH_2, C^5), 28.8 (CH_2, C^5), 26.9 (CH_2, C^5), 26.1 (CH_2, C^5), 22.8 (CH_2, C^5), 14.3 (CH_3, C^6).

IR (ATR, cm^{-1}): $\tilde{\nu}$ = 2921 (vs), 2851 (s), 1732 (vs), 1463 (w), 1387 (vw), 1349 (w), 1298 (w), 1278 (w), 1235 (w), 1150 (s), 1123 (w), 1065 (vw), 976 (vw), 721 (w).

TGA ($T_{d,5\%}$): 332 °C.

DSC (−150 °C to 200 °C, 10 K min^{-1}): T_m = −31 °C, T_{cc} = −11°C, T_m = 16 °C.

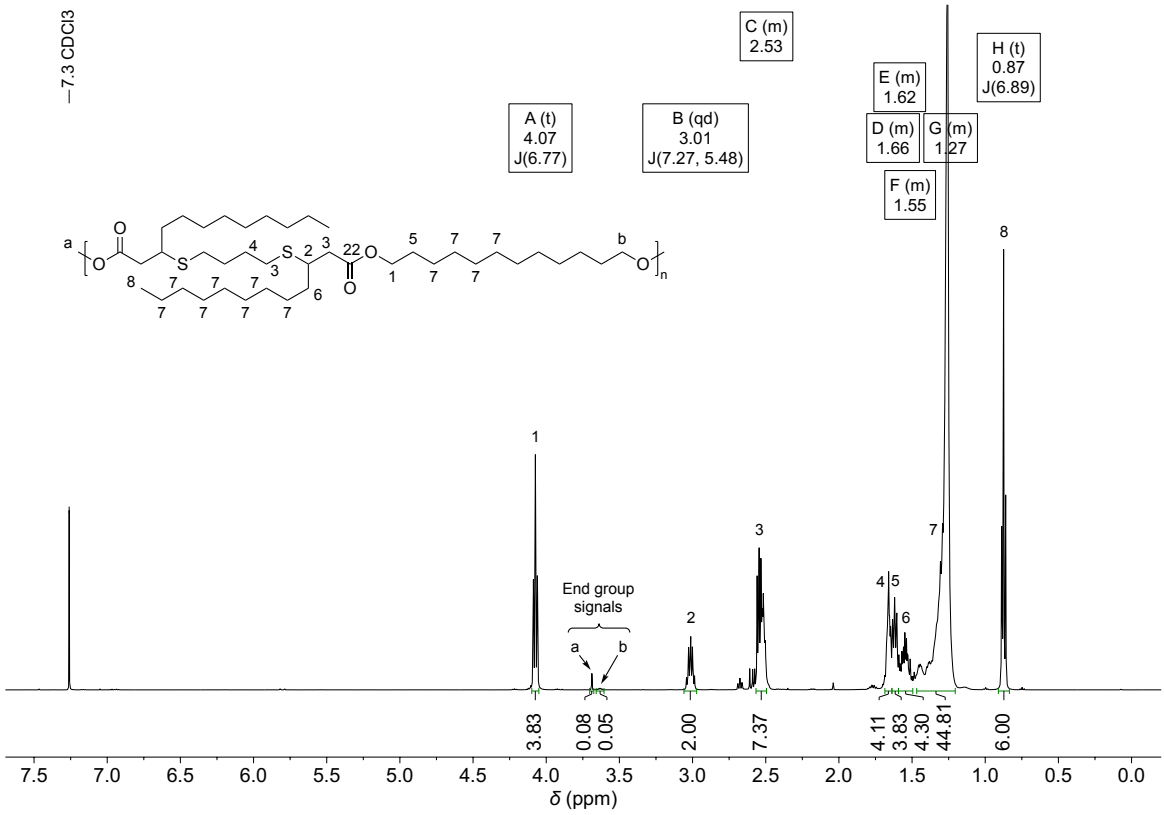

Figure 6.37: ^{1}H NMR spectrum **LD-P1** in $CDCl_3$.

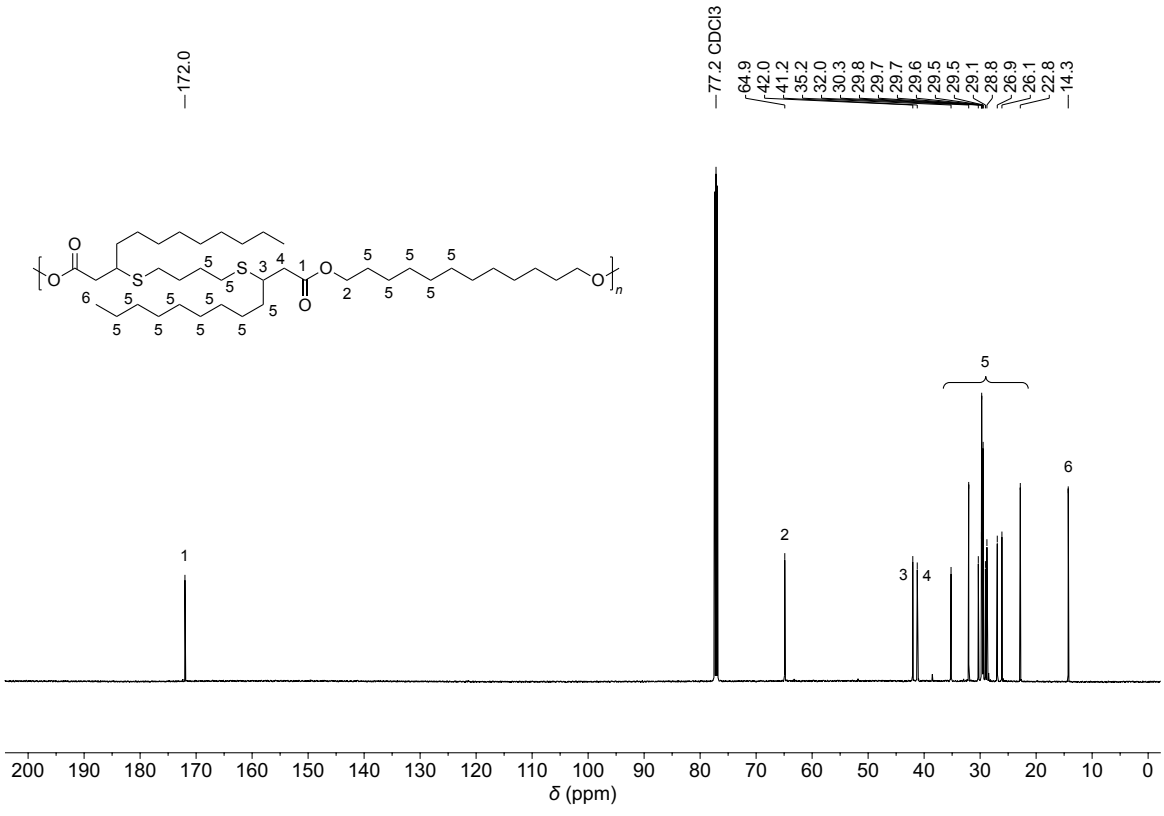

Figure 6.38: ^{13}C NMR spectrum of **LD-P1** in $CDCl_3$.

6.7.3 TGA and DSC data of CD-P1 and LD-P1

TGA: $T_{d,5\%}$ (**CD-P1**): 306 °C; $T_{d,5\%}$ (**LD-P1**): 332 °C.

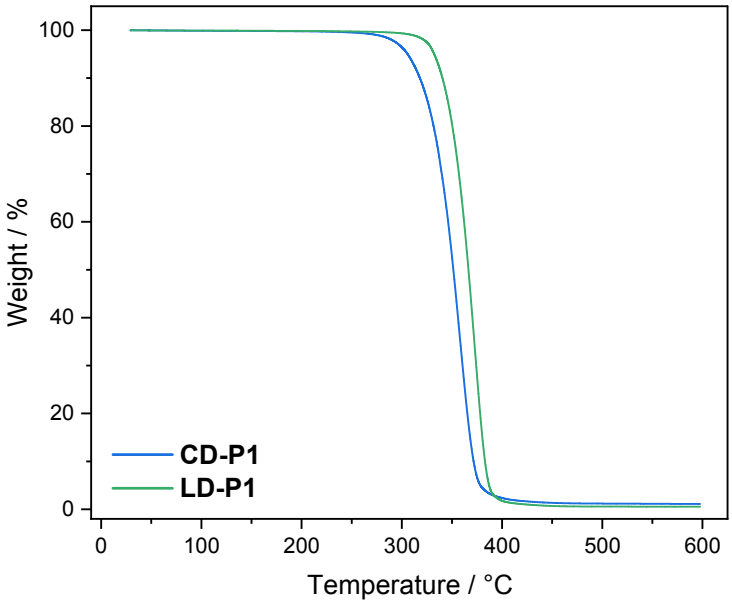

Figure 6.39: TGA measurements of **CD-P1** and **LD-P1**.

DSC: **CD-P1**: T_g = −44 °C, T_{cc} = − 29 °C, T_m = 10 °C.
LD-P1: T_m = −31 °C, T_{cc} = −11°C, T_m = 16 °C.

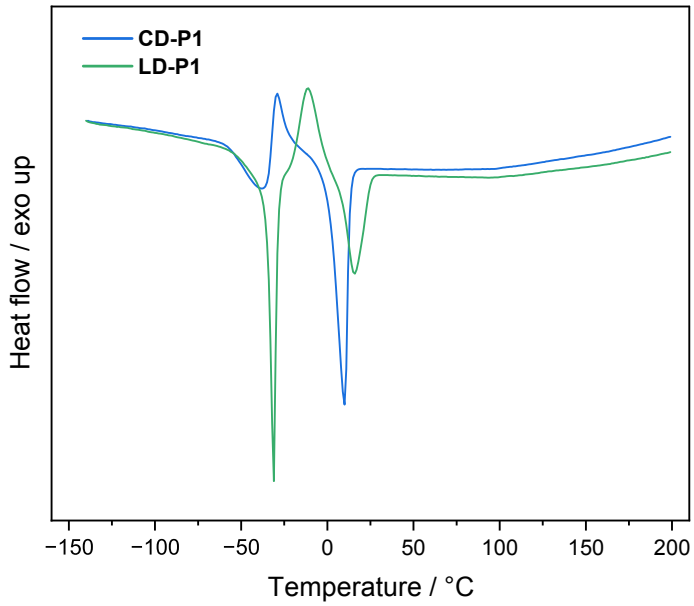

Figure 6.40: DSC measurements of **CD-P1** and **LD-P1**.

6.7.4 Polymerization of CD2 with 1,12-dodecanediol (CD-P2)

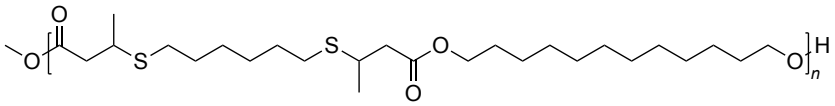

Repeating unit:
$C_{26}H_{48}O_4S_2$
M = 488.79 g/mol

1.02 g (2.90 mmol) of **CD2** was used for this reaction. After work-up, 1.18 g of polymer was obtained.

The general procedure for the polymerization is described in the beginning of this chapter (page 143).

SEC (THF): M_n = 13000 Da, M_w = 22200 Da, $Đ$ = 1.71.

^{1}H NMR (400 MHz, $CDCl_3$, ppm): δ = 4.07 (t, J = 6.8 Hz, 4H, H^1), 3.18 (dp, J = 8.4, 6.7 Hz, 2H, H^2), 2.61 (dd, J = 15.3, 6.1 Hz, 2H, H^3), 2.53 (t, J = 7.4 Hz, 4H, H^4), 2.42 (dd, J = 15.3, 8.3 Hz, 2H, H^3), 1.70−1.49 (m, 8H, H^5), 1.48−1.13 (m, 26H, H^6).

***M*$_n$ *via* ^{1}H NMR**: The end group at 3.63 ppm (signal “b” in Figure S41) shows an integral value of 0.08 if the two CH groups of the thioether moieties in the repeating unit are set to an integral value of 2. For simplicity, it is assumed that each polymer/oligomer bears one end group “a” and one end group “b”. Therefore, the integral of 0.08 corresponds to 25 repeating units on average and hence a number average molar mass of 12200 Da.

^{13}C NMR (101 MHz, $CDCl_3$, ppm): δ = 171.7 (C_q, C_{Ester}, C^1), 64.9 (CH_2, C_{Ester}, C^2), 42.5 (CH_2, α-C_{Ester}, C^3), 36.3 (CH, β-C_{Ester}, C^4), 30.7 (CH_2, C^5), 29.7 (CH_2, C^5), 29.7 (CH_2, C^5), 29.4 (CH_2, C^5), 28.7 (CH_2, C^5), 28.7 (CH_2, C^5), 26.1 (CH_2, C^5), 21.6 (CH_3, C^6).

IR (ATR, cm^{-1}): $\tilde{\nu}$ = 2922 (m), 2853 (w), 1731 (vs), 1455 (w), 1421 (vw), 1388 (vw), 1350 (w), 1285 (w), 1218 (m), 1156 (vs), 1108 (vw), 1074 (w), 1021 (w), 990 (vw), 722 (vw).

TGA ($T_{d,5\%}$): 321 °C.

DSC (−150 °C to 200 °C, 10 K min^{-1}): T_g = −52 °C, T_{cc} = −29 °C, T_m = 13 °C.

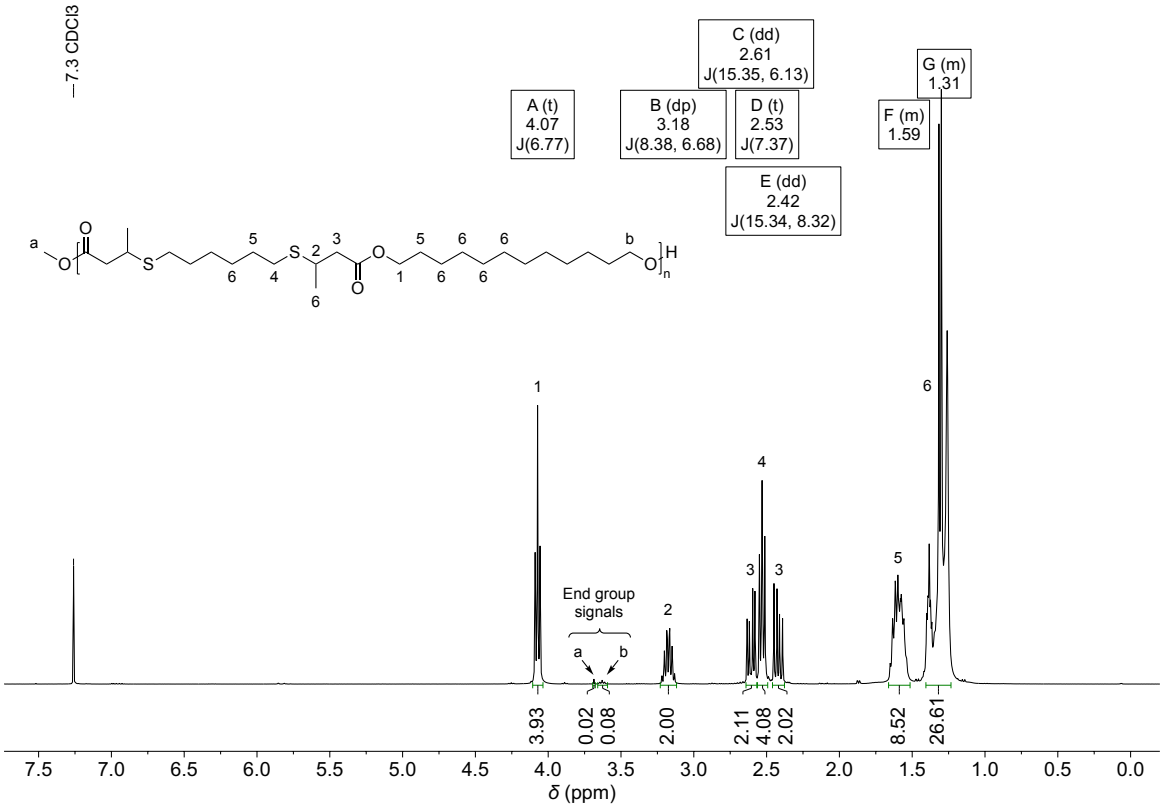

Figure 6.41: ^{1}H NMR spectrum of **CD-P2** in $CDCl_3$.

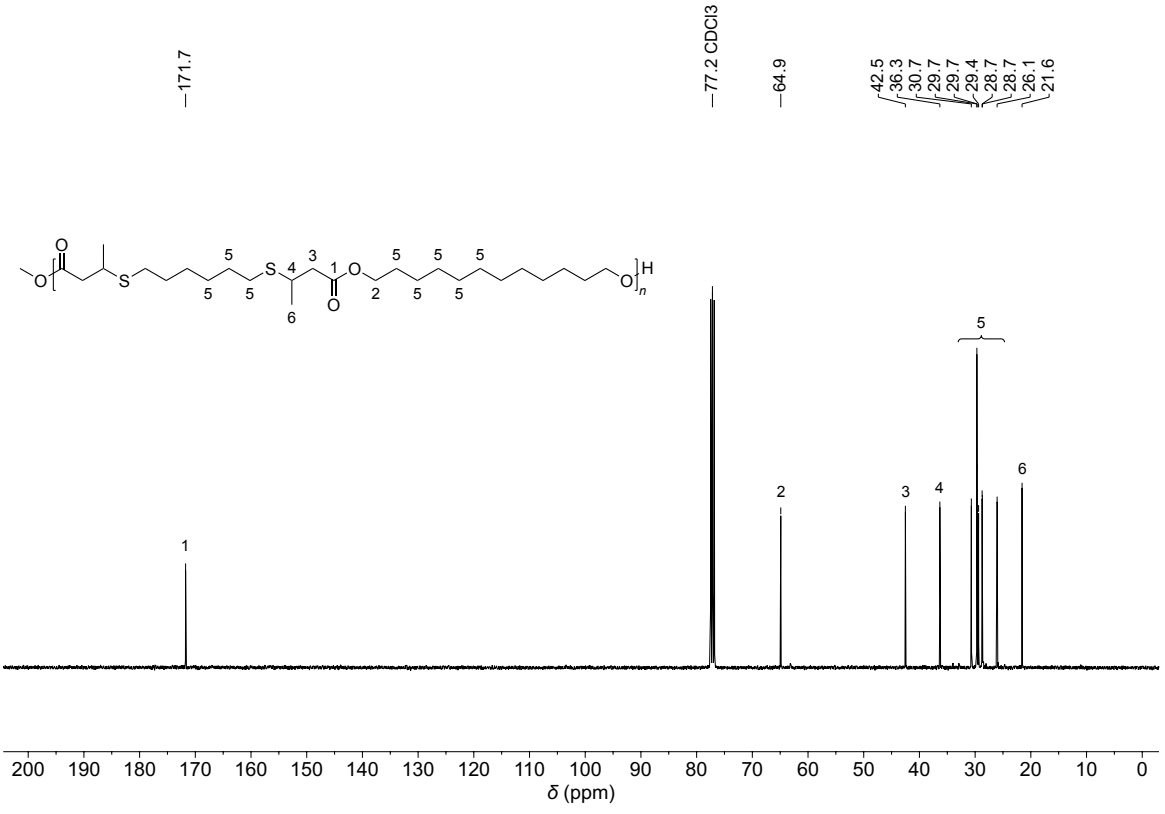

Figure 6.42: ^{13}C NMR Spectrum of **CD-P2** in $CDCl_3$.

6.7.5 Polymerization of LD2 with 1,12-dodecanediol (LD-P2)

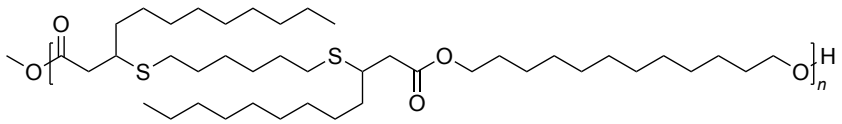

Repeating unit:
$C_{42}H_{80}O_4S_2$
M = 713.22 g/mol

1.04 g (1.80 mmol) of **LD2** was used for this reaction. After work-up, 1.04 g of polymer was obtained.

The general procedure for the polymerization is described in the beginning of this chapter (page 143).

SEC (THF): M_n = 28100 Da, M_w = 51900 Da, $Đ$ = 1.85.

^{1}H NMR (500 MHz, $CDCl_3$, ppm): δ = 4.08 (t, J = 6.8 Hz, 4H, H^1), 3.09−2.93 (m, 2H, H^2), 2.55 (t, J = 7.3 Hz, 4H, H^3), 2.50 (td, J = 7.4, 3.3 Hz, 4H, H^4), 1.65 1.59 (m, 4H, H^5), 1.60−1.51 (m, 8H, H^6), 1.42−1.18 (m, 48H, H^7), 0.87 (t, J = 6.9 Hz, 6H, H^8).

***M*$_n$ *via* ^{1}H NMR**: The end group at 3.63 ppm (signal “b” in Figure S43) shows an integral value of 0.04 if the two CH groups of the thioether moieties in the repeating unit are set to an integral value of 2. For simplicity, it is assumed that each polymer/oligomer bears one end group “a” and one end group “b”. Therefore, the integral of 0.04 corresponds to 50 repeating units on average and hence a number average molar mass of 35700 Da.

^{13}C NMR (126 MHz, $CDCl_3$, ppm): δ = 172.0 (C_q, C_{Ester}, C^1), 64.9 (CH_2, C_{Ester}, C^2), 42.0 (CH, β-C_{Ester}, C^3), 41.3 (CH_2, α-C_{Ester}, C^4), 35.2 (CH_2, C^5), 32.0 (CH_2, C^5), 30.7 (CH_2, C^5), 29.8 (CH_2, C^5), 29.8 (CH_2, C^5), 29.7 (CH_2, C^5), 29.7 (CH_2, C^5), 29.6 (CH_2, C^5), 29.5 (CH_2, C^5), 29.4 (CH_2, C^5), 28.8 (CH_2, C^5), 28.8 (CH_2, C^5), 26.9 (CH_2, C^5), 26.1 (CH_2, C^5), 22.8 (CH_2, C^5), 14.3 (CH_3, C^6).

IR (ATR, cm^{-1}): $\tilde{\nu}$ = 2921 (vs), 2851 (vs), 1734 (vs), 1463 (w), 1387 (vw), 1347 (w), 1235 (w), 1150 (s), 1123 (w), 1062 (vw), 979 (vw), 721 (w).

TGA ($T_{d,5\%}$): 341 °C.

DSC (−150 °C to 200 °C, 10 K min^{-1}): T_g = −50 °C.

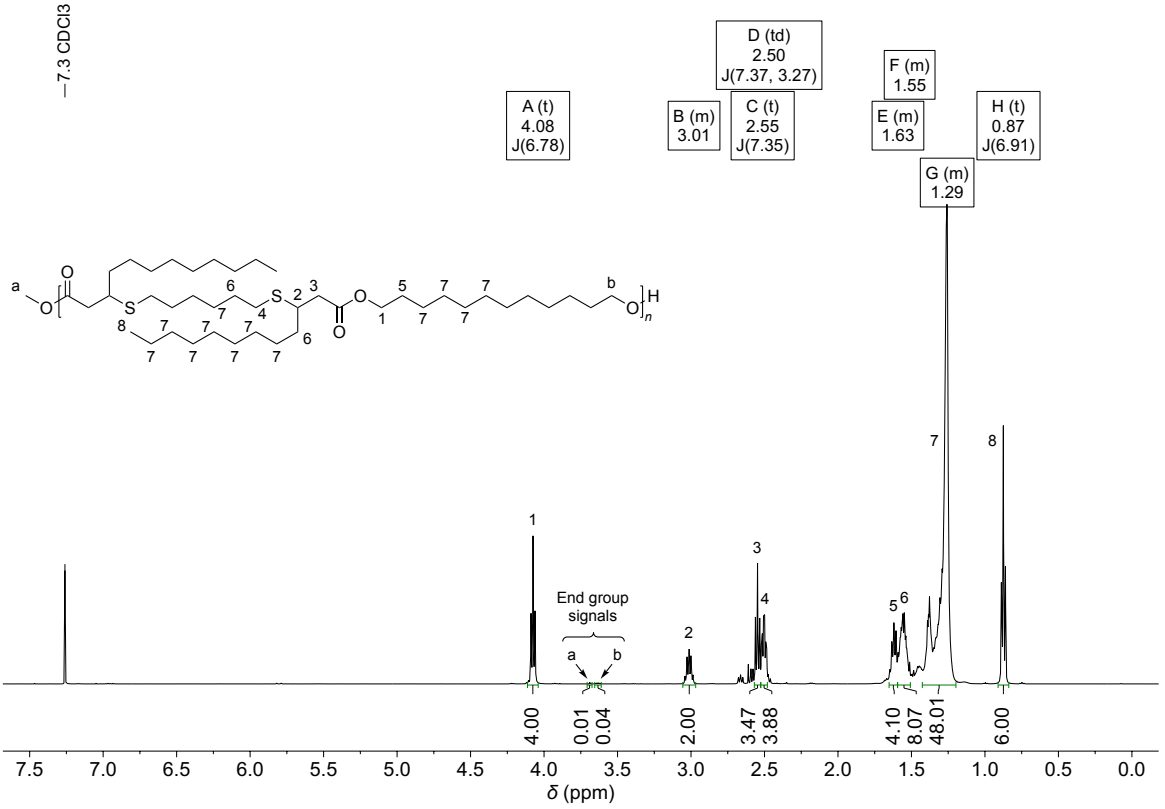

Figure 6.43: ^{1}H NMR spectrum of **LD-P2** in $CDCl_3$.

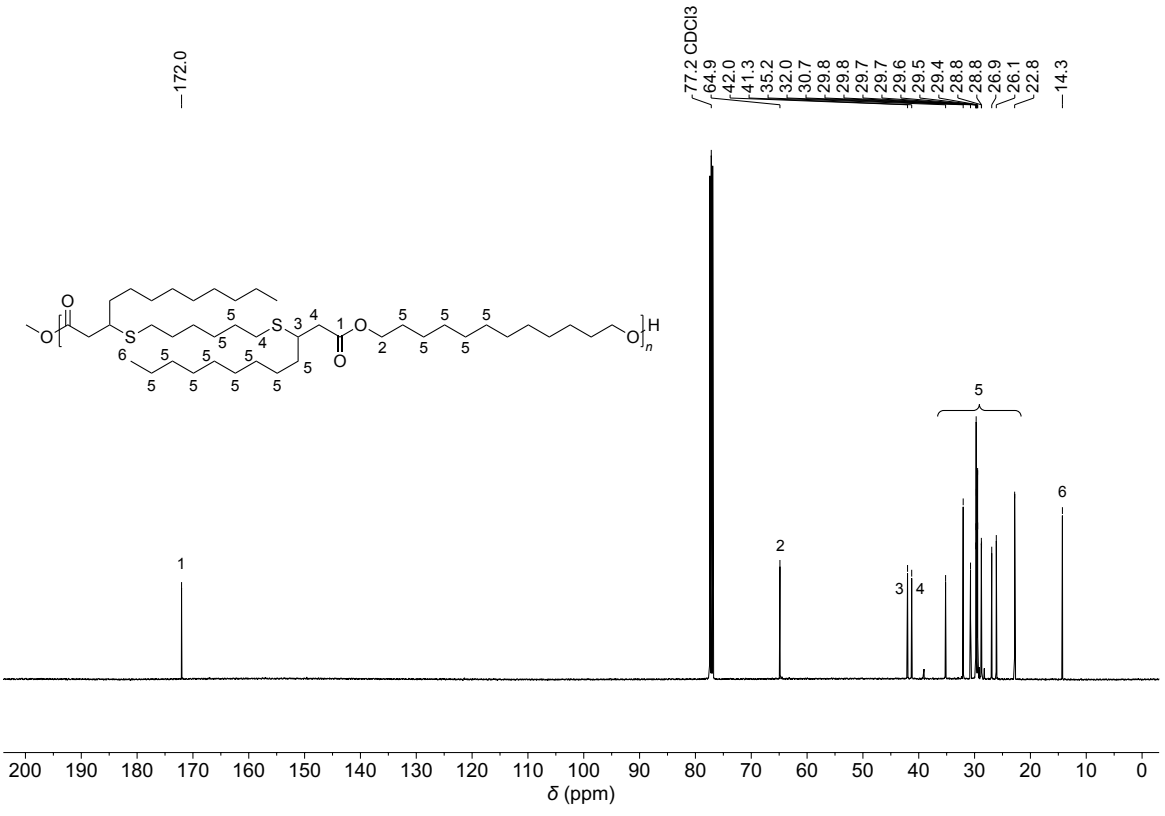

Figure 6.44: ^{13}C NMR spectrum of **LD-P2** in $CDCl_3$.

6.7.6 TGA and DSC data of CD-P2 and LD-P2

TGA: $T_{d,5\%}$ (**CD-P2**): 321 °C; $T_{d,5\%}$ (**LD-P2**): 341 °C.

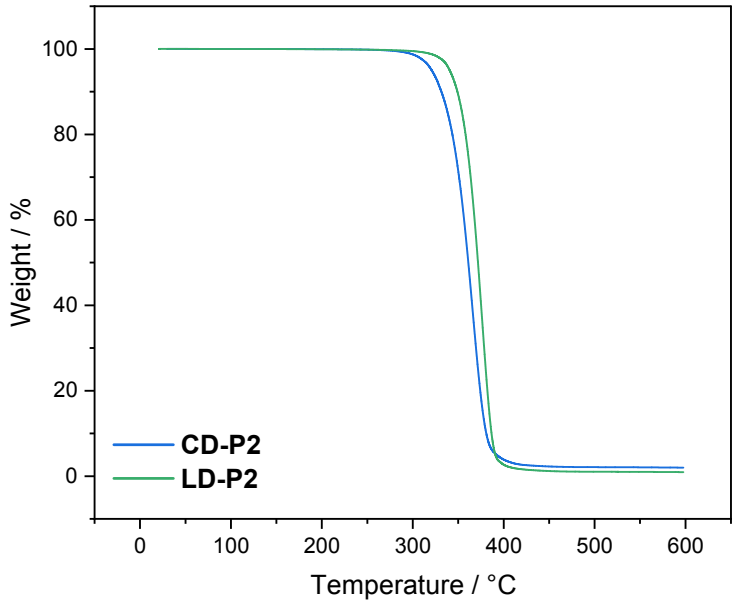

Figure 6.45: TGA measurements of **CD-P2** and **LD-P2**.

DSC: **CD-P2**: T_g = −52 °C, T_{cc} = −29 °C, T_m = 13 °C.
LD-P2: T_g = −50 °C.

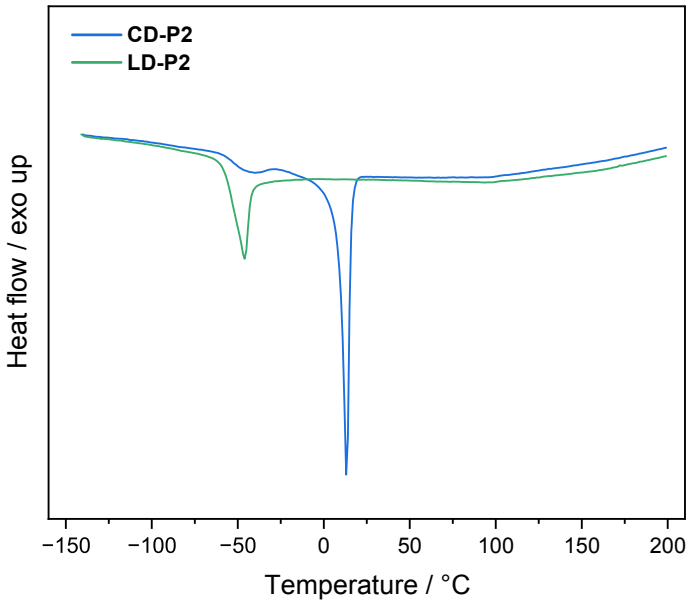

Figure 6.46: DSC measurements of **CD-P2** and **LD-P2**.

6.7.7 Polymerization of CD3 with 1,12-dodecanediol (CD-P3)

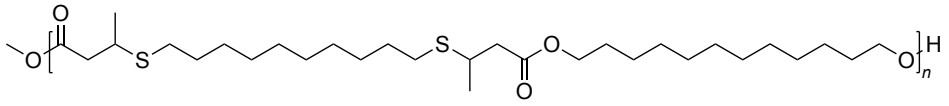

Repeating unit:
$C_{30}H_{56}O_4S_2$
M = 544.89 g/mol

1.18 g (2.90 mmol) of **CD3** was used for this reaction. After work-up, 1.38 g of polymer was obtained.

The general procedure for the polymerization is described in the beginning of this chapter (page 143).

SEC (THF): M_n = 29100 Da, M_w = 50700 Da, $Đ$ = 1.74.

^{1}H NMR (400 MHz, $CDCl_3$, ppm): δ = 4.07 (t, J = 6.8 Hz, 4H, H^1), 3.18 (dp, J = 8.5, 6.7 Hz, 2H, H^2), 2.61 (dd, J = 15.4, 6.1 Hz, 2H, H^3), 2.53 (d, J = 7.4 Hz, 4H, H^4), 2.42 (dd, J = 15.3, 8.4 Hz, 2H, H^3), 1.66−1.59 (m, 4H, H^5), 1.59−1.51 (m, 4H, H^6), 1.39−1.22 (m, 34H, H^7).

***M_n* *via* ^{1}H NMR**: The end group at 3.63 ppm (signal “b” in Figure S47) shows an integral value of 0.05 if the two CH groups of the thioether moieties in the repeating unit are set to an integral value of 2. For simplicity, it is assumed that each polymer/oligomer bears one end group “a” and one end group “b”. Therefore, the integral of 0.05 corresponds to 40.0 repeating units on average and hence a number average molar mass of 21800 Da.

^{13}C NMR (101 MHz, $CDCl_3$, ppm): δ = 171.8 (C_q, C_{Ester}, C^1), 64.9 (CH_2, C_{Ester}, C^2), 42.5 (CH_2, α-C_{Ester}, C^3), 36.3 (CH_2, β-C_{Ester}, C^4), 30.8 (CH_2, C^5), 29.8 (CH_2, C^5), 29.7 (CH_2, C^5), 29.7 (CH_2, C^5), 29.6 (CH_2, C^5), 29.4 (CH_2, C^5), 29.4 (CH_2, C^5), 29.1 (CH_2, C^5), 28.7 (CH_2, C^5), 26.1 (CH_2, C^5), 21.6 (CH_3, C^6).

IR (ATR, cm^{-1}): $\tilde{\nu}$ = 2918 (vs), 2850 (m), 1728 (vs), 1466 (w), 1418 (vw), 1374 (vw), 1351 (w), 1307 (w), 1282 (w), 1222 (m), 1157 (vs), 1118 (vw), 1075 (w), 1026 (w), 975 (vw), 721 (w).

TGA ($T_{d,5\%}$): 334 °C.

DSC (−150 °C to 200 °C, 10 K min^{-1}): T_g = −30 °C, T_m = 36 °C.

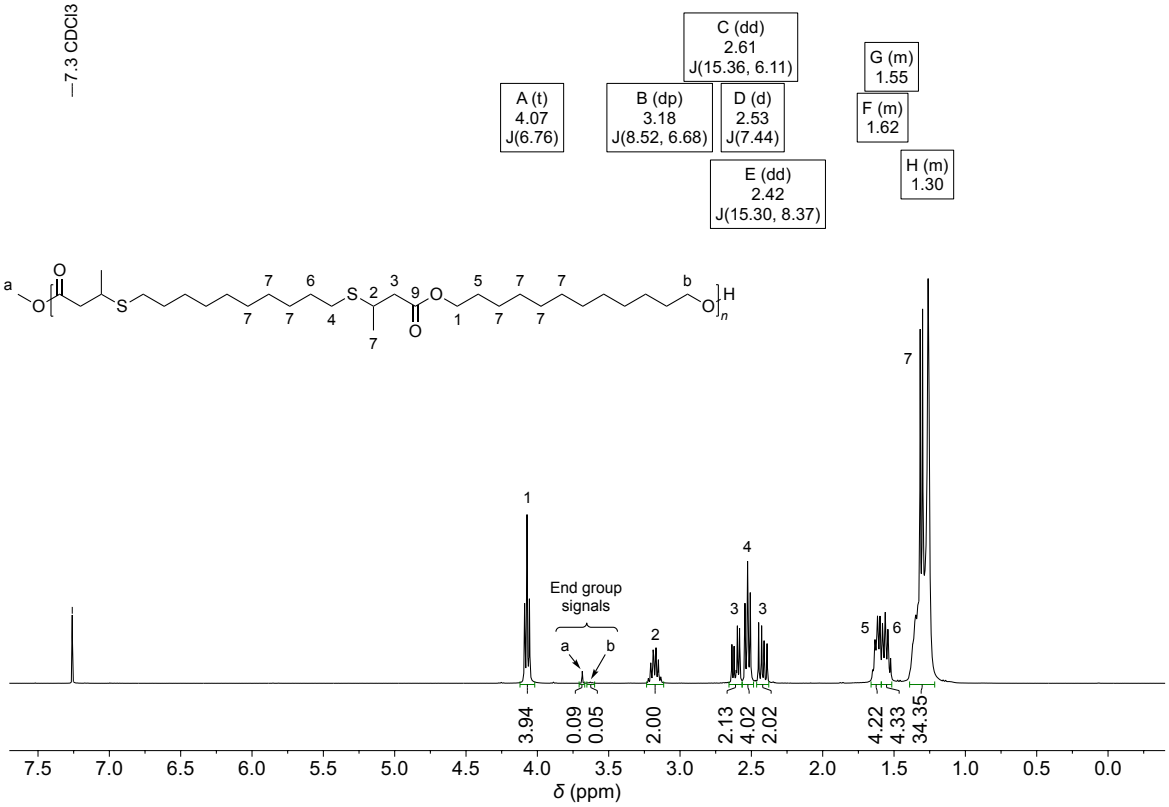

Figure 6.47: ^{1}H NMR spectrum of **CD-P3** in $CDCl_3$.

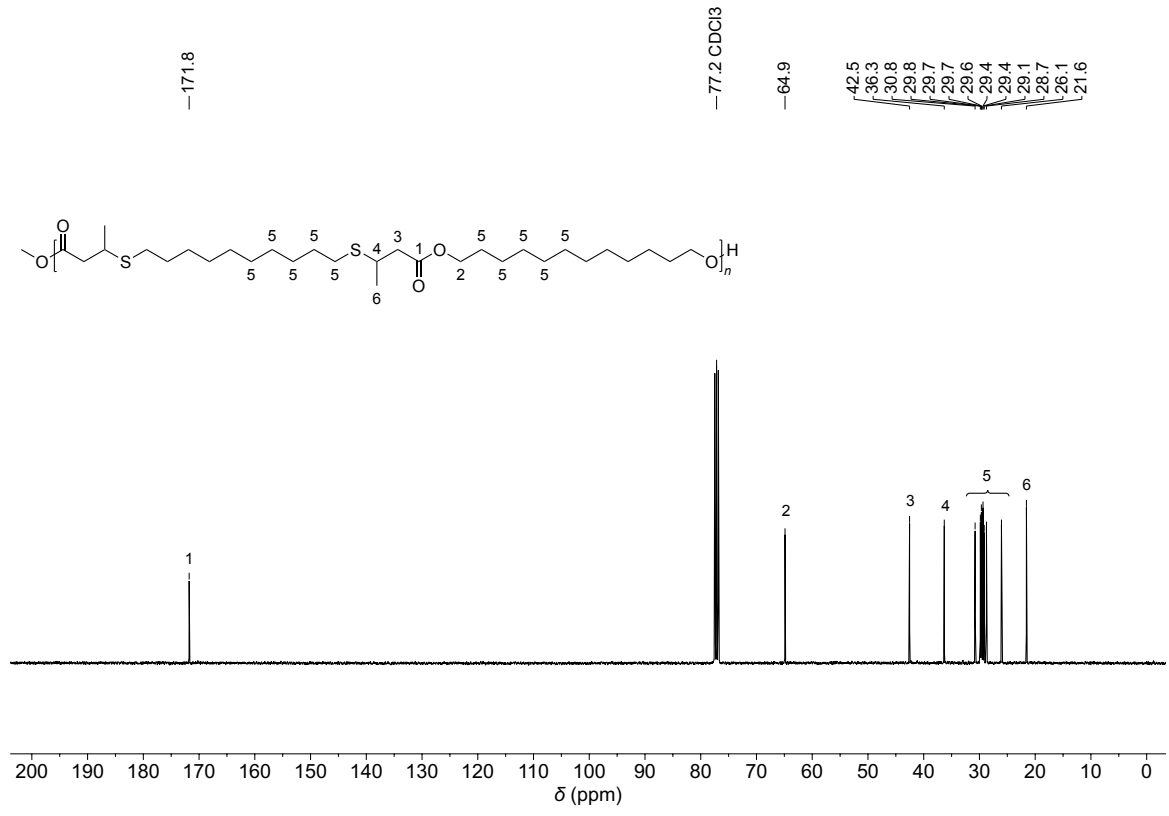

Figure 6.48: ^{13}C NMR spectrum of **CD-P3** in $CDCl_3$.

6.7.8 Polymerization of LD3 with 1,12-dodecanediol (LD-P3)

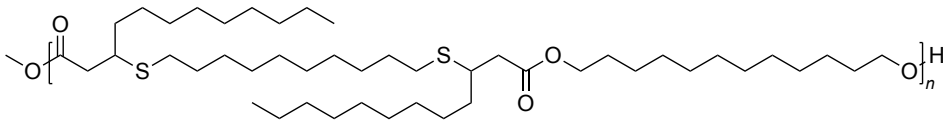

Repeating unit:
$C_{46}H_{88}O_4S_2$
M = 769.33 g/mol

1.14 g (2.90 mmol) of **LD3** was used for this reaction. After work-up, 1.17 g of polymer was obtained.

The general procedure for the polymerization is described in the beginning of this chapter (page 143).

SEC (THF): M_n = 26000 Da, M_w = 47600 Da, $Đ$ = 1.83.

^{1}H NMR (500 MHz, $CDCl_3$, ppm): δ = 4.08 (t, J = 6.8 Hz, 4H, H^1), 3.06−2.96 (m, 2H, H^2), 2.55 (t, J = 7.7 Hz, 4H, H^3), 2.50 (td, J = 7.2, 3.3 Hz, 4H, H^4), 1.63 (p, J = 6.9 Hz, 4H, H^5), 1.59−1.51 (m, 8H, H^6), 1.41−1.20 (m, 56H, H^7), 0.88 (t, J = 6.9 Hz, 6H, H^8).

***M*$_n$ *via* ^{1}H NMR**: The end group at 3.69 ppm (signal “a” in Figure S49) shows an integral value of 0.09 if the two CH groups of the thioether moieties in the repeating unit are set to an integral value of 2. For simplicity, it is assumed that each polymer/oligomer bears one end group “a” and one end group “b”. Therefore, the integral of 0.09 corresponds to 33 repeating units on average and hence a number average molar mass of 25600 Da.

^{13}C NMR (126 MHz, $CDCl_3$, ppm): δ = 172.1 (C_q, C_{Ester}, C^1), 64.9 (CH_2, C_{Ester}, C^2), 42.0 (CH, β-C_{Ester}, C^3), 41.3 (CH_2, α-C_{Ester}, C^4), 35.2 (CH_2, C^5), 32.0 (CH_2, C^5), 30.8 (CH_2, C^5), 29.9 (CH_2, C^5), 29.8 (CH_2, C^5), 29.7 (CH_2, C^5), 29.7 (CH_2, C^5), 29.7 (CH_2, C^5), 29.6 (CH_2, C^5), 29.5 (CH_2, C^5), 29.4 (CH_2, C^5), 29.4 (CH_2, C^5), 29.2 (CH_2, C^5), 28.8 (CH_2, C^5), 26.9 (CH_2, C^5), 26.1 (CH_2, C^5), 22.8 (CH_2, C^5), 14.3 (CH_3, C^6).

IR (ATR, cm^{-1}): $\tilde{\nu}$ = 2921 (vs), 2851 (vs), 1734 (vs), 1465 (w), 1387 (vw), 1347 (w), 1298 (w), 1276 (w), 1234 (w), 1150 (s), 1116 (vw), 1064 (vw), 1004 (vw), 721 (w).

TGA ($T_{d,5\%}$): 344 °C.

DSC (−150 °C to 200 °C, 10 K min^{-1}): T_g = −40 °C, T_{cc} = −24 °C, T_m = 0 °C, T_m = 15 °C.

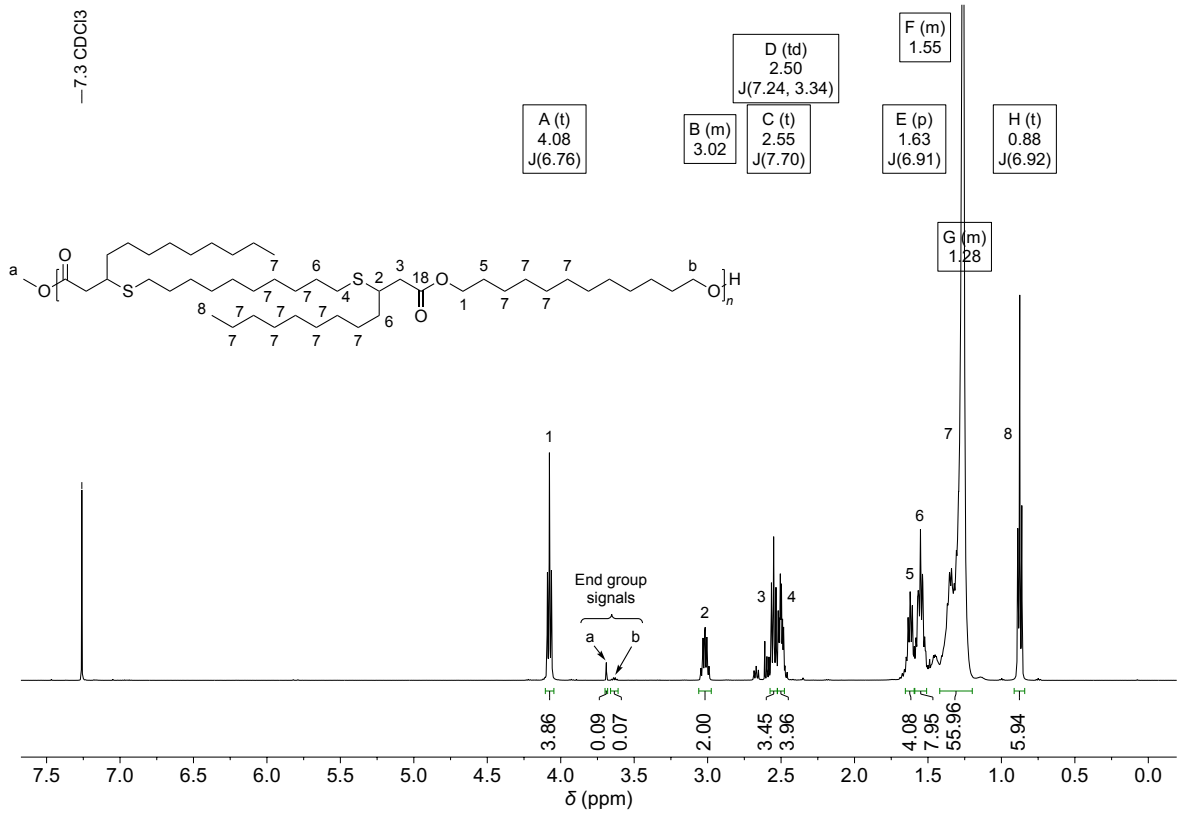

Figure 6.49: ^{1}H NMR spectrum of **LD-P3** in $CDCl_3$.

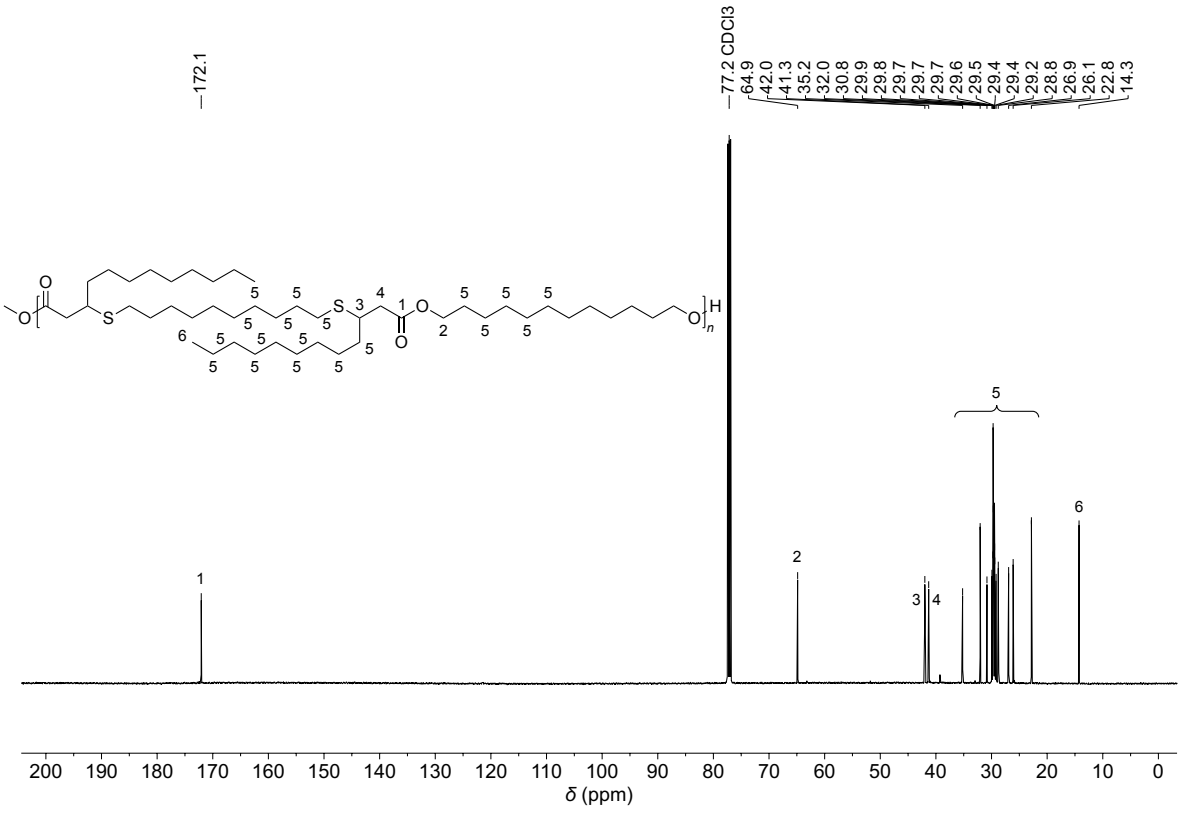

Figure 6.50: ^{13}C NMR spectrum of **LD-P3** in $CDCl_3$.

6.7.9 TGA and DSC data of CD-P3 and LD-P3

TGA: $T_{d,5\%}$ (**CD-P3**) : 334 °C; $T_{d,5\%}$ (**LD-P3**): 344 °C.

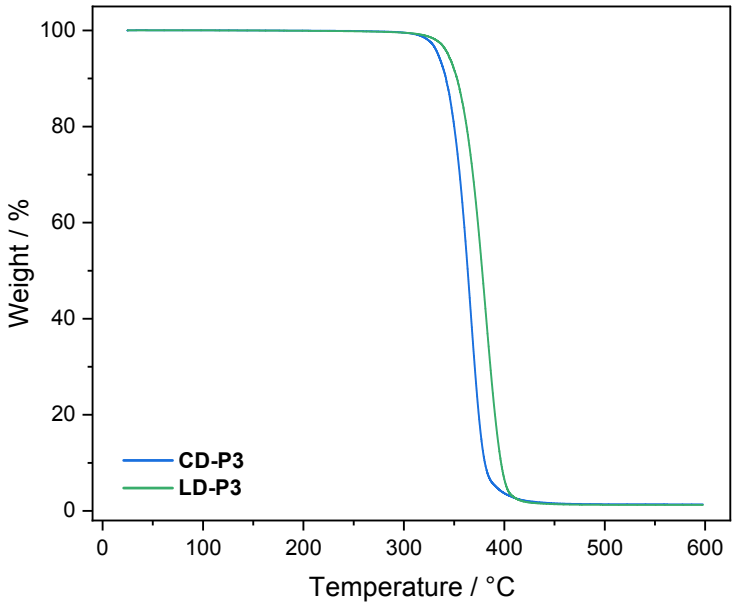

Figure 6.51: TGA measurements of **CD-P3** and **LD-P3**.

DSC: **CD-P3**: T_g = −30 °C, T_m = 36 °C.
LD-P3: T_g = −40 °C, T_{cc} = −24 °C, T_m = 0 °C, T_m = 15 °C.

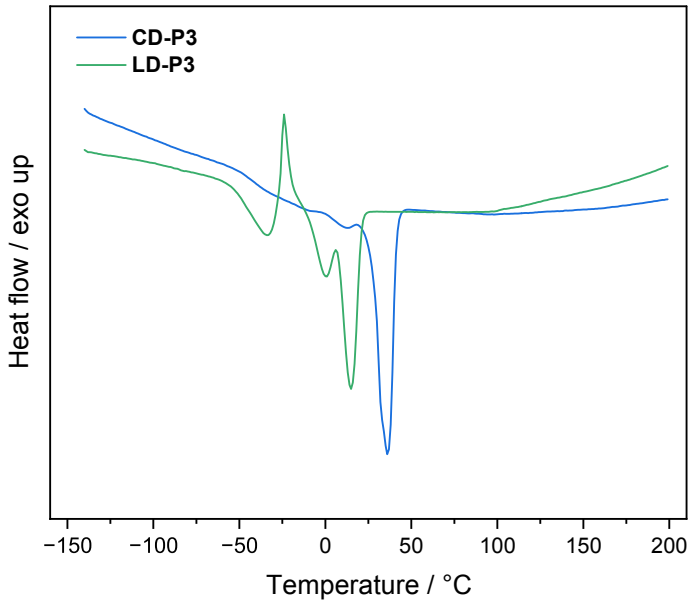

Figure 6.52: DSC measurements of **CD-P3** and **LD-P3**.

6.8 Fatty acid content determination of high oleic sunflower oils

Four different high oleic sunflower oils were bought at local supermarkets in Karlsruhe, Germany: high oleic sunflower oil 01 (**HOSO01**) and high oleic sunflower oil 02 (**HOSO02**) were bought in Alnatura, high oleic sunflower oil 03 (**HOSO03**) was bought in Scheck-in-Center, and high oleic sunflower oil 04 (**HOSO04**) was bought in dm. All four oil bottles are depicted in ascending order from left to right in Figure 6.53. The fatty acid content of each oil was determined *via* GC-MS supplemented by ^{1}H NMR spectroscopy to determine the oil with the highest content of oleic acid. This fatty acid content determination will be described in the following.

Figure 6.53: Picture of the high oleic sunflower oils HOSO01 to HOSO04 in ascending order from left to right.

6.8.1 Retention times of all investigated fatty acid methyl esters

Pure reference samples of methyl myristate (C14:0), methyl palmitate (C16:0), methyl stearate (C18:0), methyl arachidate (C20:0), methyl oleate (C18:1 cis (ω-9)), methyl elaidate (C18:1 trans (ω-9)), methyl linoleate (C18:2 cis (ω-9)), methyl linolenate (C18:3 cis (ω-3)), were measured *via* GC-MS to determine their retention times. An overlay of all chromatograms is depicted in Figure 6.54.

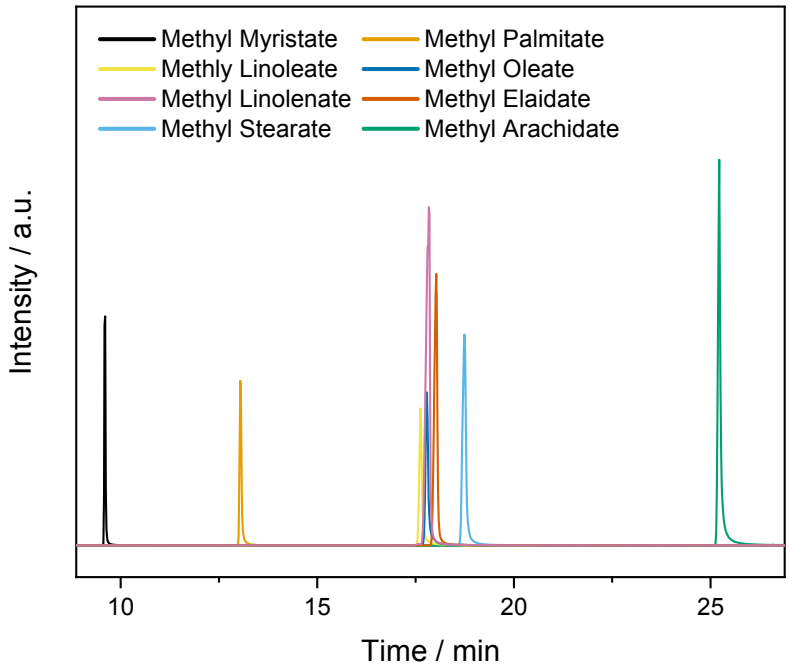

Figure 6.54: GC-MS chromatograms of all fatty acid methyl esters overlayed to show the achieved separation through the used method.

Additionally, all retention times are ordered in Table 6.5 from low retention times to high retention times.

Table 6.5: GC-MS retention times of all analyzed fatty acid methyl esters.

Fatty acid methyl ester	Retention time / min
Methyl myristate (C14:0)	9.60
Methyl palmitate (C16:0)	13.05
Methyl linoleate (C18:2 cis (ω-9))	17.63
Methyl oleate (C18:1 cis (ω-9))	17.79
Methyl linolenate (C18:3 cis (ω-3))	17.83
Methyl elaidate (C18:1 trans (ω-9))	18.02
Methyl stearate (C18:0)	18.74
Methyl arachidate (C20:0)	25.22

As can be seen from the overlayed chromatograms and the retention times, all fatty acid methyl esters except for methyl oleate and methyl linolenate could be separated. It was therefore only possible to integrate the sum of both fatty acids. It was however noticed, that the terminal methyl group of methyl linolenate is shifted towards a lower field (0.97 ppm) in a ^{1}H NMR measurement, compared to all other fatty acid methyl esters (0.88 ppm). Additionally, the CH_2-groups between two double bonds of methyl linolenate (C18:3) are shifted to 2.80 ppm. The CH_2-group between two double bonds of methyl linoleate (C18:2) is also shifted towards a lower field (2.77ppm). An overlay of all ^{1}H NMR spectra is depicted in Figure 6.55. The fatty acid composition of the sunflower oils was hence determined *via* GC-MS by analysis of the methyl esters of each fatty acid. The ratio of methyl oleate to methyl linolenate was determined by ^{1}H NMR. This ratio was subsequently used to calculate the content of methyl oleate and methyl linolenate using the integration result obtained by GC-MS.

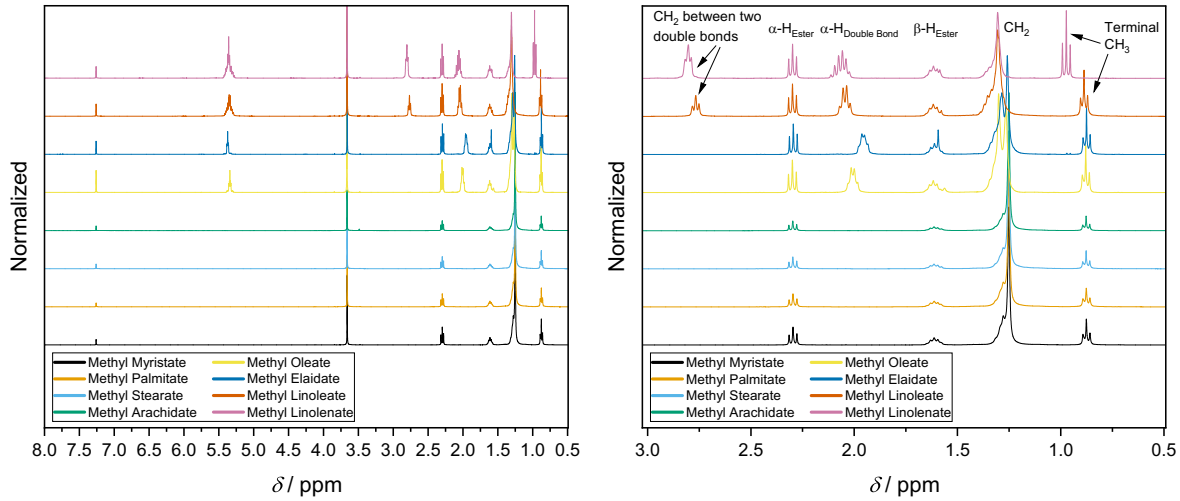

Figure 6.55: ^{1}H NMR spectra of all fatty acid methyl esters; **left:** whole spectrum; **right:** region between 3.00 and 0.50 ppm.

6.8.2 Fatty acid content of high oleic sunflower oils

Each high oleic sunflower oil was analyzed as methyl esters according to a modified procedure of the one published by Ruffo et al.[272] Sunflower oil (400 mg), methanol (10 ml, 247 mmol), and sulfuric acid (100 µl, 1.88 mmol) were added into a 25 ml round bottom flask. The reaction solution was stirred at 65 °C for 4 h. Afterwards, the reaction mixture was concentrated under reduced pressure to a volume of 1 ml and diluted with ethyl acetate (10 ml). The organic phase was washed with water (3 × 15 ml), dried over anhydrous sodium sulfate, filtered, and the solvent was removed under reduced pressure. The GC-MS sample was prepared by dilution of the transesterified oil (10 mg) with ethyl acetate (990 µl). The fatty acid composition of the sample was determined *via* GC-MS. An exemplary ^{1}H NMR spectrum of **HOSO02** after transesterification is depicted in Figure 6.56. After 4 h of reaction, there is no visible residue of glycerol esters between 4.00 ppm and 5.00 ppm and hence a full conversion of all ester moieties is observed. In Figure 6.57 to Figure 6.64 all GS-MS chromatograms of the transesterified oils and all ^{1}H NMRs of the pristine oils (normalized to one glyceryl moiety) are depicted.

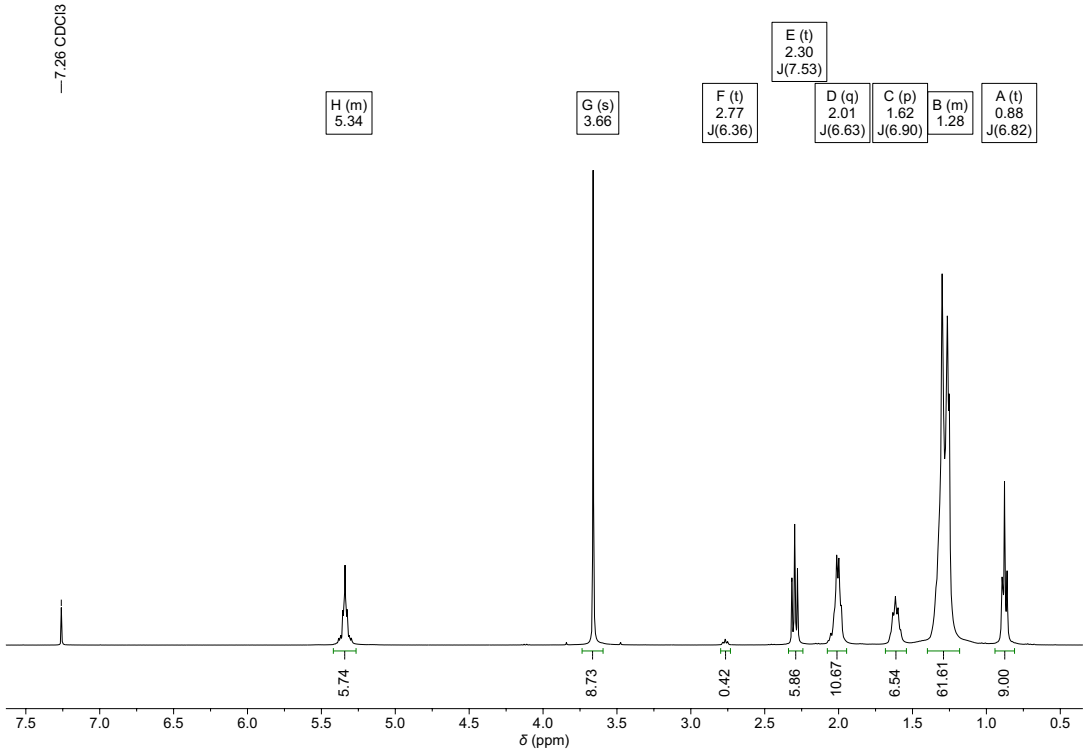

Figure 6.56: ^{1}H NMR spectrum of transesterified **HOSO02** after work-up.

GC-MS chromatograms of sunflower oils

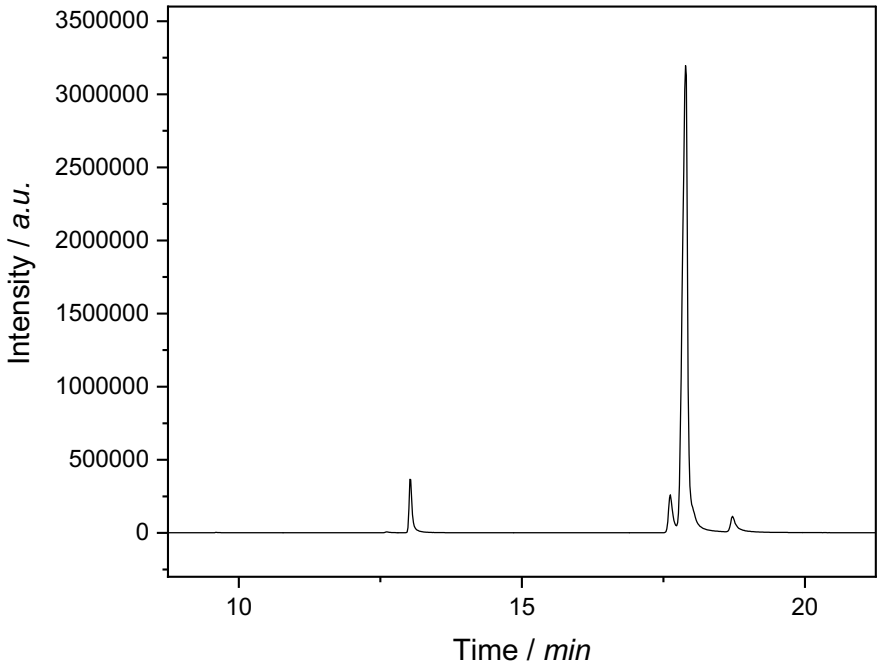

Figure 6.57: GC-MS chromatogram of transesterified **HOSO01**.

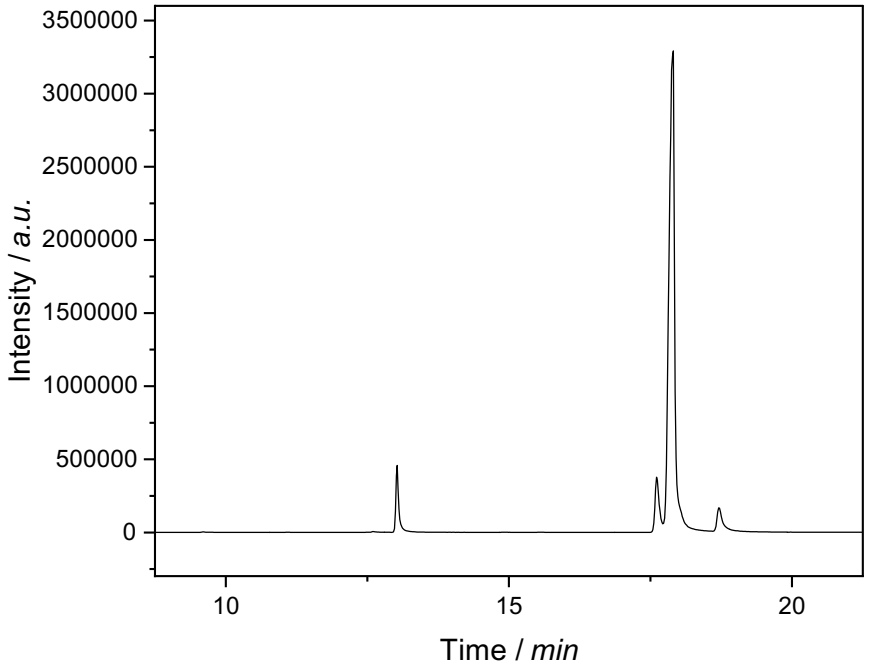

Figure 6.58: GC-MS chromatogram of transesterified **HOSO02**.

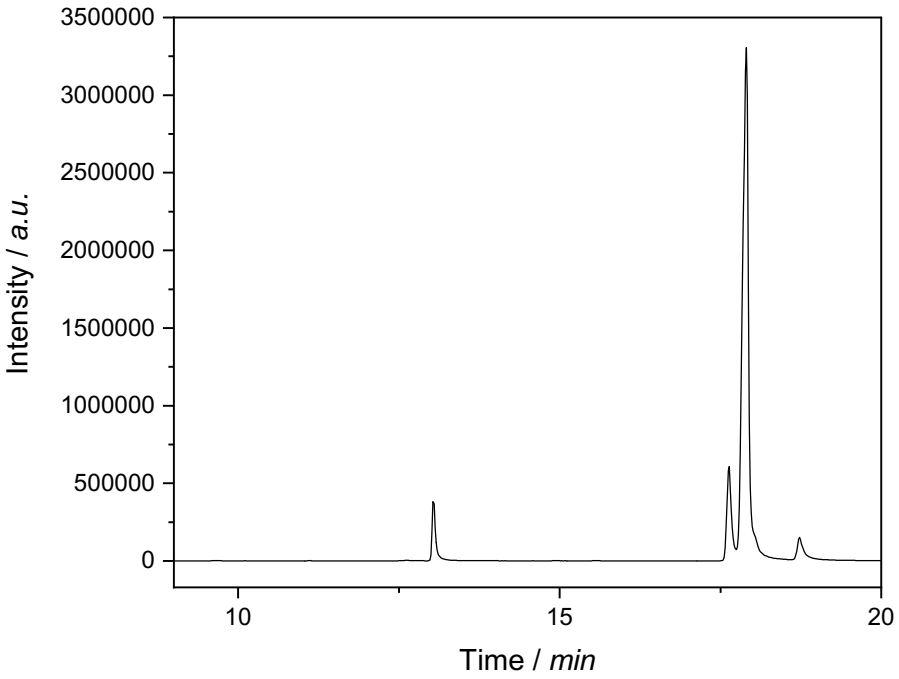

Figure 6.59: GC-MS chromatogram of transesterified **HOSO03**.

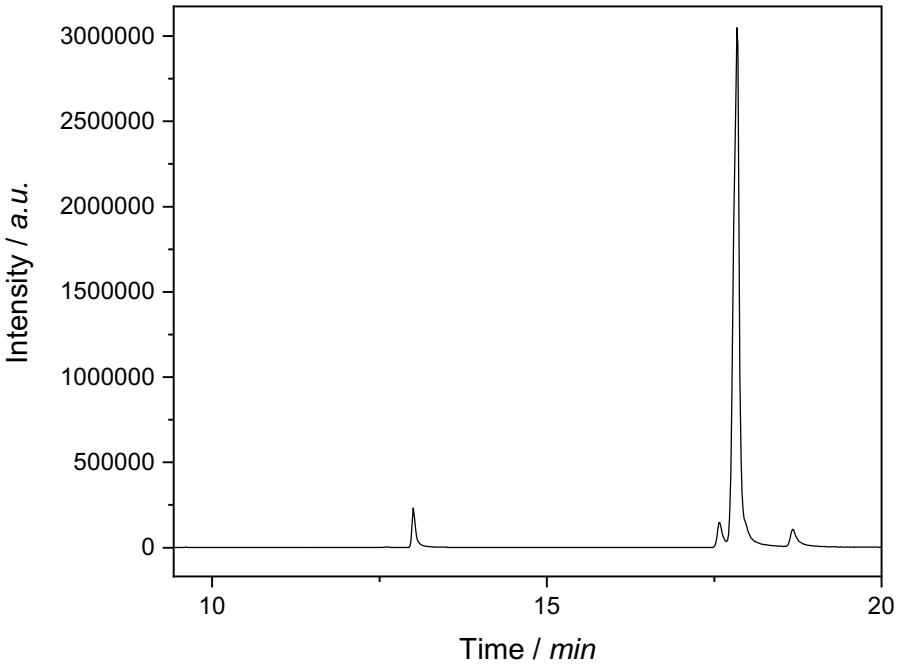

Figure 6.60: GC-MS chromatogram of transesterified **HOSO04**.

^{1}H NMR spectra of pristine sunflower oils

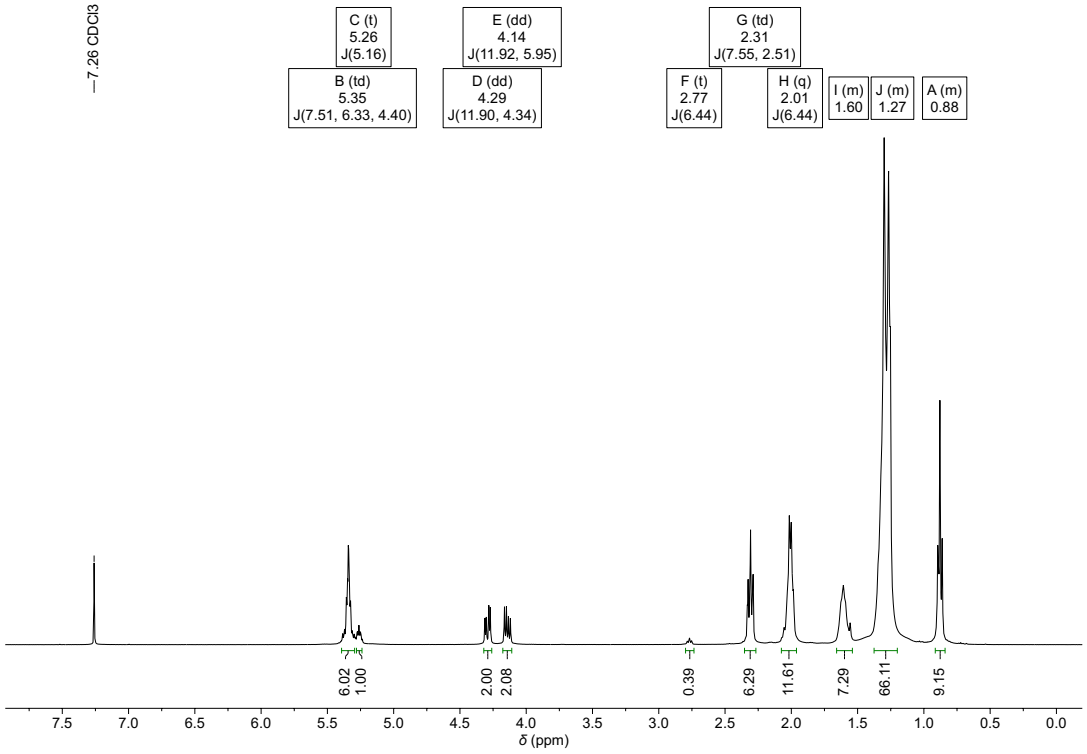

Figure 6.61: ^{1}H NMR spectrum of **HOSO01** in $CDCl_3$.

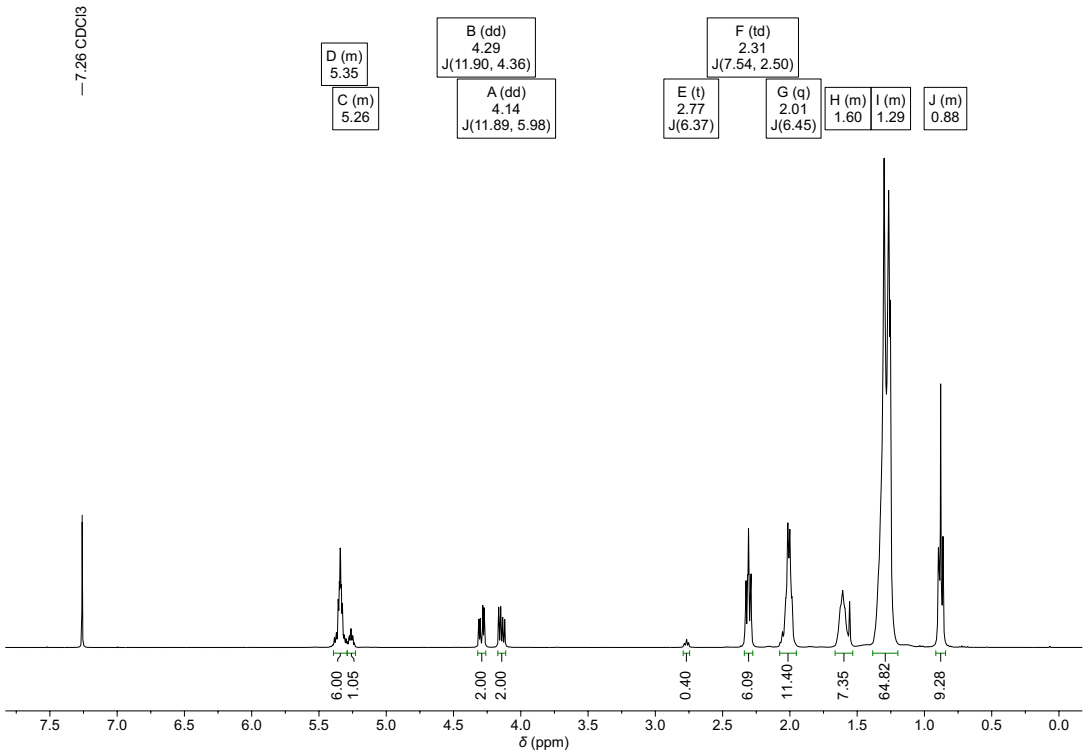

Figure 6.62: ^{1}H NMR spectrum of **HOSO02** in $CDCl_3$.

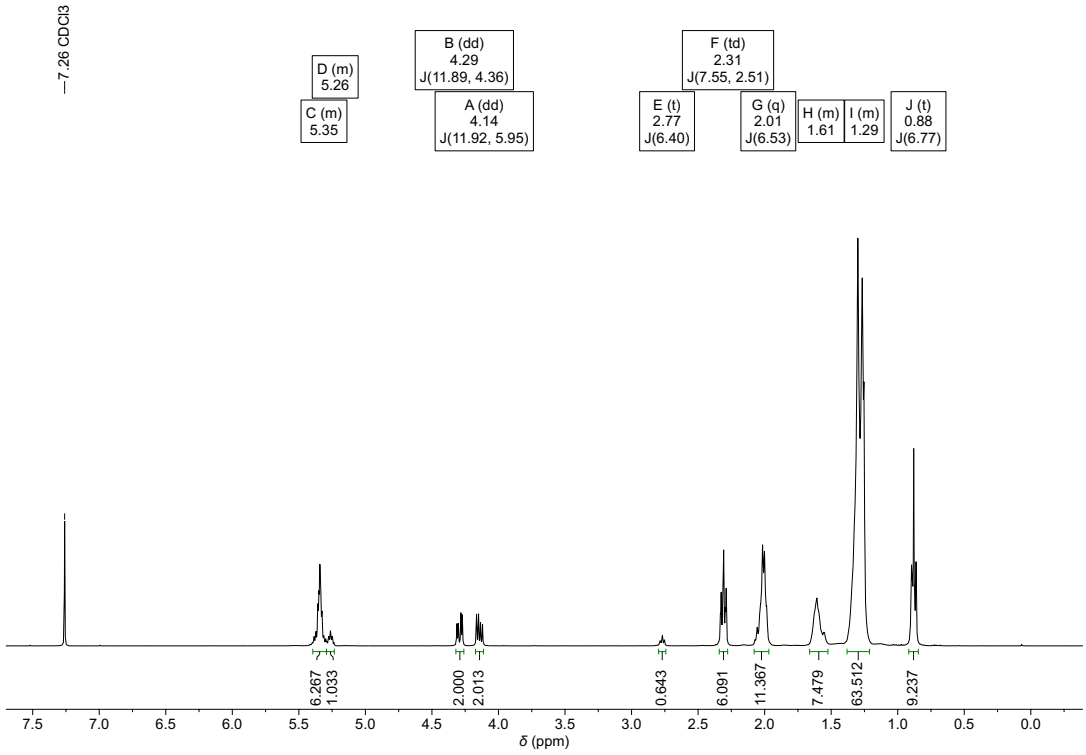

Figure 6.63: ^{1}H NMR spectrum of **HOSO03** in $CDCl_3$.

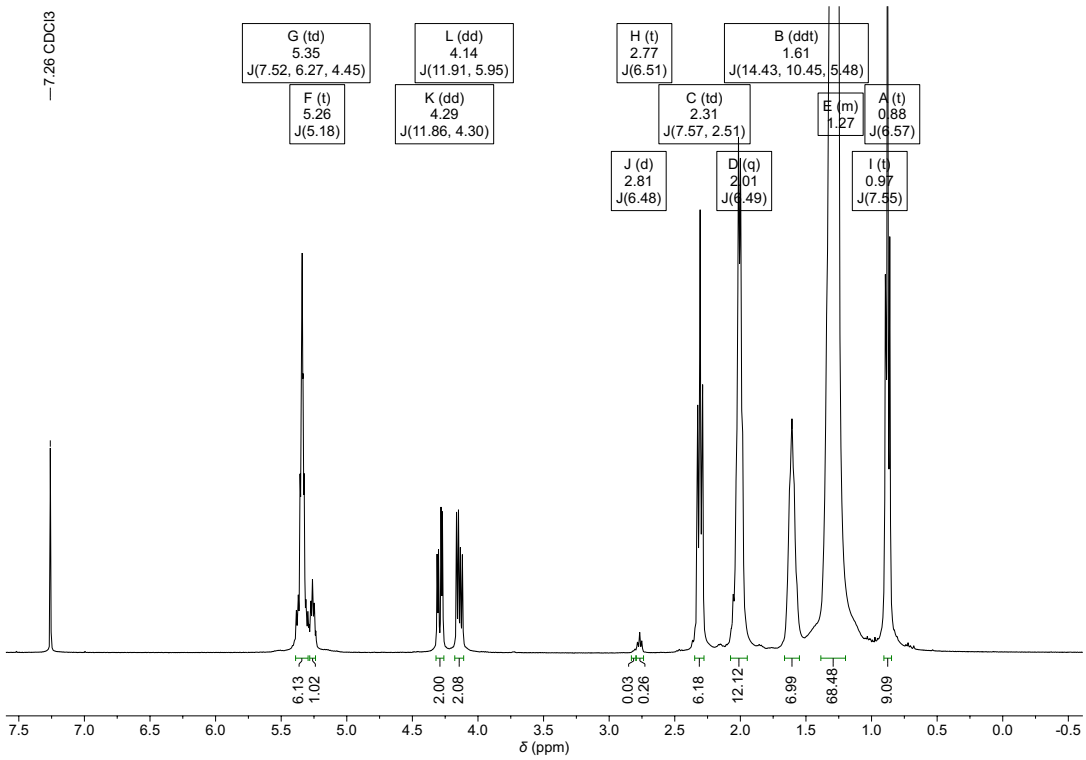

Figure 6.64: ^{1}H NMR spectrum of **HOSO04** in $CDCl_3$.

Table 6.6: Fatty acid content determination of high oleic sunflower oils *via* GC-MS.

Fatty Acid		% FA in HOSO01	% FA in HOSO02	% FA in HOSO03	% FA in HOSO04
Myristic	C14:0	0.02	0.02	0.02	0.02
Palmitic	C16:0	5.47	5.59	5.10	3.89
Stearic	C18:0	2.97	4.05	3.73	3.43
Arachidic	C20:0	0.02	0.02	0.02	0.02
Oleic and linolenic	C18:1 cis (ω-9) C18:3 cis (ω-3)	85.97	83.38	79.77	88.93
Elaidic	C18:1 trans (ω-9)	–	–	–	–
Linoleic	C18:2 cis (ω-6)	5.55	6.93	11.36	3.71
SFAs	C14:0, C16:0, C18:0, C20:0	8.49	9.69	8.87	7.36
UFAs	C18:1, C18:2, C18:3	91.51	90.31	91.13	92.64
MUFAs	C18:1	85.97	83.38	79.77	88.93
PUFAs	C18:2, C18:3	5.55	6.93	11.36	3.71

The fatty acid (FA) content of the analyzed oils was determined *via* GC-MS by integration of a respective fatty acid methyl ester signal and dividing it by the sum of all integrals (Table 6.6). The integration result for oleic acid methyl ester and linolenic acid methyl ester was supplemented as discussed above by ^{1}H NMR spectroscopy of the corresponding oil in $CDCl_3$. The signal of one CH_2 group of the glyceryl moiety was normalized to 2. Afterwards, the characteristic signals of linoleic acid (CH_2 group between two double bonds at 2.77 ppm), linolenic acid (CH_2 groups between two double bonds at 2.80 ppm) were integrated to calculate their content with equations Eq (11) and Eq (12). The number 3 in the denominator corresponds to 3 fatty acid residues per triglyceride. The other number is used to convert the integral into the number of fatty acid molecules. For instance, if the signal was one CH_2 group, the integral would be divided by 2.

$$\text{content linoleic acid } (\%) = \frac{\text{integral } (CH_2)}{2 \times 3} \tag{11}$$

$$\text{content linolenic acid } (\%) = \frac{\text{integral } (CH_2)}{4 \times 3} \tag{12}$$

The oleic acid content was then calculated by integration of all double bond protons and subtraction of the integral that should be generated by the content of linoleic and linolenic acid (Eq (13)). The calculations from the ^{1}H NMR data are summarized in Table 6.7.

$$\text{oleic acid } (\%) = \frac{\text{Int(double bond protons)} - \text{Int(linoleic)} \times 2 - \text{Int(linolenic)} \frac{6}{4}}{2 \times 3} \tag{13}$$

Table 6.7: Unsaturated fatty acid content determination of sunflower oils *via* ^{1}H NMR.

Fatty Acid		**% FA in HOSO01**	**% FA in HOSO02**	**% FA in HOSO03**	**% FA in HOSO04**
Oleic	C18:1 cis (ω-9)	87.33	86.67	83.02	92.75
Linoleic	C18:2 cis (ω-6)	6.50	6.67	10.72	4.33
Linolenic	C18:3 cis (ω-3)	–	–	–	0.25
Ratio linolenic to oleic acids		–	–	–	0.0027

Eventually, the quantitative GC-MS results were supplemented by splitting the integral of oleic acid methyl ester and linolenic acid methyl ester of HOSO04 into both fatty acids through multiplication of the integral with the integration ratio determined by ^{1}H NMR spectroscopy (Table 6.8).

Table 6.8: Fatty Acid content determination of sunflower oils *via* GC-MS supplemented by ^{1}H NMR.

Fatty Acid		**% FA in HOSO01**	**% FA in HOSO02**	**% FA in HOSO03**	**% FA in HOSO04**
Myristic	C14:0	0.02	0.02	0.02	0.02
Palmitic	C16:0	5.47	5.59	5.10	3.89
Stearic	C18:0	2.97	4.05	3.73	3.43
Arachidic	C20:0	0.02	0.02	0.02	0.02
Oleic	C18:1 cis (ω-9)	85.97	83.38	79.77	88.69
Elaidic	C18:1 trans (ω-9)	–	–	–	–
Linoleic	C18:2 cis (ω-6)	5.55	6.93	11.36	3.71
Linolenic	C18:3 cis (ω-3)	–	–	–	0.24
SFAs	C14:0, C16:0, C18:0, C20:0	8.49	9.69	8.87	7.36
UFAs	C18:1, C18:2, C18:3	91.51	90.31	91.13	92.64
MUFAs	C18:1	85.97	83.38	79.77	88.69
PUFAs	C18:2, C18:3	5.55	6.93	11.36	3.95

6.9 Theoretical considerations for the oxidative cleavage of sunflower oil

The theoretic considerations described herein were made to assess the applicability of an oxidative cleavage on a pristine oil. The following probability-based calculations try to estimate the amount of trifunctional carboxylic acids that will be formed depending on the oleic acid content of the oil and depending on the yield of the oxidative cleavage for a monofunctional derivative (e.g. methyl oleate). First, triolein was used as model substrate as it simplifies the calculation. Afterwards, the heterogeneity of the oil was taken into consideration by variation of the oleic acid content and by inclusion of uncleavable residues like stearic acid.

6.9.1 Oxidative cleavage of triolein

The first calculation of the oxidative cleavage of triolein was conducted with the assumption that every double bond has an 80% probability (P) to be cleaved into a carboxylic acid and a 20% probability for no reaction or, more realistically, to be transformed into possible side products (e.g., diol, acyloin, diketone). Moreover, triolein was used as model substrate as it simplifies the calculation. A tree diagram is depicted in Figure 6.65 to illustrate these statistical considerations. The expected yield of tricarboxylic acid for an overall reaction yield of 80% is hence only 51.2%, as the cleavages distribute statistically among all molecules. The triacid yield is exponentially dependent on P (cleavage) to the power of 3, rendering it difficult to obtain high yields of triacid without an oxidative cleavage reaction having a yield higher than 80% for monofunctional derivatives.

The possible permutations of monoacids, diacids, triacid and unreacted starting material (or side products bearing no carboxylic acid) can be calculated with binomial coefficients (Equations (14) to (17)).

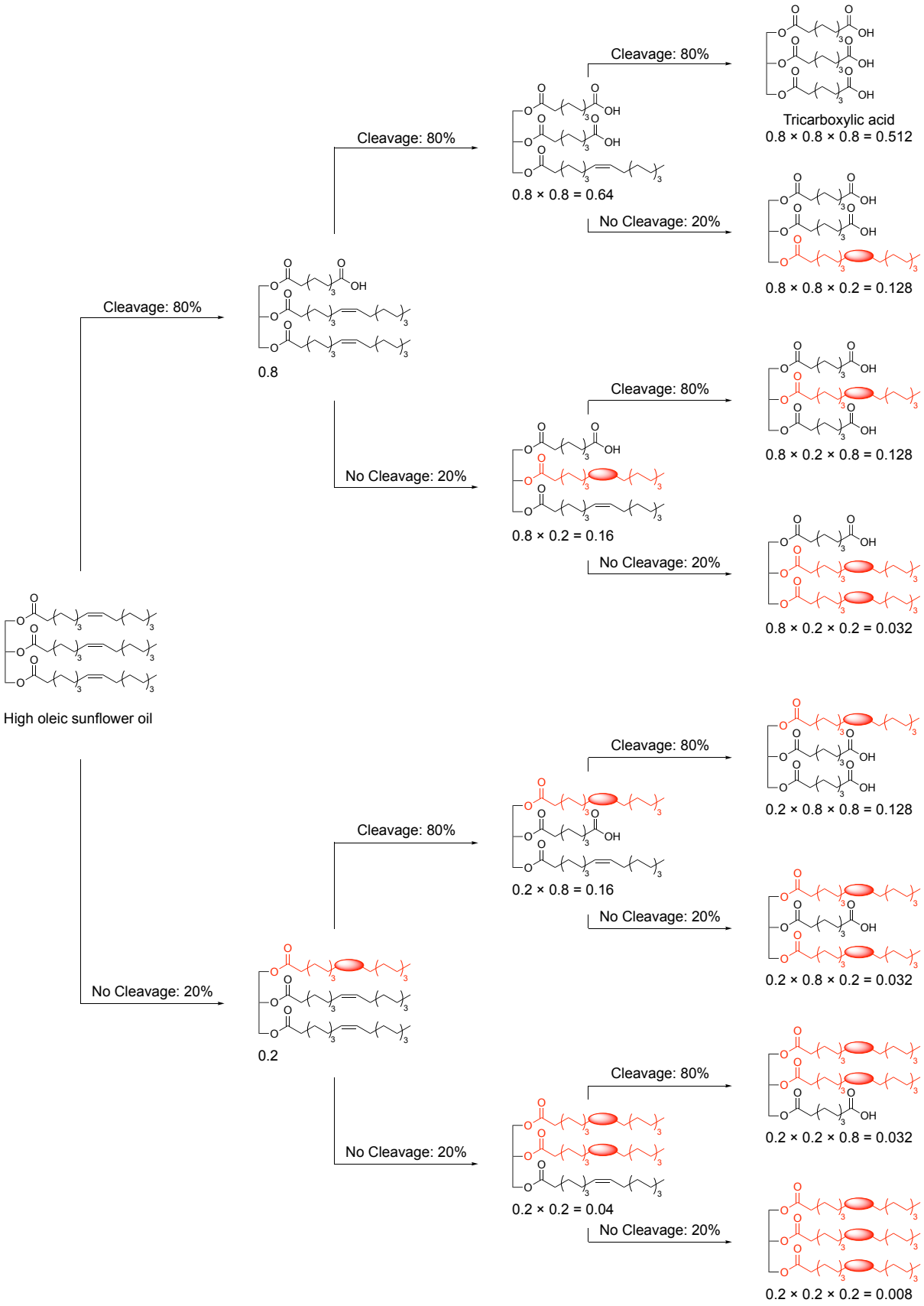

Figure 6.65: Tree diagram of the oxidative cleavage of triolein. The possible product acids are calculated with a probability of 80% for an oxidative cleavage and a probability of 20% for a side reaction or no reaction. The red spheres depict an uncleaved chain bearing any functional groups (e.g., diol, acyloin, diketone).

$$\text{Permutations (0 cleavages)} = \binom{3}{0} = \frac{3!}{1 \times 3!} = 1 \quad (14)$$

$$\text{Permutations (1 cleavages)} = \binom{3}{1} = \frac{3!}{1! \times 2!} = 3 \quad (15)$$

$$\text{Permutations (2 cleavages)} = \binom{3}{2} = \frac{3!}{2! \times 1!} = 3 \quad (16)$$

$$\text{Permutations (3 cleavages)} = \binom{3}{3} = \frac{3!}{3! \times 1} = 1 \quad (17)$$

The product distribution can finally be statistically predicted as a function of the overall conversion of double bonds into carboxylic acids (CDBCA):

f(x; triolein, 0 cleavages) = permutations × P (0 cleavages) = 1 × $(1-x)^3$

f(x; triolein, 1 cleavage) = permutations × P (1 cleavage) = 3 × x^1 × $(1-x)^2$

f(x; triolein, 2 cleavages) = permutations × P (2 cleavages) = 3 × x^2 × $(1-x)^1$

f(x; triolein, 3 cleavages) = permutations × P (3 cleavages) = 1 × x^3

The distribution of one specific product is hence calculated by multiplication of possible permutations with the probability of the respective cleavage pattern with x as CDBCA (0 ≤ x ≤ 1).

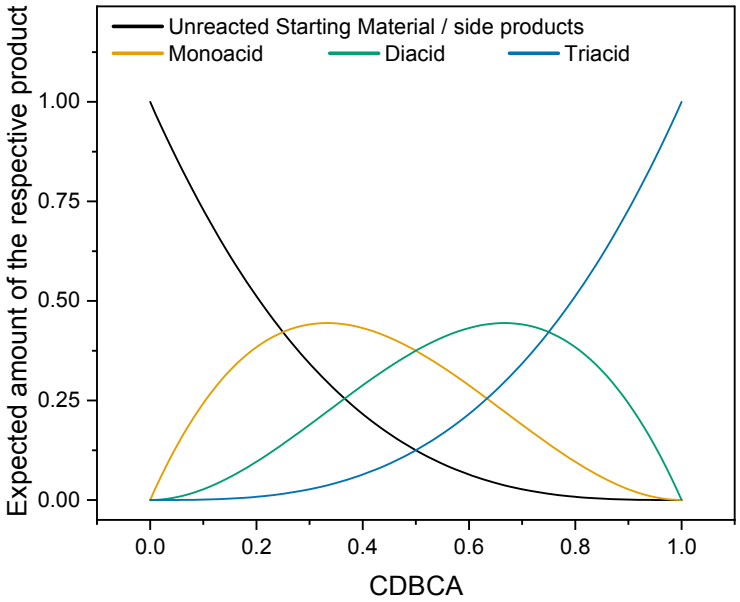

Figure S1: Statistical product distribution for the oxidative cleavage of triolein; CDBCA = conversion of double bonds into carboxylic acids.

6.9.2 Triglyceride composition

The above used statistical approach can also be used for the calculation of a composition distribution of fatty acids of triglycerides in oils. As a simplification, it was assumed that the glyceride moiety either receives an oleic acid residue or saturated fatty acid. The resulting functions are hence analogues to the ones devised for the oxidative cleavage of triolein (distribution of two objects on three places). For each possible triglyceride (3 saturated fatty acids, 1 oleic acid, 2 oleic acids, or 3 oleic acids (triolein)) a function of the amount of molecule inside the mixture was devised with y as the overall oleic acid content of the used oil having values between 0 and 1:

$f(y;\ 0\ \text{oleic acids}) = \text{permutations} \times P\ (0\ \text{oleic acids}) = 1 \times (1-y)^3$

$f(y;\ 1\ \text{oleic acid}) = \text{permutations} \times P\ (1\ \text{oleic acid}) = 3 \times y^1 \times (1-y)^2$

$f(y;\ 2\ \text{oleic acids}) = \text{permutations} \times P\ (2\ \text{oleic acids}) = 3 \times y^2 \times (1-y)^1$

$f(y;\ 3\ \text{oleic acids}) = \text{permutations} \times P\ (3\ \text{oleic acids}) = 1 \times y^3$

It should be noted that the above-mentioned functions f(x) (in chapter 6.9.1) for the triolein cleavage can only be applied to molecules containing three reactive chains. However, the triolein cleavage functions can easily be modified for oils containing 2 oleic acids and 1 oleic acid:

$f(x;\ 2\ \text{oleic acids, 0 cleavages}) = \text{permutations} \times P\ (0\ \text{cleavages}) = 1 \times (1-x)^2$

$f(x;\ 2\ \text{oleic acids, 1 cleavage}) = \text{permutations} \times P\ (1\ \text{cleavage}) = 2 \times x^1 \times (1-x)^1$

$f(x;\ 2\ \text{oleic acids, 2 cleavages}) = \text{permutations} \times P\ (2\ \text{cleavages}) = 1 \times x^2$

$f(x;\ 1\ \text{oleic acid, 0 cleavages}) = \text{permutations} \times P\ (0\ \text{cleavages}) = 1 \times (1-x)^1$

$f(x;\ 1\ \text{oleic acid, 1 cleavage}) = \text{permutations} \times P\ (1\ \text{cleavage}) = 1 \times x^1$

The final function to estimate each product distribution therefore consists of multiple parts. The amount of each triglyceride containing a different number of oleic acids must be multiplied with the oxidative cleavage function for the respective number of cleavages. The sum of all parts then corresponds to the final function f(x,y):

f(x,y; 0 cleavages) = f(y; 0 oleic acids) × 1 +
f(y; 1 oleic acid) × f(x; 1 oleic acid, 0 cleavages) +
f(y; 2 oleic acids) × f(x; 2 oleic acids, 0 cleavages) +
f(y; 3 oleic acids) × f(x; triolein, 0 cleavages)

$$\mathbf{f(x,y;\ 0\ cleavages) = (1-y)^3 + 3 \times y^1 \times (1-y)^2 \times (1-x)^1 + 3 \times y^2 \times (1-y)^1 \times (1-x)^2 + y^3 \times (1-x)^3}$$

f(x,y; 1 cleavage) = f(y; 1 oleic acid) × f(x; 1 oleic acid, 1 cleavage) +
f(y; 2 oleic acids) × f(x; 2 oleic acids, 1 cleavage) +
f(y; 3 oleic acids) × f(x; Triolein, 1 cleavage)

$$\mathbf{f(x,y;\ 1\ cleavage) = 3 \times y^1 \times (1-y)^2 \times x^1 + 3 \times y^2 \times (1-y)^1 \times 2 \times x^1 \times (1-x)^1 + y^3 \times 3 \times x^1 \times (1-x)^2}$$

f(x,y; 2 cleavages) = f(y; 2 oleic acids) × f(x; 2 oleic acids, 2 cleavages) +
f(y; 3 oleic acids) × f(x; Triolein, 2 cleavages)

$$\mathbf{f(x,y;\ 2\ cleavages) = 3 \times y^2 \times (1-y)^1 \times x^2 + y^3 \times 3 \times x^2 \times (1-x)^1}$$

f(x,y; 3 cleavages) = f(y; 3 oleic acids) × f(x; Triolein, 3 cleavages)

$$\mathbf{f(x,y;\ 3\ cleavages) = y^3 \times x^3}$$

The devised functions f(x,y) are plotted in Figure 6.66.

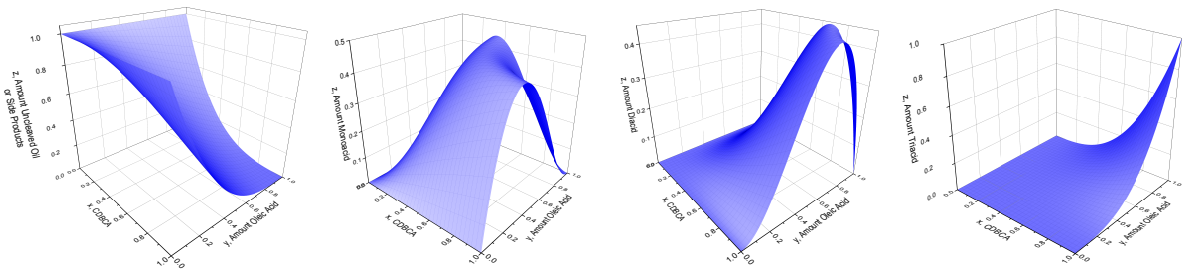

Figure 6.66: 3D plots of the product distribution of the oxidative cleavage of high oleic sunflower oil with x as the overall CDBCA and y as the amount of oleic acid inside the used oil. **Left:** amount uncleaved oil / side products; **Middle left:** amount monoacid; **Middle right:** amount diacid; **Right:** triacid.

Table 6.9 demonstrates the product distribution for an oleic acid content of 80%, 90% and pure triolein with varying CDBCA.

Table 6.9: Calculated distribution of products for the oxidative cleavage of HOSO using a statistical approach.

Oleic Acid content (y)	CDBCA (x)	Unreacted Starting Material and side products / %	Monoacid / %	Diacid / %	Triacid / %	Sum / %	Carboxylic Acids per Molecule
0.8	0.1	77.87	20.31	1.77	0.05	100	0.240
0.8	0.2	59.27	33.87	6.45	0.41	100	0.480
0.8	0.3	43.90	41.59	13.13	1.38	100	0.720
0.8	0.4	31.44	44.39	20.89	3.28	100	0.960
0.8	0.5	21.60	43.20	28.80	6.40	100	1.200
0.8	0.6	14.06	38.93	35.94	11.06	100	1.440
0.8	0.7	8.52	32.52	41.40	17.56	100	1.680
0.8	0.8	4.67	24.88	44.24	26.21	100	1.920
0.8	0.9	2.20	16.93	43.55	37.32	100	2.160
0.8	1	0.80	9.60	38.40	51.20	100	2.400
0.9	0.1	75.36	22.36	2.21	0.07	100	0.270
0.9	0.2	55.14	36.31	7.97	0.58	100	0.540
0.9	0.3	38.90	43.16	15.97	1.97	100	0.810
0.9	0.4	26.21	44.24	24.88	4.67	100	1.080
0.9	0.5	16.64	40.84	33.41	9.11	100	1.350
0.9	0.6	9.73	34.28	40.24	15.75	100	1.620
0.9	0.7	5.07	25.87	44.06	25.00	100	1.890
0.9	0.8	2.20	16.93	43.55	37.32	100	2.160
0.9	0.9	0.69	8.77	37.40	53.14	100	2.430
0.9	1	0.10	2.70	24.30	72.90	100	2.700
1	0.1	72.90	24.30	2.70	0.1	100	0.300
1	0.2	51.20	38.40	9.60	0.8	100	0.600
1	0.3	34.30	44.10	18.90	2.7	100	0.900
1	0.4	21.60	43.20	28.80	6.4	100	1.200
1	0.5	12.50	37.50	37.50	12.5	100	1.500
1	0.6	6.40	28.80	43.20	21.6	100	1.800
1	0.7	2.70	18.90	44.10	34.3	100	2.100
1	0.8	0.80	9.60	38.40	51.2	100	2.400
1	0.9	0.10	2.70	24.30	72.9	100	2.700
1	1	0	0	0	100	100	3.000

6.10 Oxidative cleavage of high oleic sunflower oil

Important note: This procedure was used two times within this thesis. Once for the optimization of the oxidative cleavage itself (chapter 4.2) and once for the polymerization of the sunflower oil based triacid *via* Passerini three component reaction (chapter 4.3). For both projects, triacid samples with a different carboxylic acid content have been used as the compound had to be resynthesized during this thesis. Therefore, two different experimental sections will be given here for both projects.

HOSO04 was chosen as the appropriate oil for all experiments as it contains the highest amount of oleic acid. The fatty acid content was used to calculate the number of double bond protons per triglyceride with Equation (18) (see chapter 6.8.2 for fatty acid composition of oil).

$$\frac{\text{double bond protons}}{\text{triglyceride}} = \text{oleic acid} \times 2 + \text{linoleic acid} \times 4 + \text{linolenic acid} \times 6 = 5.81 \quad (18)$$

This number will be used to calculate the yield of the employed oxidative cleavage on high oleic sunflower oil 04 (chapter 6.10.1 and 6.10.3). For one double bond cleavage, two carboxylic acids form. Hence, for a yield of 100%, the integral of *α*-CH_2 protons of carboxylic acids (2.18 ppm) in the ^{1}H NMR spectrum should duplicate. The conversion of double bonds into carboxylic acids, that is, the yield estimated by ^{1}H NMR spectroscopy can be calculated with Equation (19) by division of the integral of *α*-CH_2 protons of carboxylic acids by 2 and the calculated number of vinylic protons inside the oil, after normalizing the spectrum relative to the signal of the glyceryl moiety.

$$\text{NMR-Yield}\ (\%) = \frac{\text{integral}\ (\alpha\text{-}CO_2H)}{2 \times 5.81} \times 100 \quad (19)$$

6.10.1 Optimization of the oxidative cleavage of sunflower oil

In a 100 ml three-necked flask, high oleic sunflower oil **HOSO04** (4.43 g, 5.00 mmol (based on the molecular weight of triolein (885 g/mol)), 1.00 equiv.), ruthenium(III) acetylacetonate (39.8 mg, 100 µmol, 2 mol%) and pyridine-2,6-dicarboxylic acid (334 mg, 2.00 mmol, 40 mol%) were dissolved in *tert*-butanol (45.0 ml) and water (15.0 ml). The reaction mixture was stirred magnetically (400 rpm with a cross shaped stirring bar) at 80 °C for 24 h. After the reaction temperature reached 80 °C, hydrogen peroxide (35% aq. sol., 10.3 ml, 120 mmol, 24.0 equiv.) was dissolved in *tert*-butanol (12.0 ml) and added slowly to the reaction solution by a syringe pump with a flow rate of 18.6 µl min^{-1} over a period of 20 h. After the entire reaction time passed, the reaction solution was diluted with water (45 ml) and *tert*-butanol was removed under reduced pressure to ensure easier phase separation during extraction. The aqueous phase was extracted with ethyl acetate (3 × 40 ml) and the combined organic layers were washed with saturated sodium chloride solution (50 ml), dried over sodium sulfate, filtered and the solvent was removed under reduced pressure. The crude product was then purified by different procedures.

6.10.1.1 First purification procedure

The reaction was conducted twice. After extraction, ^{1}H NMR analysis of both reactions resulted in an NMR-Yield/overall conversion of double bonds into carboxylic acids of 83.13%. The reactions were combined and purified by flash column chromatography (cyclohexane/EtOAc, 4:1 + 1% formic acid, then 2:1 + 1% formic acid, then 1:1 without formic acid) to obtain three fractions (Fraction 1: nonanoic acid, 3.40 g, 21.5 mmol, 81%, GC-purity: 89%; Fraction 2: sunflower polyacid sample 1, 2.26 g, 35%; Fraction 3: sunflower polyacid sample 2, 2.85 g, 44%) after removal of solvent and formic acid under reduced pressure.

Yield Calculation:

The yield of the fractions will be calculated in the following by using some approximations:

1. The used sunflower oil has the molar mass of triolein. Therefore, in two reactions, exactly 10 mmol sunflower oil were used. The amount of oleic acid substituents, which corresponds to the theoretically possible yield of nonanoic acid, was calculated with Equation (20). The factor 0.8869 corresponds to the content of oleic acid that was determined by GC-MS (Table 6.8).

$$\text{Oleic acid substituents (mmol)} = 10\ \text{mmol} \times 3 \times 0.8869 = 26.61\ \text{mmol} \quad (20)$$

$$\text{Theoretical yield (nonanoic acid)} = 26.61\ \text{mmol} \times 158.24\ \text{g/mol} = 4211\ \text{mg} \quad (21)$$

2. After extraction, ^{1}H NMR spectroscopy was performed to calculate the conversion of double bonds into carboxylic acids (Equation (19)). The two spectra of both reactions resulted in an overall conversion of 83.13%. This conversion was used to calculate the maximum possible yield of nonanoic acid out of this purification according to Equation (22).

$$\text{NMR-Yield (nonanoic acid)} = 26.61\ \text{mmol} \times 158.24\ \text{g/mol} \times 0.8313 = 3500\ \text{mg} \quad (22)$$

3. The product yield calculation is only possible by calculation of a new mixed molar mass of the product. It is expected to calculate yields higher than 100% if the yield is calculated by diving the isolated mass through the molecular mass of the pure triacid product. This is explained by the loss of molecular weight of the starting material by cleavage of the double bonds (triolein: 885.45 g/mol; pure triacid: 602.72 g/mol). The isolated mass will therefore always be calculated too high if there are still some uncleaved residues on the isolated product. A new molecular mass was calculated based on the already calculated conversion of double bonds into carboxylic acids *via* ^{1}H NMR spectroscopy. The new molecular mass therefore consists of the sum of the starting material's molar mass multiplied by the factor "1 − NMR-Yield" and pure triacid molar mass multiplied by NMR-Yield (Equation (23)).

$$M_{Product} = 885.45\ \text{g/mol} \times 0.1687 + 602.72\ \text{g/mol} \times 0.8313 = 650.42\ \text{g/mol} \quad (23)$$

The yield of the isolated nonanoic acid was calculated in comparison to the theoretical yield and the NMR-Yield:

$$\frac{\text{isolated mass (nonanoic acid)}}{\text{theoretical yield (nonanoic acid)}} \times 100 = \frac{3.40\ \text{g}}{4.21\ \text{g}} \times 100 = 80.8\% \quad (24)$$

$$\frac{\text{isolated mass (nonanoic acid)}}{\text{NMR-Yield (nonanoic acid)}} \times 100 = \frac{3.40\ \text{g}}{3.50\ \text{g}} \times 100 = 97.1\% \quad (25)$$

The yield of fractions 2 and 3 was finally calculated by dividing the isolated mass by $M_{Product}$ and the used amount of starting oil (10.0 mmol):

$$\text{Yield (F2)} = \frac{\text{isolated mass (F2)}}{\text{M}_{\text{Product}} \times 0.01\ \text{mol}} \times 100 = \frac{2.26\ \text{g}}{650.42\ \frac{\text{g}}{\text{mol}} \times 0.01\ \text{mol}} \times 100 = 34.8\% \quad (26)$$

$$\text{Yield (F3)} = \frac{\text{Isolated mass (F3)}}{\text{M}_{\text{Product}} \times 0.01\ \text{mol}} \times 100 = \frac{2.85\ \text{g}}{650.42\ \frac{\text{g}}{\text{mol}} \times 0.01\ \text{mol}} \times 100 = 43.8\% \quad (27)$$

Isolated triacid yield:

Triacid yield is calculated from the purity of 85.7% determined *via* ^{1}H NMR (Figure 4.10, Methyl proton integral of 0.5 corresponds to 14.3% diacid impurity):

$$\text{Yield (triacid)} = \frac{\text{mass (F3)} \times \text{purity}}{\text{M(triacid)} \times 0.01\ \text{mol}} \times 100 = \frac{2.85\ \text{g} \times 0.86}{602.72\ \frac{\text{g}}{\text{mol}} \times 0.01\ \text{mol}} \times 100 = 40.5\% \quad (28)$$

However, based on the theoretical considerations, the maximum obtainable yield can be calculated from the NMR-Yield and the oleic acid content. It was decided to calculate a range of possible yields, because it is possible that linoleic acid and linolenic acid can also be cleaved to carboxylic acids. It will be assumed that linoleic acid and linolenic acid have the same probabilities for a cleavage to simplify the calculation. Therefore, two values were calculated. One lower limit (only oleic acid) and one upper limit (all unsaturated fatty acids)

Possible yield (triacid, lower limit) = NMR-Yield^3 × oleic acid content^3 × 100
= $0.8313^3 \times 0.8869^3 \times 100$
= 40.1%

Possible yield (triacid, upper limit) = NMR-Yield^3 × unsaturated fatty acids content^3 × 100
= $0.8313^3 \times 0.9264^3 \times 100$
= 45.7%

Hence, the isolated amount of triacid corresponds to 88.6%−101% of the theoretically possible yield.

Fraction 1: Nonanoic acid

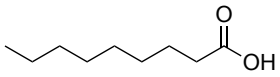

$C_9H_{18}O_2$

M = 158.24 g/mol

R_f (Fraction 1) = 0.69 (cyclohexane/EtOAc, 2:1 + 1% formic acid).

^{1}H NMR (400 MHz, DMSO-d_6, ppm): δ = 11.95 (s, 1H, CO_2H, H^1), 2.18 (t, J = 7.4 Hz, 2H, CH_2, α-$H_{\text{carboxylic acid}}$, H^2), 1.48 (p, J = 7.4 Hz, 2H, CH_2, β-$H_{\text{carboxylic acid}}$, H^3), 1.24 (s, 10H, CH_2, H^4), 0.85 (t, J = 6.8 Hz, 3H, CH_3, H^5).

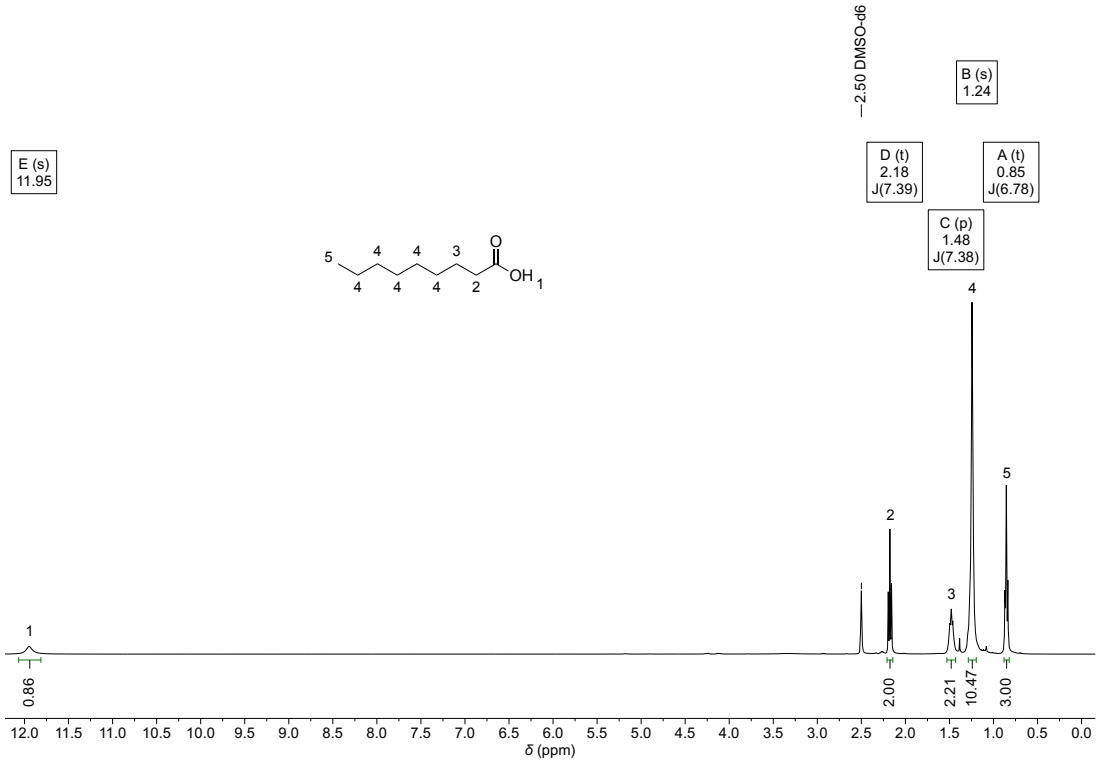

Figure 6.67: ^{1}H NMR spectrum of the isolated nonanoic acid by flash column chromatography of the oxidative cleavage of **HOSO04** (in DMSO-d_6).

Fraction 2: High oleic sunflower oil-based polyacid sample 1

Representative Structures:

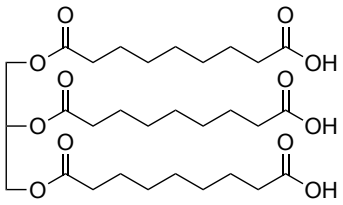

$C_{30}H_{50}O_{12}$

M = 602.72 g/mol

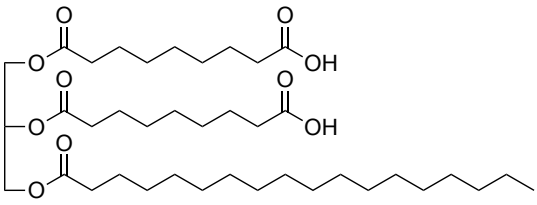

$C_{39}H_{70}O_{10}$

M = 698.98 g/mol

R_f (Fraction 2) = 0.26 (cyclohexane/EtOAc, 2:1 + 1% formic acid).

^{1}H NMR (400 MHz, DMSO-d_6, ppm): δ = 11.99 (s, 3H, CO_2H, H^1), 5.18 (tt, J = 7.0, 3.7 Hz, 1H, CH, $H_{Glyceryl}$, H^2), 4.25 (dd, J = 12.0, 3.7 Hz, 2H, CH_2, $H_{Glyceryl}$, H^3), 4.12 (dd, J = 12.0, 6.5 Hz, 2H, CH_2, $H_{Glyceryl}$, H^3), 3.97 (d, J = 5.4 Hz, not further oxidized O*H* group), 2.30−2.24 (m, 6H, CH_2, α-H_{Ester}, H^4), 2.18 (td, J = 7.4, 3.7 Hz, 6H, CH_2, α-$H_{Carboxylic\ acid}$, H^5), 1.57−1.42 (m, 15H, CH_2, H^6), 1.31−1.14 (m, 43H, CH_2, H^7), 0.85 (t, J = 6.8 Hz, 4H, CH_3, H^8).

^{13}C NMR (101 MHz, DMSO-d_6, ppm): δ = 174.5 (C_q, CO_2H, C^1), 174.4 (C_q, CO_2H, C^1), 174.4 (C_q, CO_2H, C^1), 172.5 (C_q, C_{Ester}, C^2), 172.2 (C_q, C_{Ester}, C^2), 68.7 (+, CH, $C_{Glyceryl}$, C^3), 61.8 (–, CH_2, $C_{Glyceryl}$, C^4), 33.6 (−, CH_2, C^5), 33.4 (−, CH_2, C^5), 33.3 (−, CH_2, C^5), 33.3 (−, CH_2, C^5), 31.3 (−, CH_2, C^6), 31.2 (−, CH_2, C^6), 29.0 (−, CH_2, C^6), 29.0 (−, CH_2, C^6), 28.9 (−, CH_2, C^6), 28.7 (−, CH_2, C^6), 28.7 (−, CH_2, C^6), 28.6 (−, CH_2, C^6), 28.4 (−, CH_2, C^6), 28.4 (−, CH_2, C^6), 28.4 (−, CH_2, C^6), 28.3 (−, CH_2, C^6), 28.2 (−, CH_2, C^6), 24.4 (−, CH_2, C^6), 24.4 (−, CH_2, C^6), 24.3 (−, CH_2, C^6), 22.1 (−, CH_2, C^6), 22.1 (−, CH_2, C^6), 13.9 (+, CH_3, C^7).

IR (ATR, cm^{-1}): $\tilde{\nu}$ = 3192 (vw), 2925 (s), 2855 (m), 1738 (vs), 1705 (vs), 1460 (w), 1413 (w), 1368 (w), 1279 (w), 1234 (m), 1160 (vs), 1096 (m), 940 (w), 726 (w) cm^{-1}.

ESI-MS ([M−H]$^-$, $C_{30}H_{49}O_{12}$, deprotonated triacid): calcd.: 601.3230, found: 601.3229.

ESI-MS ([M−H]$^-$, $C_{37}H_{65}O_{10}$, deprotonated diacid with palmitic acid residue): calcd.: 669.4583, found: 669.4583.

ESI-MS ([M−H]$^-$, $C_{39}H_{69}O_{10}$, deprotonated diacid with stearic acid residue): calcd.: 697.4896, found: 697.4896.

ESI-MS ([M−H]$^-$, $C_{41}H_{73}O_{10}$, deprotonated diacid with arachidic acid residue): calcd.: 725.5209, found: 725.5209.

ESI-MS ([M−H]$^-$, $C_{39}H_{69}O_{12}$, deprotonated diacid with one oleic acid residue oxidized to diol): calcd.: 729.4795, found: 729.4796.

ESI-MS ([M−H]$^-$, $C_{39}H_{67}O_{12}$, deprotonated diacid with one oleic acid residue oxidized to acyloin): calcd.: 727.4638, found: 727.4638.

ESI-MS ([M−H]$^-$, $C_{39}H_{65}O_{12}$, deprotonated diacid with one oleic acid residue oxidized to diketone): calcd.: 725.4482, found: 725.4482.

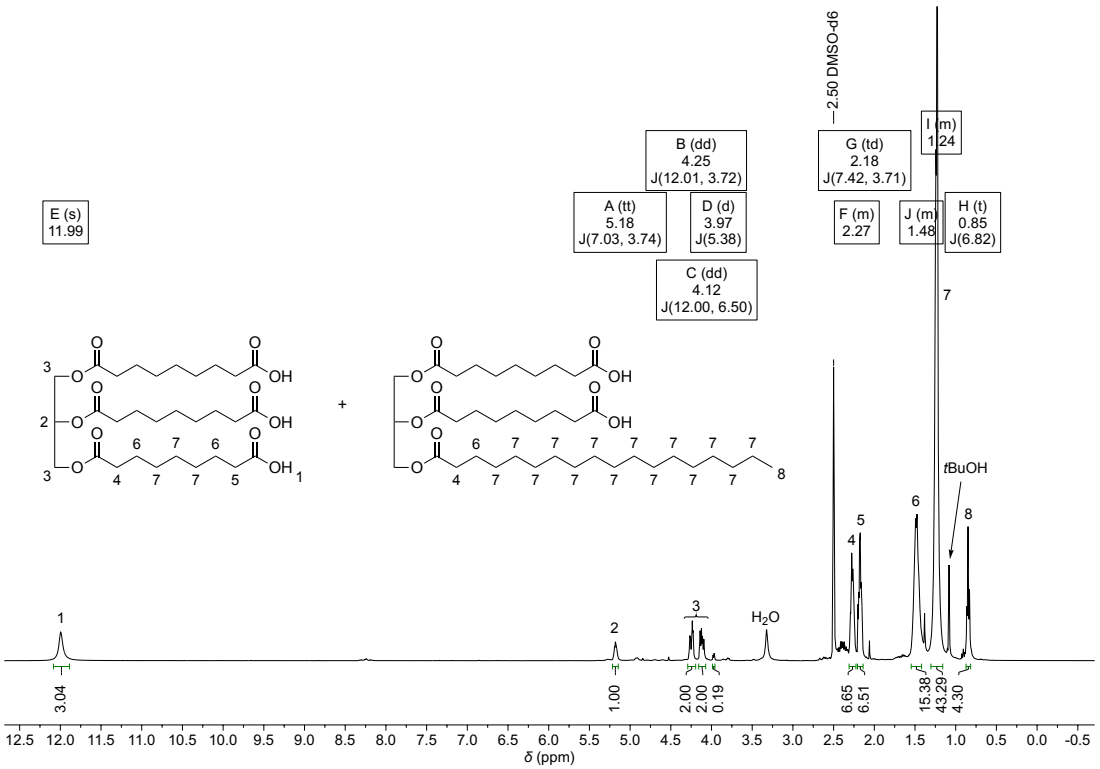

Figure 6.68: ^{1}H NMR spectrum of fraction 2 isolated by flash column chromatography of the oxidative cleavage of **HOSO 04** (in DMSO-d_6).

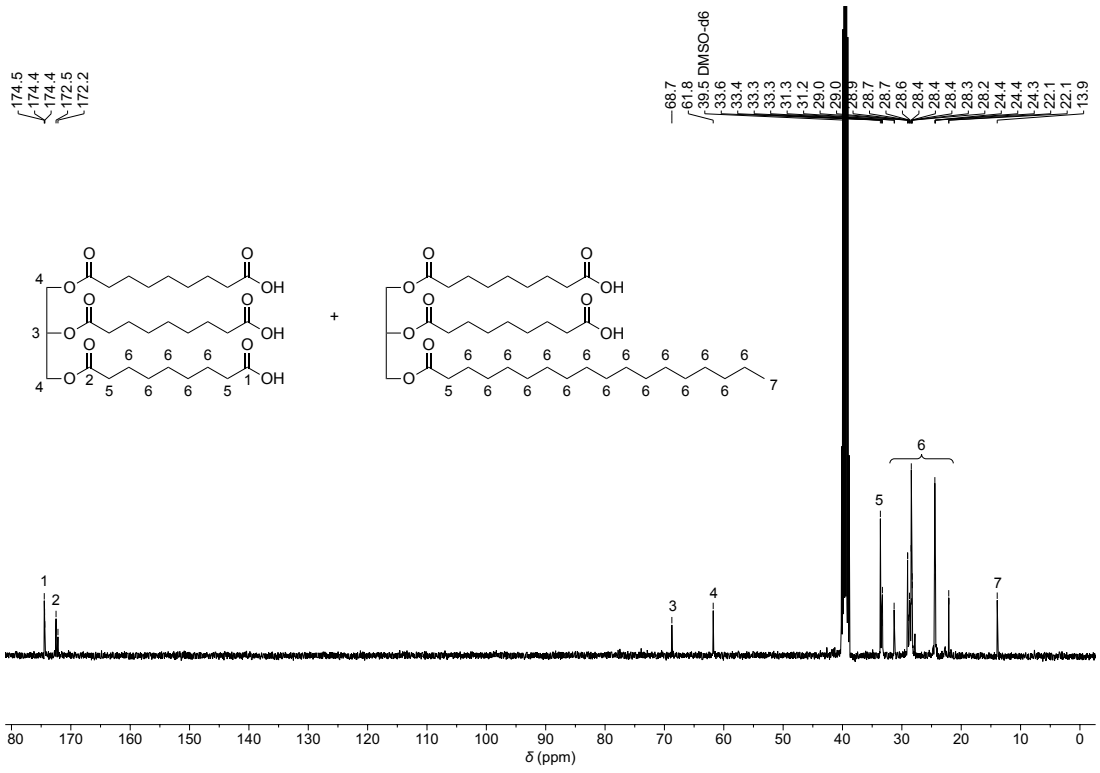

Figure 6.69: ^{13}C NMR spectrum of fraction 2 isolated by flash column chromatography of the oxidative cleavage of **HOSO04** (in DMSO-d_6).

Fraction 3: High oleic sunflower oil-based polyacid sample 2

Representative Structures:

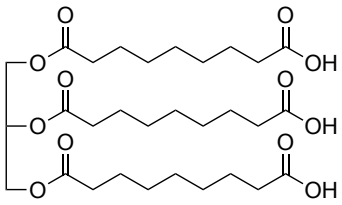

$C_{30}H_{50}O_{12}$

M = 602.72 g/mol

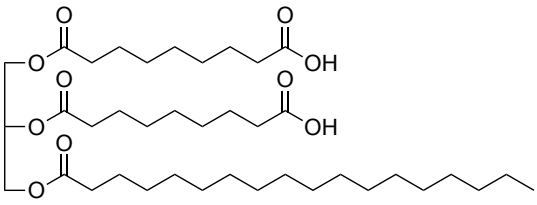

$C_{39}H_{70}O_{10}$

M = 698.98 g/mol

R_f (Fraction 3) = 0.14 (cyclohexane/EtOAc, 2:1 + 1% formic acid).

^{1}H NMR (400 MHz, DMSO-d_6, ppm): δ = 11.95 (s, 3H, CO_2H, H^1), 5.18 (tt, J = 6.9, 3.7 Hz, 1H, CH, $H_{Glyceryl}$, H^2), 4.25 (dd, J = 12.0, 3.7 Hz, 2H, CH_2, $H_{Glyceryl}$, H^3), 4.12 (dd, J = 12.0, 6.5 Hz, 2H, CH_2, $H_{Glyceryl}$, H^3), 3.98 (d, J = 5.4 Hz, not further oxidized OH group), 2.28 (td, J = 7.3, 4.2 Hz, 6H, CH_2, α-H_{Ester}, H^4), 2.18 (t, J = 7.4 Hz, 6H, CH_2, α-$H_{Carboxylic\ acid}$, H^5), 1.58−1.37 (m, 13H, CH_2, H^6), 1.24 (s, 22H, CH_2, H^7), 0.85 (t, J = 6.7 Hz, 0.5H, CH_3, H^8).

^{13}C NMR (101 MHz, DMSO-d_6, ppm): δ = 174.5 (C_q, CO_2H, C^1), 174.4 (C_q, CO_2H, C^1), 172.5 (C_q, C_{Ester}, C^2), 172.2 (C_q, C_{Ester}, C^2), 68.8 (+, CH, $C_{Glyceryl}$, C^3), 61.8 (–, CH_2, $C_{Glyceryl}$, C^4), 33.6 (−, CH_2, C^5), 33.6 (−, CH_2, C^5),33.5 (−, CH_2, C^5), 33.3 (−, CH_2, C^5), 28.4 (−, CH_2, C^6), 28.3 (−, CH_2, C^6), 28.2 (−, CH_2, C^6), 24.4 (−, CH_2, C^6), 24.4 (−, CH_2, C^6), 24.3 (−, CH_2, C^6).

IR (ATR, cm^{-1}): $\tilde{\nu}$ = 3223 (vw), 2929 (m), 2857 (w), 1738 (vs), 1703 (vs), 1456 (w), 1413 (w), 1378 (w), 1232 (m), 1160 (vs), 1133 (s), 1094 (m), 1033 (w), 938 (w), 728 (w) cm^{-1}.

ESI-MS ([M−H]$^-$, $C_{30}H_{49}O_{12}$, deprotonated triacid): calcd.: 601.3230, found: 601.3229.

ESI-MS ([M−H]$^-$, $C_{39}H_{69}O_{12}$, deprotonated diacid with one oleic acid residue oxidized to diol): calcd.: 729.4795, found: 729.4796.

ESI-MS ([M−H]$^-$, $C_{39}H_{67}O_{12}$, deprotonated diacid with one oleic acid residue oxidized to acyloin): calcd.: 727.4638, found: 727.4638.

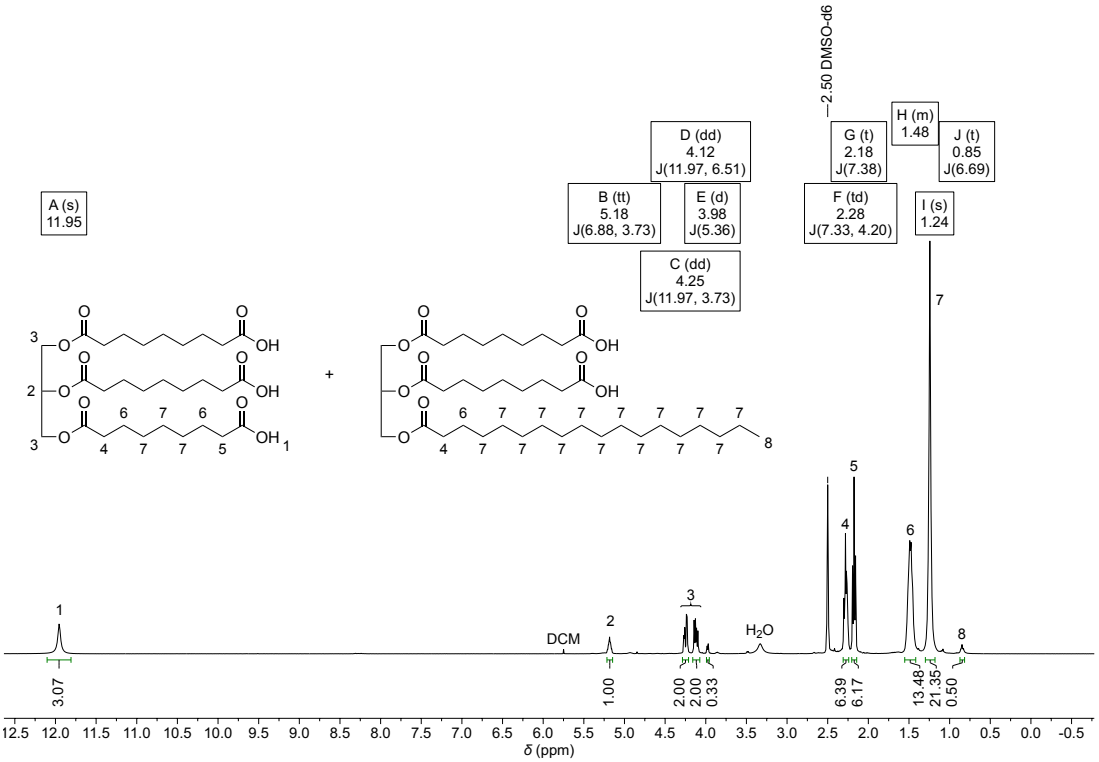

Figure 6.70: ^{1}H NMR spectrum of fraction 3 isolated by flash column chromatography of the oxidative cleavage of **HOSO04** (in DMSO-d_6).

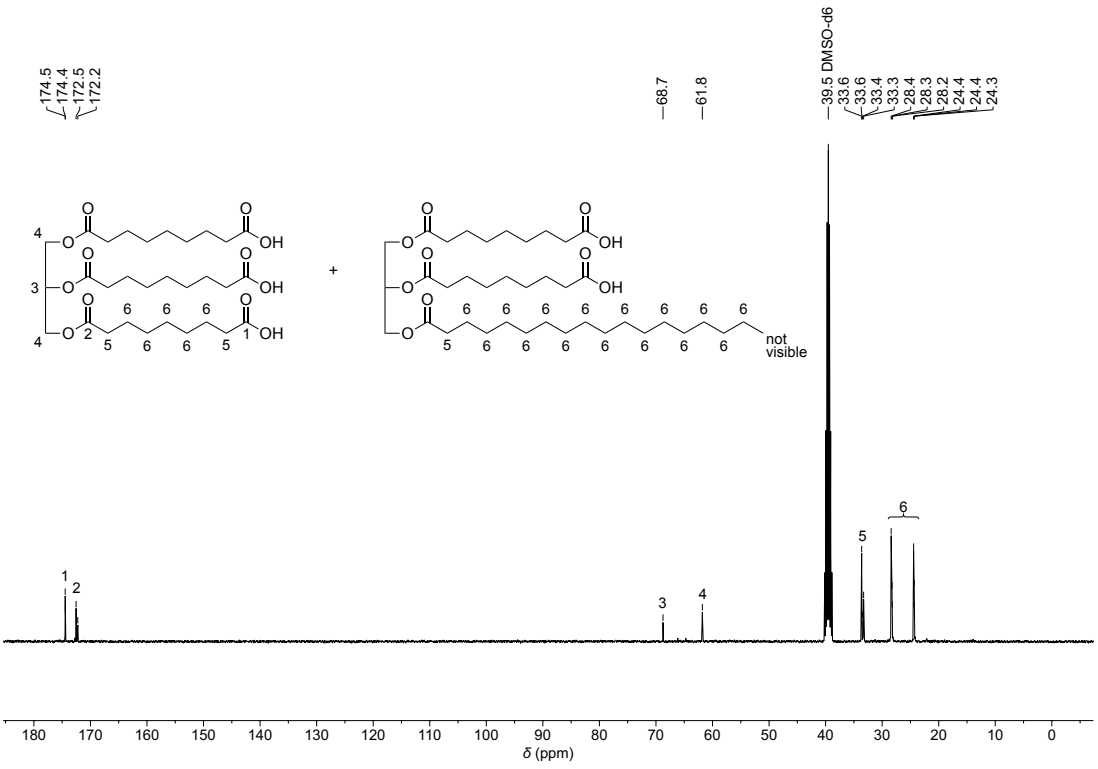

Figure 6.71: ^{13}C NMR spectrum of fraction 3 isolated by flash column chromatography of the oxidative cleavage of **HOSO04** (in DMSO-d_6).

6.10.1.2 Second purification procedure

The reaction was conducted twice. After extraction, the ^{1}H NMR analysis of both reactions resulted in an overall conversion of double bonds into carboxylic acids of 84.51%. The reactions were combined and purified by filter flash column chromatography (5 cm height, 8 cm width, cyclohexane/EtOAc, 4:1) to obtain one fraction (8.48 g). The crude product was then distilled in a Kugelrohr oven *in vacuo* (100 °C, 0.1 mbar) to remove the cleavage product nonanoic acid (3.16 g, 20.0 mmol, 75%, GC-purity: 88%) and to obtain the sunflower polyacid sample 3 (5.32 g, 82%) as residue.

Yield Calculation (chapter 6.10.1.1 explains the used equations):

$$\text{NMR Yield (nonanoic acid)} = 26.61\ \text{mmol} \times 158.24\ \text{g/mol} \times 0.8451 = 3559\ \text{mg} \quad (29)$$

$$M_{Product} = 885.45\ \text{g/mol} \times 0.1549 + 602.72\ \text{g/mol} \times 0.8451 = 646.51\ \text{g/mol} \quad (30)$$

$$\frac{\text{Isolated mass (nonanoic acid)}}{\text{theoretical yield (nonanoic acid)}} \times 100 = \frac{3.16\ \text{g}}{4.21\ \text{g}} \times 100 = 75.1\% \quad (31)$$

$$\frac{\text{Isolated mass (nonanoic acid)}}{\text{NMR yield (nonanoic acid)}} \times 100 = \frac{3.16\ \text{g}}{3.56\ \text{g}} \times 100 = 88.8\% \quad (32)$$

$$\text{Yield (polyacid)} = \frac{\text{Isolated mass}}{M_{Product} \times 0.01\ \text{mol}} \times 100 = \frac{5.32\ \text{g}}{646.51\ \frac{\text{g}}{\text{mol}} \times 0.01\ \text{mol}} \times 100 = 82.3\% \quad (33)$$

Isolated compound: High oleic sunflower oil based polyacid 3

Representative Structures:

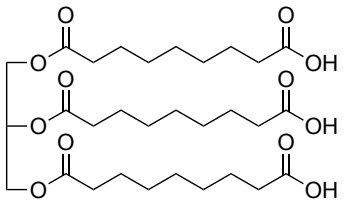

$C_{30}H_{50}O_{12}$

M = 602.72 g/mol

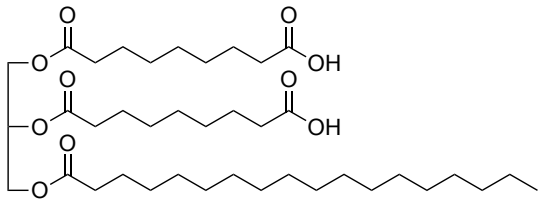

$C_{39}H_{70}O_{10}$

M = 698.98 g/mol

^{1}H NMR (400 MHz, DMSO-d_6, ppm): δ = 11.96 (s, 3H, CO_2H, H^1), 5.18 (tt, J = 6.9, 3.8 Hz, 1H, CH, $H_{Glyceryl}$, H^2), 4.25 (dd, J = 12.0, 3.7 Hz, 2H, CH_2, $H_{Glyceryl}$, H^3), 4.12 (dd, J = 11.9, 6.5 Hz, 2H, CH_2, $H_{Glyceryl}$, H^3), 3.98 (d, J = 5.3 Hz, 0H, not further oxidized O*H* group), 2.28 (td, J = 7.4, 3.9 Hz, 6H, CH_2, α-H_{Ester}, H^4), 2.17 (t, J = 7.4 Hz, 6H, CH_2, α-$H_{Carboxylic\ acid}$, H^5), 1.54−1.41 (m, 14H, CH_2, H^6), 1.33−1.17 (m, 33H, CH_2, H^7), 0.85 (t, J = 6.8 Hz, 3H, CH_3, H^8).

^{13}C NMR (101 MHz, DMSO-d_6, ppm): δ = 174.5 (C_q, CO_2H, C^1), 174.4 (C_q, CO_2H, C^1), 174.4 (C_q, CO_2H, C^1), 172.5 (C_q, C_{Ester}, C^2), 172.2 (C_q, C_{Ester}, C^2), 68.7 (+, CH, $C_{Glyceryl}$, C^3), 61.8 (–, CH_2, $C_{Glyceryl}$, C^4), 33.6 (−, CH_2, C^5), 33.4 (−, CH_2, C^5), 33.3 (−, CH_2, C^5), 33.3 (−, CH_2, C^5), 31.3 (−, CH_2, C^6), 31.2 (−, CH_2, C^6), 29.0 (−, CH_2, C^6), 28.9 (−, CH_2, C^6), 28.7 (−, CH_2, C^6), 28.7 (−, CH_2, C^6), 28.6 (−, CH_2, C^6), 28.4 (−, CH_2, C^6), 28.3 (−, CH_2, C^6), 28.2 (−, CH_2, C^6), 24.4 (−, CH_2, C^6), 24.4 (−, CH_2, C^6), 24.3 (−, CH_2, C^6), 22.1 (−, CH_2, C^6), 22.1 (−, CH_2, C^6), 13.9 (+, CH_3, C^7).

IR (ATR, cm^{-1}): $\tilde{\nu}$ = 3209 (vw), 2925 (m), 2855 (m), 1738 (vs), 1705 (vs), 1458 (w), 1413 (w), 1368 (w), 1232 (m), 1160 (vs), 1096 (m), 1031 (w), 938 (w), 734 (w) cm^{-1}.

ESI-MS ($[M-H]^-$, $C_{30}H_{49}O_{12}$, deprotonated triacid): calcd.: 601.3230, found: 601.3226.

ESI-MS ($[M-H]^-$, $C_{37}H_{65}O_{10}$, deprotonated diacid with palmitic acid residue): calcd.: 669.4583, found: 669.4581.

ESI-MS ($[M-H]^-$, $C_{39}H_{69}O_{10}$, deprotonated diacid with stearic acid residue): calcd.: 697.4896, found: 697.4893.

ESI-MS ($[M-H]^-$, $C_{41}H_{73}O_{10}$, deprotonated diacid with arachidic acid residue): calcd.: 725.5209, found: 725.5208.

ESI-MS ($[M-H]^-$, $C_{39}H_{69}O_{12}$, deprotonated diacid with one oleic acid residue oxidized to diol): calcd.: 729.4795, found: 729.4796.

ESI-MS ($[M-H]^-$, $C_{39}H_{67}O_{12}$, deprotonated diacid with one oleic acid residue oxidized to acyloin): calcd.: 727.4638, found: 727.4636.

ESI-MS ($[M-H]^-$, $C_{39}H_{65}O_{12}$, deprotonated diacid with one oleic acid residue oxidized to diketone): calcd.: 725.4482, found: 725.4482.

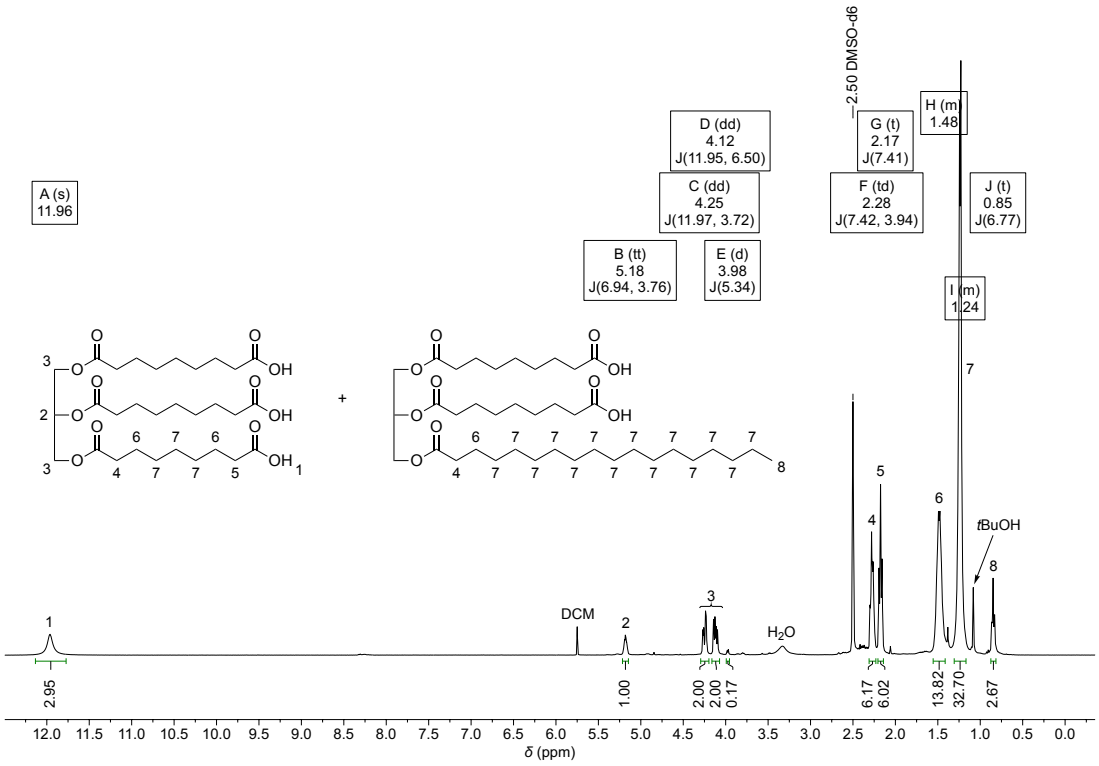

Figure 6.72: ^{1}H NMR spectrum of sunflower polyacid 3 isolated by filter flash column chromatography and subsequent vacuum distillation of the oxidative cleavage of **HOSO04** (in DMSO-d_6).

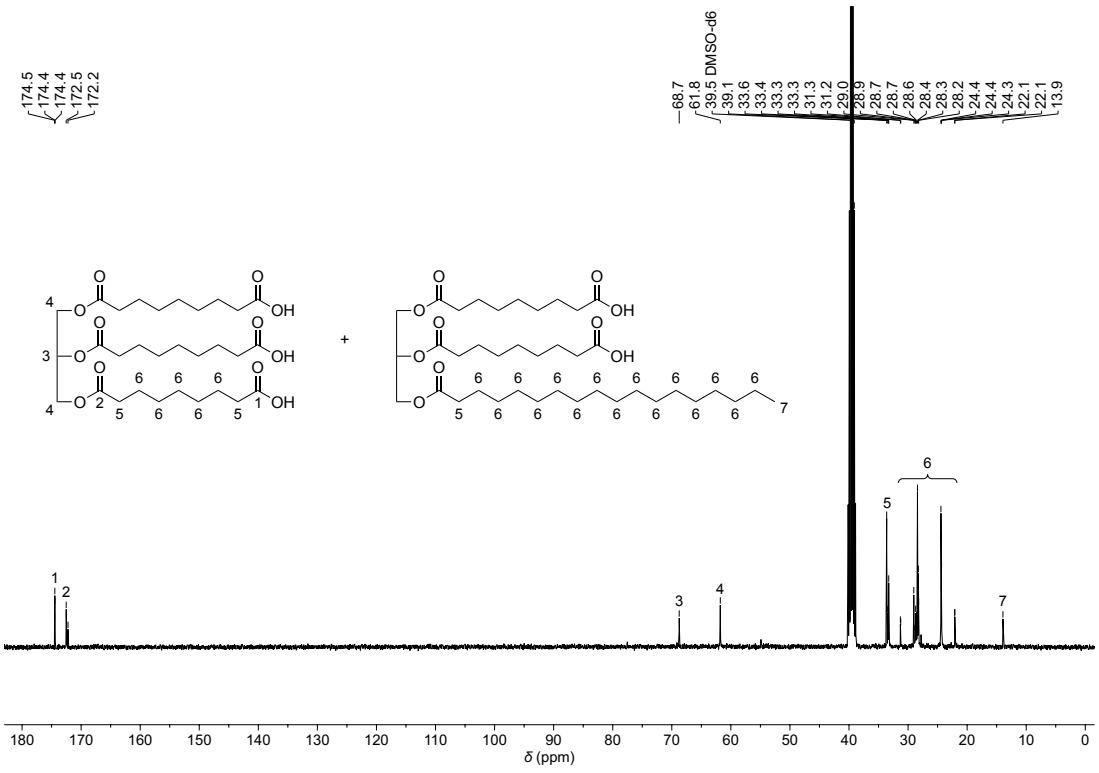

Figure 6.73: ^{13}C NMR spectrum of sunflower polyacid 3 isolated by filter flash column chromatography and subsequent vacuum distillation of the oxidative cleavage of **HOSO04** (in DMSO-d_6).

6.10.1.3 Third purification procedure

The reaction was conducted twice with 15 mol% 2,6-pyridine-dicarboxylic acid (125 mg, 750 µmol) instead of 40 mol%. After extraction ^{1}H NMR analysis of both reactions result in an overall conversion of double bonds into carboxylic acids of 76.03%. The crude product was then distilled in a Kugelrohr oven in vacuo (100 °C, 0.1 mbar) to remove the cleavage product nonanoic acid (3.05 g, 19,3 mmol, 72%, GC-purity: 88%) and obtain the sunflower polyacid sample 4 (6.82 g, 98%) as residue.

Yield Calculation (chapter 6.10.1.1 explains the used equations):

$$\text{NMR Yield (nonanoic acid)} = 26.61\ \text{mmol} \times 158.24\ \text{g/mol} \times 0.7603 = 3201\ \text{mg} \quad (34)$$

$$M_{Product} = 885.45\ \text{g/mol} \times 0.2397 + 602.72\ \text{g/mol} \times 0.7603 = 670.49\ \text{g/mol} \quad (35)$$

$$\frac{\text{Isolated mass (nonanoic acid)}}{\text{theoretical yield (nonanoic acid)}} \times 100 = \frac{3.05\ \text{g}}{4.21\ \text{g}} \times 100 = 72.4\% \quad (36)$$

$$\frac{\text{Isolated mass (nonanoic acid)}}{\text{NMR yield (nonanoic acid)}} \times 100 = \frac{3.05\ \text{g}}{3.20\ \text{g}} \times 100 = 95.3\% \quad (37)$$

$$\text{Mass(pure product)} = \text{isolated mass} - \text{mass (DPA)} = 6.82\ \text{g} - 0.25\ \text{g} = 6.57\ \text{g} \quad (38)$$

$$\text{Yield(F3)} = \frac{\text{Isolated mass}}{M_{Product} \times 0.01\ \text{mol}} \times 100 = \frac{6.57\ \text{g}}{670.49\ \frac{\text{g}}{\text{mol}} \times 0.01\ \text{mol}} \times 100 = 97.7\% \quad (39)$$

Isolated compound: High Oleic sunflower oil based polyacid 4

Representative Structures:

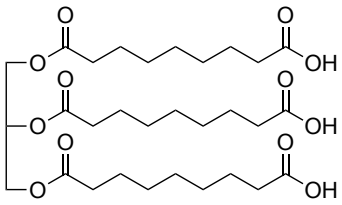

$C_{30}H_{50}O_{12}$

M = 602.72 g/mol

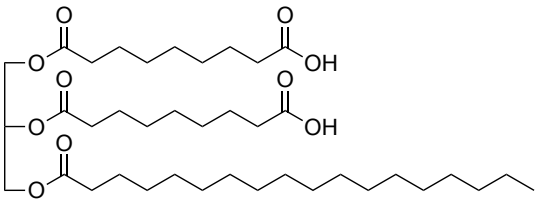

$C_{39}H_{70}O_{10}$

M = 698.98 g/mol

^{1}H NMR (400 MHz, DMSO-d_6, ppm): δ = 12.00 (s, 2.6H, CO_2H, H^1), 8.35−8.14 (m, 0.2H, H_{Ar}, 2,6-pyridine-dicarboxylic acid), 5.18 (tt, J = 7.0, 3.8 Hz, 1H, CH, $H_{Glyceryl}$, H^2), 4.25 (dd, J = 12.0, 3.7 Hz, 2H, CH_2, $H_{Glyceryl}$, H^3), 4.12 (dd, J = 11.9, 6.5 Hz, 2H, CH_2, $H_{Glyceryl}$, H^3), 3.98 (d, J = 5.4 Hz, not further oxidized OH group), 2.28 (td, J = 7.4, 3.9 Hz, 6H, CH_2, α-H_{Ester}, H^4), 2.18 (t, J = 7.4 Hz, 5H, CH_2, α-$H_{Carboxylic\ acid}$, H^5), 1.58−1.40 (m, 13H, CH_2, H^6), 1.31−1.16 (m, 31H, CH_2, H^7), 0.85 (t, J = 6.8 Hz, 3H, CH_3, H^8).

^{13}C NMR (101 MHz, DMSO-d_6, ppm): δ = 174.5 (C_q, CO_2H, C^1), 174.4 (C_q, CO_2H, C^1), 174.4 (C_q, CO_2H, C^1), 172.5 (C_q, C_{Ester}, C^2), 172.2 (C_q, C_{Ester}, C^2), 68.7 (+, CH, $C_{Glyceryl}$, C^3), 61.8 (–, CH_2, $C_{Glyceryl}$, C^4), 33.6 (−, CH_2, C^5), 33.4 (−, CH_2, C^5), 33.3 (−, CH_2, C^5), 33.3 (−, CH_2, C^5), 31.3 (−, CH_2, C^6), 31.2 (−, CH_2, C^6), 29.0 (−, CH_2, C^6), 28.9 (−, CH_2, C^6), 28.7 (−, CH_2, C^6), 28.6 (−, CH_2, C^6), 28.6 (−, CH_2, C^6), 28.4 (−, CH_2, C^6), 28.3 (−, CH_2, C^6), 28.2 (−, CH_2, C^6), 24.4 (−, CH_2, C^6), 24.4 (−, CH_2, C^6), 24.3 (−, CH_2, C^6), 22.1 (−, CH_2, C^6), 22.1 (−, CH_2, C^6), 13.9 (+, CH_3, C^7).

IR (ATR, cm^{-1}): $\tilde{\nu}$ = 3205 (vw), 2927 (s), 2855 (m), 1738 (vs), 1705 (vs), 1458 (w), 1413 (w), 1368 (w), 1234 (m), 1162 (vs), 1094 (m), 942 (w), 726 (w) cm^{-1}.

ESI-MS ([M−H]$^-$, $C_{30}H_{49}O_{12}$, deprotonated triacid): calcd.: 601.3230, found: 601.3224.

ESI-MS ([M−H]$^-$, $C_{37}H_{65}O_{10}$, deprotonated diacid with palmitic acid residue): calcd.: 669.4583, found: 669.4581.

ESI-MS ([M−H]$^-$, $C_{39}H_{69}O_{10}$, deprotonated diacid with stearic acid residue): calcd.: 697.4896, found: 697.4892.

ESI-MS ([M−H]$^-$, $C_{41}H_{73}O_{10}$, deprotonated diacid with arachidic acid residue): calcd.: 725.5209, found: 725.5209.

ESI-MS ([M−H]$^-$, $C_{39}H_{69}O_{12}$, deprotonated diacid with one oleic acid residue oxidized to diol): calcd.: 729.4795, found: 729.4794.

ESI-MS ([M−H]$^-$, $C_{39}H_{67}O_{12}$, deprotonated diacid with one oleic acid residue oxidized to acyloin): calcd.: 727.4638, found: 727.4636.

ESI-MS ([M−H]$^-$, $C_{39}H_{65}O_{12}$, deprotonated diacid with one oleic acid residue oxidized to diketone): calcd.: 725.4482, found: 725.4481.

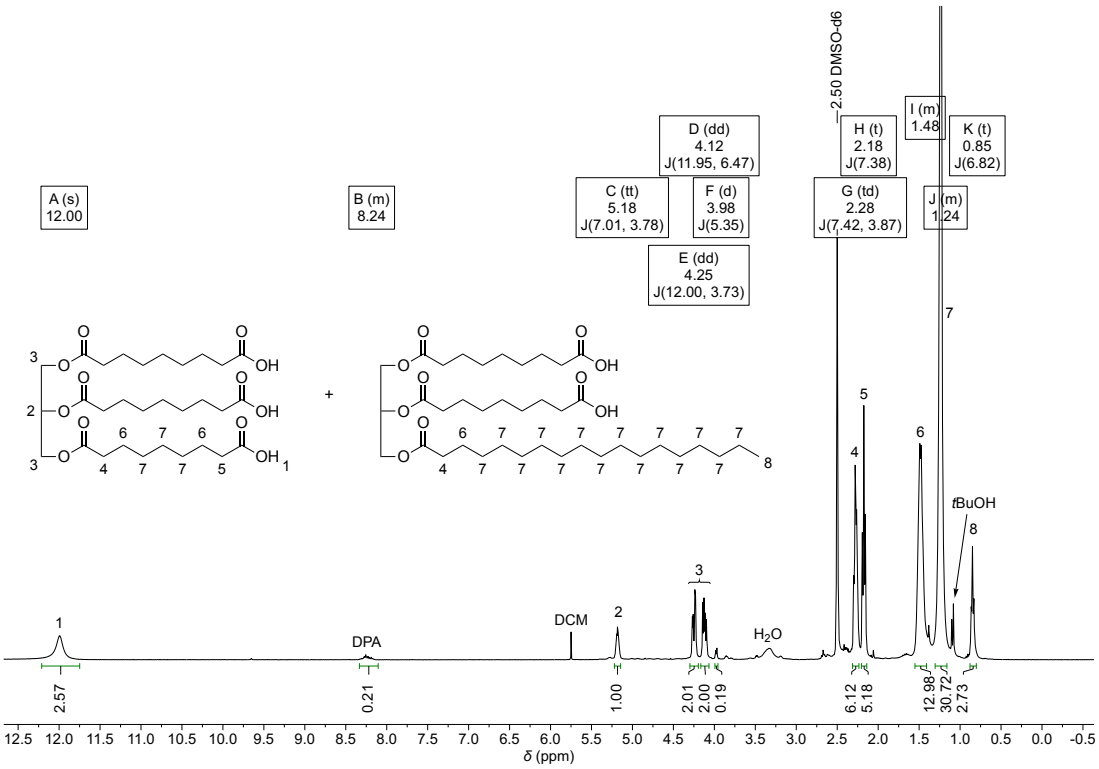

Figure 6.74: ^{1}H NMR spectrum of sunflower polyacid 4 purified by vacuum distillation of the oxidative cleavage of **HOSO04** (in DMSO-d_6).

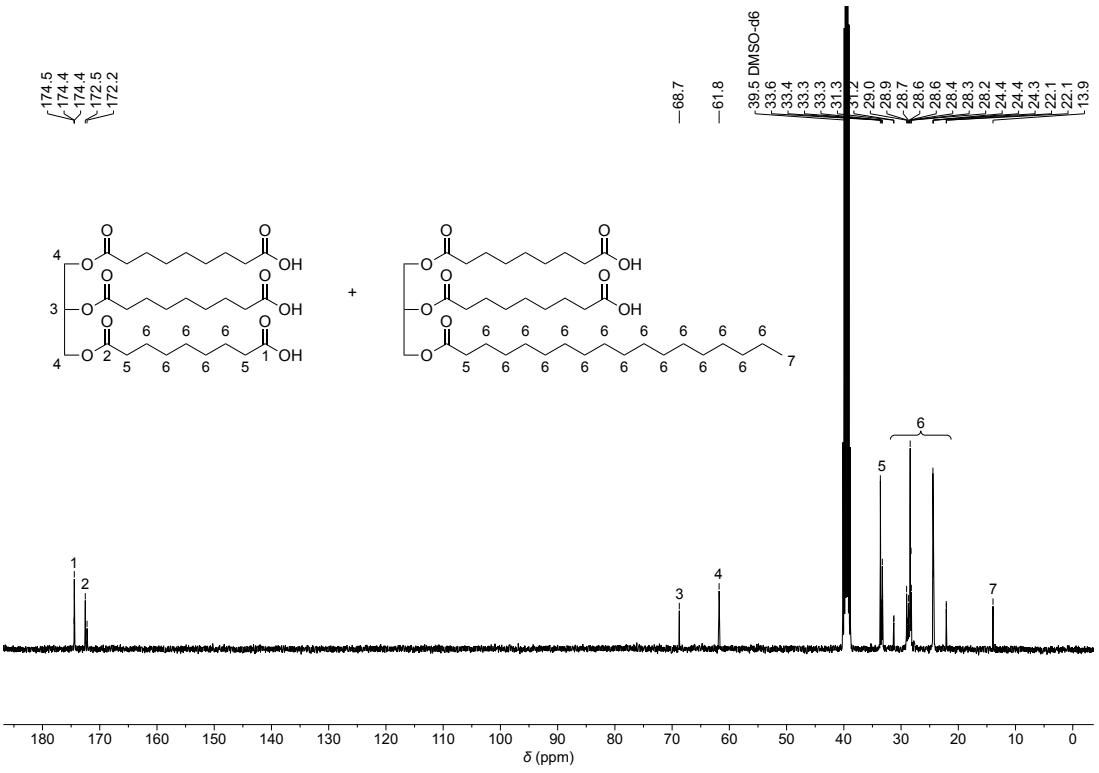

Figure 6.75: ^{13}C NMR spectrum of sunflower polyacid 4 purified by vacuum distillation of the oxidative cleavage of **HOSO 04** (in DMSO-d_6).

6.10.1.4 Picture of all isolated sunflower polyacids

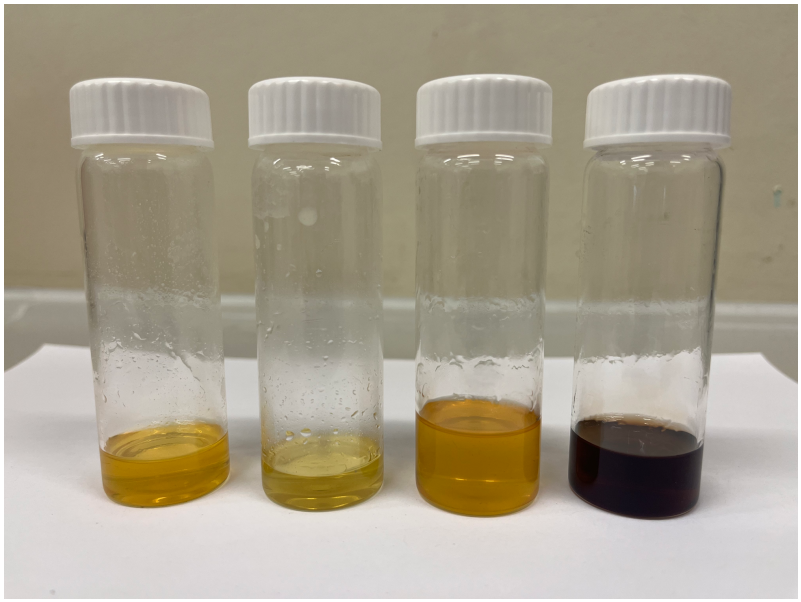

Figure 6.76: High oleic sunflower oil-based polyacid samples 1 to 4 from left to right.

6.10.2 ^{31}P NMR spectroscopy of sunflower polyacid samples 1 to 4

6.10.2.1 Calculation of carboxylic acid and hydroxyl content

The amount of carboxylic acids and hydroxyl groups per mg of sample was determined by derivatization of the respective sunflower polyacid sample using the phosphitylation agent 2-chloro-4,4,5,5-tetramethyl-1,3,2-dioxaphospholane (2-Cl-TMDP), according to a modified procedure of the one published by Kilpeläinen *et al*.[273] First, the internal standard solution was prepared by dissolving endo-N-hydroxy-5-norbornene-2,3-dicarboximide (550 mg, 3.07 mmol) in pyridine (15 ml) and CDCl3 (10 ml). This results in a final concentration of 22 mg ml^{-1} or 123 mmol l^{-1}. Then, under standard atmosphere (no argon box), 28 to 32 mg of the analyte was weighed into a 10 ml screw-top vial. CDCl3 (1 ml), Pyridine (200 µl, 2.48 mmol) and the internal standard solution of endo-*N*-hydroxy-5-norbornene-2,3-dicarboximide (650 µl) were added and the mixture was agitated with a vortex mixer until the sample was fully dissolved (approximately 1 min). At last, 2-Cl-TMDP (200 µl, 1.26 mmol) was added and the mixture was agitated for 1 min. Then, 1.0 ml of the solution was transferred to an NMR tube. 31P NMR measurements were performed immediately after the sample had been prepared.

Note: all compounds of the internal standard solution were weighed to enable the calculation of a weight percentage of internal standard inside the solution. A weight percentage was considered more accurate than a molarity, since volatile substances such as $CDCl_3$ are used. Furthermore, the use of a weight percentage erases the dependency of an accurate volume transfer.

The amount of carboxylic acids and hydroxyl groups in the samples was calculated in analogy to the calculation reported by Argyropoulos *et al*.[274] During the preparation of the ^{31}P samples, the added volume of internal standard solution is weighed in to allow the calculation of internal standard mass that was added, by multiplication of the mass with the weight percentage of the solution. The carboxylic acid and hydroxyl group content of the respective sample was then calculated using equations (40) and (41). The first term in the numerator corresponds to the amount of IS in mmol and the second term corresponds to the molar ratio of carboxylic acids (or hydroxyl groups) to internal standard (determined by integration in the ^{31}P NMR spectrum).

$$\frac{\text{mmol } CO_2H}{\text{mg sample}} = \frac{\frac{\text{mass (mg of IS solution)} \times \text{wt\% (IS solution)}}{179.18\frac{\text{g}}{\text{mol}}\ \text{(Molar mass of } e\text{-HNDI)}} \times \frac{\text{Integral } CO_2H}{\text{Integral IS}}}{\text{mg sample}} \tag{40}$$

$$\frac{\text{mmol OH}}{\text{mg sample}} = \frac{\frac{\text{mass (mg of IS solution)} \times \text{wt\% (IS solution)}}{179.18\frac{\text{g}}{\text{mol}}\ \text{(Molar mass of } e\text{-HNDI)}} \times \frac{\text{Integral OH}}{\text{Integral IS}}}{\text{mg sample}} \tag{41}$$

The final evaluation of all samples is summarized in Table 6.10.

Table 6.10: Carboxylic acid and hydroxyl group content of sunflower polyacids samples 1 to 4 determined *via* ^{31}P NMR spectroscopy.

Sample	$\frac{\boldsymbol{\mu mol\ CO_2H}}{\boldsymbol{mg\ sample}}$	$\frac{\boldsymbol{\mu mol\ OH}}{\boldsymbol{mg\ sample}}$
Sample 1 (flash column fraction 1)	3.342±0.039	0.237±0.026
Sample 2 (flash column fraction 2)	4.621±0.023	0.303±0.034
Sample 3 (filter column and removal of cleavage products *via* distillation)	3.731±0.052	0.166±0.025
Sample 4 (removal of cleavage products *via* distillation)	3.592±0.035	0.516±0.032

6.10.2.2 ^{31}P NMR spectra of sunflower polyacid sample 1 (flash column fraction 2)

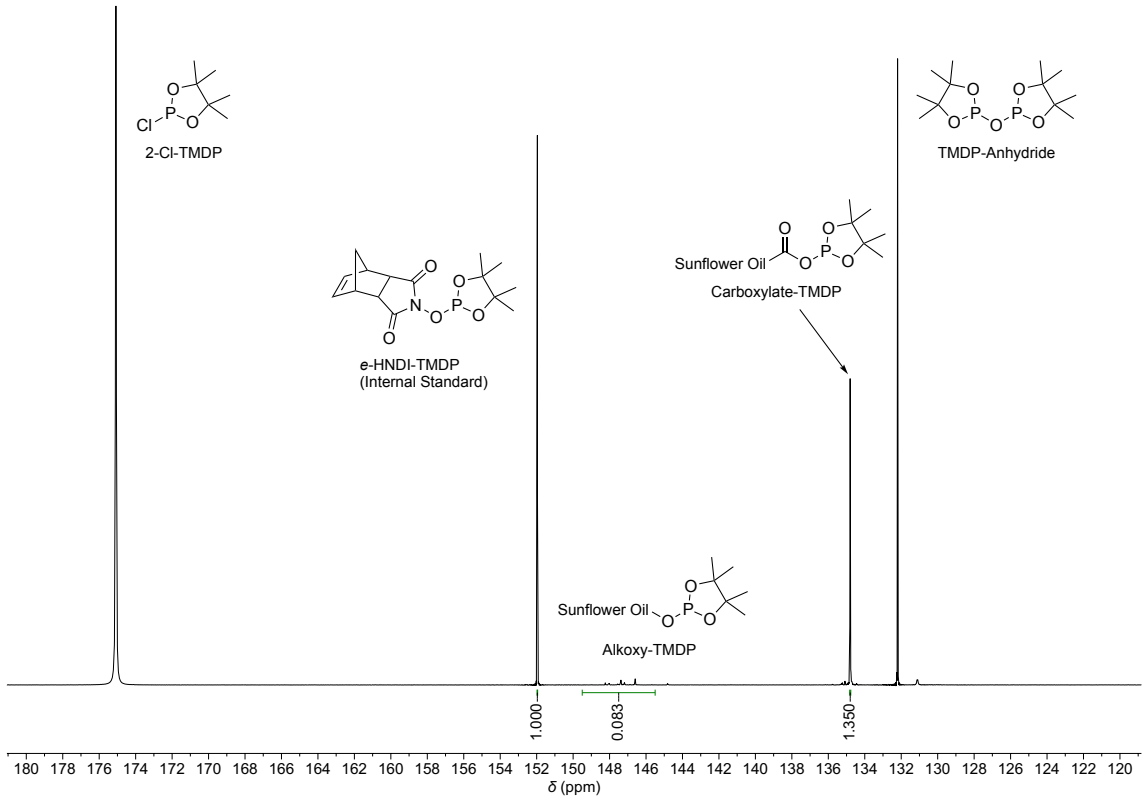

Figure 6.77: Quantitative ^{31}P NMR spectrum of phosphitylated sunflower polyacid sample 1 (measurement 1 as example).

Measurement 1: 30.9 mg sample, 752.6 mg IS solution (1.838 wt%);
alkoxy integral: 0.083, carboxy integral: 1.350;
result: 3.373 mmol CO_2H per mg sample; 0.207 mmol OH per mg sample.

Measurement 2: 30.6 mg sample, 750.6 mg IS solution (1.838 wt%);
alkoxy integral: 0.098, carboxy integral: 1.311;
result: 3.299 mmol CO_2H per mg sample; 0.247 mmol OH per mg sample.

Measurement 3: 31.2 mg sample, 755.8 mg IS solution (1.838 wt%);
alkoxy integral: 0.103, carboxy integral: 1.350;
result: 3.355 mmol CO_2H per mg sample; 0.256 mmol OH per mg sample.

6.10.2.3 ^{31}P NMR spectra of sunflower polyacid sample 2 (flash column fraction 3)

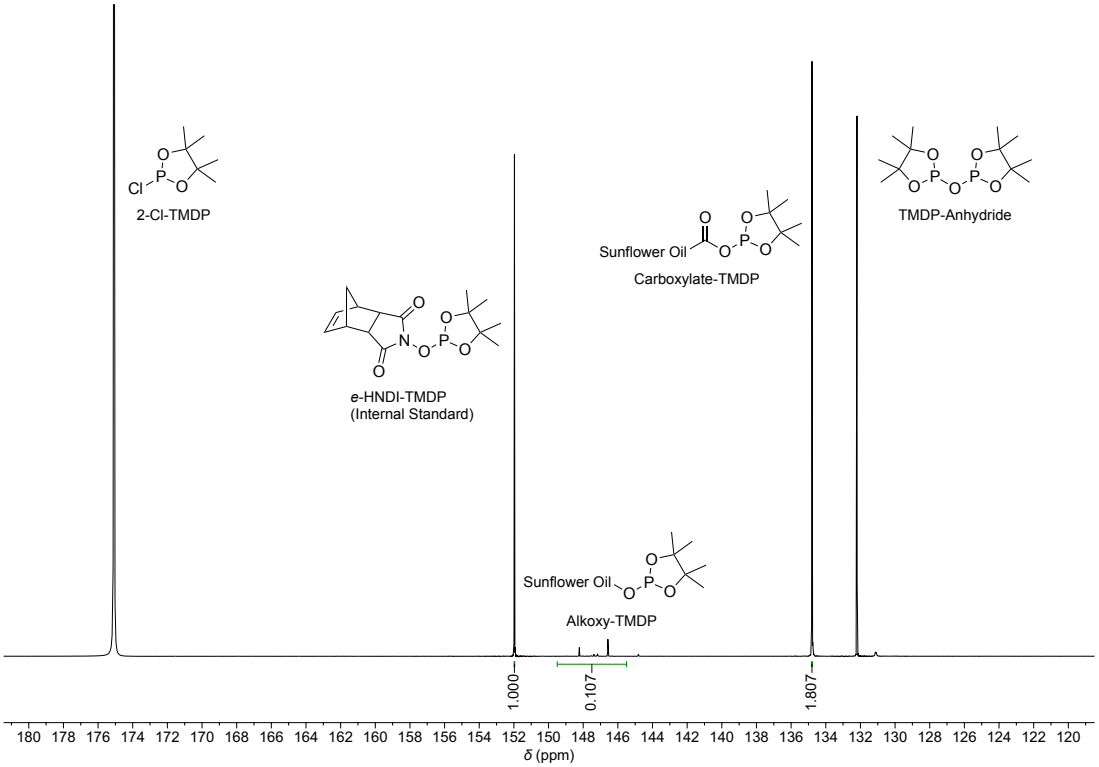

Figure 6.78: Quantitative ^{31}P NMR spectrum of phosphitylated sunflower polyacid sample 2 (measurement 1 as example).

Measurement 1: 30.6 mg sample, 758.4 mg IS solution (1.838 wt%);
alkoxy integral: 0.107, carboxy integral: 1.807;
result: 4.594 mmol CO_2H per mg sample; 0.272 mmol OH per mg sample.

Measurement 2: 30.5 mg sample, 760 mg IS solution (1.838 wt%);
alkoxy integral: 0.116, carboxy integral: 1.813;
result: 4.634 mmol CO_2H per mg sample; 0.297 mmol OH per mg sample.

Measurement 3: 31.1 mg sample, 756.9 mg IS solution (1.838 wt%);
alkoxy integral: 0.136, carboxy integral: 1.856;
result: 4.634 mmol CO_2H per mg sample; 0.340 mmol OH per mg sample.

6.10.2.4 ^{31}P NMR spectra of sunflower polyacid sample 3 (filter column, distillation)

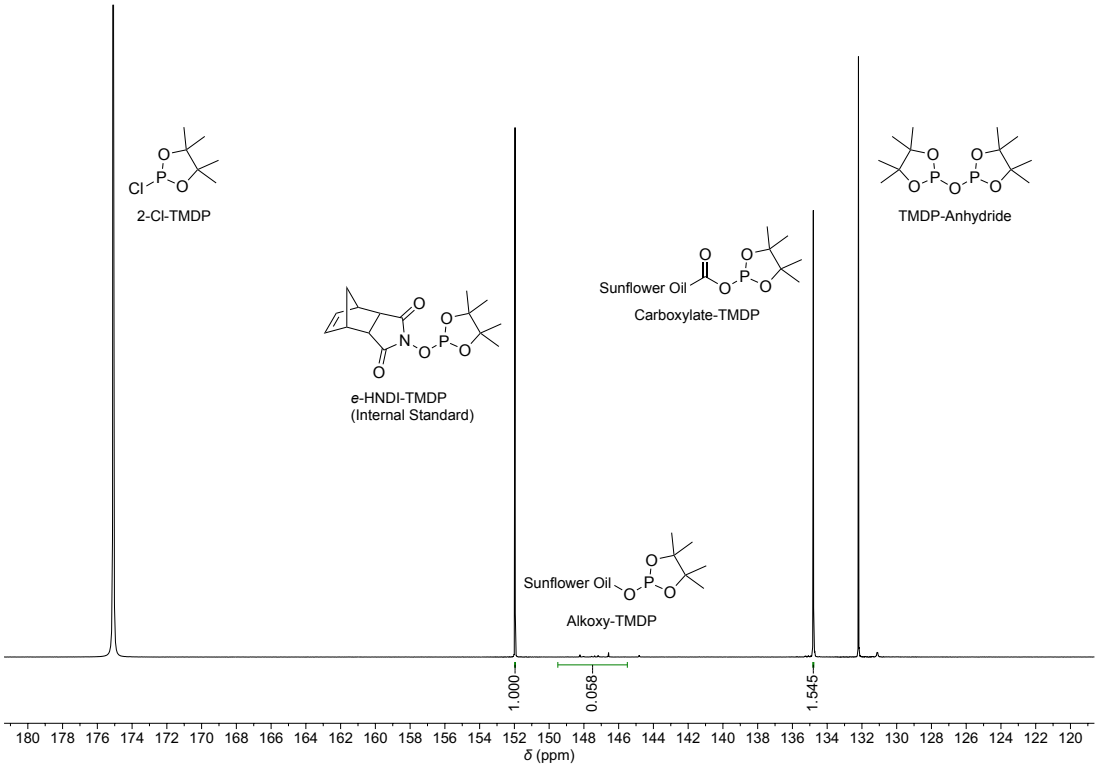

Figure 6.79: Quantitative ^{31}P NMR spectrum of phosphitylated sunflower polyacid sample 3 (measurement 1 as example).

Measurement 1: 31.7 mg sample, 749.2 mg IS solution (1.838 wt%);
alkoxy integral: 0.058, carboxy integral: 1.545;
result: 3.746 mmol CO_2H per mg sample; 0.141 mmol OH per mg sample.

Measurement 2: 30.3 mg sample, 745.8 mg IS solution (1.838 wt%);
alkoxy integral: 0.066, carboxy integral: 1.495;
result: 3.775 mmol CO_2H per mg sample; 0.167 mmol OH per mg sample.

Measurement 3: 29.8 mg sample, 748.4 mg IS solution (1.838 wt%);
alkoxy integral: 0.074, carboxy integral: 1.426;
result: 3.674 mmol CO_2H per mg sample; 0.191 mmol OH per mg sample.

6.10.2.5 ^{31}P NMR spectra of sunflower polyacid sample 4 (distillation)

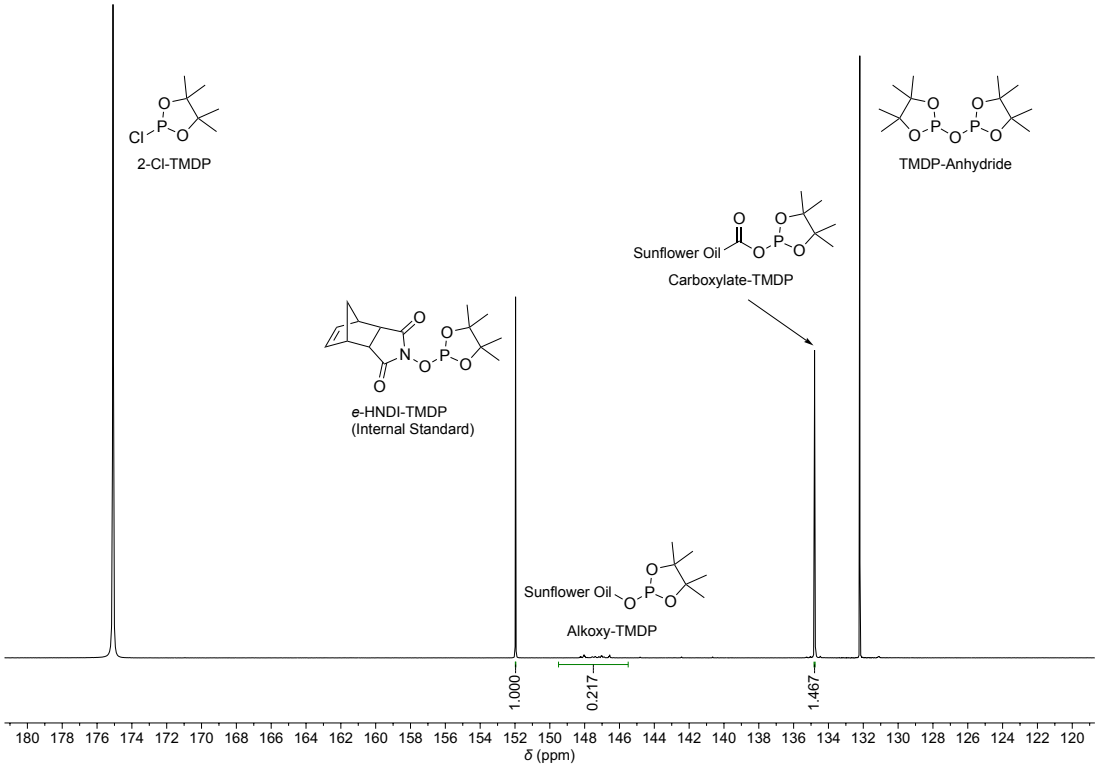

Figure 6.80: Quantitative ^{31}P NMR spectrum of phosphitylated sunflower polyacid sample 4 (measurement 1 as example).

Measurement 1: 31.3 mg sample, 752.1 mg IS solution (1.838 wt%);
alkoxy integral: 0.217, carboxy integral: 1.467;
result: 3.616 mmol CO_2H per mg sample; 0.535 mmol OH per mg sample.

Measurement 2: 39.8 mg sample, 748.2 mg IS solution (1.838 wt%);
alkoxy integral: 0.186, carboxy integral: 1.379;
result: 3.552 mmol CO_2H per mg sample; 0.479 mmol OH per mg sample.

Measurement 3: 29.9 mg sample, 754 mg IS solution (1.838 wt%);
alkoxy integral: 0.207, carboxy integral: 1.395;
result: 3.609 mmol CO_2H per mg sample; 0.535 mmol OH per mg sample.

6.10.3 Oxidative cleavage of sunflower oil for Passerini polymerizations

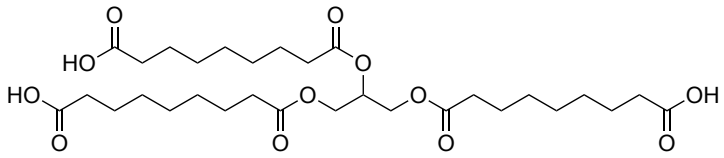

$C_{30}H_{50}O_{12}$
M = 602.72 g/mol

In a 100 ml three-necked flask, high oleic sunflower oil **HOSO04** (39.8 g, 45.00 mmol (based on the molecular weight of triolein (885.45 g/mol)), 1.00 equiv.), ruthenium(III)acetylacetonate (359 mg, 900 µmol, 2 mol%) and pyridine-2,6-dicarboxylic acid (3.01 g, 18.0 mmol, 40 mol%) were dissolved in *tert*-butanol (405 ml) and water (135 ml). The reaction mixture was stirred magnetically (400 rpm with a cross shaped stirring bar) at 80 °C for 24 h. After the reaction temperature reached 80 °C, hydrogen peroxide (35% aq. sol., 92.9 ml, 1.08 mol, 24.0 equiv.) was added slowly to the reaction solution by a syringe pump with a flow rate of 77.4 µl min^{-1} over a period of 20 h. After the entire reaction time passed, the reaction solution was diluted with water (200 ml) and *tert*-butanol was removed under reduced pressure to ensure easier phase separation during extraction. The aqueous phase was extracted with ethyl acetate (3 × 150 ml) and the combined organic layers were washed with saturated sodium chloride solution (3 × 100 ml), dried over sodium sulfate, filtered and the solvent was removed under reduced pressure. The reaction was conducted twice. After extraction, ^{1}H NMR analysis of both reactions resulted in an overall conversion of double bonds into carboxylic acids of 85.71%. Both reactions were combined and distilled in a Zinke apparatus to remove the cleavage products. Nonanoic acid (29.2g, 185 mmol, 90%) was isolated by distillation in vacuo (100 °C, 0.1 mbar). The residue of the distillation was purified by flash column chromatography (cyclohexane/EtOAc, 4:1 + 1% formic acid, then 2:1 + 1% formic acid, then 2:1 without formic acid) to obtain three fractions (Fraction 1: residue nonanoic acid (2.50 g, 15.80 mmol, 8%), Fraction 2: side product with low carboxylic acid content (18.0 g, 31%), Fraction 3: sunflower polyacid (20.8 g, 36%)) after removal of solvent and formic acid under reduced pressure.

Yield Calculation (chapter 6.10.1.1 explains the used equations):

Oleic acid substituents (mmol) = 90 mmol × 3 × 0.8869 = 239.46 mmol (42)

Theoretical Yield (nonanoic acid) = 239.46 mmol × 158.24 g/mol = 37.90 g (43)

NMR-Yield (nonanoic acid) = 239.46 mmol × 158.24 g/mol × 0.8571 = 32.5 g (44)

$M_{Product}$ = 885.45 g/mmol × 0.1429 + 602.72 g/mol × 0.8571 = 643.12 g/mol (45)

$$\frac{\text{isolated mass (nonanoic acid)}}{\text{theoretical yield (nonanoic acid)}} \times 100 = \frac{31.7\ \text{g}}{37.9\ \text{g}} \times 100 = 83.6\% \quad (46)$$

$$\frac{\text{isolated mass (nonanoic acid)}}{\text{NMR-Yield (nonanoic acid)}} \times 100 = \frac{31.7\ \text{g}}{32.5\ \text{g}} \times 100 = 97.5\% \quad (47)$$

$$\text{Yield (F2)} = \frac{\text{isolated mass (F2)}}{\text{M}_{\text{Product}} \times 0.01\ \text{mol}} \times 100 = \frac{18.0\ \text{g}}{643.12\ \frac{\text{g}}{\text{mol}} \times 0.09\ \text{mol}} \times 100 = 31.1\% \quad (48)$$

$$\text{Yield (F3)} = \frac{\text{Isolated mass (F3)}}{\text{M}_{\text{Product}} \times 0.01\ \text{mol}} \times 100 = \frac{20.8\ \text{g}}{643.12\ \frac{\text{g}}{\text{mol}} \times 0.09\ \text{mol}} \times 100 = 35.9\% \quad (49)$$

Fraction 1: Nonanoic acid

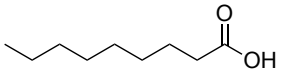

$C_9H_{18}O_2$

M = 158.24 g/mol

R_f (Fraction 1) = 0.69 (cyclohexane/EtOAc, 2:1 + 1% formic acid).

^{1}H NMR (400 MHz, $CDCl_3$, ppm): δ = 11.95 (s, 1H, H^1), 2.18 (t, J = 7.4 Hz, 2H, H^2), 1.54−1.42 (m, 3H, H^3), 1.24 (s, 10H, H^4), 0.95−0.76 (m, 3H. H^5).

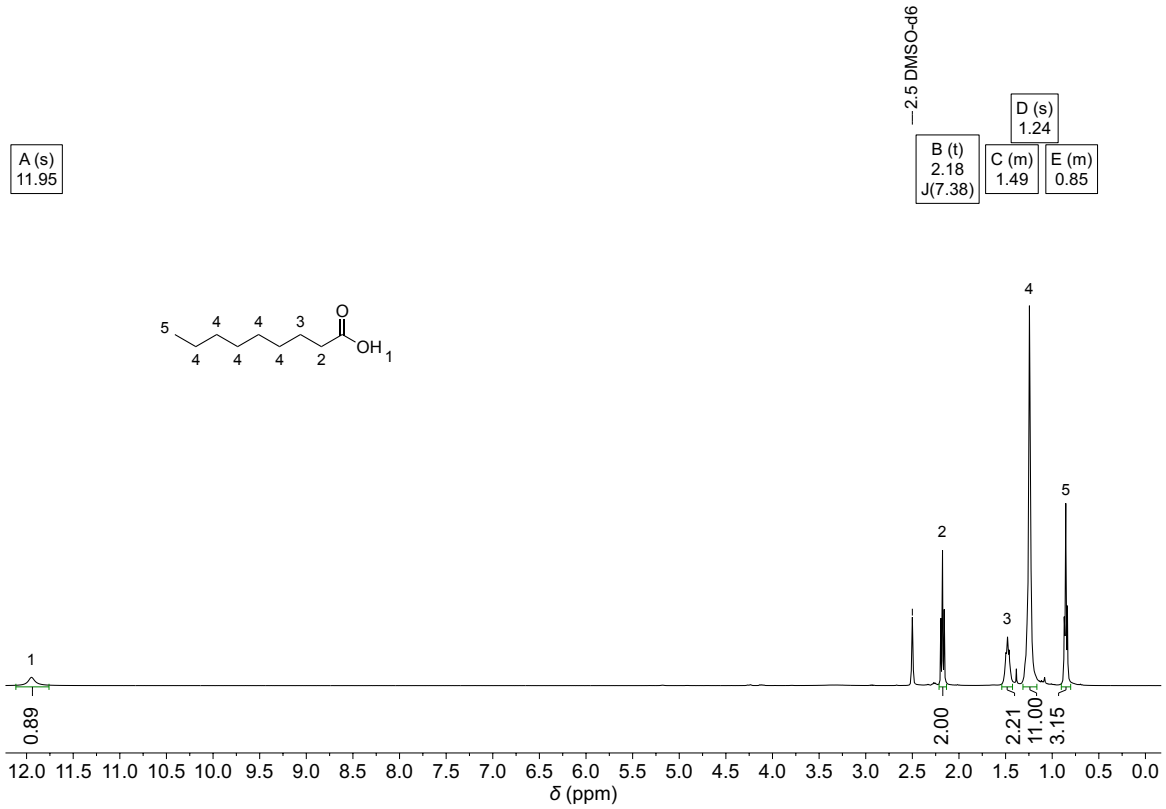

Figure 6.81: ^{1}H NMR spectrum of the isolated nonanoic acid by flash column chromatography (in DMSO-d_6).

Fraction 2: Sunflower oil based polyacid with low carboxylic acid content

Representative Structures:

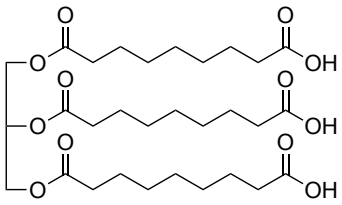

$C_{30}H_{50}O_{12}$
M = 602.72 g/mol

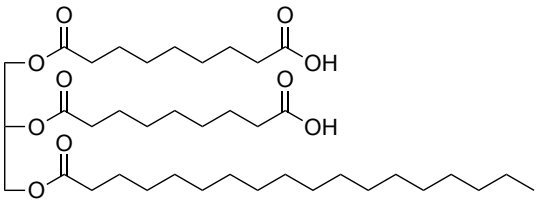

$C_{39}H_{70}O_{10}$
M = 698.98 g/mol

R_f (Fraction 2) = 0.26 (cyclohexane/EtOAc, 2:1 + 1% formic acid).

^{1}H NMR (400 MHz, DMSO-d_6, ppm): δ = 11.99 (s, 3H, H^1), 5.18 (tt, J = 7.0, 3.7 Hz, 1H, H^2), 4.25 (dd, J = 12.0, 3.7 Hz, 2H, H^3), 4.12 (dd, J = 12.0, 6.5 Hz, 2H, H^3), 3.97 (d, J = 5.4 Hz, not further oxidized O*H* group), 2.30−2.24 (m, 6H, H^4), 2.18 (td, J = 7.4, 3.7 Hz, 6H, H^5), 1.57−1.42 (m, 16H, H^6), 1.31−1.14 (m, 45H, H^7), 0.85 (t, J = 6.8 Hz, 5H, H^8).

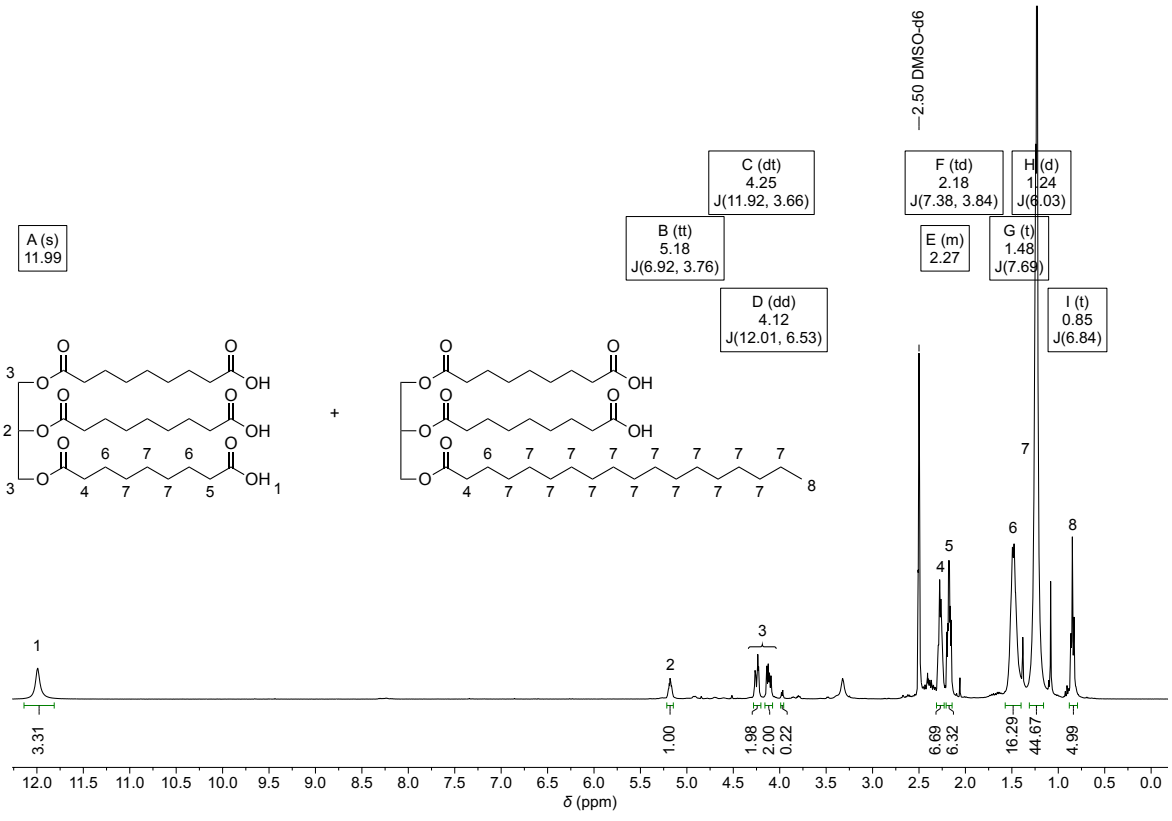

Figure 6.82: ^{1}H NMR spectrum of fraction 2 isolated by flash column chromatography (in DMSO-d_6).

Fraction 3: Sunflower oil based polyacid sample 5

Representative Structures:

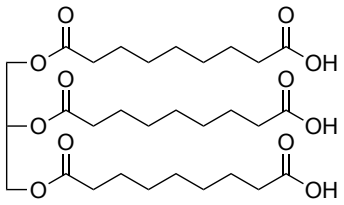

$C_{30}H_{50}O_{12}$
M = 602.72 g/mol

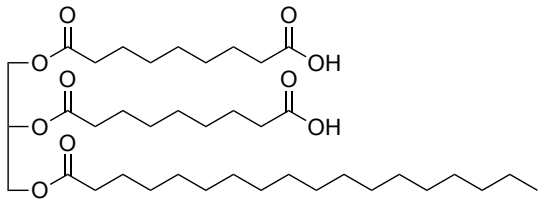

$C_{39}H_{70}O_{10}$
M = 698.98 g/mol

R_f (fraction 3) = 0.14 (cyclohexane/EtOAc, 2:1 + 1% formic acid).

^{1}H NMR (400 MHz, DMSO-d_6, ppm): δ = 11.95 (s, 3H, H^1), 5.18 (tt, J = 6.9, 3.7 Hz, 1H, H^2), 4.25 (dd, J = 12.0, 3.7 Hz, 2H, H^3), 4.12 (dd, J = 12.0, 6.5 Hz, 2H, H^3), 2.34−2.22 (m, 6H, H^4), 2.17 (t, J = 7.4 Hz, 6H, H^5), 1.49 (ddd, J = 14.6, 9.6, 5.5 Hz, 12H, H^6), 1.25 (d, J = 3.8 Hz, 18H, H^7), 0.89−0.78 (m, 0.17H, H^8).

^{13}C NMR (101 MHz, DMSO-d_6, ppm): δ = 174.5 (C_q, CO_2H, C^1), 174.4 (C_q, CO_2H, C^1), 172.5 (C_q, C_{Ester}, C^2), 172.2 (C_q, C_{Ester}, C^2), 68.8 (+, CH, $C_{Glyceryl}$, C^3), 61.8 (–, CH_2, $C_{Glyceryl}$, C^4), 33.6 (−, CH_2, C^5), 33.6 (−, CH_2, C^5),33.5 (−, CH_2, C^5), 33.3 (−, CH_2, C^5), 28.4 (−, CH_2, C^6), 28.3 (−, CH_2, C^6), 28.2 (−, CH_2, C^6), 24.4 (−, CH_2, C^6), 24.4 (−, CH_2, C^6), 24.3 (−, CH_2, C^6).

IR (ATR, cm^{-1}): $\tilde{\nu}$ = 3223 (vw), 2929 (m), 2857 (w), 1738 (vs), 1703 (vs), 1456 (w), 1413 (w), 1378 (w), 1232 (m), 1160 (vs), 1133 (s), 1094 (m), 1033 (w), 938 (w), 728 (w) cm^{-1}.

ESI-MS ($[M-H]^-$, $C_{30}H_{49}O_{12}$, deprotonated triacid): calcd.: 601.3230, found: 601.3229.

ESI-MS ($[M-H]^-$, $C_{39}H_{69}O_{12}$, deprotonated diacid with one oleic acid residue oxidized to diol): calcd.: 729.4795, found: 729.4796.

ESI-MS ($[M-H]^-$, $C_{39}H_{67}O_{12}$, deprotonated diacid with one oleic acid residue oxidized to acyloin): calcd.: 727.4638, found: 727.4638.

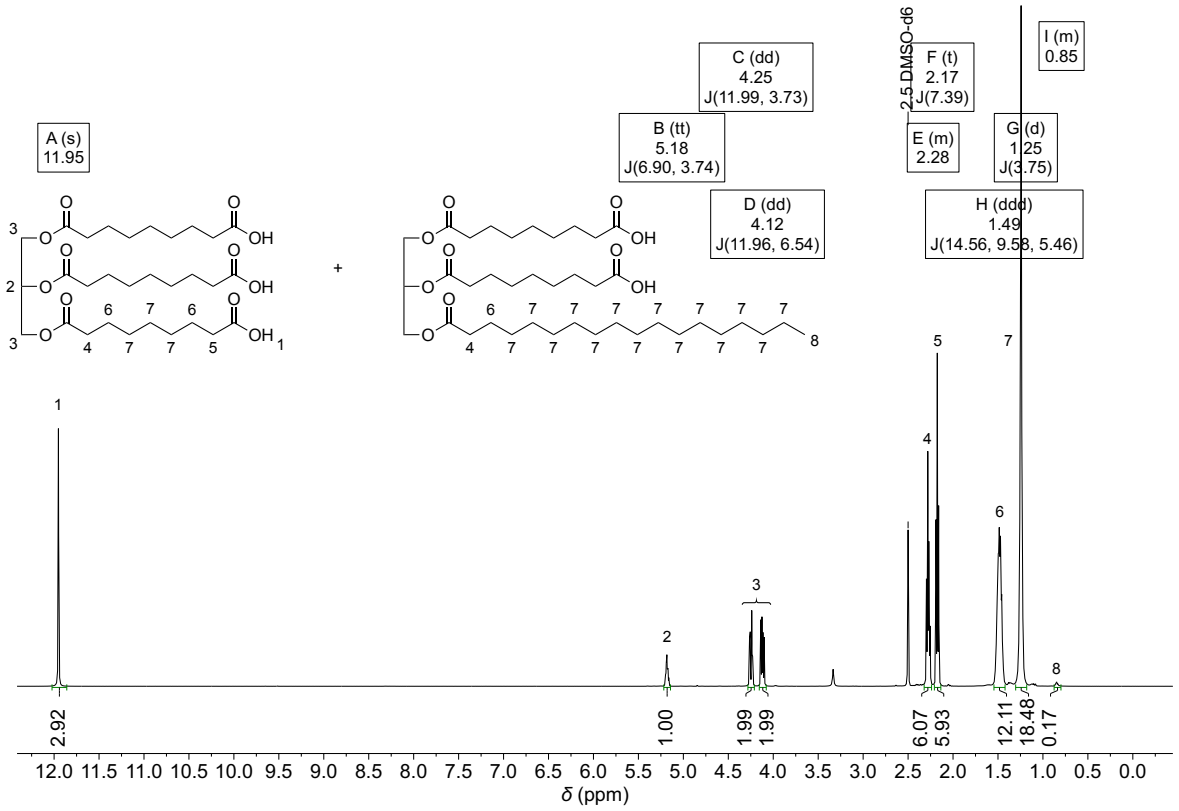

Figure 6.83: ^{1}H NMR spectrum of sunflower polyacid sample 5 in DMSO-d_6.

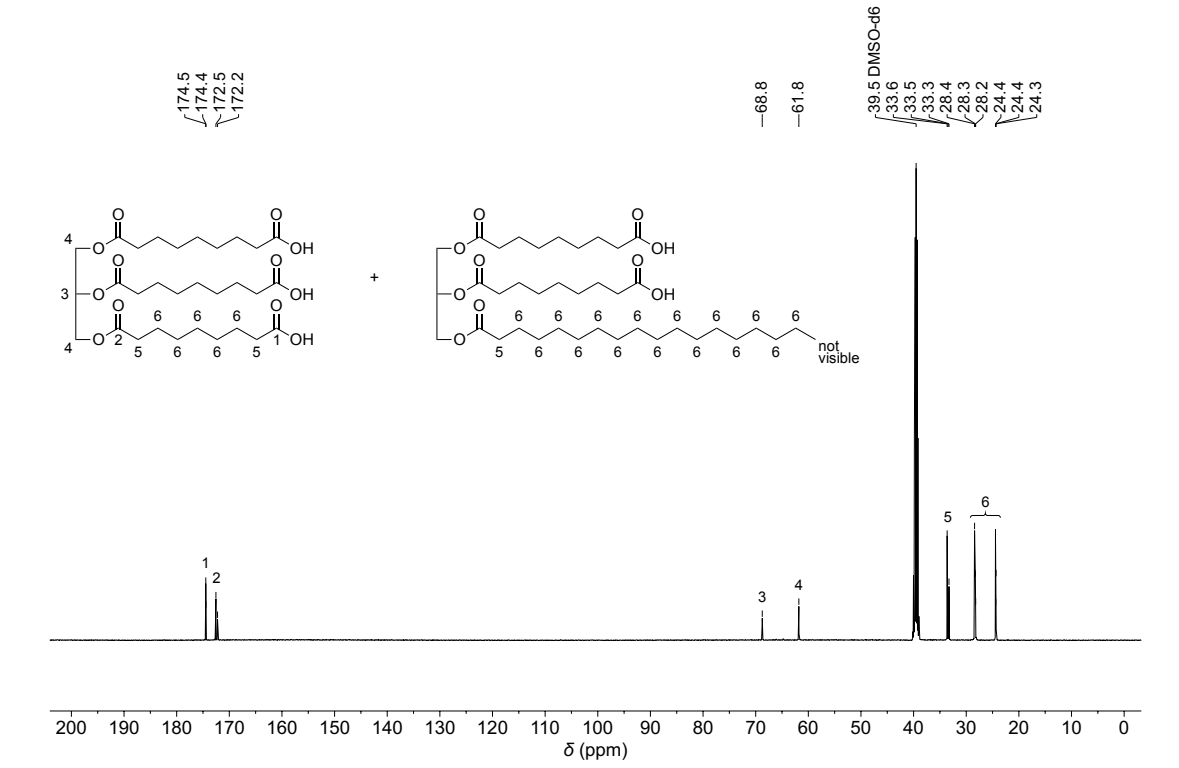

Figure 6.84: ^{13}C NMR spectrum of sunflower polyacid sample 5 in DMSO-d_6.

6.10.4 ^{31}P NMR spectroscopy of sunflower polyacid sample 5

The procedure for the preparation of the internal solution as well as the calculation are already described in chapter 6.10.2. The final evaluation of sunflower polyacid sample 5 is summarized in Table 6.11. One exemplary ^{31}P NMR spectrum is depicted in Figure 6.85

Table 6.11: Carboxylic acid and hydroxyl group content of sunflower polyacid sample 5 determined *via* ^{31}P NMR spectroscopy.

Sample	$\frac{\mu mol\ CO_2H}{mg\ sample}$	$\frac{\mu mol\ OH}{mg\ sample}$
Sunflower polyacid sample 5	4.952±0.036	0.078±0.005

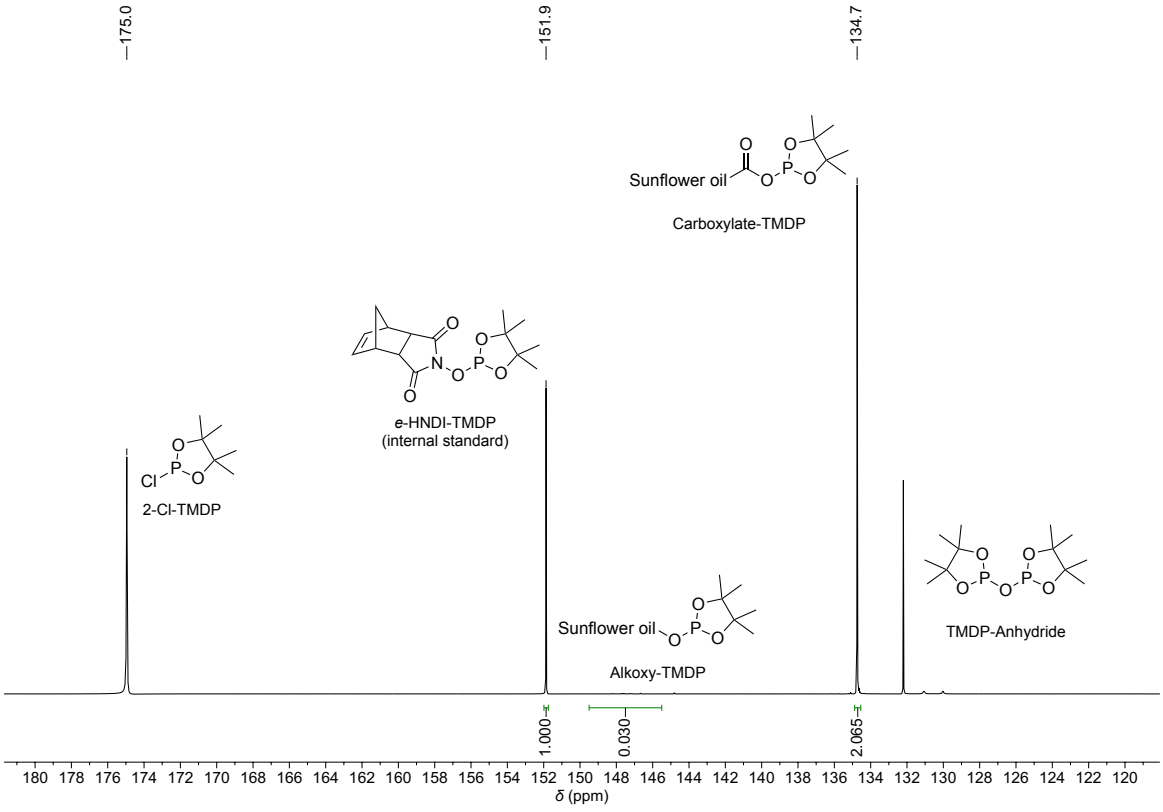

Figure 6.85: Quantitative ^{31}P NMR spectrum of phosphitylated sunflower polyacid sample 5 (measurement 1 as example).

Measurement 1: 30.2 mg sample, 813.8 mg IS solution (1.652 wt%);
alkoxy integral: 0.03, carboxy integral: 2.065;
result: 4.977 µmol CO_2H per mg sample; 0.0745 µmol OH per mg sample.

Measurement 2: 28.5 mg sample, 813.4 mg IS solution (1.652 wt%);
alkoxy integral: 0.031, carboxy integral: 1.93;
result: 4.926 µmol CO_2H per mg sample; 0.0816 µmol OH per mg sample.

6.11 Synthesis of Isocyanides

All isocyanides were synthesized according to the procedure published by Meier *et al*.[306]

6.11.1 *n*-Hexylisocyanide

Synthesis of *n*-Hexylformamide:

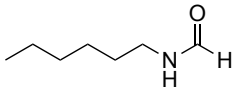

$C_7H_{15}NO$
M = 129.20 g/mol

Hexyl amine (20.4 g, 200 mmol, 1.00 eq.) and ethyl formate (322 mL, 296 g, 4.00 mol, 20.0 eq.) were stirred at 54 °C for 16 h. Afterwards, the remaining ethyl formate and ethanol were removed under reduced pressure and the crude product (21.7 g, 168 mmol, 84%) was used without further purification.

^{1}H NMR (400 MHz, $CDCl_3$, ppm): δ = 8.20−7.58 (m, 2H, H^1), 3.05 (q, J = 6.6 Hz, 2H, H^2), 1.39 (p, J = 7.0 Hz, 2H, H^3), 1.33−1.16 (m, 6H, H^4), 0.86 (t, J = 6.3 Hz, 3H, H^5).

^{13}C NMR (101 MHz, $CDCl_3$, ppm): δ = 164.4 (*C*HO, C^1), 160.8 (*C*HO, C^1), 40.8 (CH_2, α-$C_{Formamide}$, C^2), 37.0 (CH_2, α-$C_{Formamide}$, C^2), 30.9 (CH_2, C^3), 30.9 (CH_2, C^3), 29.0 (CH_2, C^3), 26.0 (CH_2, C^3), 25.5 (CH_2, C^3), 22.0 (CH_2, C^3), 13.9 (CH_3, C^4).

IR (ATR, cm^{-1}): $\tilde{\nu}$ = 3276 (w), 3055 (vw), 2956 (w), 2928 (m), 2857 (m), 1656 (vs), 1536 (m), 1466 (w), 1381 (s), 1306 (vw), 1241 (w), 1200 (w), 812 (vw), 762 (w), 724 (w), 652 (vw).

ESI-MS ($[M+H]^+$, $C_7H_{16}NO$) calcd.: 130.1226; found: 130.1227.

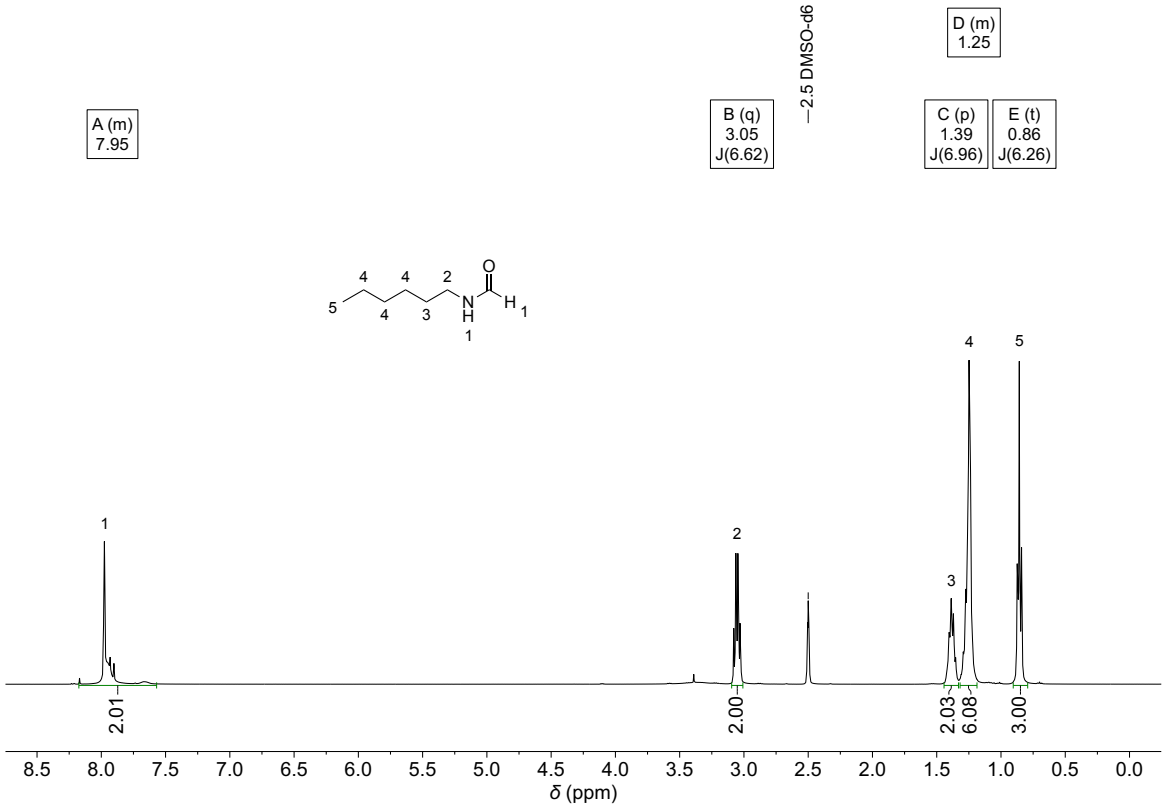

Figure 6.86: ^{1}H NMR Spectrum of *n*-hexylformamide in DMSO-d_6.

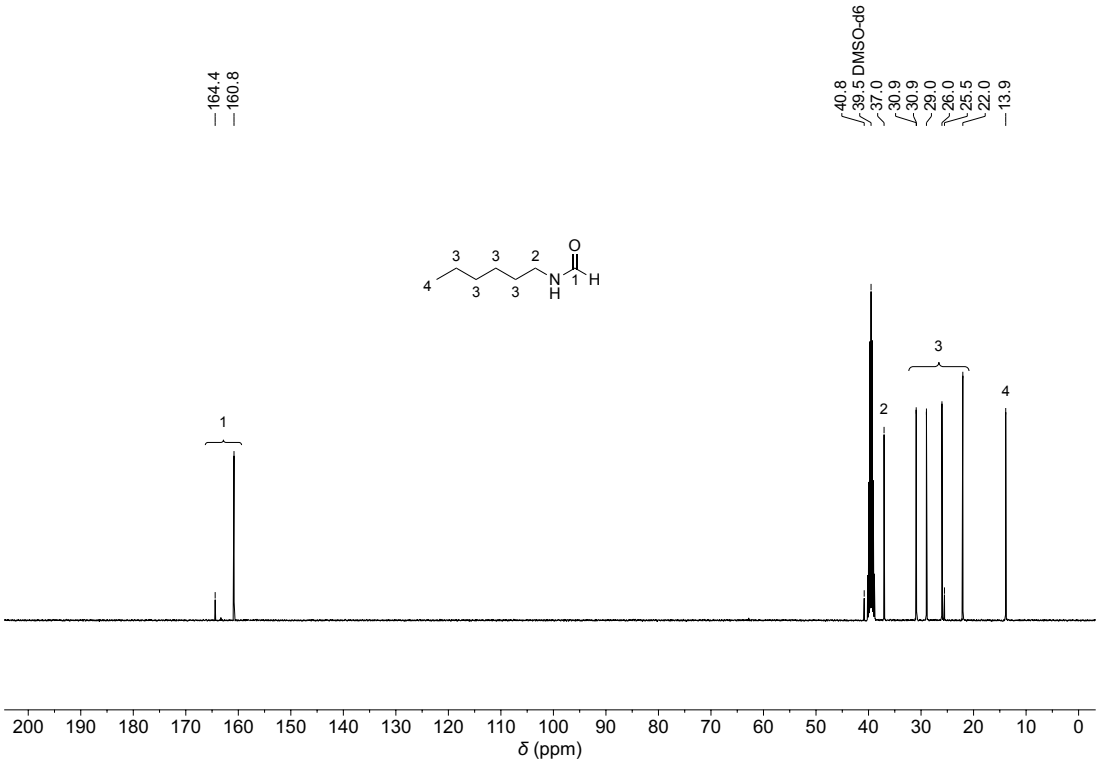

Figure 6.87: ^{13}C NMR Spectrum of *n*-hexylformamide in DMSO-d_6

Synthesis of *n*-Hexylisocyanide:

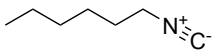

$C_7H_{13}N$
M = 111.19 g/mol

n-Hexylformamide (5.17 g, 40.0 mmol, 1.00 equiv.) was dissolved in dichloromethane (60 ml, 666 mmol/l) and pyridine (9.71 ml, 120 mmol, 3.00 equiv.) was added. Subsequently, *p*-toluenesulfonyl chloride (11.4 g, 60.0 mmol, 1.50 equiv.) was added under cooling with a water bath. The cooling was removed, and the reaction mixture was stirred for 24 h at room temperature. Afterwards, aqueous saturated sodium carbonate solution (40 ml) was added, and the biphasic mixture was stirred for another 60 minutes. Water (80 ml) and dichloromethane (80 ml) were added, and the organic phase was separated. The aqueous phase was extracted with dichloromethane (3 × 40 ml), the organic extracts were combined and washed with saturated sodium chloride solution (2 × 40 ml). The organic phase was dried over sodium sulfate, filtered and the solvent was removed under reduced pressure. The crude product was purified by vacuum distillation in a Kugelrohr oven (70 °C, 60 mbar) to obtain the title compound (2.50 g, 22.5 mmol, 56%).

^{1}H NMR (400 MHz, $CDCl_3$, ppm): δ = 3.36 (tt, J = 6.7, 2.1 Hz, 2H, H^1), 1.74−1.57 (m, 2H, H^2), 1.42 (p, J = 7.0 Hz, 2H, H^3), 1.36−1.23 (m, 4H, H^4), 0.89 (t, J = 6.9 Hz, 3H, H^5).

^{13}C NMR (101 MHz, $CDCl_3$, ppm): δ = 155.65 (t, J = 6.1 Hz, C^1), 41.62 (t, J = 6.1 Hz, CH_2, C^2), 30.9 (CH_2, C^3), 29.1 (CH_2, C^3), 26.0 (CH_2, C^3), 22.5 (CH_2, C^{3s}), 14.0 (CH_3, C^4).

IR (ATR, cm^{-1}): $\tilde{\nu}$ = 2956 (m), 2929 (s), 2860 (m), 2146 (vs), 1456 (m), 1380 (w), 1351 (w), 892 (w), 727 (w).

ESI-MS (ESI, $[M+H]^+$, $C_7H_{14}N$) calcd.: 112.1121; found: 112.1123.

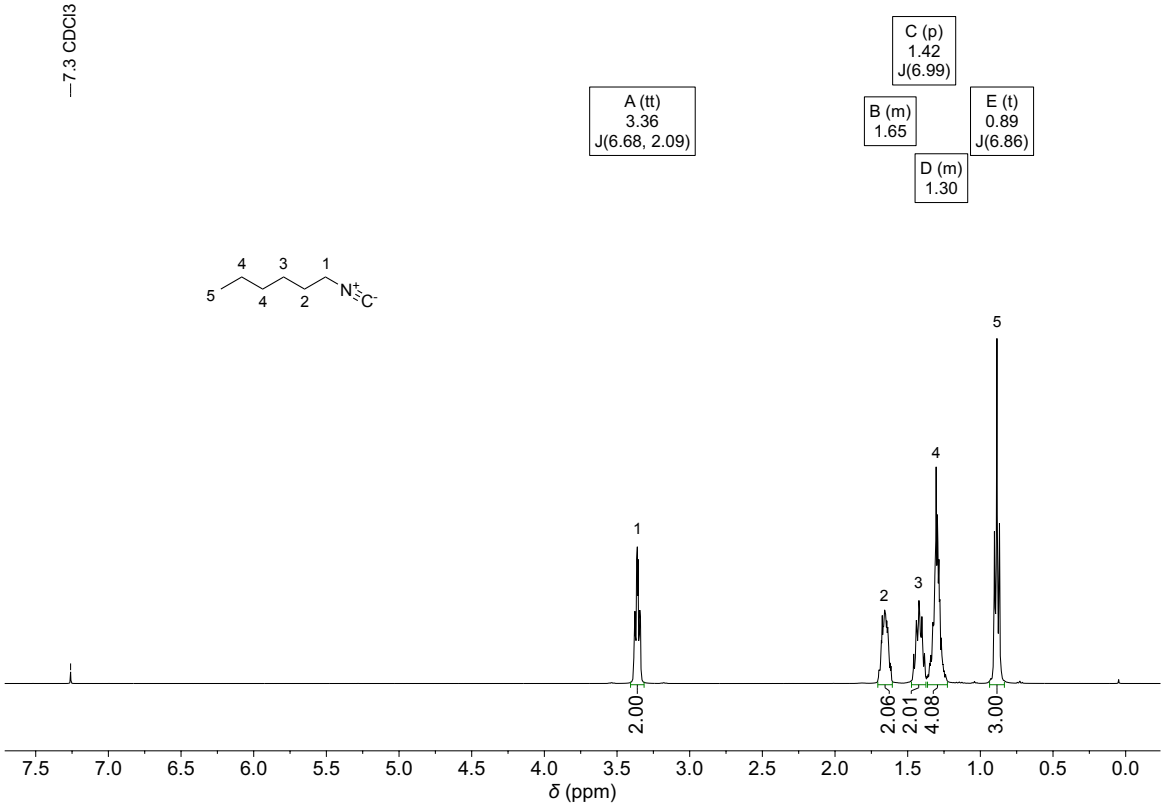

Figure 6.88: ^{1}H NMR spectrum of *n*-hexylisocyanide in $CDCl_3$.

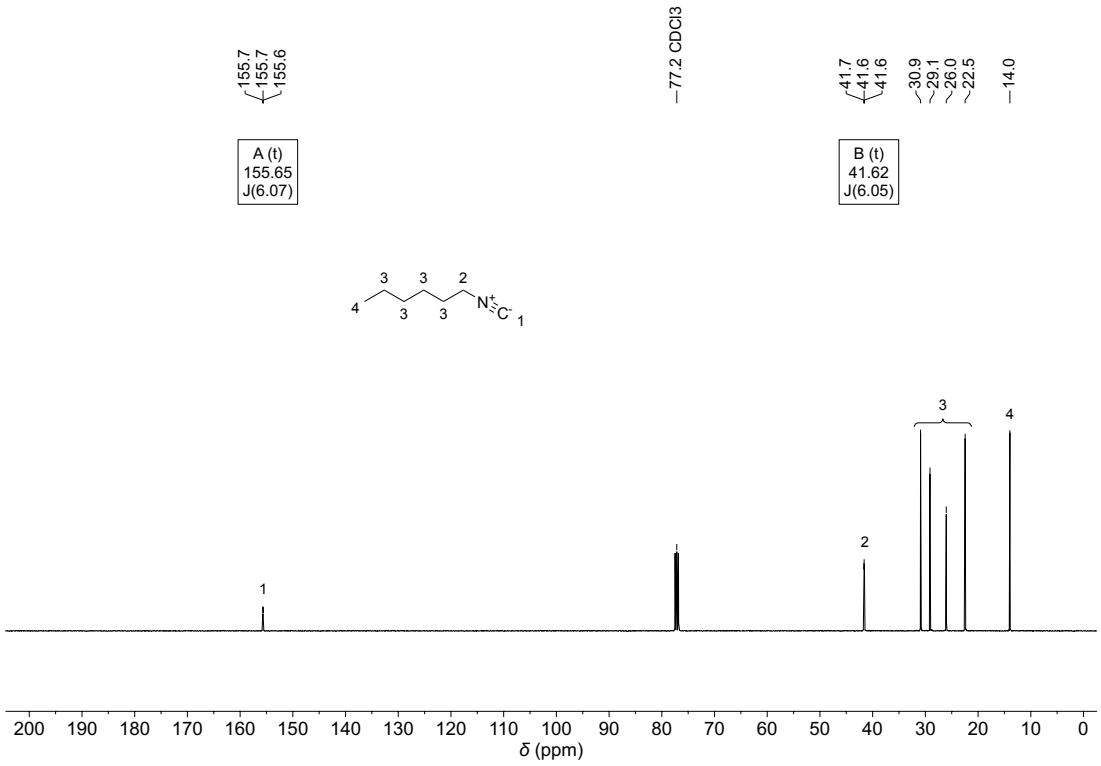

Figure 6.89: ^{13}C NMR spectrum of *n*-hexylisocyanide in $CDCl_3$.

6.11.2 1,6-Diisocyanohexane

Synthesis of 1,6-Diformamidohexane:

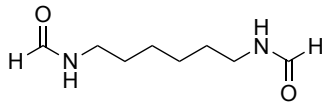

$C_8H_{16}N_2O_2$
M = 172.23 g/mol

1,6-Diaminohexane (15.0 g, 129 mmol, 1.00 eq.) and ethyl formate (209 mL, 191 g, 2.58 mol, 20.0 eq.) were stirred at 54 °C for 16 h. Afterwards, the remaining ethyl formate and ethanol were removed under reduced pressure and the crude product (21.5 g, 125 mmol, 97%) was used without further purification.

^{1}H NMR (400 MHz, $CDCl_3$, ppm): δ = 8.04−7.63 (m, 4H, H^1), 3.05 (q, J = 6.7 Hz, 4H, H^2), 1.39 (p, J = 6.5 Hz, 4H, H^3), 1.30−1.20 (m, 4H, H^4).

^{13}C NMR (101 MHz, $CDCl_3$, ppm): δ = 164.4 (*C*HO, C^1), 160.9 (*C*HO, C^1), 40.7 (CH_2, C^2), 37.0 (CH_2, C^2), 30.8 (CH_2, C^3), 28.9 (CH_2, C^3), 26.0 (CH_2, C^3), 25.5 (CH_2, C^3).

IR (ATR, cm^{-1}): $\tilde{\nu}$ = 3275 (s), 3182 (vw), 3030 (vw), 2943 (w), 2913 (w), 2863 (w), 2853 (w), 1641 (vs), 1627 (vs), 1528 (vs), 1475 (m), 1460 (w), 1442 (w), 1386 (vs), 1236 (s), 1212 (s), 1082 (w), 778 (s), 740 (w), 708 (vs), 461 (w).

ESI-MS ($[M+H]^+$, $C_8H_{17}N_2O_2$) calcd.: 173.1285; found: 173.1283.

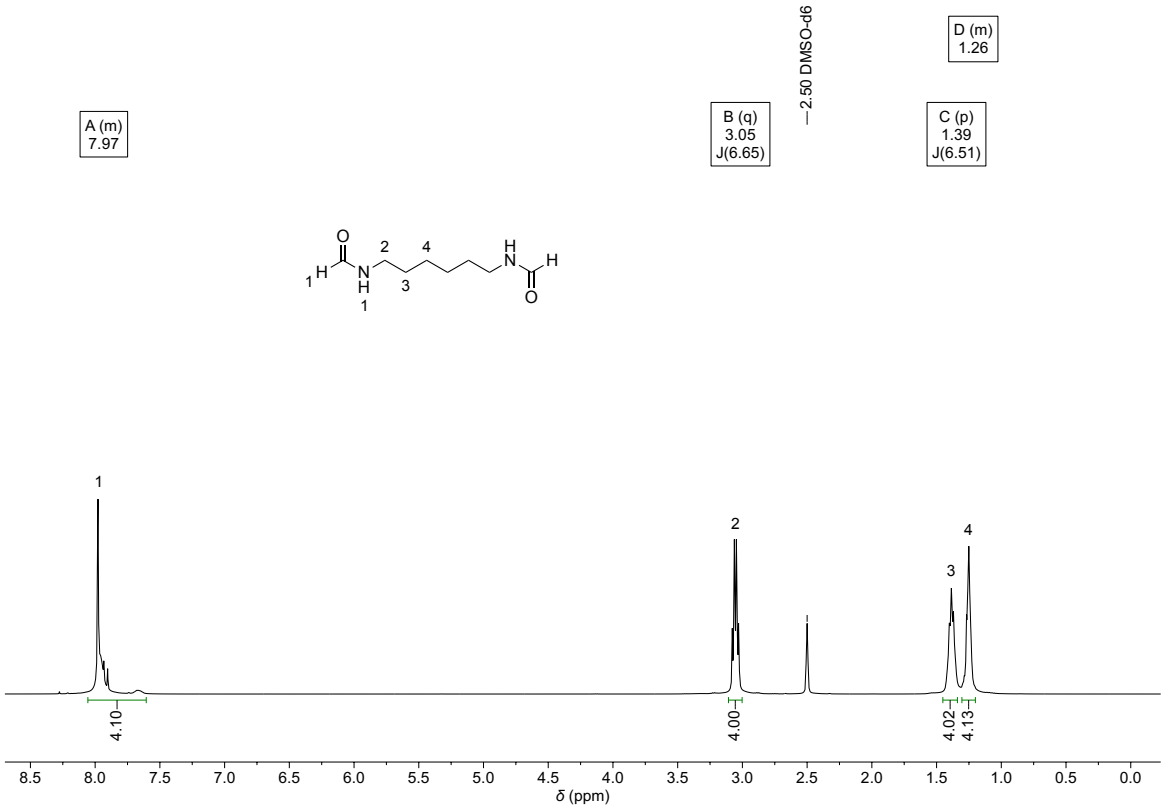

Figure 6.90: ^{1}H NMR spectrum of 1,6-diformamidohexane in DMSO-d_6.

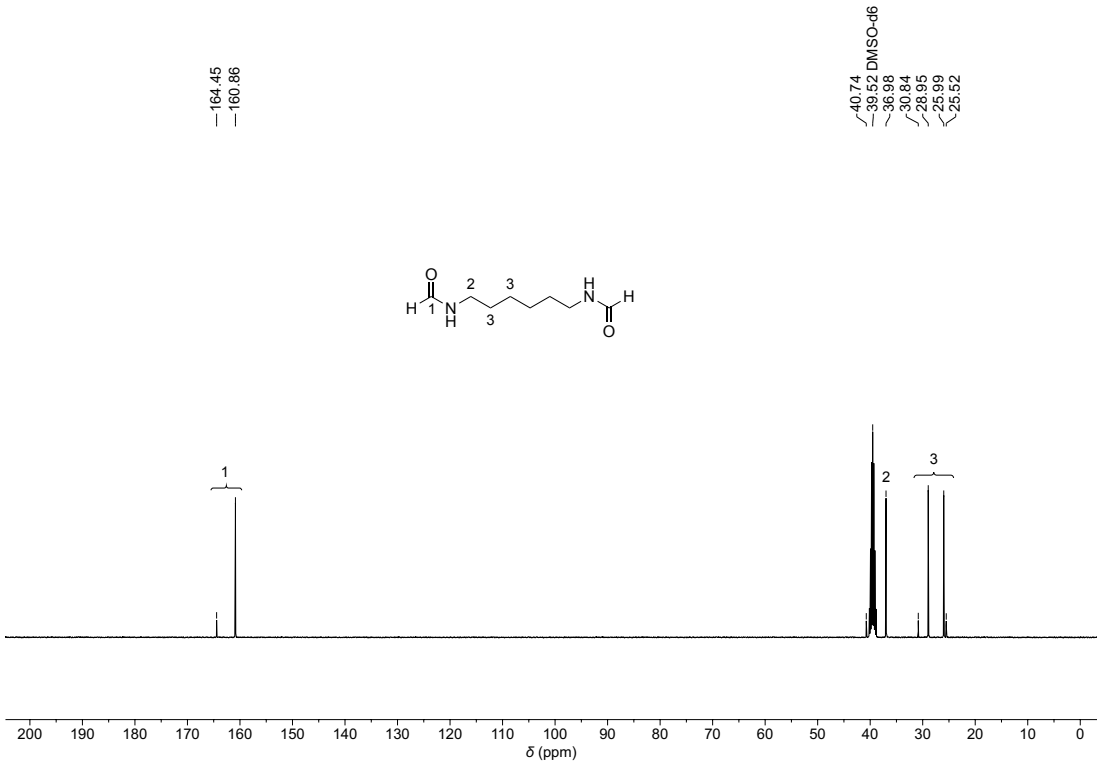

Figure 6.91: ^{13}C NMR spectrum of 1,6-diformamidohexane in DMSO-d_6.

Synthesis of 1,6-Diisocyanohexane:

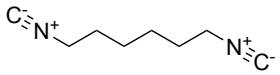

$C_8H_{12}N_2$
M = 136.20 g/mol

1,6-Diformamidohexane (30.0 mmol, 5.17 g, 1.00 eq.) was dissolved in dimethyl carbonate (60 ml) and pyridine (14.6 ml, 180 mmol, 6.00 eq.) was added. Subsequently, *p*-toluenesulfonyl chloride (17.2 g, 90.0 mmol, 3.00 eq.) was added under water bath cooling and the reaction mixture was stirred for 18 h at room temperature. Afterwards, aqueous saturated sodium carbonate solution (60 ml) was added, and thes biphasic mixture was stirred for another 30 minutes. Water (100 ml) and dimethyl carbonate (100 ml) were added, and the organic phase was separated. The aqueous phase was extracted with dimethyl carbonate (3 × 60 ml), the organic extracts were combined and washed with water (2 × 50 ml) and saturated sodium chloride solution (2 × 50 mL). The organic extract was dried over sodium sulfate, filtered and the solvent was removed under reduced pressure. The crude product was purified by flash column chromatography (cyclohexane/ethyl acetate, 2:1) to obtain the title compound (4.30 g, 25.0 mmol, 83%).

R_f (cyclohexane/ethyl acetate, 2:1) = 0.36.

^{1}H NMR (400 MHz, $CDCl_3$, ppm): δ = 3.49 (tt, J = 6.6, 1.9 Hz, 4H, H^1), 1.72−1.53 (m, 4H, H^2), 1.43−1.30 (m, 4H, H^3).

^{13}C NMR (101 MHz, $CDCl_3$, ppm): δ = 155.5 (t, J = 5.6 Hz, C^1), 41.0 (t, J = 5.5 Hz, C^2), 28.2 (CH_2, C^3), 24.9 (CH_2, C^4).s

IR (ATR, cm^{-1}): $\tilde{\nu}$ = 2944 (w), 2863 (vw), 2146 (vs), 1453 (w), 1351 (w), 958 (vw), 935 (vw), 820 (vw), 728 (vw).

ESI-MS ($[M+H]^+$, $C_8H_{13}N_2$) calcd.: 137.1073; found: 137.1073.

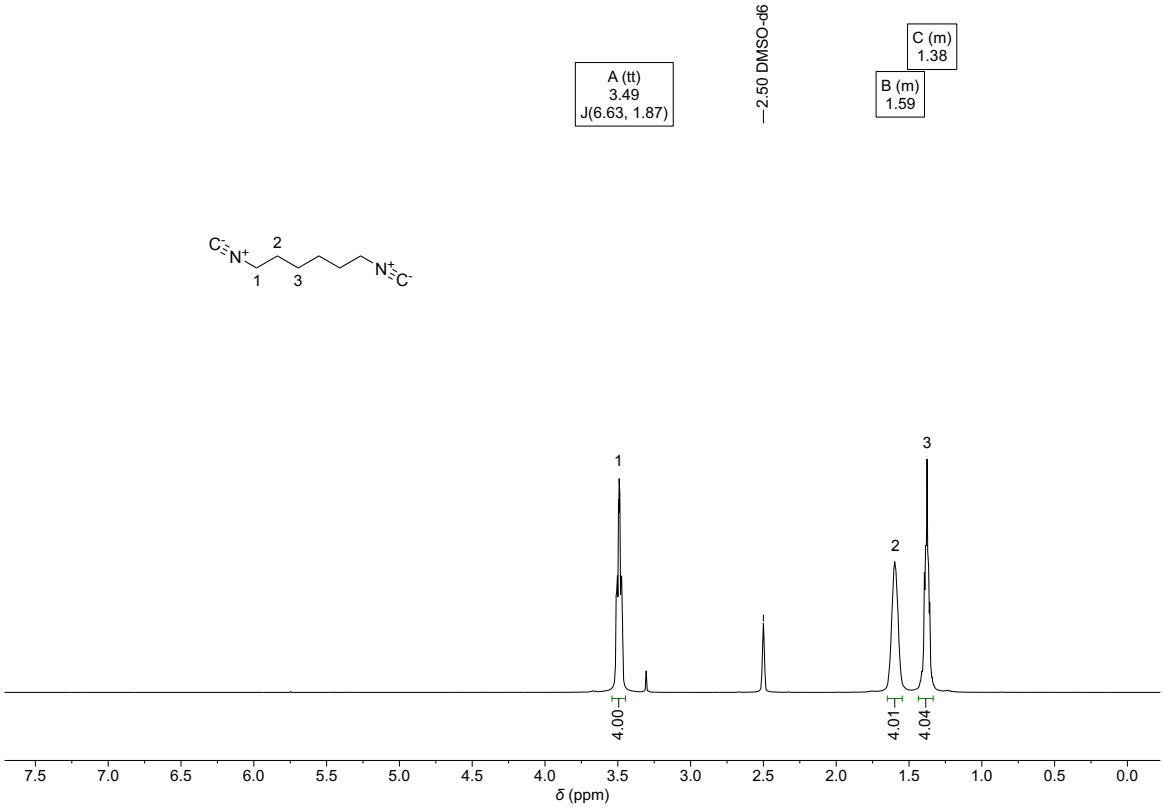

Figure 6.92: ^{1}H NMR spectrum of 1,6-diisocyanohexane in DMSO-d_6.

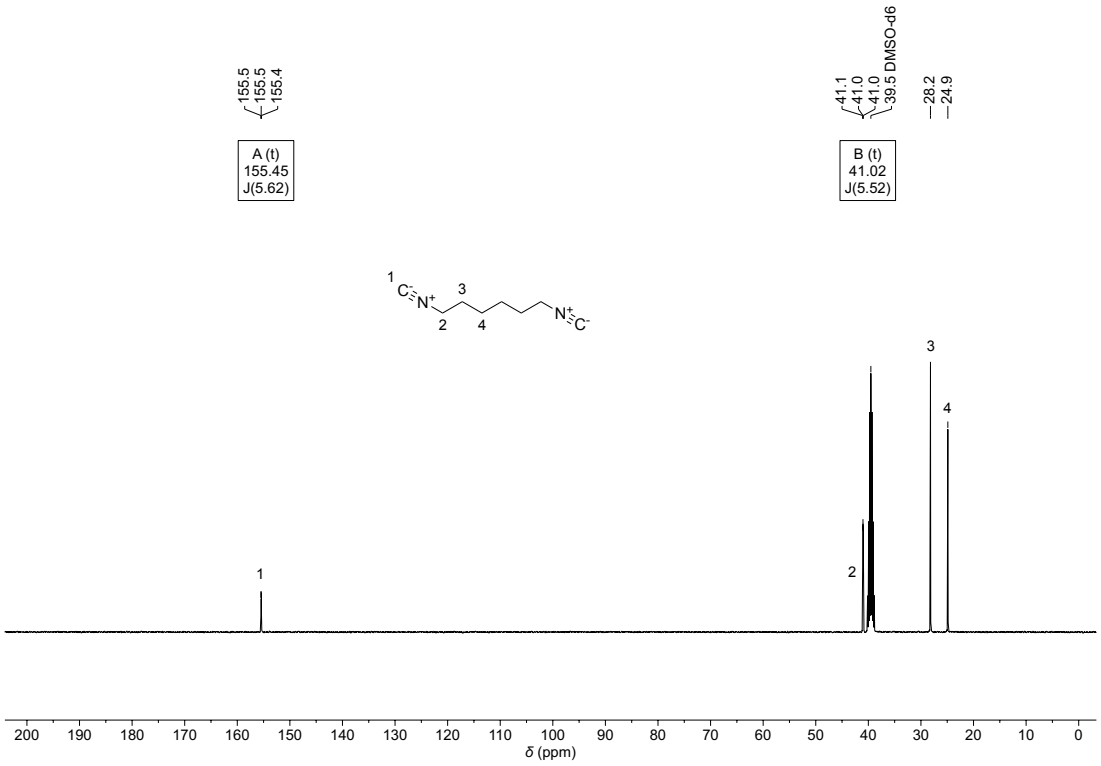

Figure 6.93: ^{13}C NMR spectrum of 1,6-diisocyanohexane in DMSO-d_6.

6.11.3 1,9-Diisocyanononane

Synthesis of 1,9-Diformamidononane:

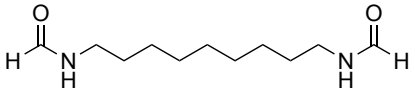

$C_{11}H_{22}N_2O_2$
M = 214.31 g/mol

1,9-Diaminononane (20.0 g, 124 mmol, 1.00 eq.) and ethyl formate (200 mL, 184 g, 2.48 mol, 20.0 eq.) were stirred at 54 °C for 16 h. Afterwards, the remaining ethyl formate and ethanol were removed under reduced pressure and the crude product (26.4 g, 123 mmol, 99%) was used without further purification.

^{1}H NMR (400 MHz, $CDCl_3$, ppm): δ = 8.06−7.59 (m, 4H, H^1), 3.05 (q, J = 6.6 Hz, 4H, H^2), 1.38 (p, J = 6.8 Hz, 4H, H^3), 1.24 (s, 10H, H^4).

^{13}C NMR (101 MHz, $CDCl_3$, ppm): δ = 164.4 (*C*HO, C^1), 160.8 (*C*HO, C^1), 40.8 (CH_2, C^2), 37.0 (CH_2, C^2), 30.9 (CH_2, C^3), 29.0 (CH_2, C^3), 28.9 (CH_2, C^3), 28.6 (CH_2, C^3), 28.6 (CH_2, C^3), 26.3 (CH_2, C^3), 25.8 (CH_2, C^3).

IR (ATR, cm^{-1}): $\tilde{\nu}$ = 3278 (m), 2928 (m), 2891 (w), 2874 (w), 2850 (w), 1628 (vs), 1520 (s), 1476 (w), 1463 (m), 1384 (s), 1313 (w), 1276 (w), 1245 (w), 1215 (s), 1198 (m), 1064 (w), 779 (m), 748 (w), 731 (w), 687 (s), 398 (w).

ESI-MS ($[M+H]^+$, $C_{11}H_{23}N_2O_2$) calcd.: 215.1754; found: 215.1754.

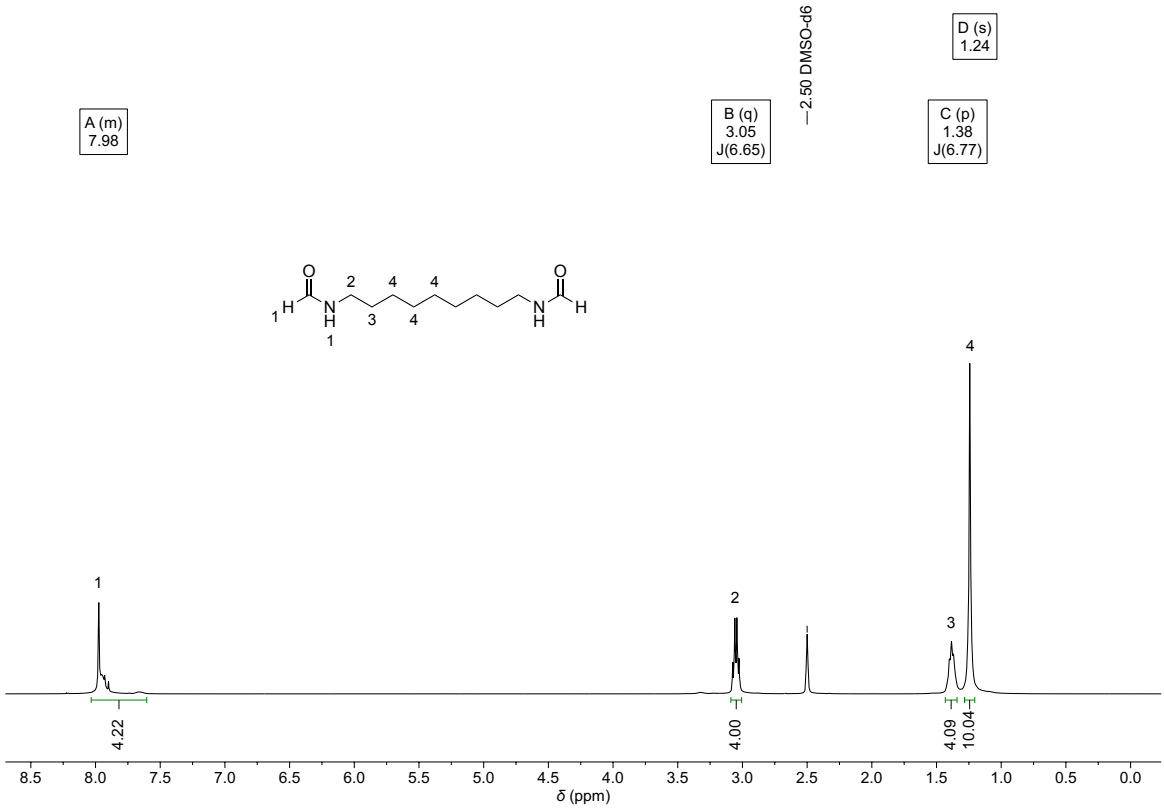

Figure 6.94: ^{1}H NMR spectrum of 1,9-diformamidononane in DMSO-d_6.

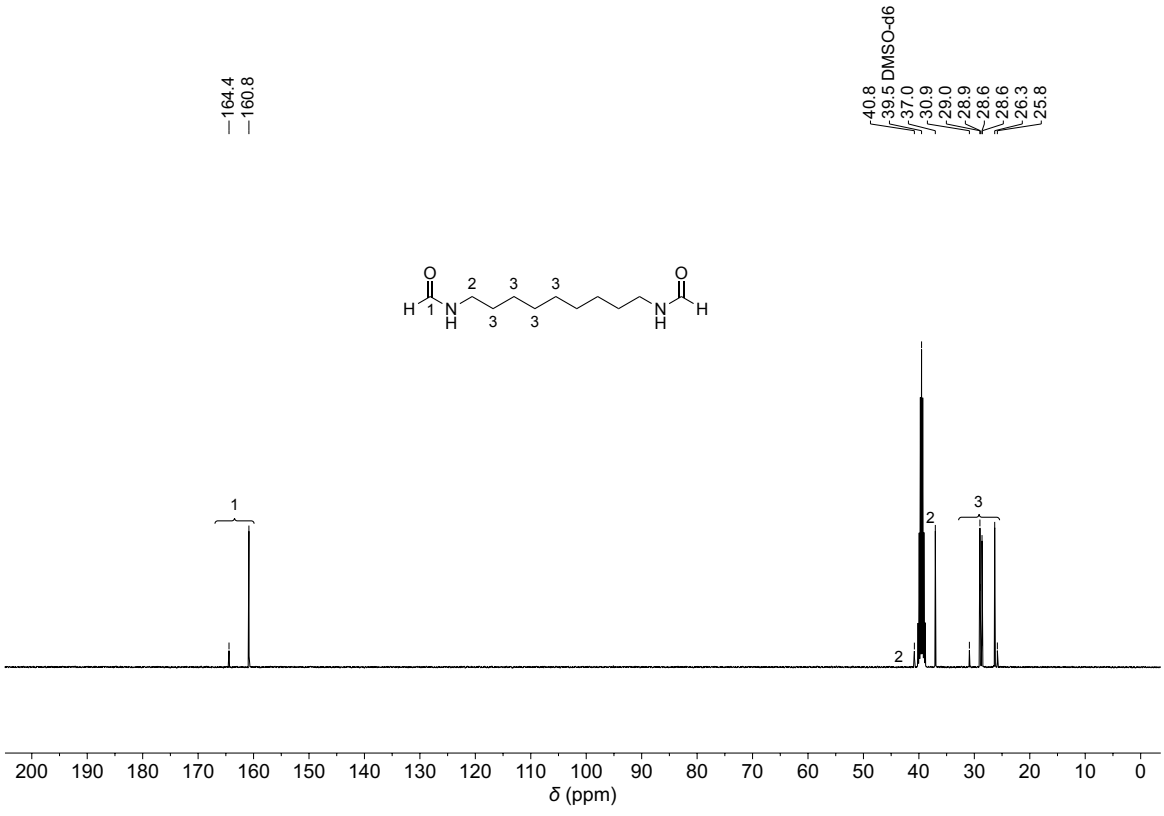

Figure 6.95: ^{13}C NMR spectrum of 1,9-diformamidononane in DMSO-d_6.

Synthesis of 1,9-Diisocyanononane:

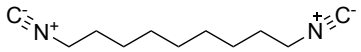

$C_{11}H_{18}N_2$
M = 178.28 g/mol

1,9-Diformamidononane (5.36 g, 25.0 mmol, 1.00 eq.) was dissolved in dimethyl carbonate (75 ml) and pyridine (12.1 ml, 150 mmol, 6.00 eq.) was added. Subsequently, *p*-toluenesulfonyl chloride (14.3 g, 75.0 mmol, 3.00 eq.) was added under cooling with a water bath. The cooling was removed, and the reaction mixture was stirred for 24 h at room temperature. Afterwards, aqueous sodium carbonate solution (30 ml, 20 wt%) was added and the biphasic mixture was stirred for another 60 minutes. Water (60 ml) and dimethyl carbonate (60 ml) were added, and the organic phase was separated. The aqueous phase was extracted with dimethyl carbonate (3 × 30 ml), the organic extracts were combined and washed with water (2 × 50 ml) and saturated sodium chloride solution (50 ml). The organic extract was dried over sodium sulfate, filtered and the solvent was removed under reduced pressure. The crude product was purified by flash column chromatography (cyclohexane/ethyl acetate, 10:1 until 5:1) to obtain the title compound (4.20 g, 23.6 mmol, 94%) as a colorless liquid.

R_f (cyclohexane/ethyl acetate, 4:1) = 0.34.

^{1}H NMR (400 MHz, $CDCl_3$, ppm): δ = 3.37 (tt, J = 6.7, 2.0 Hz, 4H, H^1), 1.73−1.58 (m, 4H, H^2), 1.48−1.38 (m, 4H, H^3), 1.36−1.27 (m, 6H, H^4).

^{13}C NMR (101 MHz, $CDCl_3$, ppm): δ = 155.7 (t, J = 5.8 Hz, C^1), 41.62 (t, J = 6.6 Hz, C^2), 29.2 (CH_2, C^3), 29.1 (CH_2, C^3), 28.6 (CH_2, C^3), 26.3 (CH_2, C^3).

IR (ATR, cm^{-1}): $\tilde{\nu}$ = 2928 (m), 2857 (w), 2146 (vs), 1455 (w), 1351 (w), 939 (vw), 836 (vw), 722 (vw), 534 (vw).

ESI-MS ($[M+H]^+$, $C_{11}H_{19}N_2$) calcd.: 179.1543; found: 179.1543.

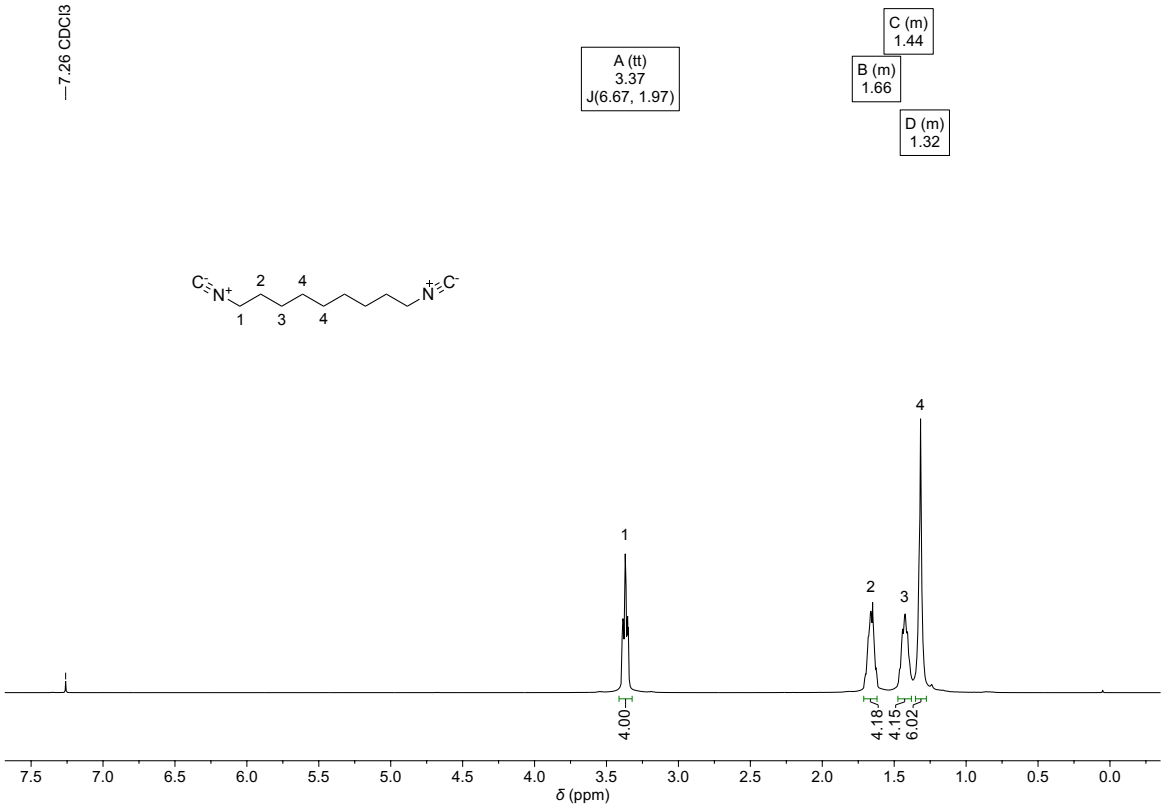

Figure 6.96: ^{1}H NMR Spectrum of 1,9-diisocyanononane in $CDCl_3$.

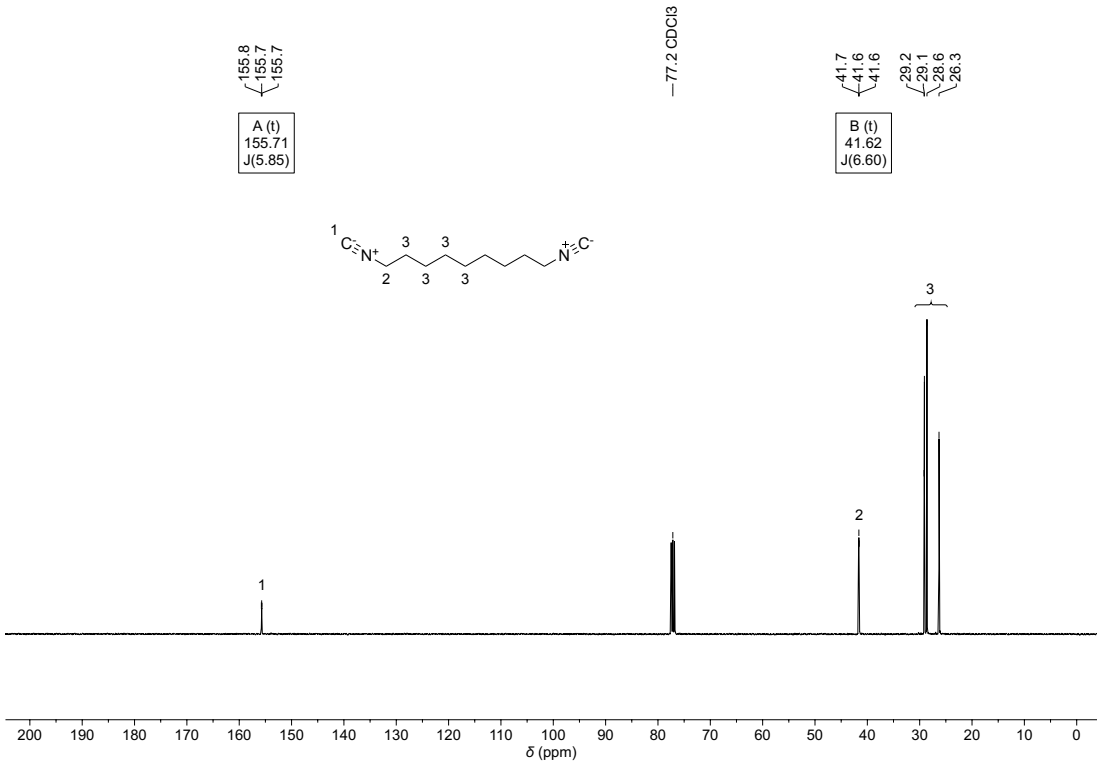

Figure 6.97: ^{13}C NMR Spectrum of 1,9-diisocyanononane in $CDCl_3$.

6.12 Synthesis of P-3CR-model compounds

6.12.1 Model Compound M1

Passerini reaction of triacid, acetaldehyde, and hexylisocyanide

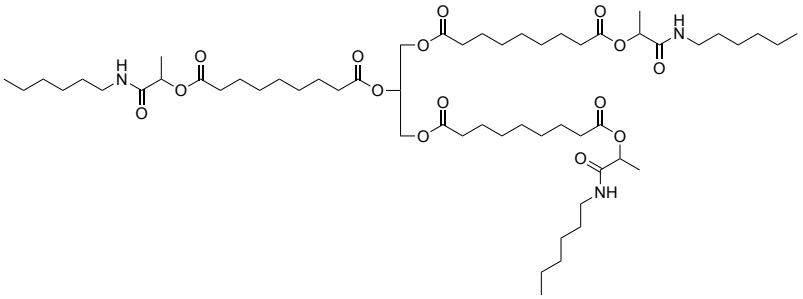

$C_{57}H_{101}N_3O_{15}$
M = 1068.44 g/mol

Sunflower oil-based triacid (200 mg, 990 µmol CO_2H, 1.00 equiv.), and *n*-hexylisocyanide (132 mg, 1.19 mmol, 1.20 equiv. based on CO_2H) were weighed into a glass vial. The vial was then cooled to −20°C and acetaldehyde (87.3 mg, 1.98 mmol, 2.00 equiv. based on CO_2H) was weighed into the vial and the vial was sealed. Then dichloromethane (1 ml) was added, and the reaction was stirred at room temperature for 2 days. The solvent was removed under reduced pressure and the crude product was purified *via* flash column chromatography (cyclohexane/ethyl acetate, 2:1, then 1:1) to obtain the title compound as colorless oi (229 mg, 214 µmol, 64%).

R_f (cyclohexane/ethyl acetate, 1:1) = 0.2.

$T_{d,5\%}$: 342 °C.

DSC (−70 °C to 250 °C, 10 K min^{-1}): T_g: −37 °C.

^{1}H NMR (400 MHz, $CDCl_3$, ppm): δ = 6.12 (t, J = 6.0 Hz, 3H, H^1), 5.23 (p, J = 5.3 Hz, 1H, H^2), 5.17 (q, J = 6.8 Hz, 3H, H^3), 4.27 (dd, J = 11.9, 4.4 Hz, 2H, H^4), 4.12 (dd, J = 11.9, 5.9 Hz, 2H, H^4), 3.24 (q, J = 6.7 Hz, 6H, H^5), 2.35 (t, J = 7.5 Hz, 6H, H^6), 2.29 (td, J = 7.6, 2.2 Hz, 6H, H^6), 1.67−1.54 (m, 12H, H^7), 1.52−1.46 (m, 6H, H^8), 1.43 (d, J = 6.8 Hz, 9H, H^9), 1.36−1.21 (m, 36H, H^{10}), 0.86 (d, J = 6.4 Hz, 9H, H^{11}).

^{13}C NMR (101 MHz, $CDCl_3$, ppm): δ = 173.2 (C_q, C_{Ester}, C^1), 172.8 (C_q, C_{Ester}, C^1), 172.3 (C_q, C_{Ester}, C^1), 170.4 (C_q, C_{Amide}, C^2), 70.6 (CH, C^3), 69.0 (CH, $C_{Glyceryl}$,C^4), 62.2(CH_2, $C_{Glyceryl}$, C^5), 39.3 (CH_2, C^6), 34.3 (CH_2, C^7), 34.2 (CH_2, C^7), 34.0 (CH_2, C^7), 31.5 (CH_2, C^8), 29.6 (CH_2, C^8), 29.0 (CH_2, C^8), 28.9 (CH_2, C^8), 28.9 (CH_2, C^8), 26.6 (CH_2, C^8), 24.9 (CH_2, C^8), 24.8 (CH_2, C^8), 24.8 (CH_2, C^8), 22.6 (CH_2, C^8), 18.1 (CH_3, C^9), 14.1 (CH_3, C^{10}).

IR (ATR, cm^{-1}): $\tilde{\nu}$ = 3308 (vw), 2929 (s), 2857 (w), 1738 (vs), 1657 (vs), 1537 (m), 1456 (w), 1418 (w), 1371 (w), 1300 (w), 1238 (m), 1160 (vs), 1132 (vs), 1094 (vs), 1040 (w), 725 (w), 645 (vw).

ESI-MS ($[M+H]^+$, $C_{57}H_{102}N_3O_{15}$): calcd.: 1068.7305, found: 1068.7312.

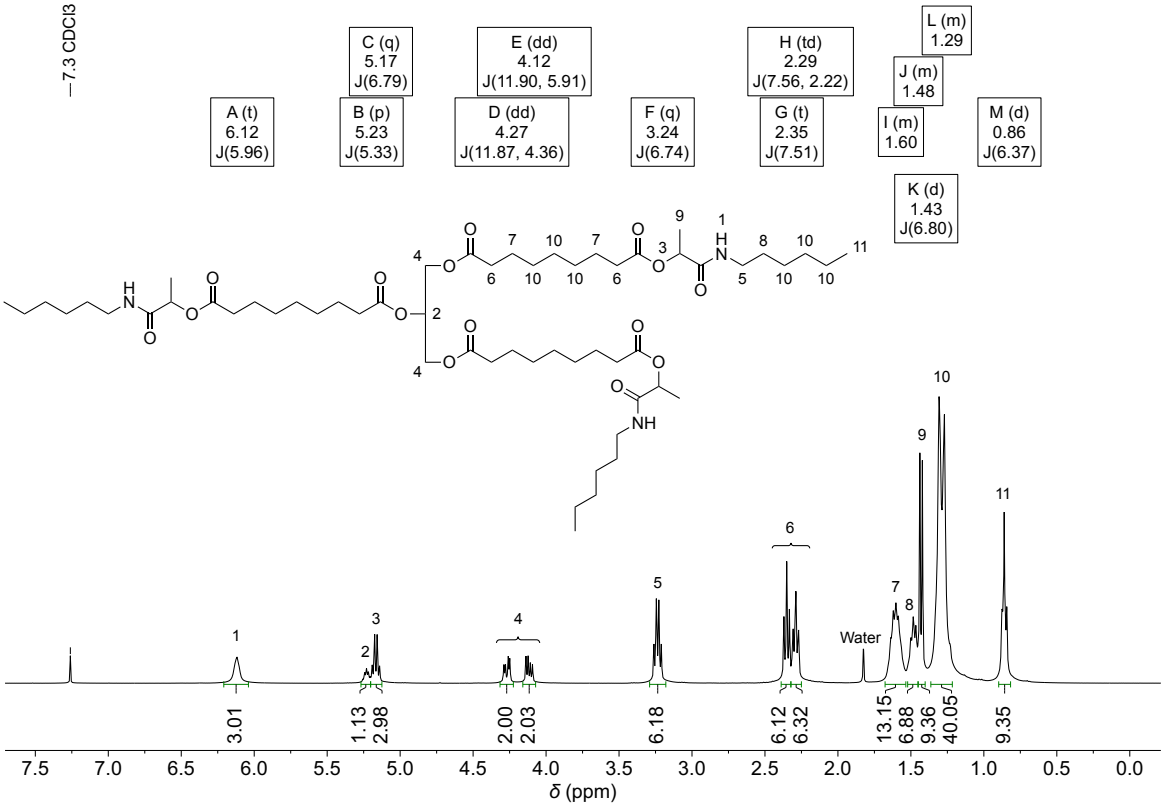

Figure 6.98: ^{1}H NMR spectrum of compound **M1** in $CDCl_3$.

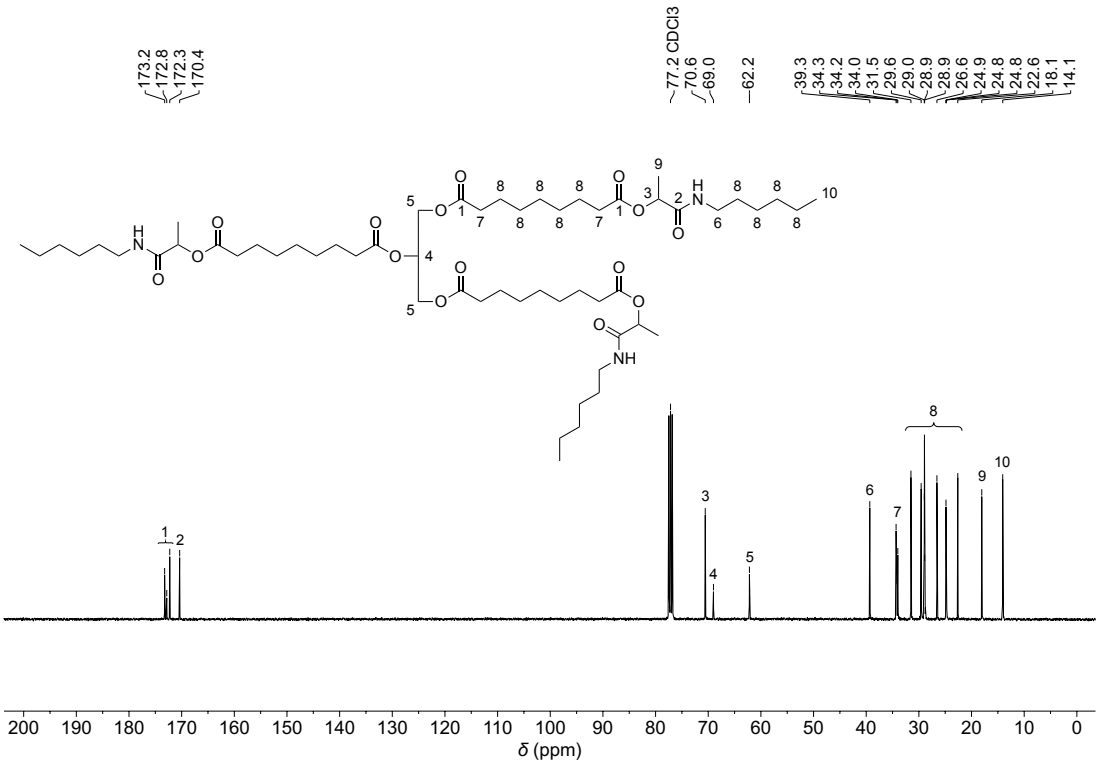

Figure 6.99: ^{13}C NMR spectrum of compound **M1** in $CDCl_3$.

6.12.2 Model Compound M2

Passerini reaction of triacid, butanal, and hexylisocyanide

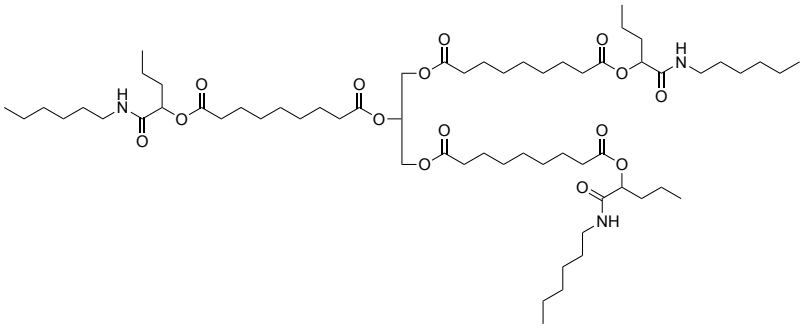

$C_{63}H_{113}N_3O_{15}$
M = 1152.60 g/mol

Sunflower oil-based triacid (200 mg, 990 µmol CO2H, 1.00 equiv.), and n-hexylisocyanide (165 mg, 1.49 mmol, 1.50 equiv. based on CO2H) were weighed into a glass vial. The vial was then cooled to 0 °C and butanal (107 mg, 1.49 mmol, 1.50 equiv. based on CO2H) was weighed into the vial and the vial was sealed. Then dichloromethane (1 ml) was added, and the reaction was stirred at room temperature for 3 days. Then, the solvent was removed under reduced pressure and the crude product was purified via flash column chromatography (cyclohexane/ethyl acetate, 2:1, then 1:1) to obtain the title compound as colorless oil (230 mg, 200 µmol, 60%).

Rf (cyclohexane/ethyl acetate, 2:1) = 0.2.

***T*$_{d,5\%}$:** 337 °C.

DSC (−70 °C to 250 °C, 10 K min^{-1}): T_g: −37 °C.

^{1}H NMR (400 MHz, $CDCl_3$, ppm): δ = 6.21−6.08 (m, 3H, H^1), 5.22−5.12 (m, 1H, H^2), 5.07 (dd, J = 7.1, 5.1 Hz, 3H, H^3), 4.22 (dd, J = 11.8, 4.3 Hz, 2H, H^4), 4.06 (dd, J = 11.9, 5.9 Hz, 2H, H^4), 3.24−3.07 (m, 6H, H^5), 2.31 (t, J = 7.5 Hz, 6H, H^6), 2.23 (td, J = 7.5, 2.1 Hz, 6H, H^6), 1.81−1.64 (m, 6H, H^7), 1.61−1.48 (m, 12H, H^8), 1.41 (p, J = 7.1 Hz, 6H, H^9), 1.34−1.14 (m, 42H, H^{10}), 0.88−0.75 (m, 18H, H^{11}).

^{13}C NMR (101 MHz, $CDCl_3$, ppm): δ = 173.0 (C_q, C_{Ester}, C^1), 172.6 (C_q, C_{Ester}, C^1), 172.3 (C_q, C_{Ester}, C^1), 169.8 (C_q, C_{Amide}, C^2), 73.7 (CH, C^3), 68.9 (CH, $C_{Glyceryl}$, C^4), 62.0 (CH_2, $C_{Glyceryl}$, C^5), 39.1 (CH_2, C^6), 34.1 (CH_2, C^7), 34.0 (CH_2, C^7), 33.9 (CH_2, C^7), 33.8 (CH_2, C^7), 31.4 (CH_2, C^7), 29.4 (CH_2, C^7), 28.8 (CH_2, C^7), 28.8 (CH_2, C^7), 28.7 (CH_2, C^7), 26.4 (CH_2, C^7), 24.8 (CH_2, C^7), 24.7 (CH_2, C^7), 24.6 (CH_2, C^7), 22.5 (CH_2, C^7), 18.1 (CH_2, C^7), 13.9 (CH_3, C^8), 13.7 (CH_3, C^8).

IR (ATR, cm^{-1}): $\tilde{\nu}$ = 3305 (w), 2956 (m), 2929 (s), 2857 (m), 1740 (vs), 1656 (vs), 1536 (m), 1460 (w), 1441 (w), 1418 (w), 1377 (w), 1299 (w), 1234 (m), 1160 (vs), 1132 (vs), 1109 (s), 1094 (s), 1026 (w), 977 (w), 727 (w), 656 (vw).

ESI-MS ($[M+H]^+$, $C_{63}H_{114}N_3O_{15}$) calcd.: 1152.8245; found: 1152.8242.

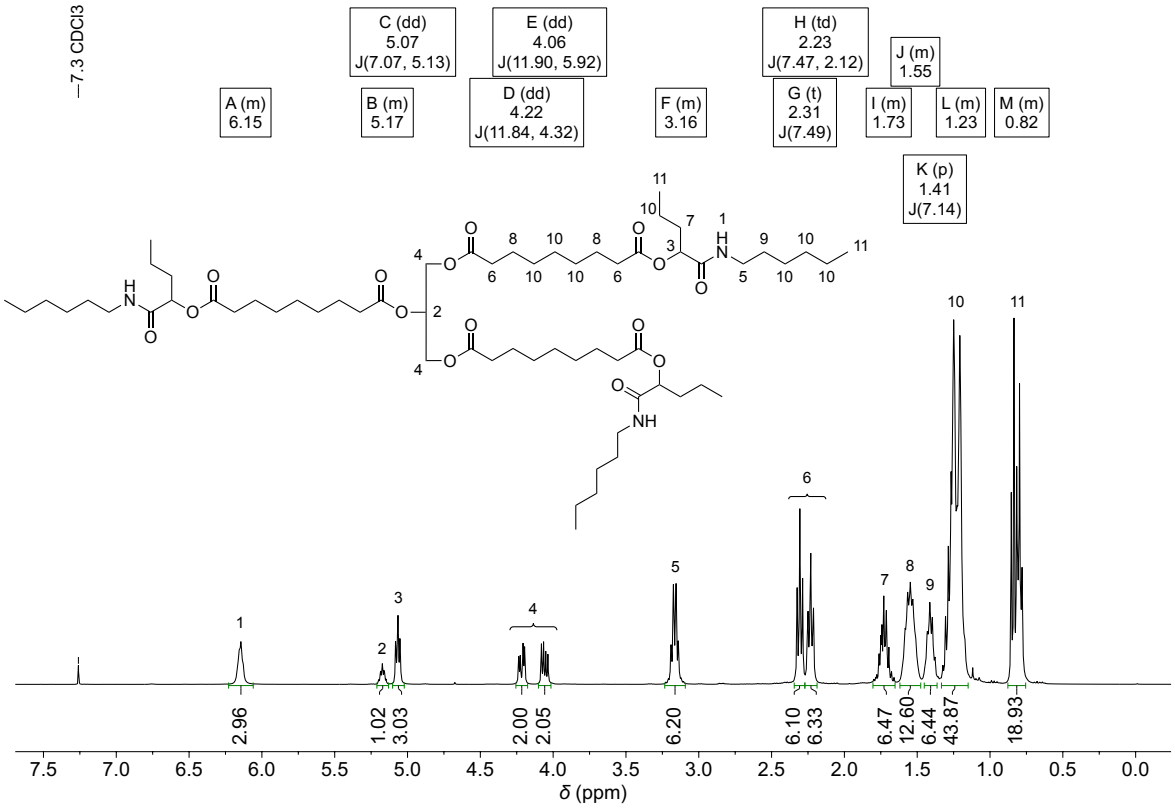

Figure 6.100: ^{1}H NMR spectrum of compound **M2** in $CDCl_3$.

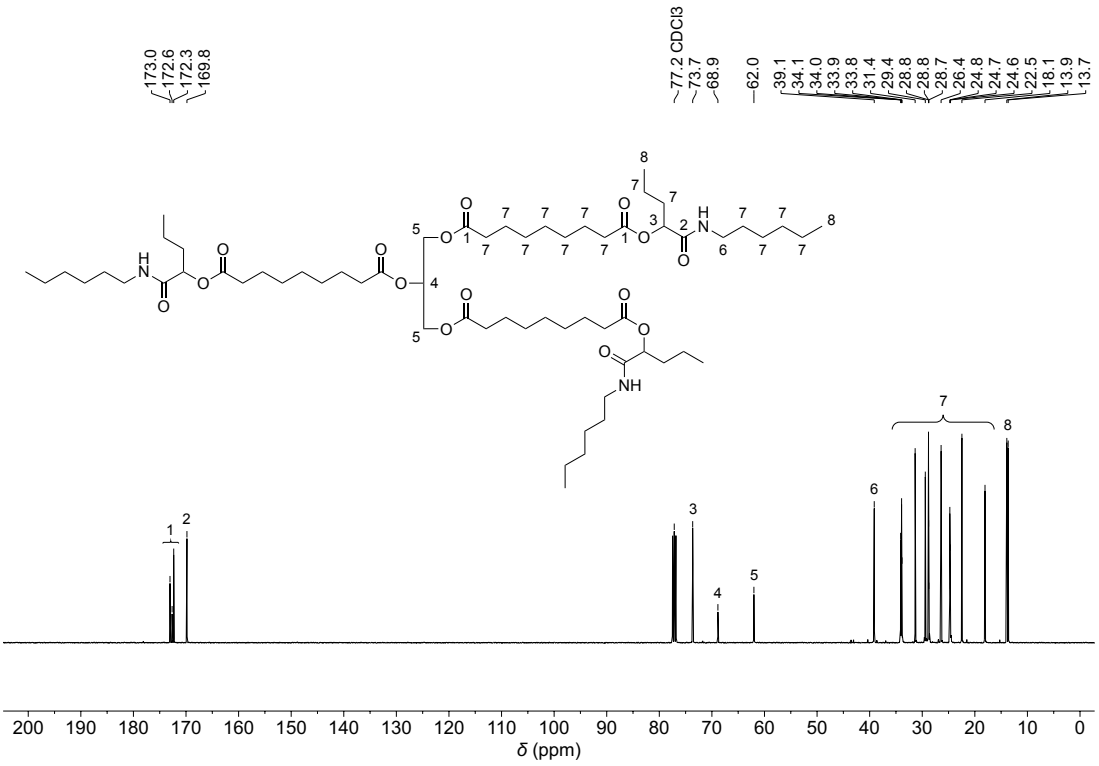

Figure 6.101: ^{13}C NMR spectrum of compound **M2** in $CDCl_3$.

6.12.3 Model Compound M3

Passerini reaction of triacid, hexanal, and hexylisocyanide

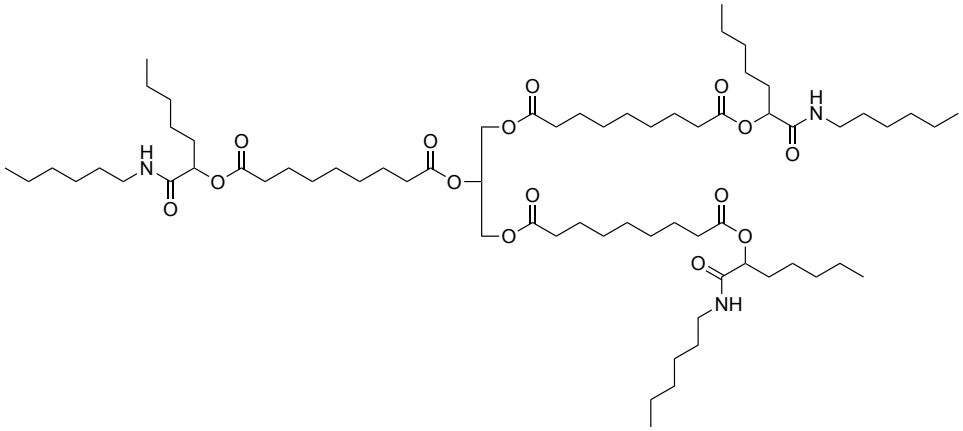

$C_{69}H_{125}N_3O_{15}$
M = 1236.77 g/mol

Sunflower oil-based triacid (200 mg, 990 µmol CO_2H, 1.00 equiv.), *n*-hexylisocyanide (165 mg, 1.49 mmol, 1.50 equiv. based on CO_2H), and hexanal (149 mg, 1.49 mmol, 1.50 equiv. based on CO_2H) were weighed into a glass vial. Then, dichloromethane (1 ml) was added, and the reaction was stirred at room temperature for 3 days. The solvent was removed under reduced pressure and the crude product was purified *via* flash column chromatography (cyclohexane/ethyl acetate, 2:1, then 1:1) to obtain the title compound as colorless oil (282 mg, 0.228 mmol, 69%).

R_f (cyclohexane/ethyl acetate, 2:1) = 0.36.

$T_{d,5\%}$**:** 344 °C.

DSC (−70 °C to 250 °C, 10 K min^{-1}): T_g: −43 °C.

^{1}H NMR (400 MHz, $CDCl_3$, ppm): δ = 6.09−5.93 (m, 3H, H^1), 5.24 (p, J = 5.1 Hz, 1H, H^2), 5.13 (t, J = 6.0 Hz, 3H, H^3), 4.27 (dd, J = 11.9, 4.4 Hz, 2H, H^4), 4.12 (dd, J = 11.9, 5.9 Hz, 4H, H^4), 3.32−3.15 (m, 6H, H^5), 2.37 (t, J = 7.5 Hz, 6H, H^6), 2.29 (td, J = 7.5, 2.2 Hz, 6H, H^6), 1.89−1.71 (m, 6H, H^7), 1.62 (dq, J = 15.4, 7.5 Hz, 12H, H^8), 1.48 (p, J = 7.0 Hz, 6H, H^9), 1.37−1.19 (m, 54H, H^{10}), 0.86 (td, J = 6.6, 3.8 Hz, 18H, H^{11}).

^{13}C NMR (101 MHz, $CDCl_3$, ppm): δ = 173.2 (C_q, C_{Ester}, C^1), 172.8 (C_q, C_{Ester}, C^1), 172.5 (C_q, C_{Ester}, C^1), 169.9 (C_q, C_{Amide}, C^2), 74.1 (CH, C^3), 69.0 (CH, $C_{Glyceryl}$, C^4), 62.2 (CH_2, $C_{Glyceryl}$, C^5), 39.3 (CH_2, C^6), 34.3 (CH_2, C^7), 34.2 (CH_2, C^7), 34.0 (CH_2, C^7), 32.0 (CH_2, C^8), 31.5 (CH_2, C^8), 31.5 (CH_2, C^8), 29.6 (CH_2, C^8), 29.0 (CH_2, C^8), 29.0 (CH_2, C^8), 28.9 (CH_2, C^8), 26.6 (CH_2, C^8), 24.9 (CH_2, C^8), 24.8 (CH_2, C^8), 24.8 (CH_2, C^8), 24.5 (CH_2, C^8), 22.6 (CH_2, C^8), 22.5 (CH_2, C^8), 14.1 (CH_3, C^9), 14.1 (CH_3, C^9).

IR (ATR, cm^{-1}): $\tilde{\nu}$ = 3306 (vw), 2953 (m), 2927 (s), 2857 (m), 1740 (vs), 1656 (vs), 1537 (m), 1459 (w), 1418 (w), 1377 (w), 1299 (w), 1235 (m), 1160 (vs), 1132 (vs), 1094 (s), 1062 (w), 1021 (w), 725 (w)

ESI-MS ($[M+H]^+$, $C_{69}H_{126}N_3O_{15}$) calcd.: 1236.9184; found: 1236.9183.

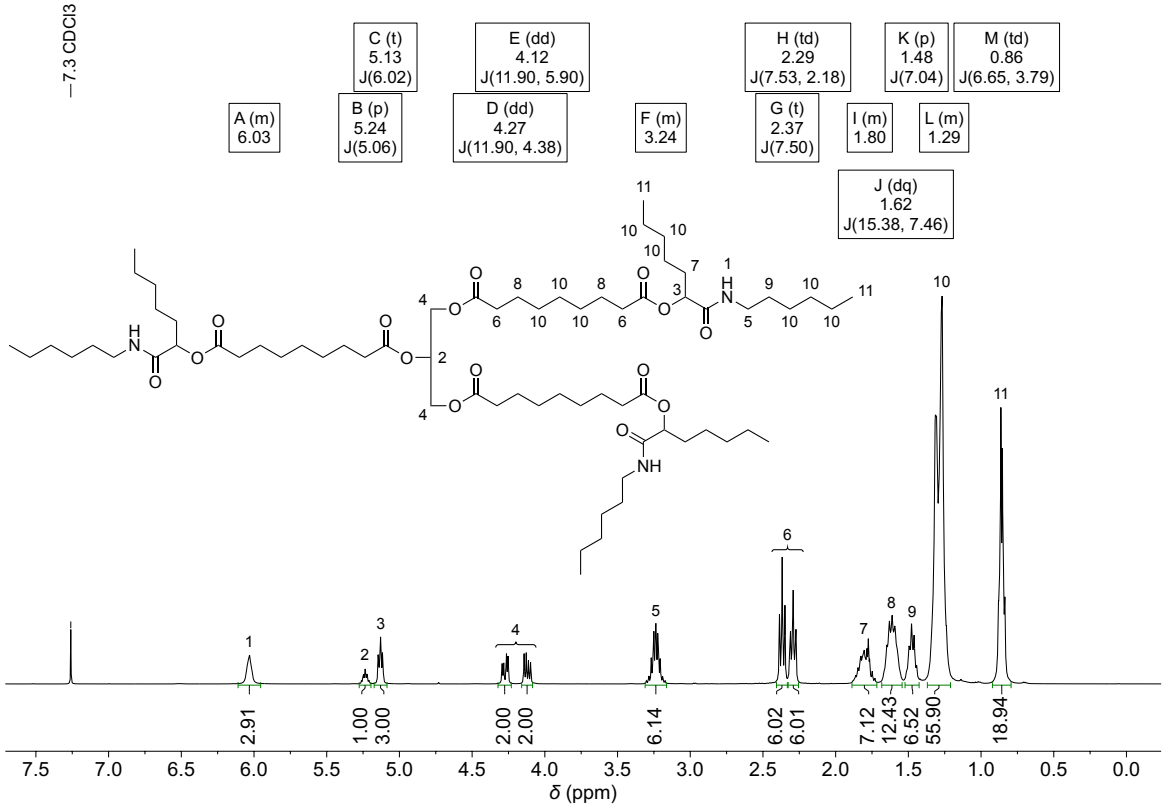

Figure 6.102: ^{1}H NMR spectrum of compound **M3** in $CDCl_3$.

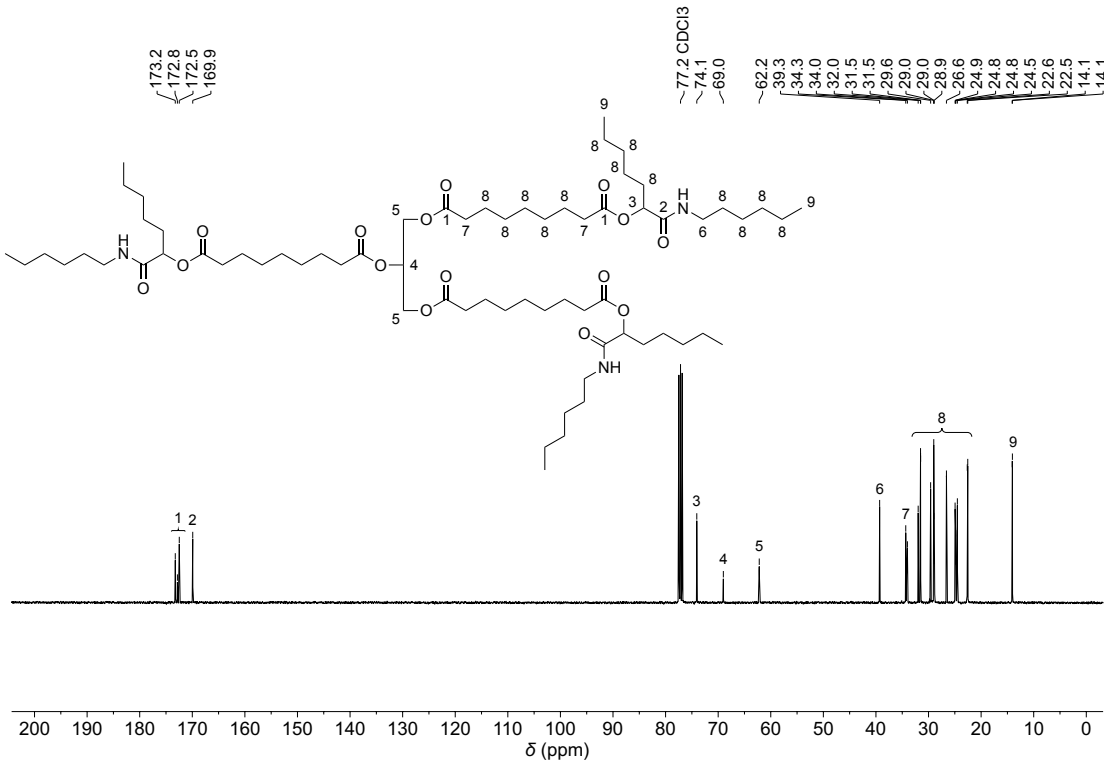

Figure 6.103: ^{13}C NMR spectrum of compound **M3** in $CDCl_3$.

6.12.4 Model Compound M4

Passerini reaction of triacid, nonanal, and hexylisocyanide

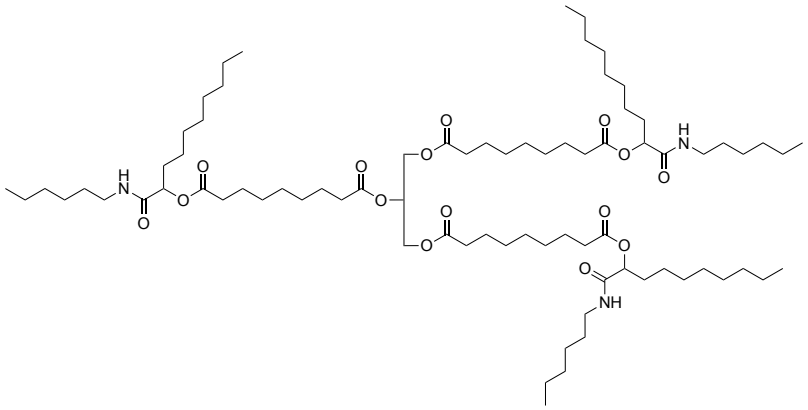

$C_{78}H_{143}N_3O_{15}$
M = 1363.01 g/mol

Sunflower oil-based triacid (300 mg, 1.49 mmol CO_2H, 1.00 equiv.) and hexylisocyanide (248 mg, 2.23 mmol, 1.50 equiv. based on CO_2H) were dissolved in dichloromethane (1.5 ml). Then, nonanal (95% purity, 404 µl, 334 mg, 2.23 mmol, 1.50 equiv. based on CO_2H) was added and the solution was stirred for 72 h at room temperature. Afterwards, the solvent was removed under reduced pressure. The crude product was purified by flash column chromatography (cyclohexane/ethyl acetate) to obtain the title compound (358 mg, 263 mmol, 53%).

R_f (cyclohexane/ethyl acetate, 2:1): 0.29.

$T_{d,5\%}$**:** 338 °C.

DSC (−70 °C to 250 °C, 10 K min^{-1}): T_g: −44 °C.

^{1}H NMR (400 MHz, $CDCl_3$, ppm): δ = 6.10−5.89 (m, 3H, N*H*, H^1), 5.23 (p, J = 5.0 Hz, CH, $H_{Glyceryl}$, 1H, H^2), 5.13 (t, J = 6.0 Hz, 3H, CH, H^3), 4.27 (dd, J = 11.9, 4.4 Hz, 2H, $H_{Glyceryl}$, H^4), 4.12 (dd, J = 11.9, 5.9 Hz, 2H, $H_{Glyceryl}$, H^4), 3.34−3.13 (m, 6H, CH_2, H^5), 2.36 (t, J = 7.5 Hz, 6H, CH_2, α-H_{Ester}, H^6), 2.29 (t, J = 7.4 Hz, 6H, CH_2, α-H_{Ester}, H^6), 1.89−1.72 (m, 6H, CH_2, H^7), 1.69−1.54 (m, 12H, CH_2, β-H_{Ester}, H^8), 1.48 (p, J = 7.0 Hz, 6H, CH_2, H^9), 1.34−1.00 (m, 72H, CH_2, H^{10}), 0.95–0.78 (m, 18H, CH_3, H^{11}).

^{13}C NMR (101 MHz, $CDCl_3$, ppm): δ = 173.2 (2C, C_q, C_{Ester}, C^1), 172.8 (C_q, C_{Ester}, C^1), 172.5 (3C, C_q, C_{Ester}, C^1), 169.9 (3C, C_q, C_{Amide}, C^2), 74.1 (3C, CH, C^3), 69.0 (CH, $C_{Glyceryl}$, C^4), 62.2 (2C, CH_2, $C_{Glyceryl}$, C^5), 39.3 (3C, CH_2, C^6), 34.3 (3C, CH_2, α-C_{Ester}, C^7), 34.2 (CH_2, α-C_{Ester}, C^7), 34.0 (2C, CH_2, α-C_{Ester}, C^7), 32.0 (CH_2), 31.9 (CH_2), 31.5 (CH_2), 29.6 (CH_2), 29.5 (CH_2), 29.4 (CH_2), 29.3 (CH_2), 29.0 (CH_2), 29.0 (CH_2), 28.9 (CH_2), 26.6 (CH_2), 24.9 (CH_2), 24.8 (CH_2), 24.8 (CH_2), 22.7 (CH_2), 22.6 (CH_2), 14.2 (3C, CH_3, C^8), 14.1 (3C, CH_3, C^8).

IR (ATR, cm^{-1}): $\tilde{\nu}$ = 3303 (w), 2952 (m), 2924 (vs), 2854 (s), 1741 (vs), 1656 (vs), 1537 (m), 1460 (m), 1418 (w), 1377 (w), 1299 (w), 1237 (m), 1159 (vs), 1132 (s), 1094 (s), 724 (w).

ESI-MS ($[M+H]^+$, $C_{78}H_{144}N_3O_{15}$): calcd.: 1363.0592, found: 1363.0494.

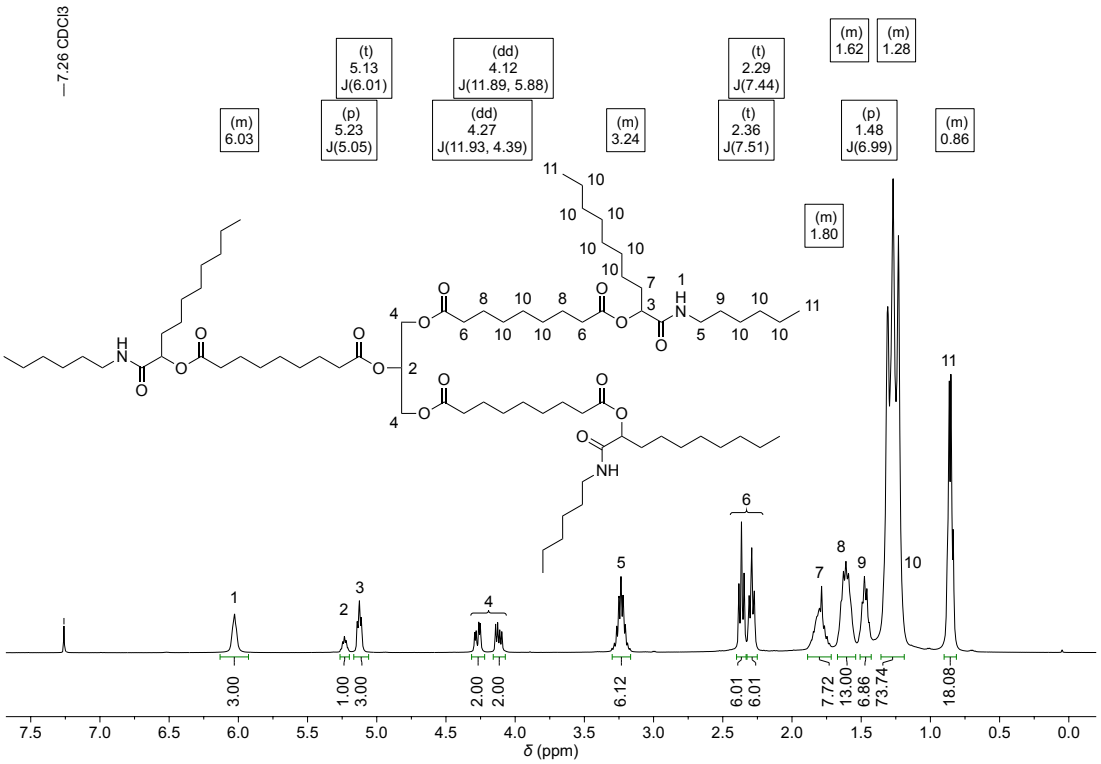

Figure 6.104: ^{1}H NMR spectrum of compound **M4** in $CDCl_3$.

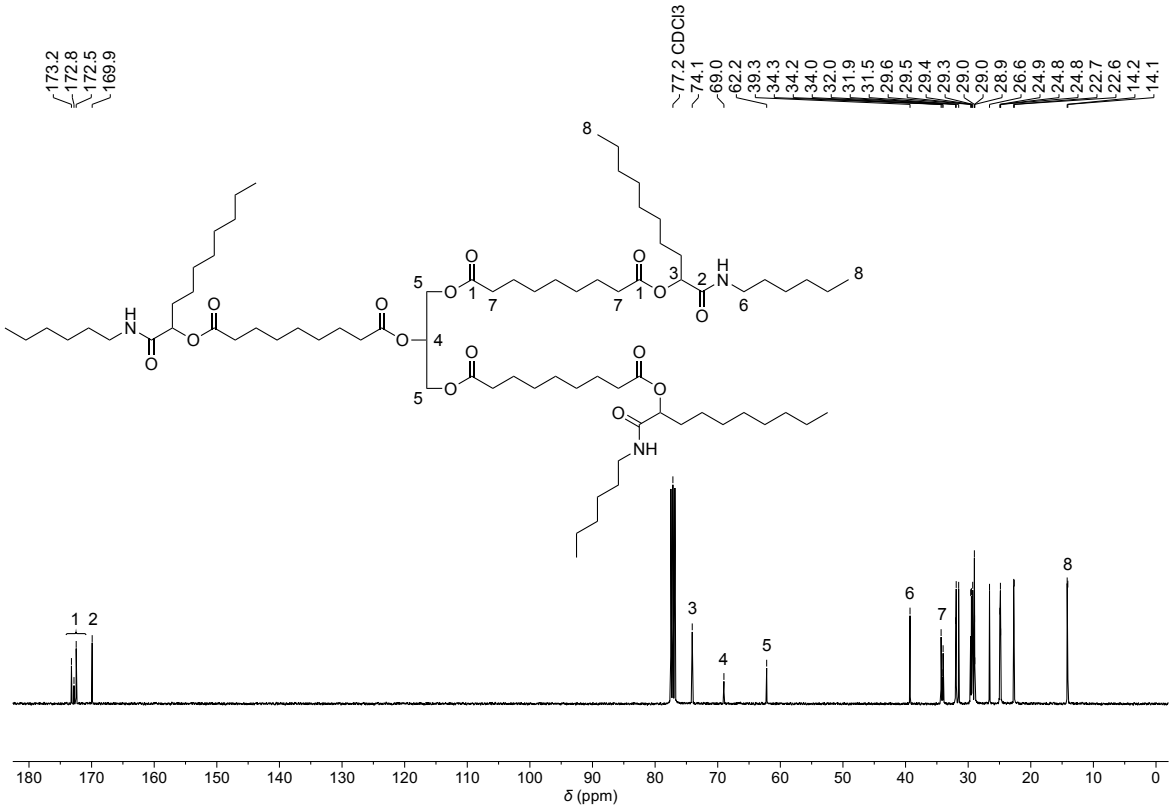

Figure 6.105: ^{13}C NMR spectrum of compound **M4** in $CDCl_3$.

6.12.5 Model Compound M5

Passerini reaction of triacid, 2-ethylbutyraldehyde, and hexylisocyanide

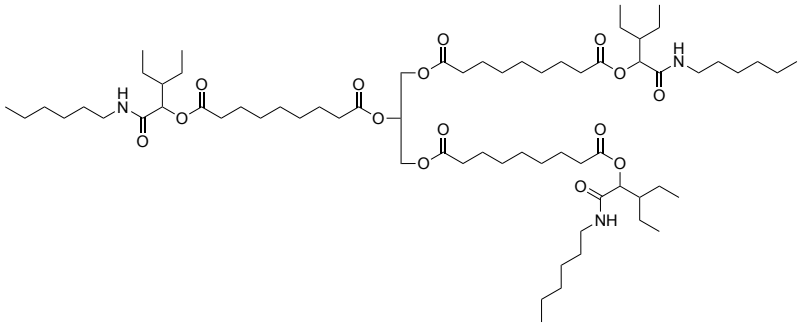

$C_{69}H_{125}N_3O_{15}$
M = 1236.77 g/mol

Sunflower oil-based triacid (200 mg, 990 µmol CO_2H, 1.00 equiv.), *n*-hexylisocyanide (165 mg, 1.49 mmol, 1.50 equiv. based on CO_2H), and 2-ethylbutyraldehyde (149 mg, 1.49 mmol, 1.50 equiv. based on CO_2H) were weighed into a glass vial. Then, dichloromethane (1.0 ml) was added, and the reaction was stirred at room temperature for 3 days. The solvent was removed under reduced pressure and the crude product was purified *via* flash column chromatography (cyclohexane/ethyl acetate, 2:1, then 1:1) to obtain the title compound as colorless oil (220 mg, 178 µmol, 54%).

R_f (cyclohexane/ethyl acetate, 2:1) = 0.36.

$T_{d,5\%}$**:** 313 °C.

DSC (−70 °C to 250 °C, 10 K min^{-1}): T_g: −27 °C.

^{1}H NMR (400 MHz, CD_2Cl_2, ppm): δ = 6.03 (d, J = 6.6 Hz, 3H, H^1), 5.23 (ddd, J = 6.0, 5.1, 3.0 Hz, 1H, H^2), 5.19 (d, J = 3.9 Hz, 3H, H^3), 4.26 (dd, J = 11.9, 4.5 Hz, 2H, H^4), 4.13 (dd, J = 11.9, 5.9 Hz, 2H, H^4), 3.31−3.07 (m, 6H, H^5), 2.44−2.34 (m, 6H, H^6), 2.30 (t, J = 7.5 Hz, 6H, H^6), 1.85−1.73 (m, 3H, H^7), 1.69−1.54 (m, 12H, H^8), 1.52−1.15 (m, 54H, H^9), 0.97−0.68 (m, 27H, H^{10}).

^{13}C NMR (101 MHz, CD_2Cl_2, ppm): δ = 173.6 (C_q, C_{Ester}, C^1), 173.2 (C_q, C_{Ester}, C^1), 172.9 (C_q, C_{Ester}, C^1), 170.0 (C_q, C_{Amide}, C^2), 75.5 (CH, C^3), 69.4 (CH, $C_{Glyceryl}$, C^4), 62.6 (CH_2, $C_{Glyceryl}$, C^5), 44.2 (CH, C^6), 39.6 (CH_2, C^7), 34.8 (CH_2, C^8), 34.6 (CH_2, C^8), 34.4 (CH_2, C^8), 32.0 (CH_2, C^8), 30.1 (CH_2, C^8), 29.5 (CH_2, C^8), 29.5 (CH_2, C^8), 29.4 (CH_2, C^8), 29.4 (CH_2, C^8), 27.1 (CH_2, C^8), 25.5 (CH_2, C^8), 25.3 (CH_2, C^8), 25.3 (CH_2, C^8), 23.1 (CH_2, C^8), 22.8 (CH_2, C^8), 22.4 (CH_2, C^8), 14.3 (CH_3, C^9), 12.0 (CH_3, C^9), 11.9 (CH_3, C^9).

IR (ATR, cm^{-1}): $\tilde{\nu}$ = 3323 (vw), 2958 (w), 2929 (s), 2859 (w), 1740 (vs), 1653 (s), 1531 (m), 1460 (w), 1417 (w), 1377 (w), 1237 (m), 1157 (vs), 1126 (vs), 1095 (m), 1047 (w), 1007 (w), 727 (w), 652 (vw).

ESI-MS ($[M+H]^+$, $C_{69}H_{126}N_3O_{15}$) calcd.: 1236.9184; found: 1236.9180.

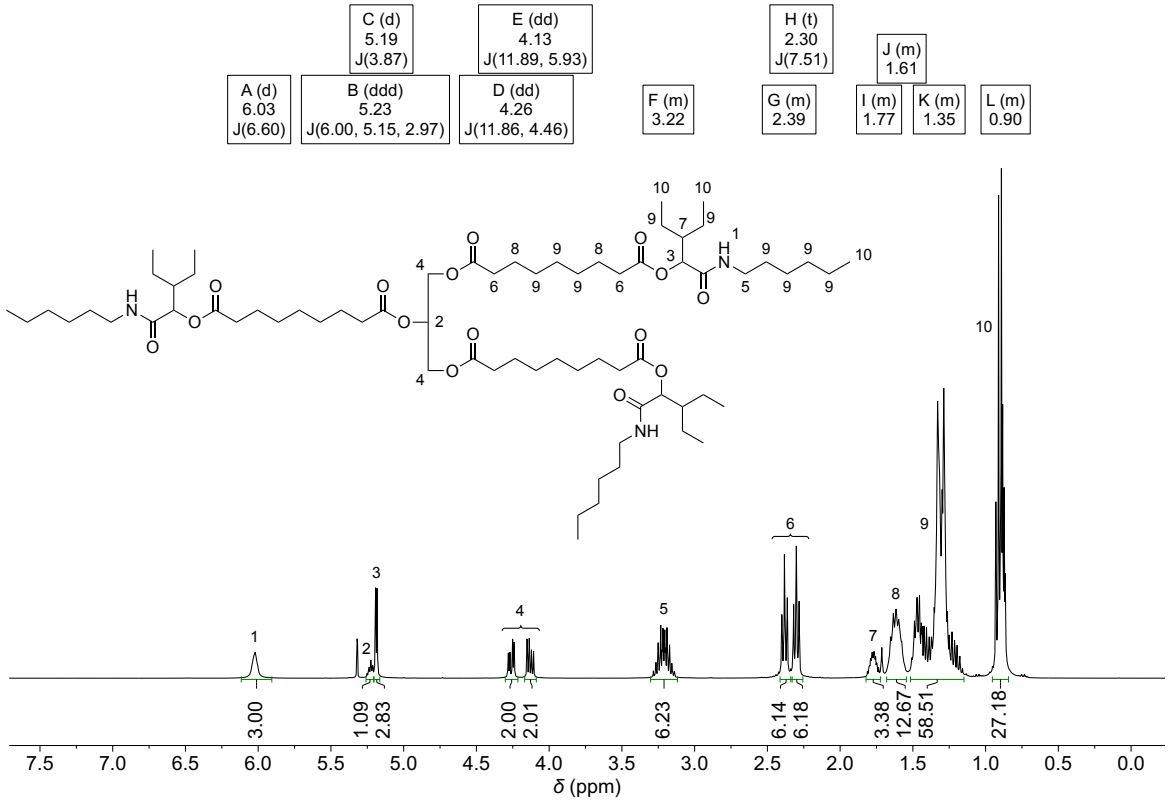

Figure 6.106: ^{1}H NMR spectrum of compound **M5** in CD_2C_2.

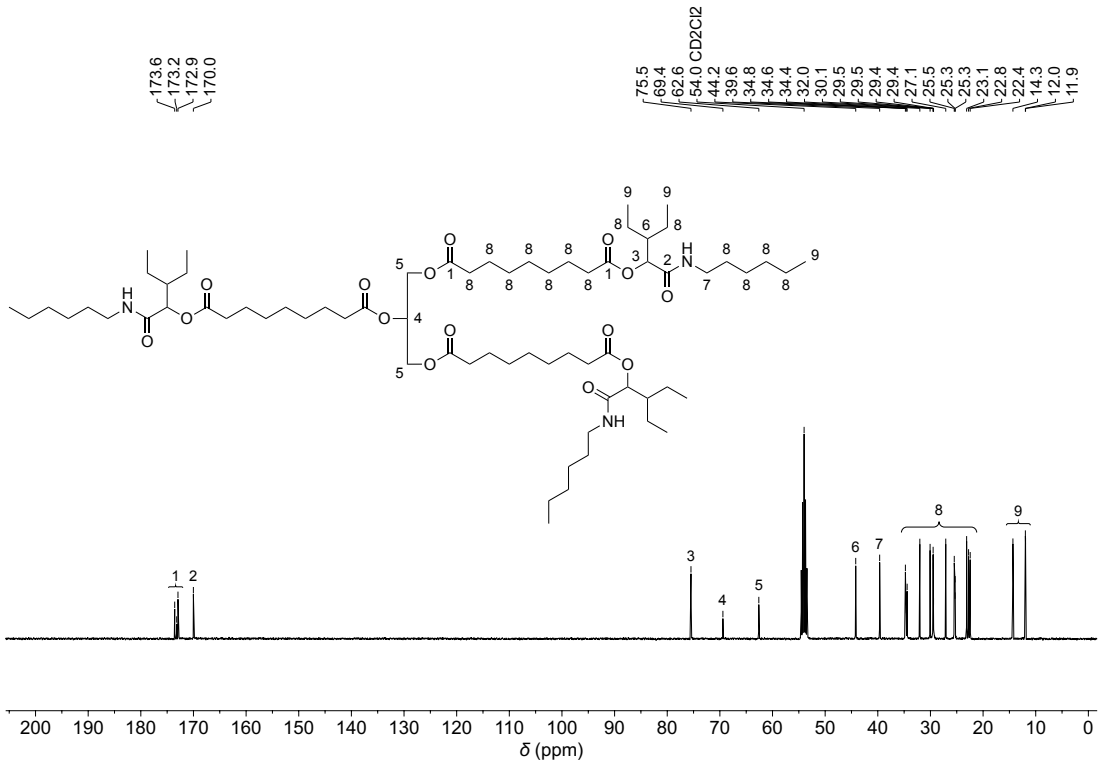

Figure 6.107: ^{13}C NMR spectrum of compound **M5** in CD_2Cl_2.

TGA of compounds M1 to M5:

The conducted TGA measurements and the determined $T_{d,5\%}$ values of compounds **M1**–**M5** are depicted in Figure 6.108 and Table 6.12, respectively.

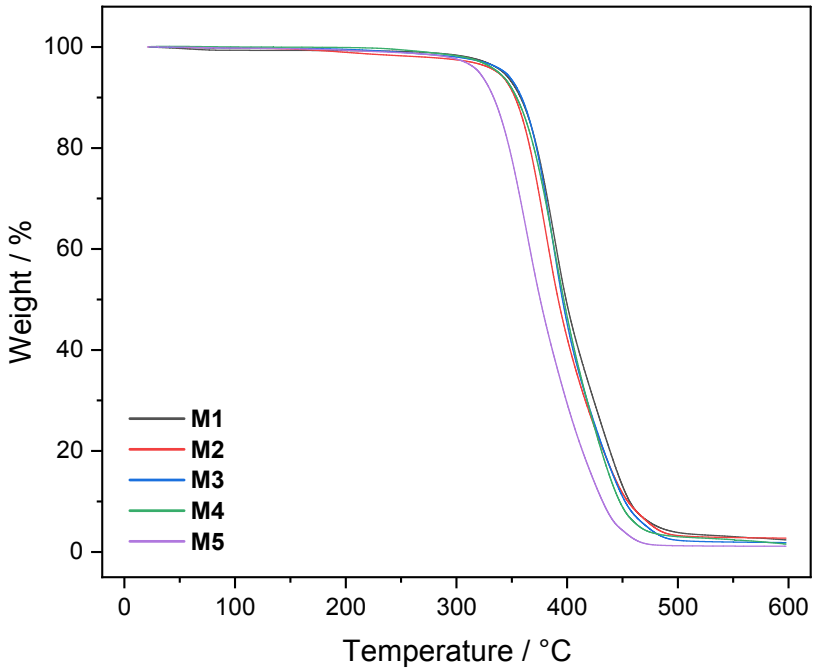

Figure 6.108: TGA Measurements of compounds **M1** to **M5**.

Table 6.12: Determined degradation temperatures $T_{d,5\%}$ of all polymers.

Polymer	$T_{d,5\%}$ / °C
1	342
2	337
3	344
4	338
5	313

DSC of compounds M1 to M5:

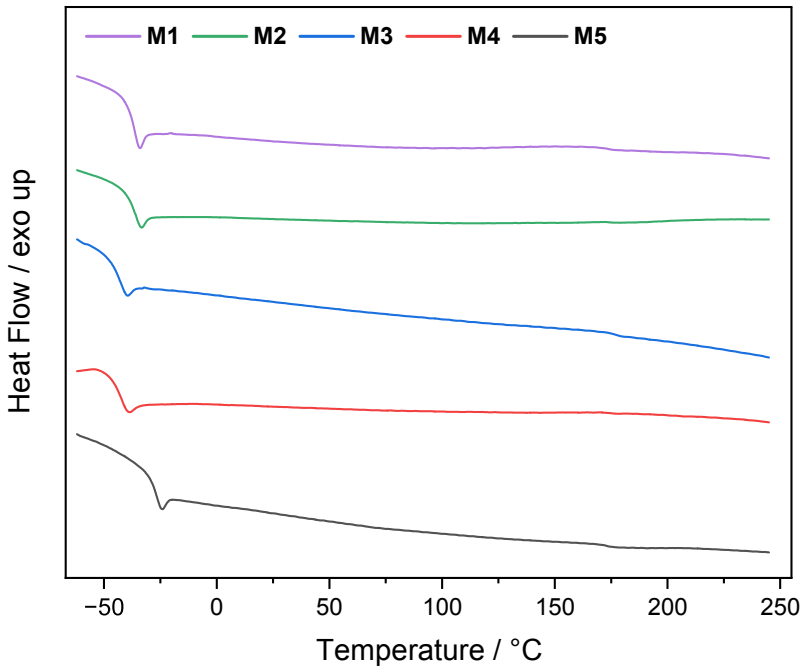

Figure 6.109: DSC Measurements of **M1** to **M5**.

Table 6.13: Determined glass transition temperatures T_g of compounds **M1** to **M5**.

Polymer	T_g / °C
1	−37
2	−37
3	−43
4	−44
5	−27

6.13 P-3CR polymerization of sunflower oil-based triacid

6.13.1 General procedure for P-3CR polymerization

Sunflower oil-based polyacid and the respective diisocyanide component were weighed into a 10 ml screw cap vial and cooled to −20 °C with a sodium chloride ice cooling bath. The aldehyde component was freshly distilled and then weighed into the cooled vial. All compounds were mixed while cooling was maintained. The mixture was then poured into a bone shaped Teflon form (see chapter 6.13.6) and cured inside a fridge (5 °C) for 30 minutes. Afterwards the thermosets were cured at 50 °C for 24 h.

The exact amount of all compounds used for the respective polymers is listed in Table 6.14. Acetaldehyde and Butanal were used in excess due to their low boiling points leading to loss of substance during the curing time.

Table 6.14: Amount of monomer compounds used for each Passerini-3CR polymerization.

Polymer	HOSOIC Acid	Aldehyde	Diisocyanide
P1a	600 mg (2.97 mmol CO_2H)	Acetaldehyde (170 mg, 3.86 mmol, 1.30 equiv.)	1,6-Diisocyanidohexane (202 mg, 1.49 mmol, 0.50 equiv.)
P1b	600 mg (2.97 mmol CO_2H)	Acetaldehyde (170 mg, 3.86 mmol, 1.30 equiv.)	1,9-Diisocyanidononane (265 mg, 1.49 mmol, 0.50 equiv.)
P2a	600 mg (2.97 mmol CO_2H)	Butanal (236 mg, 3.27 mmol, 1.10 equiv.)	1,6-Diisocyanidohexane (202 mg, 1.49 mmol, 0.50 equiv.)
P2b	600 mg (2.97 mmol CO_2H)	Butanal (236 mg, 3.27 mmol, 1.10 equiv.)	1,9-Diisocyanidononane (265 mg, 1.49 mmol, 0.50 equiv.)
P3a	550 mg (2.72 mmol CO_2H)	Hexanal (273 mg, 2.72 mmol, 1.00 equiv.)	1,6-Diisocyanidohexane (186 mg, 1.36 mmol, 0.50 equiv.)
P3b	550 mg (2.72 mmol CO_2H)	Hexanal (273 mg, 2.72 mmol, 1.00 equiv.)	1,9-Diisocyanidononane (243 mg, 1.36 mmol, 0.50 equiv.)
P4a	600 mg (2.97 mmol CO_2H)	Nonanal (423 mg, 2.97 mmol, 1.00 equiv.)	1,6-Diisocyanidohexane (202 mg, 1.49 mmol, 0.50 equiv.)
P4b	600 mg (2.97 mmol CO_2H)	Nonanal (423 mg, 2.97 mmol, 1.00 equiv.)	1,9-Diisocyanidononane (265 mg, 1.49 mmol, 0.50 equiv.)
P5a	550 mg (2.72 mmol CO_2H)	2-Ethylbutyraldehyde (273 mg, 2.72 mmol,1.00 equiv.)	1,6-Diisocyanidohexane (186 mg, 1.36 mmol, 0.50 equiv.)
P5b	500 mg (2.48 mmol CO_2H)	2-Ethylbutyraldehyde (248 mg, 2.48 mmol, 1.00 equiv.)	1,9-Diisocyanidononane (221 mg, 1.24 mmol, 0.50 equiv.)

6.13.2 Infrared spectroscopy

All P-3CR polymers were characterized *via* IR spectroscopy. All spectra are depicted in Figure 6.110.

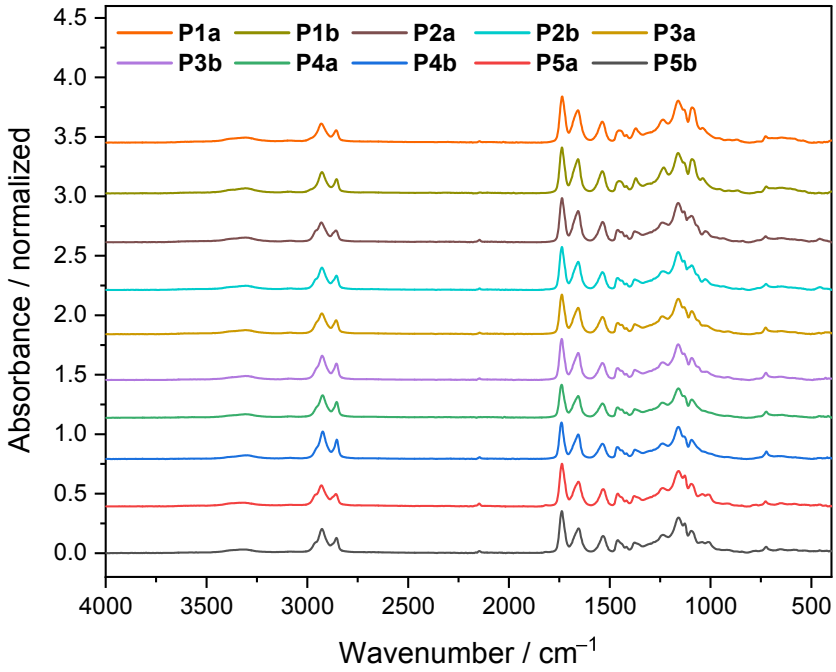

Figure 6.110: IR spectra of all P-3CR polymers.

6.13.3 Swelling tests

The gel content of all P-3CR polymers was determined to assess the overall degree of cross-linking. Each polymer sample (50−100 mg) was weighed and immersed in tetrahydrofuran for 3 days at room temperature to allow the complete solubilization of residual unreacted monomeric and oligomeric chains inside the material. The polymers were then removed from the solvent, dried at 70 °C and 10 mbar, and weighed again. The gel content is the percentage of mass that is insoluble in THF and is therefore calculated by division of the dried sample's mass m_1 by the initial sample's mass m_0 (Equation (50)).

$$\text{Gel content } (\%) = \frac{m_1}{m_0} \times 100 \tag{50}$$

The determined values for the gel content of all polymers are listed in Table 6.15.

Table 6.15: Gel content of all P-3CR polymers.

Polymer	Gel content / %
P1a	98 ± 2
P1b	96 ± 2
P2a	96 ± 1
P2b	98 ± 1
P3a	97 ± 2
P3b	96 ± 2
P4a	97 ± 1
P4b	97 ± 1
P5a	98 ± 1
P5b	99 ± 1

6.13.4 Thermogravimetric analysis

TGA measurements of all P-3CR polymers are depicted in Figure 6.111 and the corresponding $T_{d,5\%}$ values are listed in Table 6.16.

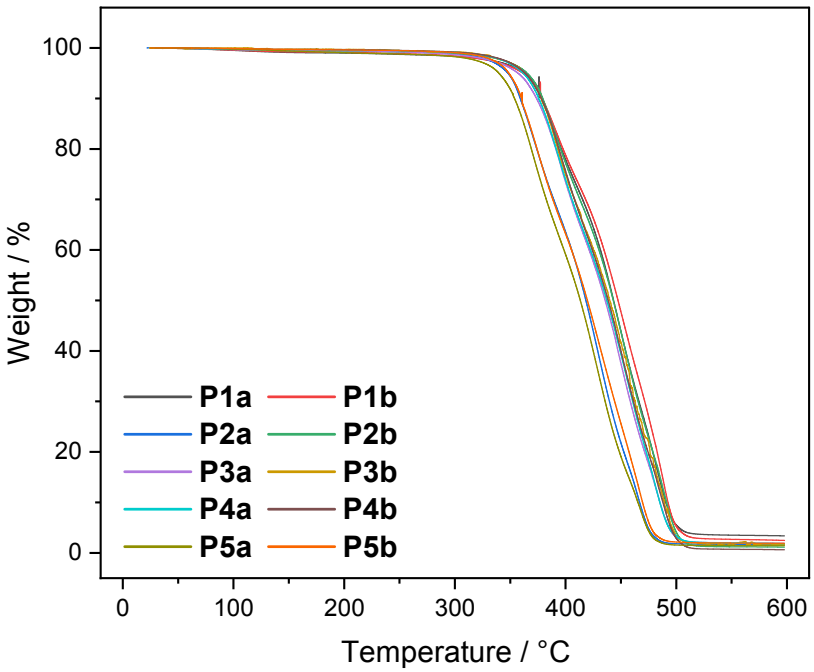

Figure 6.111: TGA Measurements of all P-3CR polymers.

Table 6.16: Determined degradation temperature (5% weight loss) of all P-3CR polymers.

Polymer	$T_{d,5\%}$ / °C
P1a	363
P1b	362
P2a	346
P2b	365
P3a	357
P3b	363
P4a	362
P4b	364
P5a	333
P5b	343

6.13.5 Differential scanning calorimetry

DSC measurements of all P-3CR polymers are depicted in Figure 6.112 and the corresponding T_g values are listed in Table 6.17.

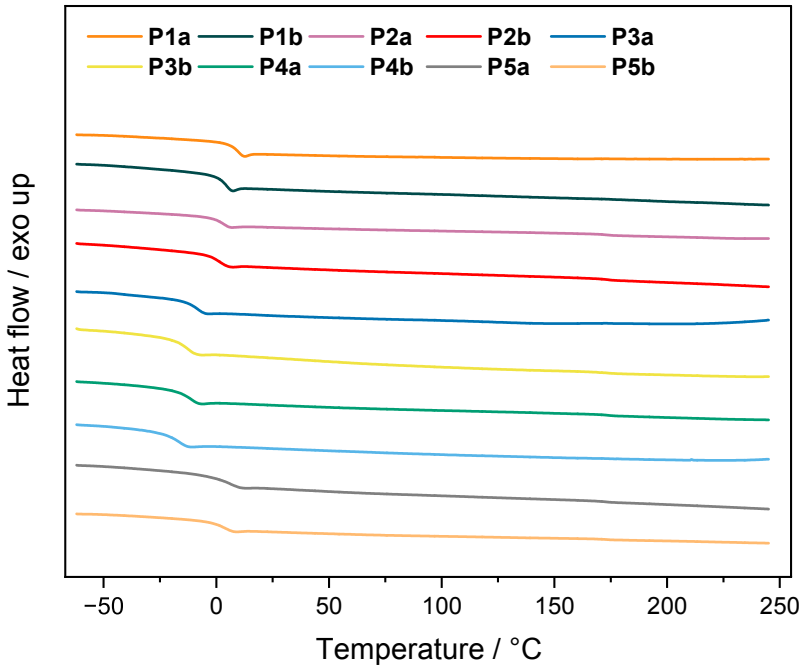

Figure 6.112: DSC Measurements of all P-3CR polymers.

Table 6.17: Determined glass transition temperatures T_g of all P-3CR polymers.

Polymer	T_g / °C
P1a	9
P1b	4
P2a	3
P2b	1
P3a	−8
P3b	−12
P4a	−12
P4b	−18
P5a	3
P5b	0

6.13.6 Tensile strength measurements

A Teflon form was manufactured to allow casting of customized tensile test samples. The dimensions of the prepared samples are depicted in Figure 6.113 and are given in millimeters. For each polymer, three samples were measured to determine the average Young's modulus, ultimate tensile strength, elongation at break and their standard deviations. All tensile strength measurements are depicted in Figure 6.114−Figure 6.123.

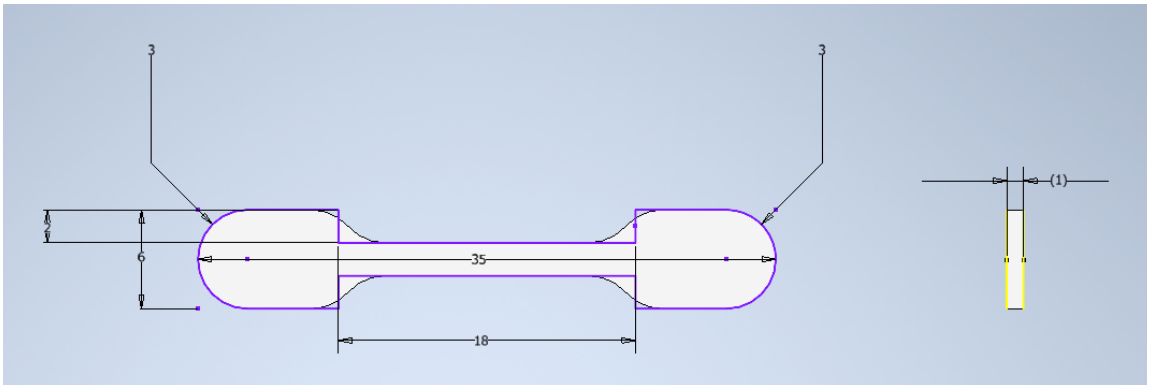

Figure 6.113: Dimensions of the manufactured tensile test samples (in millimeters). This drawing was made with Autodesk Inventor.

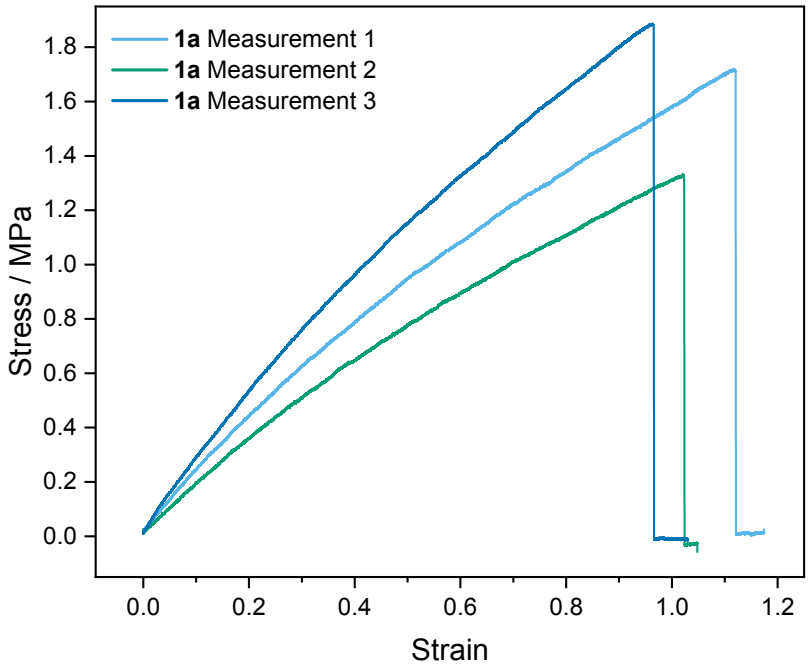

Figure 6.114: Tensile strength measurements of **P1a**.

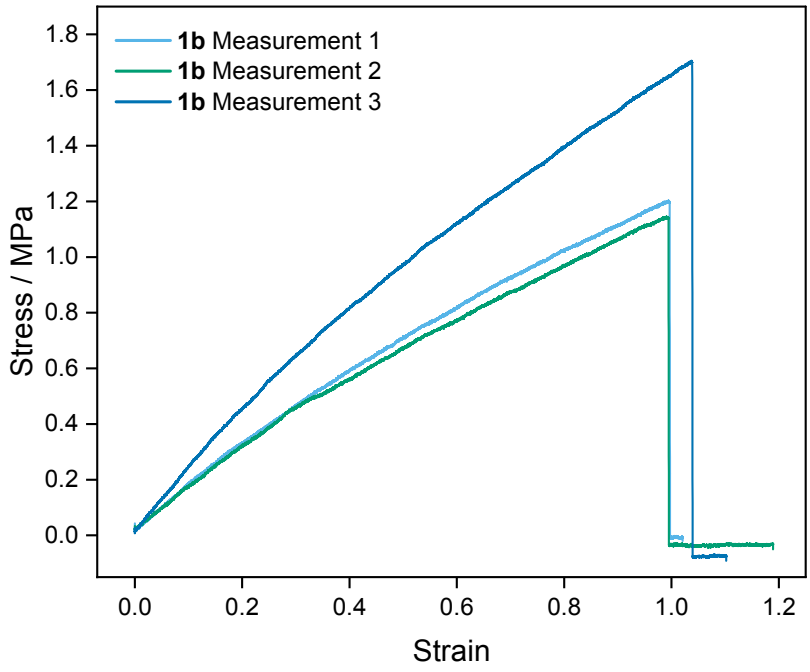

Figure 6.115: Tensile strength measurements of **P1b**.

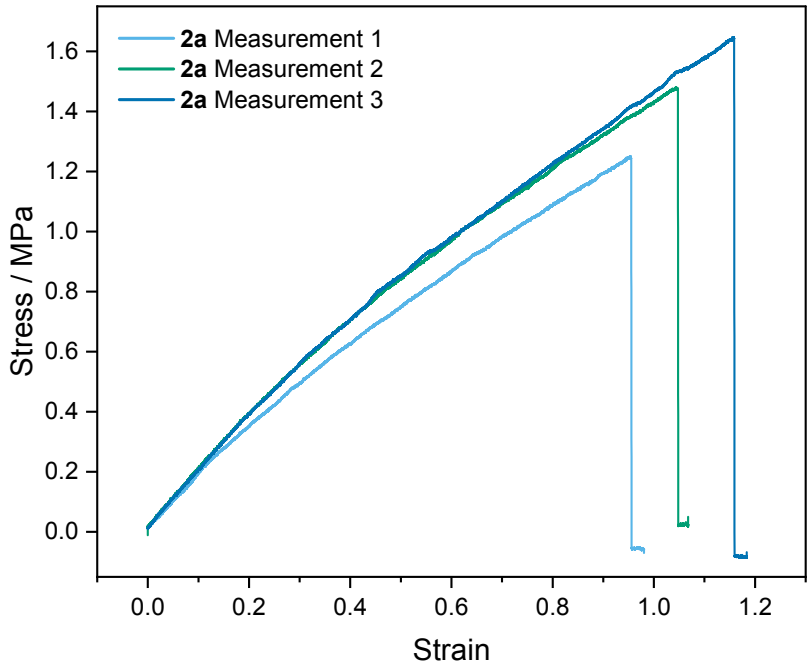

Figure 6.116: Tensile strength measurements of **P2a**.

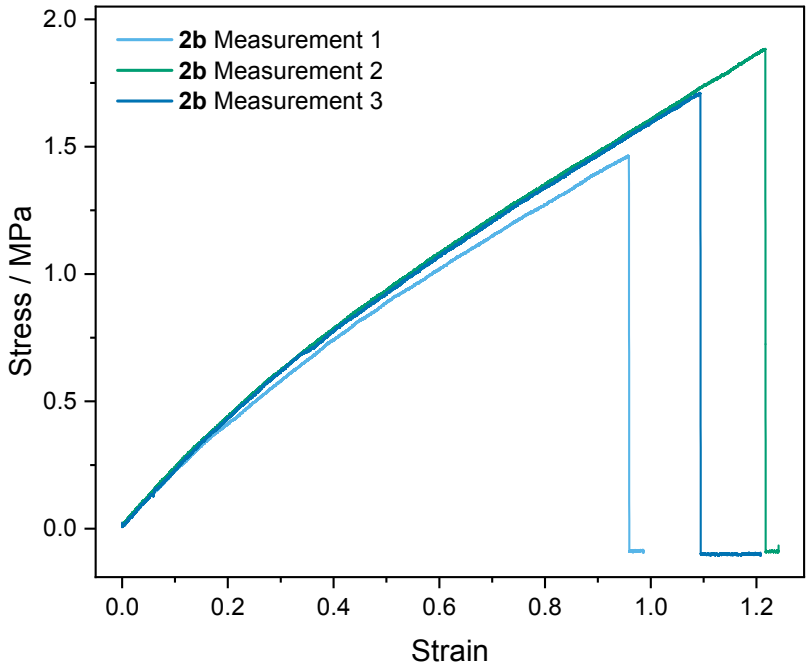

Figure 6.117: Tensile strength measurements of **P2b**.

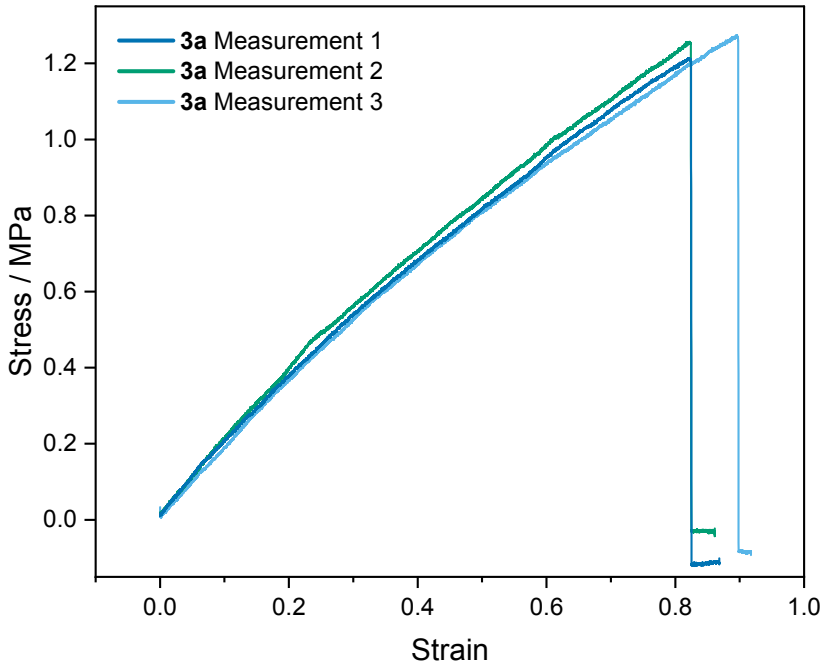

Figure 6.118: Tensile strength measurements of **P3a**.

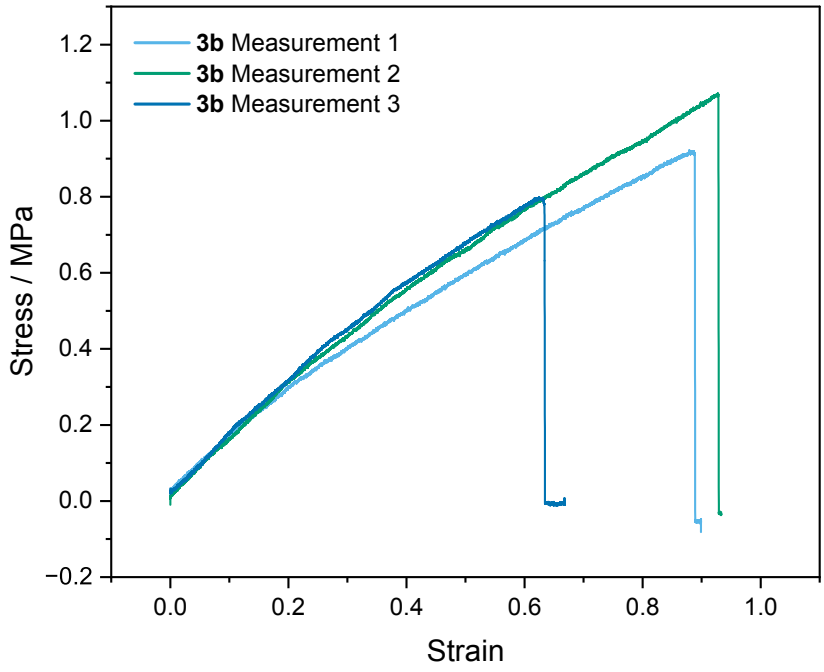

Figure 6.119: Tensile strength measurements of **P3b**.

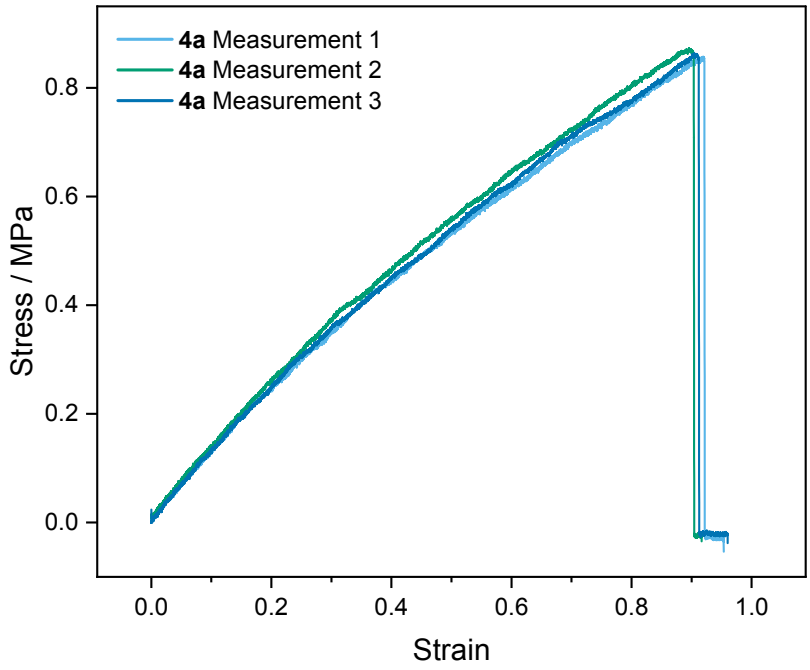

Figure 6.120: Tensile strength measurements of **P4a**.

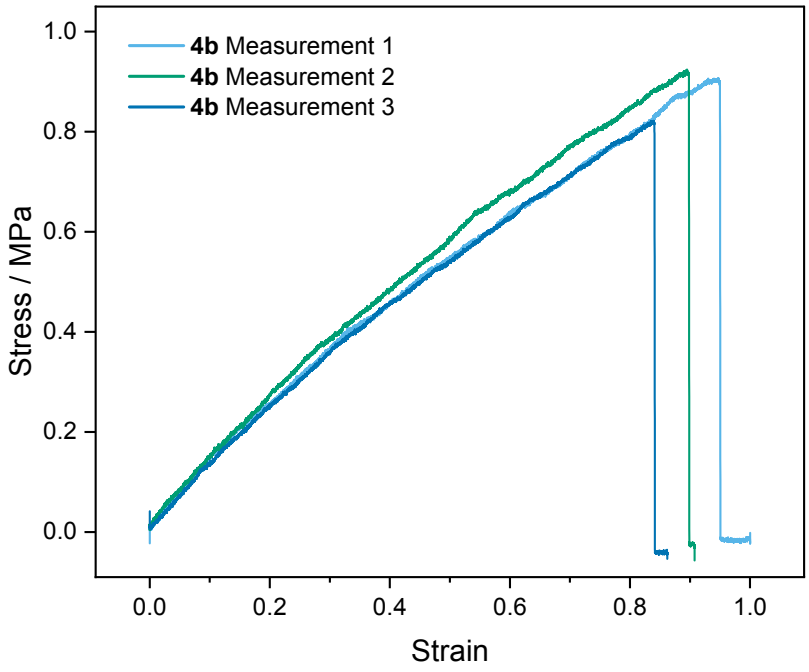

Figure 6.121: Tensile strength measurements of **P4b**.

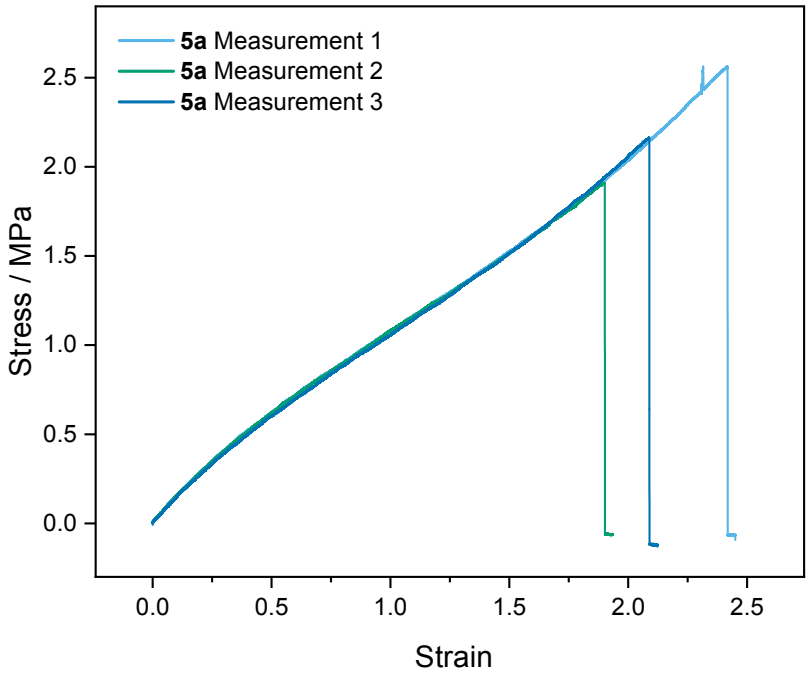

Figure 6.122: Tensile strength measurements of **P5a**.

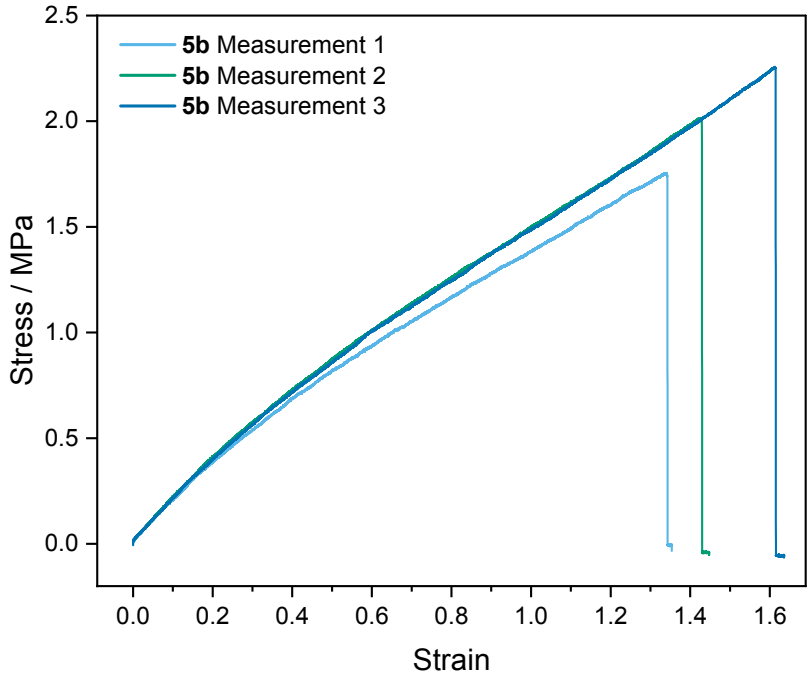

Figure 6.123: Tensile strength measurements of **P5b**.

6.13.7 Lap shear force adhesive tests

Testing samples were prepared by cutting each material into rectangular pieces.

1. Aluminum alloy (5754, or $AlMg_3$): 6 cm × 1.5 cm × 0.1 cm
2. Stainless-steel (S235JR): 6 cm × 1.5 cm × 0.1 cm
3. Wood (common ash): 6 cm × 1.5 cm × 0.5 cm
4. Poly(methyl methacrylate): 6 cm × 1.5 cm × 0.4 cm
5. Borosilicate glass: 6 cm × 1.5 cm × 0.4 cm

For sample preparation, polymer **P5a** was premixed at 0 °C and then applied onto two rectangular pieces of the same substrate (glueing area of 2.25 cm^2). The two surfaces were pressed together and cured at room temperature for 2 h. Each substrate was measured in triplicate to determine the average ultimate tensile strength and its standard deviation (Table 6.18). All adhesive test measurements are depicted in Figure 6.124−Figure 6.129.

Table 6.18: Determined ultimate tensile strengths with standard deviations of all adhesive tests with polymer **P5a**. Each sample was measured in triplicate.

Surface	Ultimate Tensile Strength / MPa
Aluminum alloy	1.12 ± 0.07
Stainless-steel	1.88 ± 0.09
Wood	1.03 ± 0.04
Poly (methyl methacrylate)	0.94 ± 0.11
Borosilicate glass	1.17 ± 0.07

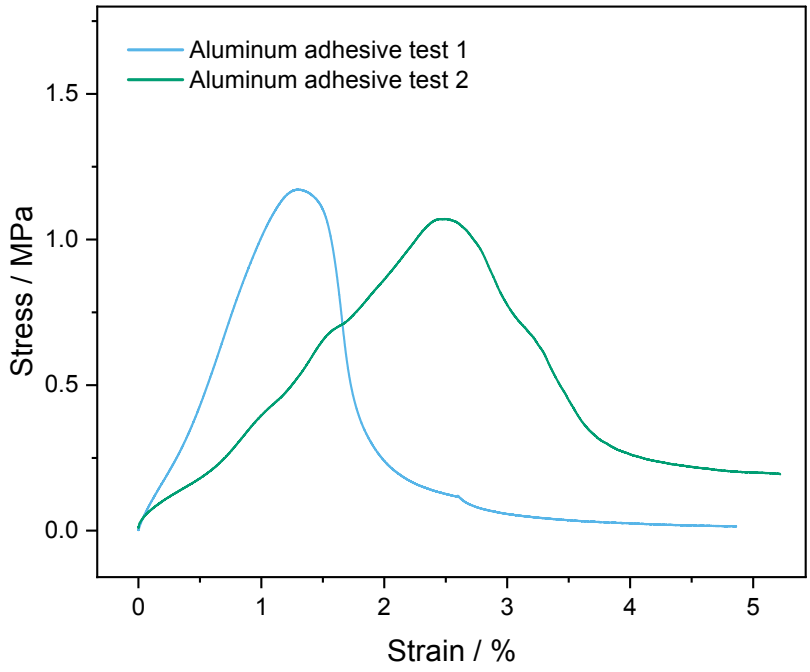

Figure 6.124: Adhesive test measurements of **P5a** on aluminum.

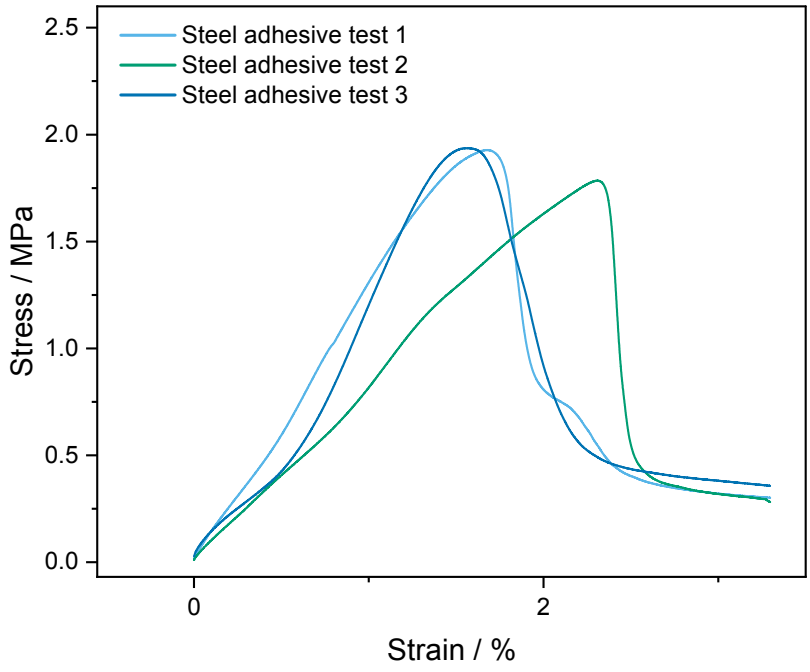

Figure 6.125: Adhesive test measurements of **P5a** on stainless-steel.

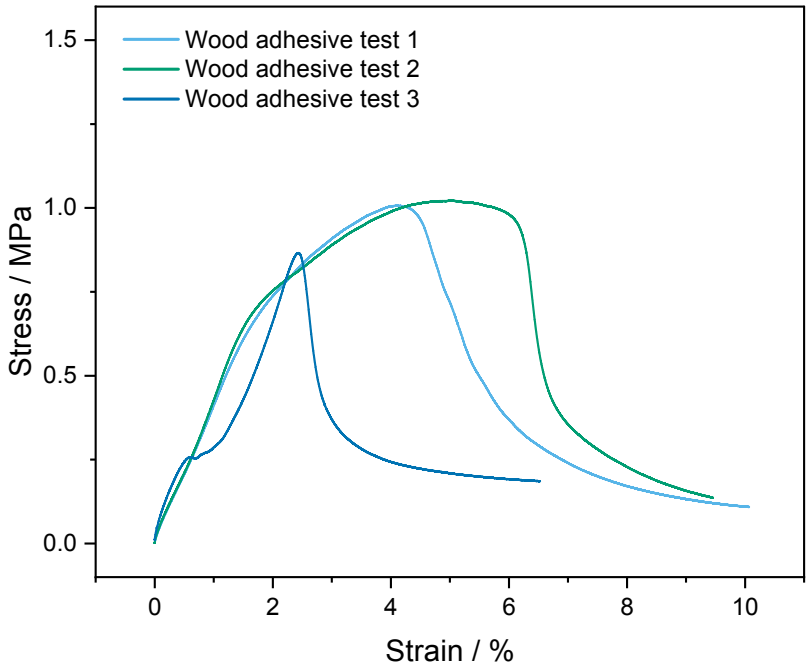

Figure 6.126: Adhesive test measurements of **P5a** on wood.

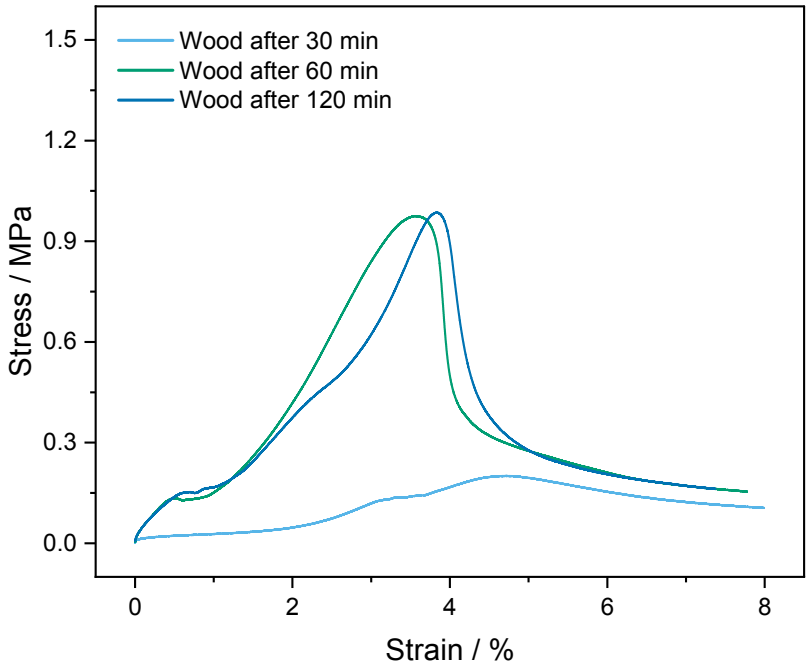

Figure 6.127: Adhesive test measurements of **P5a** on wood with different curing times.

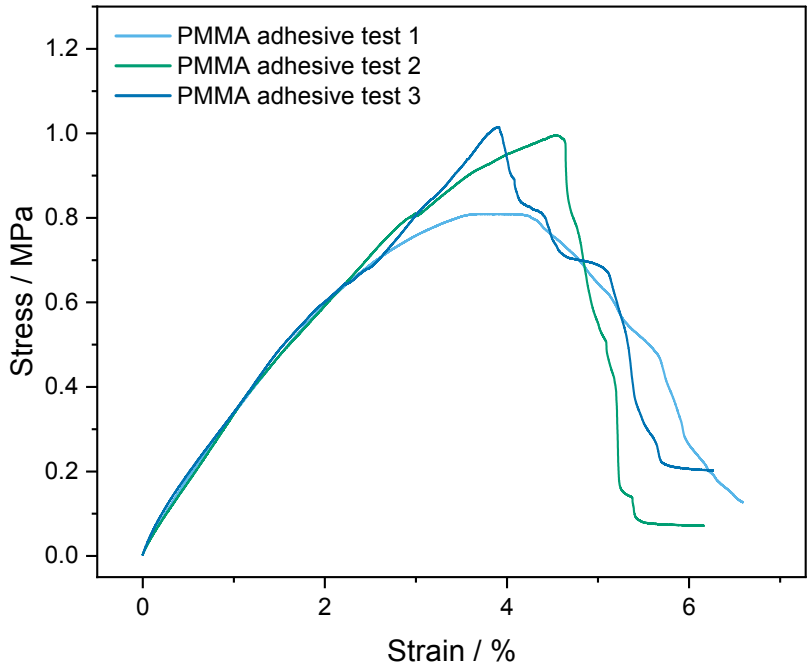

Figure 6.128: Adhesive test measurements of **P5a** on PMMA.

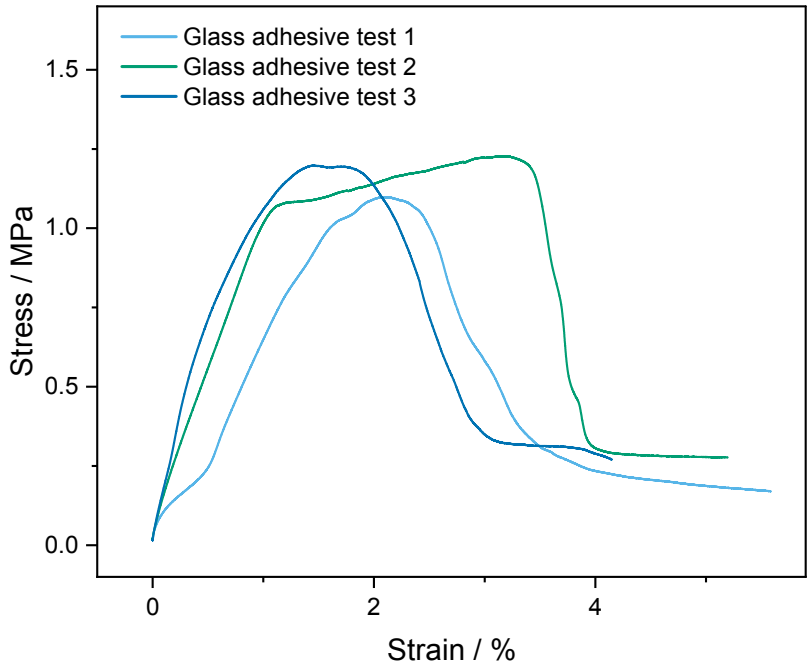

Figure 6.129: Adhesive test measurements of **P5a** on glass.

6.13.8 Chemical recycling of polymer P4b

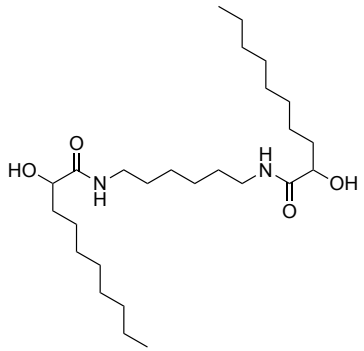

Diol **6**

$C_{26}H_{52}N_2O_4$

M = 456.71 g/mol

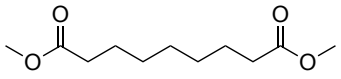

Azelaic acid dimethyl ester

$C_{11}H_{20}O_4$

M = 216.28 g/mol

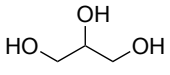

Glycerol

$C_3H_8O_3$

M = 92.09 g/mol

Polymer **P4a** (3.00 g, 14.6 mmol Ester groups, 1.00 equiv.) was suspended in methanol (120 ml, 2.96 mol, 203 equiv.) and sulfuric acid (96%, ´286 mg, 2.91 mmol, 0.20 equiv.) was added. The reaction mixture was stirred for 5 h at 65 °C until polymer **P4a** dissolved completely. While cooling down to room temperature, the diol compound precipitated. The reaction volume was reduced to 60 ml and then filtrated to isolate the diol (1.23 g, 2.69 mmol, 74%). The solvent methanol was removed from the filtrate and ethyl acetate (60 ml) was added. The organic phase was washed with water (3 ×40 ml) to remove glycerol and sulfuric acid, dried over sodium sulfate, and the solvent was removed under reduced pressure. The residue was then distilled in a Kugelrohr oven (10 mbar, 150 °C) to isolate dimethyl azelate (1.18 g, 5.45 mmol, 75%). At last, the aqueous phase from the washing step before was neutralized with sodium hydroxide (116 mg, 2.91 mmol, 0.20 equiv.) and distilled in a Kugelrohr oven to obtain glycerol (68 mg, 738 µmol, 30%).

Diol:

***T*m:** 162 °C

^{1}H NMR (500 MHz, TFA-*d*, ppm): δ = 4.63 (dd, *J* = 8.7, 3.5 Hz, 2H, H^1), 3.44 (t, *J* = 7.3 Hz, 4H, H^2), 1.96−1.83 (m, 2H, H^3), 1.81−1.68 (m, 2H, H^3), 1.68−1.56 (m, 4H, H^4), 1.48−1.39 (m, 4H, H^5), 1.39 (s, 4H, H^6), 1.34−1.15 (m, 20H, H^7), 0.79 (t, *J* = 6.6 Hz, 6H, H^8).

^{13}C NMR (126 MHz, TFA-*d*, ppm): δ = 180.7 (C_q, C_{Amide}, C^1), 73.8 (CH, C^2), 43.4 (CH_2, C^3), 35.9 (CH_2, C^3), 33.6 (CH_2, C^3), 31.1 (CH_2, C^3), 30.9 (CH_2, C^3), 30.8 (CH_2, C^3), 29.9 (CH_2, C^3), 27.9 (CH_2, C^3), 26.7 (CH_2, C^3), 24.3 (CH_2, C^3), 14.7 (CH_3, C^4).

IR (ATR, cm^{-1}): $\tilde{\nu}$ = 3242 (s), 2953 (m), 2918 (vs), 2873 (w), 2849 (vs), 1638 (vs), 1622 (vs), 1543 (vs), 1468 (s), 1441 (w), 1373 (s), 1334 (m), 1327 (m), 1268 (w), 1176 (w), 1136 (w), 1082 (vs), 1034 (w), 815 (w), 802 (w), 722 (m), 679 (s), 552 (w), 507 (w), 480 (w), 466 (w).

ESI-MS ($[M+H]^+$, $C_{26}H_{53}N_2O_4$): calcd.: 457.4000, found: 457.3996.

Dimethyl azelate:

^{1}H NMR (400 MHz, $CDCl_3$, ppm): δ = 3.65 (s, 6H, H^1), 2.29 (t, *J* = 7.5 Hz, 4H, H^2), 1.61 (qd, *J* = 7.6, 4.1 Hz, 4H, H^3), 1.31 (d, *J* = 4.5 Hz, 6H, H^4).

Glycerol:

^{1}H NMR (400 MHz, DMSO-d_6, ppm): δ = 4.45 (d, *J* = 4.7 Hz, 1H, H^1), 4.38 (t, *J* = 5.6 Hz, 2H, H^2), 3.49−3.17 (m, 5H, H^3).

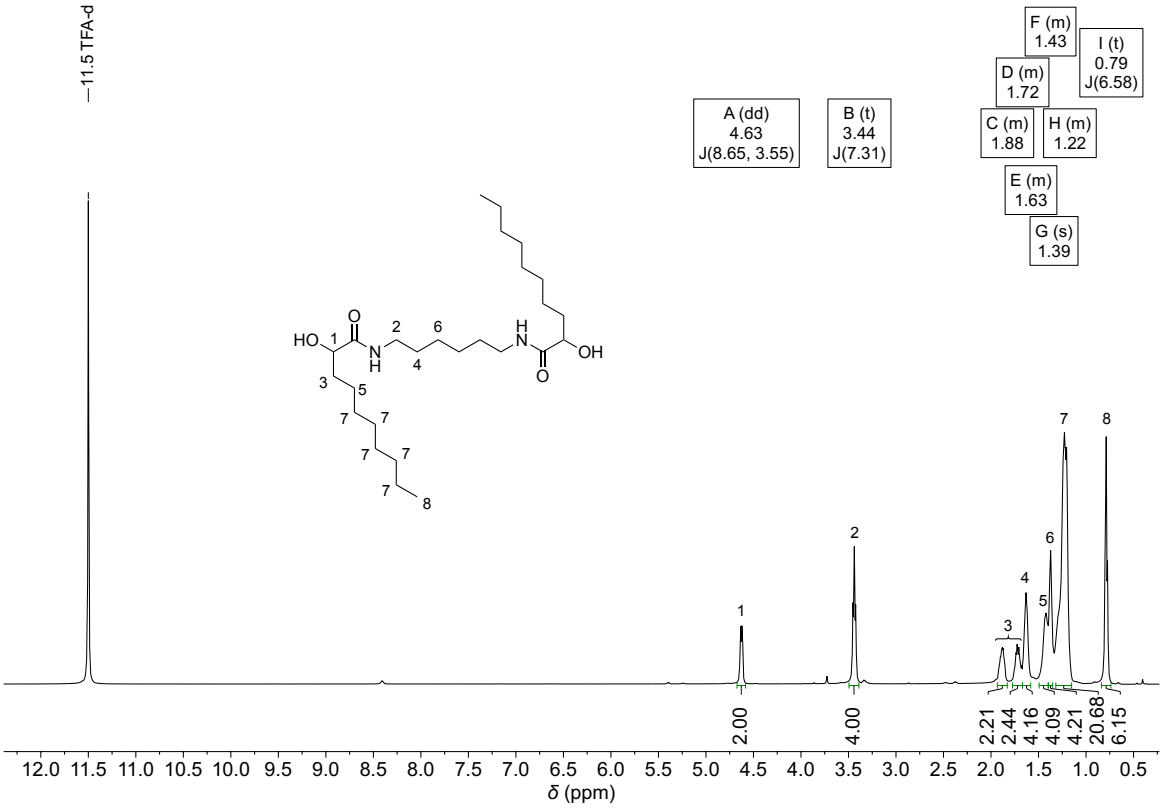

Figure 6.130: ^{1}H NMR Spectrum of diol **6** in TFA-*d*.

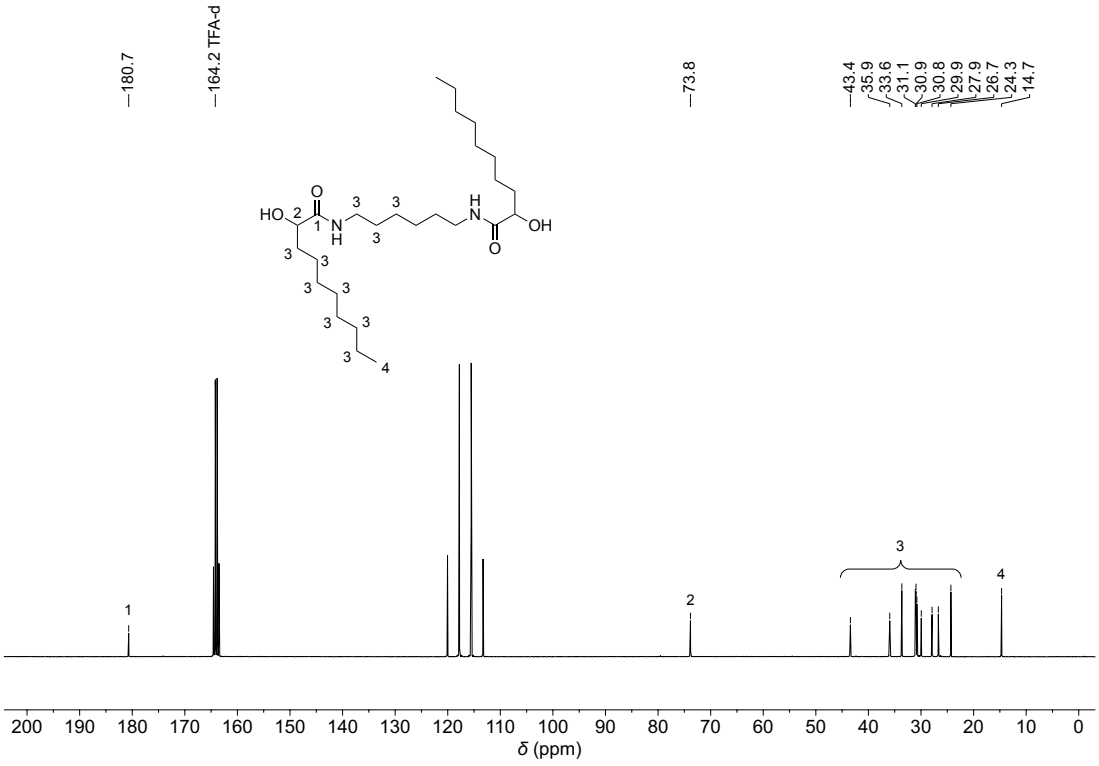

Figure 6.131: ^{13}C NMR Spectrum of diol **6** in TFA-*d*.

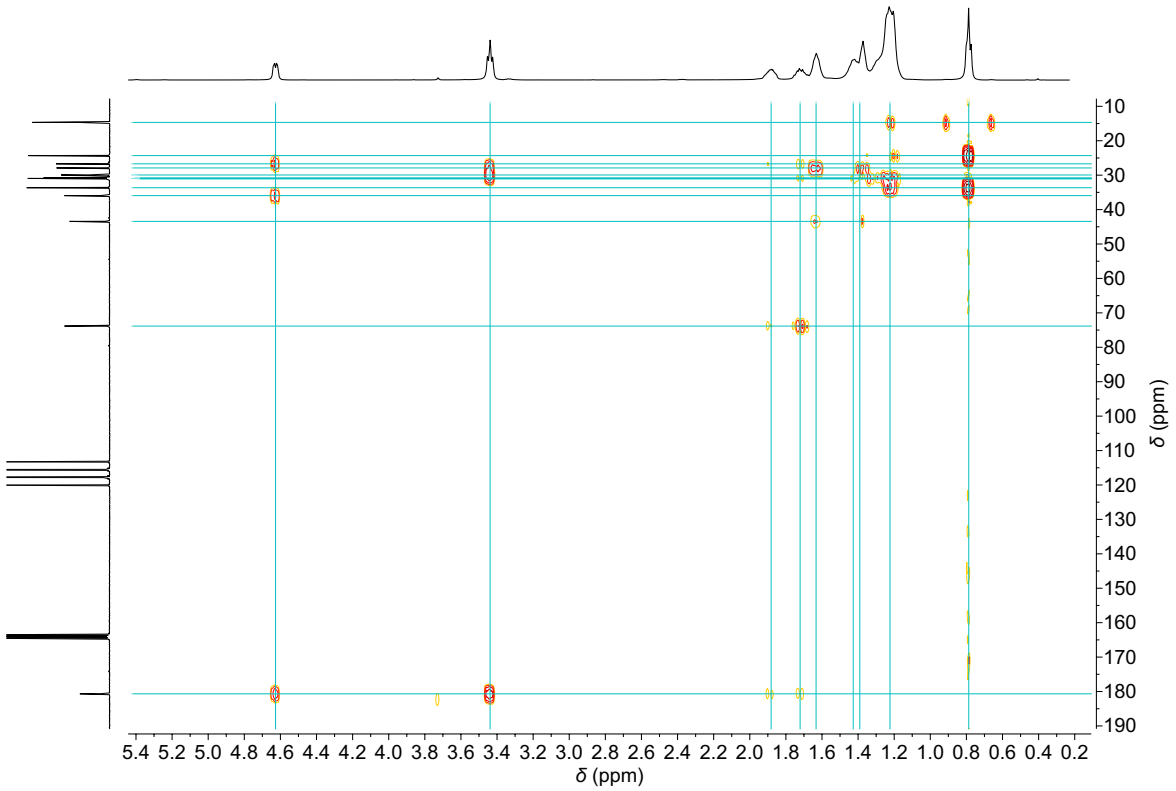

Figure 6.132: HMBC NMR spectrum of diol **6** in TFA-*d*.

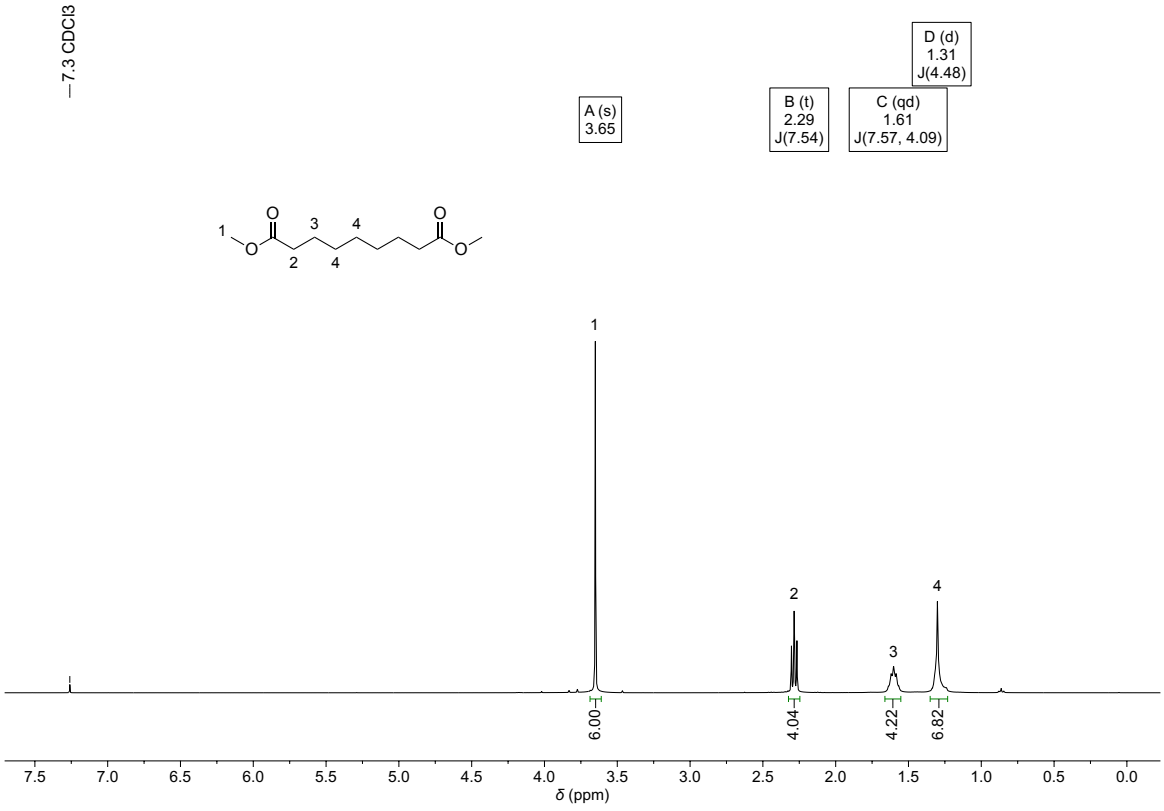

Figure 6.133: ^{1}H NMR spectrum of distilled dimethyl azelate in $CDCl_3$.

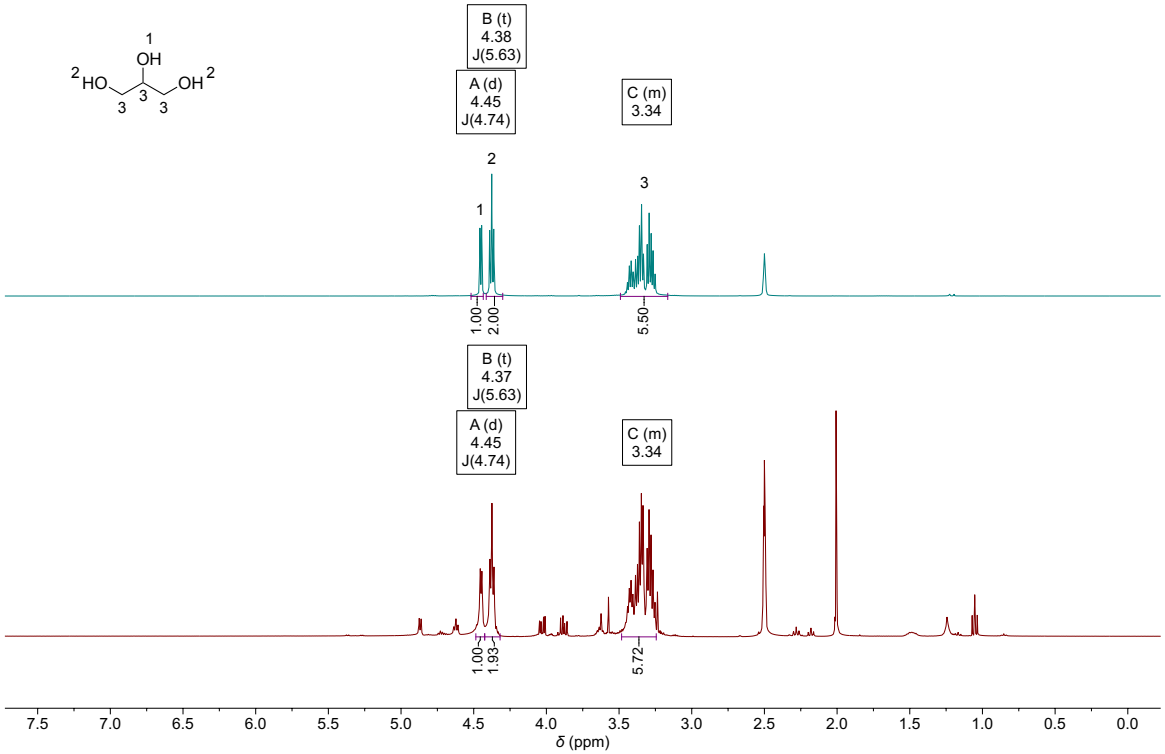

Figure 6.134: ^{1}H NMR spectrum of pure glycerol (top) and distilled glycerol (bottom) in DMSO-d_6.

6.14 Repolymerization of diol compound

6.14.1 Polymerization attempt with azelaic acid dimethyl ester

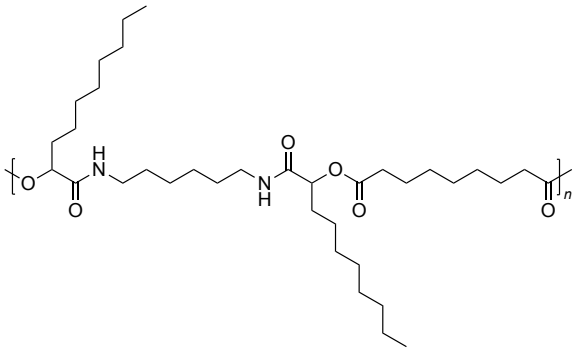

Repeating unit:
$C_{35}H_{64}N_2O_6$
M = 608.91 g/mol

Diol **6** (200 mg, 438 µmol, 1.00 equiv.), dimethyl azelate (94.7 mg, 438 µmol, 1.00 equiv.), and 1,5,7-triazabicyclo[4.4.0]dec-5-ene (3.05 mg, 21.9 µmol, 5.00 mol%) were added into a 1.5 ml screw-cap vial. The mixture was heated to 160 °C for 16 h and the pressure was reduced to 800 mbar to remove the condensation product methanol. Afterwards the pressure was further reduced to 10 mbar and the reaction was stirred for another 6 h at 160 °C. After cooling to room temperature, the residue was dissolved in tetrahydrofuran and precipitated in cold methanol. The precipitate was filtrated, washed with methanol and dried at 70 °C and 10 mbar to obtain the oligomer.

SEC (DMAc): M_n = 1900 Da, M_w = 3600 Da, $Đ$ = 1.90.

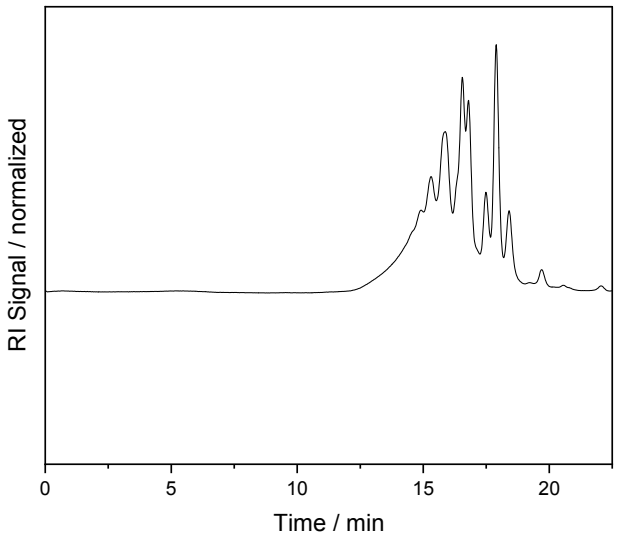

Figure 6.135: SEC (Oligo THF) after precipitation of polymerization attempt with azelaic acid dimethyl ester and TBD catalysis.

6.14.2 Polymerization with hexamethylene diisocyanate

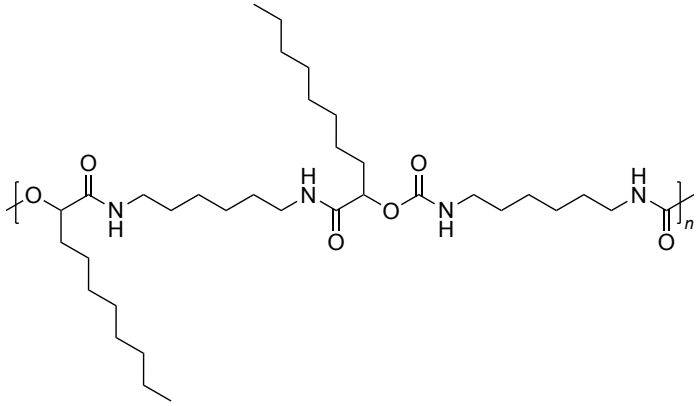

Repeating unit:
$C_{34}H_{64}N_4O_6$
M = 624.91 g/mol

Diol **6** (200 mg, 438 µmol, 1.00 equiv.) and hexamethylene diisocyanate (70.8 µl, 73.7 mg, 438 µmol, 1.00 equiv.) were added into a 1.5 ml screw cap vial. The mixture was heated to 160 °C until a homogeneous solution formed and was then stirred for another 1 h. After cooling down to room temperature, the reaction mixture was dissolved in hexafluoroisopropanol and precipitated in cold methanol. The precipitate was filtrated, washed with methanol and dried at 70 °C and 10 mbar to obtain 125 mg of polymer (46%).

SEC (DMAc): M_n = 16700 Da, M_w = 53000 Da, $Đ$ = 3.17.

^{1}H NMR (500 MHz, $CDCl_3$, ppm): δ = 7.09−6.27 (m, 2H, H^1), 6.02−5.33 (m, 2H, H^2), 5.09−4.91 (m, 2H, H^3), 3.33−3.18 (m, 4H, H^4), 3.18−3.00 (m, 4H, H^4), 1.88−1.78 (m, 2H, H^5), 1.74 (m, 2H, H^5), 1.49 (s, 8H, H^6), 1.39−1.09 (m, 32H, H^7), 0.86 (t, J = 6.8 Hz, 6H, H^8).

^{13}C NMR (126 MHz, $CDCl_3$, ppm): δ = 171.5 (C_q, C_{Amide}, C^1), 155.8 (C_q, $C_{Carbamate}$, C^2), 74.4 (CH, C^3), 41.0 (CH_2, C^4), 38.3 (CH_2, C^4), 32.5 (CH_2, C^5), 32.0 (CH_2, C^5), 29.8 (CH_2, C^5), 29.6 (CH_2, C^5), 29.5 (CH_2, C^5), 29.4 (CH_2, C^5), 29.3 (CH_2, C^5), 26.3 (CH_2, C^5), 26.1 (CH_2, C^5), 25.6 (CH_2, C^5), 25.1 (CH_2, C^5), 22.8 (CH_2, C^5), 14.2 (CH_3, C^6).

IR (ATR, cm^{-1}): $\tilde{\nu}$ = 3302 (w), 2922 (vs), 2853 (m), 1700 (vs), 1656 (vs), 1530 (vs), 1465 (m), 1438 (w), 1375 (w), 1306 (w), 1252 (vs), 1181 (w), 1136 (s), 1102 (w), 1074 (w), 1037 (w), 982 (w), 781 (w), 721 (w), 650 (w), 595 (w).

TGA ($T_{d,5\%}$): 318 °C.

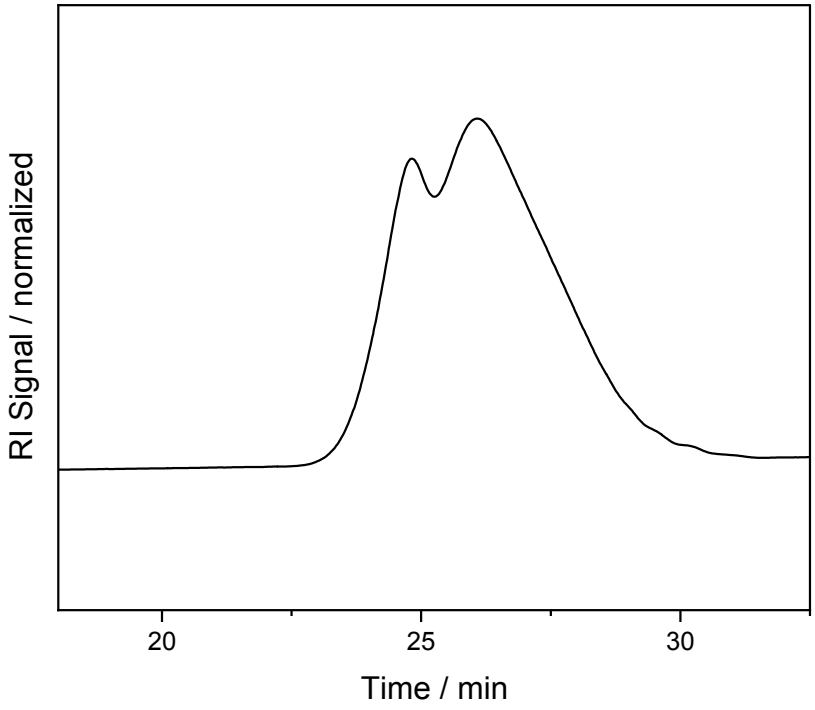

Figure 6.136: SEC (DMAc) of polyurethane made from diol **6** and hexamethylene diisocyanate.

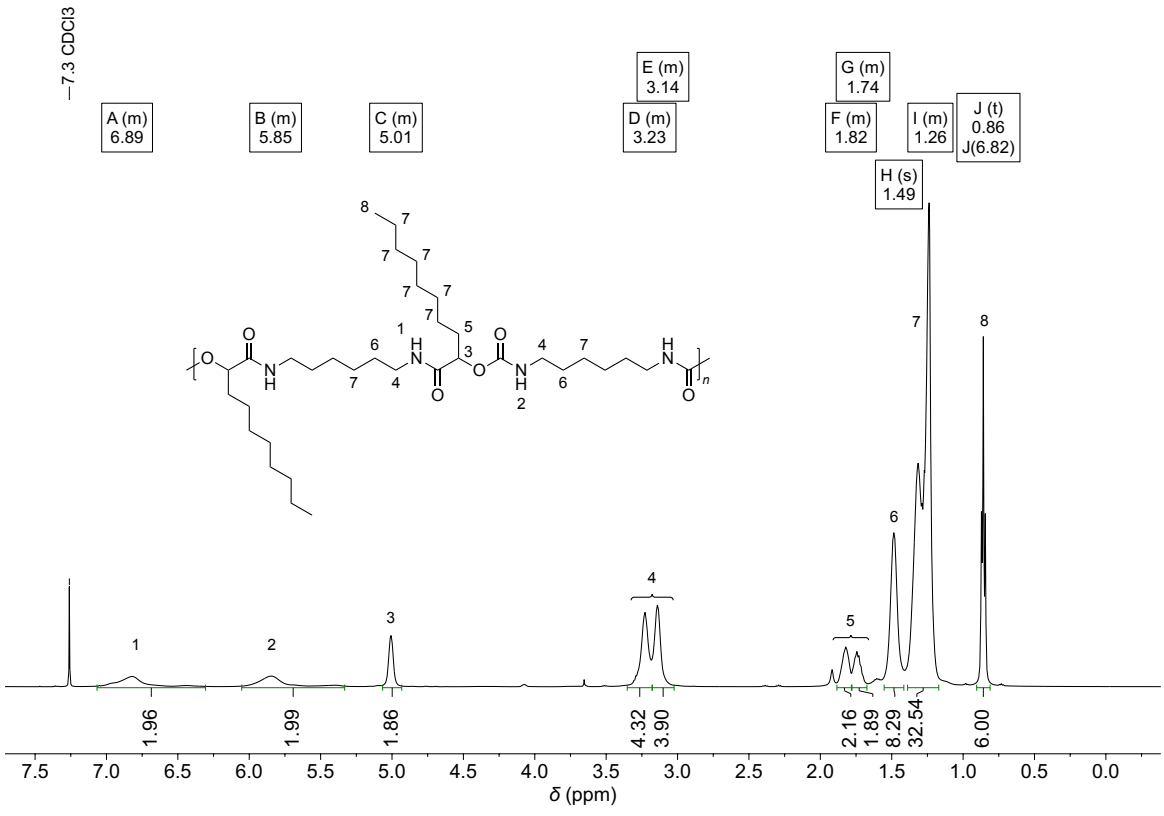

Figure 6.137: ^{1}H NMR spectrum of polyurethane made from diol **6** and hexamethylene diisocyanate in $CDCl_3$.

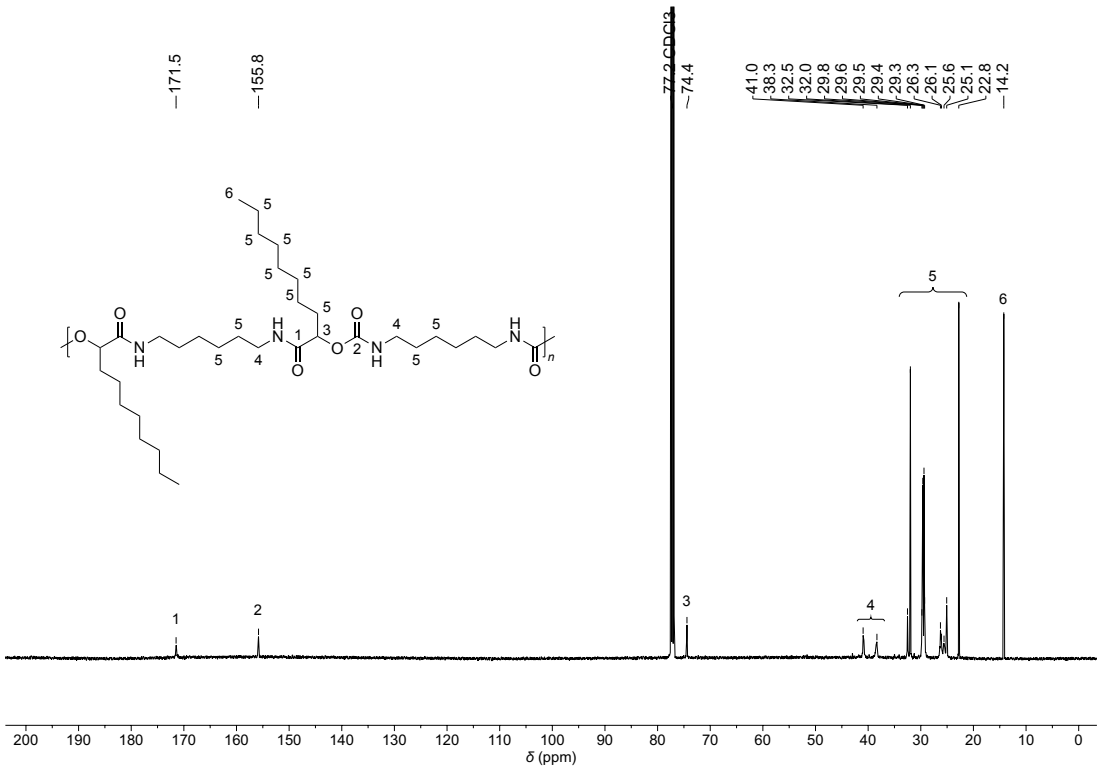

Figure 6.138: ^{13}C NMR spectrum of polyurethane made from diol **6** and hexamethylene diisocyanate in $CDCl_3$.

6.15 Functionalization of lignin with succinic anhydride

6.15.1 SEC measurement and ^{1}H NMR spectrum of organosolv lignin

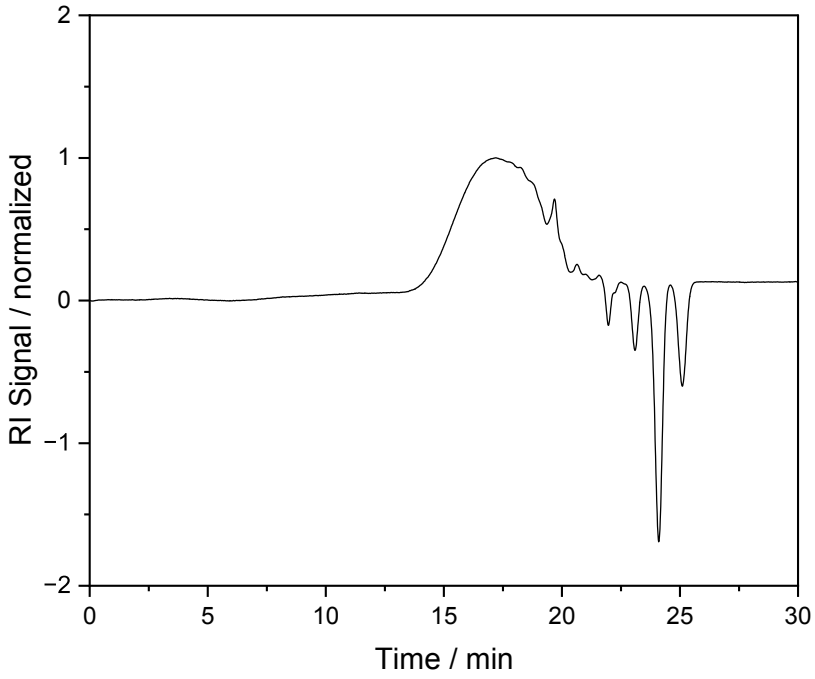

Figure 6.139: SEC (Oligo THF) measurement of organosolv lignin.

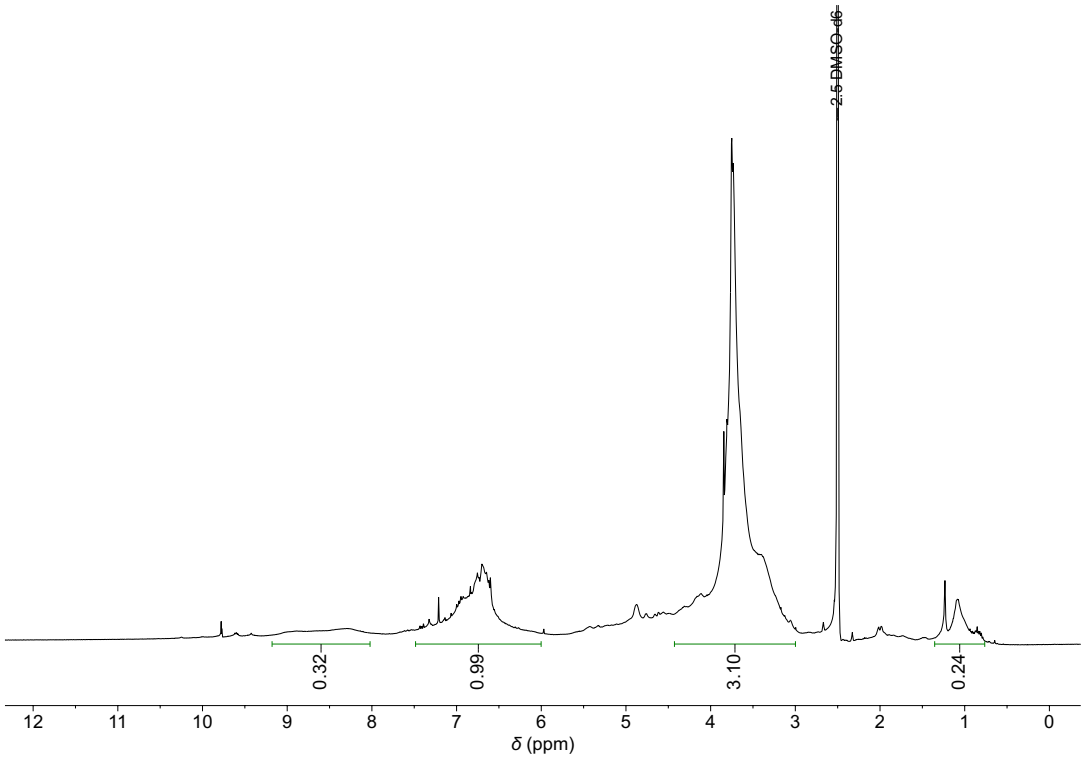

Figure 6.140: ^{1}H NMR spectrum of organosolv lignin in DMSO-d_6.

6.15.2 Quantitative ^{31}P NMR spectroscopy of lignin samples

The amount of hydroxyl and carboxylic acid groups per mg of lignin sample was determined by derivatization of the lignin sample using the phosphitylation agent 2-chloro-4,4,5,5-tetramethyl-1,3,2-dioxaphospholane (2-Cl-TMDP), according to a modified procedure of the one published by Argyropoulos *et al*.[274] First, the internal standard solution was prepared by dissolving endo-N-hydroxy-5-norbornene-2,3-dicarboximide (500 mg, 2.79 mmol) and chromium(III) acetylacetonate (125 mg, 358 µmol) in pyridine (15 ml) and $CDCl_3$ (10 ml). This results in a final concentration of 20 mg ml^{-1} or 112 mmol l^{-1} of the internal standard. Then, under standard atmosphere (no argon box), 28 to 32 mg of the analyte was weighed into a 10 ml screw-top vial. $CDCl_3$ (300 µl), Pyridine (300 µl, 3.71 mmol) and the internal standard solution of endo-*N*-hydroxy-5-norbornene-2,3-dicarboximide (700 µl) were added and the mixture was agitated with a vortex mixer until the sample was fully dissolved (approximately 1 min). At last, 2-Cl-TMDP (100 µl, 629 µmol) was added and the mixture was agitated for 1 min. Then, 1.0 ml of the solution was transferred to an NMR tube. 31P NMR measurements were performed immediately after the sample had been prepared.

Note: all compounds of the internal standard solution were weighed to enable the calculation of a weight percentage of internal standard inside the solution.

The amount of hydroxyl and carboxylic acid groups in the sample was calculated with Equations (51) and (52). The first term in the numerator corresponds to the amount of internal standard (IS) in µmol and the second term corresponds to the molar ratio of hydroxyl groups (or carboxylic acids) to internal standard (determined by integration in the ^{31}P NMR spectrum).

$$\frac{\mu\text{mol OH}}{\text{mg sample}} = \frac{\frac{\text{mass (mg of IS solution)} \times \text{wt\% (IS solution)}}{179.18\,\frac{\text{g}}{\text{mol}}\ \text{(Molar mass of } e\text{-HNDI)}} \times 1000 \times \frac{\text{Integral OH}}{\text{Integral IS}}}{\text{mg sample}} \tag{51}$$

$$\frac{\mu\text{mol } CO_2H}{\text{mg sample}} = \frac{\frac{\text{mass (mg of IS solution)} \times \text{wt\% (IS solution)}}{179.18\,\frac{\text{g}}{\text{mol}}\ \text{(Molar mass of } e\text{-HNDI)}} \times 1000 \times \frac{\text{Integral } CO_2H}{\text{Integral IS}}}{\text{mg sample}} \tag{52}$$

6.15.3 OH and CO_2H value determination of organosolv lignin

The hydroxyl groups of organosolv lignin were quantitatively functionalized using the phosphitylation agent 2-Cl-TMDP as shown in Scheme 6.1.

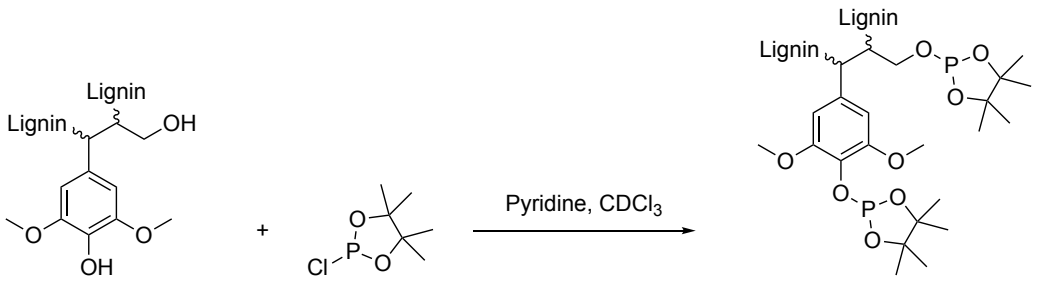

organosolv lignin representative structure | 2-Cl-TMDP | phosphitylated organosolv lignin

Scheme 6.1: Phosphitylation reaction of organosolv lignin.

Hydroxyl and carboxylic acid values of organosolv lignin were determined in triplicate applying the quantitative ^{31}P NMR method as described in chapter 6.15.2. The integrations and the corresponding ^{31}P NMR spectra are depicted in Figure 6.141. As can be seen from the shown NMR spectra, it is possible to distinguish different alcohol groups with this method.[274] For this project the alcohol groups were subdivided into aliphatic OH and aromatic OH to evaluate their different reactivity in reactions. Furthermore, the aromatic OH were divided into C_5-substituted OH (e.g., syringyl units bearing two methoxy substituents) and guaiacyl OH (1 methoxy group).

All masses and integrals of the conducted hydroxyl and carboxylic acid value determination of organosolv lignin are listed in Table 6.19 (determination was performed in triplicate).

Table 6.19: Values of sample mass (m_s), internal standard solution mass (m_{IS}), weight percentage of internal standard solution (w_{Is}), and integrals of the determination of OH and carboxylic acid value of organosolv lignin.

Entry	m_S(mg)	m_{IS}(mg)	w_{IS}	I_{allOH}	$I_{aliphaticOH}$	$I_{aromaticOH}$	$I_{C5\text{-}substitutedOH}$	$I_{GuaiacylOH}$	I_{CO2H}
1	29.8	805.0	0.0168	2.237	1.194	1.043	0.690	0.353	0.045
2	30.2	805.5	0.0168	2.263	1.209	1.054	0.699	0.355	0.059
3	30.4	807.7	0.0168	2.223	1.186	1.037	0.686	0.351	0.051

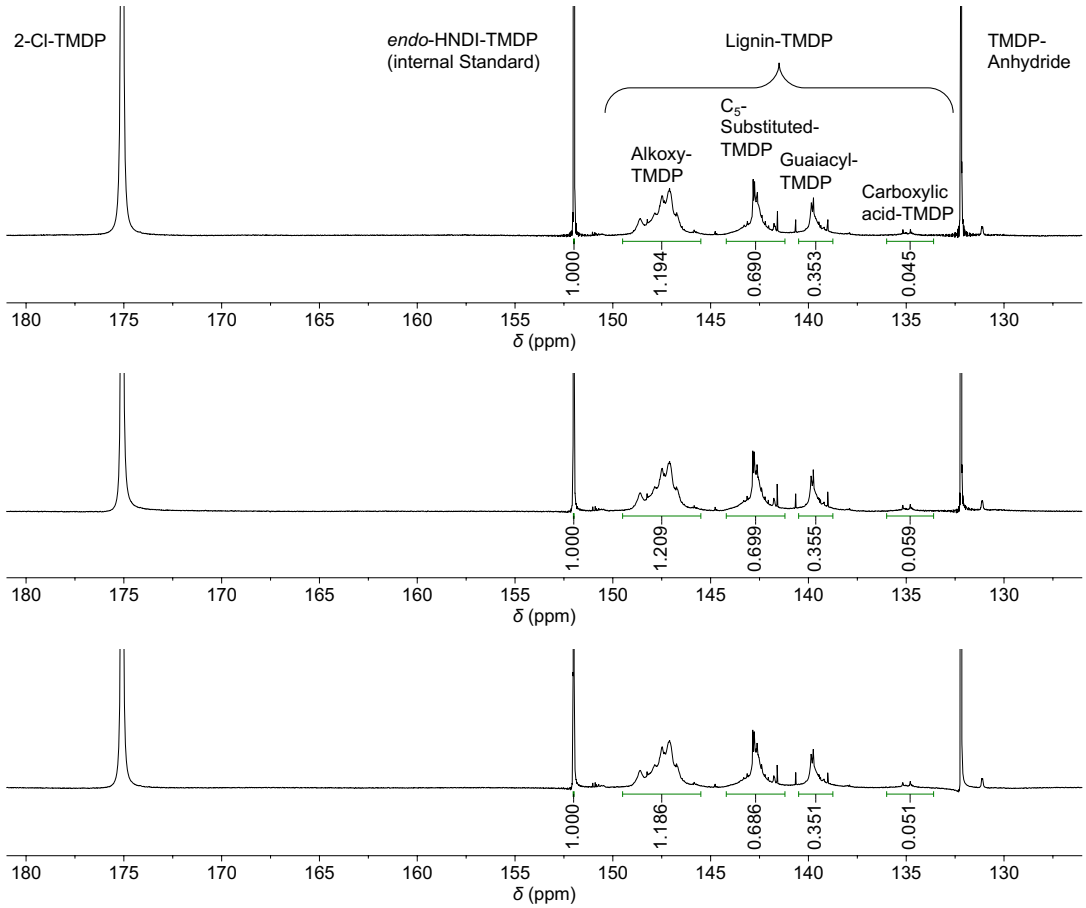

Figure 6.141: ^{31}P NMR spectra of the three phosphitylated organosolv lignin samples. The calculated *OH* and CO_2H values are listed in Table 6.20.

The determined hydroxyl and carboxylic acid values and specific *OH* values for aliphatic and aromatic alcohol groups of the organosolv lignin are listed in Table 6.20 (determination was performed in triplicate. The obtained averaged values with their corresponding standard deviations are as follows:

$OH_{\text{Organosolv lignin}}$ = 5.46 ± 0.07 µmol mg^{-1}
$OH_{\text{Aliphatic}}$ = 2.91 ± 0.04 µmol mg^{-1} (**53.4%** of all OH groups)
OH_{Aromatic} = 2.54 ± 0.03 µmol mg^{-1} (**46.6%** of all OH groups)
$OH_{\text{C5-Substituted}}$ = 1.68 ± 0.02 µmol mg^{-1} (**30.9%** of all OH groups)
OH_{Guaiacyl} = 0.86 ± 0.01 µmol mg^{-1} (**15.7%** of all OH groups)
$CO_2H_{\text{Organosolv lignin}}$ = 0.126 ± 0.016 µmol mg^{-1} (**2.25%** of all OH groups and CO_2H)

Table 6.20: Calculated *OH* and CO_2H values of organosolv lignin using Equations (51) and (52) and the values listed in Table 6.19.

Entry	$OH_{\text{Organosolv Lignin}}$ (µmol mg^{-1})	$OH_{\text{Aliphatic}}$ (µmol mg^{-1})	OH_{Aromatic} (µmol mg^{-1})	$OH_{\text{C5-substituted}}$ (µmol mg^{-1})	OH_{Guaiacyl} (µmol mg^{-1})	$CO_2H_{\text{Organosolv Lignin}}$ (µmol mg^{-1})
1	5.501	2.937	2.565	1.697	0.868	0.111
2	5.496	2.936	2.560	1.698	0.862	0.143
3	5.378	2.869	2.509	1.660	0.849	0.123

6.15.4 Calculation of degree of substitution and conversion of OH groups

For functionalizations, the degree of substitution (DS) was calculated as reported by Kilpeläinen *et al*. (for cellulose) according to the Eq (53).[273] In contrast to cellulose, the DS was calculated in percent.

$$\mathrm{DS}_{31\mathrm{P}}\,(\%) = \frac{\frac{1}{\mathrm{OH_S}} - \frac{1}{\mathrm{OH_{STM}}}}{\mathrm{M_S} + \frac{1}{\mathrm{OH_S}} - 1.008\,\frac{\mathrm{g}}{\mathrm{mol}}} \times 100 \qquad (53)$$

OH_S: free hydroxyl groups per weight unit of substrate (mol g^{-1})

OH_{STM}: free hydroxyl groups per weight unit of starting material (mol g^{-1})

for organosolv lignin: OH_{STM} = 0.0054588 mol g^{-1} (Chapter 6.15.3)

M_S: Molecular mass of the introduced substituent (not including the linking oxygen atom between the substituent and lignin; e.g., $C_4H_5O_3$ (101.081 g mol^{-1}) for reaction with succinic anhydride

1.008 g mol^{-1}: Molecular mass of a hydrogen atom

To further evaluate whether different OH groups exhibit distinct reactivity in transformations, the conversion of specific OH groups was determined as explained in the following. As depicted in Figure 6.141, it is possible to distinguish $OH_{Aliphatic}$ and $OH_{Aromatic}$. It is therefore possible to calculate ratios of particular OH groups to all OH groups with the integrals obtained in ^{31}P NMR spectroscopy (e.g., 53.4% of all organosolv lignin OH groups are aliphatic).

In an exemplary scenario, for a functionalized sample a DS of 70% is determined. Moreover, 5.0% of all unreacted OH groups are aliphatic (determined *via* ^{31}P NMR spectroscopy). Multiplication of 5.0% with 0.3 (the amount of unreacted OH groups; =1−DS) results in the amount of unreacted aliphatic OH groups of all initially present lignin OH groups (in this example = 1.5%). The conversion of aliphatic OH groups can then be calculated with Eq (54). In this example the conversion equals to 97.2% ($OH_{Aliphatic}$ (lignin) = 53.4%).

$$\mathrm{conversion}_{\mathrm{Aliphatic\,OH}}\,(\%) = \frac{OH_{\mathrm{Aliphatic}}(\mathrm{lignin}) - OH_{\mathrm{Aliphatic}}(\mathrm{unreacted})}{OH_{\mathrm{Aliphatic}}(\mathrm{lignin})} \times 100 \qquad (54)$$

6.15.5 Solventless functionalization of lignin with molten succinic anhydride

General procedure:

Organosolv lignin (1.00 g, **5.46 mmol OH**, 1.00 equiv.) was added portion wise to the respective amount of molten succinic anhydride (98% purity, see Table 6.21), while vigorously stirring at the respective temperature (Table 6.21). After complete dissolution of lignin, the mixture was stirred for either 10 min, 20 min, 40 min, 60 min or 2 h. After cooling to room temperature, the solidified mixture was dissolved in tetrahydrofuran (40 ml) and precipitated in the 15-fold volume of water (600 ml) to remove succinic anhydride. The precipitated lignin was isolated by filtration and dried under reduced pressure (20 mbar) at 50 °C for 24 h. The amount of succinic anhydride (SAn) used, the reaction temperature and the reaction time of all conducted experiments are listed in Table 6.21.

For each sample, the degree of substitution (DS) and the conversion of specific hydroxyl groups was determined *via* ^{31}P NMR spectroscopy (see chapter 6.15.4 for an exemplary calculation). Additionally, the integration ratio of carboxylic acid groups to the sum of OH groups and carboxylic acid groups was determined (*via* ^{31}P NMR spectroscopy). This ratio is approximately equal to the degree of functionalization as each OH group is transformed into a carboxylic acid moiety during this reaction. The determined values are listed in Table 6.21.

Table 6.21: Solventless Functionalization of Organosolv Lignin with molten succinic anhydride (SAn). The degree of substitution (DS) and the conversion of hydroxyl groups were determined *via* ^{31}P NMR spectroscopy.

Sample	Temperature(°C) / Reaction Time	SAn (equiv.)	DS (%)	CO_2H Integral *via* ^{31}P (%)	Conversion (%)			
					$OH_{Aliphatic}$	$OH_{Aromatic}$	$OH_{C5\text{-}substituted}$	$OH_{Guaiacyl}$
Lignin 1.1	140 / 10 min	10.0	54.9	58.2	73.1	34.0	32.2	37.3
Lignin 1.2	140 / 20 min	10.0	61.2	63.9	84.4	34.7	34.7	34.7
Lignin 1.3	140 / 40 min	10.0	66.4	68.8	91.3	37.9	37.2	39.3
Lignin 1.4	140 / 60 min	10.0	65.3	68.2	93.3	33.2	34.0	31.6
Lignin 1.5	140 / 2 h	5.00	66.0	71.1	97.7	29.8	30.0	29.4
Lignin 1.6	150 / 2 h	5.00	69.6	69.8	99.1	35.8	33.3	40.8
Lignin 1.7	160 / 2 h	5.00	68.7	68.7	99.0	34.0	29.9	42.1

6.15.6 Functionalization of lignin with succinic anhydride in solution

General procedure:

Succinic anhydride (98% purity, see Table 6.22) was dissolved in the respective solvent (THF or Me-THF) and heated to the respective reaction temperature (60 °C or 80 °C). Then, organosolv lignin (1.00 g, **5.46 mmol OH**, 1.00 equiv.) was added portion wise. After complete dissolution of lignin, the mixture was stirred for further 18 h at the given temperature. After cooling to room temperature, the mixture was added dropwise to the 15-fold volume of water to precipitate functionalized lignin and simultaneously remove succinic anhydride. The precipitated lignin was isolated by filtration and dried under reduced pressure (20 mbar) at 50 °C for 24 h. The amount of succinic anhydride used the reaction temperature and the solvent of all conducted experiments are listed in Table 6.22.

For each sample, the degree of substitution (DS) and the conversion of specific hydroxyl groups was determined *via* ^{31}P NMR spectroscopy (see chapter 6.15.4 for an exemplary calculation). Additionally, the integration ratio of carboxylic acid groups to the sum of OH groups and carboxylic acid groups was determined (*via* ^{31}P NMR spectroscopy). This ratio is approximately equal to the degree of functionalization as each OH group is transformed into a carboxylic acid moiety during this reaction. The determined values are listed in Table 6.22.

Table 6.22: Functionalization of organosolv lignin with succinic anhydride in solution. The degree of substitution (DS) and the conversion of hydroxyl groups was determined via ^{31}P NMR spectroscopy.

Sample	Temperature(°C) / Solvent / lignin concentration	SAn (equiv.)	DS (%)	CO_2H Integral *via* ^{31}P (%)	Conversion (%)			
					$OH_{Aliphatic}$	$OH_{Aromatic}$	$OH_{C5\text{-}substituted}$	$OH_{Guaiacyl}$
Lignin 1.8	60 / THF / 25 mg ml^{-1}	5.00	14.9	10.5	10.3	20.3	21.7	17.6
Lignin 1.9	80 / Me-THF / 25 mg ml^{-1}	5.00	26.3	24.6	33.8	17.8	17.5	18.5
Lignin 1.10	80 / Me-THF / 25 mg ml^{-1}	2.50	24.6	20.9	30.6	17.7	17.8	17.6
Lignin 1.11	80 / Me-THF / 25 mg ml^{-1}	1.00	18.3	10.7	27.5	7.6	6.7	9.4
Lignin 1.12	80 / Me-THF / 50 mg ml^{-1}	1.00	29.6	22.7	38.4	19.7	19.6	19.7
Lignin 1.13	80 / Me-THF / 75 mg ml^{-1}	1.00	30.3	24.9	41.4	17.7	16.8	19.3
Lignin 1.14	80 / Me-THF / 100 mg ml^{-1}	1.00	33.8	28.4	46.4	19.4	18.0	22.0

6.15.7 Large Scale reaction of solventless functionalization of organosolv lignin with succinic anhydride (Lignin 1.15)

Organosolv lignin (4.00 g, **21.8 mmol OH**, 1.00 equiv.) was added portion wise to molten succinic anhydride (98% purity, 11.2 g, 109 mmol, 5.00 equiv.), while vigorously stirring. After complete dissolution of lignin, the mixture was stirred for 2 h at 150 °C. After cooling to room temperature, the solidified mixture was dissolved in tetrahydrofuran (160 ml) and precipitated in the 15-fold volume of water (2.40 l) to remove succinic anhydride. The precipitated lignin was isolated by filtration and dried under reduced pressure (20 mbar) at 50 °C to obtain 3.29 g product.

The degree of functionalization (DS) and the amount of hydroxyl and carboxylic acid groups per mg of sample were determined *via* ^{31}P NMR spectroscopy (see chapters 6.15.2 and 6.15.4):

DS = 69.2%
CO_2H_{sample} = 2.63 µmol mg^{-1}
OH_{sample} = 1.22 µmol mg^{-1}
$OH_{Aliphatic}$ = 0.185 µmol mg^{-1}
$OH_{Aromatic}$ = 1.03 µmol mg^{-1}
$OH_{C5\text{-}Substituted}$ = 0.682 µmol mg^{-1}
$OH_{Guaiacyl}$ = 0.353 µmol mg^{-1}
CO_2H and OH_{sample} = 3.85 µmol mg^{-1}

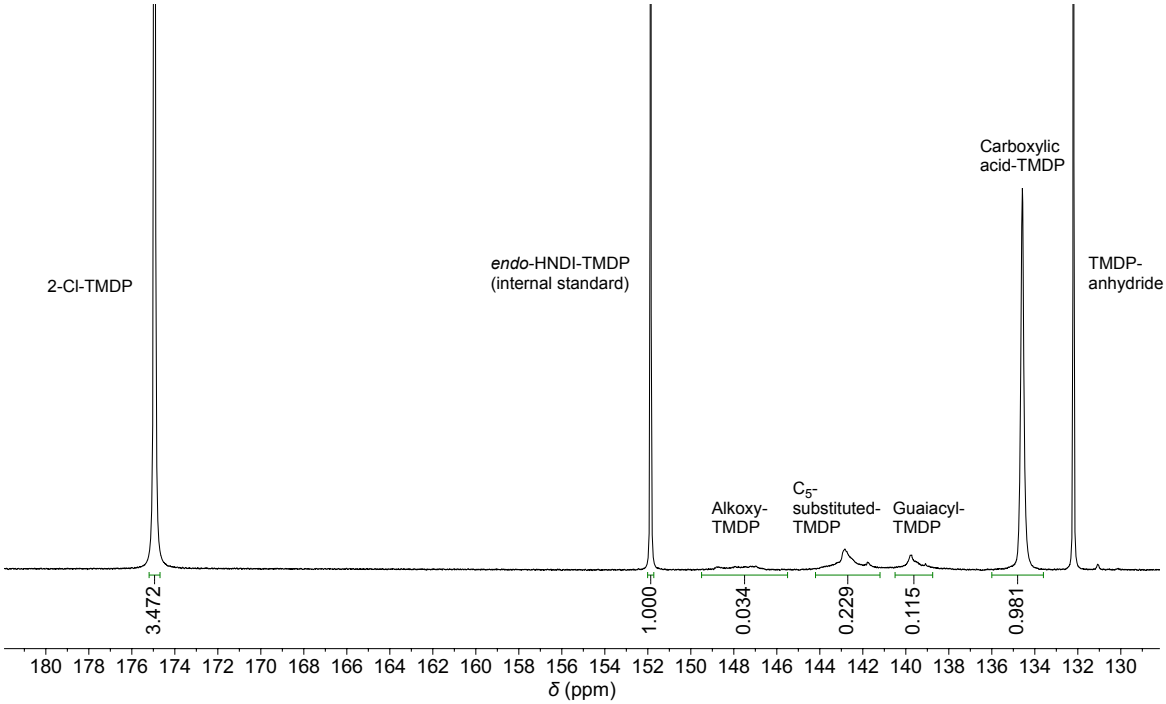

Figure 6.142: ^{31}P NMR spectrum of phosphitylated **Lignin 1.15**. The calculated Degree of substitution and *OH* and *CO_2H* values are listed above.

Lignin 1.15 was further characterized *via* ^{1}H NMR spectroscopy (Figure 6.143), IR spectroscopy (Figure 6.144) and SEC (Figure 6.145).

SEC (Oligo THF): M_n = 2000 Da, M_w = 8900 Da, $Đ$ = 4.45.

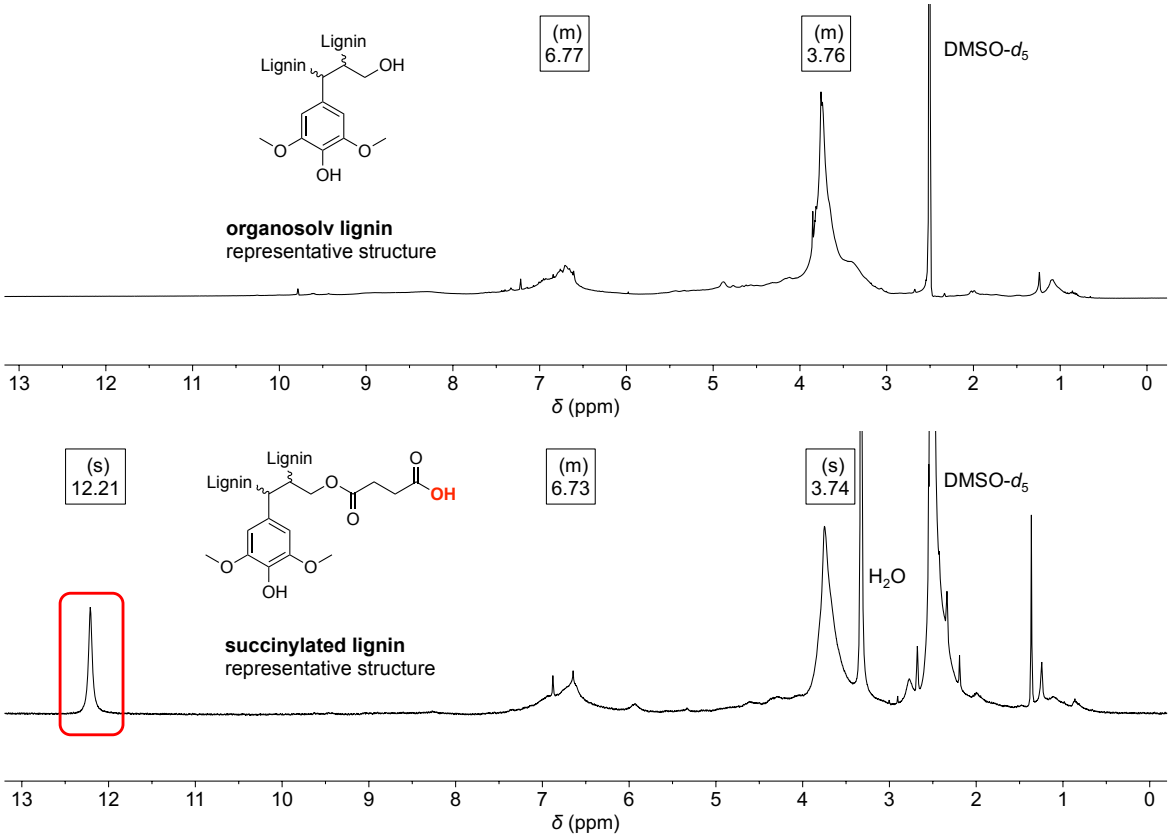

Figure 6.143: ^{1}H NMR spectra (in DMSO-d_6) of organosolv lignin (top) and **Lignin 1.15** (bottom).

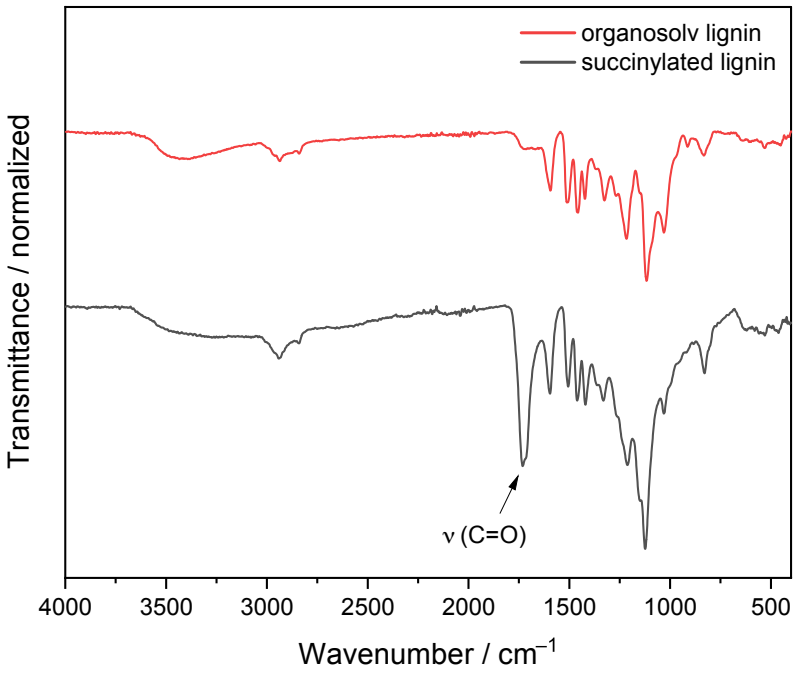

Figure 6.144: IR spectra of organosolv lignin (top) and **Lignin 1.15** (bottom).

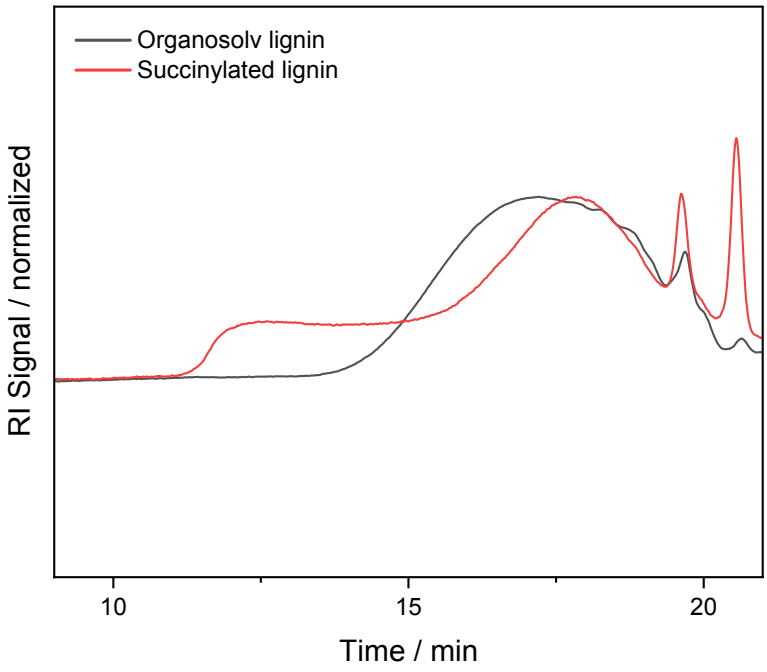

Figure 6.145: SEC (Oligo THF) measurements of organosolv lignin and **Lignin 1.15**.

6.15.8 Large Scale reaction of functionalization of organosolv lignin with succinic anhydride in solution (Lignin 1.16)

Succinic anhydride (98% purity, 5.58 g, 54.6 mmol, 1.00 equiv.) was dissolved in Me-THF (133 ml, 75 mg ml^{-1} lignin concentration) and heated to 80 °C. Then, organosolv lignin (10.0 g, **54.6 mmol OH**, 1.00 equiv.) was added portion wise. After complete dissolution of lignin, the mixture was stirred for further 18 h at 80 °C. After cooling down to room temperature the mixture was added dropwise to the 15-fold volume of water (2.00 l) to precipitate functionalized lignin and simultaneously remove succinic anhydride. The precipitated lignin was isolated by filtration and dried under reduced pressure (20 mbar) at 50 °C to obtain 10.3 g product.

The degree of functionalization (DS) and the amount of hydroxyl and carboxylic acid groups per mg of sample were determined *via* ^{31}P NMR spectroscopy (see chapters 6.15.2 and 6.15.4):

DS = 34.1%
CO_2H_{sample} = 1.27 µmol mg^{-1}
OH_{sample} = 3.03 µmol mg^{-1}
$OH_{Aliphatic}$ = 1.37 µmol mg^{-1}
$OH_{Aromatic}$ = 1.66 µmol mg^{-1}
$OH_{C5\text{-}Substituted}$ = 1.11 µmol mg^{-1}
$OH_{Guaiacyl}$ = 0.550 µmol mg^{-1}
CO_2H and OH_{sample} = 4.30 µmol mg^{-1}

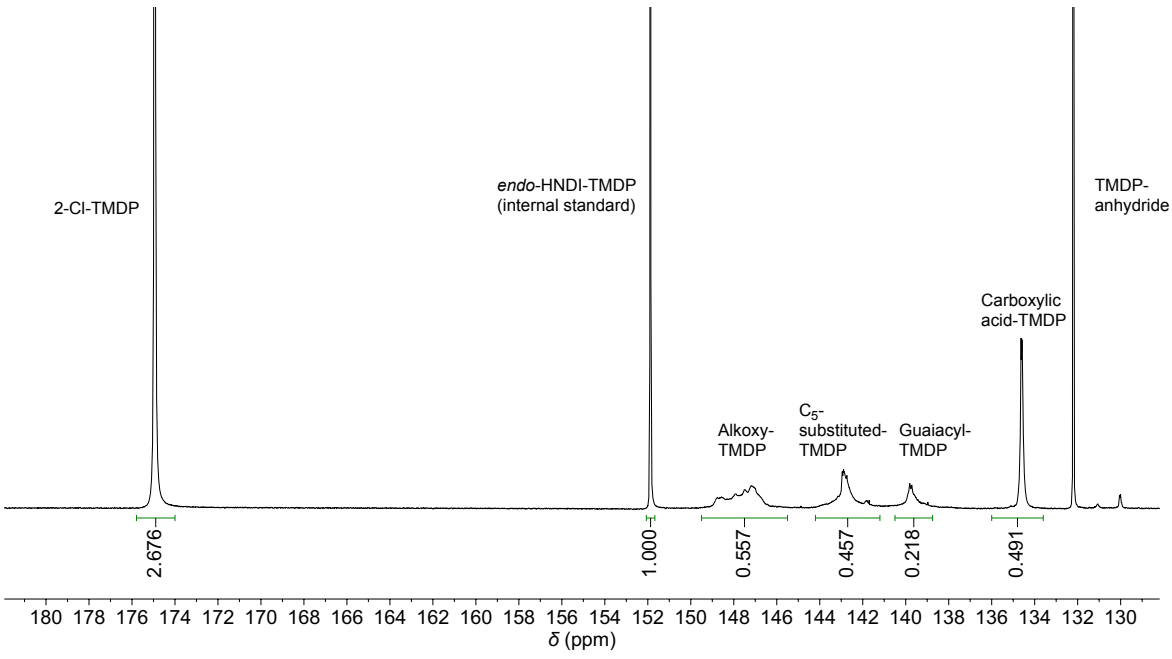

Figure 6.146: ^{31}P NMR spectrum of phosphitylated **Lignin 1.16**. The calculated Degree of substitution and *OH* and *CO_2H* values are listed above.

Lignin 1.16 was further characterized *via* ^{1}H NMR spectroscopy (Figure 6.147), IR spectroscopy (Figure 6.148) and SEC (Figure 6.149).

SEC (Oligo THF): M_n = 2200 Da, M_w = 6500 Da, $Đ$ = 2.95.

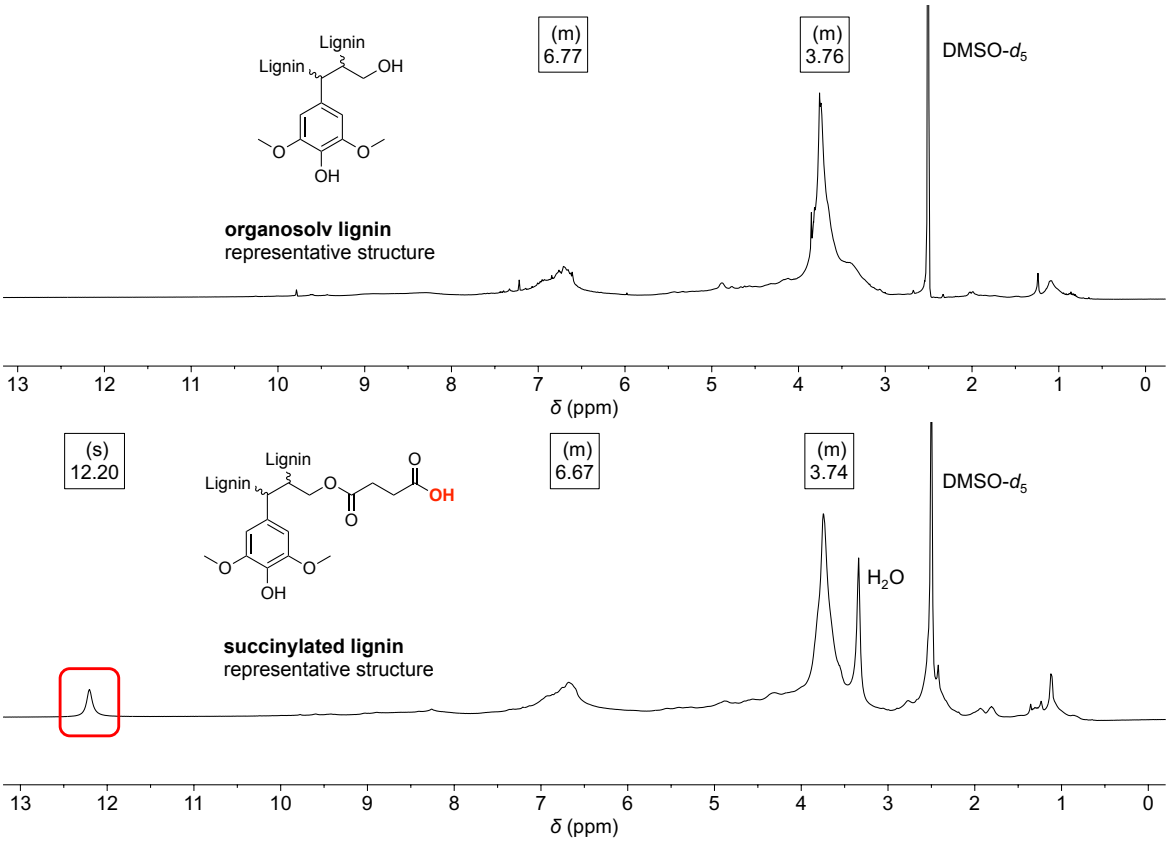

Figure 6.147: ^{1}H NMR spectra (in DMSO-d_6) of organosolv lignin (top) and **Lignin 1.16** (bottom).

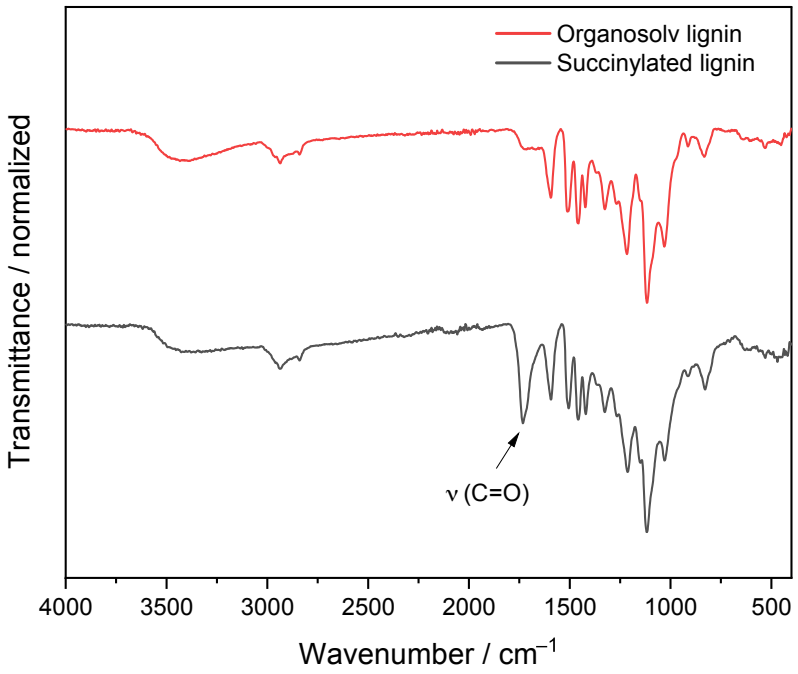

Figure 6.148: IR spectra of organosolv lignin (top) and **Lignin 1.16** (bottom).

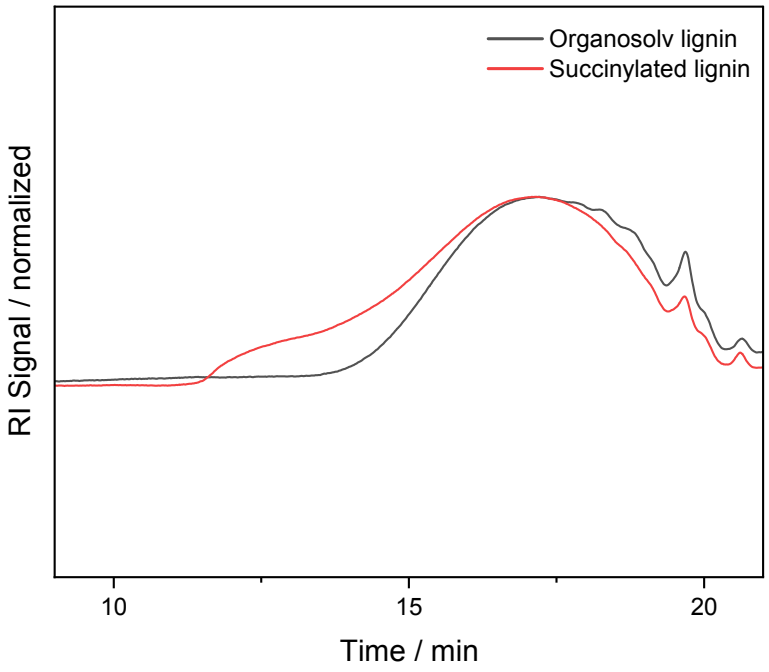

Figure 6.149: SEC (Oligo THF) measurements of organosolv lignin and **Lignin 1.16**.

6.15.9 Hydroxyethylation of lignin (Lignin 1.17)

Ethylene carbonate (180 g, 2.04 mol, 7.50 equiv.) and potassium carbonate (3.77 g, 27.3 mmol, 10.0 mol%) were heated to 90 °C. Then, organosolv lignin (50.0 g, **273 mmol OH**, 1.00 equiv.) was added portion wise. After complete dissolution of lignin, the mixture was stirred for another 4 h at 90 °C. After cooling to room temperature, the mixture was diluted with tetrahydrofuran (50 ml) and added dropwise to 0.01 molar hydrochloric acid (4.00 l) to precipitate functionalized lignin and simultaneously remove ethylene carbonate. The precipitated lignin was isolated by filtration and dried under reduced pressure (20 mbar) at 50 °C to obtain 51.4 g of product.

The amount of hydroxyl and carboxylic acid groups per mg of sample were determined *via* ^{31}P NMR spectroscopy (see chapters 6.15.2 and 6.15.4):

CO_2H_{sample} = 0.04 µmol mg^{-1}
OH_{sample} = 3.85 µmol mg^{-1}
$OH_{Aliphatic}$ = 3.80 µmol mg^{-1}
$OH_{Aromatic}$ = 0.05 µmol mg^{-1}
$OH_{C5\text{-}Substituted}$ = 0.05 µmol mg^{-1}
$OH_{Guaiacyl}$ = 0.00 µmol mg^{-1}
CO_2H and OH_{sample} = 3.89 µmol mg^{-1}

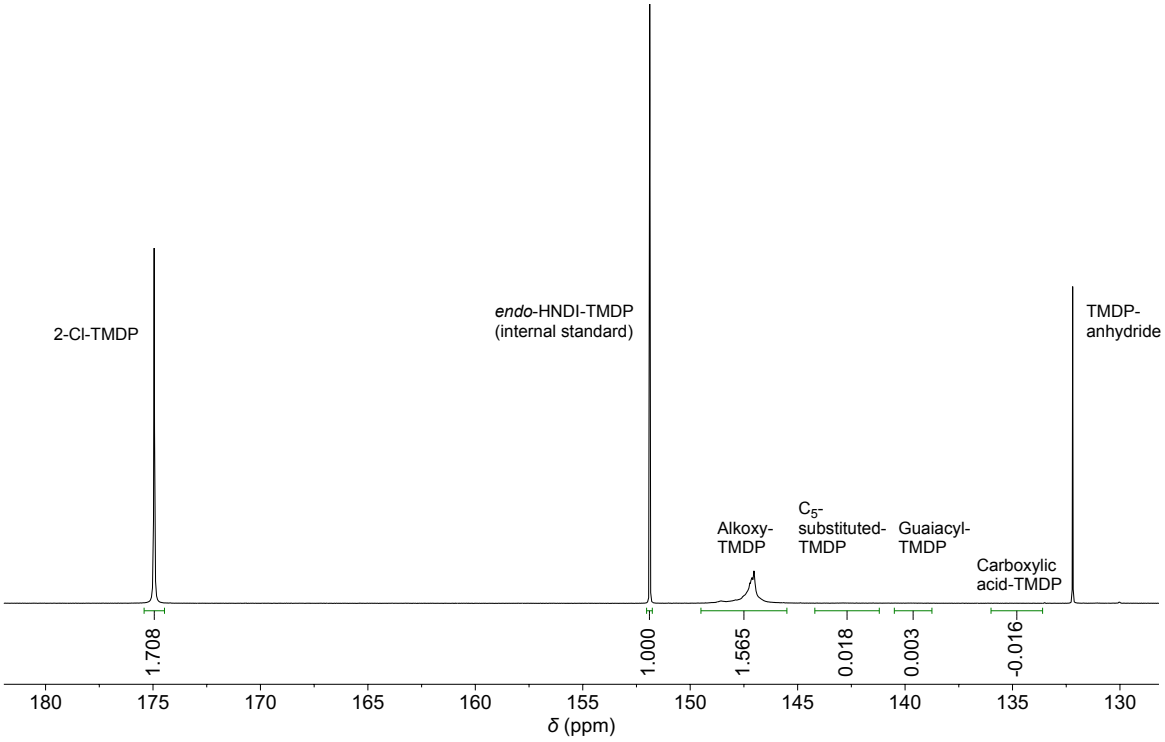

Figure 6.150: ^{31}P NMR spectrum of phosphitylated **Lignin 1.17**. The calculated *OH* and *CO_2H* values are listed above.

Lignin 1.17 was further characterized *via* ^{1}H NMR spectroscopy (Figure 6.147), IR spectroscopy (Figure 6.148) and SEC (Figure 6.149).

SEC (Oligo THF): M_n = 1100 Da, M_w = 3000 Da, $Đ$ = 2.67.

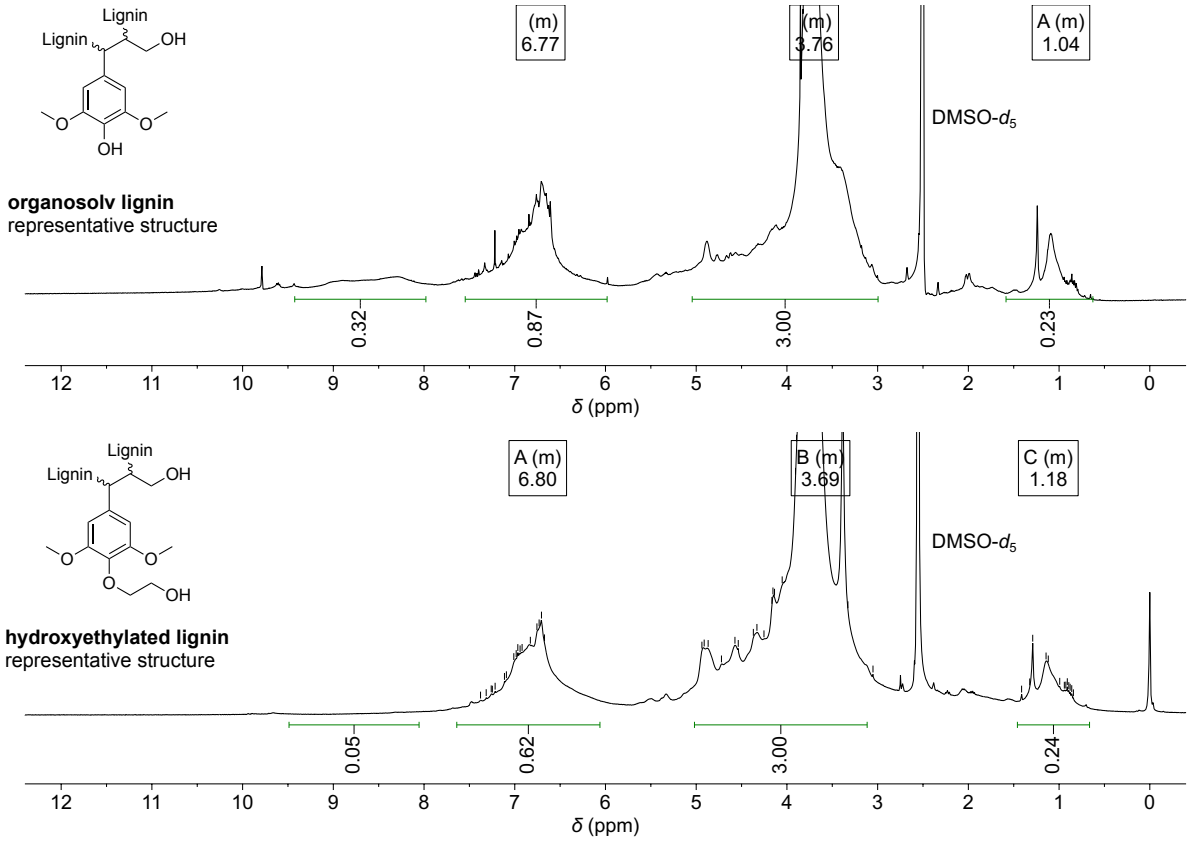

Figure 6.151: ^{1}H NMR spectra (in DMSO-d_6) of organosolv lignin (top) and **Lignin 1.17** (bottom).

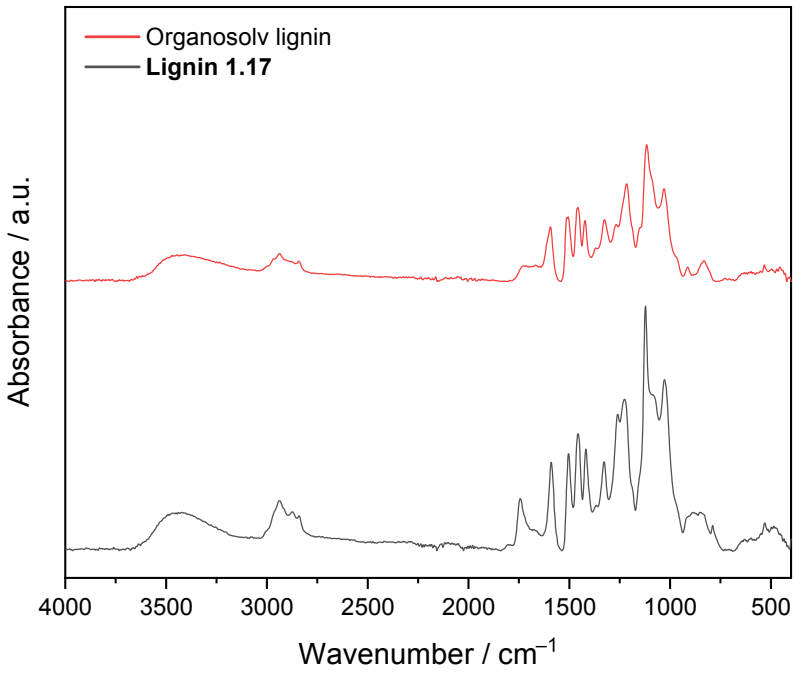

Figure 6.152: IR spectra of organosolv lignin (top) and **Lignin 1.17** (bottom).

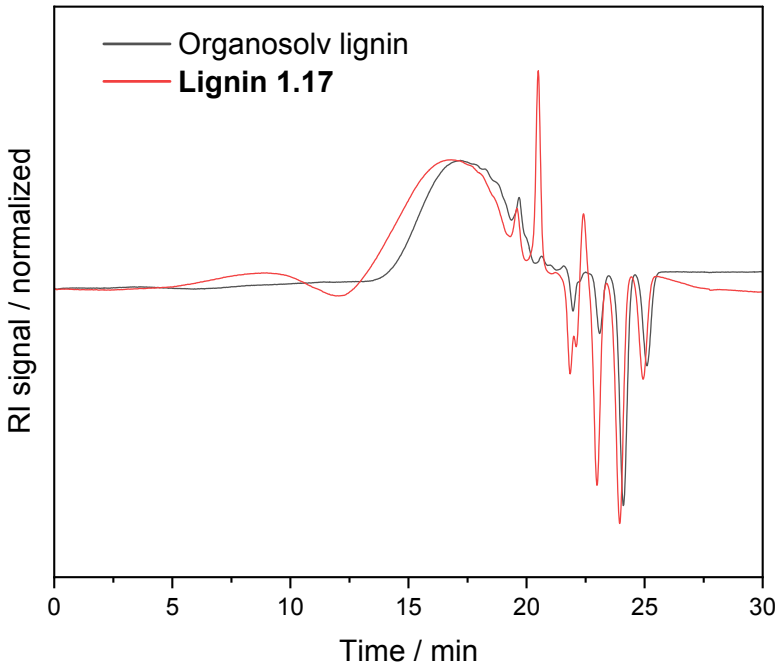

Figure 6.153: SEC (Oligo THF) measurements of organosolv lignin and **Lignin 1.17**.

6.15.10 Succinylation of hydroxyethylated lignin (Lignin 1.18)

Hydroxyethylated lignin (1.00 g, **3.85 mmol OH**, 1.00 equiv.) was added portion wise to molten succinic anhydride (98% purity, 3.93 g, 38.5 mmol, 10.0 equiv.), while vigorously stirring. After complete dissolution of lignin, the mixture was stirred for 2 h at 150 °C. After cooling to room temperature, the solidified mixture was dissolved in tetrahydrofuran (30 ml) and precipitated in the 15-fold volume of water (450 ml) to remove succinic anhydride. The precipitated lignin was isolated by filtration and dried under reduced pressure (20 mbar) at 50 °C to obtain 1.25 g product.

The degree of functionalization (DS) and the amount of hydroxyl and carboxylic acid groups per mg of sample were determined *via* ^{31}P NMR spectroscopy (see chapters 6.15.2 and 6.15.4):

DS = 99.6%
CO_2H_{sample} = 2.85 µmol mg^{-1}
OH_{sample} = 0.01 µmol mg^{-1}
$OH_{Aliphatic}$ = 0.00 µmol mg^{-1}
$OH_{Aromatic}$ = 0.01 µmol mg^{-1}
$OH_{C5\text{-}Substituted}$ = 0.01 µmol mg^{-1}
$OH_{Guaiacyl}$ = 0.00 µmol mg^{-1}
CO_2H and OH_{sample} = 2.86 µmol mg^{-1}

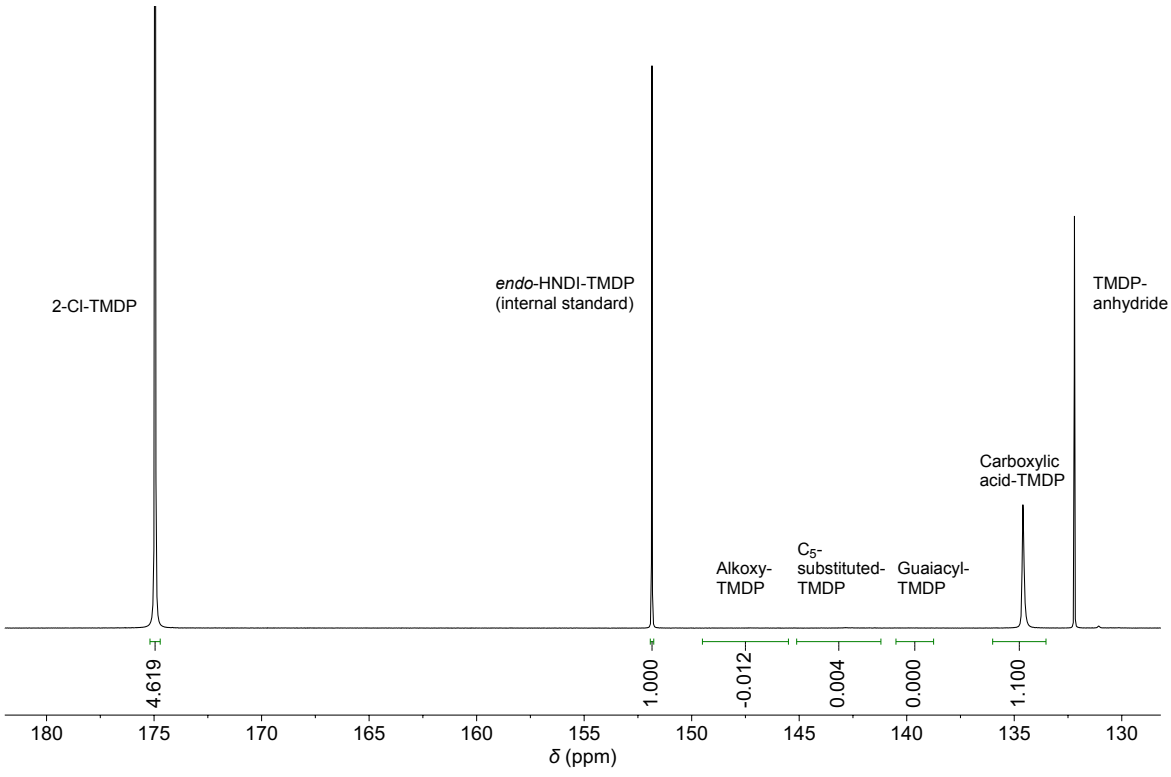

Figure 6.154: ^{31}P NMR spectrum of phosphitylated **Lignin 1.18**. The calculated Degree of substitution and *OH* and *CO_2H* values are listed above.

Lignin 1.18 was further characterized *via* ^{1}H NMR spectroscopy (Figure 6.155), IR spectroscopy (Figure 6.156) and SEC (Figure 6.157).

SEC (Oligo THF): M_n = 1100 Da, M_w = 3000 Da, $Đ$ = 2.67.

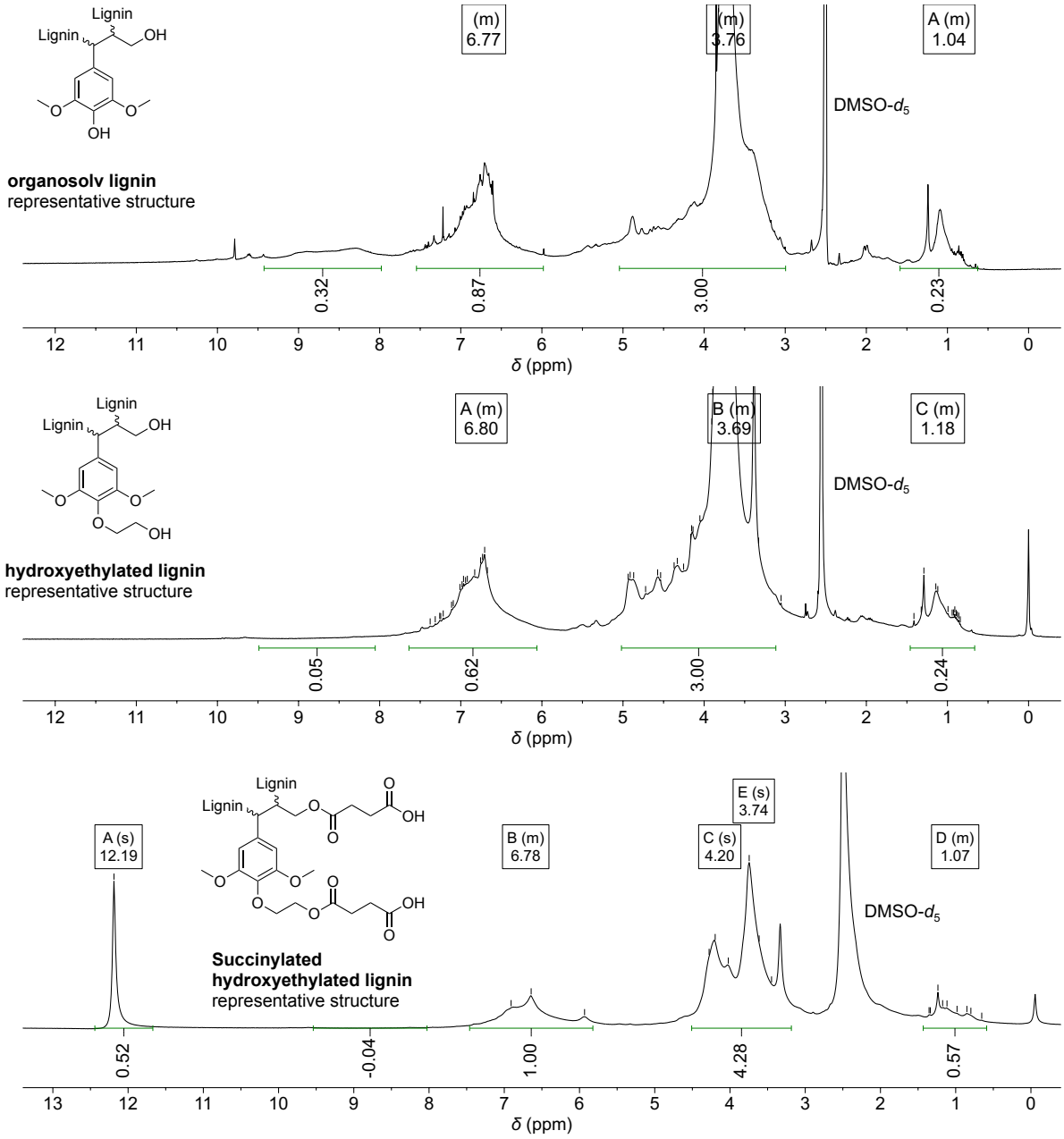

Figure 6.155: Stacked ^{1}H NMR spectra (in DMSO-d_6) of organosolv lignin (top), **Lignin 1.17** (middle) and **Lignin 1.18** (bottom).

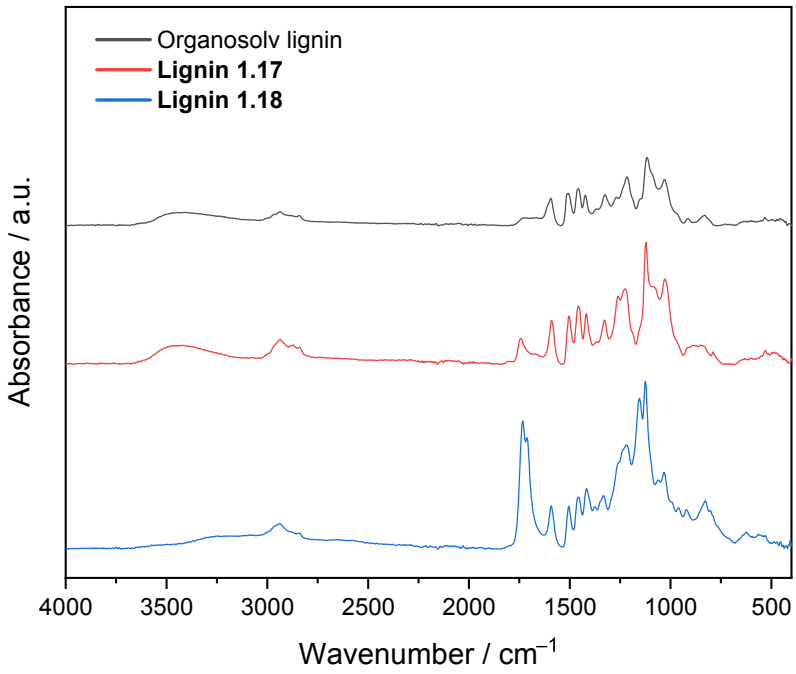

Figure 6.156: Stacked IR spectra of organosolv lignin (top), **Lignin 1.17** (middle) and **Lignin 1.18** (bottom).

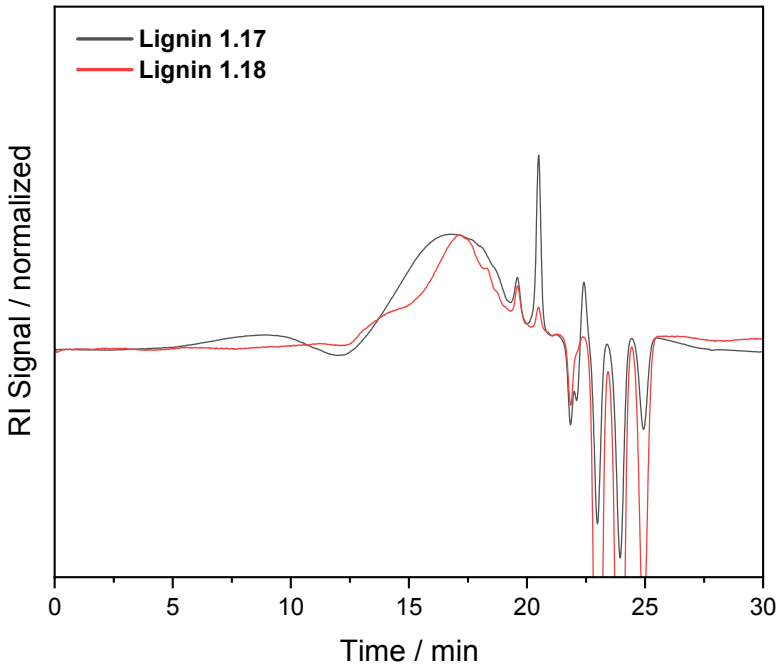

Figure 6.157: SEC (Oligo THF) measurements of **Lignin 1.17** and **Lignin 1.18**.

6.15.11 Synthesis of a P-3CR thermoset from succinylated Lignin 1.18

Succinylated **Lignin 1.18** (200 mg, **567 µmol OH**, 1.00 equiv.) was added to a 10 ml screw-cap vial and dissolved in 2-methyltetrahydrofuran (1.20 ml). Nonanal (80.7 mg, 567 µmol, 1.00 equiv.) and 1,9-diisocyanononane (50.5 mg, 284 µmol, 0.50 equiv.) were added into a separate vial and dissolved in 2-methyltetrahydrofuran (300 µl). The solution of aldehyde and isocyanide was then added to the succinylated lignin solution under vigorous stirring to achieve a homogeneous solution. The solution was casted into a Teflon mold and cured at room temperature for 48 h until the solvent 2-methyltetrahydrofuran had completely evaporated to obtain 260 mg of polymer in form of a black solid.

Gel-content (Me-THF): 95%

DSC (−70 °C to 200 °C, 10 K min^{-1}): T_g: 59 °C.

IR (ATR, cm^{-1}): $\tilde{\nu}$ = 3403 (vw), 3298 (vw), 2924 (m), 2854 (w), 1737 (vs), 1659 (m), 1592 (w), 1536 (w), 1507 (w), 1459 (w), 1418 (w), 1373 (w), 1349 (w), 1332 (w), 1259 (m), 1235 (s), 1214 (s), 1186 (m), 1150 (vs), 1126 (vs), 1067 (m), 1034 (m), 969 (w), 922 (w), 885 (vw), 854 (vw), 829 (vw), 806 (vw), 722 (vw).

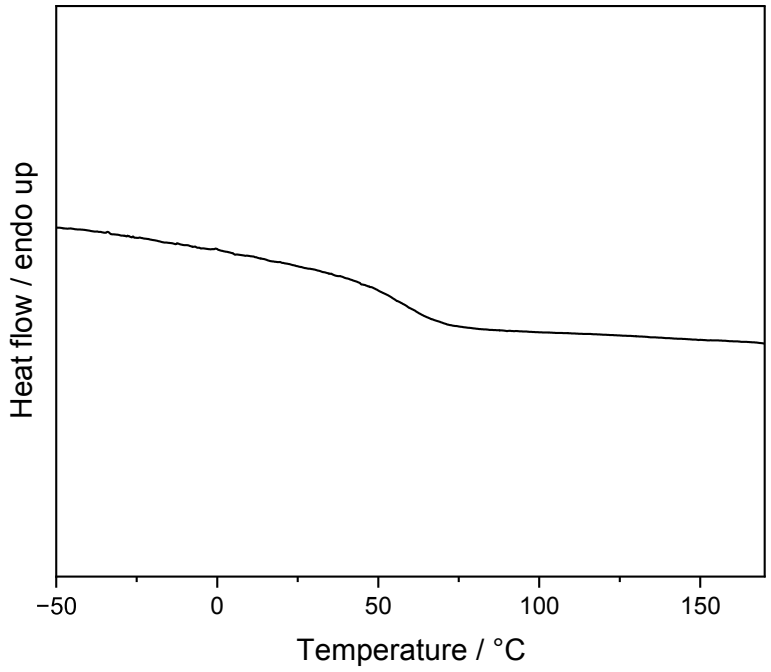

Figure 6.158: DSC measurement of P-3CR thermoset made from **Lignin 1.18**, nonanal, and 1,9-diisocyanononane.

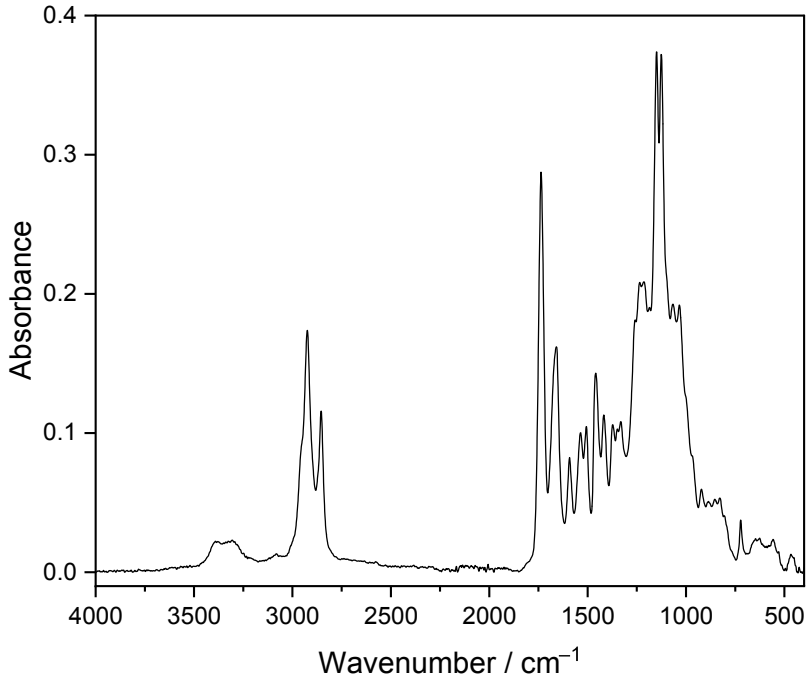

Figure 6.159: IR spectrum of P-3CR thermoset made from **Lignin 1.18**, nonanal, and 1,9-diisocyanononane.

6.15.12 SEC data of all lignin functionalizations

Table 6.23: SEC (Oligo THF) data of all lignin functionalizations.

Sample	M_n / Da	M_w / Da	$Đ$
Organosolv Lignin	800	1100	1.50
Lignin 1.1	1000	1100	1.68
Lignin 1.2	1000	1100	1.11
Lignin 1.3	900	1100	1.14
Lignin 1.4	1000	1200	1.16
Lignin 1.5	2800	25000	9.01
Lignin 1.6	2900	28100	9.56
Lignin 1.7	2900	26000	8.95
Lignin 1.8	2200	4100	1.83
Lignin 1.9	1900	3500	1.83
Lignin 1.10	2000	4200	2.09
Lignin 1.11	2000	3500	1.73
Lignin 1.12	2100	4700	2.27
Lignin 1.13	2100	5500	2.58
Lignin 1.14	2200	5800	2.67
Lignin 1.15	2000	8900	4.40
Lignin 1.16	2200	6500	2.98
Lignin 1.17	1100	3000	2.67
Lignin 1.18	1100	3000	2.67

7 Bibliography

[1] C. Okkerse, H. van Bekkum, *Green Chem.* **1999**, *1*, 107-114.

[2] P. Gallezot, *Chem. Soc. Rev.* **2012**, *41*, 1538-1558.

[3] R. Mülhaupt, *Macromol. Chem. Phys.* **2013**, *214*, 159-174.

[4] The World Commision on Environment and Development, *Our Common Future*, Oxford University Press, Oxford, **1987**.

[5] P. T. Anastas, J. C. Warner, *Green Chemistry: Theory and Practice*, Oxford University Press, New York, **1998**.

[6] P. T. Anastas, J. B. Zimmerman, *Environ. Sci. Technol.* **2003**, *37*, 94A-101A.

[7] S. Y. Tang, R. A. Bourne, R. L. Smith, M. Poliakoff, *Green Chem.* **2008**, *10*, 268-269.

[8] T. Keijer, V. Bakker, J. C. Slootweg, *Nat. Chem.* **2019**, *11*, 190-195.

[9] K. Kümmerer, J. H. Clark, V. G. Zuin, *Science* **2020**, *367*, 369-370.

[10] PlasticsEurope Deutschland e. V., *Plastics – the fast Facts 2023*, **2023**, https://plasticseurope.org/knowledge-hub/plastics-the-fast-facts-2023/; access date: 07.11.2024.

[11] D. Lithner, Å. Larsson, G. Dave, *Sci. Total Environ.* **2011**, *409*, 3309-3324.

[12] P. T. Anastas, M. M. Kirchhoff, *Acc. Chem. Res.* **2002**, *35*, 686-694.

[13] R. L. Carson, *Silent Spring*, Houghton Mifflin, Boston, **1962**.

[14] B. A. Rattner, *Ecotoxicology* **2009**, *18*, 773-783.

[15] P. T. Anastas, C. A. Farris, *Benign by Design: Alternative Synthetic Design for Pollution Prevention*, ACS Symposium Series 577, American Chemical Society, Washington, DC, **1994**.

[16] P. T. Anastas, T. C. Williamson, *Green Chemistry: Designing Chemistry for the Environment*, ACS Symposium Series 626 Washington, DC, **1996**.

[17] P. Anastas, N. Eghbali, *Chem. Soc. Rev.* **2010**, *39*, 301-312.

[18] S. L. Y. Tang, R. L. Smith, M. Poliakoff, *Green Chem.* **2005**, *7*, 761-762.

[19] Andrew P. Dicks, A. Hent, *Green Chemistry Metrics: A Guide to Determining and Evaluating Process Greenness*, Springer Cham, Heidelberg, **2015**.

[20] R. A. Sheldon, *ACS Sustainable Chem. Eng.* **2018**, *6*, 32-48.

[21] J. Andraos, *Org. Process Res. Dev.* **2005**, *9*, 404-431.

[22] B. M. Trost, *Science* **1991**, *254*, 1471-1477.

[23] B. M. Trost, *Angew. Chem. Int. Ed. Engl.* **1995**, *34*, 259-281.

[24] B. M. Trost, *Acc. Chem. Res.* **2002**, *35*, 695-705.

[25] A. Maercker, in *Org. React.*, **2011**, pp. 270-490.

[26] R. A. Sheldon, *Chem. Ind. (London)* **1992**, 903-906.

[27] R. A. Sheldon, *Green Chem.* **2007**, *9*, 1273-1283.

[28] R. A. Sheldon, *Chem. Commun.* **2008**, 3352-3365.

[29] R. A. Sheldon, *Green Chem.* **2017**, *19*, 18-43.

[30] F. Roschangar, R. A. Sheldon, C. H. Senanayake, *Green Chem.* **2015**, *17*, 752-768.

[31] R. A. Sheldon, in *Industrial Environmental Chemistry*, Ed.: D. T. Sawyer, A. E. Martell, Plenum Press, New York, **1992**, pp. 99-119.

[32] R. A. Sheldon, in *Precision Process Technology*, Ed.: M. P. C. Weijnen, A. A. H. Drinkenburg, Kluwer, Dordrecht, **1993**, pp. 125-138.

[33] R. A. Sheldon, *J. Mol. Catal. A: Chem.* **1996**, *107*, 75-83.

[34] P. A. Wender, *Tetrahedron* **2013**, *69*, 7529-7550.

[35] P. A. Wender, V. A. Verma, T. J. Paxton, T. H. Pillow, *Acc. Chem. Res.* **2008**, *41*, 40-49.

[36] F. G. Calvo-Flores, *ChemSusChem* **2009**, *2*, 905-919.

[37] D. J. C. Constable, A. D. Curzons, V. L. Cunningham, *Green Chem.* **2002**, *4*, 521-527.

[38] C. Jimenez-Gonzalez, C. S. Ponder, Q. B. Broxterman, J. B. Manley, *Org. Process Res. Dev.* **2011**, *15*, 912-917.

[39] J. B. Guinée, R. Heijungs, G. Huppes, A. Zamagni, P. Masoni, R. Buonamici, T. Ekvall, T. Rydberg, *Environ. Sci. Technol.* **2011**, *45*, 90-96.

[40] G. Finnveden, M. Z. Hauschild, T. Ekvall, J. Guinée, R. Heijungs, S. Hellweg, A. Koehler, D. Pennington, S. Suh, *J. Environ. Manage.* **2009**, *91*, 1-21.

[41] L. M. Tufvesson, P. Tufvesson, J. M. Woodley, P. Börjesson, *Int. J. Life Cycle Assess.* **2013**, *18*, 431-444.

[42] S. Hellweg, L. Milà i Canals, *Science* **2014**, *344*, 1109-1113.

[43] D. Kralisch, D. Ott, D. Gericke, *Green Chem.* **2015**, *17*, 123-145.

[44] G. Koller, U. Fischer, K. Hungerbühler, *Ind. Eng. Chem. Res.* **2000**, *39*, 960-972.

[45] H. Röper, *Starch - Stärke* **2002**, *54*, 89-99.

[46] Nova-Institut GmbH, *For the first time: Growth rate for bio-based polymers with 8% CAGR far above overall polymer market growth*, **2021**, http://nova-institute.eu/press/?id=237; access date: 09.28.2021.

[47] E. S. Lipinsky, *Science* **1981**, *212*, 1465-1471.

[48] D. R. Dodds, R. A. Gross, *Science* **2007**, *318*, 1250-1251.

[49] F. Cherubini, *Energy Convers. Manage.* **2010**, *51*, 1412-1421.

[50] Ó. J. Sánchez, C. A. Cardona, *Bioresour. Technol.* **2008**, *99*, 5270-5295.

[51] L. Avérous, in *Monomers, Polymers and Composites from Renewable Resources*, Ed.: M. N. Belgacem, A. Gandini, Elsevier, Amsterdam, **2008**, pp. 433-450.

[52] Y. Zhu, C. Romain, C. K. Williams, *Nature* **2016**, *540*, 354-362.

[53] J. Liu, S. Willför, C. Xu, *Bioact. Carbohydr. Diet. Fibre* **2015**, *5*, 31-61.

[54] J. A. Galbis, M. d. G. García-Martín, M. V. de Paz, E. Galbis, *Chem. Rev.* **2016**, *116*, 1600-1636.

[55] G.-Q. Chen, M. K. Patel, *Chem. Rev.* **2012**, *112*, 2082-2099.

[56] T. Werpy, G. Petersen, *Top Value Added Chemicals from Biomass: Volume I -- Results of Screening for Potential Candidates from Sugars and Synthesis Gas*, **2004**.

[57] J. J. Bozell, G. R. Petersen, *Green Chem.* **2010**, *12*, 539-554.

[58] S. K. Burgess, J. E. Leisen, B. E. Kraftschik, C. R. Mubarak, R. M. Kriegel, W. J. Koros, *Macromolecules* **2014**, *47*, 1383-1391.

[59] Avantium, *Avantium Celebrates the Official Opening of its FDCA Flagship Plant*, **2024**, https://newsroom.avantium.com/avantium-celebrates-the-official-opening-of-its-fdca-flagship-plant/; access date: 20.12.2024.

[60] D. S. Bajwa, G. Pourhashem, A. H. Ullah, S. G. Bajwa, *Ind. Crops Prod.* **2019**, *139*, 111526.

[61] M. Abhilash, D. Thomas, in *Biopolymer Composites in Electronics*, Ed.: K. K. Sadasivuni, D. Ponnamma, J. Kim, J. J. Cabibihan, M. A. AlMaadeed, Elsevier, **2017**, pp. 405-435.

[62] G. Gellerstedt, G. Henriksson, in *Monomers, Polymers and Composites from Renewable Resources*, Ed.: M. N. Belgacem, A. Gandini, Elsevier, Amsterdam, **2008**, pp. 201-224.

[63] J. Zakzeski, P. C. A. Bruijnincx, A. L. Jongerius, B. M. Weckhuysen, *Chem. Rev.* **2010**, *110*, 3552-3599.

[64] H.-R. Bjørsvik, F. Minisci, *Org. Process Res. Dev.* **1999**, *3*, 330-340.

[65] X. Si, J. Chen, F. Lu, X. Liu, Y. Ren, R. Lu, H. Jiang, H. Liu, S. Miao, Y. Zhu, X. Luo, J. Xu, *ACS Sustainable Chem. Eng.* **2019**, *7*, 19034-19041.

[66] M. P. Pandey, C. S. Kim, *Chem. Eng. Technol.* **2011**, *34*, 29-41.

[67] C. O. Tuck, E. Pérez, I. T. Horváth, R. A. Sheldon, M. Poliakoff, *Science* **2012**, *337*, 695-699.

[68] R. J. Khan, C. Y. Lau, J. Guan, C. H. Lam, J. Zhao, Y. Ji, H. Wang, J. Xu, D.-J. Lee, S.-Y. Leu, *Bioresour. Technol.* **2022**, *346*, 126419.

[69] D. Kai, M. J. Tan, P. L. Chee, Y. K. Chua, Y. L. Yap, X. J. Loh, *Green Chem.* **2016**, *18*, 1175-1200.

[70] C. Libretti, L. Santos Correa, M. A. R. Meier, *Green Chem.* **2024**, *26*, 4358-4386.

[71] S. Sen, S. Patil, D. S. Argyropoulos, *Green Chem.* **2015**, *17*, 4862-4887.

[72] L. C. Over, E. Grau, S. Grelier, M. A. R. Meier, H. Cramail, *Macromol. Chem. Phys.* **2017**, *218*, 1600411.

[73] J. Xin, M. Li, R. Li, M. P. Wolcott, J. Zhang, *ACS Sustainable Chem. Eng.* **2016**, *4*, 2754-2761.

[74] S. Laurichesse, C. Huillet, L. Avérous, *Green Chem.* **2014**, *16*, 3958-3970.

[75] M. Kurańska, J. A. Pinto, K. Salach, M. F. Barreiro, A. Prociak, *Ind. Crops Prod.* **2020**, *143*, 111882.

[76] L. Ruzicka, *Experientia* **1953**, *9*, 357-367.

[77] G. P. Moss, P. A. S. Smith, D. Tavernier, *Pure Appl. Chem.* **1995**, *67*, 1307-1375.

[78] E. Breitmaier, *Terpenes: Flavors, Fragrances, Pharmaca, Pheromones*, WILEY-VCH Verlag GmbH & Co. KGaA, Weinheim, **2006**.

[79] T. J. Maimone, P. S. Baran, *Nat. Chem. Biol.* **2007**, *3*, 396-407.

[80] W. Schwab, C. Fuchs, F.-C. Huang, *Eur. J. Lipid Sci. Technol.* **2013**, *115*, 3-8.

[81] A. Gandini, T. M. Lacerda, *Prog. Polym. Sci.* **2015**, *48*, 1-39.

[82] J. G. Speight, *Chemical and Process Design Handbook*, The McGraw-Hill Companies, New York, **2002**.

[83] A. J. D. Silvestre, A. Gandini, in *Monomers, Polymers and Composites from Renewable Resources*, Ed.: M. N. Belgacem, A. Gandini, Elsevier, Amsterdam, **2008**, pp. 17–38.

[84] F. M. Kerton, in *Alternative Solvents for Green Chemistry*, Ed.: J. H. Clark, G. A. Kraus, RSC Green Chemistry Book Series, The Royal Society of Chemistry, Cambridge, **2009**, pp. 97–117.

[85] A. Severino, J. Vital, L. S. Lobo, *Stud. Surf. Sci. Catal.* **1993**, *78*, 685-692.

[86] I. L. Simakova, Y. S. Solkina, B. L. Moroz, O. A. Simakova, S. I. Reshetnikov, I. P. Prosvirin, V. I. Bukhtiyarov, V. N. Parmon, D. Y. Murzin, *Appl. Catal., A* **2010**, *385*, 136-143.

[87] A. Corma, S. Iborra, A. Velty, *Chem. Rev.* **2007**, *107*, 2411-2502.

[88] S. D. Tetali, *Planta* **2019**, *249*, 1-8.

[89] M. S. I. El Alami, M. A. El Amrani, F. Agbossou-Niedercorn, I. Suisse, A. Mortreux, *Chem. Eur. J.* **2015**, *21*, 1398-1413.

[90] F. C. M. Scheelje, F. C. Destaso, H. Cramail, M. A. R. Meier, *Macromol. Chem. Phys.* **2023**, *224*, 2200403.

[91] P. A. Wilbon, F. Chu, C. Tang, *Macromol. Rapid Commun.* **2013**, *34*, 8-37.

[92] M. Winnacker, B. Rieger, *ChemSusChem* **2015**, *8*, 2455-2471.

[93] F. Della Monica, A. W. Kleij, *Polym. Chem.* **2020**, *11*, 5109-5127.

[94] *The Lipid Handbook*, Ed.: F. D. Gunstone, J. L. Harwood, A. J. Dijkstra, Taylor & Francis Group, LLC, New York, **2007**.

[95] M. A. R. Meier, J. O. Metzger, U. S. Schubert, *Chem. Soc. Rev.* **2007**, *36*, 1788-1802.

[96] *Fatty Acids: Chemistry, Synthesis, and Applications*, Ed.: Moghis U. Ahmad, Elsevier Inc., London, United Kingdom, **2017**.

[97] A. Fitton, K. L. Goa, *Drugs* **1991**, *41*, 780-798.

[98] R. Uppar, P. Dinesha, S. Kumar, *Environment, Development and Sustainability* **2023**, *25*, 9011-9046.

[99] P. Foley, A. Kermanshahi pour, E. S. Beach, J. B. Zimmerman, *Chem. Soc. Rev.* **2012**, *41*, 1499-1518.

[100] M. Alam, D. Akram, E. Sharmin, F. Zafar, S. Ahmad, *Arabian Journal of Chemistry* **2014**, *7*, 469-479.

[101] A. Hofland, *Prog. Org. Coat.* **2012**, *73*, 274-282.

[102] U. Poth, in *Ullmann's Encyclopedia of Industrial Chemistry*, **2001**.

[103] U. Biermann, U. T. Bornscheuer, I. Feussner, M. A. R. Meier, J. O. Metzger, *Angew. Chem. Int. Ed.* **2021**, *60*, 20144-20165.

[104] R. Halim, M. K. Danquah, P. A. Webley, *Biotechnol. Adv.* **2012**, *30*, 709-732.

[105] N. Pragya, K. K. Pandey, P. K. Sahoo, *Renewable Sustainable Energy Rev.* **2013**, *24*, 159-171.

[106] Z. Xue, F. Wan, W. Yu, J. Liu, Z. Zhang, X. Kou, *Eur. J. Lipid Sci. Technol.* **2018**, *120*, 1700428.

[107] A. Beopoulos, J.-M. Nicaud, *OCL* **2012**, *19*, 22-28.

[108] S. Papanikolaou, G. Aggelis, *Eur. J. Lipid Sci. Technol.* **2011**, *113*, 1052-1073.

[109] K. V. Probst, L. R. Schulte, T. P. Durrett, M. E. Rezac, P. V. Vadlani, *Crit. Rev. Biotechnol.* **2016**, *36*, 942-955.

[110] F. D. Gunstone, *Fatty Acid and Lipid Chemistry*, Springer Science+Business Media Dordrecht, New York, **1996**.

[111] Y. Chisti, *Biotechnol. Adv.* **2007**, *25*, 294-306.

[112] T. M. Mata, A. A. Martins, N. S. Caetano, *Renewable Sustainable Energy Rev.* **2010**, *14*, 217-232.

[113] M. A. R. Meier, *Macromol. Rapid Commun.* **2019**, *40*, 1800524.

[114] C. E. Hoyle, C. N. Bowman, *Angew. Chem. Int. Ed.* **2010**, *49*, 1540-1573.

[115] M. Firdaus, *Asian J. Org. Chem.* **2017**, *6*, 1702-1714.

[116] O. Türünç, M. A. R. Meier, *Macromol. Rapid Commun.* **2010**, *31*, 1822-1826.

[117] M. Unverferth, M. A. R. Meier, *Eur. J. Lipid Sci. Technol.* **2016**, *118*, 1470-1474.

[118] P. H. Nguyen, S. Spoljaric, J. Seppälä, *Polymer* **2018**, *153*, 183-192.

[119] O. Kreye, S. Oelmann, M. A. R. Meier, *Macromol. Chem. Phys.* **2013**, *214*, 1452-1464.

[120] C. Lluch, G. Lligadas, J. C. Ronda, M. Galià, V. Cadiz, *Macromol. Rapid Commun.* **2011**, *32*, 1343-1351.

[121] A. Sehlinger, R. Schneider, M. A. R. Meier, *Eur. Polym. J.* **2014**, *50*, 150-157.

[122] O. Türünç, M. Firdaus, G. Klein, M. A. R. Meier, *Green Chem.* **2012**, *14*, 2577-2583.

[123] M. A. R. Meier, *Macromol. Chem. Phys.* **2009**, *210*, 1073-1079.

[124] A. Rybak, P. A. Fokou, M. A. R. Meier, *Eur. J. Lipid Sci. Technol.* **2008**, *110*, 797-804.

[125] A. Rybak, M. A. R. Meier, *Green Chem.* **2007**, *9*, 1356-1361.

[126] Y. Schrodi, T. Ung, A. Vargas, G. Mkrtumyan, C. W. Lee, T. M. Champagne, R. L. Pederson, S. H. Hong, *Clean: Soil, Air, Water* **2008**, *36*, 669-673.

[127] K. A. Burdett, L. D. Harris, P. Margl, B. R. Maughon, T. Mokhtar-Zadeh, P. C. Saucier, E. P. Wasserman, *Organometallics* **2004**, *23*, 2027-2047.

[128] B. R. Moser, K. M. Doll, S. C. Peterson, *J. Am. Oil Chem. Soc.* **2019**, *96*, 825-837.

[129] B. R. Moser, K. E. Vermillion, B. N. Banks, K. M. Doll, *J. Am. Oil Chem. Soc.* **2020**, *97*, 517-530.

[130] C. G. Goebel, A. C. Brown, H. F. Oehlschlaeger, R. P. Rolfes, *Method of making azelaic acid*, US 2813113, **1957**.

[131] B. R. Moser, K. M. Doll, N. P. J. Price, *J. Am. Oil Chem. Soc.* **2023**, *100*, 149-162.

[132] B. W. Michel, L. D. Steffens, M. S. Sigman, in *Org. React.*, **2014**, pp. 75-414.

[133] M. Eckert, G. Fleischmann, R. Jira, H. M. Bolt, K. Golka, in *Ullmann's Encyclopedia of Industrial Chemistry*, **2006**.

[134] J. Smidt, W. Hafner, R. Jira, R. Sieber, J. Sedlmeier, A. Sabel, *Angew. Chem. Int. Ed. Engl.* **1962**, *1*, 80-88.

[135] T. Mitsudome, K. Mizumoto, T. Mizugaki, K. Jitsukawa, K. Kaneda, *Angew. Chem. Int. Ed.* **2010**, *49*, 1238-1240.

[136] T. Mitsudome, T. Umetani, N. Nosaka, K. Mori, T. Mizugaki, K. Ebitani, K. Kaneda, *Angew. Chem. Int. Ed.* **2006**, *45*, 481-485.

[137] M. Winkler, M. A. R. Meier, *Green Chem.* **2014**, *16*, 1784-1788.

[138] J. Twilton, C. Le, P. Zhang, M. H. Shaw, R. W. Evans, D. W. C. MacMillan, *Nat. Rev. Chem.* **2017**, *1*.

[139] D. S. Ogunniyi, *Bioresour. Technol.* **2006**, *97*, 1086-1091.

[140] M. Van der Steen, C. V. Stevens, *ChemSusChem* **2009**, *2*, 692-713.

[141] H. Mutlu, M. A. R. Meier, *Eur. J. Lipid Sci. Technol.* **2010**, *112*, 10-30.

[142] X. Mao, Q. Xie, Y. Duan, S. Yu, Y. Nie, *Materials* **2022**, *15*, 1565.

[143] M. Genas, *Angew. Chem.* **1962**, *74*, 535-540.

[144] M. Winnacker, B. Rieger, *Macromol. Rapid Commun.* **2016**, *37*, 1391-1413.

[145] Arkema S. A., *RILSAN® POLYAMIDE 11: A Proven Legacy, an Exciting Future (Rilsan PA11 Brochure)*, https://hpp.arkema.com/en/product-families/rilsan-polyamide-11-resins/download-brochure/; access date: 13.12.2024.

[146] Arkema S. A., *Rilsan® Polyamide 11 (PA-11)*, https://hpp.arkema.com/en/product-families/rilsan-polyamide-11-resins; access date: 13.12.2024.

[147] Arkema S. A., *Rilsan® PA 11 resin – a 70 year legacy*, https://hpp.arkema.com/en/product-families/rilsan-polyamide-11-resins/rilsan-70th-anniversary/; access date: 13.12.2024.

[148] M. von Czapiewski, M. A. R. Meier, *Macromol. Chem. Phys.* **2017**, *218*, 1700153.

[149] H. Mutlu, M. A. R. Meier, *Macromol. Chem. Phys.* **2009**, *210*, 1019-1025.

[150] M. Stemmelen, F. Pessel, V. Lapinte, S. Caillol, J.-P. Habas, J.-J. Robin, *J. Polym. Sci., Part A: Polym. Chem.* **2011**, *49*, 2434-2444.

[151] M. Desroches, S. Caillol, V. Lapinte, R. Auvergne, B. Boutevin, *Macromolecules* **2011**, *44*, 2489-2500.

[152] U. Biermann, J. O. Metzger, M. A. R. Meier, *Macromol. Chem. Phys.* **2010**, *211*, 854-862.

[153] A. Zlatanić, Z. S. Petrović, K. Dušek, *Biomacromolecules* **2002**, *3*, 1048-1056.

[154] N. Boquillon, C. Fringant, *Polymer* **2000**, *41*, 8603-8613.

[155] S. G. Tan, W. S. Chow, *Polymer-Plastics Technology and Engineering* **2010**, *49*, 1581-1590.

[156] R. Auvergne, S. Caillol, G. David, B. Boutevin, J.-P. Pascault, *Chem. Rev.* **2014**, *114*, 1082-1115.

[157] C. Ding, A. S. Matharu, *ACS Sustainable Chem. Eng.* **2014**, *2*, 2217-2236.

[158] E. A. Baroncini, S. Kumar Yadav, G. R. Palmese, J. F. Stanzione III, *J. Appl. Polym. Sci.* **2016**, *133*.

[159] A. Zlatanić, C. Lava, W. Zhang, Z. S. Petrović, *J. Polym. Sci., Part B: Polym. Phys.* **2004**, *42*, 809-819.

[160] Z. S. Petrović, *Polymer Reviews* **2008**, *48*, 109-155.

[161] N. Karak, S. Rana, J. W. Cho, *J. Appl. Polym. Sci.* **2009**, *112*, 736-743.

[162] S. Thakur, N. Karak, *Prog. Org. Coat.* **2013**, *76*, 157-164.

[163] L. D. Antonino, G. E. S. Garcia, J. R. Gouveia, A. N. B. Santos, M. P. da Silva Bisneto, D. J. dos Santos, *J. Appl. Polym. Sci.* **2022**, *139*, e52477.

[164] R. J. Slocombe, E. E. Hardy, J. H. Saunders, R. L. Jenkins, *J. Am. Chem. Soc.* **1950**, *72*, 1888-1891.

[165] H. J. Twitchett, *Chem. Soc. Rev.* **1974**, *3*, 209-230.

[166] J. Wolfs, I. Ribca, M. A. R. Meier, M. Johansson, *ACS Sustainable Chem. Eng.* **2023**, *11*, 3952-3962.

[167] L. Montero de Espinosa, M. A. R. Meier, *Eur. Polym. J.* **2011**, *47*, 837-852.

[168] S. Pandey, B. S. Rajput, S. H. Chikkali, *Green Chem.* **2021**, *23*, 4255-4295.

[169] W. S. Port, J. E. Hansen, E. F. Jordan JR., T. J. Dietz, D. Swern, *J. Polym. Sci.* **1951**, *7*, 207-220.

[170] H. M. Teeter, *J. Am. Oil Chem. Soc.* **1963**, *40*, 143-156.

[171] D. Heinze, T. Mang, C. Popescu, O. Weichold, *Thermochim. Acta* **2016**, *637*, 143-153.

[172] H. Mutlu, M. A. R. Meier, *J. Polym. Sci., Part A: Polym. Chem.* **2010**, *48*, 5899-5906.

[173] G. Çayli, M. A. R. Meier, *Eur. J. Lipid Sci. Technol.* **2008**, *110*, 853-859.

[174] N. Kolb, M. A. R. Meier, *Green Chem.* **2012**, *14*, 2429-2435.

[175] R. R. Briese, S. M. McElvain, *J. Am. Chem. Soc.* **1933**, *55*, 1697-1700.

[176] N. Kolb, M. A. R. Meier, *Eur. Polym. J.* **2013**, *49*, 843-852.

[177] L. Maisonneuve, A.-L. Wirotius, C. Alfos, E. Grau, H. Cramail, *Polym. Chem.* **2014**, *5*, 6142-6147.

[178] R. Quermann, R. Maletz, H. J. Schäfer, *Liebigs Ann. Chem.* **1993**, *1993*, 1219-1223.

[179] T. Hirao, *J. Org. Chem.* **2019**, *84*, 1687-1692.

[180] S. Gnaim, J. C. Vantourout, F. Serpier, P.-G. Echeverria, P. S. Baran, *ACS Catalysis* **2021**, *11*, 883-892.

[181] P.-F. Dai, Q.-Q. Li, J.-P. Qu, Y.-B. Kang, *Synthesis* **2024**, *56*, 2213-2222.

[182] Q.-Q. Li, P.-F. Dai, J.-P. Qu, Y.-B. Kang, *Eur. J. Org. Chem.* **2024**, *27*, e202301267.

[183] H. Chen, L. Liu, T. Huang, J. Chen, T. Chen, *Adv. Synth. Catal.* **2020**, *362*, 3332-3346.

[184] Y. Zhao, Y. Chen, T. R. Newhouse, *Angew. Chem. Int. Ed.* **2017**, *56*, 13122-13125.

[185] A. Shibatani, Y. Kataoka, Y. Ura, *Asian J. Org. Chem.* **2021**, *10*, 3285-3289.

[186] G. Meng, L. Hu, H. S. S. Chan, J. X. Qiao, J.-Q. Yu, *J. Am. Chem. Soc.* **2023**, *145*, 13003-13007.

[187] Z. Wang, L. Hu, N. Chekshin, Z. Zhuang, S. Qian, J. X. Qiao, J.-Q. Yu, *Science* **2021**, *374*, 1281-1285.

[188] Y. Xu, R. Zhang, B. Zhou, G. Dong, *J. Am. Chem. Soc.* **2024**, *146*, 22899-22905.

[189] Z. Li, Y. Tang, M. Lei, *ACS Catalysis* **2024**, *14*, 14263-14273.

[190] D. P. Nair, M. Podgórski, S. Chatani, T. Gong, W. Xi, C. R. Fenoli, C. N. Bowman, *Chem. Mater.* **2014**, *26*, 724-744.

[191] B. D. Mather, K. Viswanathan, K. M. Miller, T. E. Long, *Prog. Polym. Sci.* **2006**, *31*, 487-531.

[192] C. Gimbert, M. Lumbierres, C. Marchi, M. Moreno-Mañas, R. M. Sebastián, A. Vallribera, *Tetrahedron* **2005**, *61*, 8598-8605.

[193] A. Y. Rulev, *Russ. Chem. Rev.* **2011**, *80*, 197.

[194] C. F. Nising, S. Bräse, *Chem. Soc. Rev.* **2008**, *37*, 1218-1228.

[195] C. F. Nising, S. Bräse, *Chem. Soc. Rev.* **2012**, *41*, 988-999.

[196] P. Wadhwa, A. Kharbanda, A. Sharma, *Asian J. Org. Chem.* **2018**, *7*, 634-661.

[197] M. Bandini, P. G. Cozzi, M. Giacomini, P. Melchiorre, S. Selva, A. Umani-Ronchi, *J. Org. Chem.* **2002**, *67*, 3700-3704.

[198] S. K. Garg, R. Kumar, A. K. Chakraborti, *Tetrahedron Lett.* **2005**, *46*, 1721-1724.

[199] R. Katla, R. Katla, C. D. G. da Silva, B. F. dos Santos, T. A. Branquinho, C. T. B. Ferro, N. L. C. Domingues, *ChemistrySelect* **2019**, *4*, 13304-13306.

[200] S. Lauzon, M. Li, H. Keipour, T. Ollevier, *Eur. J. Org. Chem.* **2018**, *2018*, 4536-4540.

[201] H. Firouzabadi, N. Iranpoor, A. A. Jafari, *Synlett* **2005**, *2005*, 299-303.

[202] D. M. Pore, M. S. Soudagar, U. V. Desai, T. S. Thopate, P. P. Wadagaonkar, *Tetrahedron Lett.* **2006**, *47*, 9325-9328.

[203] N. Azizi, A. Khajeh-Amiri, H. Ghafuri, M. Bolourtchian, *Green Chem. Lett. Rev.* **2009**, *2*, 43-46.

[204] M. Winkler, Y. S. Raupp, L. A. M. Köhl, H. E. Wagner, M. A. R. Meier, *Macromolecules* **2014**, *47*, 2842-2846.

[205] O. Daglar, B. Ozcan, U. S. Gunay, G. Hizal, U. Tunca, H. Durmaz, *Polymer* **2019**, *182*, 121844.

[206] J. W. Chan, C. E. Hoyle, A. B. Lowe, M. Bowman, *Macromolecules* **2010**, *43*, 6381-6388.

[207] D. Zhang, M.-J. Dumont, A. Cherestes, *RSC Advances* **2016**, *6*, 83466-83470.

[208] W. Xi, C. Wang, C. J. Kloxin, C. N. Bowman, *ACS Macro Letters* **2012**, *1*, 811-814.

[209] J. W. Chan, B. Yu, C. E. Hoyle, A. B. Lowe, *Chem. Commun.* **2008**, 4959-4961.

[210] J. W. Chan, B. Yu, C. E. Hoyle, A. B. Lowe, *Polymer* **2009**, *50*, 3158-3168.

[211] G.-Z. Li, R. K. Randev, A. H. Soeriyadi, G. Rees, C. Boyer, Z. Tong, T. P. Davis, C. R. Becer, D. M. Haddleton, *Polym. Chem.* **2010**, *1*, 1196-1204.

[212] H. C. Kolb, M. G. Finn, K. B. Sharpless, *Angew. Chem. Int. Ed.* **2001**, *40*, 2004-2021.

[213] P. Spannring, P. C. A. Bruijnincx, B. M. Weckhuysen, R. J. M. Klein Gebbink, *Catal. Sci. Technol.* **2014**, *4*, 2182-2209.

[214] A. Enferadi Kerenkan, F. Béland, T.-O. Do, *Catal. Sci. Technol.* **2016**, *6*, 971-987.

[215] P. S. Bailey, *Ozonation in Organic Chemistry, Volume I: Olefinic Compounds*, Academic Press, New York, **1978**.

[216] S. G. Van Ornum, R. M. Champeau, R. Pariza, *Chem. Rev.* **2006**, *106*, 2990-3001.

[217] T. J. Fisher, P. H. Dussault, *Tetrahedron* **2017**, *73*, 4233-4258.

[218] *Chem. Eng. News* **1959**, *37*, 25-26.

[219] R. Criegee, *Angew. Chem. Int. Ed. Engl.* **1975**, *14*, 745-752.

[220] J. Kubitschke, H. Lange, H. Strutz, in *Ullmann's Encyclopedia of Industrial Chemistry*, **2014**.

[221] A. Köckritz, A. Martin, *Eur. J. Lipid Sci. Technol.* **2011**, *113*, 83-91.

[222] B. Cornils, P. Lappe, in *Ullmann's Encyclopedia of Industrial Chemistry*, **2014**.

[223] M. K. Pulfer, R. C. Murphy, *J. Biol. Chem.* **2004**, *279*, 26331-26338.

[224] M. L. Bell, R. D. Peng, F. Dominici, *Environ. Health Perspect.* **2006**, *114*, 532-536.

[225] P. M. Gordon, *Chem. Eng. News* **1990**, *68*, 2-3.

[226] J. Kula, *Chem. Health Saf.* **1999**, *6*, 21-22.

[227] B. Zaldman, A. Kisilev, Y. Sasson, N. Garti, *J. Am. Oil Chem. Soc.* **1988**, *65*, 611-615.

[228] R. U. Lemieux, E. V. Rudloff, *Can. J. Chem.* **1955**, *33*, 1701-1709.

[229] C.-M. Ho, W.-Y. Yu, C.-M. Che, *Angew. Chem. Int. Ed.* **2004**, *43*, 3303-3307.

[230] D. Yang, C. Zhang, *J. Org. Chem.* **2001**, *66*, 4814-4818.

[231] P. H. J. Carlsen, T. Katsuki, V. S. Martin, K. B. Sharpless, *J. Org. Chem.* **1981**, *46*, 3936-3938.

[232] P. Daw, R. Petakamsetty, A. Sarbajna, S. Laha, R. Ramapanicker, J. K. Bera, *J. Am. Chem. Soc.* **2014**, *136*, 13987-13990.

[233] R. Pappo, J. D. Allen, R. Lemieux, W. Johnson, *J. Org. Chem.* **1956**, *21*, 478-479.

[234] F. Zimmermann, E. Meux, J.-L. Mieloszynski, J.-M. Lecuire, N. Oget, *Tetrahedron Lett.* **2005**, *46*, 3201-3203.

[235] B. R. Travis, R. S. Narayan, B. Borhan, *J. Am. Chem. Soc.* **2002**, *124*, 3824-3825.

[236] A. Behr, N. Tenhumberg, A. Wintzer, *RSC Advances* **2013**, *3*, 172-180.

[237] A. Behr, N. Tenhumberg, A. Wintzer, *Eur. J. Lipid Sci. Technol.* **2012**, *114*, 905-910.

[238] M. Passerini, *Gazz. Chem. Ital.* **1921**, *51*, 126–129.

[239] A. Dömling, I. Ugi, *Angew. Chem. Int. Ed.* **2000**, *39*, 3168-3210.

[240] I. Ugi, *Angew. Chem. Int. Ed. Engl.* **1962**, *1*, 8-21.

[241] R. H. Baker, D. Stanonis, *J. Am. Chem. Soc.* **1951**, *73*, 699-702.

[242] S. Maeda, S. Komagawa, M. Uchiyama, K. Morokuma, *Angew. Chem. Int. Ed.* **2011**, *50*, 644-649.

[243] O. Kreye, T. Tóth, M. A. R. Meier, *J. Am. Chem. Soc.* **2011**, *133*, 1790-1792.

[244] X.-X. Deng, L. Li, Z.-L. Li, A. Lv, F.-S. Du, Z.-C. Li, *ACS Macro Letters* **2012**, *1*, 1300-1303.

[245] Y.-Z. Wang, X.-X. Deng, L. Li, Z.-L. Li, F.-S. Du, Z.-C. Li, *Polym. Chem.* **2013**, *4*, 444-448.

[246] J. Zhang, M. Zhang, F.-S. Du, Z.-C. Li, *Macromolecules* **2016**, *49*, 2592-2600.

[247] L.-J. Zhang, X.-X. Deng, F.-S. Du, Z.-C. Li, *Macromolecules* **2013**, *46*, 9554-9562.

[248] A. E. J. de Nooy, G. Masci, V. Crescenzi, *Macromolecules* **1999**, *32*, 1318-1320.

[249] V. Crescenzi, A. Francescangeli, D. Capitani, L. Mannina, D. Renier, D. Bellini, *Carbohydr. Polym.* **2003**, *53*, 311-316.

[250] A. E. J. de Nooy, D. Capitani, G. Masci, V. Crescenzi, *Biomacromolecules* **2000**, *1*, 259-267.

[251] S. König, I. Ugi, *Zeitschrift für Naturforschung B* **1991**, *46*, 1261-1266.

[252] H. Bu, A.-L. Kjøniksen, K. D. Knudsen, B. Nyström, *Biomacromolecules* **2004**, *5*, 1470-1479.

[253] H. Bu, A.-L. Kjøniksen, B. Nyström, *Eur. Polym. J.* **2005**, *41*, 1708-1717.

[254] N. Hauck, N. Seixas, S. P. Centeno, R. Schlüßler, G. Cojoc, P. Müller, J. Guck, D. Wöll, L. A. Wessjohann, J. Thiele, *Polymers* **2018**, *10*, 1055.

[255] W. Lin, T. Sun, M. Zheng, Z. Xie, Y. Huang, X. Jing, *RSC Advances* **2014**, *4*, 25114-25117.

[256] L. Santos Correa, E. Stapf, T. Nonner, M. A. R. Meier, *Eur. J. Lipid Sci. Technol.* **2025**, e70003.

[257] Sigma-Aldrich Chemie GmbH, *N,N-Dimethylformamide; MSDS Product Number 227056*, **2024**, https://www.sigmaaldrich.com/DE/en/product/sial/227056; access date: 2024.11.14.

[258] Sigma-Aldrich Chemie GmbH, *p-Benzoquinone; MSDS Product Number B10358*, **2024**, https://www.sigmaaldrich.com/DE/en/product/sial/b10358; access date: 13.11.2024.

[259] R. K. Henderson, C. Jiménez-González, D. J. C. Constable, S. R. Alston, G. G. A. Inglis, G. Fisher, J. Sherwood, S. P. Binks, A. D. Curzons, *Green Chem.* **2011**, *13*, 854-862.

[260] C. M. Alder, J. D. Hayler, R. K. Henderson, A. M. Redman, L. Shukla, L. E. Shuster, H. F. Sneddon, *Green Chem.* **2016**, *18*, 3879-3890.

[261] W.-X. Wu, *Polym. Int.* **2019**, *68*, 1848-1855.

[262] R. Sanaa, D. Portinha, R. Medimagh, E. Fleury, *Eur. Polym. J.* **2024**, *220*, 113498.

[263] Sigma-Aldrich Chemie GmbH, *1,8-Diazabicyclo[5.4.0]undec-7-ene; MSDS Product Number 8.03282*, **2024**, https://www.sigmaaldrich.com/DE/en/product/mm/803282; access date: 2024.11.17.

[264] Sigma-Aldrich Chemie GmbH, *1,1,3,3-Tetramethylguanidine; MSDS Product Number 241768*, **2023**, https://www.sigmaaldrich.com/DE/en/product/aldrich/241768; access date: 2024.11.17.

[265] R. K. Henderson, A. P. Hill, A. M. Redman, H. F. Sneddon, *Green Chem.* **2015**, *17*, 945-949.

[266] I. Galleano, M. Schiedel, M. Jung, A. S. Madsen, C. A. Olsen, *J. Med. Chem.* **2016**, *59*, 1021-1031.

[267] M. M. Ahsan, S. Sung, H. Jeon, M. D. Patil, T. Chung, H. Yun, *Catalysts* **2018**, *8*, 4.

[268] E. Hempel, H. Huth, M. Beiner, *Thermochim. Acta* **2003**, *403*, 105-114.

[269] L. Santos Correa, M. A. R. Meier, *Eur. J. Lipid Sci. Technol.* **2023**, *125*, 2200171.

[270] L. Santos Correa, *Ruthenium Catalyzed Oxidative Cleavage of Unsaturated Renewable Resources*, Master thesis, Karlsruhe Institute of Technology (KIT), **2021**.

[271] A. Chernova, R. Gubaev, P. Mazin, S. Goryunova, Y. Demurin, L. Gorlova, A. Vanushkina, W. Mair, N. Anikanov, E. Martynova, D. Goryunov, S. Garkusha, Z. Mukhina, P. Khaytovich, *Biomolecules* **2019**, *9*, 9.

[272] M. Melchiorre, V. Benessere, M. E. Cucciolito, C. Melchiorre, F. Ruffo, R. Esposito, *ChemistrySelect* **2020**, *5*, 1396-1400.

[273] A. W. T. King, J. Jalomäki, M. Granström, D. S. Argyropoulos, S. Heikkinen, I. Kilpeläinen, *Analytical Methods* **2010**, *2*, 1499-1505.

[274] X. Meng, C. Crestini, H. Ben, N. Hao, Y. Pu, A. J. Ragauskas, D. S. Argyropoulos, *Nature Protocols* **2019**, *14*, 2627-2647.

[275] B. D. Herzog, R. A. Smiley, in *Ullmann's Encyclopedia of Industrial Chemistry*, **2012**.

[276] M. T. Musser, in *Ullmann's Encyclopedia of Industrial Chemistry*, **2000**.

[277] J. Rios, J. Lebeau, T. Yang, S. Li, M. D. Lynch, *Green Chem.* **2021**, *23*, 3172-3190.

[278] R. A. Sheldon, *J. Mol. Catal. A: Chem.* **2016**, *422*, 3-12.

[279] S.-Y. Hwang, J.-M. Woo, G. E. Choi, D.-K. Oh, J.-H. Seo, J.-B. Park, *ACS Catalysis* **2024**, *14*, 4130-4138.

[280] D. K. Raff, in *Ullmann's Encyclopedia of Industrial Chemistry*, **2013**.

[281] C. Kohlpaintner, M. Schulte, J. Falbe, P. Lappe, J. Weber, G. D. Frey, in *Ullmann's Encyclopedia of Industrial Chemistry*, **2013**.

[282] Y.-T. Guo, C. Shi, T.-Y. Du, X.-Y. Cheng, F.-S. Du, Z.-C. Li, *Macromolecules* **2022**, *55*, 4000-4010.

[283] Z. Söyler, K. N. Onwukamike, S. Grelier, E. Grau, H. Cramail, M. A. R. Meier, *Green Chem.* **2018**, *20*, 214-224.

[284] R. M. Carrillo, A. G. Neo, L. López-García, S. Marcaccini, C. F. Marcos, *Green Chem.* **2006**, *8*, 787-789.

[285] M. Shiri, Z. Gholami-Koupaei, F. Bandehali-Naeini, M.-S. Tonekaboni, S. Soheil-Moghaddam, D. Ebrahimi, S. Karami, B. Notash, *Synthesis* **2020**, *52*, 3243-3252.

[286] H. A. Schenck, P. W. Lenkowski, I. Choudhury-Mukherjee, S.-H. Ko, J. P. Stables, M. K. Patel, M. L. Brown, *Biorg. Med. Chem.* **2004**, *12*, 979-993.

[287] M. R. Wood, K. M. Schirripa, J. J. Kim, S. D. Kuduk, R. K. Chang, C. N. Di Marco, R. M. DiPardo, B.-L. Wan, K. L. Murphy, R. W. Ransom, R. S. L. Chang, M. A. Holahan, J. J. Cook, W. Lemaire, S. D. Mosser, R. A. Bednar, C. Tang, T. Prueksaritanont, A. A. Wallace, Q. Mei, J. Yu, D. L. Bohn, F. C. Clayton, E. D. Adarayn, G. R. Sitko, Y. M. Leonard, R. M. Freidinger, D. J. Pettibone, M. G. Bock, *Bioorganic & Medicinal Chemistry Letters* **2008**, *18*, 716-720.

[288] *Lignocellulose biorefinery "final report"*, https://www.cbp.fraunhofer.de/en/reference-projects/lignocellulose-biorefinery.html; access date: 04.12.2024.

[289] *Lignocellulose biorefinery Product sheet "Organosolv lignin"*, https://www.cbp.fraunhofer.de/en/range-of-services/processing-of-raw-materials/lignocellulose-biorefinery.html; access date: 04.12.2024.

[290] F. H. Isikgor, C. R. Becer, *Polym. Chem.* **2015**, *6*, 4497-4559.

[291] I. Bechthold, K. Bretz, S. Kabasci, R. Kopitzky, A. Springer, *Chem. Eng. Technol.* **2008**, *31*, 647-654.

[292] J. Sun, J. Hu, G. Liu, D. Xiao, G. He, R. Lu, *J. Polym. Sci., Part A: Polym. Chem.* **2011**, *49*, 1282-1288.

[293] M. W. Halloran, L. Danielczak, J. A. Nicell, R. L. Leask, M. Marić, *ACS Appl. Polym. Mater.* **2022**, *4*, 3608-3617.

[294] M. Novotný, A. Hrabálek, B. Janůšová, J. Novotný, K. Vávrová, *Bioorg. Med. Chem. Lett.* **2009**, *19*, 344-347.

[295] G. H. Schenk, in *Quantitative Organic Analysis via Functional Groups*, Pergamon Press, Oxford, England, **1968**, pp. 30-44.

[296] J. L. Cohen, G. P. Fong, *Anal. Chem.* **1975**, *47*, 313-316.

[297] P. Ballinger, F. A. Long, *J. Am. Chem. Soc.* **1960**, *82*, 795-798.

[298] A. Kütt, V. Movchun, T. Rodima, T. Dansauer, E. B. Rusanov, I. Leito, I. Kaljurand, J. Koppel, V. Pihl, I. Koppel, G. Ovsjannikov, L. Toom, M. Mishima, M. Medebielle, E. Lork, G.-V. Röschenthaler, I. A. Koppel, A. A. Kolomeitsev, *J. Org. Chem.* **2008**, *73*, 2607-2620.

[299] T. C. Bruice, U. K. Pandit, *Proc. Natl. Acad. Sci. U. S. A.* **1960**, *46*, 402-404.

[300] F. Monteil-Rivera, L. Paquet, *Ind. Crops Prod.* **2015**, *65*, 446-453.

[301] C. Scarica, R. Suriano, M. Levi, S. Turri, G. Griffini, *ACS Sustainable Chem. Eng.* **2018**, *6*, 3392-3401.

[302] L.-Y. Liu, M. Cho, N. Sathitsuksanoh, S. Chowdhury, S. Renneckar, *ACS Sustainable Chem. Eng.* **2018**, *6*, 12251-12260.

[303] H. Jork, W. Funk, W. Fischer, H. Wimmer, *Thin-Layer Chromatography: Reagents and Detection Methods, Vol. 1*, VCH Verlagsgesellschaft Weinheim, **1990**.

[304] W. C. Still, M. Kahn, A. Mitra, *J. Org. Chem.* **1978**, *43*, 2923-2925.

[305] J. Kim, D. N. Kim, S. H. Lee, S.-H. Yoo, S. Lee, *Food Chem.* **2010**, *118*, 398-402.

[306] K. A. Waibel, R. Nickisch, N. Möhl, R. Seim, M. A. R. Meier, *Green Chem.* **2020**, *22*, 933-941.

List of Abbreviations

Abbreviations for chemical compounds and groups

α	The first carbon atom next to a functional group
β	The second carbon atom next to a functional group
ω	The carbon atom furthest away from the functional group
Ac	Acetyl
Aliquat 336	Methyltrioctylammonium chloride
^{t}Amyl-OH	*tert*-Amyl alcohol
bpy	2,2'-Bipyridine
^{t}BuOH	*tert*-Butanol
CDI	1,1'-Carbonyldiimidazole
DBN	1,5-Diazabicyclo[4.3.0]non-5-ene
DBU	1,8-Diazabicyclo[5.4.0]undec-7-ene
DDT	Dichlorodiphenyltrichloroethane
DMAc	*N*,*N*-Dimethylacetamide
DMC	Dimethyl carbonate
DMF	*N*,*N*-Dimethylformamide
DMPA	2,2-Dimethoxy-2-phenylacetophenone
DMSO	Dimethyl sulfoxide
DPA	Pyridine-2,6-dicarboxylic acid, Dipicolinic acid
EBIB	Ethyl 2-bromoisobutyrate
Et	Ethyl
FA	Formic acid
FAME	Fatty acid methyl ester
FDCA	2,5-Furandicarboxylic acid
HOSO	High oleic sunflower oil
LDA	Lithium diisopropylamide
MDI	Methylene diphenyl diisocyanate
Me-THF	2-Methyltetrahydrofuran
NBM	5-Norbornene-2-methanol
PEF	Poly(ethylene furanoate)

PMDETA	Pentamethyldiethylenetriamine
PMMA	Poly(methyl methacrylate)
PTFE	Poly(tetrafluoroethylene)
PU	Polyurethane
$Ru(acac)_3$	Ruthenium(III) acetylacetonate
SAn	Succinic anhydride
TBD	1,5,7-Triazabicyclo[4.4.0]dec-5-ene
THF	Tetrahydrofuran
TMG	1,1,3,3-Tetramethylguanidine
$Zn(TMP)_2$	Bis(2,2,6,6,-tetramethylpiperidinyl)zinc

Other abbreviations

δ	Chemical shift
λ	Wavelength
$\tilde{\nu}$	Wavenumber (1/λ)
ADMET	Acyclic diene metathesis
AAE	Actual atom economy
AE	Atom economy
ATR	Attenuated total reflection
ATRP	Atom transfer radical polymerization
c	Concentration
CDBCA	Conversion of double bonds into carboxylic acids
cEF	Complete environmental factor
Đ	Dispersity
DFT	Density functional theory
DS	Degree of substitution
DSC	Differential scanning calorimetry
E factor	Environmental factor
equiv.	Equivalents
ESI	Electrospray ionization
FID	Flame ionization detector
GC	Gas chromatography

COSY	Gradient selected correlation spectroscopy
HMBC	Heteronuclear multiple bond correlation
$HSQC_{ed}$	Phase-edited heteronuclear single quantum coherence
IR	Infrared
LCA	Life Cycle Assessment
MI	Mass intensity
M_n	Number average molar mass
MS	Mass spectrometry
M_w	Mass average molar mass
MW	Molecular weight
NMR	Nuclear magnetic resonance
P	Probability
P-3CR	Passerini three-component reaction
p.a.	Pro analysis (degree of purity)
PMI	Process mass intensity
r.t.	Room temperature
R_f	Retardation factor
RME	Reaction mass efficiency
ROMP	Ring-opening metathesis polymerization
SEC	Size exclusion chromatography
sEF	Simple environmental factor
$T_{d,5\%}$	Temperature of 5 weight% loss
T_g	Glass transition temperature
TGA	Thermogravimetric analysis
T_m	Melting temperature
TLC	Thin-layer chromatography
UV	Ultraviolet

Scientific Contributions

List of publications

[6] L. Santos Correa, E. Stapf, T. Nonner, M. A. R. Meier, Catalytic Dehydrogenation of Lauric Acid and a Potential Use in Polyester Synthesis, *Eur. J. Lipid Sci. Technol.* **2025**, e70003.

[5] L. Santos Correa, S. Leidenheimer, M. A. R. Meier, Sunflower oil-based thermosets via the Passerini three-component reaction, *Polym. Chem.* **2025**, *16*, 821-832.

[4] J. O. Wenzel, L. Santos Correa, S. Schmidt, M. A. R. Meier, Benign synthesis of terpene-based 1,4-*p*-menthane diamine, *Sci. Rep.* **2024**, *14*, 8055.

[3] C. Libretti, L. Santos Correa, M. A. R. Meier, From waste to resource: advancements in sustainable lignin modification, *Green Chem.* **2024**, *26*, 4358-4386.

[2] L. Santos Correa, M. A. R. Meier, Ruthenium Catalyzed Oxidative Cleavage of High Oleic Sunflower Oil: Considerations Regarding the Synthesis of a Fully Biobased Triacid, *Eur. J. Lipid Sci. Technol.* **2023**, *125*, 2200171.

[1] M. Dahlen, J. Vázquez Quesada, L. Santos Correa, L. Münzfeld, N. Reinfandt, W. Klopper, P. W. Roesky, Investigation of the Coordination Chemistry of a Bisamidinate Ferrocene Ligand with Cu, Ag, and Au, *ACS Omega* **2022**, *7*, 4683-4693.

List of conference contributions

[3] Presentation: “Sunflower oil based thermosets *via* the Passerini three component reaction” at the *50th IUPAC World Polymer Congress* held at the University of Warwick, Coventry, England, **July 2024**.

[2] Poster: “Sunflower oil based thermosets *via* the Passerini three component reaction” at the *12th Workshop on Fats and Oils as Renewable Feedstocks for the Chemical Industry*, Dortmund, Germany, **June 2024**.

[1] Poster: “Ruthenium Catalyzed Oxidative Cleavage of High Oleic Sunflower Oil” at the *11th Workshop on Fats and Oils as Renewable Feedstocks for the Chemical Industry*, Dortmund, Germany, **May 2022**.

Danksagung

Ich möchte mich bei allen Personen bedanken, welche mich in den letzten acht Jahren vom Anfang des Studiums bis hin zum Ende dieser Doktorarbeit begleitet und unterstützt haben.

Als erstes möchte ich mich bei Prof. Michael Meier dafür bedanken, dass er mir die Möglichkeit gegeben hat, sowohl meine Masterarbeit, als auch meine Doktorarbeit in seiner Arbeitsgruppe anzufertigen. Seine offene und freundliche Art hat ein schönes Arbeitsklima geschaffen, für welches ich sehr dankbar bin. Ich möchte mich besonders für das Vertrauen bedanken, welches er mir entgegengebracht hat.

Des Weiteren möchte ich mich bei allen Personen bedanken, mit denen ich während meiner Promotion zusammengearbeitet habe: Leon Bartlewski, Philipp Bohn, Qianyu Cai, Peter Conen, Francesca Destaso, Benjamin Felker, Federico Ferrari, Luca Filippi, Andreas Ganzbuhl, Nichollas Jaques, Anja Kirchberg, Hendrik Kirchhoff, Silas Leidenheimer, Celeste Libretti, Jiangling (Caitlyn) Liu, Federico Mundo, Hatice Mutlu, Luca Narducci, Roman Nickisch, Timo Nonner, Michael Rhein, Pinar Sancar, Clara Scheelje, Timo Sehn, Severin Stalter, Emma Stapf, Sandra Wegelin, Jonas Wenzel, Julian Windbiel und Jonas Wolfs.

Außerdem möchte ich mich bei allen Personen, welche mich bei meiner Forschung unterstützt haben, bedanken: Richard von Budberg für die spezialangefertigten Kugelrohr Kolben, Birgit Huber für TGA Messungen, Alexander Jaks für die spezialangefertigte Teflon Form, Azra Kocaarslan für DSC Messungen, Carlos Miguelez-Böbel und Christoph Götz und Nathalie Schmitt für die Chemikalienausgabe, Andreas Rapp und Despina Savvidou für die Wartung der NMR-Geräte, Angelika Mösle und Lara Hirsch für Massenspektrometrie Messungen, Klara Urbschat und Katharina Kuppinger für GPC Messungen, und Valerian Hirschberg und Max Schußmann für Zug-Dehn Messungen.

Ich möchte mich ferner auch für die großartige Zeit mit meinen Kollegen während wissenschaftlichen Konferenzen bedanken. Ich bedanke mich bei Anja, Francesca, Timo und Hatice für die Zeit in Dortmund beim „11th Workshop on Fats and Oils as Renewable Feedstocks for the Chemical Industry“, bei Anja, Clara, Qianyu, Federico, Jonas und Philipp für die Zeit in Freiburg bei der Makro 2023, bei Clara, Nichollas, Timo und Philipp für die Zeit in Coventry beim „50th IUPAC World Polymer Congress“, und bei Celeste und Iuliana für die Zeit in Turku beim „17th European Workshop on Lignocellulosics and Pulp“.

Ich möchte mich speziell bei Silas, Emma und Timo für die äußerst produktive Zusammenarbeit bedanken. Ohne sie wäre ich mit meinen Forschungsprojekten nicht so weit gekommen. Ich möchte mich darüber hinaus für die gute Zeit, welche ich mit ihnen außerhalb der Arbeit verbringen konnte, bedanken.

Ein besonderer Dank gilt meinen Arbeitskollegen und Freunden Pete und Timo, welche meine Zeit während der Promotion in vielerlei Hinsicht bereichert haben.

Auch möchte ich mich bei Jonas, mit welchem ich das Chemie Studium vor 8 Jahren begonnen habe, bedanken. Die unzähligen Wochen in denen wir während dem Studium zusammen gelernt haben, haben meine fachliche Kompetenz enorm erweitert. Ich möchte mich für die Freundschaft und die vielen schönen Momente bedanken.

Ich möchte mich bei meinen Eltern Carlos und Ivone dafür bedanken, dass sie mich schon in jungen Jahren für die Wissenschaft begeistern konnten und mich zu jeder Zeit auf diesem Weg begleitet und unterstützt haben.

Zuletzt möchte ich mich bei Maya für die unglaubliche Unterstützung während meiner gesamten Promotion bedanken. Sie hat einen erheblichen Teil dazu beigetragen, dass ich es so weit geschafft habe. Dafür bin ich ihr sehr dankbar.